Caractérisation structurale d'enzymes hydrolysant les organophosphorés et rationalisation de leur amélioration en vue d'applications biotechnologiques

Guillaume Gotthard

THESE

Pour obtenir le grade de

DOCTEUR DE L'UNIVERSITE D'AIX-MARSEILLE

Spécialité : Biochimie structurale

Présenté par

Guillaume GOTTHARD

Caractérisation structurale d'enzymes hydrolysant les organophosphorés et rationalisation de leur amélioration en vue d'applications biotechnologiques

---

Jury composé de

Rapporteurs	Patrick MASSON
	Claude DIDIERJEAN
Examinateurs	Miguel ORTIZ-LOMBARDIA
	Laurent VERDIER
Directeur de thèse	Eric CHABRIERE
Co-encadrant de thèse	Mikael ELIAS

Remerciements

Je tiens tout d'abord à remercier mon directeur de thèse, le Pr. Eric Chabrière, qui m'a accueilli au sein de son équipe, m'accordant sa confiance et des responsabilités tout au long de mon parcours. Je le remercie également pour la liberté qu'il m'a laissée dans l'orientation de mes travaux, me permettant de prendre rapidement confiance, contribuant ainsi à ma formation. Je remercie également le Dr. Mikael Elias, pour la formation qu'il m'a prodiguée, pour tout son soutien et ses précieux conseils tout au long de ma thèse.

Je remercie les Dr. Yves Bourne et le Pr. Didier Raoult, directeurs respectifs des laboratoires AFMB et URMITE au sein desquels j'ai effectué mes travaux de thèse. Je remercie aussi l'ensemble des enseignants qui ont participé à ma formation académique à l'Université de la Méditerranée et qui ont su me donner goût à la Recherche.

Je tiens à remercier nos partenaires et collaborateurs qui ont contribué à nos travaux. En particulier, je remercie la DGA qui a financé ma thèse et les travaux au sein du groupe.

Je remercie également les membres du jury qui m'ont fait l'honneur d'accepter d'évaluer mes travaux de thèse.

La Recherche étant un travail d'équipe, je remercie les différents membres du groupe qui ont apporté l'ambiance de travail et la cohésion nécessaire à cette période difficile qu'est la thèse. En particulier je remercie le Dr. Julien Hiblot avec qui nous avons rapidement formé un duo complémentaire nous permettant à tous deux d'être plus efficaces.

Je remercie toute ma famille pour tout le soutien qu'ils m'ont apporté tout au long de ces années, pour leurs encouragements et pour l'aide qu'ils m'ont prodiguée.

Enfin, je tiens à remercier ma Cynthia, qui m'a toujours soutenu, encouragé et supporté dans mes succès comme dans mes échecs.

Avant-propos

Les recherches du groupe sont axées autour de trois principales thématiques, le développement de bio-épurateurs d'organosphosphorés, l'inhibition de la virulence bactérienne par interférence au *quorum* sensing, et l'étude de la famille des protéines DING. Malgré l'apparente absence de lien entre ces différents projets, ceux-ci ont pour origine commune les travaux initiés sur l'étude de la paraoxonase humaine hPON1 au cours du service militaire du Pr. Eric Chabrière. En effet, alors que celui-ci fut chargé d'obtenir la structure de cette enzyme, c'est son partenaire physiologique, une protéine DING nommée HPBP qui cristallisa. De cette découverte débuta les travaux d'étude de cette famille protéique aux propriétés biologiques étonnantes.

Plus tard, la thématique de décontamination des organophosphorés pris son envol avec l'étude de l'enzyme hyperthermostable *Sso*Pox. Egalement capable de dégrader les molécules utilisées dans la communication interbactérienne, l'étude de *Sso*Pox devint un projet très important du fait de ses propriétés biotechnologiques exceptionnelles, qui en font le candidat idéal pour le développement de bio-produits à fort potentiel de valorisation. Ainsi mes travaux de thèse se sont tout naturellement articulés autour de ces différentes thématiques avec pour objectifs principaux d'étudier l'enzyme *Sso*Pox et ses homologues, caractériser de nouvelles enzymes d'intérêt biotechnologique afin de rationaliser l'ingénierie enzymatique par l'approche structurale. C'est pourquoi, j'ai choisi d'intituler ma thèse :

Caractérisation structurale d'enzymes hydrolysant les organophosphorés et rationalisation de leur amélioration en vue d'applications biotechnologiques

Les travaux présentés dans ce manuscrit furent initiés au sein du laboratoire AFMB, dont la spécialité est l'étude structurale et fonctionnelle des protéines, puis se sont poursuivis au sein de l'URMITE, spécialisé dans l'étude des maladies infectieuses. L'environnement matériel et humain de ces deux laboratoires permet ainsi d'expliquer, en tout cas en partie, les différentes orientations prises par le sujet. Le manuscrit comprend une introduction sur le projet, une partie résultats présentée sous forme d'articles scientifiques publiés. Ceux-ci sont accompagnés d'une conclusion rappelant les principaux résultats obtenus ainsi que d'une partie perspective sur les résultats en cours d'étude et les orientations prises par le projet. En fin de manuscrit sont également fournis un bilan du travail et une fiche résumé de la thèse. Enfin, les travaux annexes auxquels j'ai pu participer activement tout au long de mon travail au sein du groupe sont présentés sous forme d'articles scientifiques publiés et de manuscrits soumis dans des journaux à comité de lecture.

Table des matières

Abréviations :

CWA : Chemical Warfare Agents (agents chimiques de guerre)

N(R)BC : Nucléaire, Radiologique, Bactériologique et Chimique

AChE : AcétylCholinEstérase

BuChE : ButyrylCholinEstérase

SNC : Système Nerveux Central

PTE : PhosphoTriEstérases

ISOR : “Incorporating Synthetic Oligonucleotide via gene Reassembly”

PCR : réaction de polymérisation en chaine

QM/MM : Quantum Mechanics / Molecular Mechanics

DDT : DichloroDiphenylTrichloroethane

DFP : Diisopropyl FluoroPhosphate

HDL : High Density Lipoparticules

LDL : Low Density Lipoparticules

rePON1 : recombinant Paraoxonase 1

PEG : PolyEthylène Glycol

OPAA : OrganoPhosphorus Acid Anhydrolase

MPH : Methyl Parathion Hydrolase

PLL : Phosphotriestérase-Like Lactonase

QS : *quorum* sensing

QQ : *quorum* quenching

AHL : Acyl Homosérine Lactone

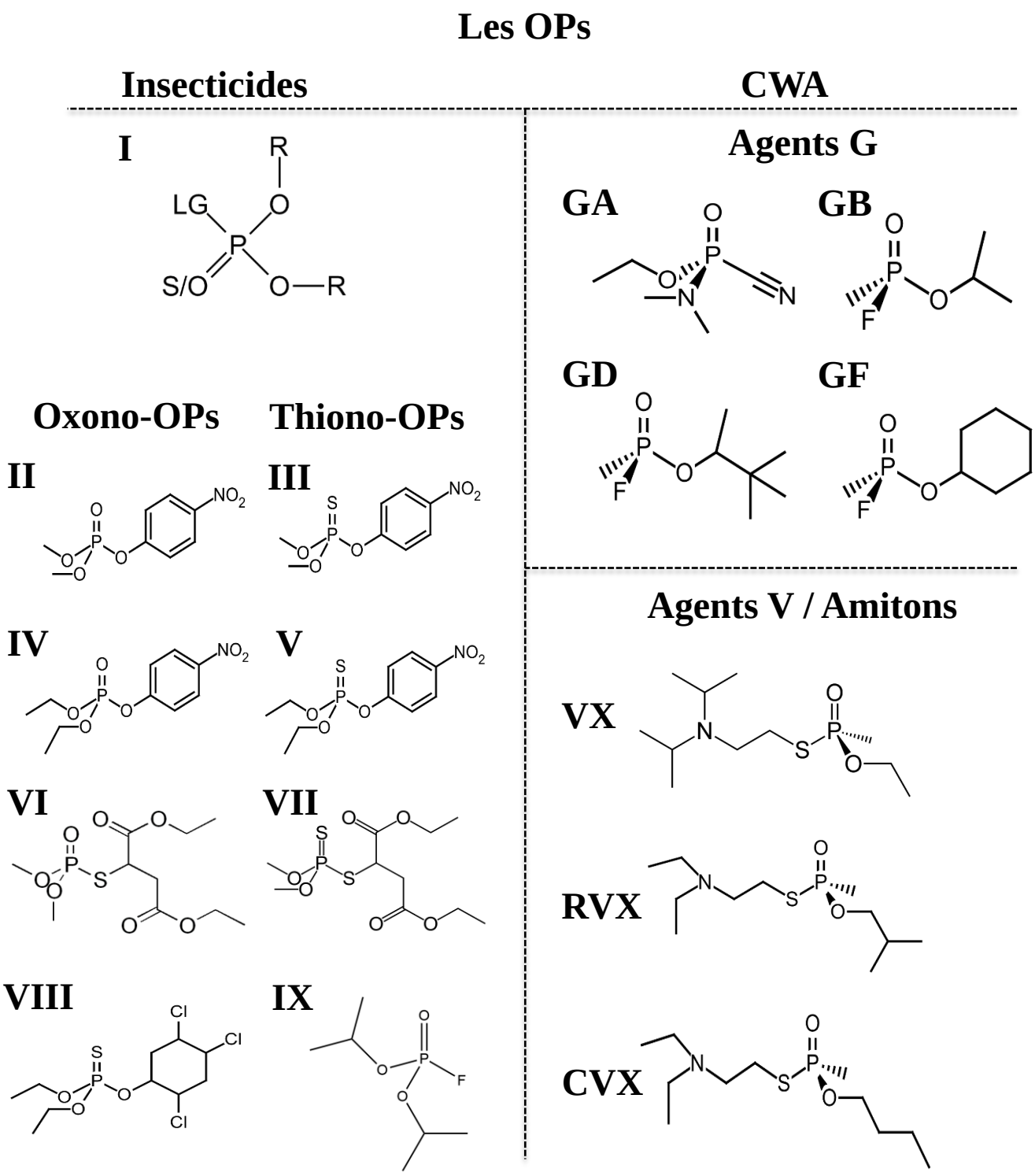

Figure I.1 : *Structure chimique des principaux insecticides et CWA*

Structure chimique générale des insecticides OPs montrant le groupement partant (LG), les différentes décorations R et l'atome terminal S (thiono-OPs) ou O (oxono-OPs) (**I**). Différents exemples d'insecticides : methyl-paraoxon (**II**), methyl-paraothion (**III**), ethyl-paraoxon (**IV**), ethyl-parathion (**V**), malaoxon (**VI**), malathion (**VII**), chlorpyrifos (**VIII**), diisopropyl fluorophosphate (**IX**). Différents exemples de CWA : agents G : tabun (**GA**), sarin (**GB**), soman (**GD**), cyclosarin (**GF**); agents V : VX (**VX**), Russian-VX (**RVX**), Chinese-VX (**CVX**).

I. Synthèse bibliographique :

A. Les Composés organophosphorés

1. Historique des organophosphorés

Les agents chimiques de guerre (CWA) sont des composés hautement toxiques dont le but est de blesser, tuer, mettre hors de combat ou contrôler l'adversaire (1). L'utilisation de tels agents chimiques remonterait au V^{ème} siècle avant Jésus Christ (lors de la guerre du Péloponnèse) mais leur utilisation moderne ne date que de la 1ère guerre mondiale avec l'utilisation d'ypérite (gaz moutarde) et de phosgène, deux agents chimiques à base de chlore (1). Ce n'est finalement qu'avec l'amélioration des connaissances en science et plus particulièrement en chimie au XIX^{ème}, que la possibilité de produire à grande échelle des armes chimiques de guerre a été exploitée. Peu avant le début de la 2nde guerre mondiale, la production massive d'armes chimiques à base d'OrganoPhosphorés (OPs) a pu être développée par l'Allemagne. Ainsi, le développement des agents G (Germany) débuta dès 1937 avec le Tabun, suivi du Sarin en 1939 et du Soman en 1944 (tous trois étant des agents G, voir **Figure I.1**). Après la 2nde guerre mondiale, les agents V (selon les sources pour Victory, Venomous, Viscous) comme le VX ont été développés par différentes nations comme les Etats-Unis, la Russie (Russian-VX) et plus récemment la Chine (CVX) (**Figure I.1**). Les agents V furent également commercialisés en tant qu'insecticides par l'ICI (Imperial Chemical Industries) dans les années 50 et appelés alors Amitons. La production d'OPs a ainsi atteint son paroxysme au cours de la guerre froide pendant laquelle d'énormes quantités d'agents chimiques furent accumulées (1).

Au cours du XX^{ème} siècle les armes chimiques furent utilisées par différents dictateurs, extrémistes, sectes et groupes terroristes. Les agents neurotoxiques à base d'OPs ont pour la première fois été utilisés lors de la Guerre Iran - Irak en 1980 et l'on estime qu'entre 1980 et 1988, 387 attaques à l'arme chimique ont été commanditées par le régime Irakien (2). Le nombre de victimes militaires estimé est de plus de 100 000 auquel s'ajoute un nombre de victimes civiles élevé qui subissent encore aujourd'hui les effets à long terme de l'exposition. L'année 1988 est marquée par l'attaque au gaz Sarin commanditée par Saddam Hussein, le leader Irakien, contre la ville Irakienne Halabja où étaient présente la minorité Kurde (1). Cette attaque tua plus de 10 % de la population de la ville soit plus de 5 000 personnes. Durant la guerre du Golfe, de nombreux soldats américains furent exposés aux OP lors de la destruction de stocks de munitions contenant des OPs tels que le sarin et le cyclosarin. En revanche, aucune exposition aigue ne fut recensée, mais de nombreux soldats présentaient et présentent encore des effets à long terme : le « syndrome de la guerre du Golfe » (1). Le syndrome de la guerre du Golfe est

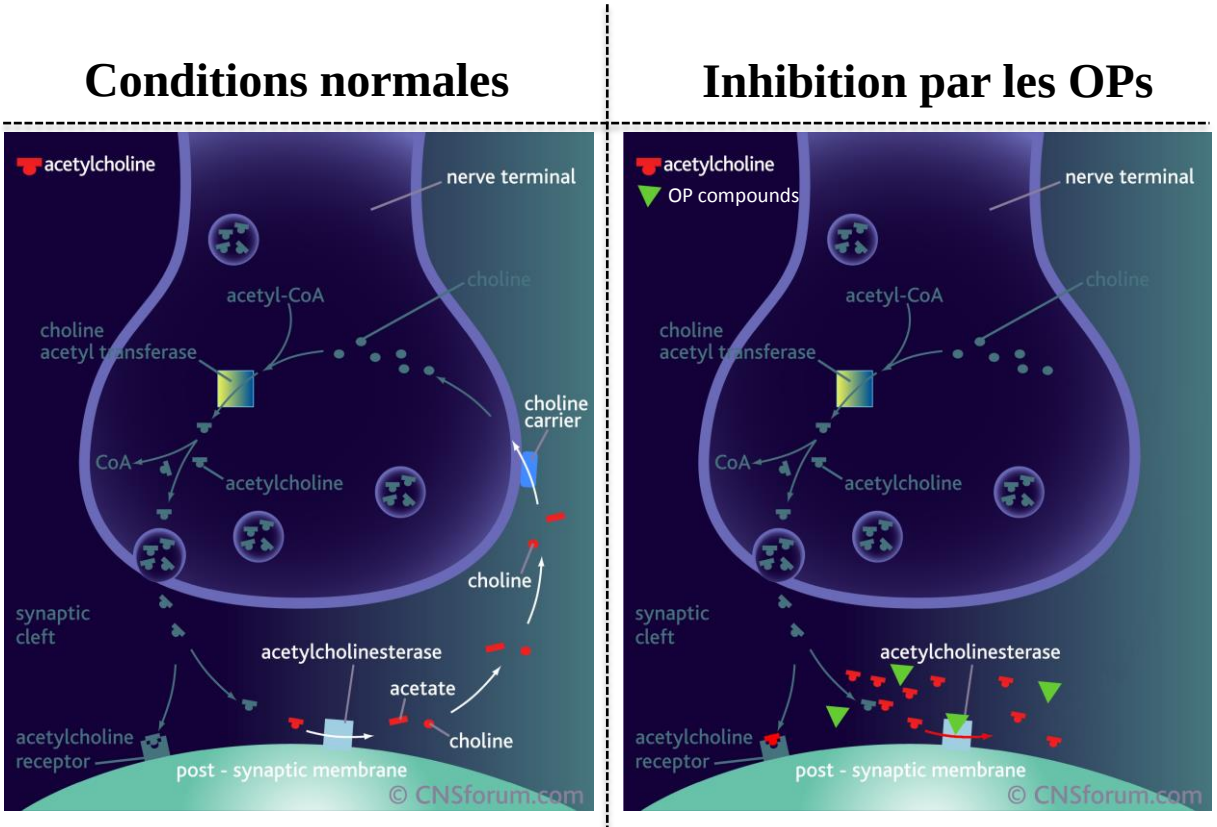

Adapté de CNSforum, Lundbeck Institute

Figure I.2 : *Inhibition de la transmission du message nerveux*

Les OPs inhibent l'AchE, une enzyme clé dans la transmission du message nerveux. Lorsqu'elle est inhibée, l'AchE ne peut plus dégrader l'acetylcholine qui s'accumule dans la fente synaptique et sature les récepteurs (à droite), empêchant ainsi la transmission d'un nouveau signal.

une affection dont l'origine semble multifactorielle impliquant probablement le stress post-traumatique, une exposition à de faibles doses de CWA (*i.e* OPs, gaz moutarde), aux pesticides, à la pyridostigmine bromide (inhibiteur réversible de l'Acétylcholinestérase (AchE) utilisé en prévention) et aux adjuvants utilisés dans les vaccins administrés aux soldats (3, 4). Plus récemment, l'utilisation terroriste d'OPs (*i.e* sarin) dans les évènements liés aux attaques dans la ville de Matsumoto et le métro de Tokyo, respectivement en 1994 et 1995, firent à eux deux plus de 20 morts, 6000 blessés et l'objectif principal de mettre en place la terreur fut réalisé.

En 1993, une convention visant à interdire le développement et le stockage des CWA fut ratifiée par plus d'une centaine de pays, ceux-ci devant être éliminés avant 2007 (1, 5). Aujourd'hui encore, des quantités importantes s'étant accumulées lors des conflits passés restent stockées, attendant des moyens efficaces d'élimination (**voir partie I. A. 5. a.**) (5). Leur destruction étant, de plus, ralentie par les risques de contamination encourus lors de leur manipulation ou de leur transport (1).

2. Mécanisme d'action des organophosphorés

Lors d'une exposition, les OPs peuvent circuler librement dans la circulation sanguine puis se disséminent rapidement dans les autres compartiments du corps (*e.g* cœur, foie, rein, poumons et cerveau). Le pouvoir neurotoxique des OPs provient de leur capacité à inhiber irréversiblement l'activité de l'AcetylCholinEstérase (AChE), une enzyme clé dans la transmission du message nerveux (**Figure I.2**) (1, 6). En effet, le message nerveux est transmis sous la forme d'un signal électrique (*i.e* un potentiel d'action) au sein du système nerveux périphérique et se propage le long de l'axone jusqu'à atteindre la terminaison nerveuse pré-synaptique. A cet endroit, le message électrique est transformé en message chimique par exocytose, libérant dans la fente synaptique des neurotransmetteurs (ex : l'acétylcholine, dopamine). Ces molécules transmettent le signal en se fixant sur des récepteurs spécifiques présents à la surface de la cellule suivante (ex : neurone ou muscle), qui va ensuite propager à son tour le potentiel d'action ou engendrer la contraction musculaire. L'acétylcholine présente à la jonction synaptique doit alors être dégradée ou recaptée afin de (i) réguler la durée et l'intensité du signal, (ii) permettre à un nouveau signal d'être transmis. Lorsque l'AChE est inhibée, elle ne peut plus exercer son rôle qui est de dégrader l'acétylcholine présente dans la fente. L'acétylcholine va alors s'accumuler et saturer les récepteurs cholinergiques, entraînant ainsi une hyperstimulation responsable des symptômes cholinergiques observés (1). Les sujets intoxiqués (exposition aigue) présentent alors des symptômes caractéristiques rappelés par le moyen mnémotechnique anglophone « SLUDGEM » (hyper-salivation, larmoiement, émission d'urine, défécation, hypermotricité gastrique, vomissements, myosis).

Classe		Nom	DL et DL_{50}				Persistance
			IV	PC	SC	R	
CWA	Agents G	Tabun (GA)	70	25840	162	150-400	1,5 – 2,5 jours
		Sarin (GB)	45-53	8750	103-108	75-100	1,5 – 2,5 jours
		Soman (GD)	44,5	9930	70-165	35 - 50	1 à 2 jours
	Agents V	VX	7-10	34	12	10	4-42 jours
Insecticides	Thiono	Malathion	~ 1000 [2]				1 – 25 jours
		Ethyl-Parathion	2 - 10				30 – 180 jours
		Chlorpyrifos	135 – 163				16 à 120 jours
	Oxono	Ethyl-Paraoxon	0.85 [2]				N.D
		DFP	4,85 [2]				N.D

Tableau I.1 : *Toxicité de quelques agents chimiques de guerre et insecticides OPs*
D'après Singh *et al.*, 2009
[2] D'après le "Handbook of Toxicology of Chemical Warfare Agents", Ramesh C. Gupta
DL_{50} = dose létale 50, quantité de molécule à laquelle la moitié des animaux testés ne survivent pas
Les valeurs données pour les insecticides concernent les contaminations par ingestion en mg/kg
La dose létale mesurée par inhalation (R) est donnée en mg/min/m3
Les données en intraveineux (IV), percutané (PC) et sous-cutané (SC) sont données en µg/kg respectivement chez le rat, le cobaye, le rat et la souris.

Bien que la fonction biologique de l'AChE soit de dégrader l'acétylcholine, les OPs peuvent être accommodés dans le site actif de l'enzyme, agissant ainsi comme des antagonistes. Ils réagissent rapidement avec la sérine de la triade catalytique (Ser 200, Glu 327, His 440) (1, 6, 7) (**voir partie I. B. 1. a.** et **Figure I.4**). Il y a alors formation d'un intermédiaire covalent de type phospho-enzyme qui est extrêmement stable. Lorsque l'intermédiaire phospho-enzyme est formé, un processus de vieillissement par déalkylation peut survenir après un certain délai en fonction de l'OP (1, 8). Ainsi, le phospho-enzyme ne peut plus être spontanément régénéré et est irréversiblement inhibée (**Figure I.3**). La cinétique de vieillissement est un facteur très important à prendre en compte pour le traitement des empoisonnements aux OPs car celui-ci peut survenir au bout de seulement quelques minutes après l'exposition (3 min pour le soman) (1, 6, 9).

3. Les agents chimiques de guerre organophosphorés

Les CWAs de type OPs sont des composés comportant selon le type de molécule, une, deux ou trois liaisons phosphoester, alors appelés phospho-, phosphodi- et phosphotri-ester. On recense plus d'une centaine de composés qui varient principalement par la taille et la nature des groupements décorant l'atome de phosphore. Ainsi, selon le composé, la molécule peut comporter des liaisons P-C, P-N, P-CN P-S ou P-F, tous ces éléments influant sur la persistance et la nocivité du composé (**Tableau I.1**). Les CWA de type OPs peuvent pénétrer l'organisme par voie percutanée (à travers la peau) ou par voie aérienne (inhalation de vapeurs) (1). Ils sont regroupés en deux catégories (**Figure I.2**): (i) les agents G (*i.e* sarin, soman, tabun), le sarin étant volatil, il constitue ainsi un risque d'inhalation ou « risque vapeur » et (ii) les agents V (*i.e* VX, R-VX, C-VX) qui s'évaporent plus lentement et ont la consistance d'huiles. Purs, ces composés ont été rapportés comme inodores et incolores. L'intoxication aigue à ces CWAs se manifeste rapidement (dans les minutes suivant l'intoxication) par des symptômes caractéristiques (SLUDGEM) pouvant aller jusqu'à la mort du sujet (1).

4. Les insecticides organophosphorés

Les composés OPs furent également largement utilisés en agriculture en tant qu'insecticide où ils ont remplacé le DichloroDiphenylTrichloroethane (DDT), un organochloré interdit dans les années 70 de par ses propriétés cancérigènes suspectées et sa persistance dans l'environnement (1). Cependant, moins persistants mais plus toxiques que le DDT, l'utilisation d'OPs en tant qu'insecticides est restreinte dans les pays de l'Union Européenne (UE) depuis quelques années. En dépit des mesures prises, une étude récente montre la présence résiduelle d'insecticides OPs à la surface de certains fruits et légumes sur les étalages de supermarchés (rapport de l'Autorité Européenne de Sécurité des Aliments (EFSA))

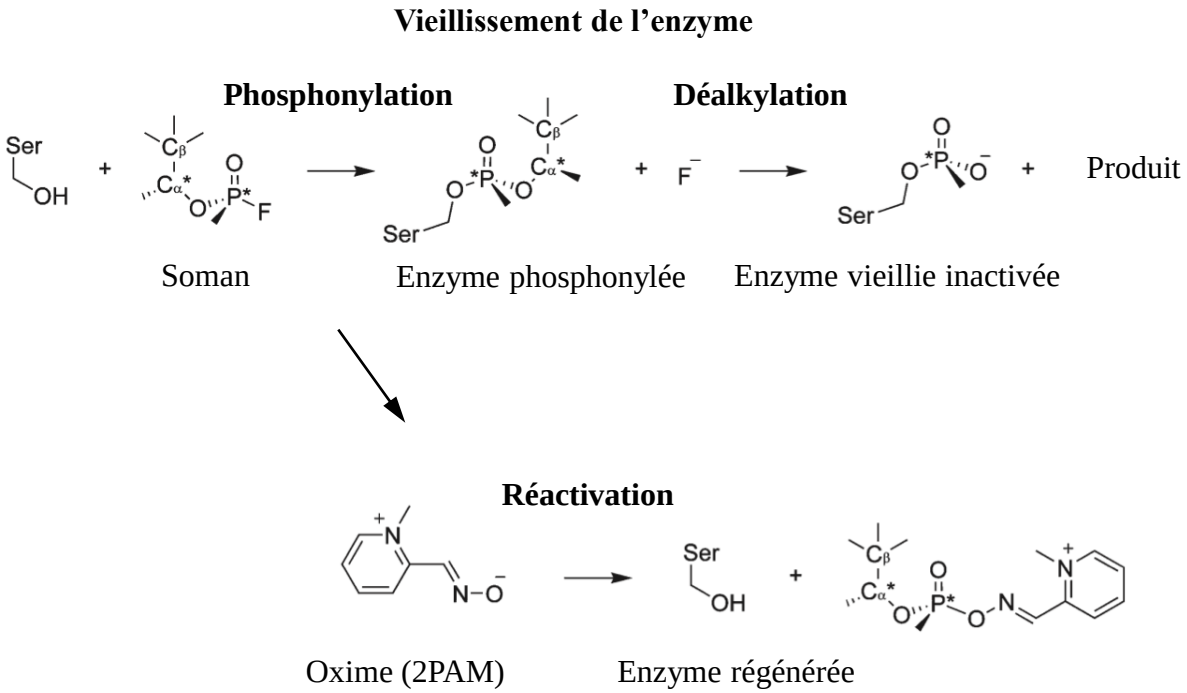

Adapté de Sanson *et. al* J. Med. Chem. (2009).

Figure I.3 : *Inhibition irréversible, vieillissement et réactivation par les oximes*

Le mécanisme d'inhibition et de vieillissement de l'AchE a en grande partie été déterminé grâce à l'utilisation de la cristallographie aux rayons X. Le soman forme un adduit covalent avec la Sérine du site catalytique (en haut à gauche). Le processus de vieillissement intervient plus ou moins rapidement selon l'inhibiteur (en haut à droite) avec le départ du groupement alkyle. Les oximes permettent de régénérer en partie la sérine phosphorylée avant le vieillissement (en bas à gauche).

(10). De plus, en dépit de ces restrictions d'utilisation, une étude récente rapporte la présence de métabolites d'OPs dans des échantillons sanguins de la population Française (présence de métabolites d'OPs, rapport de l'InVS) (11). En effet, de nombreux insecticides OPs sont utilisés quotidiennement dans les foyers sans que le public exposé n'en soit correctement averti (*e.g* présence d'OPs dans les bombes anti-insectes, les colliers anti-puces pour chien, shampoings anti-poux). De plus, ils restent largement utilisés dans le reste du monde, notamment en agriculture intensive où ils constituent parfois le seul rempart disponible contre les insectes ravageurs.

Ainsi, les insecticides OPs sont responsables d'intoxications insidieuses en raison de leur présence à large échelle dans l'environnement. En 2007, environ 15 000 tonnes d'insecticides OPs ont été utilisés aux Etats-Unis, dont 80 % épandus en agriculture (données de l' « Environmental Protection Agency ») (12). Parmi les insecticides les plus utilisés de par le monde, on compte : le malathion, le l'éthyl-parathion/paraoxon, le methyl-parathion/paraoxon ou bien le chlorpyrifos (**Figure I.2** et **Tableau I.1**). Depuis les années 50, plus de 100 000 OPs différents ont été synthétisés et plus de 350 ont bénéficié d'une autorisation de mise sur le marché (1). Les insecticides OPs sont responsables de la plus grande part des pollutions environnementales et l'on estime qu'ils conduisent chaque année à plus de 3 millions d'intoxications, volontaires ou accidentelles, conduisant a plus de 300 000 décès (données de l'OMS, comprenant également les cas de suicides par ingestion d'OPs) (13, 14). Les agriculteurs constituent ainsi une population particulièrement soumise aux contaminations aigues et chroniques aux insecticides OPs. Ainsi, une étude réalisée chez les femmes d'agriculteurs enceintes mit en évidence des effets importants sur le développement du cerveau chez les enfants exposés, résultant en des risques d'hyperactivité et de retard mental accrus (source : UIPP « Union des industries de la protection des plantes ») (6, 15, 16).

5. Les solutions actuelles de protection ou de décontamination

Pour se prémunir des expositions, les principales solutions consistent au port d'une combinaison de protection. Les personnels militaires (*e.g* soldats) disposent d'une combinaison N(R)BC (Nucléaire, Radiologique, Bactériologique et Chimique) dont l'objectif est d'empêcher l'exposition aux OPs à travers la peau et leur inhalation en filtrant l'air respiré (1). Les agriculteurs disposent également de tenues de protection contre les insecticides leur permettant d'éviter les contaminations bien qu'il n'existe aucune règlementation en la matière au niveau Européen (avis de l'agence nationale de sécurité sanitaire de l'alimentation (ANSES)) (17). En revanche, aucun moyen n'est disponible pour assurer le lavage correct de ces tenues, ni même la protection des habitations jouxtant parfois les parcelles traitées par les insecticides.

En prévention des expositions aux OPs, l'armée dispose également de prétraitements tels que la pyridostigmine visant à empêcher l'inhibition de l'AChE, en inhibant de façon réversible environ 50 % des AChEs libres (1). Malgré tout, l'un des problèmes majeurs de cette solution est que la pyridostigmine ne passe pas la barrière hémato-encéphalique alors que le système nerveux central (SNC) constitue l'une des cibles principales des OPs. D'autres pré-traitements (*e.g* physostigmine) capables de protéger également les AChEs du SNC sont en cours d'étude (9). Par ailleurs, ces traitements ne semblent pas sans effets secondaires puisque des études les ont partiellement reliés au syndrome de la guerre du golfe (18).

En cas d'exposition, il existe un traitement symptomatique d'urgence des empoisonnements aux OPs (*i.e* la seringue tri-compartimentée), devant être pris le plus rapidement possible après l'exposition. Ce traitement contient de l'atropine (antagoniste cholinergique qui se fixe sur les récepteurs muscariniques de l'acétylcholine), du contrathion (ou pralidoxime, permettant la réactivation des AChEs inhibées) et du diazépam (anti-convulsivant). La pralidoxime est une oxime permettant de régénérer les AChEs inhibées par les OPs. Les oximes agissent en attaquant l'intermédiaire phosphorylé de la sérine (**Figure I.3**) (1, 9) mais ne sont en revanche pas efficaces sur les AChE vieillies.

Une fois exposés aux OPs, les différents matériels (*e.g* vêtements de protection, véhicules, bâtiments) doivent être décontaminés pour ne plus constituer à leur tour une source de contamination. Ainsi, les méthodes disponibles reposent sur l'utilisation de molécules chimiques telles que la soude (NaOH) qui peuvent être délicates d'utilisation sur certains matériaux de pointe ou sur les éléments électroniques. Par ailleurs, la destruction des stocks d'armes chimiques étant un enjeu international majeur, différentes méthodes d'élimination furent envisagées telles que l'incinération à ciel ouvert, leur enfouissement ou leur dissémination dans les grand fonds océaniques. L'incinération fut néanmoins la solution retenue, bien que freinée par son coût et les pollutions secondaires engendrées (19). De plus, bien que les insecticides OPs présentent une persistance limitée dans l'environnement (du fait de leur bio-dégradation), la dépollution des sols agricoles par l'utilisation de soude est d'autant plus problématique puisque celle-ci poserait plus de problèmes écologiques qu'elle n'en résoudrait (20). Enfin, les personnes exposées constituant également une source de contamination potentielle, celles-ci doivent faire également l'objet d'une décontamination appropriée. Néanmoins, ces méthodes sont archaïques et consistent en l'utilisation de Javel diluée rincée abondamment avec du savon et de l'eau (1). Les militaires et la sécurité civile disposent également du gant poudreur à la terre à foulon (ou argile smectique) permettant d'absorber par son application abondante en partie les liquides contaminants. Il existe également une lotion nommée RSDL® (Reactive Skin Decontamination Lotion) permettant de neutraliser les OPs en cas de contamination sur la peau. En revanche, aucune de ces méthodes n'est satisfaisante pour la décontamination des muqueuses, des yeux ou des cheveux (1, 6).

Bien que d'importants progrès aient été réalisés ces dernières années dans la prophylaxie, le traitement et la protection contre les empoisonnements aux OPs, ces méthodes restent insatisfaisantes. Elles ne permettent pas de couvrir les différents besoin de décontamination, des solutions innovantes et écologiques furent ainsi envisagées pour répondre à cet enjeu sociétal d'intérêt majeur. Ainsi, la bio-épuration (bio-remédiation), c'est à dire l'utilisation de protéines ou d'enzymes capables de piéger ou de dégrader les OPs avant qu'ils n'atteignent leur cible, a suscité l'intérêt des forces de défense pour une utilisation en prophylaxie et la décontamination des personnels après exposition. L'organisation américaine DTRA (Defense Threat Reduction Agency) a placé officiellement le développement d'enzymes permettant la destruction des stocks et la protection des personnes comme étant une priorité (19). Ainsi, plusieurs protéines sont envisagées pour répondre aux différentes problématiques de protection et décontamination : des protéines d'origine humaine pour une utilisation prophylactique (décontamination interne) et des protéines d'origine bactériennes très actives et robustes pour la décontamination externe.

B. La bio-remédiation des organophosphorés

Les bio-épurateurs d'OPs (21) peuvent être classés en deux catégories : (i) les bio-épurateurs non-catalytiques, dont le mode d'action sera de piéger stoechiométriquement les molécules; (ii) les bio-épurateurs catalytiques, capables d'hydrolyser les molécules toxiques. Ces différents bio-épurateurs sont étudiés pour une utilisation dans les deux voies principales de décontamination (*i.e* la décontamination externe et la décontamination interne). Ces différents moyens de bio-remédiation seront abordés au cours des chapitres suivants en fonction de leur capacité à hydrolyser ou non les OPs.

1. Les bio-épurateurs non catalytiques

Les bio-épurateurs non catalytiques sont des pièges stoechiométriques d'OPs dont le rôle va être de capturer les molécules d'OP avant qu'elles n'atteignent leurs cibles dans la fente synaptique (22). Les protéines impliquées sont les cibles privilégiées des OPs en cas de contamination : *i.e* les cholinestérases, les carboxylestérases et d'autres protéines sériques telles les lipases et l'albumine.

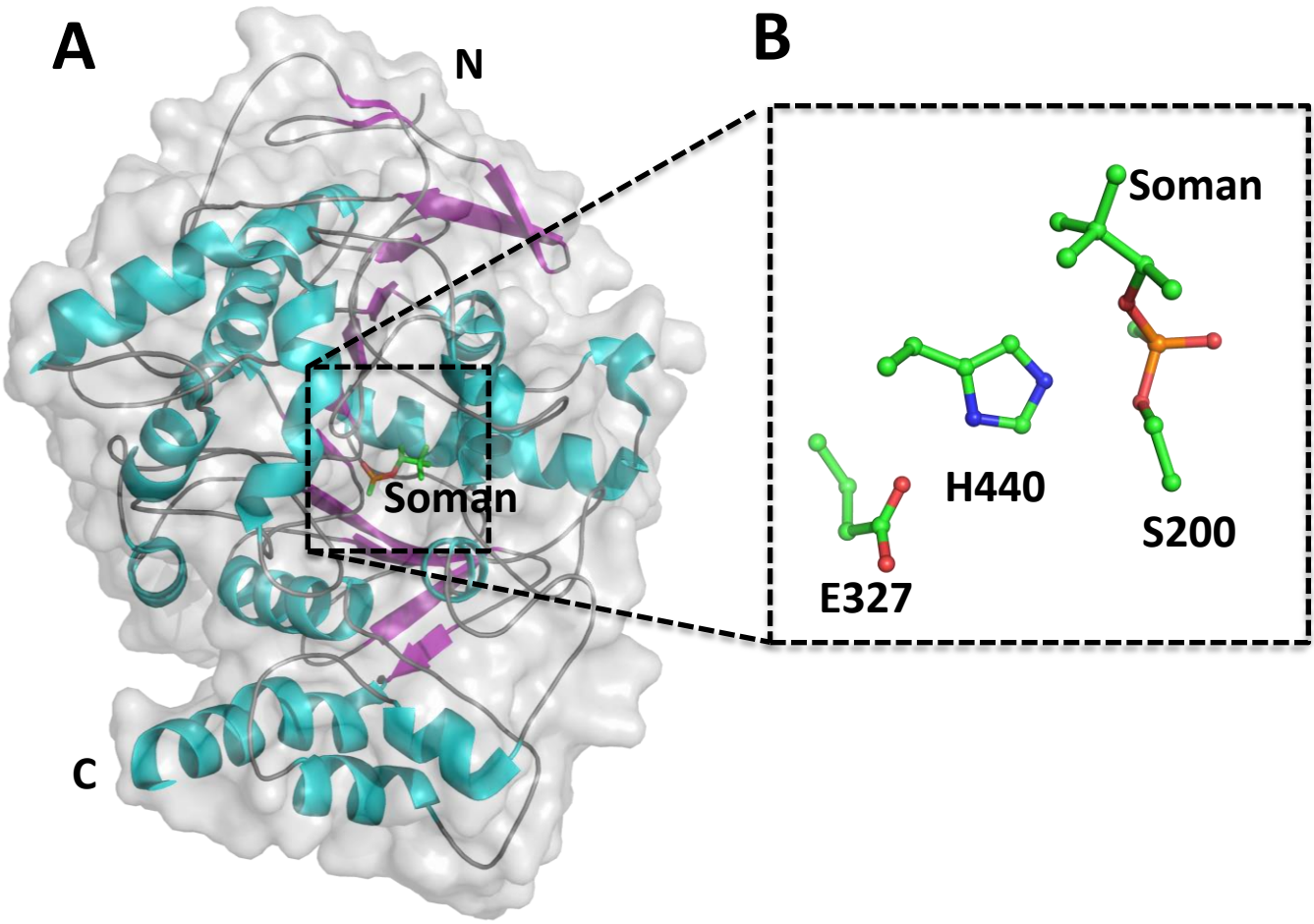

Figure I.4 : *Les bio-épurateurs non catalytiques*

A – Structure d'un monomère d'AchE (code PDB : 2WFZ) conjuguée au Soman **B** – Vue rapprochée de la poche du site catalytique de l'AchE conjuguée Soman.

a. Les cholinestérases

Les cholinestérases (AChE et ButyrylCholinEstérase (BuChE)) sont des enzymes présentes chez l'homme et constituant l'une des cibles principales des OPs (voir partie **I. A. 2.**). Ainsi, elles furent rapidement envisagées dans le traitement prophylactique des contaminations aux OPs. Leur site catalytique est constitué d'une triade (Ser, His, Glu) qui est incapable de terminer la réaction d'hydrolyse des OPs. En effet, le phosphore des OPs mime la géométrie de l'état de transition de la réaction native (celui-ci étant tétraédrique), l'un des substituants prend la place de la molécule d'eau qui doit régénérer l'enzyme. Alors, lors de l'attaque, la sérine catalytique va former un adduit covalent extrêmement stable avec le groupement phosphoré, la régénération de la sérine phosphorylée étant une étape extrêmement lente. Enfin, la déalkylation de l'intermédiaire phosphorylé inactivera définitivement l'enzyme (processus de vieillissement ou « aging ») (**Figure I.3**).

L'AChE (E.C. 3.1.1.7) est une protéine très étudiée de par l'importance de sa fonction physiologique qui est de dégrader l'acétylcholine afin de stopper le message nerveux. Elle fait également l'objet de nombreux travaux de par son implication dans la maladie d'Alzheimer (23, 24). En effet, un déficit en AChE due à la perte des neurones cholinergiques est observé chez les malades. Sa structure cristallographique fut obtenue à partir de l'AChE issue de la raie électrique, *Torpedo californica*, révélant un homodimère dont chaque monomère est composé de 537 résidus adoptants une topologie de type α/β (7) (**Figure I.4 A**). La structure est composée de 12 brins β et 14 hélices α. L'AChE et la BuChE sont des enzymes présentant une homologie structurale qui fut exploitée pour le développement des bio-épurateurs stœchiométriques. Le site actif de l'AChE est situé dans une profonde gorge composé de la triade catalytique Glu 327, Ser 200 et His 440 et d'acides aminés principalement hydrophobes adaptés à l'accommodation de l'acétylcholine, son substrat naturel (**Figure I.4 B et Figure I.5**). L'AChE étant la cible majeure des OPs, elle présente un potentiel d'utilisation en prophylaxie plus intéressant que la BuChE du fait de sa stéréosélectivité envers les énantiomères de CWA les plus toxiques (9). Cependant, étant non-catalytique (stœchiométrique), les quantités nécessaires en injection seraient trop importantes et occasionneraient un coût de traitement trop élevé; son développement en tant que tel a été arrêté (9).

La BuChE (EC 3.1.1.8) est une enzyme d'origine hépatique faisant partie des « sérum cholinestérases ». Son rôle physiologique est encore mal connu mais présentant la capacité de dégrader la cocaïne dans le sang et pourrait constituer un traitement en cas d'intoxication (25). Elle se distingue de l'AChE par sa capacité à hydrolyser la butyrylcholine, molécule synthétique qui n'est pas présente à l'état naturel dans le corps. Elle présente une structure cristallographique comparable à l'AChE (**Figure I.6 A**) (26) (topologie α/β composée de 12 brins entouré de 14 hélices). C'est une protéine glycosylée d'environ 90 kDa s'associant sous forme de tétramères. Le site actif de l'enzyme est constitué d'une triade catalytique (*i.e* Ser 198, Glu 325 et His 438) située au fond d'une cavité hydrophobe comparable

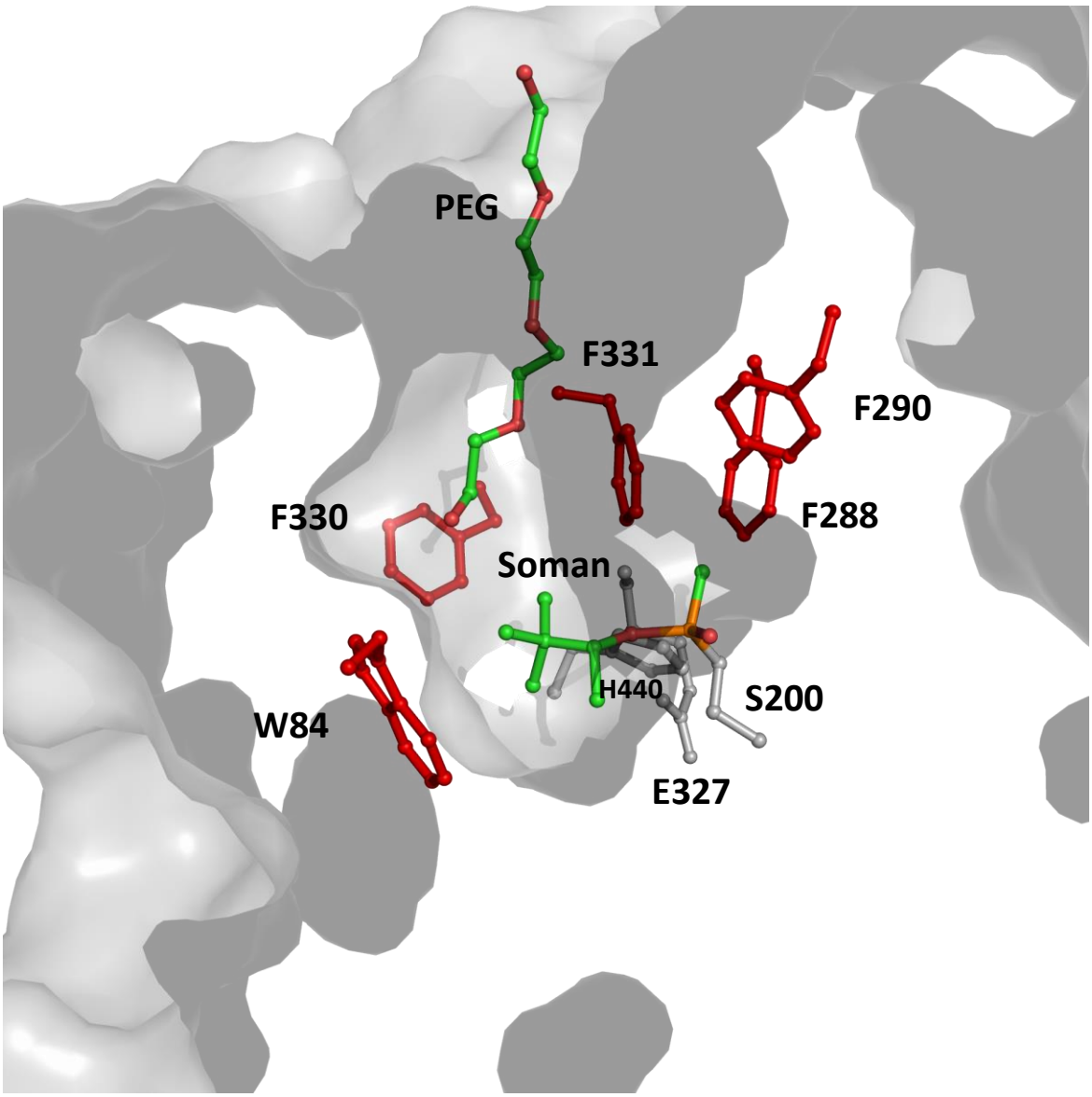

Figure I.5 : *Vue en coupe de la cavité du site catalytique de l'AChE*

Le site catalytique de l'AChE est formé d'une profonde cavité hydrophobe constituée principalement par des résidus tryptophane et phenylalanine. Dans cette structure, le groupement pinacolyl du soman interagit avec les résidus formant un sous-site (W84 et F330).

à celle de l'AChE (**Figure I.6 B**). Ainsi, elle constitue un piège stœchiométrique naturel (27) à OPs mais sa concentration dans le sérum est trop faible pour assurer une protection efficace en cas d'exposition importante. De cette capacité émergea l'idée de développer des traitements à base de BuChE afin de piéger les OPs avant qu'ils n'atteignent leur cible (28-30). Néanmoins, les quantités de protéine nécessaire pour une protection sont importantes (évalué à 240 mg de BuChE pour un homme de 70 kg) (31). Le coût de production de telles quantités est très important, mais cela n'a pas découragé l'armée américaine pour qui elle constitue une alternative viable aux traitements actuels. En effet, l'injection de BuchE est en phase I d'essai clinique pour le traitement des empoisonnements aux OPs (31). Elle fut commercialisée jusqu'en 2012 sous la marque Protexia ^{Tm}, qui la produisait grâce à des chèvres transgéniques. Elle est désormais purifiée à partir de poches de plasma périmées, occasionnant des coûts d'autant plus élevés.

Une autre approche concernant ces bio-épurateurs non-catalytiques vise à les transformer en bio-épurateurs pseudo-catalytiques soit en développant des molécules capables de réactiver l'enzyme, soit en développant des mutants résistants au vieillissement et/ou capables de s'auto-réactiver. Ainsi, l'étude du mécanisme de vieillissement de ces enzymes reste un champ de recherche important (9, 32). Notamment, il a été proposé que la BuChE puisse être injectée en combinaison avec des oximes dont le but est de réactiver la protéine en cas de traitement prophylactique (33, 34). De plus, d'autres études, guidés par les modélisations moléculaires, ont permis de développer des mutants présentant une résistance plus élevée à la déalkylation et une réactivation plus rapide (35, 36). Cette approche permettrait ainsi de donner une activité catalytique partielle diminuant ainsi la quantité d'enzyme nécessaire. Néanmoins, il n'existe toujours pas d'oxime à large spectre capable de réactiver efficacement tous les types d'intermédiaire OP-BuChE. De plus, la cinétique de réactivation étant très lente, cette solution est considérée comme inenvisageable d'un point de vue pharmacocinétique (37). Une autre solution pourrait être de disposer de mutants de BuChE capables de s'auto-réactiver, présentant ainsi une activité enzymatique envers les OPs (38). Ainsi, par ingénierie protéique, des mutants capables de régénérer la sérine phosphorylée (k_{cat}/K_M envers le paraoxon 1.8 x 10^2 $M^{-1}.s^{-1}$ (39)) ont pu être obtenus. Récemment, des mutants plus actifs de la BuChE ont été produits et permettraient de réduire les coûts tout en augmentant l'efficacité de cette solution (40-42). Cependant, leur capacité à protéger efficacement l'AChE reste à évaluer.

Ainsi, l'utilisation d'enzyme semblant être la solution la plus efficace, la conversion par mutagénèse de bio-épurateurs stoechiométrique (*i.e* AChE et BuChE) en bio-épurateurs catalytique reste un champ de recherche important (9).

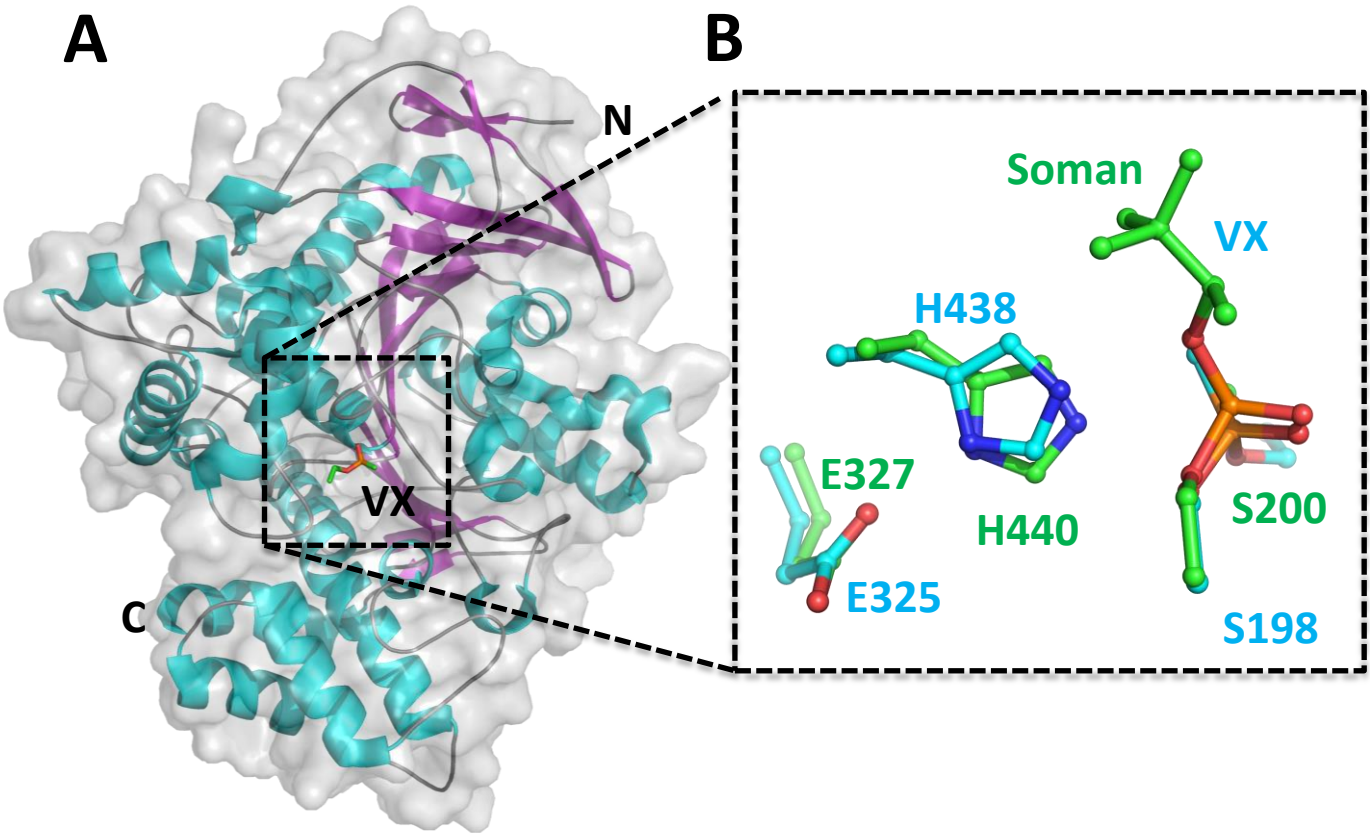

Figure I.6 : *Les bio-épurateurs non catalytiques*

A – Structure d'un monomère de BuchE (code PDB : 2XQF) conjuguée au VX
B – Superposition des acides aminés catalytiques de l'AchE (vert) et de la BuchE (bleu), conjuguée au Soman et au VX respectivement.
L'AChE et la BuChE ont une topologie similaire de type Rossman fold. La BuchE, qui est naturellement circulante dans le sang, constitue un bio-épurateur stoechiométrique de choix. Néanmoins, les quantités nécessaires d'enzymes sont très importantes et ne permettraient pas de traiter toute une population. Les deux protéines ont un site catalytique similaire permettant l'hydrolyse de leur substrat naturel et le « piégeage » stoechiométrique des OPs.

b. Les Carboxylestérases

Les carboxylestérases (EC 3.1.1.1) sont des enzymes retrouvées chez les eucaryotes (insectes, plantes, animaux), les bactéries et les archaea (*e.g Sulfolobus tokodai* (43)). Elles interviennent dans de nombreux processus métaboliques (44-47). Chez l'Homme, la carboxylesterase hCE1 est principalement présente dans les tissus hépatiques où elle est impliquée dans la dégradation d'ester, de thioesters et de certaines liaisons amides de différents composés endogènes et exogènes comme la cocaïne et l'héroïne (48, 49). hCE1 est une protéine de 62 kDa possédant une topologie α/β hydrolases comparable cholinestérases (50) dont le cœur catalytique est également composé d'une triade catalytique (Ser 221, Glu 354 et His 468) (**Figure I.7 A**). Ainsi, elles sont inhibées de la même manière que les cholinestérases, lors de l'étape de régénération de la sérine phosphorylée (**Figure I.7 B**).

Le mécanisme de résistance aux insecticides OPs observé chez certains insectes fut élucidé récemment. Chez la mouche du mouton, *Lucilia cuprina*, les carboxylestérases sont organisées en un cluster de gènes. L'un de ces gènes, αE7 (ou E3) fut largement étudié pour son implication dans la résistance aux insecticides OPs (51). Les études structure-fonction effectuée sur l'enzyme (*Lc*αE7) permirent de montrer qu'elle présente un site actif similaire à l'AChE avec une complémentarité plus élevée pour les OPs (affinité environ 10 fois supérieure). De plus, *Lc*αE7 présente des différences spécifiques dans le site actif lui conférant une résistante à l'aging des OPs lorsque le complexe phospho-sérine est formé. Ainsi, l'enzyme est capable d'effectuer une hydrolyse lente sans être irréversiblement inhibée (52). Enfin, les carboxylestérases d'insectes peuvent présenter des mutations dans le site actif de l'enzyme (*e.g* Gly 137 Asp) responsables d'une augmentation de l'efficacité catalytique (53). Ces mutations entrainent une diminution de l'activité naturelle (carboxylestérase) de l'enzyme au profit d'une activité de promiscuité (hydrolyse des OPs) qui devient alors suffisante pour assurer un avantage sélectif à ces organismes (53).

De ce fait, les carboxylestérases dotées d'une activité catalytique envers certains OPs constituent ainsi un champ d'investigation important pour l'obtention d'un traitement prophylactique des empoisonnements aux OPs. Des mutants de hCE1 actifs envers les agents neurotoxiques de guerre ont par exemple été obtenus par dessein rationnel (54).

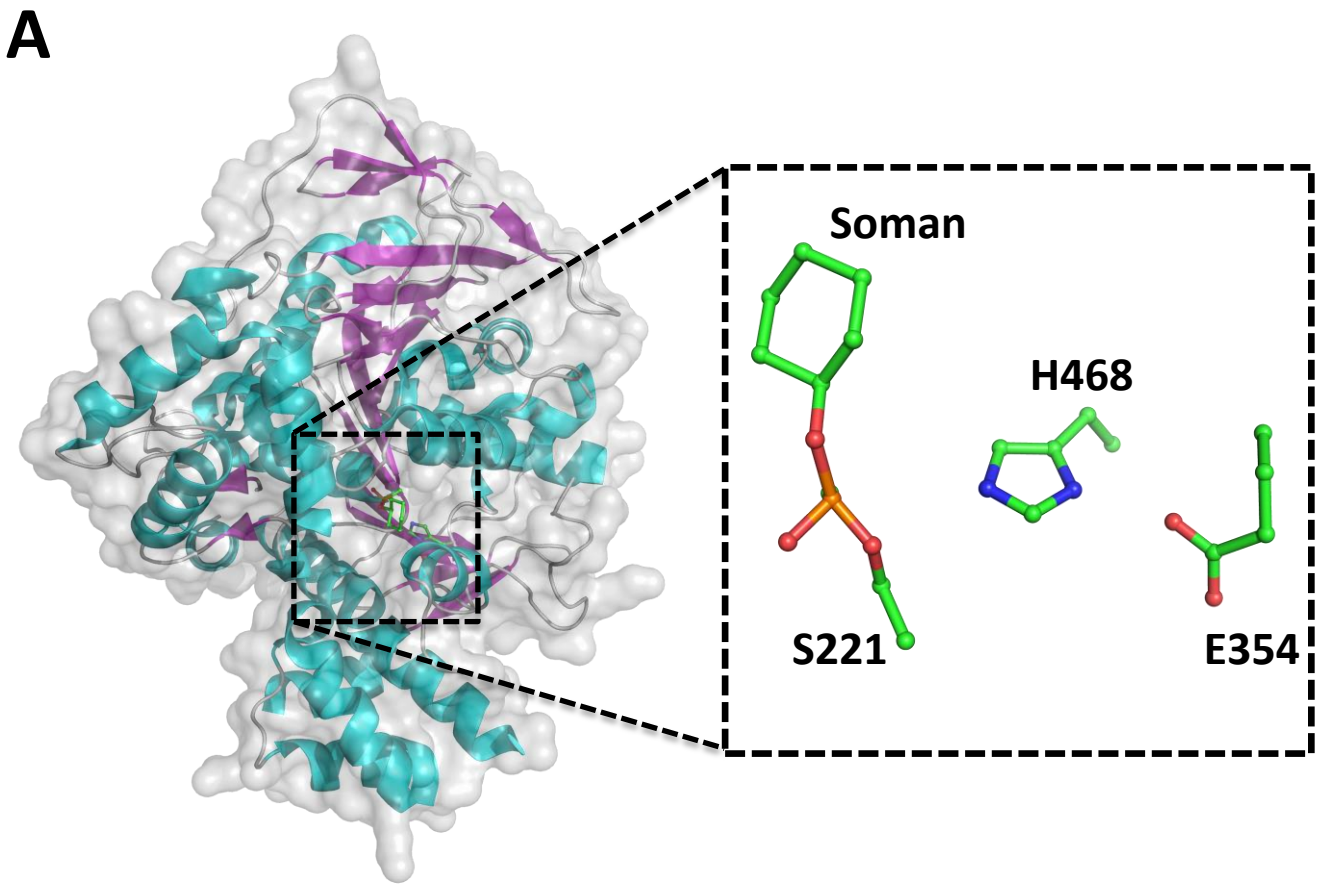

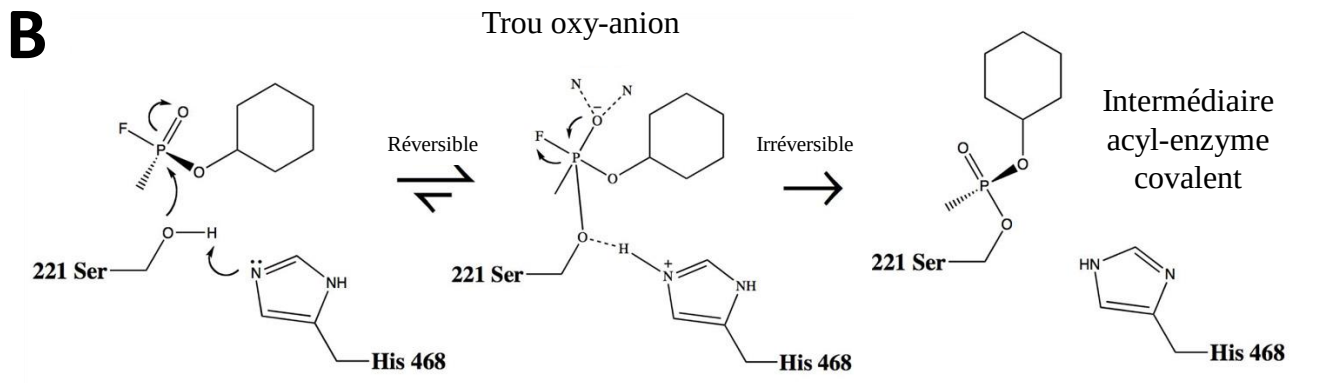

Adapté d'Hemmert *et al.*, 2010

Figure I.7 : *Mécanisme des Carboxylestérases*

A – Structure d'un monomère de hCE1 (pdb id 3K9B) (à gauche) et vue rapprochée du site catalytique (à droite). La triade catalytique est composée des résidus de Ser 221, His 468 et Glu 354

B – Le schéma réactionnel proposé se déroule en plusieurs étapes : (i) lors de la liaison de l'OP dans le site actif, il y a formation d'une liaison hydrogène particulière (« low barrier hydrogen bond ») entre le Glu 354 et l'Histidine 468, accentuant ainsi son pKa, (ii) l'His 468 agit alors comme une base et déprotonne la Ser 221, (iii) l'oxygène de la Ser 221, alors très nucléophile, attaque le centre phosphoré avec le développement d'une charge négative sur l'oxygène terminal (iv) la charge négative étant stabilisée par les azotes de la chaine principale, il y a alors formation d'un intermédiaire acylenzyme avec le départ du groupement partant (F^-). De façon comparable aux sérum estérases, les carboxylestérases sont bloquées par la formation de cet intermédiaire covalent qui, souvent, ne peut être régénéré.

c. Les autres cibles plasmatiques

D'autres protéines plasmatiques possèdent naturellement la capacité de fixer les d'OPs. Ces protéines, telles que les lipases ou l'albumine (49), constituent des pièges naturels aux molécules exogènes telles que les OPs. Cependant, en dépit des efforts qui ont été produits ces dernières années, ces protéines ne présentent qu'un intérêt pratique limité (9). Ainsi, que ce soit pour une utilisation en prophylaxie ou en décontamination interne ou externe, les recherches se sont désormais majoritairement tournées vers des enzymes présentant une activité catalytique envers les OPs. Ces bio-épurateurs catalytiques pouvant ainsi répondre aux différentes problématiques liées à la décontamination, constituent ainsi une alternative viable aux méthodes disponibles à ce jour.

2. Les bio-épurateurs catalytiques

Il existe dans la nature des enzymes naturellement capables de dégrader les composés OPs et portants alors le nom d'OP hydrolases ou PhosphoTriEstérases (PTE). Elles se regroupent en 4 principaux types de repliement structural ou topologies différentes (**Figure I.8**) : les *β-propeller (*hélice de bateau), les *pita bread*, les *TIM-Barrel* (tonneaux $(\beta/\alpha)_8$) et les *metallo-β-lactamases* (sandwich αβ/βα).

a. Les OP hydrolases à topologie « β-propeller »

Cette famille structurale d'OP hydrolase fut découverte pour la première fois dans les années 50 de par la capacité d'hydrolyse des OPs qu'elle confère aux tissus les exprimant (55, 56). Néanmoins, ce n'est que plus tard que ces enzymes ont pris le nom de Paraoxonases ou DFPases pour leur capacité respective à hydrolyser le paraoxon et le Diisopropyl FluoroPhosphate (DFP) (57).

Description structurale

L'étude structurale de cette famille enzymatique constitua un point clé pour la mise au point d'un traitement capable de dégrader les OPs dans la circulation sanguine. Du fait de son homologie avec les paraoxonases, les DFPases constituèrent pendant longtemps des modèles essentiels aux études

β-propellers

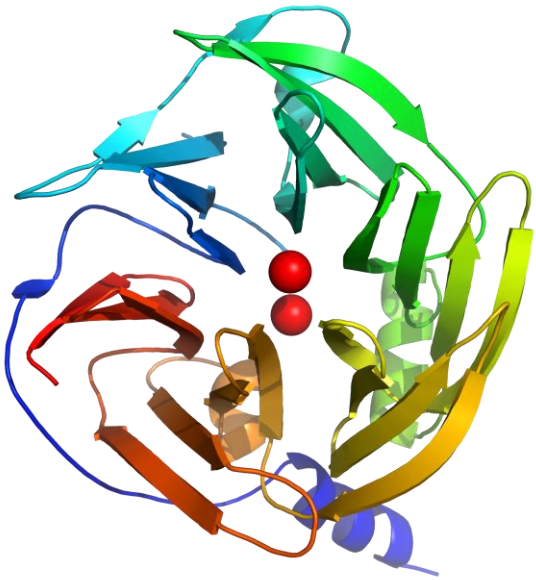

PDB ID 1V04

Pita bread

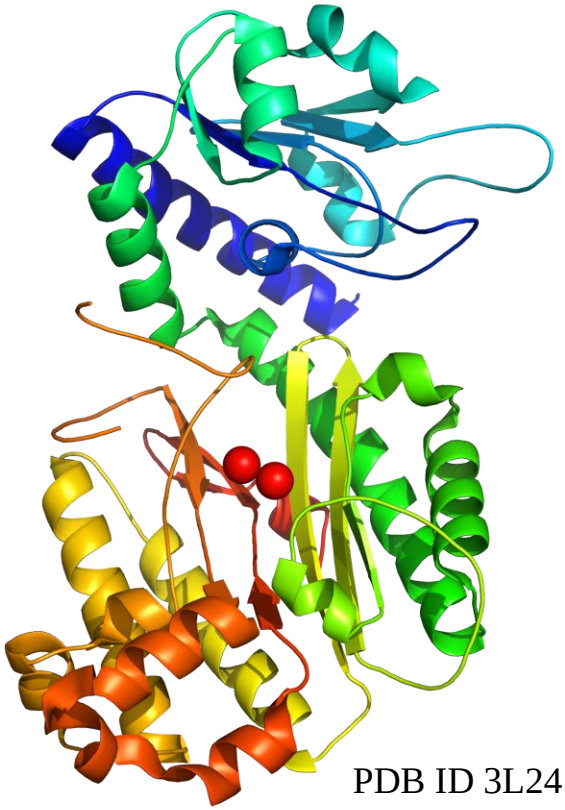

PDB ID 3L24

Sandwichs αβ/βα

PDB ID 1P9E

Tonneau $(\beta/\alpha)_8$

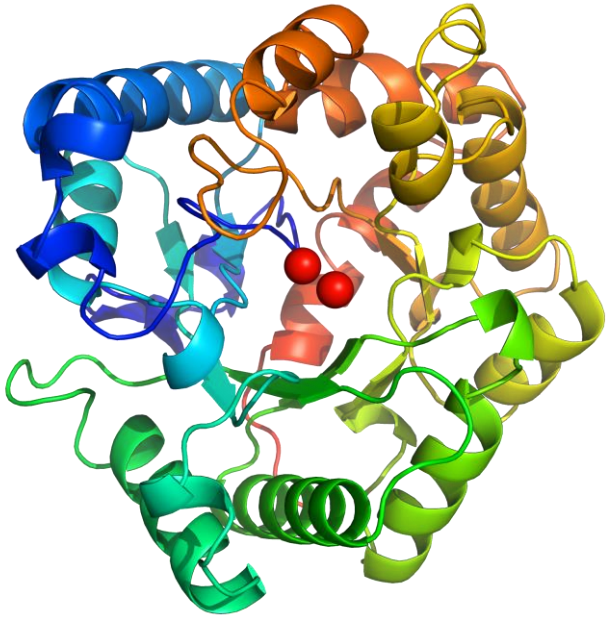

PDB ID 1DPM

Figure I.8 : *Représentations structurales des 4 types de topologies d'OP hydrolases*

mécanistiques de cette famille structurale d'OPs hydrolases (58, 59). Enfin, l'obtention d'une paraoxonase chimérique recombinante (rePON1) par évolution dirigée (60, 61), permit de surmonter les nombreux problèmes de solubilité et de stabilité de l'enzyme.

Les enzymes de cette famille présentent des structures généralement « tout β » formant 6 pales constituant l'hélice de bateau (**Figure I.9 A**). C'est un repliement dont la symétrie peut varier de 4 à 10 pales permettant ainsi de faire varier le diamètre du tunnel central selon la fonction biologique de la protéine (*e.g* hydrolase, réductase, déshydrogénase, porine) (62, 63). Le motif structural répété est un feuillet β composé de 4 brins antiparallèles, les extrémités N- et C-terminales étant en interaction à la manière d'un velcro (62). Chez les OPs hydrolases de cette famille structurale, un tunnel dans lequel se trouvent deux atomes de calcium se situe au centre de l'enzyme (**Figure I.9 B**). L'atome le plus enfoui au fond de la cavité dit structural est coordonné par trois molécules d'eau, la chaine principale et les chaines latérales de deux résidus (*i.e* Asp 232 et His 274 pour la DFPase et Asp 169 et Asp 54 pour hPON1). Le second atome de Ca est impliqué dans le mécanisme catalytique, coordonné par deux molécules d'eau et les chaines latérales des résidus Asp 229, Glu 21, Asn 120 et Asn 175 chez la DFPase et par une molécule d'eau et les chaines latérales des résidus Asp 269, Glu 53, Asn 168, Asn 224, Asn 270 (59, 62) (**Figure I.10 A**).

Comme la plupart des OP hydrolases, les enzymes de cette famille présentent une énantio-préférence pour les énantiomères (*S*) d'OPs dus aux sous-sites de spécificité de la poche du site actif. La DFPase présente deux sous-sites latéraux (Tyr 144, Met 90, Ileu 72, Glu 37 et Trp 244, Thr 195, Phe 173, Met 148) et deux résidus centraux (Arg 146 et His 287) (58). hPON1 présente un large sous-site latéral (Tyr 71, His 115, His 134, Ser 137, Ser 166, Asp 183, His 184 et Lys 192), un second sous-site latéral (Leu 69, Leu 240, His 285, Ile 291, Ile 332, Val 346, Phe 347) et un sous-site central (Ser 193, Met 196, Phe 222, Phe 292, Phe 293) (**Figure I.10 B**).

Mécanisme catalytique

Le mécanisme catalytique des OP hydrolases de cette famille fut pendant longtemps sujet à débat (*e.g* dyade d'histidine, attaque directe par l'Asp 269) (61, 64). Récemment, Ben-David *et al.*, (65, 66) proposa un mécanisme d'hydrolyse plus parcimonieux : (i) une molécule d'eau coordonnant l'ion Ca^{++} catalytique est positionnée et activée par l'assistance des résidus d'Asp 269 et de Glu 53, (ii) l'un des deux résidus joue le rôle de catalyseur acide en arrachant un proton de la molécule d'eau, (iii) la molécule d'eau ainsi activée peut effectuer une attaque nucléophile sur le centre phosphore (**Figure I.10 C**). Ce mécanisme n'impliquant pas la formation d'un intermédiaire phospho-enzyme (58, 64), est soutenu par des expériences de mutagénèse dirigée, docking et dynamique moléculaire (65). Il est par

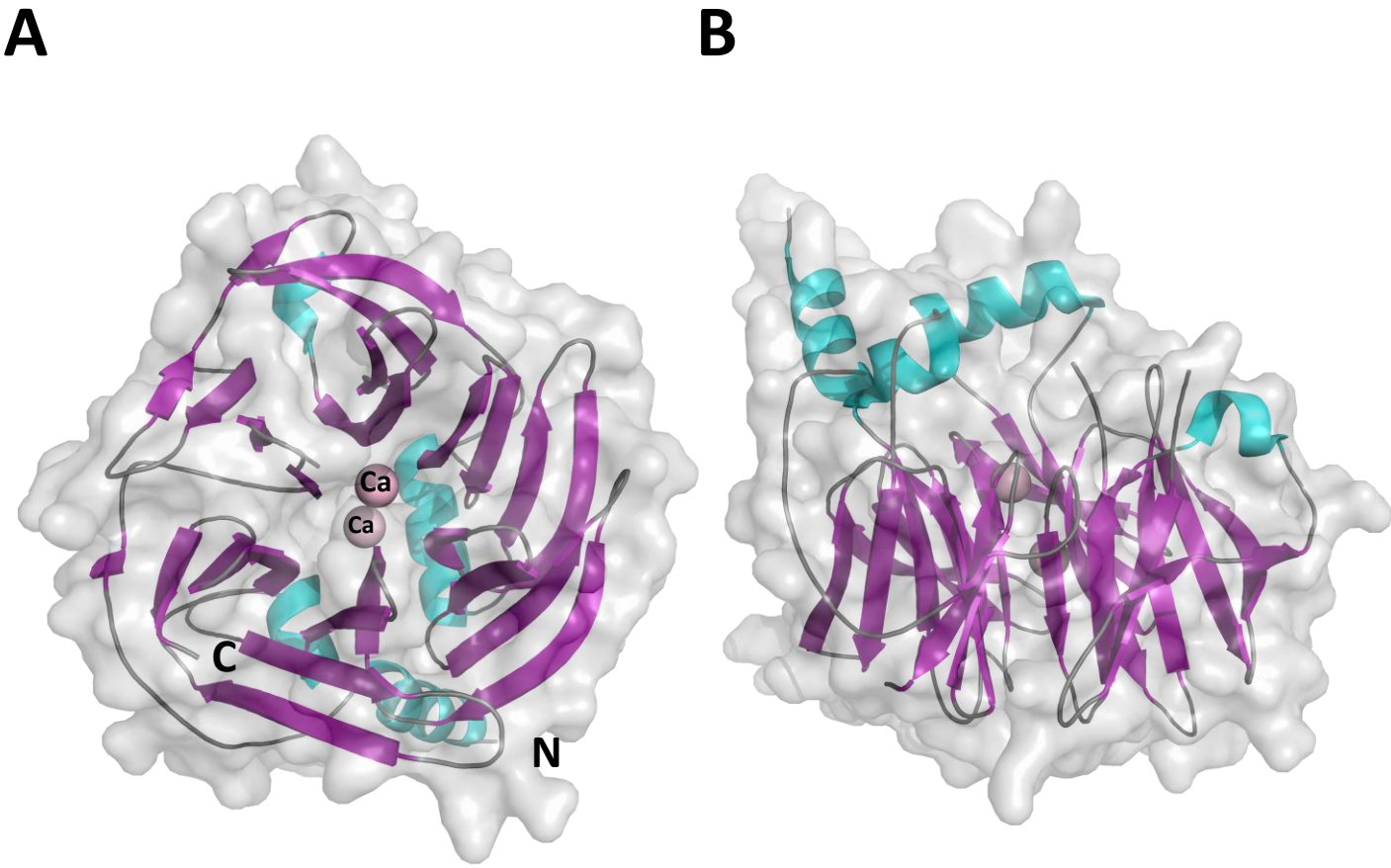

Figure I.9 : *Structure de la Paraoxonase, une OP hydrolase à repliement β-propeller*

A – Structure d'un monomère de paraoxonase (code PDB : 1V04)

B – Vue de profil de la paraoxonase

ailleurs cohérent avec l'observation d'une molécule d'eau activée, coordonnée à l'atome de calcium, dans la structure à résolution sub-atomique de la DFPase (67). Enfin, il fut montré que l'activité de promiscuité phosphotriestérase de hPON1 est permise grâce à une re-localisation de l'ion Ca^{++} catalytique dans une position différente de celle permettant l'activité lactonase (65).

Représentants principaux

a. DFPase

Les DFPases furent identifiées dans les tissus d'animaux en vertu de leur capacité à hydrolyser efficacement le DFP. Ces enzymes peuvent être classées en deux sous-familles selon leur masse moléculaire: (i) les « Mazur-type DFPase », pouvant varier de 40 à 96 kDa (ii) les « Squid-type DFPase », dont la taille peut varier de 35-40 kDa (57). Ces deux types d'enzymes présentent également des topologies différentes (repliement de type pita-bread pour les Mazur-type DFPases (**voir partie I. A. 2. b.**)). Les principales « Squid-type DFPases » (E.C 3.1.8.2) décrites ont été détecté dans le ganglion cervical de céphalopodes tels que *Octopus vulgaris*, *Loligo pealei*, *L. opalescens* et *Todarodes pacificus* (68). L'enzyme modèle a été isolée à partir du calamar, *L. vulgaris*, pour son activité particulièrement élevée envers le DFP (k_{cat}/K_M ~ 5.6 x 10^4 $M^{-1}.s^{-1}$) (69, 70). L'enzyme est également capable de détoxiquer de nombreux OPs tel que le tabun, le sarin et le soman. L'enzyme pouvant être obtenue de façon recombinante en grande quantités (69), elle devint l'objet d'intenses recherches dans l'objectif de développer son application potentielle dans le traitement des empoisonnements aux OPs (71). Sa structure cristallographique à ultra haute résolution a été résolue et a permis de poser les bases structurales du mécanisme catalytique des OP hydrolases à β-propeller (72, 73).

b. Paraoxonases

Les paraoxonases sont des enzymes semblables aux DFPases et qui sont retrouvées principalement dans le sérum des animaux (55, 56). Ce sont des enzymes très conservées chez les mammifères, absentes chez les poissons, les oiseaux et les invertébrés qui sont ainsi d'autant plus exposés aux pollutions environnementales aux OPs (74).

Chez l'homme, il existe trois gènes codants des paraoxonase (hPON1, 2 et 3) (75). hPON1 (E.C.3.1.8.1) suscita un intérêt tout particulier pour son implication dans l'étiologie des maladies

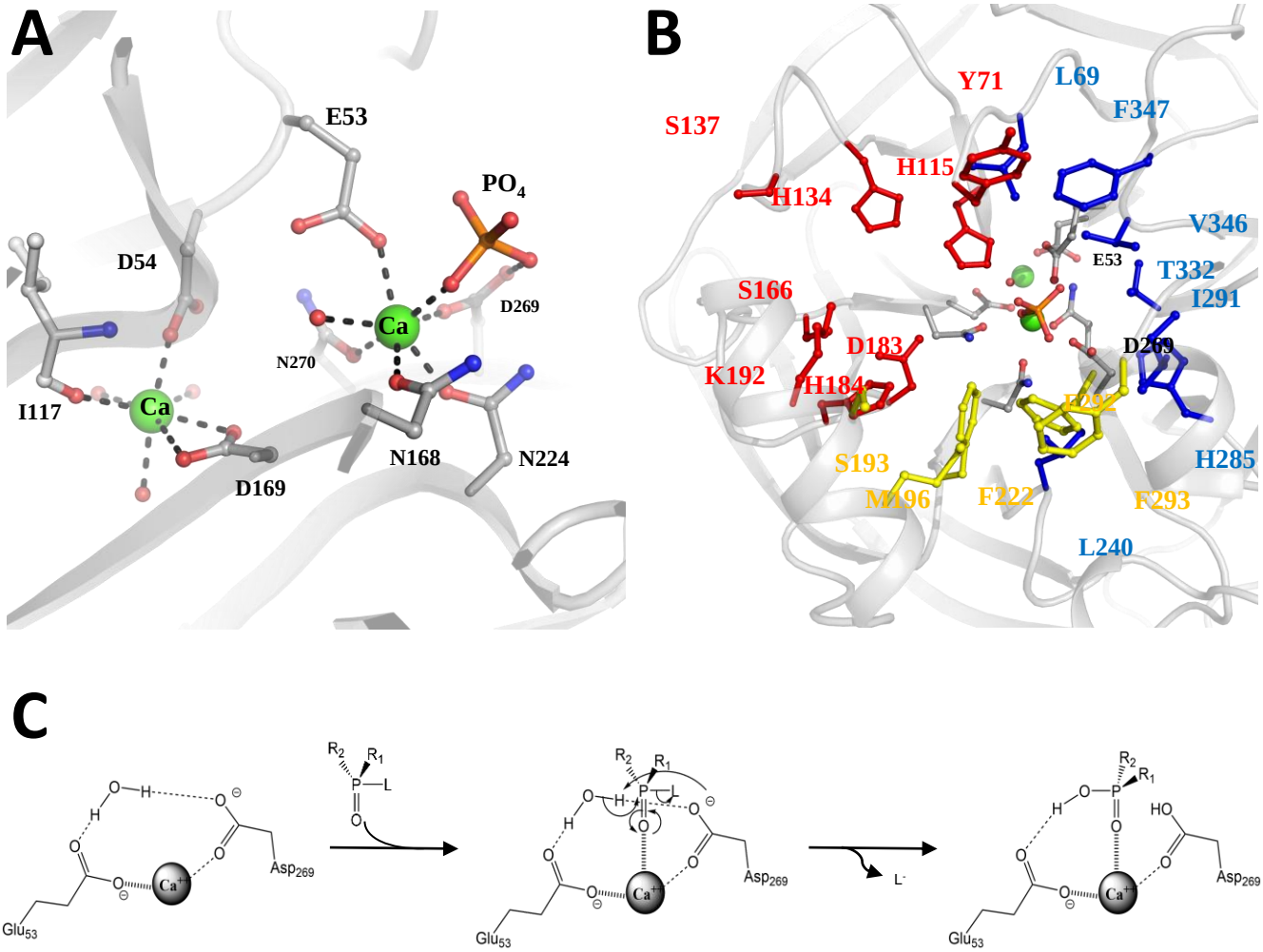

Figure I.10 : *Structure du site actif de la Paraoxonase et mécanisme catalytique*

A – Vue du site catalytique de hPON1 et sphère de coordination des ions calcium

B – Vue du site actif de la paraoxonase, les acides aminés du site actif sont représentés en sticks. Les trois sous-sites de spécificité de l'enzyme sont représentés : un large sous-site latéral (Y71, H115, H134, S137, S166, D183, H184 et K192), un second sous-site latéral (L69, L240, H285, I291, I332, V346, F347) et un sous-site central (Ser 193, Met 196, Phe 222, Phe 292, Phe 293)

C – Mécanisme catalytique phosphotriestérase des PONs d'après Ben David *et., al* 2012.

cardiovasculaires (75, 76). hPON1 est une enzyme présente sous différentes glycoformes allant de 40 à 45 kDa et principalement associée aux « high-density lipoproteins » (HDL) (77). C'est une lactonase naturelle présentant des activités de promiscuité phosphotriestérase et arylestérases (77, 78). Il fut récemment proposé que les PONs eucaryotes auraient évolué à partir de lactonases bactériennes ancestrales (79). Bien que le rôle physiologique de hPON1 ne soit pas encore clair, elle serait impliquée dans la protection contre l'oxydation des « low-density lipoproteins » (LDL) et l'athérosclérose (74, 80). hPON1 s'associe aux HDL grâce à la présence d'une hélice transmembranaire hydrophobe lui permettant de s'ancrer à la surface des lipoparticules (81). Elle s'associe dans le sérum à la « Human Phosphate-Binding Protein » (HPBP) (**voir articles annexes VII. C. D. E. et F.**), une protéine DING co-purifiée avec hPON1 et qui est nécessaire à sa stabilité (82, 83).

hPON1 conférant une protection naturelle des animaux contre les insecticides et les agents neurotoxiques, son potentiel d'utilisation prophylactique fut évident (80, 84). Cependant, cette approche fut ralentie par son hydrophobicité, son instabilité et les difficultés liées à l'obtention de la protéine impliquant une purification à partir de poches de plasma périmées (85). Afin de résoudre ces problèmes et faciliter son étude, sa production en système hétérologue nécessita des travaux de pointe en biologie moléculaire qui permirent de solubiliser l'enzyme et d'en obtenir sa structure cristallographique (60, 61, 86). L'enzyme, nommée rePON1 (pour recombinant PON1) présente des efficacités catalytiques aux alentours de $k_{cat}/K_M \sim 10^3$ $M^{-1}.s^{-1}$ envers la plupart des agents G. Au cours d'un travail d'amélioration de près de 10 ans, l'activité de l'enzyme fut optimisée pour hydrolyser les énantiomères les plus toxiques de différents agents G, atteignant des efficacités proches de $k_{cat}/K_M \sim 10^6$ $M^{-1}.s^{-1}$ (87, 88) (**Tableau I.2**). L'efficacité catalytique élevée de ces variants, permet de les envisager pour le traitement des empoisonnements aux OPs puisqu'il est considéré qu'une efficacité catalytique proche de 10^6 $M^{-1}.s^{-1}$ est nécessaire pour une détoxification *in vivo* efficace (89). Néanmoins, les différents variants de PON1 présentant des mutations de surface, celles-ci peuvent constituer un risque d'immunogénicité devant être pris en compte. Plusieurs solutions sont ainsi à l'étude comme la ré-humanisation des variants ou la décoration de l'enzyme avec des chaines poly-ethylène glycol (PEG) (87, 90).

.

c. Autres représentants

D'autres représentants de cette famille structurale, principalement décrits pour d'autres activités, ont été envisagés pour la mise au point d'un traitement prophylactique aux empoisonnements aux OPs (9). Chez les mammifères, la « Senescence Marker Protein 30 » (SMP30) (E.C 3.1.1.17) est une enzyme présente dans le foie et qui hydrolyse le DFP (21, 91). Sa fonction physiologique la relie au

	k_{cat}/K_M ($M^{-1}.s^{-1}$)			
	rePON1	**PON-2D8**	**PON IIG1**	**DFPase**
Paraoxon	2,3 x 10^3	N.D	N.D	N.D
Sarin	1,33 x 10^3	4,17 x 10^3	5,33 x 10^4	4,7 x 10^4
Soman	9,17 x 10^2	6,67 x 10^4	8,5 x 10^5	N.D
Cyclosarin	2,17 x 10^3	7,67 x 10^4	5,67 x 10^5	7,2 x 10^5
Tabun	7,17 x 10^3	1,37 x 10^4	3,83 x 10^4	N.D

Tableau I.2 : *Efficacités catalytiques de différents variants de PON1 et de la DFPase envers différents OPs*
Les efficacités catalytiques des différents variants de PON1 sont issues de *Gupta et al.*, 2011 et de *Goldsmith et al.*, 2012. Le variant rePON1 correspond au variant soluble qui fut utilisé afin d'obtenir la structure tridimensionnelle de la paraoxonase (*Harel et al.*, 2004). Le variant 2D8 correspond au meilleur variant issu de l'évolution *in vitro* de la rePON1 (Gupta et al., 2011) et le variant IIG1 correspond au variant issu de l'amélioration *in vitro* de la stéréospécificité du variant 2D8). Les valeurs concernant la DFPase sont données envers l'énantiomère le mieux hydrolysé par l'enzyme (d'après *Melzer et al.*, 2009).

métabolisme de la vitamine C (acide L-ascorbique) (92, 93) et son expression diminuant avec l'âge en fait un marqueur important de la sénescence cellulaire (92).

Chez les bactéries, d'autres enzymes furent envisagées telles que la Gluconolactonase (XC5397) (E.C 3.1.1.17) issue de *Xanthomonas campestris* et impliquée dans le métabolisme secondaire du glucose (94); la « Drug resistance protein » (Drp-35) identifiée chez *Staphylococcus aureus*, principalement étudiées pour son activité lactonase naturelle (95). Néanmoins, le développement de ces enzymes dans le cadre d'une utilisation en prophylaxie, en traitement des empoisonnements aux OPs ou même en décontamination externe n'en est qu'à ses balbutiements.

b. Les OP hydrolases à topologie « pita-bread »

Les prolidases (E.C. 3.4.13.9) sont des di-peptidases reconnaissant le motif Xaa-Proline (Proline en position C-terminale d'un dipeptide). Bien que le rôle physiologique de ces enzymes soit encore sujet à discussion, elles pourraient être impliquées dans le métabolisme des dipeptides chez les bactéries, les céphalopodes et l'homme (96, 97). Le représentant le plus étudié de cette famille de protéines est l'« Organophosphorus Acid Anhydrolase » (OPAA) (E.C 3.1.8.2) retrouvée chez plusieurs souches d'*Alteromonas* : *Alteromonas sp.*, *Alteromonas* JD6.5, *Alteromonas haloplanktis* et *Alteromonas undina* (OPAA-2) (98, 99). Les enzymes appartenant à cette famille sont particulièrement intéressantes du fait de leur capacité à hydrolyser les liaisons P-F et P-CN des agents chimiques de guerre (agents G) (19, 100).

Description structurale

Les enzymes de cette famille structurale sont décrites comme des dimères de dimères. Chaque monomère s'organise en deux domaines composés d'hélices α et de brins β (**Figure I.11 A**). Le domaine N-terminal, plus petit est composé d'un feuillet β twisté comportant deux brins centraux anti-parallèles flanqués de chaque côté de 2 brins β parallèles et de 4 petites hélices α de chaque côté du feuillet. Le domaine C-terminal, plus gros, est composé d'un feuillet β à 5 brins anti-parallèles formant une surface incurvée rappelant la forme du pain grec duquel la topologie tire son nom : « pita bread ». La face convexe du feuillet est tapissée d'hélices α. Le site actif de ces enzymes est composé d'un centre bimétallique qui se trouve dans la cavité formée par le domaine C-terminal (**Figure I.11 A et B**). Le site catalytique est constitué de deux ions métalliques de type Mn^{2+} qui sont coordonnés par les résidus

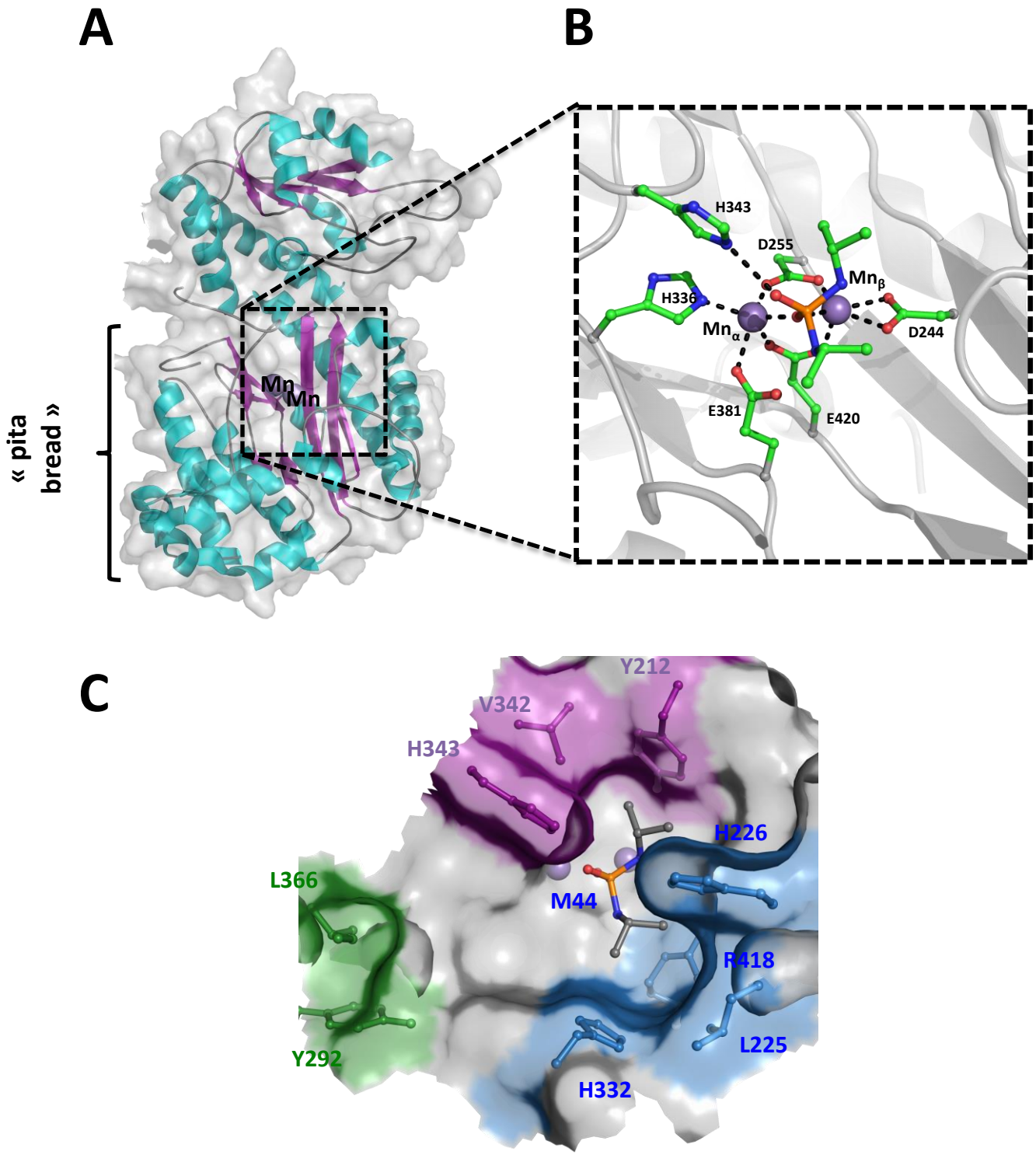

Figure I.11 : *Structure des prolidases « pita bread »*

A – Représentation cartoon d'un monomère de prolidase à repliement de type pita bread.

B – Vue rapprochée du site catalytique : les deux métaux, ici des ions Mn^{2+}, sont coordonnés par les résidus Asp244, Asp255, His336, Glu381, and Glu420. Le métal le plus exposé au solvant (Mn_α) est liés par les résidus Glu381, His336 et Asp255 et Glu420 qui pontent les deux métaux. Le métal Mn_β, quant à lui plus enfoui, est lié par les oxygènes du carboxylate de l'Asp244 en plus des résidus Asp255 et Glu420.

C – Vue en surface de la poche du site actif. Les couleurs représentent les différents sous-sites tels qu'ils sont décrits dans Vyas et al., 2010 : le grand sous-site est en bleu, le petit sous-site en violet et le site du groupement partant en vert.

Glu381, His336 et Asp255 et Glu420 (Mn_{α}, le plus exposé au solvant) et par Asp 244, Asp 255, and Glu 420 (Mn_{β}, le plus enfoui). Dans la structure cristallographique d'OPAA résolue par Vyas *et al.*, les deux métaux pontent l'atome d'oxygène d'une molécule de glycolate co-cristallisée avec l'enzyme (101). La structure d'OPAA également co-cristallisée en présence d'un inhibiteur permit ainsi de définir la structure du site de fixation des substrats (**Figure I.11 C**) (101). On distingue ainsi un grand sous-site (His 332, Leu 225, Arg 418 et His 226), un petit sous-site (His 343, Val 342, Tyr 212) et le sous-site du groupement partant (Leu 366 et Tyr 292).

Mécanisme catalytique

Le mécanisme d'hydrolyse des OPs par les prolidases fut établi par analogie avec les phosphotriestérases bactériennes (**voir partie I. B. 2. d.**) qui constituent le modèle principal des OP hydrolases à site bi-métallique. Ce mécanisme implique une attaque nucléophile par une molécule d'eau activée sous la forme d'un ion hydroxyde qui ponte les deux métaux du site actif (58). Lors de la fixation d'un OP, l'oxygène libre du centre phosphoré (oxygène terminal) interagit avec le métal α et l'His 343 alors que l'oxygène de l'ester est lié au métal β. Ce positionnement permet une attaque nucléophile directe de l'ion hydroxyde sur le phosphore occasionnant le départ du groupement partant sans dissociation des oxygènes des métaux (**Figure I.12**). Enfin, l'enzyme est régénérée avec le départ du produit et l'arrivée d'une nouvelle molécule d'eau (58, 101).

Représentants principaux

Les principaux représentants de cette famille structurale d'OP hydrolases sont les OPAA identifiées chez les *Alteromonas*. Des enzymes homologues furent également caractérisées chez *Escherichia coli* (aminopeptidase P (AMPP)) et l'homme (102). L'enzyme d'origine humaine étant facilement exprimable chez *E. coli*, celle-ci est envisagée dans le traitement prophylactique des empoisonnements aux OPs (9, 21). En dépit de leur activité importante envers les OPs possédant un groupement partant fluoré (*i.e* $k_{cat}/K_M = 6{,}1 \times 10^4\ M^{-1}.s^{-1}$ envers le soman) (**Tableau I.3**). (103) et de leur relative stabilité (activité à pH 6-9.5, optimum de température 55°C) (98, 101), les études concernant ces enzymes n'en sont encore qu'à leurs débuts.

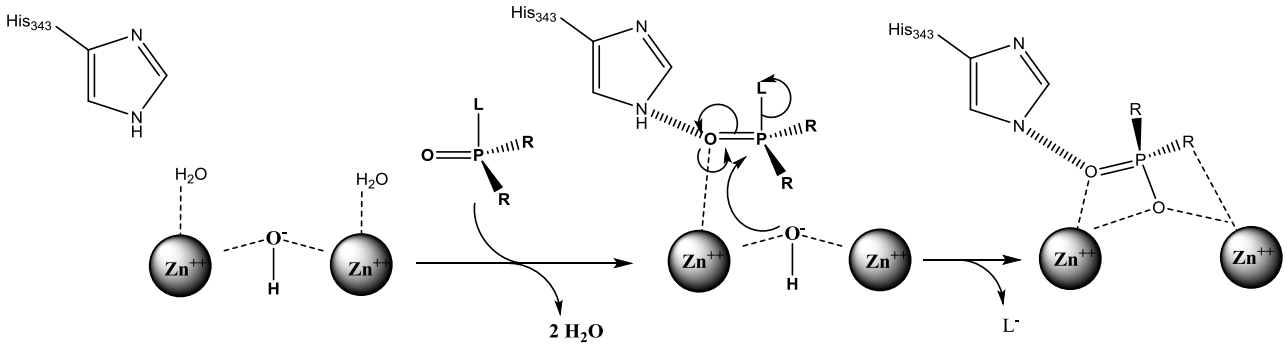

Adapté de Bigley *et al.*, 2012

Figure I.12 : *Mécanisme catalytique des « pita bread »*

Représentation schématique du mécanisme catalytique des OP hydrolases à repliement de type pita bread. Une molécule d'eau activée sous forme d'ion hydroxyde ponte les deux métaux. Lors de la fixation d'un OP, la présence d'une Histidine permet d'orienter l'oxygène terminal du phosphoryle sur le métal α, alors que l'oxygène de l'ester se positionne sur le métal β. L'ion hydroxyde peut ainsi attaquer le centre phosphoré, provoquant le départ du groupement partant (L). Lors de l'attaque, il y a formation d'un état de transition pentavalent. L'enzyme est ensuite régénérée avec l'arrivée d'une nouvelle molécule d'eau du solvant.

	k_{cat}/K_M ($M^{-1}.s^{-1}$)
Paraoxon	N.D
Parathion	N.D
DFP	$7{,}7 \times 10^{4}$ *
Sarin	$2{,}8 \times 10^{5}$ *
Soman	$6{,}1 \times 10^{4}$ *
VX	N.D

Tableau I.3 : *Efficacités catalytiques d'OPAA envers divers phosphotriesters*
Les données marquées d'une * sont issues de *Theriot et al*., 2011, celles indiquées N.D correspondent aux valeurs non déterminées dans la littérature.

c. Les OP hydrolases à topologie « sandwich αβ/βα »

Les OP hydrolases appartenant à cette famille structurale furent parmi les premières à être décrites (104, 105). Elles furent reliées à la superfamille des métallo-β-lactamases largement étudiée pour leurs implications dans la résistance des bactéries pathogènes contre les antibiotiques (104, 106, 107). Deux gènes différents (*ophc2* et *mph*) furent identifiés principalement chez des bactéries issues de sols pollués près d'usines de production (*e.g* Compagnie de Pesticides « Shanongda », Hubei, Chine) (104, 108).

Description structurale

Les enzymes appartenant à cette famille structurale se présentent sous la forme d'un sandwich αβ/βα composé de deux feuillets-β centraux, entouré par 5 hélices α exposées au solvant (109) (**Figure I.13 A**). Les deux feuillets centraux peuvent se superposer par un axe de symétrie d'ordre deux passant par les métaux du site actif, suggérant que la structure complète de ces enzymes provient de la duplication d'un gène (110). Chez la Methyl Parathion Hydrolase (MPH), l'enzyme modèle de cette topologie, le site actif est constitué de deux ions métalliques formant un centre bi-nucléaire localisé à l'une des extrémité du sandwich de feuillets β où se trouvent les boucles permettant l'accommodation des substrats (109). Le métal le plus enfoui (métal α) est coordonné par deux aspartates (Asp 151, Asp 255), deux histidines (His 152 et His 302) et une molécule d'eau. Le métal exposé est coordonné par trois histidines (His 147, His 149, His 234) et partagent le résidu d'Asp 255 et la molécule d'eau (106) (**Figure I.13 B**). Les deux métaux adoptent ainsi des coordinations octaédriques impliquant la présence d'un motif structural caractéristique des métallo-β-lactamases : le motif His-X-His-X-Asp-His, conservé chez dans cette topologie d'enzymes (109). Trois sous-sites présents dans la poche du site actif définissent la stéréospécificité de l'enzyme : un patch de résidus aromatiques (Phe 119, Trp 179 et Phe 196) facilitant la fixation du substrat, et deux sous-sites latéraux (Val 65, Leu 67 et Arg 72, Leu 258, Leu 273 respectivement) (**Figure I.13 C**) (58).

Mécanisme catalytique

Le mécanisme catalytique supposé de ces OP hydrolases implique l'attaque d'une molécule d'eau pontante, activée sous la forme d'un ion hydroxyde par l'assistance de l'Asp 255, sur le centre phosphore du substrat (111). En effet, l'oxygène terminal interagit avec le métal β alors que l'hydroxyde

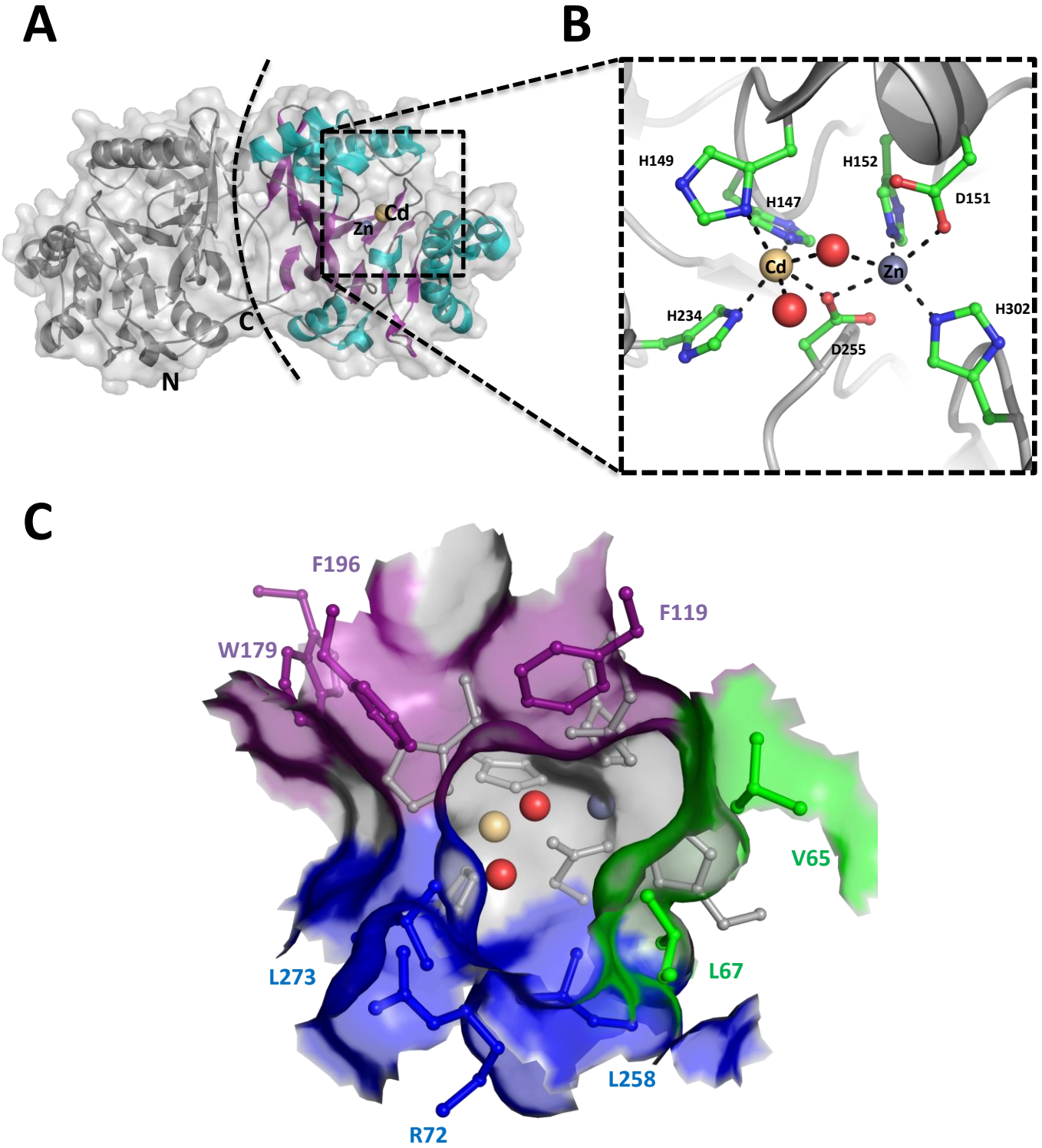

Figure I.13 : *Structure de la Methyl Parathion Hydrolase, un représentant des OP hydrolases à repliement de type metallo-β-lactamase*

A – Représentation cartoon d'un dimère de MPH, l'interface dimérique est symbolisée par la ligne en tirets. Les deux métaux sont coordonnés dans une cavité à l'opposé de l'interface du dimère.

B – Vue rapprochée du site catalytique et du réseau de coordination des métaux.

C – Représentation en surface de la poche du site actif. Le cluster hydrophobe tel que décrit dans l'article Dong et al., 2005, est coloré en violet.

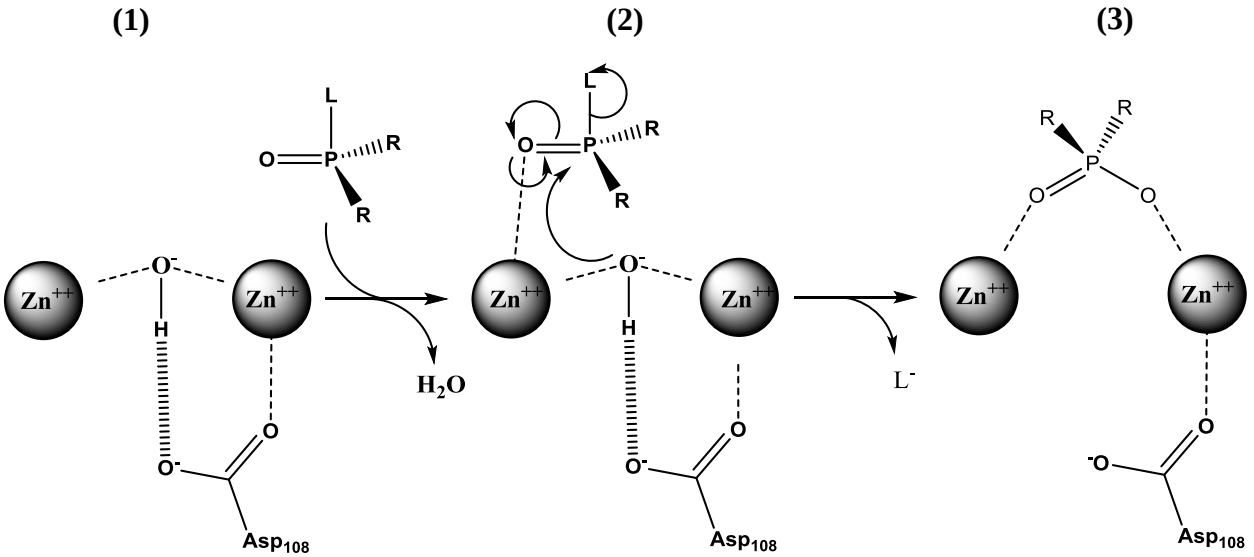

Figure I.14 : *Mécanisme catalytique des phosphotriesters par MPH*

(1) La molécule d'eau catalytique est activée en ion hydroxyde positionné grâce à l'Asp 108. Le substrat interagit *via* l'oxygène terminal du phosphore sur le centre bimétallique. **(2)** L'ion hydroxyde réalise alors une attaque nucléophile sur l'ion phosphore entrainant ainsi la rupture de la liaison phosphoester la plus labile (L) **(3)**.

effectue l'attaque nucléophile sur le centre phosphore. Lors de l'attaque, il y a formation d'un état de transition pentavalent qui, après rabattement du doublet présent sur l'oxygène terminal entraine le départ du groupement partant. L'enzyme est ensuite régénérée avec l'arrivée d'une nouvelle molécule d'eau (58, 111) (**Figure I.14**).

Représentants principaux

MPH fut la première OP hydrolase de cette famille structurale à avoir été décrite suite à l'identification du gène *mpd* (AY029773) issu de *Pseudomonas putida* (104). Depuis, d'autres séquences homologues ont été identifiées soit à partir d'ADN chromosomique soit à partir d'éléments transposables acquis par les bactéries du sol par transfert horizontal d'ADN (112-116). L'enzyme la plus étudiée de cette famille, avant mon travail, est la MPH issue de la bactérie *Pseudomonas sp.* WBC-3 (114) dont la structure cristallographique a été résolue à 2.4 Å de résolution (106). L'enzyme est dimérique avec un centre bi-métallique (Cd^{2+} / Zn^{2+} ou Zn^{2+} / Zn^{2+}) (106). L'enzyme présente des efficacités catalytique intéressantes envers les OPs ($k_{cat}/K_M \sim 10^5$ $M^{-1}.s^{-1}$ envers le methyl-parathion) pouvant être modulées par des mutations dans les sous-sites de spécificité. Cependant, MPH étant d'origine mésophile, elle ne présente pas les avantages biotechnologiques liés aux protéines hyperthermostables (*e.g* bas coût de production, stabilité dans le temps, maniabilité industrielle, **voir partie I. C. 1**) (117). Ainsi, des études furent menées afin d'améliorer les propriétés de stabilité de l'enzyme (*e.g* mutagénèse dirigée guidée par la comparaison avec des enzymes homologues thermorésistantes (OPHC2) ou par la dynamique moléculaire) (117, 118).

d. Les OP hydrolases à topologie « tonneau $(\beta/\alpha)_8$ »

Des enzymes extrêmement efficaces envers les OPs furent découvertes chez des bactéries du sol quelques décennies seulement après l'introduction des insecticides OPs dans la nature. Ces bactéries sont capables d'utiliser les OPs comme source de carbone et de phosphore, ce dernier étant très souvent limitant dans l'environnement (119). De plus, il a été montré que l'épandage répété d'insecticides OPs conduit à terme à une meilleure capacité de bio-dégradation par les sols (120, 121). Ainsi, certaines bactéries telles que *Brevundimonas diminuta*, ont évolué pour dégrader spécifiquement les OPs atteignant pour l'une d'elles une vitesse d'hydrolyse ~10^8 $M^{-1}.s^{-1}$ (122). Celles-ci ont ainsi été nommées phosphotriestérases (PTE) pour leur capacité à dégrader les phosphotriesters (**Tableau I.4**) (122). Ces

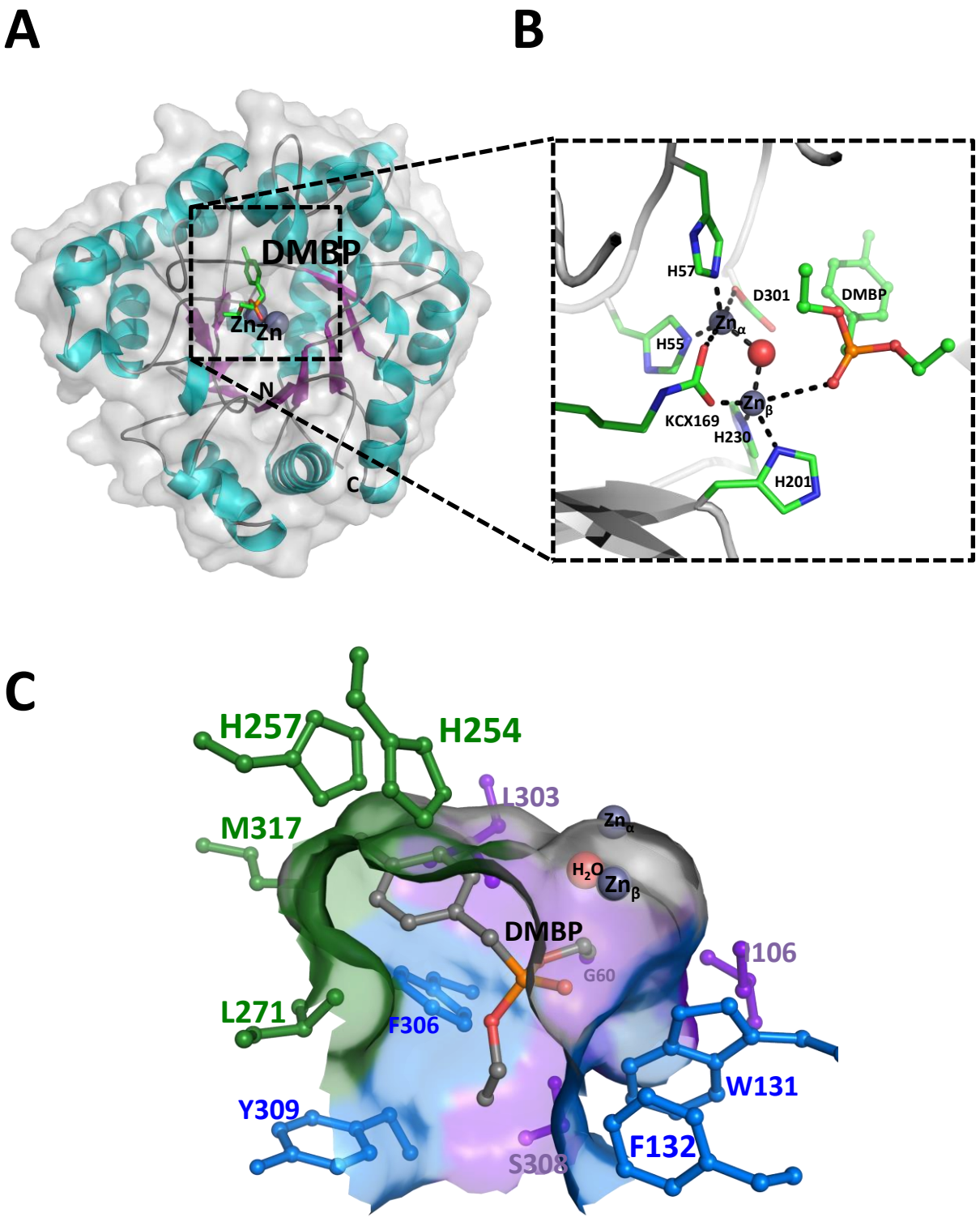

Figure I.15 : *Structure de la PTE de P. diminuta (1DPM)*

A – Représentation cartoon d'un monomère du *Bd*PTE en complexe avec un analogue du paraoxon.

B – Vue rapprochée du site de catalytique de la *Bd*PTE et du réseau de coordination des métaux.

C – Les différents sous-sites de la PTE tels qu'ils sont décrit par Vanhooke et al., 1996, le grand sous-site est colorié en vert, le petit sous site en violet et la poche du groupement partant est colorée en bleu.

enzymes possèdent un repliement de type TIM-barrel ou tonneau-$(\beta/\alpha)_8$, un repliement très populaire, présent dans de nombreuses enzymes et catalysant plus de 100 réactions enzymatiques (123). Le principal représentant est la PTE issue de *Brevundimonas diminuta (ex-Pseudomonas diminuta)* (*Bd*PTE), également retrouvée chez *Flavobacterium sp.*, et *Agrobacterium radiobacter* (OpdA) qui présentent respectivement 100 % et plus de 90 % d'identité de séquence (124, 125).

Description structurale

La *Bd*PTE présente un repliement de type TIM-barrel constitué de 8 brins β formant un tonneau entouré de 8 hélices α, chaque élément étant reliés par des boucles (**Figure I.15 A**). Les OPs hydrolases appartenant à cette famille structurale sont des enzymes homodimériques (123, 126). Le site actif est constitué de deux ions métalliques situés dans une cavité du côté C-terminal du tonneau dont l'entrée est régie par la présence de boucles 7 et 8 accommodants le substrat (123, 126). Les deux cations métalliques, deux atomes de Zn, sont coordonnés grâce à la présence d'une lysine carboxylée, 4 résidus histidine, d'un résidu aspartate et d'une molécule d'eau pontant les deux métaux. Le métal α, le plus enfoui, adopte une géométrie de type bi-pyramide trigonale constituée par His 55, His 57, Asp 301, Lys 169 (lysine carboxylée) et la molécule d'eau pontante. Le métal β, exposé au solvant, est coordonné par His 201, His 230, Lys 169, la molécule d'eau pontante auxquels s'ajoute une seconde molécule d'eau selon une géométrie bi-pyramide trigonale distordue (**Figure I.15 B**). La poche de fixation du substrat, se décompose en trois sous-sites imposant la stéréo préférence de l'enzyme pour les énantiomères *(S)* : (i) le petit sous-site (Gly 60, Leu 303, Ser 308 et Ile 106) accommodant le substituant le plus encombrant, (ii) le grand sous-site (His 254, His 257, Leu 271 et Met 317) accommodant un second substituant de l'OP (iii) le groupement partant étant accommodé par des résidus hydrophobes (Phe 306, Phe 132, Trp 131 et Tyr 309) (**Figure I.15 C**)(58, 127-130).

Mécanisme catalytique

Le mécanisme catalytique de la PTE et plus généralement des OPs hydrolases appartenant à la superfamille des amido-hydrolases est identique à celui de MPH (famille des métallo-β-lactamases) (58). La réaction se déroule selon une attaque nucléophile de type S_N2 de la molécule d'eau activée pontant les deux métaux du site actif sur le centre phosphore (**Figure I.16**) (58, 131). Il y a alors formation d'un intermédiaire pentavalent fixé aux métaux. Ceux-ci, et en particulier le métal β, compensent la charge négative se développant sur l'oxygène du phosphoryle. Le rabattement du doublet de l'oxygène entraine le départ du groupement partant avec renversement de la stéréochimie (attaque

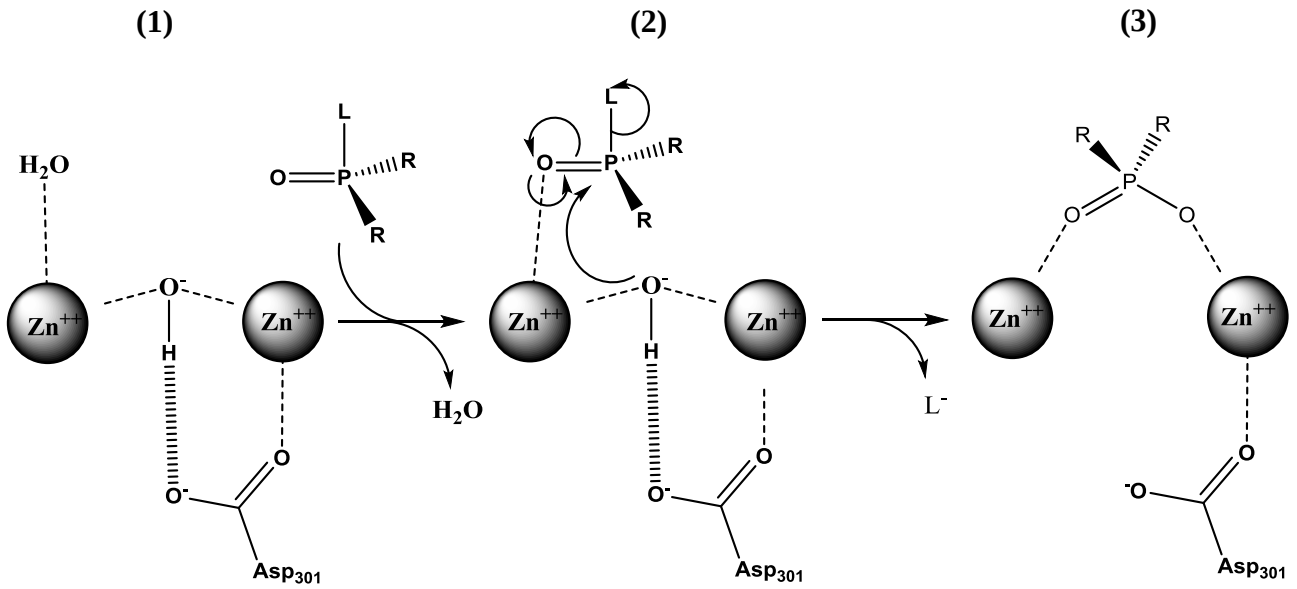

Figure I.16: *Mécanisme catalytique des phosphotriesters par les PTEs*

(1) La molécule d'eau catalytique est activée en ion hydroxyde positionné grâce à l'Asp 301. Le substrat interagit *via* l'oxygène terminal du phosphore sur le centre bimétallique. **(2)** L'ion hydroxyde réalise alors une attaque nucléophile sur l'ion phosphore entrainant ainsi la rupture de la liaison phosphoester la plus labile (L).

apicale – départ apical) et formation d'un produit de géométrie tétravalente. L'enzyme est régénérée lors du départ du produit, alors phosphodiester, remplacé par une molécule d'eau. L'acte chimique ne constitue pas l'étape limitante de la catalyse qui est limitée par les mouvements structuraux de l'enzyme impliqués dans l'entrée/sortie du substrat et du produit (132, 133).

Représentants principaux

a. La PTE (Opd)

Le représentant le mieux caractérisé est la PTE issue de *Brevundimonas diminuta* (*Bd*PTE), identifiée également chez *Flavobacterium sp.*, deux bactéries du sol (134, 135). La *Bd*PTE est encodée par le gène *opd*, présent sur un élément plasmidique au sein de ces bactéries (135, 136). Cet élément est par ailleurs partagé par de nombreuses bactéries présentes dans les sols pollués aux insecticides (136, 137). La *Bd*PTE est une enzyme extrêmement optimisée pour hydrolyser les insecticides OPs tels que le paraoxon et le parathion mais présente une efficacité catalytique plus faible envers les agents chimiques de guerre (138). Il a été proposé que la *Bd*PTE ait évolué par duplication d'un gène ancestral, puis divergé jusqu'à spécialisation de l'activité envers les OPs.

b. OpdA

OpdA fut isolée chez *Agrobacterium radiobacter* du fait de l'importante similarité de séquence qui la relie à la *Bd*PTE (*opda* possède 88.4 % d'identité avec *opd*) (125). En dépit de cette ressemblance, les variations d'acides aminés sont suffisantes pour qu'OpdA présente des différences de spécificité de substrat par rapport à la *Bd*PTE (*e.g* substitution His_{BdPTE} 254 Arg_{OpdA} et His_{BdPTE} 257 Tyr_{OpdA}) (139). La nature des métaux chez OpdA est également différente de la *Bd*PTE avec un centre hétéro-bimétallique Fer-Co (ou Zn-Co) (140). Le mécanisme catalytique proposé par Jackson *et al.*, en 2008 est légèrement différent de la PTE et implique qu'une molécule d'eau présente sur le métal α soit déprotonée par la molécule d'eau pontante, permettant ainsi la catalyse (141). OpdA a été à plusieurs reprises utilisée comme base pour des travaux d'amélioration par évolution dirigée (139, 142) ou des preuves de concept pour des applications biotechnologiques (143, 144). Ces applications biotechnologiques sont même devenues une réalité puisque la société Orica commercialise l'enzyme (Landguard^{Tm} A900, Orica) pour une utilisation principale dans la décontamination des eaux issues du traitement antiparasitaire ovin dans les pays du Commonwealth.

Afin d'améliorer les activités de *Bd*PTE et OpdA envers les agents chimiques de guerre, des travaux d'évolution dirigée ont été entrepris, permettant à l'enzyme d'atteindre une efficacité catalytique

	k_{cat}/K_M ($M^{-1}.s^{-1}$)		
	Bd*PTE	**L7ep-3**	**OpdA**
Paraoxon	$5,5 \times 10^7$	$1,3 \times 10^7$	$2,1 \times 10^{7\,\#}$
Parathion	$2,6 \times 10^6$	N.D	$5,6 \times 10^{6\,\#}$
DFP	$9,7 \times 10^6$	N.D	$55^{\,\$}$
Sarin	$8,0 \times 10^4$	N.D	N.D
Soman	$1,0 \times 10^4$	N.D	N.D
VX	45	6×10^4	N.D

Tableau I.4 : *Efficacités catalytiques de la* Bd*PTE et d'OpdA envers divers phosphotriesters*
* Les efficacités d'hydrolyse déterminés pour la *Bd*PTE sont issus de *Theriot et al.*, 2011. #Les efficacité catalytiques observées pour OpdA sont issues de *Ely et al.*, 2010, celles indiquées par un $ sont issues de *Horne et al*., 2006 et celles indiquées par N.D correspondent aux valeurs non déterminées dans la littérature pour l'enzyme sauvage. L7ep-3 correspond à l'un des variants de *Bd*PTE les plus actifs envers le VX (*Bigley et al,*. 2013)

d'environ 10^5 $M^{-1}.s^{-1}$ envers les agents G tels que le soman (130, 145). Une étude récente permis également d'améliorer l'activité de la *Bd*PTE envers le VX ($k_{cat}/K_M \sim 10^4$ $M^{-1}.s^{-1}$) en introduisant des mutations dans les résidus constituant la boucle 7 (146). Néanmoins, l'utilisation de ces enzymes dans le cadre d'une décontamination externe est tempérée par leur relative instabilité (demi-vie < 4 jours dans l'eau et stockage à 4 °C nécessaire) occasionnant un coût de production et de purification élevé (19). Outre son intérêt pour une décontamination externe, OpdA a fait l'objet de travaux visant à fonctionnaliser l'enzyme grâce des chaines de PEG dans le but d'une utilisation en prophylaxie (143).

C. Potentialités des OP hydrolases thermo-résistantes

1. Avantages biotechnologiques des enzymes thermo-résistantes

Les enzymes dites « hyper-thermophiles » sont en général issues d'organismes présentant une croissance optimale entre 80 et 110 °C (*e.g S. solfataricus*, 87 °C). En effet, les enzymes issues de tels organismes ont évolué pour fonctionner de façon efficace à haute température et possèdent des paramètres cinétiques plus faibles à des températures plus basses. Afin de répondre à ces contraintes, ces enzymes présentent des caractéristiques de thermo-stabilité exceptionnelles pouvant être soit intrinsèques (particularités structurales), soit dues à des facteurs extrinsèques (*e.g* présence de co-facteurs particuliers) (147).

La dénaturation thermique des protéines est la résultante de plusieurs mécanismes : (i) l'exposition des parties hydrophobes normalement enfouies dans le cœur protéique, (ii) des modifications chimiques comme la déamidation (Asn et Gln) et l'oxydation des cystéines, (iii) et l'hydrolyse des liaisons peptidiques (favorisée par la présence d'Asp-Pro ou Asn-Xaa). Les protéines thermo-résistantes présentent ainsi un biais d'enrichissement en résidus chargés (à la défaveur des asparagines et glutamines) favorables à la constitution de complexes réseaux de ponts salins de surface. Il est également communément admis que les protéines thermostables sont plus rigides que les protéines mésophiles. Cette rigidité est souvent liée à un raccourcissement des boucles et des extrémités protéiques, à leur ancrage au corps de la structure, à la stabilisation des structures secondaires et à la réduction des cavités. La multimérisation est également un facteur de stabilisation observé chez ces protéines, et les surfaces d'interaction entre monomères sont enrichies en interactions hydrophobes. Celles-ci étant favorisées avec la température, elles peuvent ainsi présenter un biais de séquence en résidus hydrophobes.

En dépit de ces différences, les protéines mésophiles et leurs pendants hyperthermostables présentent des structures tridimensionnelle superposables et ont des mécanismes catalytiques identiques (147). De ce fait, elles présentent de nombreux avantages biotechnologiques liés à ces propriétés. Elles peuvent souvent être exprimées chez un hôte mésophile (à moins de requérir un co-facteur particulier), sont très stables et résistantes. De plus, leur activité à hautes températures peut constituer un avantage pour certaines réactions ou éviter les contaminations microbiennes. Du fait de leur thermo-résistance supérieure, elles peuvent facilement être purifiées par la chaleur lorsqu'exprimées chez un hôte mésophile, la plupart des protéines de l'hôte étant éliminées sous l'effet de la température. Enfin, elles présentent une résistance supérieure aux agents dénaturants (*e.g* chlorure de guanidinium) et sont souvent actives, voire légèrement plus actives en présence de détergents (*e.g* Triton X-100, SDS) ou de solvants. Le potentiel biotechnologique des enzymes thermo-résistantes étant indéniable (148, 149), les enzymes étant à la fois robustes et efficaces envers les OPs constituent un champ de recherche important dans le cadre d'une utilisation en décontamination externe (*e.g* surfaces, matériaux).

2. Les OP hydrolases thermo-résistantes

L'existence d'enzymes homologues aux prolidases à topologie « pita bread » fut rapportée chez certaines archaea extrêmophiles du genre *Pyrococcus* (*Pyrococcus furiosus* et *Pyrococcus horikoshii*, température optimale de croissance 98-100 °C (150)). Bien que ces enzymes présentent 24% identité et des structures cristallographiques comparables à OPAA, elles sont extrêmement thermo-résistantes (8h à 100 °C sans perte significative d'activité) (151, 152). Elles présentent un site catalytique bimétallique avec une préférence pour les cations métalliques de type Co^{++} et Mn^{++}. L'affinité pour les métaux est également plus élevée que celle observée chez OPAA ce qui peut être un avantage pour une utilisation externe (153). La fonction naturelle de ces enzymes est liée, tout comme pour OPAA, à l'hydrolyse de dipeptides Xaa-Pro. Elles présentent des activités plus élevées à haute température (*e.g* $k_{cat}/K_M \sim 2 \times 10^6$ $M^{-1}.s^{-1}$ à 100 °C envers Met-Pro) et perdent rapidement leur activité à plus basse température (152, 154, 155). De plus, ces enzymes sont capables d'hydrolyser les liaisons P-F et P-O présentes dans les composés organophosphorés. En particulier, elles sont capables d'hydrolyser le DFP (0,73 U/mg à 50 °C) et le p-Nitrophenyl Soman (0,50 U/mg à 70 °C), un analogue de CWA. Des expériences d'évolution dirigée sont actuellement en cours afin d'améliorer les activités OP hydrolase de ces enzymes (155).

Parmi les enzymes à repliement de type sandwich αβ/βα, OPHC2 fut tout d'abord isolée chez l'organisme mésophile *Pseudomonas pseudoalcaligenes* souche C2-1 (156) puis chez *Stenotrophomonas sp.* SMSP-1 (98 % d'identité) (157). Elle partage environ 58 % de similarité de

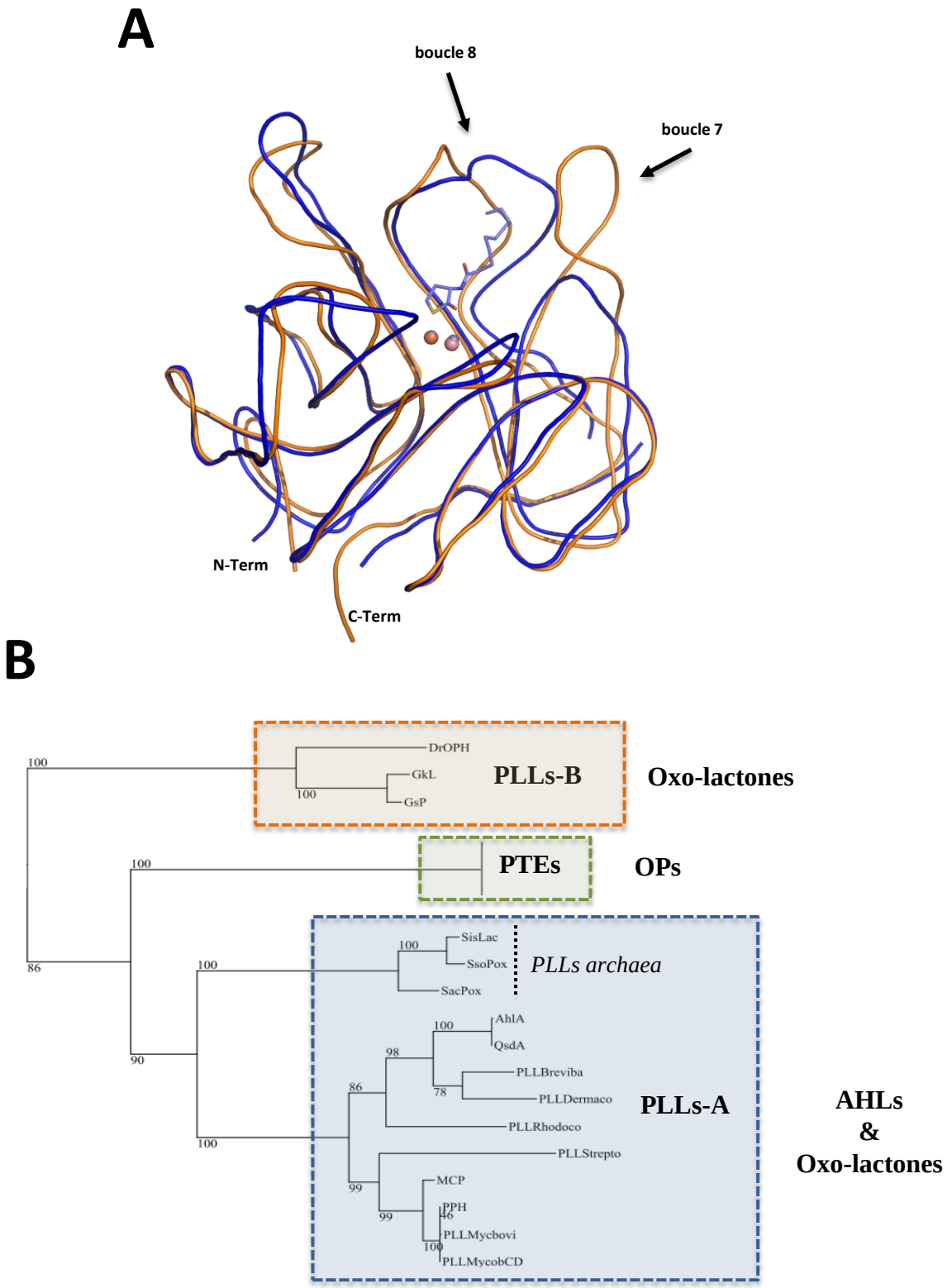

Figure I.17: *Arbre phylogénétique des PLLs*

A – Structure d'un monomère de PTE (orange) et de *Sso*Pox (bleu) superposés, la lactone présente dans le site actif de *Sso*Pox est colorée en bleu clair.

B – Arbre phylogénétique des PLLs et des PTEs. Les PLL-A constituent le groupe d'enzyme le plus proche de la *Bd*PTE. Leur préférence de substrat est indiquée.

séquence avec MPH et fut montrée comme étant résistante à la température (activité optimale à 65 °C) (158, 159). Cette similarité servit de base à l'amélioration de la thermostabilité de MPH par transfert de ponts salins présumés présent chez OPHC2 dans l'architecture de MPH (117). De plus, un autre avantage observé pour cette enzyme est qu'elle peut être obtenue de façon recombinante en grande quantités lorsqu'exprimée chez la levure *Pichia pastoris* (158). En dépit de ces caractéristiques biotechnologiques particulièrement intéressantes, l'enzyme ne fut que très peu caractérisée. L'obtention de la structure cristallographique de cette enzyme ainsi que sa caractérisation biochimique et enzymatique furent ainsi l'un de mes objectifs de thèse (**articles présentés en partie II. C. et II. D.**).

Enfin, le plus large travail de caractérisation d'enzymes thermostables hydrolysant les OPs fut effectué chez les « Phosphotriesterase-Like Lactonase » (PLLs) (160, 161). Les PLLs, constituent une large famille d'enzymes apparentées aux PTEs (homologie de séquence de l'ordre de 30 %). Les principales différences observées avec les PTEs concernent les boucles du site actif (boucles 7 et 8) permettant l'accommodation des substrats (**Figure I.17 A**). Leur activité naturelle est d'hydrolyser les fonctions lactones mais elles présentent également des activités plus faibles envers certains composés OPs (160, 161). Elles constituent un réservoir majeur d'OPs hydrolases du fait de leur origine d'organismes aussi bien mésophiles, thermophiles qu'extrémophiles (161). De plus, du fait de leur homologie avec la *Bd*PTE, elles constituent des candidats de départ idéaux pour les procédés d'évolution dirigée visant à augmenter l'activité d'hydrolyse des OPs (162). Au sein de cette famille enzymatique, deux sous-familles de PLLs ont récemment été décrites (161) (**Figure I.17 B**) : (i) les PLL-A qui sont phylogénétiquement les plus proches de la PTE, elles hydrolysent plus efficacement les AHLs et comprennent les PLL issues des *Sulfolobus* (*Sso*Pox, *Sis*Lac, *Sac*Pox) (163, 164), *Rhodococcus* (AhlA, QsdA) (160, 165), et *Mycobacterium* (MCP, PPH) (160, 166) et (ii) les PLL-B, plus éloignées des PTEs, hydrolysant plus efficacement les oxo-lactones, elles comprennent les protéines présentes chez *Geobacillus* (GkL, GkaP, GsP) (167-169) et *Deinococcus radiodurans* (Dr-OPH) (162).

Geobacillus stearothermophilus et *Geobacilus kaustophilus* sont des organismes thermophiles (température optimale de croissance 55-65 °C, (170, 171)) alors que *Deinococcus radiodurans* est mésophile (25-30 °C, (172)). Néanmoins, les PLLs issues de ces organismes présentent des thermostabilités élevées (GsP conserve plus de 70 % d'activité après 2h d'incubation à 90 °C) (162). Les archées hyperthermophiles étant également une source connue d'enzymes d'intérêt biotechnologique majeur (148, 173, 174), plusieurs PLLs furent ainsi identifiées et caractérisées chez le genre *Sulfolobus* : *Sulfolobus solfataricus* (*Sso*Pox), *Sulfolobus islandicus* (*Sis*Lac) et *Sulfolobus acidocaldarius* (*Sac*Pox). *S. solfataricus* est une archaea extrémophile hyperthermophile et acidophile (température optimale de croissance entre 50 à 80 °C, pH 3, (175)) découverte dans les sulfatares volcaniques Napolitains (176). Ainsi, les enzymes issues de ces organismes, présentent une thermostabilité exceptionnelle, évaluée à 106 °C pour *Sso*Pox (177). Ces enzymes présentent d'une

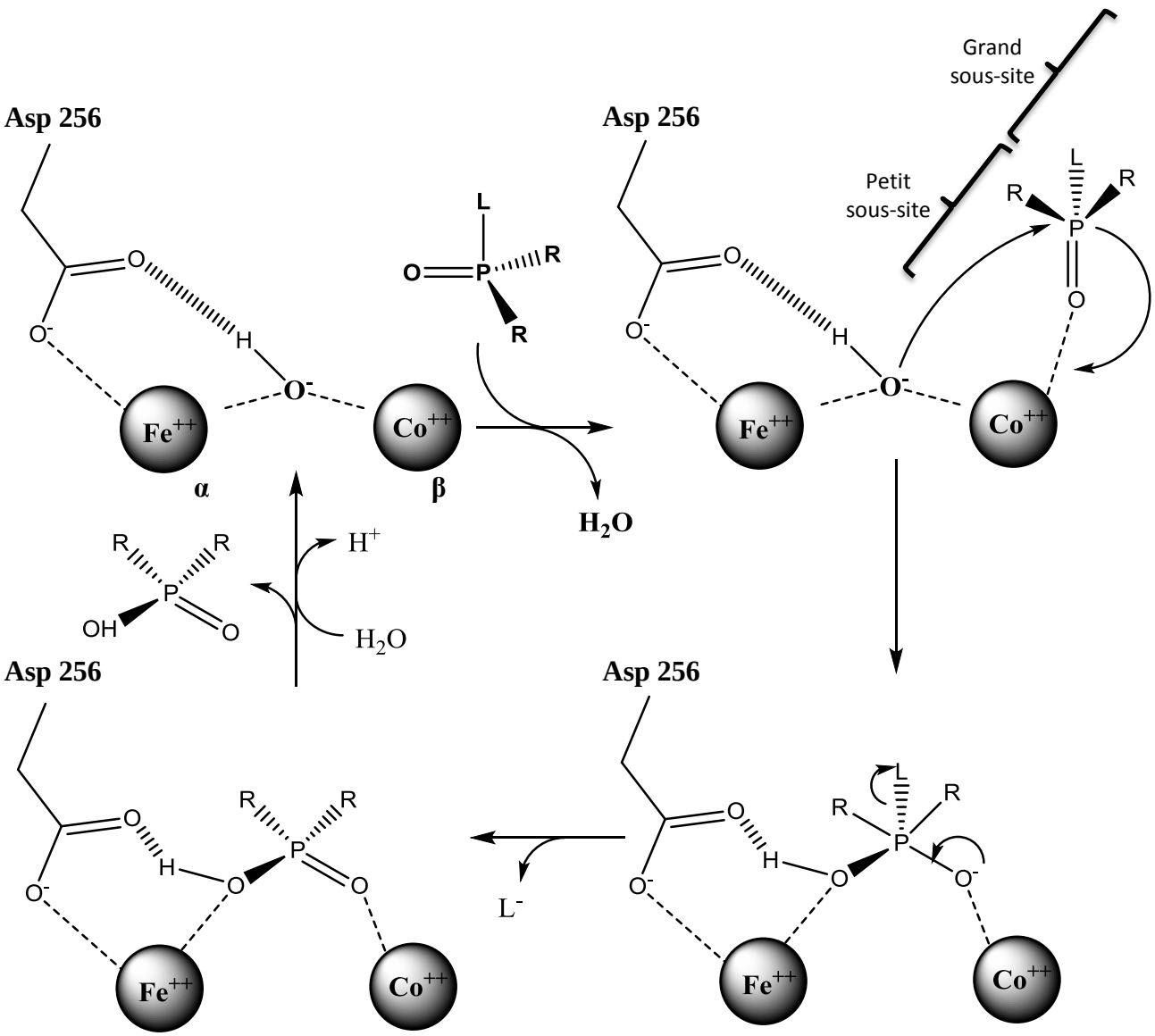

Adapté d'Elias JMB 2008

Figure I.18: *Mécanisme catalytique des PLLs*

Mécanisme catalytique de *Sso*Pox, proposé par Elias et al., 2008. Le schéma réactionnel implique la formation d'un état de transition pentavalent.

façon générale les mêmes éléments structuraux incriminés dans la thermo-stabilité que ceux observés chez d'autres enzymes thermo-résistantes (*e.g* ponts salins de surface, compaction, boucles raccourcies, surface de dimérisation importante principalement hydrophobe) (162, 163, 169, 177). Enfin, toutes ces enzymes présentent à température ambiante des efficacités d'hydrolyse variables de l'ordre de $k_{cat}/K_M \sim 10^{1-3}$ $M^{-1}.s^{-1}$ envers l'insecticide modèle paraoxon. Ce sont, en fait, des activités de promiscuité qui font l'objet de plusieurs travaux d'amélioration : amélioration de *Sso*Pox (178), plus récemment GkaP (168) et DrOPH (179). Au cours de ces travaux d'amélioration d'activité OP hydrolase, un variant fut sélectionné chez l'enzyme GkL (variant de GkL 28A8C F28I/Y99L/T171S/F228L/N269S/V270G/W271C/G273D) (168). Néanmoins, le meilleur résultat fut obtenu pour l'enzyme *Dr*OPH par une approche couplant évolution aléatoire et mutagenèse à saturation ciblant des résidus clés du site actif (variant *Dr*PLL.10 Y28L/D71N/Y97F/E101G/E179D/V235L/P274L) (179). *Dr*PLL.10 atteignant une efficacité catalytique de 2,0 x 10^4 $M^{-1}.s^{-1}$ envers le paraoxon (179).

3. Relations de promiscuité Phosphotriestérase - Lactonase

a. Origine de la promiscuité enzymatique

La promiscuité enzymatique se définit comme la capacité fortuite d'une enzyme à prendre en charge des substrats non natifs et catalyser la réaction selon un mécanisme pouvant être différent de son activité naturelle (180-182). L'activité de promiscuité n'est pas sous pression de sélection, c'est une réaction « parasite » pour laquelle l'enzyme n'est pas optimisée (180, 181). En effet, les enzymes sont optimisées pour effectuer une tache mais peuvent parfois permettre de réaliser des réactions parallèles. Ainsi, lorsqu'une nouvelle pression de sélection s'exercera, l'activité la promiscuité pourra être optimisée en réponse à cette pression (180, 181). L'un des moteurs prépondérant de l'évolution des enzymes et de l'émergence de nouvelles activités serait ainsi constitué par les activités de promiscuité qui serviraient de base de départ à l'émergence d'enzymes optimisées (181, 183, 184). Ainsi, il fut proposé que les PTEs aient émergé à partir de PLLs ancestrales présentant une activité naturelle lactonase et des activités de promiscuité phosphotriestérase (160, 161). Le mécanisme d'hydrolyse des OPs proposé pour les PLLs est de plus identique à celui des PTEs (**Figure I.18**). Par ailleurs, cette évolution ne semble pas être un cas unique puisque des enzymes optimisées pour hydrolyser les insecticides ont également été identifiées dans des lieux géographiquement éloignés et au sein d'une

Les lactones

AHLs

I

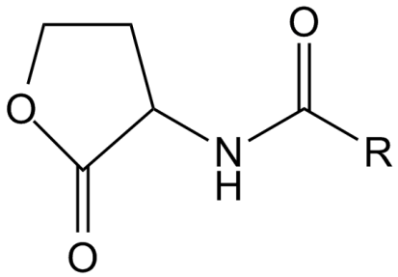

II

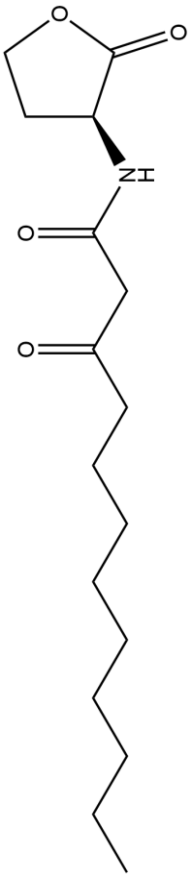

Oxo-lactones

III

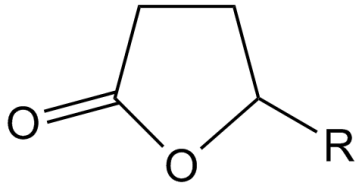

IV

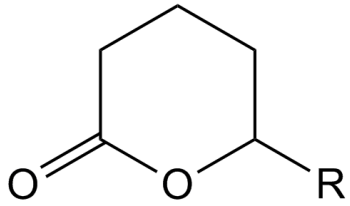

V

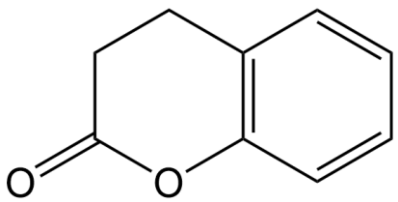

Figure I.19 : *Structure chimique des principales AHLs et oxo-lactones*

Structure générale d'une AHL (**I**), 3-oxo-C12 AHL (**II**)

Structure générale d'un oxo-lactone : γ-lactone (**III**), δ-lactone (**IV**), dihydrocoumarine (**V**)

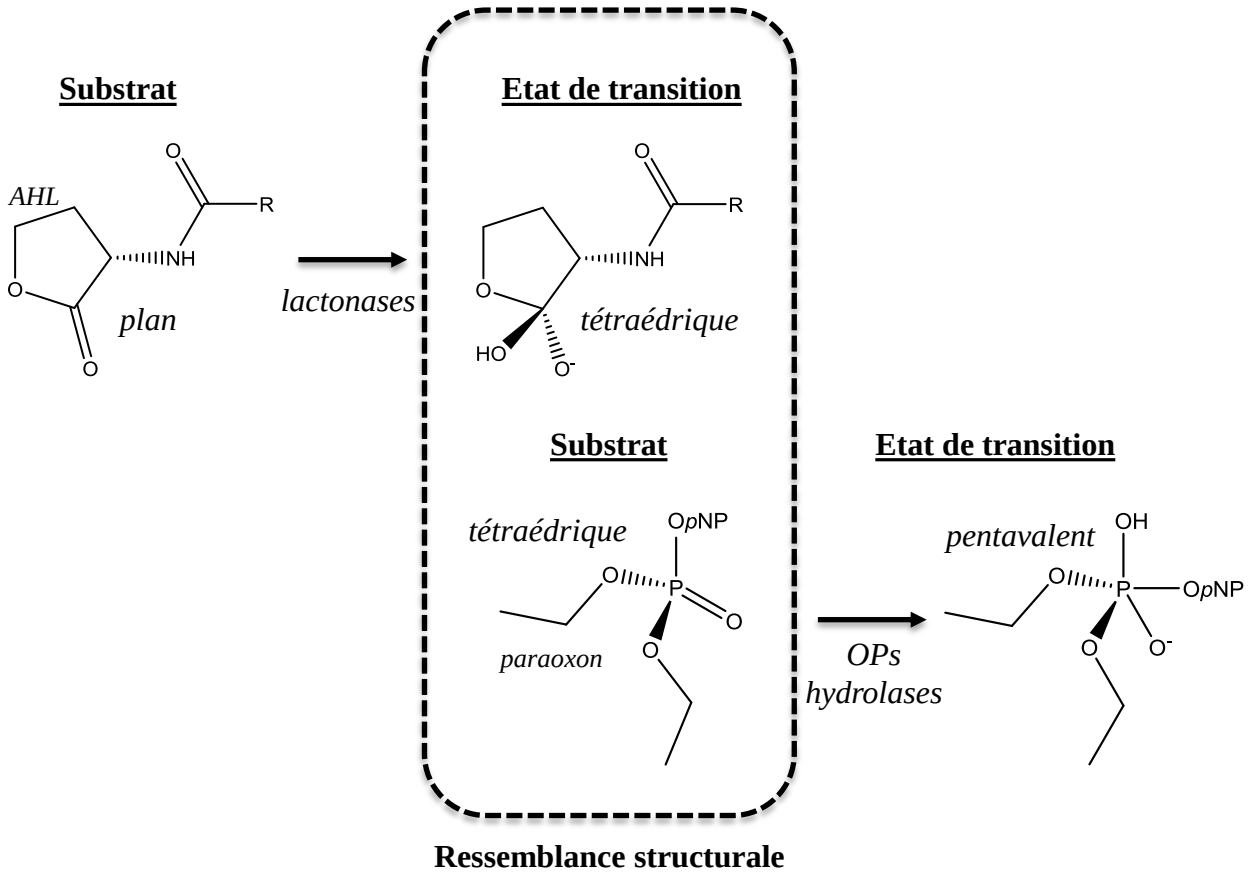

Figure I.20 : *Promiscuité enzymatique lactonase - phosphotriestérase*

La ressemblance géométrique entre l'état de transition d'hydrolyse des lactones (tétrahédrique) et la configuration des substrats phosphotriesters est à l'origine de la promiscuité d'activité lactonase – phosphotriestérase.

topologie différente (sandwich αββα, MPH) (185). Ainsi, ces phénomènes tendent à illustrer que la nature peut utiliser des solutions équivalentes, guidées par la chimie, pour produire des enzymes optimisées envers de nouveaux substrats.

b. La chimie de promiscuité phosphotriesterase - lactonase

Les lactones sont des molécules chimiquement différentes des OPs (**Figure I.19**). Ce sont des esters cycliques (configuration de type sp^2). Au cours de la réaction enzymatique d'hydrolyse, il y a formation d'un état transition tétraédrique (hybridation de type sp^3) (163) (**Figure I.20**). Or, les enzymes sont optimisées pour fixer et stabiliser l'état de transition afin de réduire la barrière d'énergie d'activation de la réaction chimique. De ce fait, les OPs tels que le paraoxon qui présentent une configuration tétraédrique peuvent être accommodés puis pris en charge « fortuitement » et de façon non optimale par les lactonases (PLLs, PONs, Metallo-β-lactamase) (163, 185). L'inverse étant également vrai, du fait que les phosphotriestérases fixent les substrats tétraédriques, elles peuvent, de façon non optimisée, prendre en charge des substrats de type lactone et ainsi présenter une activité de promiscuité lactonase (161, 185). De ce fait, toutes les lactonases décrites présentent des activités de promiscuité phosphotriestérases, et il existe dans leur famille structurale, au moins une enzyme optimisée envers les OPs. La réciproque est probablement vraie, bien que n'ayant pas été vérifiée pour toutes les phosphotriestérases, celles-ci présentent des activités de promiscuité lactonase.

Ainsi, l'activité lactonase étant intimement liée à l'activité OP hydrolase, on retrouve la même diversité structurale. En effet, de nombreuses lactonases ont été décrites au sein de différents types de repliement structuraux : (i) les paraoxonases (topologie β-propeller) (ii) les sandwich αβ/βα (iii) et les PLLs (topologie tonneau $(\beta/\alpha)_8$). De façon intéressante, certaines de ces enzymes, comme la paraoxonase humaine (hPON1) ou *Sso*Pox issue de *Sulfolobus solfataricus*, ont tout d'abord été caractérisées pour leur activité de promiscuité (*i.e* paraoxonase) avant d'être finalement attribuées comme étant des lactonases naturelles capables d'hydrolyser les molécules du *quorum* sensing (QS) (77, 78, 160).

Les Paraoxonases

Tout d'abord découvertes en vertu de leur capacité à hydrolyser le paraoxon, les PONs (**voir partie II. B. 2. a.**) ne furent que récemment caractérisées comme étant des enzymes capables d'hydrolyser divers esters et lactones. Les études phylogénétiques réalisées dans cette famille d'enzymes suggèrent qu'elles auraient évolué à partir d'un ancêtre commun présentant une activité naturelle

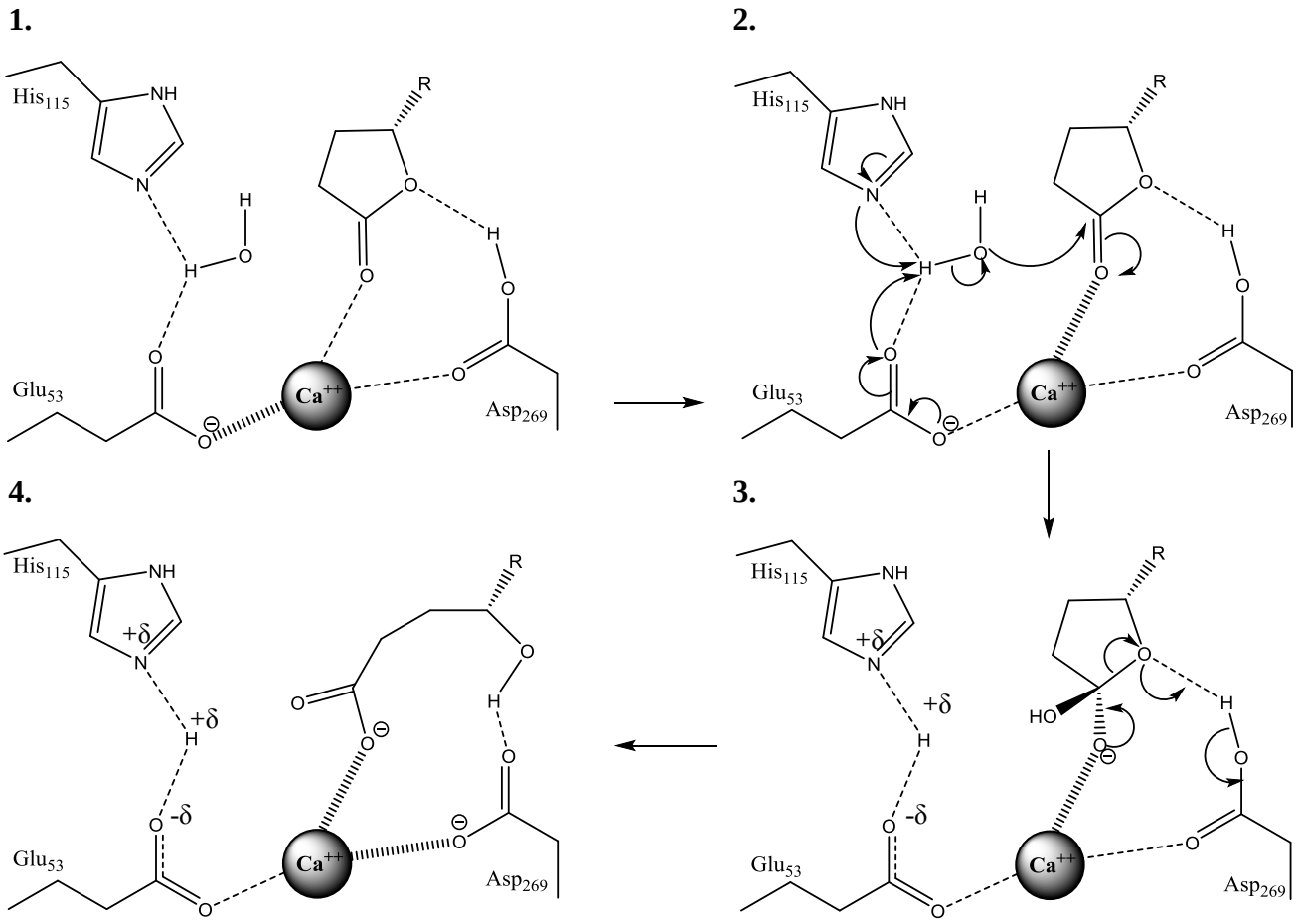

Figure I.21 : *Mécanisme d'hydrolyse des AHLs par les PONs*

Les résidus Glu 53 et Asp 269 coordonnent le Ca^{++} catalytique. L'Asp 269 permet de positionner la lactone qui interagit *via* sa fonction carbonyle avec le Ca^{++} et l'oxygène estérique avec l'Asp 269 (**1.**). Les résidus Glu 53 et His 115 positionnent et activent la molécule d'eau sous forme d'un ion hydroxyde lui permettant d'effectuer l'attaque nucléophile (**2.**) sur le carbone du carbonyle de la fonction lactone. L'intermédiaire de réaction alors formé est tétravalent dont l'oxyanion est stabilisé par l'ion Ca^{++} (**3.**). Enfin, c'est le rabattement de doublet qui entraîne la rupture de la liaison ester du cycle lactone (**4.**). Durant la catalyse, l'alcoolate naissant prend l'atome hydrogène de l'Asp 269 avec lequel il interagit tout au long de la catalyse.

lactonase (186). L'évolution *in vitro* de la PON permit néanmoins d'obtenir des variants optimisés envers les agents neurotoxiques OPs (88). Bien que principalement décrites pour leur implication dans les processus inflammatoires (187), elles sont désormais suspectées d'être les vestiges d'une immunité innée envers les bactéries utilisant les lactones comme moyen de communication.(186).

Le mécanisme catalytique lactonase proposé pour les PONs consiste en en attaque nucléophile SN_2 de la molécule d'eau catalytique. Celle-ci est positionnée et activée par les résidus de Glu 53 et d'His 115 (66) tandis que le cycle lactone est fixé par le carbonyle à l'atome de Ca^{2+} du site actif et l'oxygène estérique par l'Asp 269. Au cours de la réaction, il y a formation d'un intermédiaire de réaction tétravalent avec un oxyanion stabilisé par l'ion Ca^{2+}. Enfin, c'est le rabattement du doublet qui entraine la rupture de la liaison ester du cycle lactone par l'assistance de l'Asp 269 qui protone l'alcoolate naissant (66) (**Figure I.21**).

Les sandwichs αβ/βα

Parmi les enzymes possédant une topologie de type sandwichs αβ/βα, des enzymes optimisées envers les OPs furent précédemment décrites (*i.e* MPH, OPHC2). Cependant, c'est au sein de cette famille structurale que furent identifiées les AHL-lactonases dont le représentant le plus étudié est AiiA (**Figure I.22**) principalement isolée chez *Bacillus thuringiensis* (188), *Bacillus cereus*, *Bacillus anthracis* et *Bacillus mycoides*. Une nouvelles fois, la même famille structurale recèle aussi bien des lactonases optimisées que des phosphotriestérases optimisées.

Tout comme leur homologue phosphotriestérase, les lactonases de cette famille présentent un centre catalytique constitué de deux ions métalliques (Zn^{2+}) coordonné par 5 histidines et deux résidus d'aspartate (189) (**voir partie II. B. 2. c.**). Le mécanisme catalytique proposé pour les lactones débute par la fixation des atomes d'oxygène des groupements ester de la lactone sur le centre bimétallique. L'oxygène du carbonyle interagit alors avec la Tyr 194 (chez AiiA) alors que la chaine N-acyl se positionne dans le canal hydrophobe de l'enzyme. L'attaque est ensuite réalisée par la molécule d'eau pontant les deux métaux sur le carbone sp^2 du groupement carbonyle de la lactone. Il y a ainsi formation d'un état de transition tétraédrique qui permet l'ouverture du cycle lactone suite au rabattement du doublet et à la formation d'un carboxylate et d'un alcool. Il a été proposé que la molécule d'eau est activée par l'Asp 108 qui joue le rôle de base en arrachant un proton de la molécule d'eau puis comme acide en redonnant le proton au groupement alkoxyde (**Figure I.23**) (188, 190, 191). Chez la PLL *Sso*Pox, la Tyr 194 correspond à la Tyr 97, tandis que l'Asp 108 correspond à l'Asp 256 (185). Les études enzymatiques effectuées sur AiiA montrent que la fonction naturelle de cette enzyme est l'hydrolyse des Acyl Homoserine Lactones (AHLs), molécules médiatrices de la communication inter-bactérienne (**voir partie I. C. 3. c. et Figure I.19**).

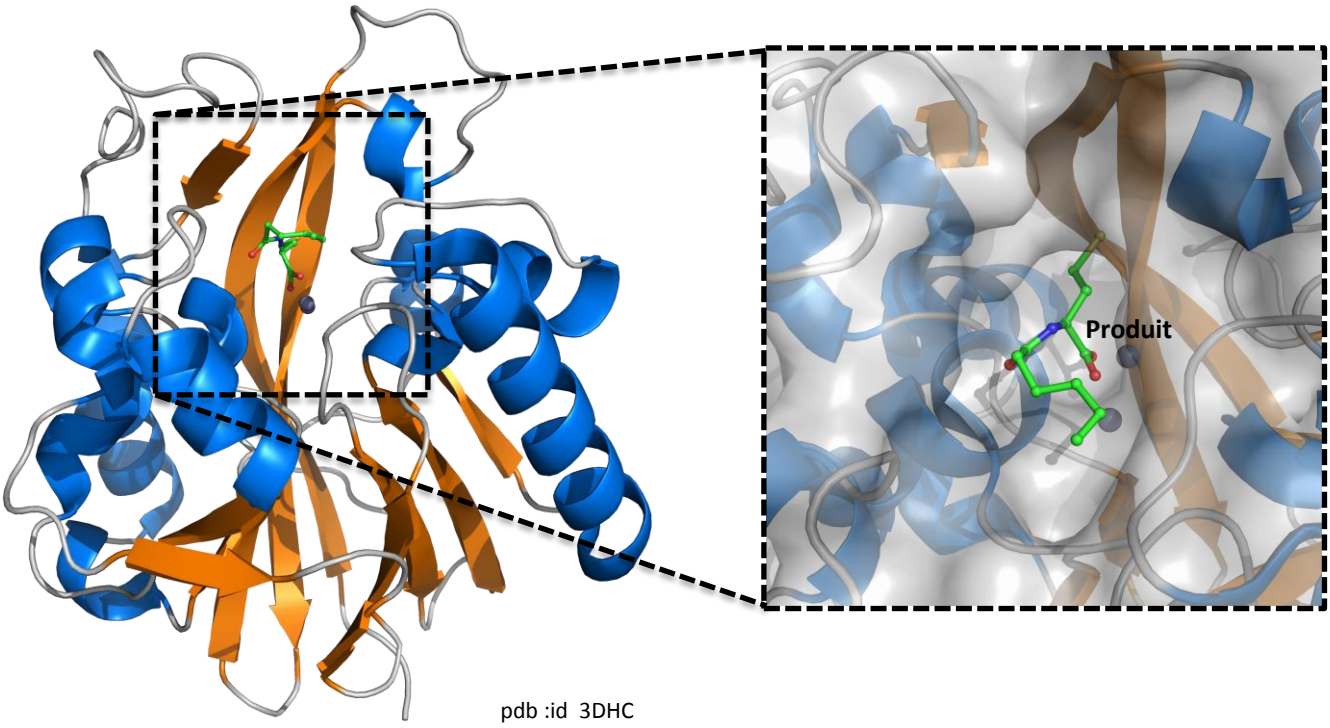

Figure I.22 : *AiiA une lactonase à toplogie αβ/βα*

La structure d'AiiA permit d'étudier le mécanisme d'hydrolyse lactonase. L'enzyme présente une topologie de type sandwich αβ/βα analogue aux β-lactamases. A droite est représentée une vue rapprochée de la poche du site actif de l'enzyme obtenue en complexe avec un produit d'hydrolyse d'AHL (pdb id : 3DHC)

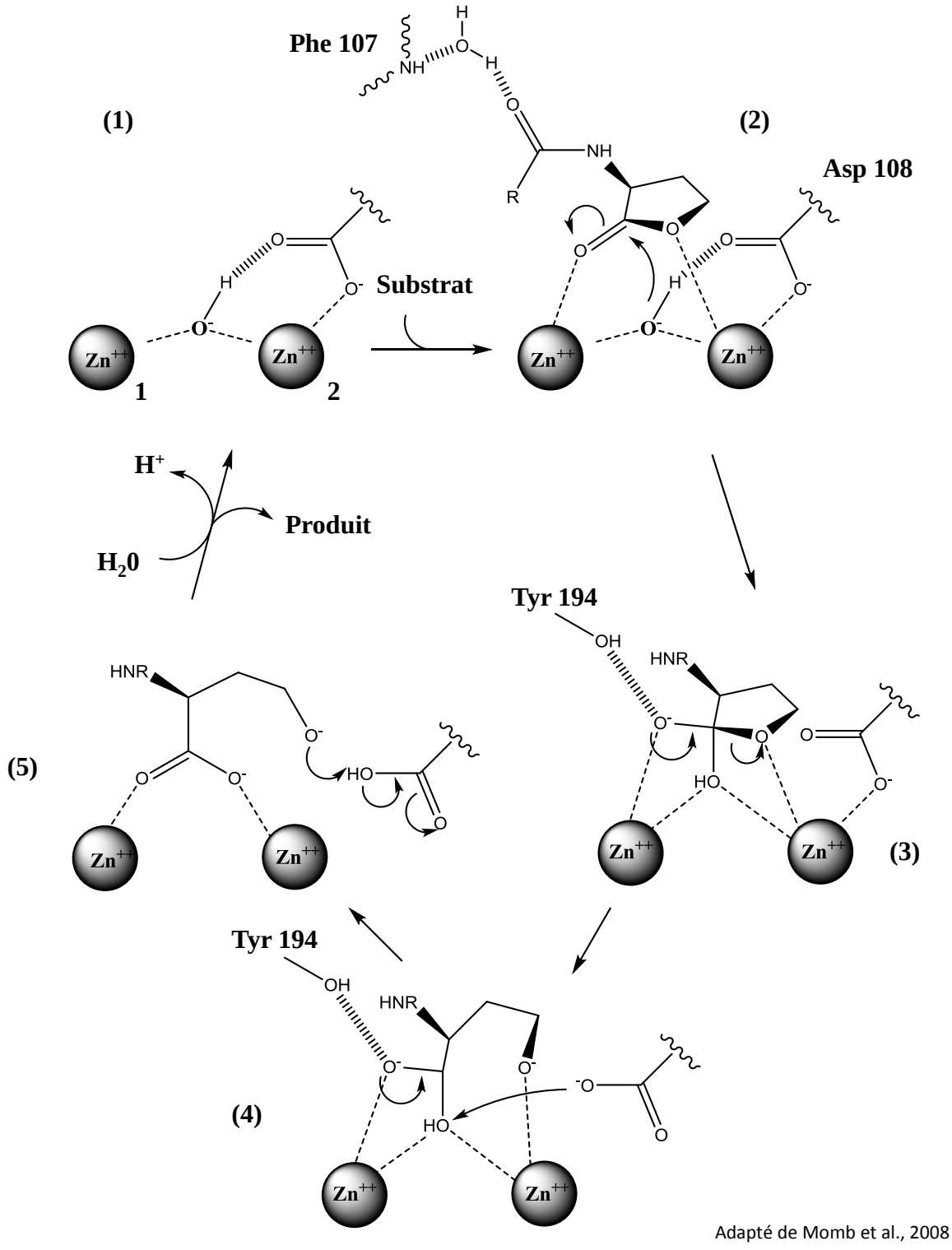

Figure I.23 : Mécanisme catalytique lactonase de *AiiA*

(1) Une molécule d'eau pontant les deux métaux est activée en ion hydroxyde et orientée par l'Asp 108. **(2)** Le substrat se fixe sur le centre bimétallique (oxygène du carbonyle avec le métal 1 (enfoui) et l'oxygène estérique avec le métal 2 (exposé)) et est accommodé grâce à la Tyr 194 et la chaine principale de la Phe 107. L'ion hydroxyde est positionné perpendiculairement au carbone du carbonyle de manière à réaliser l'attaque de type SN_2. **(3)** Il y a alors formation d'un état de transition tétravalent avec formation d'un oxyanion stabilisé par la Tyr 194. **(4)** Le rabattement du doublet entraine la rupture de la liaison ester du cycle lactone, générant un acide carboxylique et un alcoolate. **(5)** Le résidu d'Asp 108 déprotone la fonction carboxylique précédemment générée afin de transférer l'hydrogène à l'alcoolate assistant ainsi l'hydrolyse défavorable à pH physiologique.

Les PLLs

Les PLLs présentent une topologie similaire aux PTEs (*Bd*PTE et OpdA), en faisant ainsi un troisième exemple de couple phosphotriestérase optimisée et lactonase optimisée présentant le même type de repliement. Celles-ci, décrites précédemment (**voir partie I. B. 2. d.**), comprend deux groupes : les PLL-A (AhlA, QsdA, MCP, PPH) qui hydrolysent les AHL avec une efficacité élevée ($k_{cat}/K_M \sim 10^5$ $M^{-1}.s^{-1}$) et les PLL-B (GkL, GkaP, GsP, Dr-OPH) qui sont plus spécifiques des oxo-lactones (**voir Figure I.17 B**).

Le mécanisme d'hydrolyse des lactones est comparable à celui décrit pour la lactonase AiiA (190, 191). Chez *Sso*Pox, la chaine aliphatique des AHLs est accommodée au sein du canal hydrophobe de l'enzyme formé par la boucle 8, en particulier le Trp 263 positionnant le cycle lactone sur les métaux (**Figure I.24**). C'est le métal α qui accommode l'oxygène estérique du cycle lactone alors que l'oxygène du carbonyle est positionné sur le métal β. La catalyse est réalisée par la molécule d'eau activée sous forme d'hydroxyde pontant les deux métaux, qui est orientée par l'Aspartate 256. Le métal α, augmente le caractère électrophile du carbone estérique, rendant possible l'attaque par l'ion hydroxyde. Il y a alors formation d'un intermédiaire réactionnel de type tétravalent (sp3), alors qu'une charge négative se développe sur l'oxygène de la fonction cétone attaquée, charge qui est stabilisée par le métal β et la Tyrosine 97. Enfin, suite au rabattement de la charge négative, il y a formation d'une fonction acide carboxylique et d'un alcoolate (**Figure I.25**).

c. Fonction des lactonases

Certains organismes (bactéries, champignons, animaux) ont développé une stratégie dite de *quorum* quenching (QQ) visant à couper la communication bactérienne en éliminant la molécule messagère (192). C'est une stratégie naturellement employée par les bactéries entrant dans la compétition pour les ressources environnementales ou par les mêmes bactéries qui les produisent afin de réguler le signal et recycler ces molécules.

La perception du *quorum* aussi appelée *quorum* sensing (QS) désigne à la capacité de certaines bactéries à coordonner un comportement de groupe grâce à la perception de molécules de communication émises par les autres bactéries présentes dans son environnement (193). C'est un mode de communication leur permettant, en coordonnant leurs activités, de fonctionner comme des systèmes multicellulaires (193). Le QS permet aux bactéries de répondre aux *stimuli* environnementaux (*e.g*

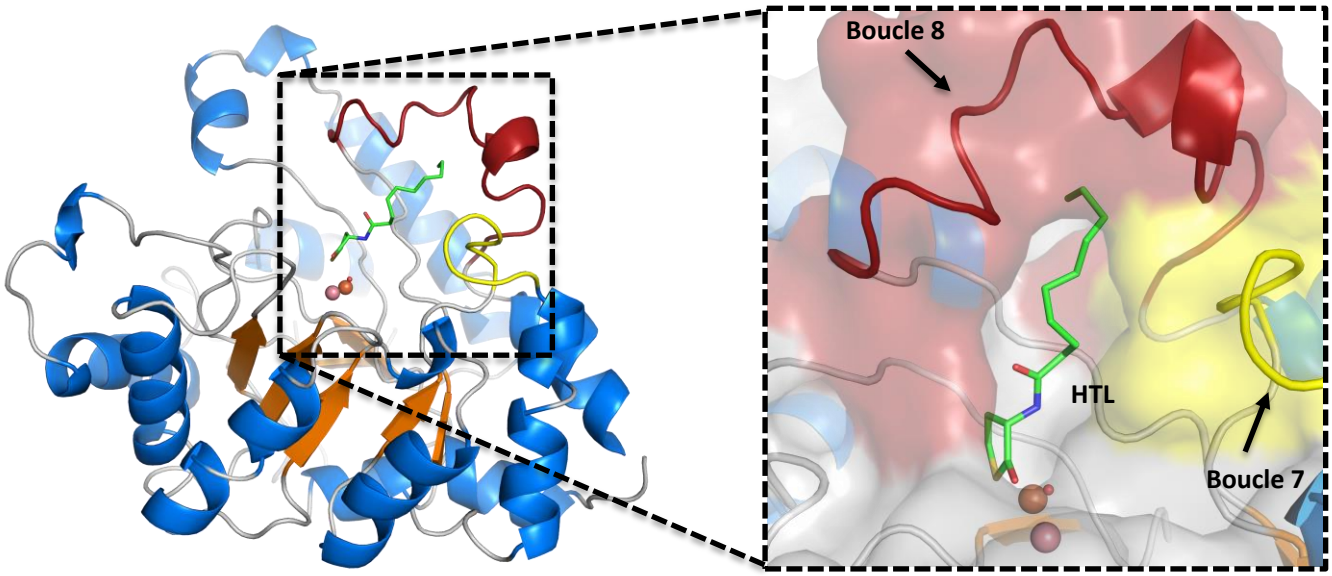

*Sso*Pox en complexe avec HTL (pdb id : 2VC7)

Figure I.24 : Sso*Pox comme exemple de PLL*

A – Représentation cartoon de la fixation d'un mime de lactone au sein de l'enzyme *Sso*Pox (pdb id 2vc7). Le cycle lactone se fixe sur les métaux alors que la chaine aliphatique emprunte le canal hydrophobe formé par les résidus des boucles 7 et 8.

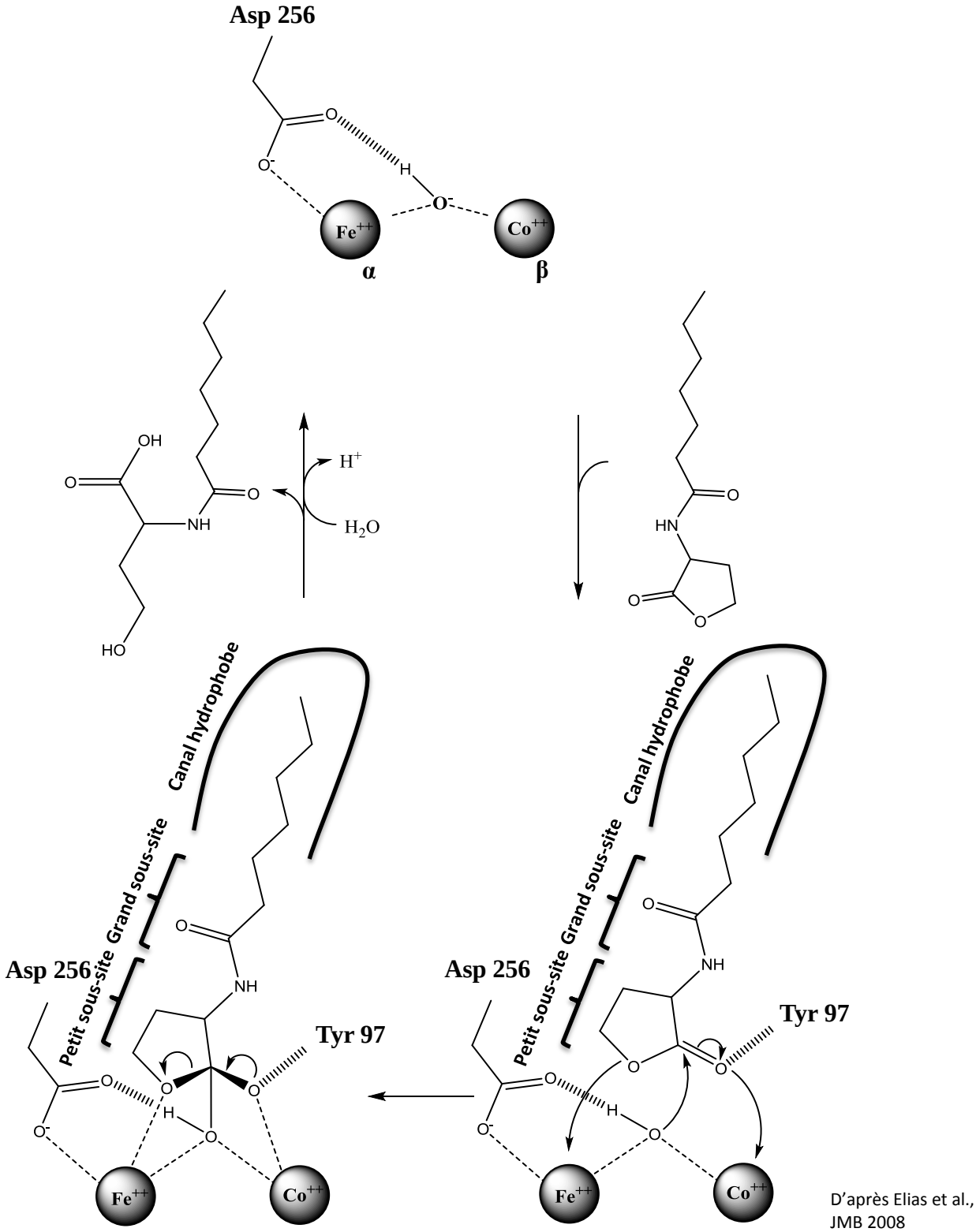

Figure I.25 : *Représentation schématique du mécanisme d'hydrolyse des lactones par la PLL* Sso*Pox*

La molécule d'eau catalytique est activée sous forme d'un ion hydroxyde. L'oxygène de la cétone du cycle lactone est accommodé par le métal β et la Tyr 97 tandis que l'oxygène estérique est accommodé par le métal α. La chaine aliphatique de la lactone se positionne dans le canal hydrophobe formé par les boucle 7 et 8. L'acte catalytique est réalisé par l'hydroxyde sur le carbone estérique, entrainant la formation d'un intermédiaire tétravalent. L'oxyanion formé est stabilisé par la Tyr 97 et le métal β. Enfin, le rabattement de la charge négative entraine la rupture du cycle de la lactone, formant ainsi un acide carboxylique et un alcoolate. L'arrivée d'une molécule d'eau permet de régénérer le site catalytique.

établissement de la virulence) (194-196). Parmi les nombreux systèmes découverts chez les bactéries, on distingue 3 principaux systèmes de communication caractérisés. Ces principaux systèmes sont basés sur des molécules chimiquement différentes, on distingue ainsi :

- le QS à base d'N-acyl homoserine lactones (AHL), utilisé par les bactéries gram négative, spécifique d'espèce/souche
- le QS à base de diesters de furanosyl borate (AI-2), système de communication universel partagé à la fois par les bactéries gram positive et les grams négatifs,
- et le QS à base de peptides (AIP), utilisé par les bactéries à gram positive, spécificité d'espèces/souche.

Les molécules médiatrices sont excrétées et s'accumulent dans le milieu extracellulaire jusqu'à atteindre une concentration seuil (le *quorum*, de l'ordre du pM au µM). Lorsque le *quorum* est atteint, la fixation de ces molécules sur des récepteurs spécifiques va engendrer une cascade de signalisation influant sur l'état transcriptionnel de nombreux gènes de la bactérie (*e.g* de virulence de la bactérie) (194). Les lactonases hydrolysent le cycle lactone, ouvrant ainsi le cycle, la molécule n'étant alors plus reconnue par le récepteur. Ainsi, les organismes exprimant des AHL-lactonases vont présenter un avantage sélectif sur les autres bactéries de leur environnement puisqu'elles seront capables de perturber les signaux perçus par celles-ci ou les signaux ennemis qu'elles vont percevoir.

II. Projets de recherche :

Historiquement, le projet fut initié par le Pr. Eric Chabrière dès son service militaire sous la direction du Pharmacien-Général Patrick Masson au Centre de Recherche du Service de Santé des Armées (C.R.S.S.A, Grenoble) où il fut chargé de l'étude structurale de hPON1. Au cours de ce projet fut découverte la Human Phosphate Binding Protein (HPBP) (82) qui devint plus tard une thématique importante du groupe (**voir articles annexes VII. C. à VII. H.**). Le projet fut poursuivi lorsque plus tard, le Pr. Eric Chabrière obtint un poste de Maître de conférences à l'Université Henry Pointcaré (Nancy) dans le laboratoire du Pr. Claude Lecomte (CRM2, Nancy). Il continua de travailler sur les deux thématiques, puis fut contacté par le Gal. Masson et G. Manco qui lui proposa de participer à la résolution de la structure d'une enzyme issue de l'archaea extrémophile *Sulfolobus solfataricus*, apparentée aux PTEs et capable de dégrader certains OPs : la *Sso*Pox. En effet, les enzymes originaires d'organismes extrêmophiles présentent des propriétés biologiques exceptionnelles (*i.e* résistance à la dénaturation) leur conférant un intérêt bio-technologique majeur gage de leur maniabilité industrielle.

La thématique pris de l'ampleur lorsque l'équipe d'Eric Chabrière fut transférée au laboratoire d'Architecture et Fonctions des Macromolécules Biologiques (AFMB) où il obtint un poste de Professeur à l'Université de la Méditerranée. Il confia cette thématique à son doctorant de l'époque, Mikael Elias, qui avait résolu la structure de *Sso*Pox (163). Du fait de la grande similarité structurale entre *Sso*Pox et la *Bd*PTE, le Pr. Chabrière et Mikael Elias eurent l'idée de développer une base de données de mutations en vue d'améliorer l'activité phosphotriestérase de *Sso*Pox. Cette première base de données, basée sur le concept de transfert de site actif de la *Bd*PTE (optimisé pour l'activité OP hydrolase), dans l'architecture hyperthermostable de *Sso*Pox, fut l'objet d'un brevet (n° 07/0304 ; PCT/FR2008/000596).

Une base de données de 14 mutations établie par Mikael Elias, permis d'obtenir une chimère de *Sso*Pox mimant le site actif de la *Bd*PTE. Néanmoins, cette chimère était très active mais s'agrégeait assez rapidement. Il devint ainsi évident qu'une combinaison de ces 14 mutations devait être obtenue afin de converger plus rapidement vers un produit biotechnologique d'intérêt. Alors, de nouveaux protocoles d'évolution permettant le brassage aléatoire de ces 14 mutations et leur criblage devaient être établis.

Ainsi, ma thèse s'inscrivit dans ce contexte scientifique et eu pour objectif d'identifier et de caractériser de nouvelles enzymes hydrolysant les OPs ainsi que les différents mutants obtenus au cours des protocoles d'évolution afin de rationaliser par la structure l'ingénierie rapide de l'enzyme. J'ai donc commencé par chercher dans les bases de données génomiques des enzymes présentant des intérêts

biotechnologiques potentiels et pouvant apporter des informations structurales susceptibles d'optimiser et soutenir l'amélioration.

J'ai alors identifié par alignements de séquences un gène homologue à *Sso*Pox, présent chez plusieurs souches de *S. islandicus*. *S. islandicus* étant également une archaea extrémophile, le gène identifié avec plus de 91 % d'identité de séquence présentait un intérêt en vue de l'amélioration des connaissances sur les PLLs, l'ingénierie de *Sso*Pox et leurs applications en biotechnologie. Bien que très similaire à *Sso*Pox l'enzyme présentait potentiellement des différences dans les ponts salins de surface, pouvant influer sur la thermophilicité de l'enzyme. Après m'être confronté un à un problème de macle (article présenté en **III. A.**) la structure de l'enzyme fut finalement obtenue à 2.7 Å de résolution. Le modèle obtenu permis de mettre en évidence les éléments structuraux présents chez *Sis*Lac et contribuant aux différences biochimiques et enzymatiques observées avec *Sso*Pox (articlé présenté en **III. B.**).

Je me suis également intéressé à un membre de la famille des OP hydrolases à repliement de type sandwich αβ/βα. Cette enzyme, nommée OPHC2, présentait un intérêt biotechnologique potentiel du fait de son optimum d'activité à 65 °C et de sa forte similarité de séquence avec MPH. Néanmoins, très peu de travaux avaient été effectués sur cette enzyme. Nous avons alors résolu sa structure cristallographique (article présenté en **III. C.**) et réalisé une étude des relations structure-fonction d'OPHC2 (article présenté en **III. D.**).

En parallèle j'ai également poursuivis les travaux initiés par le Dr. Mikael Elias sur la résolution de la structure de la protéine *Sso*Pox en complexe avec un insecticide inhibiteur (le fensulfothion). Des cristaux et un jeu de données avaient été collectés par Mikael Elias au cours de sa thèse. Celui-ci a pu être phasé et la structure résolue, montrant pour la première fois une structure d'une PLL complexée avec le substrat de promiscuité phosphotriester. De façon étonnante, le fensulfothion est fixé dans le site actif de l'enzyme de telle manière que le groupement sulfinyl mime la fixation des lactones. Au cours de l'étude, nous avons également caractérisé les activités de *Sso*Pox envers divers OPs à 25 °C et montré que l'enzyme possède une activité à température ambiante envers les OPs. Enfin, il fut montré que *Sso*Pox est non seulement active en présence de détergents mais également qu'à faible concentration, ceux-ci permettent même de stimuler les activités (article présenté en **III. E.**).

Enfin, le travail d'amélioration de *Sso*Pox fut débuté en réalisant une mutagénèse à saturation sur la position Trp 263 (article présenté en **III. F.**), une position que nous avons identifié (article présenté en **III. E.**) comme étant clé dans l'accommodation des substrats. Au cours de ce travail, l'efficacité catalytique de l'enzyme fut améliorée envers les OPs et envers les AHLs du *quorum* sensing. La résolution des structures des différents mutants sélectionnés permis de mieux comprendre l'origine des améliorations.

Enfin, en perspective seront brièvement présenté les résultats préliminaires d'amélioration ainsi que certaines explications structurales du premier cycle d'évolution rationalisée par la structure (**voir partie perspectives IV. A.**).

A. Cristallisation et collectes de données de *Sis*Lac

Crystallization and preliminary X-ray diffraction analysis of the hyperthermophilic *Sulfolobus islandicus* lactonase

Gotthard Guillaume, Hiblot Julien, Elias Mikael, Chabrière Eric

Dans les travaux décrits, j'ai réalisé :

- partie expérimentale : expression de la protéine, purification de l'enzyme, cristallisation, collecte des données, traitement des données, résolution du macle et phasage
- rédaction de l'article

Résumé : Ce travail concerne la mise au point de conditions expérimentales permettant l'expression et la purification de *Sis*Lac. Il décrit en particulier les travaux de cristallisation de l'enzyme qui ont nécessité l'identification de nouvelles conditions de cristallisation. Il est également rapporté les conditions de diffraction (cryoprotectant) et la qualité du jeu de données obtenu. Enfin, ce travail traite également de l'identification et la résolution d'un problème courant en cristallographie des protéines, la présence d'une macle. Ce travail intervient en amont de la caractérisation biochimique, enzymatique et structurale de la protéine *Sis*Lac présentée dans la partie **III. B.**

Acta Crystallographica Section F
Structural Biology and Crystallization Communications
ISSN 1744-3091

Crystallization and preliminary X-ray diffraction analysis of the hyperthermophilic *Sulfolobus islandicus* lactonase

Guillaume Gotthard,[a] Julien Hiblot,[a] Mikael Elias[b] and Eric Chabrière[a]*

[a]Architecture et Fonction des Macromolécules Biologiques, CNRS–Aix Marseille Université, 13288 Marseille, France, and [b]Department of Biological Chemistry, Weizmann Institute of Science, Rehovot, Israel

Correspondence e-mail: eric.chabriere@afmb.univ-mrs.fr

Received 9 November 2010
Accepted 22 December 2010

Phosphotriesterase-like lactonases (PLLs) constitute an interesting family of enzymes that are of paramount interest in biotechnology with respect to their catalytic functions. As natural lactonases, they may act against pathogens such as *Pseudomonas aeruginosa* by shutting down their quorum-sensing system (quorum quenching) and thus decreasing pathogen virulence. Owing to their promiscuous phosphotriesterase activity, which can inactivate toxic organophosphorus compounds such as pesticides and nerve agents, they are equally appealing as potent bioscavengers. A new representative of the PLL family has been identified (*Sis*Pox) and its gene was cloned from the hyperthermophilic archeon *Sulfolobus islandicus*. Owing to its hyperthermostable architecture, *Sis*Pox appears to be a good candidate for engineering studies. Here, production, purification, crystallization conditions and data collection to 2.34 Å resolution are reported for this lactonase from the hyperthermophilic *S. islandicus*.

1. Introduction

*Sis*Pox is an enzyme from the archaeal organism *Sulfolobus islandicus*, which is found in extreme environments such as Yellowstone National Park in the USA and the Mutnovsky volcano in Kamchatka, Russia (Reno *et al.*, 2009). *Sis*Pox belongs to the phosphotriesterase-like lactonase (PLL) family of proteins (Afriat *et al.*, 2006) and displays 91% sequence identity to *Sso*Pox isolated from *Sulfolobus solfataricus* (Merone *et al.*, 2005). The PLL family contains several representatives, which include *Dr*OPH from *Deinoccocus radiodurans* (Hawwa, Larsen *et al.*, 2009), Gsp from *Geobacillus stearothermophilus* (Hawwa, Aikens *et al.*, 2009) and *Sso*Pox from *S. solfataricus* (Merone *et al.*, 2005). These proteins are natural quorum-quenching lactonases that exhibit promiscuous phosphotriesterase acitivity. This promiscuous activity might be a consequence of the divergence of PLLs from optimized phosphotriesterases (PTEs) (Afriat *et al.*, 2006) such as the PTE from *Pseudomonas diminuta* or OpdA found in *Agrobacterium radiobacter*.

All PLLs exhibit lactonase and phosphotriesterase activities, but to different extents. PLLs are natural lactonases that possess promiscuous weak phosphotriesterase activity (Afriat *et al.*, 2006). In contrast, the PTE from *P. diminuta* exhibits a phosphotriesterase activity towards the pesticide paraoxon which reaches the diffusion-limited rate of the substrate in water ($k_{cat}/K_M = 10^8\ M^{-1}\ s^{-1}$) (Omburo *et al.*, 1992) and possesses some lactonase activity (Draganov, 2010). Structural insights into this family of proteins are of great interest in order to understand the origin of the differences in substrate specificity that are observed between these two families.

The amidohydrolase superfamily (Seibert & Raushel, 2005) that encompasses PLLs and PTEs exhibits a classical $(\alpha/\beta)_8$-barrel fold with two divalent metal cations in the active site, which is located at the C-terminus of the barrel. The catalytic mechanism involves a nucleophilic attack by a water molecule activated as a hydroxide ion by the bimetallic centre (Elias *et al.*, 2008). The hydrolysis of phosphotriester substrates is performed *via* a pentacoordinate transition

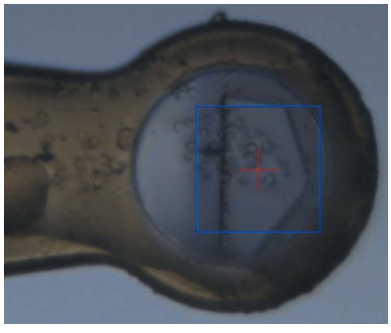

state (Elias *et al.*, 2008). The PLL active site presents three subsites that are remarkably well adapted for lactone binding: a small subsite, a large subsite and a hydrophobic channel (Elias *et al.*, 2008; Del Vecchio *et al.*, 2009). The aliphatic chain of the lactones binds within the hydrophobic channel, the large subsite adapts the carbonyl group of the chain and the small subsite positions the lactone ring. During catalysis, the bridging hydroxide ion attacks the carbonyl carbon of the lactone ring, forming a tetrahedral transition state. The ability of PLLs, including *Sis*Pox, to hydrolyze lactones, and especially acyl-homoserine lactones (AHLs), is interesting. Indeed, several pathogens use AHLs to communicate and to coordinate the transcription of some genes (Popat *et al.*, 2008). This communication behaviour is known as a quorum-sensing system (QS). The perturbation of bacterial communication using lactonases, a process that is known as quorum quenching (QQ), is seen as a potent antibiotic strategy (Reimmann *et al.*, 2002). Moreover, the presence of QQ lactonases in archaea raises the question of the utilization of QS by these organisms (Elias *et al.*, 2008). Another hypothesis would involve the advantage provided by such a QQ enzyme in controlling the QS of concurrent organisms in the natural biotope.

*Sis*Pox, like *Sso*Pox, also exhibits phosphotriesterase activity (unpublished data). Such enzymes are able to hydrolyze neurotoxic organophosphate (OP) pesticides, as well as OP nerve agents such as sarin, soman and VX (Raushel, 2002). Current methods for removal of these compounds, which include bleach treatment and incineration, are slow, expensive and harmful to the environment. Therefore, enzymes that are able to hydrolyze these compounds are appealing (LeJeune *et al.*, 1998). Because of their intrinsic thermal stability, enzymes such as *Sis*Pox represent interesting candidates for the engineering of an OP bioscavenger (Demirjian *et al.*, 2001).

In this report, we describe the purification, crystallization, data collection and preliminary X-ray diffraction analysis of *Sis*Pox, a new member of the PLL family.

2. Expression and purification

The *sispox* gene was synthesized with an N-terminal linker containing a Strep-tag and a TEV cleavage site (GeneArt, Germany). The construct was subcloned in the plasmid pET22b (Novagen). The protein was produced in *Escherichia coli* Rosetta (DE3) pLysS strain (Invitrogen).

Protein production was performed in 8 l ZYP medium (Studier, 2005) (100 µg ml^{-1} ampicillin, 34 µg ml^{-1} chloramphenicol) inoculated with an overnight pre-culture at a 1:20 ratio. Cultures were grown at 310 K until they reached an $OD_{600\,nm}$ of 1.5. Induction of the protein took place on consumption of the lactose in the ZYP medium with the addition of 0.2 m*M* $CoCl_2$ and a temperature transition to 298 K for 20 h. Cells were harvested by centrifugation (3000*g*, 277 K, 10 min), resuspended in lysis buffer (50 m*M* HEPES pH 8, 150 m*M* NaCl, 0.2 m*M* $CoCl_2$, 0.25 mg ml^{-1} lysozyme, 10 µg ml^{-1} DNAse, 20 m*M* $MgSO_4$ and 0.1 m*M* PMSF) and stored at 193 K overnight. Suspended frozen cells were thawed at 310 K for 15 min and disrupted by three 30 s sonication steps (Branson Sonifier 450; 80% intensity and microtip limit of 8). Cell debris was removed by centrifugation (12 000*g*, 277 K, 30 min).

The crude extracts clarified by centrifugation were charged onto a StrepTrap HP chromatography column (GE Healthcare). The bound proteins on the column were eluted by competition with elution buffer (50 m*M* HEPES pH 8, 150 m*M* NaCl, 0.2 m*M*$CoCl_2$, 4 m*M* desthiobiotin). The eluted protein was cleaved by TEV protease (van den Berg *et al.*, 2006) at a 1:20(*w*:*w*) ratio during overnight incubation at 303 K. Precipitated TEV protease was harvested by centrifugation (12 000*g*, 277 K, 30 min). The sample was reloaded onto a StrepTrap chromatography column (GE Healthcare) and cleaved *Sis*Pox was obtained in the flowthrough fraction. The protein obtained was subsequently loaded onto a size-exclusion chromatography column (Superdex 75 16/60, GE Healthcare) and fractions containing pure protein were pooled. About 5 mg protein was obtained from 8 l culture medium. The purity of the protein was checked by 15% SDS–PAGE separation under reducing conditions at 250 V for 40 min. The gel was stained using the Coomassie Blue method (0.3% Coomassie Blue, 0.2 *M* citric acid) and destained in water.

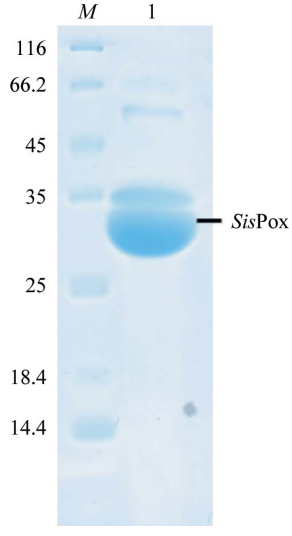

Figure 1
15% SDS–PAGE of the *Sis*Pox protein. Lane *M*, molecular-weight markers (Euromedex 06U-0511; labelled in kDa). Lane 2, 8 µl *Sis*Pox protein at 5 mg ml^{-1}.

3. Crystallization

*Sis*Pox was concentrated to 5.44 mg ml^{-1} using a centrifugation device (Amicon Ultra centrifugal units with 10 kDa cutoff; Millipore, Carrigtwohill, County Cork, Ireland) and its purity was checked on SDS–PAGE (Fig. 1). Crystallization was performed using a sitting-drop vapour-diffusion setup in 96-well plates at 293 K. The best hit was obtained using the commercial screens Wizard I and II (Emerald BioSystems) in a condition consisting of 2 *M* ammonium sulfate,

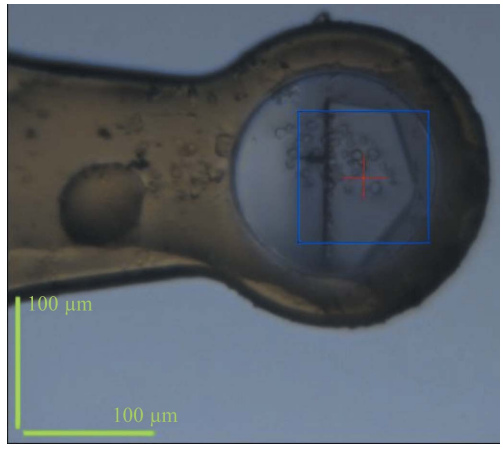

Figure 2
A crystal of the *Sis*Pox protein mounted in a MiTeGen MicroLoop.

0.1 *M* Tris pH 7.0 and 0.2 *M* lithium sulfate. A single crystal appeared after one month at 293 K in a drop containing a 3:1 protein:reservoir ratio (Fig. 2).

4. Data collection

A cryoprotectant solution consisting of the crystallization solution supplemented with 20%(*v*/*v*) glycerol was added to the drop in order to exchange the solution containing the crystal. The crystal was mounted on a MicroLoop (MiTeGen) and flash-frozen in liquid nitrogen at 100 K. X-ray diffraction intensities were collected on the ID14-EH1 beamline at the ESRF (Grenoble, France) using a wavelength of 0.933 Å and an ADSC Quantum Q210 detector with 12 s exposures. Diffraction data were collected from 92 images using the oscillation method; individual frames consisted of 1.0° oscillation steps over a range of 92° (Fig. 3).

5. Results and conclusions

X-ray diffraction data were integrated, scaled and merged using the *XDS* program (Kabsch, 2010) and the *CCP*4 program suite (Collaborative Computational Project, Number 4, 1994). The best result with the highest symmetry suggested that the *Sis*Pox crystal belonged to the hexagonal space group $P6_222$, with unit-cell parameters $a = 47.8$, $b = 47.8$, $c = 239.5$ Å (quality of fit = 6.0). The $R_{\rm merge}$ of 7.1% and the multiplicity of 9.16 confirmed that symmetry operators were present: a sixfold axis (z) and two twofold axes (x, y). Nevertheless, the Matthews coefficient ($V_{\rm M}$; Matthews, 1968) calculated for a monomer of *Sis*Pox (35.6 kDa) corresponded to a very low value of 1.11 Å^3 Da^{-1} with an impossible solvent content of −11.2% (calculated with http://csb.wfu.edu/tools/vmcalc/vm.html). Data quality was assessed using *phenix.xtriage* (Zwart *et al.*, 2005) from the *PHENIX* refinement-program suite (Adams *et al.*, 2002). An *L* test was performed on the data and the results (Fig. 4) suggested possible merohedral twinning. Although a molecular-replacement solution was unlikely in this space group, it was tested with *Phaser* (McCoy *et al.*, 2007) using the structure of *Sso*Pox as a model (PDB code 2vc5; Elias *et al.*, 2007). Robust solutions for the rotation and translation functions (RFZ = 9.5 and TFZ = 12.4) were found, but the solution was rejected owing to the large number of clashes (143). All of these results suggested supplementary symmetry arising from twinning.

The data were reprocessed in $P3_221$ using *XDS* (Table 1). This space group contains fewer asymmetric units in the unit cell and was of the highest symmetry that retains coherency in term of $V_{\rm M}$. The $V_{\rm M}$ and solvent content were calculated and gave more typical values (2.21 Å^3 Da^{-1} and 44.4%, respectively, with one molecule in the asymmetric unit). A *phenix.xtriage* analysis estimated the twin fraction to be 0.487 (*H* test). A twofold axis (z) arising from the twinning and the twin law ($-h$, $-k$, l) were proposed. The twin operator explained how $P3_221$ could be confused with $P6_222$.

Molecular replacement was performed with *Phaser* using the *Sso*Pox structure as a model (PDB code 2vc5). One robust solution was found with one molecule in the asymmetric unit (RFZ = 6.2 and TFZ = 12.7). The electron-density map was calculated with model phases obtained from molecular replacement, but the best solution

Table 1
Diffraction data collected on the ID14-EH1 beamline at the ESRF, Grenoble, France.

Values in parentheses are for the highest resolution shell.

Wavelength (Å)	0.9334	
Detector	ADSC Quantum Q210	
Crystal-to-detector distance (mm)	262.50	
No. of crystals	1	
Temperature (K)	100	
Exposure per frame (s)	12	
Oscillation (°)	1	
Total rotation range (°)	92	
Resolution (Å)	79.71–2.34 (2.50–2.34)	
Space group	$P3_221$	$P6_222$
Unit-cell parameters (Å, °)	a = 47.8, b = 47.8, c = 239.5, α = 90.0, β = 90.0, γ = 120.0	a = 47.8, b = 47.8, c = 239.5, α = 90.0, β = 90.0, γ = 120.0
No. of observed reflections	69183 (8477)	69274 (8494)
No. of unique reflections	14077 (2381)	7560 (1287)
Completeness (%)	98.6 (95.1)	99.6 (98.3)
$R_{\rm merge}$† (%)	9.4 (60.9)	7.1 (48.4)
$R_{\rm meas}$‡ (%)	5.8 (47.2)	6.0 (48.1)
$\langle I/\sigma(I)\rangle$	20.13 (2.56)	26.44 (3.42)
Multiplicity	4.91 (3.56)	9.16 (6.60)
Mosaicity (°)	0.134	0.134

† $R_{\rm merge} = \sum_{hkl}\sum_i |I_i(hkl) - \langle I(hkl)\rangle| / \sum_{hkl}\sum_i I_i(hkl)$. ‡ $R_{\rm meas} = \sum_{hkl}[N/(N-1)]^{1/2} \times \sum_i |I_i(hkl) - \langle I(hkl)\rangle| / \sum_{hkl}\sum_i I_i(hkl)$.

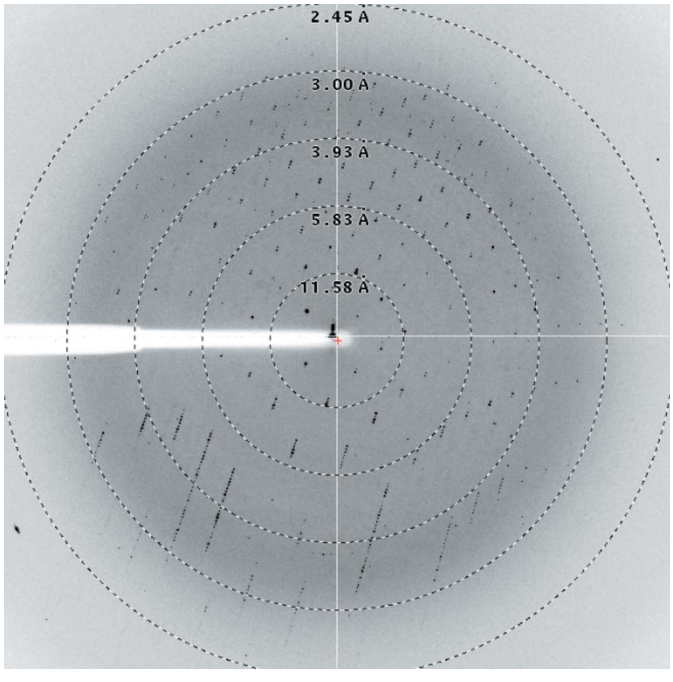

Figure 3
A diffraction pattern from a crystal of *Sis*Pox. The edge of the frame is at 2.5 Å resolution.

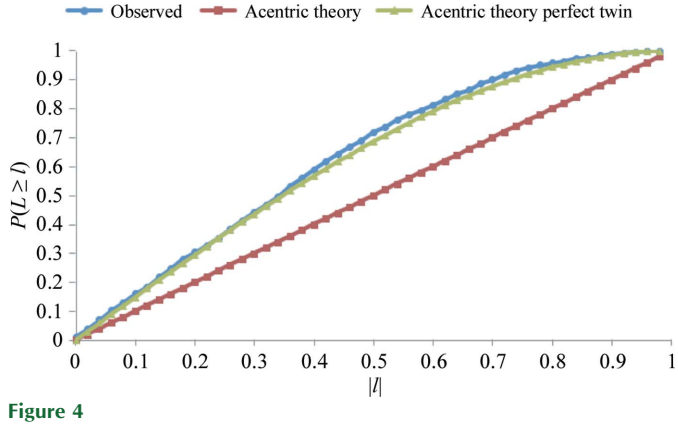

Figure 4
The *L* test indicates that the intensity statistics are significantly different from those that would be expected for good to reasonable untwinned data.

was not certain because of the twinning (R factor of 55% after molecular replacement). The two metal cations (iron and cobalt) in the active site were then removed from the model and the maps were recalculated. Two strong peaks (5.7σ and 8σ, respectively) corresponding to the two metal cations were clearly visible in the $F_{obs} - F_{calc}$ map, showing that the molecular-replacement solution was correct. Use of the twin option in *REFMAC*5 (Vagin *et al.*, 2004) allowed us to obtain untwinned maps that were of sufficient quality for model building. Manual model improvement was performed using *Coot* (Emsley & Cowtan, 2004). Refinement of the structure of *Sis*Pox at 2.34 Å resolution and its interpretation are in progress.

This research was supported by grants to EC from the Délégation Générale pour l'Armement (DGA) (REI#09C7002) and from CNRS. GG is a doctoral fellow supported by the DGA. ME is a fellow supported by the IEF Marie Curie program (grant No. 252836). We thank Dr Alain Dautant for fruitful discussions about twinning.

References

Adams, P. D., Grosse-Kunstleve, R. W., Hung, L.-W., Ioerger, T. R., McCoy, A. J., Moriarty, N. W., Read, R. J., Sacchettini, J. C., Sauter, N. K. & Terwilliger, T. C. (2002). *Acta Cryst.* D**58**, 1948–1954.
Afriat, L., Roodveldt, C., Manco, G. & Tawfik, D. S. (2006). *Biochemistry*, **45**, 13677–13686.
Berg, S. van den, Löfdahl, P. A., Härd, T. & Berglund, H. (2006). *J. Biotechnol.* **121**, 291–298.
Collaborative Computational Project, Number 4 (1994). *Acta Cryst.* D**50**, 760–763.
Del Vecchio, P., Elias, M., Merone, L., Graziano, G., Dupuy, J., Mandrich, L., Carullo, P., Fournier, B., Rochu, D., Rossi, M., Masson, P., Chabriere, E. & Manco, G. (2009). *Extremophiles*, **13**, 461–470.
Demirjian, D. C., Morís-Varas, F. & Cassidy, C. S. (2001). *Curr. Opin. Chem. Biol.* **5**, 144–151.
Draganov, D. I. (2010). *Chem. Biol. Interact.* **187**, 370–372.
Elias, M., Dupuy, J., Merone, L., Lecomte, C., Rossi, M., Masson, P., Manco, G. & Chabriere, E. (2007). *Acta Cryst.* F**63**, 553–555.
Elias, M., Dupuy, J., Merone, L., Mandrich, L., Porzio, E., Moniot, S., Rochu, D., Lecomte, C., Rossi, M., Masson, P., Manco, G. & Chabrière, E. (2008). *J. Mol. Biol.* **379**, 1017–1028.
Emsley, P. & Cowtan, K. (2004). *Acta Cryst.* D**60**, 2126–2132.
Hawwa, R., Aikens, J., Turner, R. J., Santarsiero, B. D. & Mesecar, A. D. (2009). *Arch. Biochem. Biophys.* **488**, 109–120.
Hawwa, R., Larsen, S. D., Ratia, K. & Mesecar, A. D. (2009). *J. Mol. Biol.* **393**, 36–57.
Kabsch, W. (2010). *Acta Cryst.* D**66**, 125–132.
LeJeune, K. E., Wild, J. R. & Russell, A. J. (1998). *Nature (London)*, **395**, 27–28.
McCoy, A. J., Grosse-Kunstleve, R. W., Adams, P. D., Winn, M. D., Storoni, L. C. & Read, R. J. (2007). *J. Appl. Cryst.* **40**, 658–674.
Matthews, B. W. (1968). *J. Mol. Biol.* **33**, 491–497.
Merone, L., Mandrich, L., Rossi, M. & Manco, G. (2005). *Extremophiles*, **9**, 297–305.
Omburo, G. A., Kuo, J. M., Mullins, L. S. & Raushel, F. M. (1992). *J. Biol. Chem.* **267**, 13278–13283.
Popat, R., Crusz, S. A. & Diggle, S. P. (2008). *Br. Med. Bull.* **87**, 63–75.
Raushel, F. M. (2002). *Curr. Opin. Microbiol.* **5**, 288–295.
Reimmann, C., Ginet, N., Michel, L., Keel, C., Michaux, P., Krishnapillai, V., Zala, M., Heurlier, K., Triandafillu, K., Harms, H., Défago, G. & Haas, D. (2002). *Microbiology*, **148**, 923–932.
Reno, M. L., Held, N. L., Fields, C. J., Burke, P. V. & Whitaker, R. J. (2009). *Proc. Natl Acad. Sci. USA*, **106**, 8605–8610.
Seibert, C. M. & Raushel, F. M. (2005). *Biochemistry*, **44**, 6383–6391.
Studier, F. W. (2005). *Protein Expr. Purif.* **41**, 207–234.
Vagin, A. A., Steiner, R. A., Lebedev, A. A., Potterton, L., McNicholas, S., Long, F. & Murshudov, G. N. (2004). *Acta Cryst.* D**60**, 2184–2195.
Zwart, P. H., Grosse-Kunstleve, R. W. & Adams, P. D. (2005). *CCP4 Newsl.* **43**, contribution 7.

B. Etude biochimique, enzymatique et structurale de *Sis*Lac

Structural and enzymatic characterization of the lactonase *Sis*Lac from *Sulfolobus islandicus*

*Gotthard Guillaume**, Hiblot Julien*, Eric Chabrière, Mikael Elias*

* Contribution égale

Dans les travaux décrits, j'ai réalisé :

- partie expérimentale : expression et purification des protéines, caractérisations biochimiques (diffusion de lumière dynamique et réfractométrie, gel filtration, dichroïsme circulaire)
- analyses des données, analyses bioinformatiques (alignements, analyses structurales) et affinement de la structure
- écriture de parties de l'article, dépôt de la structure sur la PDB (code pdb : 4G2D)

Résumé : Ce travail concerne l'étude structurale, enzymatique et biochimique de *Sis*Lac, une protéine homologue à *Sso*Pox, issue de *S. islandicus*. *Sis*Lac est une PLLs-A, qui partage 91 % d'identité de séquence avec *Sso*Pox. De manière analogue à *Sso*Pox, *Sis*Lac présente des activités équivalentes envers les lactones (AHL et oxo-lactones $k_{cat}/K_M \sim 10^{5\text{-}6}$ $M^{-1}.s^{-1}$) ainsi que des activités de promiscuité phosphotriestérase ($10^{2\text{-}3}$ $M^{-1}.s^{-1}$) et estérase. Issue d'une archaea extrêmophile de l'ordre des *Sulfolobales*, *Sis*Lac présente également une résistance à la chaleur équivalente à celle de *Sso*Pox (T_m = 102 °C).

L'obtention de la structure cristallographique de *Sis*Lac (2.7 Å de résolution) permit de mettre en évidence un résidu impliqué dans la compaction et la thermostabilité de l'enzyme. Ce résidu, correspondant à la Gln 34 chez *Sso*Pox, qui est une Tyrosine chez *Sis*Lac, est un résidu pivot qui est en interaction avec son résidu équivalent dans l'autre monomère. Ainsi, chez *Sso*Pox, la Gln34 se trouve en interaction avec la Gln34 du monomère équivalent, alors que chez *Sis*Lac l'interaction ne peut être satisfaite, les Tyr34 se réorientent pour ne pas être en répulsion stérique. Cette réorientation à l'interface du dimère entraine une compaction plus importante de la protéine, augmentant également la surface de dimérisation. Chez les enzymes hyperthermostables, la surface et la nature de l'interface dimérique est un facteur important de thermostabilité. Nous avons également mis en évidence chez *Sis*Lac, un nombre moins élevé de ponts salins de surface comparé à *Sso*Pox.

Afin de mieux comprendre les relations structure/fonction/thermostabilité entre *Sis*Lac et *Sso*Pox, nous avons muté *Sis*Lac sur les différentes positions identifiées par les résidus correspondants chez *Sso*Pox. Ainsi, les résultats obtenus montrent que ces mutations affectent les activités et la thermostabilité de *Sso*Pox et suggèrent qu'il existe des relations épistatiques complexes influençant activités et thermostabilité dans cette famille de protéines.

OPEN ACCESS Freely available online

PLOS ONE

Structural and Enzymatic characterization of the lactonase *Sis*Lac from *Sulfolobus islandicus*

Julien Hiblot[1☯], Guillaume Gotthard[1☯], Eric Chabriere[1]*, Mikael Elias[2]*

1 URMITE UMR CNRS-IRD 6236, IFR48, Faculté de Médecine et de Pharmacie, Université de la Méditerranée, Marseille, France, **2** Weizmann Institute of Science, Biological Chemistry, Rehovot, Israel

Abstract

Background: A new member of the Phosphotriesterase-Like Lactonases (PLL) family from the hyperthermophilic archeon *Sulfolobus islandicus* (*Sis*Lac) has been characterized. *Sis*Lac is a native lactonase that exhibits a high promiscuous phosphotriesterase activity. *Sis*Lac thus represents a promising target for engineering studies, exhibiting both detoxification and bacterial *quorum* quenching abilities, including human pathogens such as *Pseudomonas aeruginosa*.

Methodology/Principal Findings: Here, we describe the substrate specificity of *Sis*Lac, providing extensive kinetic studies performed with various phosphotriesters, esters, *N*-acyl-homoserine lactones (AHLs) and other lactones as substrates. Moreover, we solved the X-ray structure of *Sis*Lac and structural comparisons with the closely related *Sso*Pox structure highlighted differences in the surface salt bridge network and the dimerization interface. *Sis*Lac and *Sso*Pox being close homologues (91% sequence identity), we undertook a mutational study to decipher these structural differences and their putative consequences on the stability and the catalytic properties of these proteins.

Conclusions/Significance: We show that *Sis*Lac is a very proficient lactonase against aroma lactones and AHLs as substrates. Hence, data herein emphasize the potential role of *Sis*Lac as *quorum* quenching agent in *Sulfolobus*. Moreover, despite the very high sequence homology with *Sso*Pox, we highlight key epistatic substitutions that influence the enzyme stability and activity.

Citation: Hiblot J, Gotthard G, Chabriere E, Elias M (2012) Structural and Enzymatic characterization of the lactonase *Sis* Lac from *Sulfolobus islandicus*. PLoS ONE 7(10): e47028. doi:10.1371/journal.pone.0047028

Editor: Fernando Rodrigues-Lima, University Paris Diderot-Paris 7, France

Received May 28, 2012; **Accepted** September 7, 2012; **Published** October 10, 2012

Funding: This work was granted by Direction Generale de l'armement (D.G.A.), France (REI. 2009 34 0045) and Vaincre La Mucoviscidose, France. J.H. and G.G. are PhD students granted by D.G.A. M.E. is a fellow supported by the IEF Marie Curie program (grant No. 252836). The funders had no role in study design, data collection and analysis, decision to publish, or preparation of the manuscript.

Competing Interests: The authors have declared that no competing interests exist.

* E-mail: Eric.chabriere@univmed.fr (EC); Mikael.elias@weizmann.ac.il (ME)

☯ These authors contributed equally to this work.

Introduction

*Sis*Lac (also known as *Sis*Pox [1]) is an enzyme isolated from the archaeon organism *Sulfolobus islandicus*, which is found in extreme environments like the Yellowstone natural park (U.S.A.) or the Mutnovksy volcano in Kamchatka (Russia) [2]. *Sis*Lac belongs to an enzyme family called Phosphotriesterase-Like Lactonase (PLL) that encompasses members from mesophilic organisms (PPH, AhlA, MCP, *Dr*OPH) [3,4,5] as well as thermophilic (*Sso*Pox, *Sac*Pox, *Gs*P, *Gk*L) [6,7,8,9] representatives. The PLL family is structurally and biochemically related to bacterial Phosphotriesterases (PTEs) [3]. Indeed, some representatives of PLLs were primarily isolated by virtue of their phosphotriesterase activity towards the insecticide paraoxon, and were named paraoxonases (Pox) as was the case with *Sis*Lac's closest homologue, *Sso*Pox, an enzyme isolated from *Sulfolobus solfataricus* [6]. However, further phylogenetic and biochemical studies has revealed that these enzymes are native lactonases endowed with promiscuous paraoxonase activity and more generally with organophosphate hydrolase activity [3]. Hyperthermophylic PLLs (hPLLs) are appealing enzymes in biotechnology because they possess an intrinsically high stability that often confer high resistance towards harsh conditions and proteases activity [10], which constitute useful properties for storage and large scale purification.

Interestingly, PTEs exhibit diffusion limit-like second order rates with paraoxon as a substrate [11], and are also endowed with promiscuous lactonase activity [3,12]. The particular link between these two families raises the hypothesis that PTEs have diverged from native lactonases like PLLs [3,13,14,15]. Indeed, both PTEs and PLLs belong to the amidohydrolase superfamily [3]. Despite the relatively low sequence identity between these two families (~30%), PTEs and PLLs exhibit the same $(\beta/\alpha)_8$ barrel fold or so-called TIM barrel [16]. At the C-terminus of the barrel, two divalent metal cations constitute the active site [13,17,18]. The phosphotriesterase activity of PTEs and PLLs is modulated in the presence of various divalent cations, the highest activity being achieved in a cobalt-containing buffer for *Pseudomonas diminuta* PTE [19], OpdA [20] and *Sso*Pox [6].The active site metal cations' chemical nature has been investigated using anomalous X-ray scattering and has revealed that both the PTE from *Agrobacterium radiobacter* (OpdA) and the PLL *Sso*Pox possess an iron/cobalt heterobinuclear center when the expression media is supplemented with cobalt ions [13,20].

The catalytic mechanisms for both the lactonase and phosphotriesterase involve a nucleophilic attack by a water molecule activated by the bi-metallic center. The major difference between the two activities consists of the respective transition state geometries: bi-pyramidal for the phosphotriesters and tetrahedral for the lactones. The fact that these two activities can be catalyzed with significant rates within the same active site suggests an overlap between the stabilization of the corresponding transitions state species, from which the enzymatic promiscuity would stem from [14,21]. The active site of PLLs possesses three sub-sites that are remarkably adapted for the lactone binding: a small sub-site, a large sub-site and a hydrophobic channel [13]. The aliphatic chain of the lactones binds within the hydrophobic channel, the large sub-site accommodates the amide group of the *N*-acyl chain, and the small sub-site positions the lactone ring. AHLs are molecules that mediate bacterial communication (*quorum* sensing) for many species. These molecules accumulate in the media to reach a certain threshold for which the transcriptional profile of the bacteria is altered [22]. Some studies report that virulence and biofilm life-style are regulated by *quorum* sensing [23,24,25,26], and suggest that quenching the *quorum* sensing (*quorum* quenching) could be an interesting strategy against multi-resistant pathogen bacteria using AHL based *quorum* sensing like *P. aeruginosa* [27,28,29,30,31]. By hydrolyzing AHLs, lactonases like PLLs can quench the AHL-mediated communication between bacteria, as seen for AiiA [28] or for human paraoxonases [30].

Because of their dual catalytic activities, lactonases and phosphotriesterases, PLLs constitute highly attractive candidate for biotechnological utilization as *quorum* quenching agent [32] or OPs biodecontaminant [33]. However, their precise biological function(s) remain(s) unknown. In many cases, PLLs are found in bacteria that do not produce or sense AHLs, which may suggest a role in interfering with the *quorum* sensing of other organisms or in the metabolism of the AHL molecules. Furthermore, some members of the PLL family efficiently hydrolyze gamma and/or delta oxo-lactones, but not AHLs [9,34]. However, the structural features that determine the lactonase specificity of these two classes remain unknown.

In this work we present a structural and biochemical analysis of *Sis*Lac. We have performed a detailed kinetic characterization and show that this enzyme hydrolyzes AHLs, but also γ and δ-lactones with high proficiency. Moreover, we provide a characterization of its thermal stability, thermophilicity and structural determinants responsible of its stability. The structural comparison with *Sso*Pox reveals an important dimer interface change. Key amino acids variations between the two close homologues were analyzed by mutagenesis study and revealed their critical involvement in the protein stability and lactonase activity.

Materials and Methods

Strain, Plasmids and Site Directed Mutagenesis

The plasmids preparations were performed in *Escherichia coli* strain DH5α (Invitrogen). Protein production was performed in *E. coli* BL21(DE_3)-pGro7/GroEL strain (TaKaRa) using plasmids pET22b-StrepTev*Sis*Lac and pET22b-*Sso*Pox (provided by GeneArt; Germany). Site directed mutagenesis was performed in 50 µL using *Pfu* polymerase (Invitrogen) on 100 ng of plasmid encoding corresponding genes and primers referenced in **Table S1**. The PCR cycle was performed using hybridization temperature of 55°C, elongation time of 12 min during 30 cycles and final elongation of 20 min. The template plasmid was eliminated by Fast Digest *Dpn*I (Fermentas) digestion of 30 min at 37°C followed by inactivation step of 20 min at 80°C. Plasmids were concentrated by classical alcoholic precipitation and then electroporated (Gene-Pulser, Bio-Rad) into *E. cloni 5alpha* cells (Lucingen), a particularly competent strain of *E. coli*. Site directed mutagenesis was finally verified by sequencing.

Production-purification of SisLac, SsoPox and SisLac's Variants

*Sis*Lac and its variants were heterologously produced and purified from the *Escherichia coli* strain BL21(DE3)-pGro7/GroEL (TaKaRa) as previously described [1] with the only difference being that 0.2% (w/v) arabinose was added at the start of the over-expression in order to induce chaperones expression. A very similar production protocol was used for *wt Sso*Pox. Briefly, protein production was performed in 2 liters of ZYP medium [35] (100 µg/ml ampicillin, 34 µg/ml chloramphenicol) inoculated by over-night pre-culture at a 1/20 ratio. Cultures grew at 37°C to reach $OD_{600nm} = 1.5$. The induction of protein production was made by starting the consumption of the lactose in ZYP medium. Subsequently, 0.2 mM $CoCl_2$ was added and the temperature was reduced to 25°C for additional 20 hours. Cells were harvested by centrifugation (3 000 g, 4°C, 10 min), re-suspended in lysis buffer (50 mM HEPES pH 8, 150 mM NaCl, $CoCl_2$ 0.2 mM, Lysozyme 0.25 mg/ml, PMSF 0.1 mM DNAseI 10 µg/ml) and stored at −80°C. The frozen cells were thawed and disrupted by three steps of 30 seconds of sonication (Branson Sonifier 450; 80% intensity and microtype limit of 8). Cell debris were removed by centrifugation (12 000 g, 4°C, 30 min). The purified protein being hyperthermostable, host proteins were precipitated by incubation of 30 min at 70°C and harvested by centrifugation (12 000 g, 4°C, 30 min). Other thermostable proteins from the host *E. coli* were eliminated by ammonium sulfate precipitation (326 g/L), and the overexpressed protein was concentrated by ammonium sulfate precipitation (476 g/L) and suspended in *activity buffer* (HEPES 50 mM pH 8, NaCl 150 mM, $CoCl_2$ 0,2 mM). The remaining ammonium sulfate was removed by dialysis against the *activity buffer* and the protein sample was subsequently concentrated prior to the size exclusion chromatography step (S75-16-60, GE Healthcare). The yield of protein production varied between 20 and 100 mg of protein per liter of culture after purification. The purity and the protein quality were verified by SDS-PAGE and mass spectrometry.

Oligomerization State Determination

Dynamic light scattering (DLS): experiments were performed at room temperature using zetasizer nano series apparatus (Malvern, UK) and the Zetasizer software. 30 µL of purified *wt Sso*Pox and *Sis*Lac (2.5 mg/mL) was used in the *activity buffer* to measure the hydrodynamic radius of particles in the protein solutions at 633 nm.

Multi-angle Light Scattering Studies: experiments were performed at room temperature using a size exclusion chromatography (KW803 column (Shodex)) carried out on an Alliance 2695 HPLC system (Waters) at a flow rate of 0.5 ml/min. The buffer used was similar to *activity buffer* despite pH was adjusted to 7.3 using NaOH. The signal was monitored by a three-angle light-scattering detector (MiniDAWNTMTREOS; Wyatt Technology), a quasi-elastic light-scattering instrument (DynaproTM, Wyatt Technology), and a differential refractometer (Optilab rEX, Wyatt Technology). Molecular weight, gyration, and hydrodynamic radii determination were performed by the ASTRA V software (Wyatt Technology) using a dn/dC (specific refractive index increment of the solution) value of 0.185 ml/g.

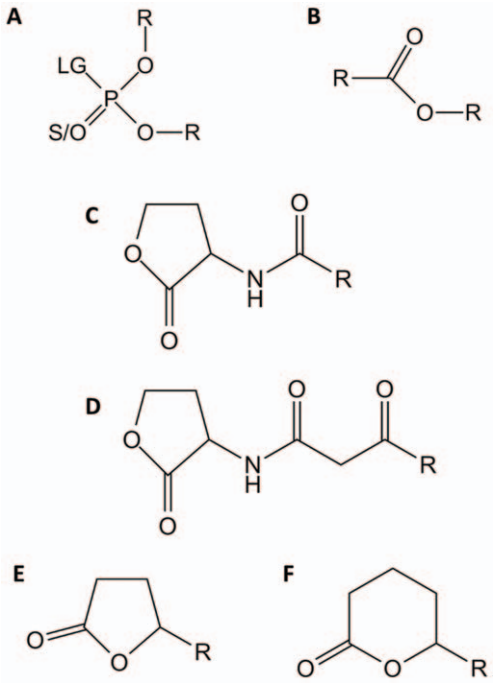

Figure 1. Chemical structure of *Sis*Lac substrates. Chemical structures of (**A.**) phosphotriesters, (**B.**) esters, (**C.**) Acyl-Homoserine Lactones, (**D.**) 3-oxo-Acyl-Homoserine Lactones (**E.**) γ-lactones and (**F.**) δ-lactones are presented. For phosphotriesters, R corresponds to different nature of substituents, LG corresponds to the leaving group which can be F, S-R, O-R or CN. The terminal substituent could be S atom if the molecule is a thionophosphotriester or an O atom if the molecule is an oxonphosphotriester. For esters, R corresponds to different nature of substituent. For AHLs and γ/δ-lactones, R corresponds to different size of acyl chain.
doi:10.1371/journal.pone.0047028.g001

Enzymatic Characterization

The time course of ethyl-paraoxon hydrolysis by *Sis*Lac at 70°C was monitored following the *p*-nitrophenolate production at 405 nm ($\varepsilon_{405nm} = 17\ 000\ M^{-1}cm^{-1}$) in 1-cm path length cell with a Cary WinUV spectrophotometer (Varian, Australia) and using the Cary WinUV software. Standard assays (500 µL) were performed in *paraoxonase buffer* CHES 50 mM pH 9, NaCl 150 mM, $CoCl_2$ 0.2 mM, EtOH 6% (v/v), with pH adjusted with NaOH at 70°C.

At 25°C, the phosphotriesterase, esterase and lactonase activities were analyzed monitoring absorbance variations in 200 µL reaction volumes using 96-well plates (6.2-mm path length cell) and a microplate reader (Synergy HT) using the Gen5.1 software at 25°C. For each substrate, assays were performed using organic solvent concentrations below 1%. The monitoring wavelength, the solvent used, the molar extinction coefficient and the concentration range for each substrate (**Fig. 1, S1 & S2**) are summarized in **Table S2**. Phosphotriesterase and esterase activities were performed in *activity buffer*. When required, DTNB at 2 mM was added to the buffer to follow hydrolysis of substrate releasing thiolate group (malathion (**Fig. S1V**)). Catalytic parameters for some phosphotriesters were also recorded using SDS at concentrations 0.01 and 0.1% (w/v). Lactone hydrolysis assays were performed in *lactonase buffer* (Bicine 2.5 mM pH 8.3, NaCl 150 mM, $CoCl_2$ 0.2 mM, Cresol purple 0.25 mM and 0.5% DMSO) using cresol purple (pK_a 8.3 at 25°C) as pH indicator to follow the acidification related to the lactone ring hydrolysis. Molar coefficient extinction was measured by recording absorbance of the buffer over a range of acetic acid concentrations (0–0.35 mM). The absorbance values *versus* acetic acid concentration were fitted to a linear regression (GraphPad Prism 5 software) with a slope corresponding to molar extinction coefficient (see **Table S2**). For all experiments, each point was made in triplicate and the Gen5.1 software was used to evaluate the initial velocity at each substrate concentration. Mean values were fitted to the Michaelis-Menten equation using Graph-Pad Prism 5 software to obtain the catalytic parameters. In the case of C4 AHL hydrolysis for which the substrate concentration that enable to determine the enzyme V_{max} could not be reached, the catalytic efficiency has been determined by fitting the linear part of the Michaelis-Menten plot to a linear regression.

Thermostability Analysis

Temperature dependence analysis. The temperature dependence of the *Sis*Lac paraoxonase activity was studied over the temperature range 25–85°C with 10°C increment. The ethyl-paraoxon (2 mM) hydrolysis was monitored in 500 µL at 405 nm ($\varepsilon_{405nm} = 17\ 000\ M^{-1}cm^{-1}$) in 1-cm path length cell with a Cary WinUV spectrophotometer (Varian, Australia) using the Cary WinUV software. Triplicate experiments were performed in *paraoxonase buffer* with pH adjusted with NaOH to 9 at each temperature.

Activity-based thermal stability. The residual paraoxonase activity of *Sis*Lac after incubation at different temperatures was performed. Incubation time and temperatures tested in this experiment were 390 min at 85°C, 90°C and 95°C in *activity buffer*. The ethyl-paraoxonase (1 mM) activity was followed at 25°C every 15 min during the first hour of incubation and every 30 min till the end of the experiment (after cooling). Paraoxon hydrolysis was monitored at 405 nm ($\varepsilon_{405nm} = 17\ 000\ M^{-1}cm^{-1}$) with a microplate reader (Synergy HT) and Gen5.1 software in a 6.2 mm path length cell for 200 µL reaction in 96-well plate. Initial velocity at 25°C was used as reference to normalize velocities obtained after incubation at high temperature. Values are represented as fraction of the reference (value 1.0). The half-life of the protein at each temperature was determined by fitting the data to an exponential decay equation using GraphPadPrism 5 software.

Melting temperature determination. Circular Dichroism (CD) spectra were recorded using Jasco J-810 spectropolarimeter equipped with Pelletier type temperature control system (Jasco PTC-4235) in 1 mm thick quartz cell and using the Spectra Manager software. Measurements were carried out in 10 mM sodium phosphate buffer at pH 8 with a protein concentration of 0.1 mg/mL. For *wt Sis*Lac, denaturation was first recorded between 190 to 260 nm with a scattering speed of 20 nm/min every 10°C at temperatures ranging between 20 to 90°C. To determine the melting temperature of proteins (*wt Sis*Lac and variants), the denaturation was recorded at 222 nm by increasing the temperature from 20 to 90°C (at 5°C/min) in 10 mM sodium phosphate buffer at pH 8 containing increasing concentrations (0.5–3.5 M) of guanidinium chloride. The theoretical T_m without guanidinium chloride was extrapolated at the y-intercept by a linear fit using the GraphPadPrism 5 software.

pH Dependence Profile Determination

The pH-dependence ethyl-paraoxonase activity (2 mM) profile of *Sis*Lac was monitored at 348 nm (the pH-independent isobestic point of *p*-nitrophenol and *p*-nitrophenoxide ion; $\varepsilon_{348nm} = 5\ 300\ M^{-1}cm^{-1}$) [6]. To explore the pH range 5–11, different buffers were prepared containing 50 mM monobasic phosphate over the pH range 5–7, 50 mM HEPES for pH 8, 50 mM CHES

Table 1. Data collection and refinement statistics of *Sis*Lac structure.

Data collection	
PDB Id	4G2D
Wavelength (Å)	0.980
Detector	ADSC Q315
Oscillation (°)	0.5
Number of frames	323
Resolution (Å) (last bin)	2.70 (2.80-2.70)
Space group	$P3_22_1$
Unit-cell parameters (Å)	a = 47.8, b = 47.8, c = 239.5 $\alpha = 90.0$, $\beta = 90.0$, $\gamma = 120.0$
No. of observed reflections (last bin)	86521 (8903)
No. of unique reflections (last bin)	9436 (959)
Completeness (%) (last bin)	99.9 (100)
R_{merge} [a] (%) (last bin)	6.2 (47.6)
R_{meas} [b] (%) (last bin)	6.6 (50.4)
I/σ(I) (last bin)	28.42 (4.71)
Redundancy (last bin)	9.17 (9.28)
Mosaicity (°)	0.103
Refinement statistics	
R_{free}/R_{work} [c]	29.25/26.49
No. of total model atoms	2517
Ramachandran favored	98.2%
Ramachandran outliers	1.8%
Rmsd from ideal	
Bond lengths (Å)	0.0021
Bond angles (°)	0.5114

[a] $R_{sym} = R_{merge} = \sum_h |\hat{I}_h - I_{h,i}| \Big/ \sum_h \sum_i^{nh} I_{h,i}$.

[b] $R_{meas} = \sum_h \sqrt{\frac{n_h}{n_h - 1}} \sum_i^{nh} |\hat{I}_h - I_{h,i}| \Big/ \sum_h \sum_i^{nh} I_{h,i}$ with $\hat{I}_h = \frac{1}{n_h} \sum_i^{nh} I_{h,i}$.

[c] $R_{work} = \sum ||F_o| - |F_c|| / = \sum |F_o|$ where F_o denotes the observed structure factor amplitude and F_c, the structure factor amplitude calculated from the model. R_{free} is as for R_{work} but calculated with 5% of randomly chosen reflections omitted from the refinement.

doi:10.1371/journal.pone.0047028.t001

over the pH range 9–10 and 50 mM dibasic phosphate at pH 11. The buffers also contained 150 mM NaCl and 0.2 mM of $CoCl_2$, and were adjusted with NaOH or HCl. The kinetic measurements were performed at 25°C with a microplate reader (Tecan) and Magellan software in a 6.2 mm path length cell for 200 µL reaction in 96-well plate. Each experiment was made in triplicate and initial velocities were evaluated using Excel software (Microsoft).

Crystallization and Structure Determination

The crystallization procedure of *Sis*Lac has been previously described [1]. Diffraction data were collected at the ESRF (Grenoble, France) BM-30A (FIP) beamline using a wavelength of 0.98 Å on an ADSC Quantum Q315 Detector. X-Ray diffraction data were integrated and scaled with the XDS program [36]. The presence of a twin was clearly established using *phenix.xtriage* [37] from the *PHENIX* refinement-program suite [38]. The Molecular replacement using the *Sso*Pox structure as model (PDB code 2vc5) was performed with *Phaser* [39]. The twin operator (*-h, -k, l*) and a twofold axis (z) arising from the twinning were determined using *phenix.xtriage*. The solution was then used for refinement performed using *REFMAC5* [40] using the twin option and *Coot* [41] for model improvement. The model and structure factor were deposited under the Protein Data Bank (PDB) code 4G2D. Despite the twinning, the electronic density maps were of good quality (**Fig. S3**; R and R_{free} values (0.2649 and 0.2925, respectively; **Table 1**)).

Structural analysis and comparison, cartoon and ribbon representation were made using PyMOL (www.pymol.org). Surface contacts and interaction analysis was performed using the PROTORP server [42]. Root mean square deviations (r.m.s.d) were computed using Swiss-pdb-viewer software [43].

Sequence Alignment

The alignment was performed using T-coffee server [44,45], manually improved with *seaview* software [46] and finally drawn with *BioEdit* 7.1.3.

Results

This study provides the characterization of *Sis*Lac isolated from *Sulfolobus islandicus* strain M.16.4. Several genomes of *S. islandicus* are available and encode highly similar (99% sequence identity) orthologs of *Sis*Lac (**Fig. S4**). Sequence comparison with close homologs *Sso*Pox (91% identical) from *Sulfolobus solfataricus* MT4 & P2 [6] and *Sac*Pox (76% identical) from *Sulfolobus acidocaldarius* DSM 639 [7] (**Fig. 2 & S4**) reveals that the sequence divergence is mainly localized at the N-terminus and C-terminus of the protein. *Sis*Lac displays lower sequence identity with other members of the PLL family of proteins (35% *Gs*P/*Gk*L from Geobacillus sp. [8,9], 28% *Dr*OPH form *Deinococcus radiodurans* [5,34], 37–38% AhlA/PPH/MCP from mesophilic organisms [3,4]) and ~ 30% with PTEs (**Fig. 2**). Despite a very high sequence homology between *Sso*Pox and *Sis*Lac, both enzymes exhibit structural and enzymatic differences.

Biochemical and Biophysical Characterization of SisLac

Oligomeric state analysis. Size exclusion chromatography, dynamic light scattering and multi angle light scattering experiments were carried out to determine the oligomeric states of *Sis*Lac and *Sso*Pox. Using a combination of static plus dynamic light scattering, UV spectrophotometry, and refractometry, *Sis*Lac and *Sso*Pox appear to be dimeric at room temperature (25°C) (**Fig. 3A–B**) (72.57±0.79 kDa and 70.46±0.97 kDa, respectively, *versus* MWs of *Sso*Pox and *Sis*Lac dimers = 71.2 kDa). Moreover, the dynamic light scattering experiments show apparent sizes for *Sis*Lac and *Sso*Pox of 80±3 kDa and 82±3 kDa, respectively (**Fig. 3C–D**). These results confirm that both proteins are dimeric at 25°C. The existence of homodimers is consistent with the crystal structures of *Sis*Lac, *Sso*Pox [47] and other PLLs (*Dr*OPH (PDB ID: 3FDK), *Gs*P (PDB ID: 3F4D) and *Gk*L (PDB ID: 3QJG)).

pH and temperature dependence. We determined the pH and temperature dependency of *Sis*Lac's catalytic activities. However, because the lactonase assay utilizes a pH indicator, these characteristics could only be determined for the paraoxonase activity. The optimal pH for *Sis*Lac's paraoxonase activity was established by measuring the velocity at pH ranging from 5 to 11 (**Fig. 4A**). The pH-rate dependence plot displays a bell-shape curve with a wide plateau between pH 7 and 10 (with maximal activity at pH 9). The same dependency what was described for *Sac*Pox at 70°C [7], and only a slightly different pattern was observed for *Sso*Pox (optimum at pH 8 [6]). The PTE from *P.*

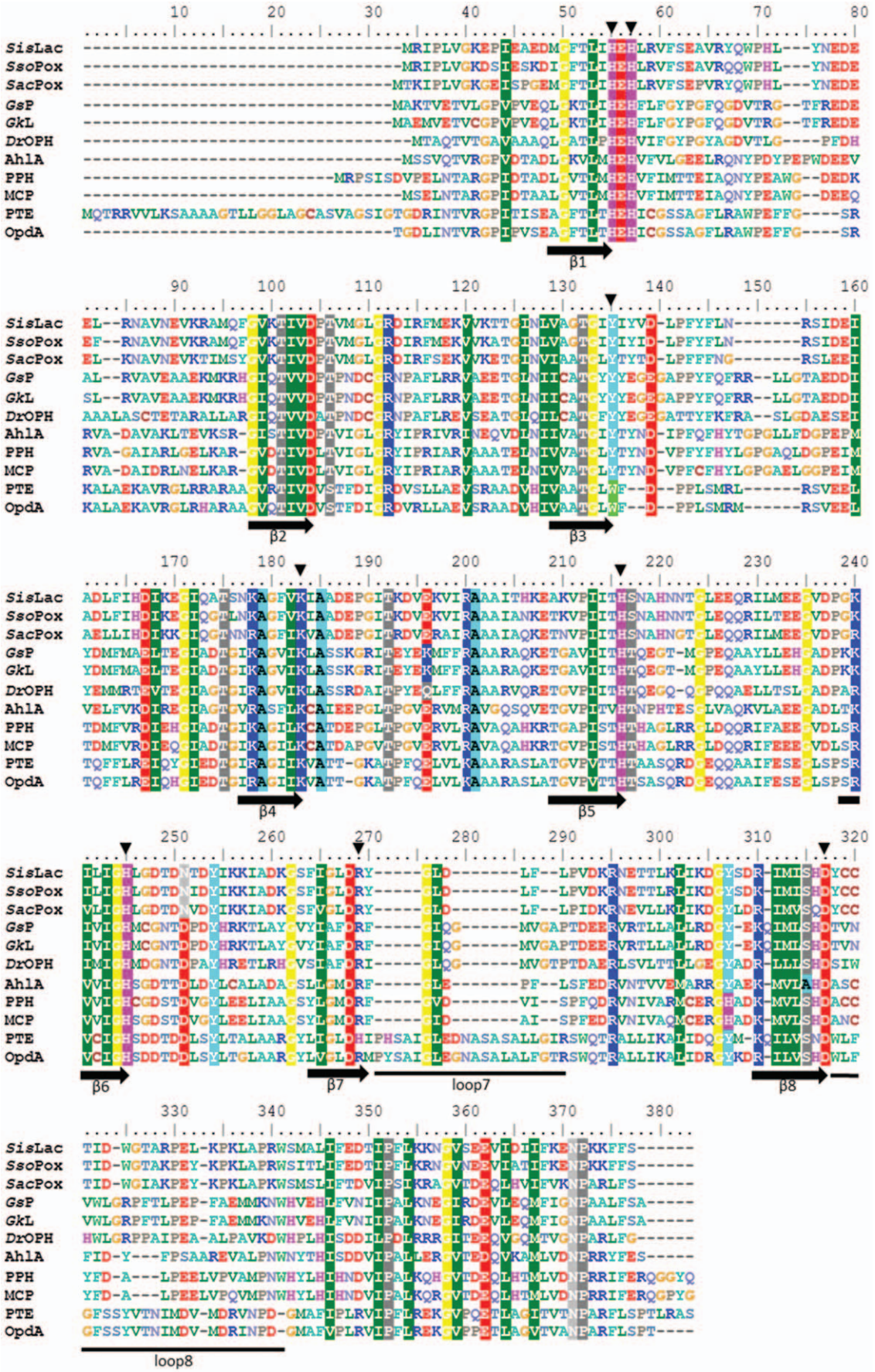
SisLac
SsoPox
SacPox
GsP
GkL
DrOPH
AhlA
PPH
MCP
PTE
OpdA
β1
β2
β3
β4
β5
β6
β7
loop7
β8
loop8

Figure 2. Sequence alignment of PLLs and PTEs. Sequence alignment of *Sis*Lac from *Sulfolobus islandicus* strain M.16.4 (ACR40964.1), *Sac*Pox from *Sulfolobus acidocaldarius* strain DSM 639 (AAY81433.1), *Sso*Pox from *Sulfolobus solfataricus* strain MT4 (AAW47234.1), *Gs*P from *Geobacillus stearothermophilus* strain 10, *Gk*L from *Geobacillus kaustophilus* strain HTA426 (YP_147359.1), *Dr*OPH from *Deinococcus radiodurans* (AAF10507.1), AhlA from *Rhodococcus erythropolis* (ACF57853.1), PPH from *Mycobacterium tuberculosis* (ACF57854.1), MCP from *Mycobacterium avium subsp. paratuberculosis* K-10 (NP_962602.1), *Pseudomonas diminuta* PTE and *Agrobacterium radiobacter* OpdA. Metal coordinating residues and important active site residues are indicated by a black vertical arrow. The β-sheets are indicated by a horizontal black arrow. An alignment of *Sulfolobal* PLL is provided in Supplementary information.
doi:10.1371/journal.pone.0047028.g002

diminuta also exhibits an activity maximum at a pH range of 8–10 [48]. This observation is consistent with the hypothesis of common mechanism shared by these enzyme families.

The temperature dependency was investigated by measuring the paraoxonase activity at temperatures ranging from 25 to 85°C (**Fig. 4B**). The highest temperature tested (85°C) presented the highest velocity. However, within the tested temperature (imposed by technical limitations), we did not find a maximum. Similarly, no maxima were found in the cases of *Sso*Pox [6], *Dr*OPH [5] and *Gs*P [8]. In contrast, *Sac*Pox presents a maximum activity around 70°C and the activity decrease above this temperature [7].

Thermostability

The thermostability of *Sis*Lac was evaluated based on its catalytic activity. The residual paraoxonase activity of the enzyme after different incubation times at 80, 90 and 95°C was measured (**Fig. 4C**). The enzyme exhibited respective half-lives of 84±20 min, 8.5±1.5 min and 3.6±0.4 min at 85, 90 and 95°C. In comparison, *Sso*Pox exhibits a half-life of 4 hours at 95°C, and 90 min at 100°C [6], and *Sac*Pox exhibits a half-life of 5 min at 90°C [7] (from *S. acidocaldarius*, living temperatures from 55 to 85°C [49]).

The thermal stability of *Sis*Lac was also determined by circular dichroism at temperatures ranging between 20°C and 90°C (**Fig. S5**). However, as previously observed for *Sso*Pox [47], the extreme thermostability of this enzyme does not allow to precisely determine a melting temperature (T_m) by this method. Different concentrations of guanidium chloride were required to further destabilize the protein and the T_m values were extrapolated to zero guanidinium chloride: T_m at 102±2°C for *Sis*Lac (**Fig. S5**) (while *Sso*Pox's T_m = 106°C [47]). These values are in the range of the other characterized thermostable PLLs, including *Dr*OPH and *Gs*P whose Tm values are 88.1°C [5] and 106.6°C [8], respectively. Notably, the extremophile *Deinoccocus radiodurans* is a

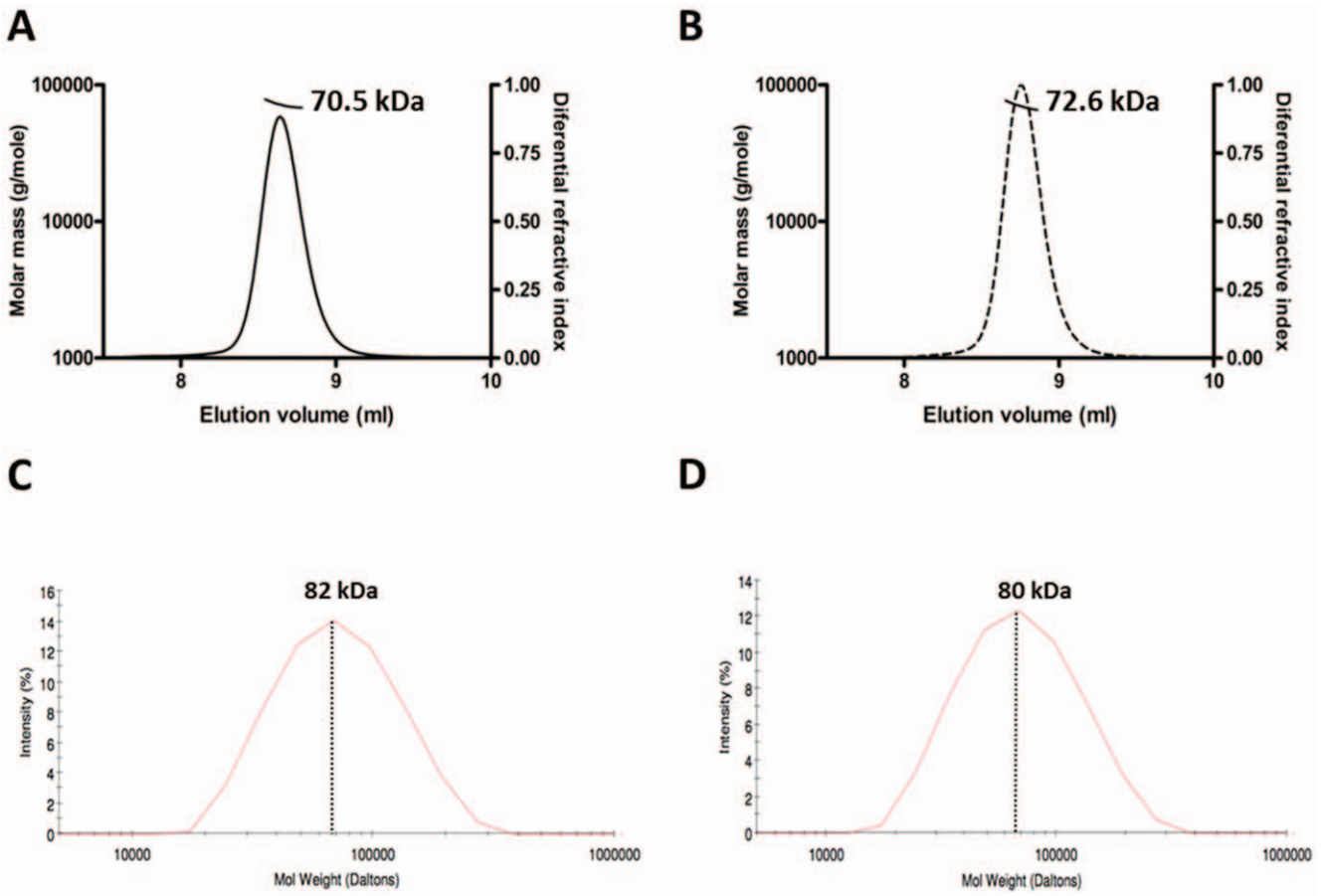

Figure 3. Oligomerization state analysis of *Sis*Lac. A–B- Multi-angle light scattering analysis of *Sso*Pox (**A.**) and *Sis*Lac (**B.**) at 25°C. The molecular weight of particules (dashed line) are represented in function of the elution profile (continuous line) during size exclusion chromatography. **C–D-** Dynamic light scattering experiments. Intensity (%) of the signal *versus* molecular weight of particles for *Sso*Pox sample (**C.**) and *Sis*Lac sample (**D.**).
doi:10.1371/journal.pone.0047028.g003

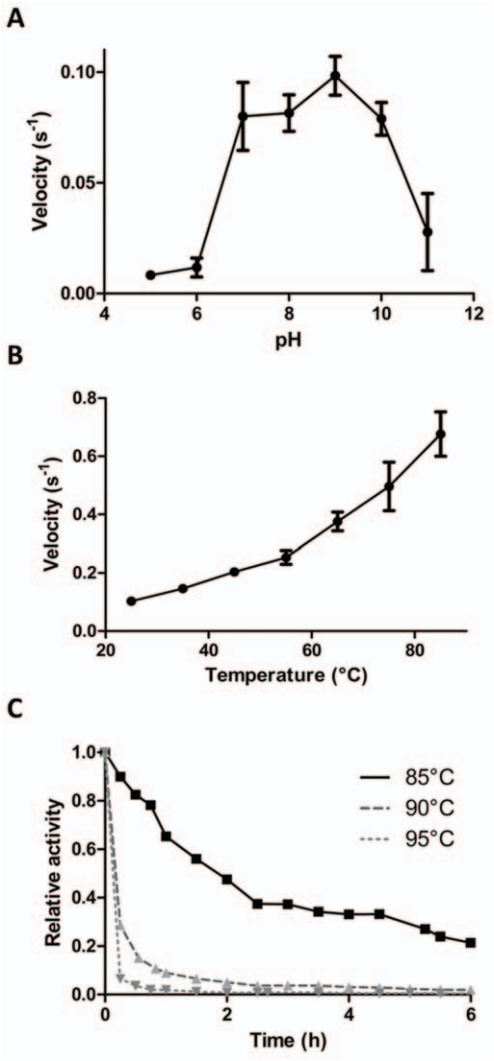

Figure 4. Biochemical analysis of *Sis*Lac. A- pH dependence of *Sis*Lac paraoxonase activity. Velocity obtained against 2 mM ethyl-paraoxon at different pH ranging between pH 5 and pH 11 (see *methods* for more details). **B**- Thermophilicity of *Sis*Lac. Initial rates for the paraoxonase activity of *Sis*Lac were measured at temperatures ranging from 25 up to 85°C. **C**- Thermal stability of *Sis*Lac. Relative residual activity of *Sis*Lac after different incubation at 85°C (*Black square*), 90°C (*grey triangle*) and 95°C (*Grey inverted triangle*) for different times yielded half-lives of 84 (±20) min for 85°C, 8.5 (±1.5) min for 90°C and 3.6 (±0.4) min for 95°C.
doi:10.1371/journal.pone.0047028.g004

mesophilic bacteria [5], and *Dr*OPH exhibits an extreme T_m, typical for enzymes from hyperthermophiles or thermophiles (*Sulfolobus solfataricus* living temperatures from 50 to 87°C [49], *Sulfolobus islandicus* from 59 to 91°C [2], *Geobacillus stearothermophilus* from 37–70°C [50,51]).

Enzymatic Characterization of SisLac

Phosphotriesterase activity. Kinetic parameters were determined for paraoxon (**Fig. S1I**) at 70°C and 25°C (**Table 2**). The catalytic efficiency obtained at 70°C for *Sis*Lac ($k_{cat}/K_M = 6.98(\pm1.56)\times10^2$ $M^{-1}s^{-1}$) is similar to that reported for *Sac*Pox [7] and *Sso*Pox [52] (**Table S3**). The catalytic efficiency at 25°C was about 2.5 folds lower than the efficiency at 70°C ($2.60(\pm0.58)\times10^2$ $M^{-1}s^{-1}$), and is higher than that of *Gs*P ($5{,}47(\pm0.47)\times10^1$ $M^{-1}s^{-1}$) [8], *Gk*L (4.5 $M^{-1}s^{-1}$; at 37°C) [9], MCP (4.1 $M^{-1}s^{-1}$) [4] and *Dr*OPH (1.39 ± 0.11 $M^{-1}s^{-1}$) [5]. These promiscuous phosphotriesterase catalytic parameters of lactonases [3,14] contrast with the diffusion limit-like second order rates of *P. diminuta* PTE with paraoxon as substrate ($k_{cat}/K_M \sim 10^8$ $M^{-1}s^{-1}$) [11].

The modulation of *Sis*Lac phosphotriester hydrolysis by Sodium Dodecyl Sulfate (SDS), which has been previously shown to act as an activator in the case of *Sso*Pox [53], was also tested (**Table 2**). Interestingly, the addition of 0.01% SDS yields to a 2.5 folds increase in the paraoxonase catalytic efficiency ($6.36(\pm2.18)\times10^2$ $M^{-1}s^{-1}$), whereas the addition of 0.1% SDS enhanced the efficiency by 25 folds ($k_{cat}/K_M = 7.14(\pm4.16)\times10^3$ $M^{-1}s^{-1}$).

Others phosphotriesters (**Fig. 1A**) were also tested as substrates at 25°C; including methyl-paraoxon (**Fig. S1II**), parathion (**Fig. S1III**), methyl-parathion (**Fig. S1IV**), malathion (**Fig. S1V**) and CMP-coumarin (**Fig. S1VI**) (methylphosphonic acid 3-cyano-4-methyl-2-oxo-2H-coumarin-7-yl ester cyclohexyl ester (a cyclosarin derivative in which the fluoro substituent of cyclosarin has been replaced by a cyanocoumarin group [54])) (**Table 3 & S4**). These assays showed that *Sis*Lac is over 10 times more efficient towards methyl-paraoxon than for (ethyl-)paraoxon ($4.26(\pm1.74)\times10^3$ $M^{-1}s^{-1}$ and $2.60(\pm0.58)\times10^2$ $M^{-1}s^{-1}$, respectively). In a similar fashion, *Sis*Lac shows a clear preference for the methyl-parathion ($3.57(\pm0.3)\times10^1$ $M^{-1}s^{-1}$), as compared with ethyl-parathion for which no catalysis could be detected. This suggests that the bulkiness of the substituent groups of some phosphotriesters affects a catalytically efficient binding. This preference has also been observed for *Sso*Pox and *Sac*Pox at 70°C [7]. Moreover, *Sis*Lac exhibits a pronounced thiono-effect; methyl-paraoxon and methyl-parathion differ by only one atom (the oxon function on the phosphorus moiety in paraoxon is a thiono in parathion), *Sis*Lac hydrolyzes methyl-paraoxon about 100 times more efficiently ($4.26(\pm1.74)\times10^3$ $M^{-1}s^{-1}$ and $3.57(\pm0.3)\times10^1$ $M^{-1}s^{-1}$, respectively). PTEs does not exhibit such a drastic difference and paraoxon is only a slightly better substrate than parathion [20,55]. Kinetics parameters were also recorded for the hydrolysis of another sulfur-containing organophosphate, the insecticide called malathion (1.88 ± 0.43 $M^{-1}s^{-1}$). *Sis*Lac exhibits a similar K_M for this substrate than for methyl-parathion, but malathion is a considerably slower substrate than parathion. Finally, *Sis*Lac hydrolyzes the nerve agent analog CMP-coumarin with moderate efficiency ($4.26(\pm1.86)\times10^3$ $M^{-1}s^{-1}$) illustrating its potential for organophosphorus detoxification.

Esterase activity. Although lactones constitute a specific class of esters (**Fig. 1B**), no esterase activity was detected within PLL family members with the exception of *Sso*Pox and *Sac*Pox (with 2-naphthyl acetate [6,7], *p*-nitrophenyl butanoate and 2-naphthyl acetate [3]). It is therefore not surprising that *Sis*Lac

Table 2. Ethyl-paraoxonase activity of *Sis*Lac.

Conditions	*Sis*Lac		
	k_{cat} (s^{-1})	K_M (μM)	k_{cat}/K_M ($s^{-1}M^{-1}$)
25°C	1.42±0.09	5439±873	$2.60(\pm0.58)\times10^2$
25°C SDS 0.1%	14.31±3.16	2005±728	$7.14(\pm4.16)\times10^3$
25°C SDS 0.01%	2.70±0.29	4248±999	$6.36(\pm2.18)\times10^2$
70°C	0.79±0.04	1131±196	$6.98(\pm1.56)\times10^2$

Data obtained with cobalt as cofactor.
doi:10.1371/journal.pone.0047028.t002

Table 3. Phosphotriesterase activity of *Sis*Lac.

Substrate	k_{cat} (s^{-1})	K_M (μM)	k_{cat}/K_M ($s^{-1}M^{-1}$)
Ethyl-Paraoxon (I)	1.42±0.09	5 439±873	$2.60(\pm0.58)\times10^{2}$
Methyl-Paraoxon (II)	7.40±1.26	1 739±417	$4.26(\pm1.74)\times10^{3}$
Ethyl-Parathion (III)	ND	ND	ND
Methyl-Parathion (IV)	$9.7(\pm0.2)\times10^{-3}$	272±17	$3.57(\pm0.30)\times10^{1}$
Malathion (*r*) (V)	$6.2(\pm0.4)\times10^{-4}$	330±54	1.88±0.43
CMP (*r*) (VI)	1.86±0.27	437±130	$4.26(\pm1.86)\times10^{3}$

r corresponds to racemic solution. Data obtained with cobalt as cofactor. ND corresponds to substrates for which no hydrolysis can be detected. Roman numeration corresponds to chemical structures of **Fig. S1**.
doi:10.1371/journal.pone.0047028.t003

hydrolyzes *p*-nitrophenyl-acetate (**Fig. S1VIII**) with $k_{cat}/K_M = 1.6(\pm0.5)\times10^{3}$ $M^{-1}s^{-1}$, a 50 times higher catalytic efficiency than *Sso*Pox (k_{cat}/K_M of $3.12(\pm0.33)\times10^{1}$ $M^{-1}s^{-1}$) (**Table 4**). However, both proteins do not exhibit any detectable activity against phenyl-acetate (**Fig. S1VII**), *p*-nitrophenyl-decanoate (**Fig. S1IX**), nitrophenyl-acetate (**Fig. S1X**) and 4-acetoxyacetophenone (**Fig. S1XI**) (**Table 4**).

Lactonase activity. PLLs are lactonases that might be involved in *quorum* quenching mechanisms [3,13]. We thus assayed the activity of *Sis*Lac on several AHLs (**Fig. 1C–D**) of different chain lengths with the aim of evaluating *Sis*Lac's specificity (**Table 5**). These experiments revealed that *Sis*Lac exhibits clear preference for AHLs with medium-length aliphatic chains (C8 and C10-AHL). Long chains are strongly disfavored, the efficiency of 3-oxo-C12-AHL hydrolysis (**Fig. S2VI**) ($8.97(\pm3.45)\times10^{2}$ $M^{-1}s^{-1}$) is 100 fold lower than that of 3-oxo-C10-AHL (**Fig. S2V**) ($9.63(\pm1.89)\times10^{4}$ $M^{-1}s^{-1}$). In addition, 3-oxo-AHLs (**Fig. 1D**) are overall better substrates for *Sis*Lac than unsubstituted (**Fig. 1C**).

Others lactones were also assayed as substrates (**Table 6**), such as the γ-lactones (5 atoms lactone ring) (**Fig. 1E**), δ-lactones (6-atoms lactone ring) (**Fig. 1F**) and ε-lactone (7 atoms lactone ring) (**Fig. S2XI**), with alkyl substituent on carbons 4 and 5 of the lactone ring (contrary to the substitution of carbon 2 in AHLs (**Fig. 1C**) (**Table 6**). Finally, dihydrocoumarin (**Fig. S2XII**), an aromatic lactone, was also tested (**Table 6**). We found that γ-lactones (**Fig. 1E**) and δ-lactones (**Fig. 1F**) comprise good substrates for *Sis*Lac, δ-lactones being the preferred substrates. Indeed, the best δ-lactone (undecanoic-δ-lactone (**Fig. S2XIV**), $1.77(\pm0.04)\times10^{6}$ $M^{-1}s^{-1}$) is hydrolyzed with over 5-times higher catalytic efficiency than the best γ-lactone (nonanoic-γ-lactone (**Fig. S2IX**), $2.04(\pm1.12)\times10^{5}$ $M^{-1}s^{-1}$). The latter is 2 times a better substrate than the best AHL substrate (3-oxo-C8-AHL (**Fig. S2IV**), $9.70(\pm1.84)\times10^{4}$ $M^{-1}s^{-1}$). Comparison of different lactones possessing different alkyl chain lengths confirmed the trend observed for AHLs, whereby acyl chains containing 7 carbons were preferred by the enzyme. For γ-lactones and δ-lactones, the alkyl chain length preferred by the enzyme is between 5 and 6 carbon atoms, and a similar specificity was observed for MCP, *Gk*L and *Dr*OPH enzymes [4,9,34]. Interestingly, whereas the short chain C4-AHL (**Fig. S2I**) is a poor substrate for *Sis*Lac, the γ-heptanolide lactone (**Fig. S2VIII**) (3 carbon atoms in the alkyl side-chain) shows a 10^{4} higher catalytic efficiency. In fact, lactones with very short or without side-chains (dihydrocoumarin (**Fig. S2XVII**), γ-butyrolactone (**Fig. S2VII**), δ-valerolactone (**Fig. S2XII**), ε-caprolactone (**Fig. S2XVI**)) constitute better substrates than C4-AHL (**Fig. S2I**).

Structural Analysis of SisLac

*Sis*Lac is homodimeric in the crystal structure with overall dimensions of the monomers of being approximately 39×48×56 Å. As for its close homolog *Sso*Pox [13] and related PLLs like *Dr*OPH [5], *Gs*P [8] and *Gk*L [9], *Sis*Lac is roughly globular and exhibits a $(\beta/\alpha)_8$ barrel topology. The active site consists of a binuclear center located at the C-Terminal of the barrel. Four histidines (His22, His24, His170, His199), one aspartic acid (Asp256) and a carboxylated lysine (residue 137) are coordinating the two metals. The two metal cations (possibly iron and cobalt, as seen for *Sso*Pox [13] and OpdA [20]) are bridged by a water molecule that is presumed to be the catalytic nucleophile. The active site includes a long hydrophobic channel that was revealed by structural studies on *Sso*Pox as the binding region of aliphatic chains for the AHL substrates [13]. Indeed, *Sis*Lac's structure is overall very similar to the structure of *Sso*Pox (root-mean-square deviation (r.m.s.d.) for α-carbon atoms (over 314 atoms) of 0.35 Å).

Salt bridge network analysis. *Sis*Lac sequence exhibits approximately the same amino acid content as *Sso*Pox, containing 14.3 *versus* 16% of uncharged polar residues and 28.7 *versus* 28% of charged residues. This is no surprising since both enzymes possess high sequence identity (91%) (see sequence alignment, **Fig. 2**). As described for *Sso*Pox, the charged residues are mainly located at the protein surface, forming complex electrostatic networks [47] that includes 28 salt bridges implicating 46 residues. This charge network mainly differs by the substitution K14E in *Sis*Lac that suppress a salt bridge network between E12-K14-D15 of *Sso*Pox,

Table 4. Esterase activity of *Sis*Lac.

Substrat	*Sis*Lac			*Sso*Pox		
	k_{cat} (s^{-1})	K_M (μM)	k_{cat}/K_M ($s^{-1}M^{-1}$)	k_{cat} (s^{-1})	K_M (μM)	k_{cat}/K_M ($s^{-1}M^{-1}$)
Phenyl-acetate (VII)	ND	ND	ND	ND	ND	ND
***p*NP-acetate(VIII)**	0.20±0.01	124±36	$1.6(\pm0.5)\times10^{3}$	0.17±0.007	5447±352	$3.12(\pm0.33)\times10^{1}$
***p*NP-decanoate (XI)**	ND	ND	ND			
***m*NP-acetate (X)**	ND	ND	ND	ND	ND	ND
4AAP (XI)	ND	ND	ND	ND	ND	ND

*p*NP corresponds to *para*-nitrophenol leaving group and *m*NP to *meta*-nitrophenol leaving group. Data obtained with cobalt as cofactor. ND corresponds to substrates for which no hydrolysis can be detected. Roman numeration corresponds to chemical structures of **Fig. S1**.
doi:10.1371/journal.pone.0047028.t004

Table 5. AHL lactonase activity of *Sis*Lac.

Substrate	*Sis*Lac		
	k_{cat} (s^{-1})	K_M (μM)	k_{cat}/K_M ($s^{-1}M^{-1}$)
C4-AHL (*r*) (I)	ND	ND	3.89±0.60
C8-AHL (*r*) (II)	0.71±0.09	677±163	1.05(±0.39)×10^3
C12-AHL (*r*) (III)	1.90±0.79	1 303±1 078	1.46(±1.81)×10^3
3-oxo-C8-AHL (*r*) (IV)	4.10±0.09	42±7	9.70(±1.84)×10^4
3-oxo-C10-AHL (*l*) (V)	10.65±0.36	111±18	9.63(±1.89)×10^4
3-oxo-C12-AHL (*l*) (VI)	0.39±0.04	435±123	8.97(±3.45)×10^2

r corresponds to racemic solution and *l* at the pure levorotatory enantiomer. Data obtained with cobalt as cofactor. ND corresponds to not determined value. Roman numeration corresponds to chemical structures of **Fig. S2**.
doi:10.1371/journal.pone.0047028.t005

and consequently creates a local concentration of 3 negative charges within 4 consecutive residues (**Fig. 5A**).

Dimer interface analysis. The dimer interface of *Sis*Lac comprises 46 residues (44 in *Sso*Pox). The contacting area is almost identical and comprise a typical value for homodimers [42] (1770 $Å^2$ for *Sis*Lac structure, 1750 $Å^2$ for *Sso*Pox structure, lower for other thermostable PLLs: 1728 $Å^2$ for *Gk*L structure, 1632 $Å^2$ for *Gs*P structure and 1473 $Å^2$ for *Dr*OPH structure). The nature of this interface is mainly hydrophobic in both enzymes, but *Sis*Lac's interface tends to be more hydrophobic (56% for *Sis*Lac, 52.6% for *Sso*Pox), more charged (*Sis*Lac 23.91%, *Sso*Pox 20.45%) and less polar (*Sis*Lac 32.61%, *Sso*Pox 36.36%). Four interface residues differ from *Sis*Lac to *Sso*Pox but these substitutions do not fully explain the observed differences. Interestingly, the superposition of *Sis*Lac and *Sso*Pox monomers shows a relative movement of the second *Sis*Lac monomer of about 5 Å relative to *Sso*Pox's, revealing that the interface area is slightly shifted (**Fig. 5B**). This reorganization of the dimer interface appears to be due to the substitution Q34Y, although it could also originate from the different crystal packing of both proteins. Whereas the two Q34 interact with each other's in *Sso*Pox structure, the bulkiness of both Y34 in *Sis*Lac imposes a reorientation of the dimer (**Fig. 5C**). This reorientation increases the monomers interpenetration, and makes one closer to the active site of the other. This trend was previously described while comparing the *P. diminuta* PTE and *Sso*Pox structures [47], although these enzymes are far more divergent in sequence (about 30% identity). Although the biological importance and catalytic influence of dimerization for these enzymes remain unclear, second shell active site residues are notably involved in dimer formation.

Key Substitutions between SisLac and SsoPox

The structural analysis revealed that the positions 14 and 34 seem to be the major impacting variations between *Sis*Lac and *Sso*Pox structures, that may relate to dimerization changes (position 34) or stability (positions 14, 34). Mutational intermediates between *Sis*Lac and *Sso*Pox have been constructed to evaluate the consequences of these substitutions (E14K and Y34Q) for the enzyme stability and activity. All the variants exhibit lower Tm as compared to *Sis*Lac (102±2°C) and *Sso*Pox (106°C) [6] while double variants (Y34Q-E14K) present the highest Tm among the variants (**Table 7**). The analysis of Tm reveals that the substitution Y34Q and E14K are destabilizing on *Sis*Lac background but the combination of both variations tends to restore partially the stability (**Table 7**). Additionally, the mutants have been characterized for catalytic activity against ethyl/methyl-paraoxon and for the best AHL, δ-lactone and γ-lactone substrates of *wt* *Sis*Lac (**Table 8**). The efficiency of methyl-paraoxon hydrolysis is similar for *wt* and the mutants, whereas the mutants exhibit higher catalytic efficiency against ethyl-paraoxon than the *wt* enzyme. However, the mutants exhibit a dramatically reduced AHLase activity (**Table 8**). A similar trend is observed with δ/γ-lactones. These results clearly highlight the critical importance of these positions for *Sis*Lac stability and activity, and validate our structural analysis.

Discussion

Catalytic Properties of *Sis*Lac

The pH dependence of *Sis*Lac was investigated and yields a bell-shaped curve with a pH optimum at pH 9, a consistent behavior with previously characterized PLLs [6,7] and PTEs [48]. This pH dependence profile is also in agreement with the commonly accepted hydrolysis mechanism where a water molecule activated

Table 6. Oxo-lactone lactonase activity of *Sis*Lac.

Family	Substrate	*Sis*Lac		
		k_{cat} (s^{-1})	K_M (μM)	k_{cat}/K_M ($s^{-1}M^{-1}$)
γ-lactone	**γ-butyrolactone (VII)**	5.75±0.63	158±38	3.64(±1.27)×10^4
	γ-heptanolide (*r*) (VIII)	5.89±0.07	128±10	4.61(±0.09)×10^4
	Nonanoic-γ-lactone (*r*) (IX)	3.10±0.13	15±8	2.04(±1.12)×10^5
	Undecanoic-γ-lactone (*r*) (X)	2.15±0.13	391±90	5.49(±1.59)×10^3
	Dodecanoic-γ-lactone (*r*) (XI)	1.49±0.08	475±83	3.14(±0.72)×10^3
δ-lactone	**δ-valerolactone (XII)**	0.43±0.09	1 949±1 056	2.20(±1.65)×10^2
	Nonanoic-δ-lactone (*r*) (XIII)	51.70±1.67	62±22	8.28(±3.14)×10^5
	Undecanoic-δ-lactone (*r*) (XIV)	17.65±0.38	<10	>1.77(±0.04)×10^6
	Dodecanoic-δ-lactone (*r*) (XV)	11.09±0.71	124±36	8.95(±3.16)×10^4
Others	**ε-caprolactone (XVI)**	7.27±0.31	367±54	1.98(±0.38)×10^4
	Dihydrocoumarin (XVII)	11.50±0.37	1 122±75	1.04(±1.02)×10^4

Data obtained with cobalt as cofactor. Roman numeration corresponds to chemical structures of **Fig. S2**.
doi:10.1371/journal.pone.0047028.t006

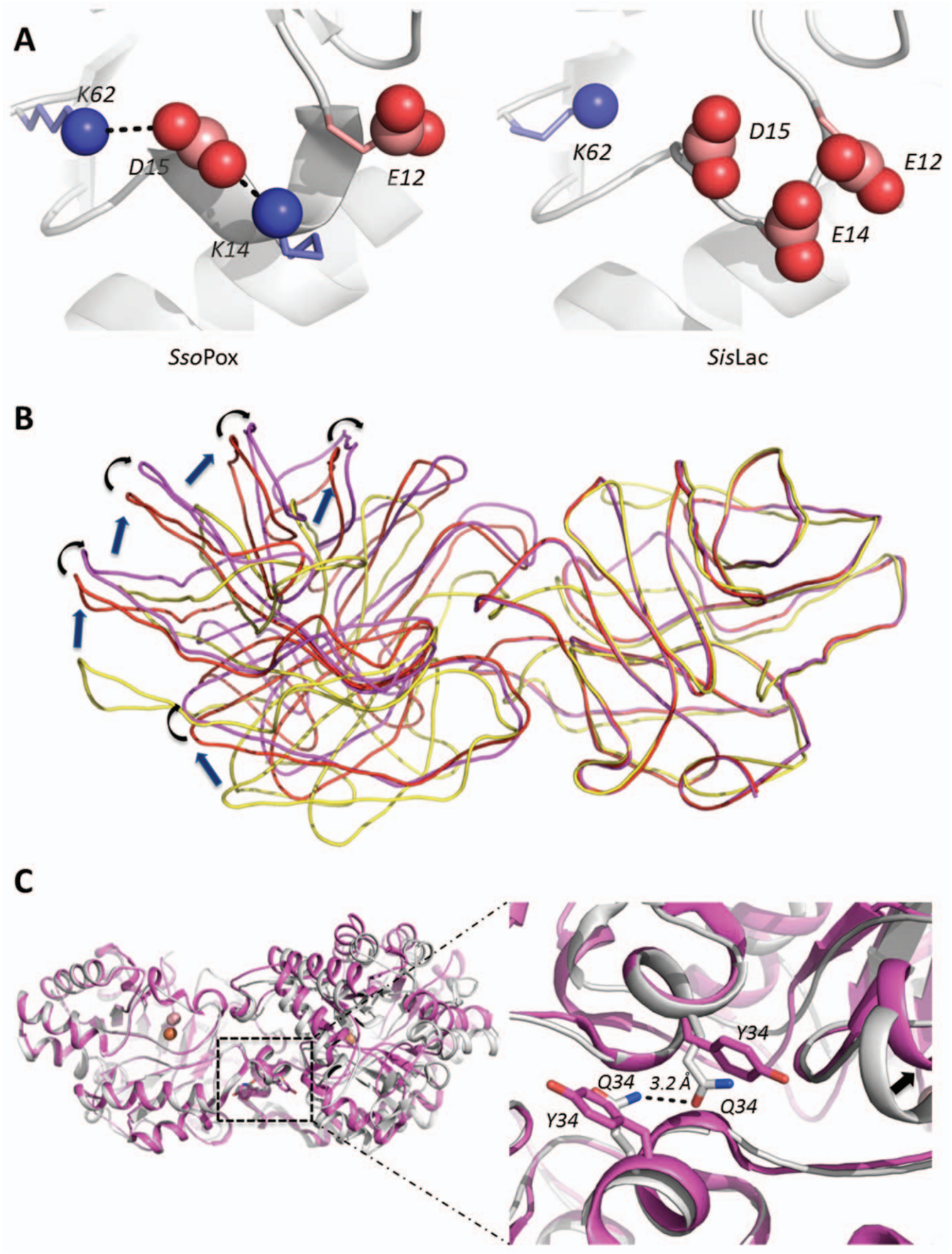
A
K62
D15
E12
K14
SsoPox
K62
D15
E12
E14
SisLac
B
C
Y34
Q34
3.2 Å
Q34
Y34

Figure 5. Structural analysis. A- Close view on position 14 in *Sso*Pox (left side) and *Sis*Lac (right side) structures. Negatively and positively charged residues are represented as red and blue spheres, respectively. Black dashed lines correspond to the putative salt-bridges in *Sso*Pox. **B**- Structural comparisons of the dimers of *Sis*Lac (*violet*), *Sso*Pox (*red*) and *P. diminuta* PTE (*yellow*). One monomer was used to superpose the three structures (shown on the right side), thus indicating the conformational shift in the position of the second monomer (left side). The differences are highlighted by blue arrows (*P. diminuta* PTE *versus Sso*Pox) or by black arrows (*Sso*Pox *versus Sis*Lac). When compared to *P. diminuta* PTE, the rotational shift observed in *Sis*Lac is more pronounced than that of *Sso*Pox. **C**- Close view on position 34 in *Sso*Pox (grey) and *Sis*Lac (violet). Black dashed lines correspond to the hydrogen bond between Q34 of each monomer of *Sso*Pox with a distance of 3.2 Å. The black arrow shows the rotational shift that seems to be induced by this substitution.
doi:10.1371/journal.pone.0047028.g005

by the bi-metallic active site serves as nucleophile [13]. Additionally, the metal dependence was assayed and the metal nature was found to modulate the catalytic activities, as previously described in PTEs [19] and PLLs [34]. Amongst the tested metals, *Sis*Lac shows preference for cobalt cations for both lactonase and paraoxonase activities (**supplementary information & Fig. S6**), as previously reported for the paraoxonase activity of *Sso*Pox [6] and the lactonase activity of *Dr*OPH [34], MCP [4] and *Gk*L [9]. The metal dependence of *Sis*Lac may be related to the relative pK_a of considered metal with H_2O, since the pK_a of Co^{2+}/H_2O is lower than that of Zn^{2+}/H_2O and Mn^{2+}/H_2O (8.9 *versus* 9.0, and 10.6, respectively [20]), thus Co^{2+} would better contribute to the activation of the nucleophile. In addition, Co^{2+} is more electronegative than Zn^{2+} and Mn^{2+} (1.88 *versus* 1.65 and 1.55, respectively [19]), thus being more efficient for stabilizing the developing negative charge on the transition state.

Phosphotriesterase Activity

The catalytic efficiency of paraoxon hydrolysis by *Sis*Lac at 25°C ($k_{cat}/k_M = 2.60(\pm 0.58)\times 10^2$ $M^{-1}s^{-1}$) shows that *Sis*Lac is endowed with one of the highest paraoxonase activity amongst PLLs [3,4,5,6,8,9]. Moreover, this activity can be considerably increased by addition of 0.1% SDS (25 folds), suggesting that the enzyme has an interesting potential for catalytic improvement. The potential of this enzyme for organophosphorus compounds bio-decontamination is further illustrated by its ability to hydrolyze the nerve agent analog CMP-coumarin with significant efficiency ($k_{cat}/K_M = 4.26(\pm 1.86)\times 10^3$ $M^{-1}s^{-1}$).

Interestingly, we observed that methyl-paraoxon is a better substrate than ethyl-paraoxon, the same trend being monitored between methyl and ethyl-parathion. The fact that smaller substituents on the phosphorus center are preferred by the enzyme is consistent with the promiscuous nature of paraoxonase activity in *Sis*Lac. Moreover, the higher compaction of the *Sis*Lac monomer makes active sites closer one to each other in the dimer as compared to *Sso*Pox structure and thus could explain the substrate preference in disfavor of bulkier substrates.

In addition, *Sis*Lac exhibits very low catalytic efficiency towards P = S containing organophosphates (*e.g.* ethyl and methyl-parathion, malathion). The K_M values are in the range of the native substrates (hundreds of μM), but the k_{cat} values are extremely low (about 3 orders of magnitude lower than P = O containing OPs), which is a typical behavior for promiscuous activities [56]. PTEs, albeit preferring paraoxon to parathion as a substrate, do not exhibit such a pronounced thiono-effect [20,55]. PTEs constitutes a protein family that are believed to have diverged from PLLs like *Sis*Lac [3] in the last few decades to specifically hydrolyzes man-made insecticides [57]. They thus may have evolved to suppress this thiono-effect in order to hydrolyze the most used pesticides (e.g. parathion).

Table 7. Melting temperature of *Sis*Lac and its variants.

Protein	Tm (°C)
*Sis*Lac *wt*	102±2
*Sis*Lac E14K	96±1
*Sis*Lac Y34Q	94±2
*Sis*Lac E14K-Y34Q	98±2

doi:10.1371/journal.pone.0047028.t007

Esterase and Lactonase Activity

PLLs have been previously characterized as poor esterases [3], and so is *Sis*Lac. Amongst the five tested esters, only *p*NP-acetate is a substrate for *Sis*Lac. The natural substrates of PLLs, lactones, being a specific class of esters, it is thus surprising that PLLs exhibit low esterase activity. It might results from a rather good binding to the active site (as suggested by observed K_M for *p*NP-acetate), but with a large fraction of non-productive binding (very low k_{cat}).

PLLs are natural lactonases that might be involved in *quorum* quenching [13]. Their precise substrates and biological function(s) are however still unknown. Lactones encompass two major families of compounds, the lipophilic aroma (oxo-lactones) and the Acyl Homoserine Lactones (AHLs) involved in *quorum* sensing. The *quorum* sensing is common in bacteria, but its existence in the archaeal world remains unclear, despite the finding of AHL-based *quorum* sensing stimulating molecules in *Natronoccocus occultus* [58], the presence of biofilms in *Sulfolobus sp.* [59] and the recent characterization of complete carboxylated-AHLs *quorum* sensing system in methanogenic archaeon [60].

Our kinetic experiments show that *Sis*Lac prefers long aliphatic chain lactones, exhibiting optimal activity when the acyl chain contains 7 carbon atoms, as seen for *Sso*Pox [52]. *Sis*Lac show also preference for 3-oxo-AHLs and hydrolyzes poorly short chain AHLs. It is interesting to notice that other PLLs, like AhlA and PPH, hydrolyze short and long chain lactones with similar catalytic efficiency [3]. It is thus possible that within the PLL family, different sub-groups of enzymes exhibit different specificities, and thus possibly different physiological functions. In addition, we show that *Sis*Lac is a proficient enzyme against oxo-lactones (best substrate: undecanoic-δ-lactone, $k_{cat}/k_M = 1.77(\pm 0.04)\times 10^6$ $M^{-1}s^{-1}$), and hydrolyzes more efficiently long chain lactones, with a preference for 5 to 6 acyl chain carbon atoms. This preference is similar to that observed for AHLs as substrates, and possibly indicates that oxo-lactones and AHLs acyl chains bind into a similar pocket, most likely the hydrophobic channel connected to the active site that was depicted for *Sso*Pox structure [13,47]. However, interestingly, whereas the short chain C4-AHL is a poor substrate for *Sis*Lac, the heptanolide-δ-lactone (3 carbon atoms in the acyl chain) shows a 10^4 higher hydrolysis efficiency. In addition, lactones with very short or without acyl chains (dihydrocoumarin, γ-butyrolactone, δ-valerolactone, ε-caprolactone) constitute better substrates than C4-AHL. Altogether, these features might reveal that γ- and δ-lactones utilize an alternate binding mode for the lactone ring than AHLs, and/or that C4-AHL does not bind in a catalytically relevant fashion to *Sis*Lac.

Table 8. Kinetic characterization of mutational intermediates between *Sis*Lac and *Sso*Pox.

Substrate	Protein	k_{cat} (s^{-1})	K_M (μM)	k_{cat}/K_M ($M^{-1}s^{-1}$)
Ethyl Paraoxon	*Sis*Lac *wt*	1.42±0.09	5439±873	$2.60(\pm0.58)\times10^2$
	*Sis*Lac E14K	0.14±0.01	30±5	$4.50(\pm0.80)\times10^3$
	*Sis*Lac Y34Q	0.13±0.01	150±12	$8.66(\pm0.89)\times10^2$
	*Sis*Lac E14K-Y34Q	0.17±0.01	132±19	$1.28(\pm0.22)\times10^3$
Methyl Paraoxon	*Sis*Lac *wt*	7.40±1.26	1739±417	$4.26(\pm1.74)\times10^3$
	*Sis*Lac E14K	0.30±0.01	50±6	$6.00(\pm0.80)\times10^3$
	*Sis*Lac Y34Q	0.42±0.01	261±24	$1.61(\pm0.19)\times10^3$
	*Sis*Lac E14K-Y34Q*	0.86±0.21	620±198	$1.39(\pm0.78)\times10^3$
3-oxo-C8-AHL (*r*)	*Sis*Lac *wt*	4.1±0.09	42±7	$9.70(\pm1.84)\times10^4$
	*Sis*Lac E14K	0.85±0.06	917±150	$9.27(\pm2.17)\times10^2$
	*Sis*Lac Y34Q	0.92±0.05	1214±135	$7.58(\pm1.25)\times10^2$
	*Sis*Lac E14K-Y34Q	0.97±0.04	1017±98	$9.54(\pm1.31)\times10^2$
nonanoic-γ- lactone (*r*)	*Sis*Lac *wt*	3.10±0.13	15±8	$2.04(\pm1.12)\times10^5$
	*Sis*Lac E14K	1.88±0.07	25±10	$7.52(\pm3.29)\times10^4$
	*Sis*Lac Y34Q	1.91±0.05	61±9	$3.13(\pm0.17)\times10^4$
	*Sis*Lac E14K-Y34Q	1.99±0.12	47±18	$4.23(\pm1.87)\times10^4$
Undecanoic-δ- lactone (*r*)	*Sis*Lac *wt*	17.65±0.38	<10	$>1.77(\pm0.04)\times10^6$
	*Sis*Lac E14K	14.09±0.59	42±16	$3.35(\pm1.41)\times10^5$
	*Sis*Lac Y34Q	12.80±0.51	121±22	$1.06(\pm0.23)\times10^5$
	*Sis*Lac E14K-Y34Q	12.91±0.58	43±13	$3.00(\pm1.04)\times10^5$

Data obtained with cobalt as cofactor. * Hydrolysis of methyl-paraoxon by *Sis*Lac E14K-Y34Q exhibits a substrate inhibition profile with $K_I = 855\pm376$ μM.
doi:10.1371/journal.pone.0047028.t008

Structural Determinants for Thermal Stability

The major structural determinants explaining the high thermal stability of hPLLs have been documented with the example of *Sso*Pox [47], the comparison with *Gs*P and *Dr*OPH enzymes [8], and are part of the classical properties described for hyperthermostable proteins [61]. The structures of these enzymes, including *Sis*Lac, exhibit a high number of salt bridges organized in complex networks of charges at the protein surface that may rigidify the global protein architecture. Moreover, the homodimer interface is larger and more hydrophobic (see Results) and the overall structure is more compact than mesophilic counterparts [47]. Here we observed that the interface area between *Sis*Lac's monomers is slightly shifted, as compared with *Sso*Pox structure. This reorganization of the dimer interface is consistent with observations made in solution. Indeed, as observed in crystals, both enzymes are dimeric at 25°C. The importance of hydrophobic contacts within the dimer interface of *Sis*Lac and *Sso*Pox explain the dimerization of the proteins. Since the hydrophobic effect increases with temperature, it is highly probable that these enzymes could be dimers at physiological temperatures (50–90°C) [2,49].

Interestingly, both *Sulfolobus* species from which *Sis*Lac and *Sso*Pox enzymes originates lives in similarly extreme environments (*S. solfataricus* from 50 to 87°C [49], *S. islandicus* from 59 to 91°C [2]) and exhibit similar thermostability ($T_m = 102\pm2$°C for *Sis*Lac and $T_m = 106$°C for *Sso*Pox [6]). Taking advantage from their high sequence identity between the two proteins, we studied the substitution K14E in *Sis*Lac (as compared to *Sso*Pox) that breaks a salt bridge network at the C-terminus of the protein, a region concentrating the highest divergences among hPLLs as revealed by sequence alignment (*i.e.* *Sso*Pox, *Sac*Pox and *Sis*Lac). E14 engenders in *Sis*Lac a cluster of 3 negatively charged residues at the surface of the structure allowing to evaluate the contribution of these electrostatic interactions to the enzyme stability and activity. Moreover, another key substitution occurred between the two enzymes in the homodimerization interface. Q34Y is indeed a key substitution in the interface since it consists in a "pivot" residue, *i.e.* a residue that contacts its equivalent in the second protein molecule while forming the dimer, and seems to be responsible for the observed dimerization shift between *Sis*Lac and *Sso*Pox structures. Q34Y is, moreover, the substitution between *Sis*Lac and *Sso*Pox that is the closest in space to the active site (second shell). We therefore studied the effects of this variation on *Sis*Lac's activity and stability.

Surprisingly, whereas K14 in *Sso*Pox is involved in a large network of charged interactions and may contribute to the overall protein rigidity [47], the variation E14K in *Sis*Lac is destabilizing (Tm is decreased by 6°C). The variation of the pivot interface residue Y34Q is also destabilizing on *Sis*Lac background (decrease of Tm by 8°C). Interestingly, the double variant E14K-Y34Q that carries two destabilizing mutations exhibits a higher Tm than the single variants, revealing the highly epistatic nature of these positions. Moreover, whereas the promiscuous phosphotriesterase activity is not altered by these substitutions, the lactonase activity, especially the AHLase activity is considerably reduced (by ~100 folds) as compared to *wt*. The influence of E14K on *Sis*Lac's catalytic activity is not obvious from a structural analysis. However, position 34 comprises a second shell residue, and the overall dimer interface is in the vicinity of the active site. Mutation of position 34 highly influences the protein dimerization and thus the degree of monomers interpenetration. Monomer active sites being close one to each other, their interpenetration could influence substrate specificities and catalytic efficiencies by fine steric or dynamic constraints which can't be evaluated by

structural analysis. These identified key substitutions, however, does not fully explain the observed different catalytic properties of *Sis*Lac and *Sso*Pox. The active site residues and configuration of these two enzymes being similar, these discrepancies might be partly mediated by yet unidentified substitutions distant from the active site.

Reconstructed mutational intermediates between *Sis*Lac and *Sso*Pox have lower fitness both in term of stability and AHLase activity. Despite the very high sequence identity between both proteins (91%), it may indicate that the evolutionary route that links them already comprise a fraction of highly epistatic mutations. In other words, the mutations that accumulate at a very early stage of divergence might not only be neutral but a fraction of them are highly cooperative.

Supporting Information

Figure S1 Chemical structure of phosphotriesters (I-VI) and esters (VII-XI).
(DOC)

Figure S2 Chemical structure of AHLs (I-VI), γ-lactones (VII-XI), δ-lactones (XII-XV) and other lactones (XVI-XVII).
(DOC)

Figure S3 Electronic density map of *Sis*Lac at 2.7 Å resolution.
(DOC)

Figure S4 Sequence alignment of PLLs from Sulfolobus species.
(DOC)

Figure S5 Thermostability analysis of *Sis*Lac by circular dichroism.
(DOC)

Figure S6 *Sis*Lac metal preference.
(DOC)

Information S1 Supplementary information for *Sis*Lac metal preferences.
(DOC)

Table S1 Primers used for site directed mutagenesis.
(DOC)

Table S2 Kinetics protocols.
(DOC)

Table S3 Ethyl-paraoxonase comparison between *Sso*Pox, *Sac*Pox and *Sis*Lac.
(DOC)

Table S4 Phosphotriesterase activity comparison between *Gs*P, *Dr*OPH and *Sso*Pox and *Sis*Lac.
(DOC)

Acknowledgments

We are grateful to Prof. Dan S. Tawfik for fruitful discussions and to Dr. Moshe Goldsmith for the kind gift of CMP-coumarin. We thank the AFMB laboratory (Marseille, France) for the access to protein production and crystallization platforms.

Accession Number

The coordinate file and the structure factors file of the *Sis*Lac structure have been deposited to the Protein Data Bank under the accession number 4G2D.

Author Contributions

Conceived and designed the experiments: ME JH EC. Performed the experiments: ME JH GG. Analyzed the data: ME JH EC. Wrote the paper: ME JH.

References

1. Gotthard G, Hiblot J, Elias M, Chabriere E (2011) Crystallization and preliminary X-ray diffraction analysis of the hyperthermophilic Sulfolobus islandicus lactonase. Acta crystallographica Section F, Structural biology and crystallization communications 67: 354–357.
2. Reno ML, Held NL, Fields CJ, Burke PV, Whitaker RJ (2009) Biogeography of the Sulfolobus islandicus pan-genome. Proc Natl Acad Sci U S A 106: 8605–8610.
3. Afriat L, Roodveldt C, Manco G, Tawfik DS (2006) The latent promiscuity of newly identified microbial lactonases is linked to a recently diverged phosphotriesterase. Biochemistry 45: 13677–13686.
4. Chow JY, Wu L, Yew WS (2009) Directed evolution of a quorum-quenching lactonase from Mycobacterium avium subsp. paratuberculosis K-10 in the amidohydrolase superfamily. Biochemistry 48: 4344–4353.
5. Hawwa R, Larsen SD, Ratia K, Mesecar AD (2009) Structure-based and random mutagenesis approaches increase the organophosphate-degrading activity of a phosphotriesterase homologue from Deinococcus radiodurans. J Mol Biol 393: 36–57.
6. Merone L, Mandrich L, Rossi M, Manco G (2005) A thermostable phosphotriesterase from the archaeon Sulfolobus solfataricus: cloning, overexpression and properties. Extremophiles 9: 297–305.
7. Porzio E, Merone L, Mandrich L, Rossi M, Manco G (2007) A new phosphotriesterase from Sulfolobus acidocaldarius and its comparison with the homologue from Sulfolobus solfataricus. Biochimie 89: 625–636.
8. Hawwa R, Aikens J, Turner RJ, Santarsiero BD, Mesecar AD (2009) Structural basis for thermostability revealed through the identification and characterization of a highly thermostable phosphotriesterase-like lactonase from Geobacillus stearothermophilus. Arch Biochem Biophys 488: 109–120.
9. Chow JY, Xue B, Lee KH, Tung A, Wu L, et al. (2010) Directed evolution of a thermostable quorum-quenching lactonase from the amidohydrolase superfamily. J Biol Chem 285: 40911–40920.
10. Demirjian DC, Moris-Varas F, Cassidy CS (2001) Enzymes from extremophiles. Curr Opin Chem Biol 5: 144–151.
11. Omburo GA, Kuo JM, Mullins LS, Raushel FM (1992) Characterization of the zinc binding site of bacterial phosphotriesterase. J Biol Chem 267: 13278–13283.
12. Draganov DI (2010) Lactonases with organophosphatase activity: structural and evolutionary perspectives. Chem Biol Interact 187: 370–372.
13. Elias M, Dupuy J, Merone L, Mandrich L, Porzio E, et al. (2008) Structural basis for natural lactonase and promiscuous phosphotriesterase activities. J Mol Biol 379: 1017–1028.
14. Elias M, Tawfik DS (2012) Divergence and Convergence in Enzyme Evolution: Parallel Evolution of Paraoxonases from Quorum-quenching Lactonases. J Biol Chem 287: 11–20.
15. Afriat-Jurnou L, Jackson CJ, Tawfik DS (2012) Reconstructing a missing link in the evolution of a recently diverged phosphotriesterase by active-site loop remodeling. Biochemistry.
16. Nagano N, Orengo CA, Thornton JM (2002) One fold with many functions: the evolutionary relationships between TIM barrel families based on their sequences, structures and functions. J Mol Biol 321: 741–765.
17. Vanhooke JL, Benning MM, Raushel FM, Holden HM (1996) Three-dimensional structure of the zinc-containing phosphotriesterase with the bound substrate analog diethyl 4-methylbenzylphosphonate. Biochemistry 35: 6020–6025.
18. Elias M, Dupuy J, Merone L, Lecomte C, Rossi M, et al. (2007) Crystallization and preliminary X-ray diffraction analysis of the hyperthermophilic Sulfolobus solfataricus phosphotriesterase. Acta Crystallogr Sect F Struct Biol Cryst Commun 63: 553–555.
19. Rochu D, Viguie N, Renault F, Crouzier D, Froment MT, et al. (2004) Contribution of the active-site metal cation to the catalytic activity and to the conformational stability of phosphotriesterase: temperature- and pH-dependence. Biochem J 380: 627–633.
20. Jackson CJ, Carr PD, Kim HK, Liu JW, Herrald P, et al. (2006) Anomalous scattering analysis of Agrobacterium radiobacter phosphotriesterase: the prominent role of iron in the heterobinuclear active site. Biochem J 397: 501–508.
21. Ben-David M, Elias M, Filippi JJ, Dunach E, Silman I, et al. (2012) Catalytic versatility and backups in enzyme active sites: the case of serum paraoxonase 1. J Mol Biol 418: 181–196.

22. Hentzer M, Wu H, Andersen JB, Riedel K, Rasmussen TB, et al. (2003) Attenuation of Pseudomonas aeruginosa virulence by quorum sensing inhibitors. EMBO J 22: 3803–3815.
23. Popat R, Crusz SA, Diggle SP (2008) The social behaviours of bacterial pathogens. Br Med Bull 87: 63–75.
24. Costerton JW, Stewart PS, Greenberg EP (1999) Bacterial biofilms: a common cause of persistent infections. Science 284: 1318–1322.
25. Dickschat JS (2009) Quorum sensing and bacterial biofilms. Nat Prod Rep 27: 343–369.
26. Jones MB, Peterson SN, Benn R, Braisted JC, Jarrahi B, et al. (2010) Role of luxS in Bacillus anthracis growth and virulence factor expression. Virulence 1: 72–83.
27. Amara N, Krom BP, Kaufmann GF, Meijler MM (2011) Macromolecular inhibition of quorum sensing: enzymes, antibodies, and beyond. Chem Rev 111: 195–208.
28. Dong YH, Wang LH, Xu JL, Zhang HB, Zhang XF, et al. (2001) Quenching quorum-sensing-dependent bacterial infection by an N-acyl homoserine lactonase. Nature 411: 813–817.
29. Dong YH, Xu JL, Li XZ, Zhang LH (2000) AiiA, an enzyme that inactivates the acylhomoserine lactone quorum-sensing signal and attenuates the virulence of Erwinia carotovora. Proc Natl Acad Sci U S A 97: 3526–3531.
30. Ma F, Wang Y, Zhang Y, Xiong N, Yang B, et al. (2009) Heterologous expression of human paraoxonases in Pseudomonas aeruginosa inhibits biofilm formation and decreases antibiotic resistance. Appl Microbiol Biotechnol 83: 135–141.
31. Reimmann C, Ginet N, Michel L, Keel C, Michaux P, et al. (2002) Genetically programmed autoinducer destruction reduces virulence gene expression and swarming motility in Pseudomonas aeruginosa PAO1. Microbiology 148: 923–932.
32. Dong YH, Wang LY, Zhang LH (2007) Quorum-quenching microbial infections: mechanisms and implications. Philos Trans R Soc Lond B Biol Sci 362: 1201–1211.
33. Singh BK (2009) Organophosphorus-degrading bacteria: ecology and industrial applications. Nat Rev Microbiol 7: 156–164.
34. Xiang DF, Kolb P, Fedorov AA, Meier MM, Fedorov LV, et al. (2009) Functional annotation and three-dimensional structure of Dr0930 from Deinococcus radiodurans, a close relative of phosphotriesterase in the amidohydrolase superfamily. Biochemistry 48: 2237–2247.
35. Studier FW (2005) Protein production by auto-induction in high density shaking cultures. Protein Expr Purif 41: 207–234.
36. Kabsch W (1993) Automatic processing of rotation diffraction data from crystals of initially unknown symmetry land cell constants. J Appl Cryst 26: 795–800.
37. Zwart PH G-KR, Adams PD (Winter 2005) Xtriage and Fest: automatic assessment of X-ray data and substructure structure factor estimation. CCP4 newsletter No.43.
38. Adams PD, Grosse-Kunstleve RW, Hung LW, Ioerger TR, McCoy AJ, et al. (2002) PHENIX: building new software for automated crystallographic structure determination. Acta Crystallogr D Biol Crystallogr 58: 1948–1954.
39. A. J. McCoy RWG-K, P. D Adams, M. D Winn, L. C Storoni and R. J Read (2007) Phaser crystallographic software. J Appl Cryst 40: 658–674.
40. Vagin A, Steiner RS, Lebedev AA, Potterton L, McNicholas S, Long F and Murshudov GN (2004) REFMAC5 dictionary: organisation of prior chemical knowledge and guidelines for its use. Acta Cryst D60: 2284–2295.
41. Emsley P, Cowtan K (2004) Coot: model-building tools for molecular graphics. Acta Crystallogr D Biol Crystallogr 60: 2126–2132.
42. Reynolds DJ Protorp: a protein-protein interaction analysis tool. Bioinformatics: Submitted.
43. Guex N, Peitsch MC (1997) SWISS-MODEL and the Swiss-PdbViewer: an environment for comparative protein modeling. Electrophoresis 18: 2714–2723.
44. Poirot O, O'Toole E, Notredame C (2003) Tcoffee@igs: A web server for computing, evaluating and combining multiple sequence alignments. Nucleic Acids Res 31: 3503–3506.
45. Notredame C, Higgins DG, Heringa J (2000) T-Coffee: A novel method for fast and accurate multiple sequence alignment. J Mol Biol 302: 205–217.
46. Gouy M, Guindon S, Gascuel O (2010) SeaView version 4: A multiplatform graphical user interface for sequence alignment and phylogenetic tree building. Mol Biol Evol 27: 221–224.
47. Del Vecchio P, Elias M, Merone L, Graziano G, Dupuy J, et al. (2009) Structural determinants of the high thermal stability of SsoPox from the hyperthermophilic archaeon Sulfolobus solfataricus. Extremophiles 13: 461–470.
48. Dumas DP, Raushel FM (1990) Chemical and kinetic evidence for an essential histidine in the phosphotriesterase from Pseudomonas diminuta. J Biol Chem 265: 21498–21503.
49. Auernik KS, Cooper CR, Kelly RM (2008) Life in hot acid: pathway analyses in extremely thermoacidophilic archaea. Curr Opin Biotechnol 19: 445–453.
50. Nazina TN, Tourova TP, Poltaraus AB, Novikova EV, Grigoryan AA, et al. (2001) Taxonomic study of aerobic thermophilic bacilli: descriptions of Geobacillus subterraneus gen. nov., sp. nov. and Geobacillus uzenensis sp. nov. from petroleum reservoirs and transfer of Bacillus stearothermophilus, Bacillus thermocatenulatus, Bacillus thermoleovorans, Bacillus kaustophilus, Bacillus thermodenitrificans to Geobacillus as the new combinations G. stearothermophilus, G. th. Int J Syst Evol Microbiol 51: 433–446.
51. McMullan G, Christie JM, Rahman TJ, Banat IM, Ternan NG, et al. (2004) Habitat, applications and genomics of the aerobic, thermophilic genus Geobacillus. Biochem Soc Trans 32: 214–217.
52. Ng FS, Wright DM, Seah SY (2010) Characterization of a phosphotriesterase-like lactonase from Sulfolobus solfataricus and its immobilization for quorum quenching. Appl Environ Microbiol.
53. Merone L, Mandrich L, Porzio E, Rossi M, Muller S, et al. (2010) Improving the promiscuous nerve agent hydrolase activity of a thermostable archaeal lactonase. Bioresour Technol 101: 9204–9212.
54. Ashani Y, Gupta RD, Goldsmith M, Silman I, Sussman JL, et al. (2010) Stereospecific synthesis of analogs of nerve agents and their utilization for selection and characterization of paraoxonase (PON1) catalytic scavengers. Chem Biol Interact 187: 362–369.
55. Dumas DP, Caldwell SR, Wild JR, Raushel FM (1989) Purification and properties of the phosphotriesterase from Pseudomonas diminuta. J Biol Chem 264: 19659–19665.
56. Khersonsky O, Tawfik DS (2010) Enzyme promiscuity: a mechanistic and evolutionary perspective. Annual review of biochemistry 79: 471–505.
57. Raushel FM (2002) Bacterial detoxification of organophosphate nerve agents. Curr Opin Microbiol 5: 288–295.
58. Paggi RA, Martone CB, Fuqua C, De Castro RE (2003) Detection of quorum sensing signals in the haloalkaliphilic archaeon Natronococcus occultus. FEMS Microbiol Lett 221: 49–52.
59. Koerdt A, Godeke J, Berger J, Thormann KM, Albers SV (2010) Crenarchaeal biofilm formation under extreme conditions. PLoS One 5: e14104.
60. Zhang G, Zhang F, Ding G, Li J, Guo X, et al. (2012) Acyl homoserine lactone-based quorum sensing in a methanogenic archaeon. ISME J.
61. Vieille C, Zeikus GJ (2001) Hyperthermophilic enzymes: sources, uses, and molecular mechanisms for thermostability. Microbiol Mol Biol Rev 65: 1–43.

C. Cristallisation et collectes des données d'OPHC2

Crystallization and preliminary X-ray diffraction analysis of the organophosphorus hydrolase OPHC2 from *Pseudomonas pseudoalcaligenes*

Guillaume GOTTHARD, Julien HIBLOT*, Daniel GONZALEZ, Eric CHABRIERE and Mikael ELIAS*

* Contribution égale

Dans les travaux décrits, j'ai réalisé :

- partie expérimentale : expression, purification de l'enzyme, cristallisation, collecte des données, traitement des données et phasage
- rédaction de l'article et soumission

Résumé : Ce travail concerne la mise au point des conditions d'expression recombinante et de purification d'OPHC2. Sont également rapportées l'identification des conditions de cristallisation de l'enzyme et l'analyse des premières données de diffraction aux rayons X de OPHC2. Enfin est rapportée la méthode utilisée pour le phasage par remplacement moléculaire qui nécessita plusieurs ajustements successifs du modèle utilisé. Ce travail intervient en amont de l'étude des relations structure-fonction de l'enzyme dans le but de mieux comprendre : (i) les détails moléculaires à l'origine de la thermo-résistance d'OPHC2 et (ii) les mécanismes moléculaires d'hydrolyse des OPs par l'enzyme.

Acta Crystallographica Section F
Structural Biology and Crystallization Communications
ISSN 1744-3091

Crystallization and preliminary X-ray diffraction analysis of the organophosphorus hydrolase OPHC2 from *Pseudomonas pseudoalcaligenes*

Guillaume Gotthard,[a]‡ Julien Hiblot,[a]‡ Daniel Gonzalez,[a] Eric Chabrière[a,b]* and Mikael Elias[c]*

[a]Aix Marseille Université, URMITE, UM63, CNRS 7278, IRD 198, Inserm 1095, 13005 Marseille, France, [b]Département de Toxicologie, Institut de Recherches Biomédicales des Armées-CRSSA, BP 87, 38702 La Tronche CEDEX, France, and [c]Biological Chemistry, Weizmann Institute of Science, Rehovot 76100, Israel

‡ These authors contributed equally.

Correspondence e-mail: eric.chabriere@univmed.fr, mikael.elias@weizmann.ac.il

Received 19 October 2012
Accepted 11 December 2012

Enzymes that are capable of degrading neurotoxic organophosphorus compounds are of increasing interest because of the lack of efficient and clean methods for their removal. Recently, a novel organophosphorus hydrolase belonging to the metallo-β-lactamase superfamily was identified and isolated from the mesophilic bacterium *Pseudomonas pseudoalcaligenes*. This enzyme, named OPHC2, is endowed with significant thermal and pH stability, making it an appealing candidate for engineering studies to develop an efficient organophosphorus biodecontaminant. Combined with biochemical studies, structural information will help decipher the catalytic mechanism of organophosphorus hydrolysis by OPHC2 and identify the residues involved in its substrate specificity. Here, the expression, purification, crystallization and X-ray data collection at 2.1 Å resolution of OPHC2 are presented.

1. Introduction

Organophosphorus compounds (OPs) are well known toxic molecules that irreversibly inhibit acetylcholinesterase, a key enzyme in the nerve message transmission system (Singh, 2009). These compounds have been widely used as agricultural insecticides (Raushel, 2002) and the most toxic compounds have also been developed as chemical warfare agents (such as tabun, sarin, soman or VX; Gupta, 2009). Current methods for removing them are slow, expensive and engender ecological concerns (LeJeune *et al.*, 1998). Novel methods of remediation, such as enzyme-mediated decontamination, are therefore under intensive research (Bigley & Raushel, 2012; Goldsmith *et al.*, 2012).

The intensive use of OPs as pesticides starting in the 1950s has resulted in the rapid emergence of microorganisms that are able to degrade OPs and can probably utilize them as carbon and phosphorus sources (Pakala *et al.*, 2007). Several organophosphorus hydrolases have been identified belonging to different protein families: the prolidases (Cheng *et al.*, 1999), the paraoxonases (PONs; Ben-David *et al.*, 2012), the phosphotriesterases (PTEs) and phosphotriesterase-like lactonases (PLLs) from the amidohydrolase superfamily and the organophosphorus hydrolases from the metallo-β-lactamase superfamily (Elias & Tawfik, 2012). The PTEs isolated from *Brevundimonas diminuta* (Omburo *et al.*, 1992) and *Agrobacterium radiobacter* (Jackson *et al.*, 2006) are the best characterized organophosphorus hydrolases so far and exhibit near-diffusion-limit rates against the insecticide paraoxon as a substrate (Omburo *et al.*, 1992). PTEs are believed to have emerged from native lactonases with promiscuous phosphotriesterase activity such as the PLLs (Afriat-Jurnou *et al.*, 2012; Elias *et al.*, 2008; Hiblot *et al.*, 2012*a*).

A novel organophosphorus hydrolase named OPHC2 (GenBank ID AJ605330) has been isolated from *Pseudomonas pseudoalcaligenes* (Chu *et al.*, 2006). This enzyme is the second characterized representative of a recently identified organophosphorus hydrolase clade. OPHC2 shares 57.9% sequence identity with methyl-parathion hydrolase (MPH), a protein isolated from *Pseudomonas* sp. WBC3 (GenBank ID AY251554), a soil bacterium living in organophosphorus-contaminated soil in China (Dong *et al.*, 2005). The structure of MPH has previously been solved (Dong *et al.*, 2005) and revealed a metallo-β-lactamase fold containing a bimetallic catalytic site and a bridging water molecule. This feature, also found in PLLs and PTEs,

might suggest a similar catalytic mechanism in which the bridging catalytic water molecule is activated by the bimetallic active site and serves as the nucleophile that attacks the phosphorus centre of the bound substrate (Dong *et al.*, 2005).

OPHC2 has been shown to exhibit methyl-parathion hydrolysing activity (Chu *et al.*, 2006). While OPHC2 originates from a mesophilic bacterium (*P. pseudoalcaligenes*), its temperature optimum for catalysis is 338 K. Possible explanations for this feature have been hypothesized, such as a putative disulfide bridge and a higher number of surface salt bridges compared with MPH (Chu *et al.*, 2010). Given its organophosphorus hydrolase activity, combined with thermal and pH stability (Chu *et al.*, 2006), OPHC2 represents an interesting target for attempts to develop an efficient OP biodecontaminant. The structure of OPHC2 will thus help to decipher the structural determinants that account for its thermal stability. Moreover, the comparative analysis of MPH and OPHC2 structures and their careful biochemical characterization will lead to the identification of key residues involved in substrate binding and enzymatic specificity. This information will serve to engineer and improve OPHC2 catalytic efficiency against organophosphorus compounds. In this report, we describe the expression, purification, crystallization and X-ray data collection of OPHC2.

2. Cloning, expression and purification of OPHC2

The full gene encoding for OPHC2 with its N-terminus periplasmic signal peptide (UniProt ID Q5W503) was optimized for *Escherichia coli* expression and synthesized by GeneArt (Life Technologies, France). The gene was subsequently cloned into a custom version of pET22-b(+) (Novagen) containing an N-terminal streptavidin peptide (for affinity chromatography purification) and a tobacco etch virus protease (TEV) cleavage site (for removal of the tag; Gotthard *et al.*, 2011) using *Nde*I and *Xho*I as cloning sites to avoid adding the plasmid's *pelB* leader sequence. Recombinant OPHC2 protein was overexpressed using a protocol similar to that used for the PLLs *Sso*Pox and *Sis*Lac (Hiblot *et al.*, 2012*a*,*b*). Briefly, recombinant OPHC2 protein was overproduced in *E. coli* BL21(DE3)-pGro7/GroEL (TaKaRa). Protein expression was performed in 2 l ZYP medium (100 µg ml^{-1} ampicillin, 34 µg ml^{-1} chloramphenicol) inoculated with a 50 ml overnight preculture. The culture was grown at 310 K until it reached an $OD_{600\,nm}$ of 1.0. The induction of the protein was conducted by consumption of the lactose in ZYP medium, a temperature transition to 298 K during 20 h and the addition of 0.2 m*M* $CoCl_2$. Cells were harvested by centrifugation (4500*g*, 277 K, 15 min). Pellets were resuspended in lysis buffer (50 m*M* HEPES pH 8, 150 m*M* NaCl, 0.2 m*M* $CoCl_2$, 0.25 mg ml^{-1} lysozyme, 10 µg ml^{-1} DNAse, 0.1 m*M* PMSF) and stored at 193 K for 2 h. Suspended frozen cells were thawed at 310 K for 15 min and disrupted by three steps of 30 s of sonication (QSonica sonicator Q700; amplitude at 50). Cell debris was removed by centrifugation (12 500*g*, 277 K, 30 min).

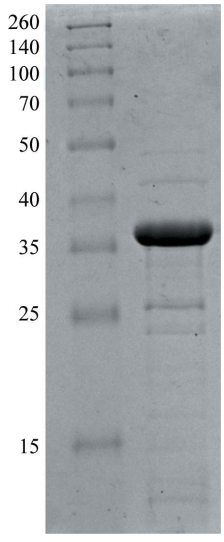

Figure 1
15% SDS–PAGE of OPHC2 protein stained with Coomassie Blue. Left lane, molecular-weight markers (Thermo Scientific Spectra Multicolor broad range protein ladder; labelled in kDa). Right lane, 11 µg OPHC2 protein.

Attempts to purify the protein using streptavidin affinity chromatography failed, indicating that the natural signal peptide of OPHC2 was recognized, processed and the protein subsequently exported to the periplasm by the *E. coli* cell machinery, which also removes the affinity tag. Consequently, another purification strategy was used: the thermal stability of OPHC2 (Chu *et al.*, 2006) was exploited for purification in combination with differential ammonium sulfate precipitation. After 30 min incubation at 342 K, host proteins that precipitated were removed by a centrifugation step (12 000*g*, 277 K, 30 min). Remaining contaminant proteins were precipitated by ammonium sulfate (2 h incubation at 277 K with 291 g l^{-1} ammonium sulfate) and discarded after a centrifugation step (12 000*g*, 277 K, 30 min). OPHC2 was then concentrated by 36 h incubation with a final ammonium sulfate concentration of 476 g l^{-1}, followed by centrifugation (15 min, 277 K, 12 000*g*) and resuspension in activity buffer (50 m*M* HEPES pH 8, 150 m*M* NaCl, 0.2 m*M* $CoCl_2$). The remaining ammonium sulfate was removed by overnight dialysis against the activity buffer. The protein was concentrated using a centrifugation device (Amicon Ultra MWCO 10 kDa; Millipore, Ireland) prior to a size-exclusion chromatography step (Superdex 75 16/60, GE Healthcare). Although the affinity tag was probably removed by the *E. coli* cell machinery while processing the signal peptide, the fractions containing the protein were pooled and submitted to a tag-removal step in order to minimize the heterogeneity of the sample. We used TEV protease [1:13(*w*:*w*) ratio for 6 h at 303 K in activity buffer] to remove the tag (van den Berg *et al.*, 2006). Precipitated TEV protease was removed by centrifugation (12 000*g*, 277 K, 10 min). The OPHC2 crystal structure did not show any tag or signal peptide. The sample was concentrated and subsequently reloaded onto a size-exclusion chromatography column in activity buffer (Superdex 75 16/60, GE Healthcare). Fractions containing pure protein were pooled and concentrated prior to crystallization trials using a centrifugation device (Amicon Ultra MWCO 10 kDa; Millipore, Ireland). The yield of production was about 8 mg per litre of culture. The purity of the protein was checked with Coomassie-stained 15% SDS–PAGE (Fig. 1).

3. Kinetic experiment

Methyl-paraoxon ($\varepsilon_{405\,nm}$ = 17 000 M^{-1} cm^{-1}) hydrolysis by OPHC2 (2 µl at 725 µg ml^{-1} in a 200 µl reaction volume) was performed in triplicates, at 298 K, in activity buffer, recorded with a microplate reader (Synergy HT, BioTek, USA) and monitored by the *Gen*5.1 software in a 6.2 mm path-length cell in 96-well plates, as described previously (Hiblot *et al.*, 2012*a*,*b*). The specific activity of OPHC2 was evaluated using *Excel* software (Microsoft, USA). The measured specific activity against methyl-paraoxon as substrate (1 m*M*) is

Table 1
Data-collection statistics.

Values in parentheses are for the last bin.

Beamline	PROXIMA-1
Wavelength (Å)	0.980
Detector	PILATUS 6M
Oscillation (°)	0.15
No. of frames	1200
Resolution (Å)	2.1 (2.2–2.1)
Space group	*C*2
Unit-cell parameters (Å, °)	a = 109.9, b = 63.8, c = 221.3, β = 101.8
No. of observed reflections	252270 (24317)
No. of unique reflections	82530 (9469)
Completeness (%)	93.7 (82.6)
$R_{\rm meas}$† (%)	6.5 (50.1)
$\langle I/\sigma(I)\rangle$	13.67 (3.07)
Multiplicity	3.06 (2.57)
Mosaicity (°)	0.508

† $R_{\rm meas} = \sum_{hkl}\{N(hkl)/[N(hkl)-1]\}^{1/2}\sum_i |I_i(hkl) - \langle I(hkl)\rangle|/\sum_{hkl}\sum_i I_i(hkl)$.

0.632 ± 0.088 µmol mg^{-1} min^{-1}. This value is slightly lower than the previously published specific activity against another substrate, methyl-parathion (1.982 µmol min^{-1} mg^{-1} at 310 K against 1.9 m*M* substrate; Chu *et al.*, 2006). This difference could be explained by the difference in the nature of the substrates, their different concentrations and the temperature of the assays, but also, as proposed previously (Ng *et al.*, 2011), by the different nature of the protein-expression system: *E. coli* in our case and *Pichia pastoris* in the previous work (Chu *et al.*, 2006).

4. Protein crystallization

OPHC2 was concentrated to 16.4 mg ml^{-1} for crystallization trials. Crystallization assays were performed using a sitting-drop vapour-diffusion method setup in a 96-well plate and the commercial screen conditions Wizard I and II (Emerald BioSystems). The plates were incubated at 293 K and monitored using a Rock Imager and Rock Maker system (Formulatrix Inc., USA). Reproducible crystals appeared after 3 months at 293 K in a condition consisting of 10% PEG 8000, 100 m*M* Tris buffer pH 7, 200 m*M* $MgCl_2$. Crystals grew in drops containing 2:1 and 1:1 protein:precipitant ratios (respective volumes of 200 nl:100 nl and 100 nl:100 nl; 200 µl reservoir volume; Fig. 2).

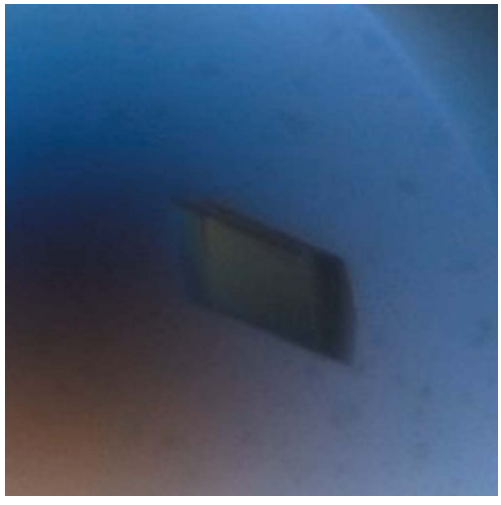

Figure 2
A typical crystal of OPHC2 (average dimensions of 170 × 80 × 40 µm).

5. Data collection

A cryoprotectant solution consisting of the crystallization solution supplemented with 20%(*v*/*v*) glycerol was added to the crystal-containing drops (1 µl cryoprotectant was added to the 200 or 300 nl drops). The crystals were then transferred in a drop (1 µl) containing the cryoprotectant solution for 1 min and flash-cooled in liquid nitrogen. X-ray diffraction intensities were collected on the PROXIMA-1 beamline at SOLEIL (Gif-Sur-Yvette, France) using a wavelength of 0.980 Å and a PILATUS 6M detector with 0.15 s exposures. Diffraction data were collected from 1200 images using the fine-slicing method; individual frames consisted of 0.15° steps over a range of 180° (Fig. 3).

6. Results and conclusions

X-ray diffraction data were integrated, scaled and merged using the *XDS* program (Kabsch, 1993; Table 1). The OPHC2 crystals belonged to the monoclinic space group *C*2, with unit-cell parameters a = 109.9, b = 63.8, c = 221.3 Å, β = 101.8°. With a molecular weight of 35 kDa for OPHC2, the calculated Matthews coefficient suggests between four and five monomers per asymmetric unit (2.71 and 2.17 Å^3 Da^{-1}, corresponding to 54.7 and 43.38% solvent content, respectively). Initial molecular replacement (MR) using a monomer of MPH as a model (PDB entry 1p9e; Y. Dong, L. Sun, M. Bartlam, Z. Rao & X. Zhang, unpublished work) was performed using *Phaser* (McCoy *et al.*, 2007). Only two molecules could initially be placed in the asymmetric unit ($R_{\rm free}$ = 50.9%), while the crystal packing was clearly incomplete and residual density corresponding to other monomers could be observed. Attempts to place additional monomers using the initial solution as a fixed input failed. The initial solution was then submitted to *ARP*/*wARP* (Morris *et al.*, 2003) for automated model construction. After 50 cycles of *ARP*/*wARP*, peptide fragments belonging to two new monomers were built and the $R_{\rm free}$ factor decreased to 39.1%, yielding electron-density maps that were sufficiently informative to evaluate the model. We identified two fragments of the protein (fragment 1, amino acids 26–166; fragment 2, amino acids 214–295) that were well defined in the initially placed monomers.

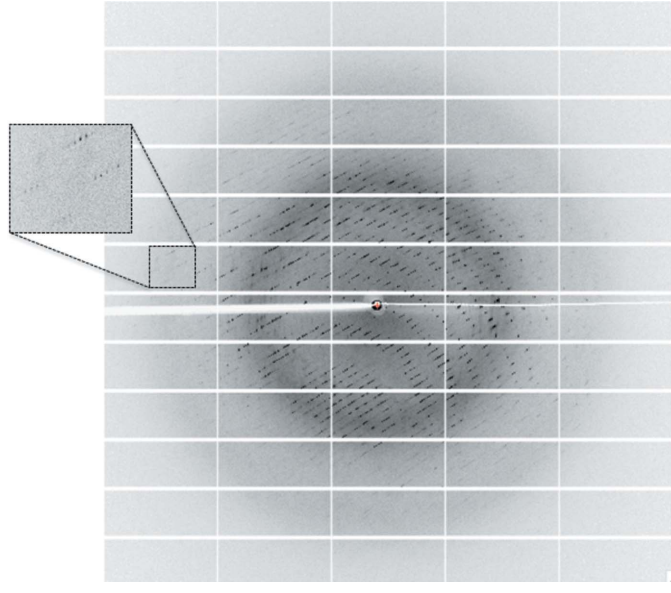

Figure 3
A diffraction pattern from a crystal of OPHC2. The edge of the diffraction frame is at 1.63 Å resolution.

However, the residues between these parts were missing from the electron-density maps, and the conformation of the equivalent residues in the starting model (PDB entry 1p9e) was incompatible with the observed crystal packing. We thus performed new MR searches by using fragments 1 and 2 as models. A total of four fragments 1 and three fragments 2 were placed using *Phaser* (R_{free} = 35.4%), revealing a total of four monomers in the asymmetric unit. The quality improvement of the maps allowed extension of the fragments using *Coot* (Emsley & Cowtan, 2004). The incomplete monomer revealed by the positioning of a fragment 1 was reconstructed by superposition of a complete monomer. Another round of MR was performed using fragments 1 and 2 as models with the previous solution as a fixed input. This allowed us to identify a fifth monomer (R_{free} = 31.7%) that forms a dimer with a symmetry-related monomer through a twofold crystallographic axis. After manual building and reconstruction of the five monomers, the current R_{free} factor is 30.21%. The asymmetric unit contains two homodimers of OPHC2 and one monomer. Notably, despite the sequence identity (57%) between MPH and OPHC2, the molecular replacement was not straightforward. Indeed, a significant fragment from OPHC2 (167–213) differs from the MPH model and is poorly defined in the OPHC2 structure. The fact that the conformation of the corresponding fragment in MPH is incompatible with the observed packing of the OPHC2 crystal explains why the MR searches with the complete MPH model failed. This structural difference between the enzymes may denote a functional difference and different substrate specificity; some residues belonging to this fragment are second-shell active-site residues in MPH (*e.g.* Phe178, Trp179, Asp190, Asp193, Phe196 and Phe197). Complete biochemical and kinetic characterization of OPHC2, as well as the construction of the structure, refinement, interpretation of the structure and the identification of the metal cations using anomalous scattering, are in progress.

This research was supported by a grant to EC from Délégation Générale pour l'Armement (REI #2009 34 0045). GG and JH are PhD students granted by Délégation Générale pour l'Armement. DG is a PhD student granted by AP-HM (Marseille, France). We thank the AFMB-CNRS UMR 6098 for full access to the expression and crystallization platform. We are grateful to Agnes Toth-Petroczy for critical reading of the manuscript.

References

Afriat-Jurnou, L., Jackson, C. J. & Tawfik, D. S. (2012). *Biochemistry*, **51**, 6047–6055.
Ben-David, M., Elias, M., Filippi, J. J., Duñach, E., Silman, I., Sussman, J. L. & Tawfik, D. S. (2012). *J. Mol. Biol.* **418**, 181–196.
Berg, S. van den, Löfdahl, P. A., Härd, T. & Berglund, H. (2006). *J. Biotechnol.* **121**, 291–298.
Bigley, A. N. & Raushel, F. M. (2012). *Biochim. Biophys. Acta*, doi: 10.1016/j.bbapap.2012.04.004.
Cheng, T.-C., DeFrank, J. J. & Rastogi, V. K. (1999). *Chem. Biol. Interact.* **119–120**, 455–462.
Chu, X.-Y., Tian, J., Wu, N.-F. & Fan, Y.-L. (2010). *Appl. Microbiol. Biotechnol.* **88**, 125–131.
Chu, X., Wu, N., Deng, M., Tian, J., Yao, B. & Fan, Y. (2006). *Protein Expr. Purif.* **49**, 9–14.
Dong, Y.-J., Bartlam, M., Sun, L., Zhou, Y.-F., Zhang, Z.-P., Zhang, C.-G., Rao, Z. & Zhang, X.-E. (2005). *J. Mol. Biol.* **353**, 655–663.
Elias, M., Dupuy, J., Merone, L., Mandrich, L., Porzio, E., Moniot, S., Rochu, D., Lecomte, C., Rossi, M., Masson, P., Manco, G. & Chabriere, E. (2008). *J. Mol. Biol.* **379**, 1017–1028.
Elias, M. & Tawfik, D. S. (2012). *J. Biol. Chem.* **287**, 11–20.
Emsley, P. & Cowtan, K. (2004). *Acta Cryst.* D**60**, 2126–2132.
Goldsmith, M., Ashani, Y., Simo, Y., Ben-David, M., Leader, H., Silman, I., Sussman, J. L. & Tawfik, D. S. (2012). *Chem. Biol.* **19**, 456–466.
Gotthard, G., Hiblot, J., Elias, M. & Chabrière, E. (2011). *Acta Cryst.* F**67**, 354–357.
Gupta, R. C. (2009). *Handbook of Toxicology of Chemical Warfare Agents*. London: Academic Press.
Hiblot, J., Gotthard, G., Chabriere, E. & Elias, M. (2012*a*). *PLoS One*, **7**, e47028.
Hiblot, J., Gotthard, G., Chabriere, E. & Elias, M. (2012*b*). *Sci. Rep.* **2**, 779.
Jackson, C. J., Carr, P. D., Kim, H.-K., Liu, J.-W., Herrald, P., Mitić, N., Schenk, G., Smith, C. A. & Ollis, D. L. (2006). *Biochem. J.* **397**, 501–508.
Kabsch, W. (1993). *J. Appl. Cryst.* **26**, 795–800.
LeJeune, K. E., Wild, J. R. & Russell, A. J. (1998). *Nature (London)*, **395**, 27–28.
McCoy, A. J., Grosse-Kunstleve, R. W., Adams, P. D., Winn, M. D., Storoni, L. C. & Read, R. J. (2007). *J. Appl. Cryst.* **40**, 658–674.
Morris, R. J., Perrakis, A. & Lamzin, V. S. (2003). *Methods Enzymol.* **374**, 229–244.
Ng, F. S. W., Wright, D. M. & Seah, S. Y. K. (2011). *Appl. Environ. Microbiol.* **77**, 1181–1186.
Omburo, G. A., Kuo, J. M., Mullins, L. S. & Raushel, F. M. (1992). *J. Biol. Chem.* **267**, 13278–13283.
Pakala, S. B., Gorla, P., Pinjari, A. B., Krovidi, R. K., Baru, R., Yanamandra, M., Merrick, M. & Siddavattam, D. (2007). *Appl. Microbiol. Biotechnol.* **73**, 1452–1462.
Raushel, F. M. (2002). *Curr. Opin. Microbiol.* **5**, 288–295.
Singh, B. K. (2009). *Nature Rev. Microbiol.* **7**, 156–164.

D. Analyse structurale et enzymatique d'OPHC2

Structural and enzymatic characterization of the phosphotriesterase from *Pseudomonas pseudoalcaligenes*

Guillaume GOTTHARD, Julien HIBLOT*, Daniel GONZALEZ, Mikael ELIAS et Eric CHABRIERE*

* Contribution égale

Article en révision dans le journal « PlosOne »

Dans les travaux décrits, j'ai réalisé :

- partie expérimentale : résolution de la structure cristallographique de l'enzyme, caractérisations biochimiques
- analyses structurales
- écriture de l'article

Résumé : Ce travail concerne la caractérisation biochimique, enzymatique et structurale d'OPHC2. Au cours de ce travail, une étude phylogénétique fut réalisée afin d'investiguer l'origine d'OPHC2 qui présente un ancêtre commun avec les lactonases de type AiiA. De plus, une caractérisation des activités enzymatiques de l'enzyme fut réalisée. OPHC2 présente principalement des activités envers les OPs (*e.g* $k_{cat}/K_M \sim 10^3\ M^{-1}.s^{-1}$ envers un dérivé coumarinique du cyclosarin). Les activités lactonases sont pour la plupart faibles excepté envers la dihydro-coumarine ($k_{cat}/K_M \sim 10^3 M^{-1}.s^{-1}$) de même que les activités estérase sont faibles ($k_{cat}/K_M \sim 10^{1-2}\ M^{-1}.s^{-1}$). L'activité OP hydrolase d'OPHC2 est néanmoins plus faible que celle de MPH (envers le parathion $k_{cat}/K_M \sim 10^5\ M^{-1}.s^{-1}$).

L'analyse structurale confirma ainsi l'appartenance d'OPHC2 à la superfamille des métallo-β-lactamases et permit de montrer qu'OPHC2 présente un site catalytique analogue à celui d'MPH. Celui-ci étant constitué d'un centre bimétallique (Zn^{++}/Co^{++}) pontant une molécule d'eau activée responsable de la catalyse. Par analogie avec MPH, l'enzyme présente des sous sites de spécificité impliqués dans l'accommodation des OPs.

Enfin, OPHC2 fut caractérisée comme étant hyper-thermostable ($T_m \sim 98$ °C), et nous avons pu identifier quelques déterminants structuraux permettant d'expliquer cette stabilité (*i.e* large interface dimérique, réseau de ponts salins et pont disulfure rigidifiant les boucles). Ainsi, de par sa thermostabilité et sa capacité à hydrolyser les OPs, OPHC2 constitue un point de départ intéressant pour le développement d'une nouvelle classe de bio-épurateur d'OPs.

OPEN ACCESS Freely available online

PLOS ONE

Structural and Enzymatic Characterization of the Phosphotriesterase OPHC2 from *Pseudomonas pseudoalcaligenes*

Guillaume Gotthard[1☯], Julien Hiblot[1☯], Daniel Gonzalez[1], Mikael Elias[2]*, Eric Chabriere[1]*

1 URMITE UMR CNRS-IRD 6236, IFR48, Faculté de Médecine et de Pharmacie, Université de la Méditerranée, Marseille, France, **2** Weizmann Institute of Science, Biological Chemistry, Rehovot, Israel

Abstract

Background: Organophosphates (OPs) are neurotoxic compounds for which current methods of elimination are unsatisfactory; thus bio-remediation is considered as a promising alternative. Here we provide the structural and enzymatic characterization of the recently identified enzyme isolated from *Pseudomonas pseudoalcaligenes* dubbed OPHC2. OPHC2 belongs to the metallo-β-lactamase superfamily and exhibits an unusual thermal resistance and some OP degrading abilities.

Principal findings: The X-ray structure of OPHC2 has been solved at 2.1 Å resolution. The enzyme is roughly globular exhibiting a αβ/βα topology typical of the metallo-β-lactamase superfamily. Several structural determinants, such as an extended dimerization surface and an intramolecular disulfide bridge, common features in thermostable enzymes, are consistent with its high T_m (97.8°C). Additionally, we provide the enzymatic characterization of OPHC2 against a wide range of OPs, esters and lactones.

Significance: OPHC2 possesses a broad substrate activity spectrum, since it hydrolyzes various phosphotriesters, esters, and a lactone. Because of its organophosphorus hydrolase activity, and given its intrinsic thermostability, OPHC2 is an interesting candidate for the development of an OPs bio-decontaminant. Its X-ray structure shed light on its active site, and provides key information for the understanding of the substrate binding mode and catalysis.

Citation: Gotthard G, Hiblot J, Gonzalez D, Elias M, Chabriere E (2013) Structural and Enzymatic Characterization of the Phosphotriesterase OPHC2 from *Pseudomonas pseudoalcaligenes*. PLoS ONE 8(11): e77995. doi:10.1371/journal.pone.0077995

Editor: Hendrik W. van Veen, University of Cambridge, United Kingdom

Received June 30, 2013; **Accepted** September 16, 2013; **Published** November 4, 2013

Funding: This work was granted by DGA, France (REI. 2009 34 0045. J.H. and G.G. are PhD students granted by DGA. D.G. is a PhD student granted by APHM. M.E. is a fellow supported by the IEF Marie Curie program (grant No. 252836). The funders had no role in study design, data collection and analysis, decision to publish, or preparation of the manuscript.

Competing Interests: The authors have declared that no competing interests exist.

* E-mail: mikael.elias@weizmann.ac.il (ME); eric.chabriere@univmed.fr (EC)

☯ These authors contributed equally to this work.

Introduction

Organophosphates (OPs; **Fig. 1A**) are well known neurotoxic compounds which irreversibly inhibit the acetylcholinesterase, a key enzyme in the nerve signal transmission [1]. OPs are widely used as agricultural insecticides [2] and their most toxic representatives have been developed as chemical warfare agents (*e.g.* tabun, sarin, soman or VX) [3]. These compounds are still massively used as pesticides resulting in considerable pollutions [4,5]. Current methods for removing them are slow, cost prohibitive [6], and generate secondary pollution. Novel methods of remediation such as enzyme-mediated decontamination, are therefore highly desirable and under intensive research [7,8].

OPs pesticides have been massively used since the 1950's, leading to the fast emergence of microorganisms that are capable of degrading OPs, and that can probably utilize them as carbon and phosphorus source [9]. Several OrganoPhosphorus Hydrolases (OPHs) have been identified so far, belonging to different protein families: the OrganoPhosphorus Acid Anhydrolases (OPAAs; EC 3.4.13.9) related to the prolidases [10,11], the paraoxonases (PONs; EC 3.1.8.1) [12], the PhosphoTriEsterases (PTEs; EC 3.1.8.1) and the Phosphotriesterase-Like Lactonases (PLLs; EC 3.1.1.81) from the amidohydrolase superfamily, and finally the OPHs from the metallo-β-lactamase superfamily [13]. PTEs, isolated from *Brevundimonas diminuta* [14] and *Agrobacterium radiobacter* [15], are the most characterized OPHs so far and exhibit near diffusion-limit rate for the insecticide paraoxon as substrate [14]. PTEs are believed to have emerged from native lactonases with promiscuous phosphotriesterase activity such as the PLLs [16–18].

A recently identified OPH, named OPHC2 (GenBank ID: AJ605330), has been isolated from *Pseudomonas pseudoalcaligenes* [19,20] but also from *Stenotrophomonas sp.* SMSP-1 (98% identity) [21]. This enzyme shares about 45% sequence identity with the Methyl-Parathion Hydrolases (MPHs; EC 3.1.8.1). MPHs enzymes are isolated from several organisms, such as *Pseudomonas putida*, *Pleisiomonas sp.* M6, *Ochrobactrum sp.* M231 or *Pseudomonas sp.* WBC3, and hydrolyze methyl-parathion with high efficiency

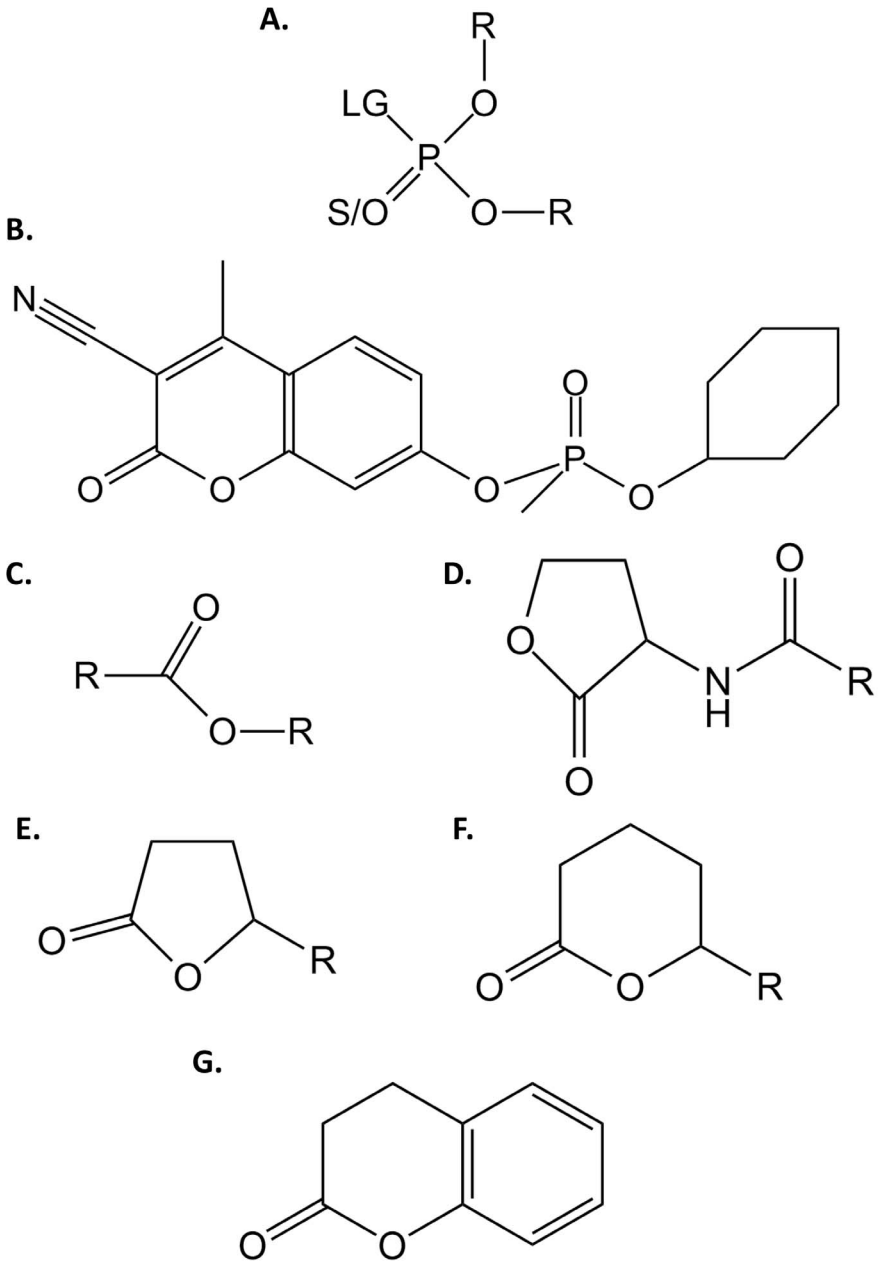

Figure 1. Chemical structure of tested substrates. Chemical structures of (**A.**) phosphotriesters, (**B.**) CMP-coumarin, (**C.**) esters, (**D.**) Acyl-Homoserine Lactones, (**E.**) γ-lactones, (**F.**) δ-lactones and (**G.**) dihydrocoumarin are presented. For phosphotriesters, R corresponds to different nature of substituents; LG corresponds to the leaving group which can be F, S-R, O-R or CN. The terminal substituent could be S atom if the molecule is a thionophosphotriester or an O atom if the molecule is an oxonophosphotriester. For esters, R corresponds to different nature of substituent. For AHLs and γ/δ-lactones, R corresponds to different size of acyl chain.
doi:10.1371/journal.pone.0077995.g001

(*i.e.* $k_{cat}/K_M \sim 10^6\ M^{-1}\ s^{-1}$) [22]. The structure of MPH from *Pseudomonas sp.* WBC3 was solved and revealed an αβ/βα sandwich fold typical of the metallo-β-lactamase superfamily, forming a homodimer [22]. Containing a Zn(II) bi-metallic catalytic site bridged by a water molecule, the MPHs catalytic mechanism is presumed to be similar to that of other OPHs [22]. The bridging catalytic water molecule is activated by the bi-metallic active site and serves as the nucleophile that attacks the phosphorus center of the bound substrate *via* a SN_2 mechanism [22].

OPHC2 has been previously shown to exhibit methyl-parathion hydrolyzing activity [19]. Although the enzyme originates from a mesophilic soil bacterium [23], its optimum temperature for catalysis is reported to be 66°C. In this article, we report the biochemical, enzymatic and structural analysis of OPHC2 from *P. pseudoalcaligenes*. In combination, these results allows us to propose possible explanations for the thermostability of OPHC2 and its substrate preference.

Materials and Methods

Sequence Alignment

The alignments were performed using the *T-coffee* server (expresso) [24,25], and subsequently manually improved. The phylogenetic tree was performed using *PhyML* [26] and default parameters. The sequence alignment was drawn with *BioEdit* 7.1.3. Protein sequence identities were calculated using *ClustalW* server [27].

Protein Production and Purification

The protein production and purification was performed as previously explained [20]. Briefly, the protein production was performed in *E. coli* strain BL21(DE_3)-pGro7/GroEL (TaKaRa). Purification was performed using a previously described procedure [18,28] that takes advantage of the high stability of the target protein by performing a heating step of 30 minutes at 70°C followed by a differential ammonium sulfate precipitation to eliminate remaining thermostable proteins. The sample is subsequently loaded on a size exclusion column [20]. Proteins were quantified using a nanospectrophotometer (nanodrop, thermofisher scientific, France) with the protein molar extinction coefficient ($\varepsilon_{280\ nm} = 38\ 390\ M^{-1}\ cm^{-1}$) calculated by the *PROTPARAM* server [29].

Determination of the Oligomerization State

Oligmerization state determination was performed using a size exclusion column S75 10/300 GL (GE-Healthcare) calibrated with the Gel Filtration Low Molecular Weight calibration kit (GE-Healthcare) in *activity buffer* (50 mM HEPES pH 8, 150 mM NaCl, 0.2 mM $CoCl_2$). 145 µg of OPHC2 enzyme was separated using a flow rate of 0.5 $ml.min^{-1}$ on an ÄKTA avant chromatography apparatus (GE-Healthcare) running with the *UNICORN 6.1* software. Dynamic light scattering (DLS) experiments were performed at room temperature using zetasizer nano series apparatus (Malvern, UK) and the Zetasizer software. 30 µL of purified OPHC2 (5 $mg.ml^{-1}$) was used in the *activity buffer* to measure the hydrodynamic radius of particles at 633 nm allowing estimation of a theoretical enzyme molecular weight.

Kinetic Characterization

Catalytic parameters were evaluated at 25°C, and recorded with a microplate reader (Synergy HT, BioTek, USA) and the Gen5.1 software in a 6.2 mm path length cell for 200 µL reaction in 96-well plate as previously explained [18]. Catalytic parameters were obtained by fitting the data to the Michaelis-Menten (MM) equation [30] using *Graph-Pad Prism 5* software. When V_{max} could not be reached in the experiments, the catalytic efficiency was obtained by fitting the linear part of MM plot to a linear regression using *Graph-Pad Prism 5* software.

Standard assays were performed in *activity buffer* by measuring the time course hydrolysis of *p*NP derivatives ($\varepsilon_{405\ nm} = 17\ 000\ M^{-1}\ cm^{-1}$) of OPs (**Fig. 1A**), esters (**Fig. 1C**). For malathion (**Fig. S1V**), 2 mM DTNB was added to the buffer ($\varepsilon_{412\ nm} = 13\ 700\ M^{-1}\ cm^{-1}$). The time course hydrolysis of phenyl-acetate (**Fig. S1VI**) and dihydrocoumarin (**Fig. 1G**) were monitored at 270 nm ($\varepsilon_{270\ nm} = 1\ 400\ M^{-1}\ cm^{-1}$) and at 412 nm for coumarin nerve agent derivative of cyclosarin (CMP-coumarin **Fig. 1B**; $\varepsilon_{412\ nm} = 37\ 000\ M^{-1}\ cm^{-1}$). The kinetics for the lactonase activities were performed using a previously described protocol [18]. The time course hydrolysis of lactones were performed in *lactonase* buffer (2.5 mM Bicine pH 8.3, 150 mM NaCl, 0.2 mM $CoCl_2$, 0.25 mM Cresol purple and 0.5% DMSO) with different AHLs (**Fig. 1D**) [*i.e.* C4-AHL (*r*), 1 mM; C6-AHL (r), 2 mM; 3-oxo-C6-AHL (*l*), 2 mM; C8-AHL (*r*), 1 mM; 3-oxo-C8-AHL (*l*), 2 mM; 3-oxo-C10-AHL (*l*), 2 mM] (**Fig. S1IX–XIV**) and oxo-lactones (**Fig. 1EF**) [*i.e.* ε-caprolactone, 5 mM; γ-heptanolide (*r*), 5 mM; Nonanoic-γ-lactone (*r*), 5 mM; Nonanoic-δ-lactone (*r*), 5 mM; Undecanoic-γ-lactone (*r*), 5 mM] (**Fig. S1XV–XIX**). Cresol purple (pK_a 8.3 at 25°C) is a pH indicator (577 nm) used to follow the lactone ring hydrolysis that cause an acidification of the medium.

Thermostability Analysis

Circular Dichroïsm (CD) spectra were recorded as previously described [18] using Jasco J-810 spectropolarimeter equipped with Pelletier type temperature control system (Jasco PTC-4235) in 1 mm thick quartz cell and using the *Spectra Manager* software. To determine the melting temperature of the protein, the denaturation was recorded at 222 nm by increasing the temperature from 20 to 95°C (at 2°C/min) in 10 mM sodium phosphate buffer at pH 8 containing increasing concentrations (1–3 M) of guanidinium chloride. The theoretical T_m without guanidinium chloride was extrapolated at the y-intercept by a linear fit using the *Graph-Pad Prism 5* software.

Crystallization

Crystallization was performed as previously published [20]. Briefly, crystals were obtained by the sitting drop vapour diffusion method set up in a 96-well plate. Crystals grow reproducibly after three months at 293 K in drops (2:1 and 1:1 protein:reservoir ratio) of condition 1 (10% PEG 8000, 100 mM Tris-HCl pH 7 and 200 mM $MgCl_2$) and condition 2 (10% PEG 3000, 100 mM Sodium cacodylate pH 6.5 and 200 mM $MgCl_2$).

Data Collection and Structure Refinement

Crystals were transferred into a cryo-protectant solution composed of the reservoir solution and 20% (v/v) glycerol prior to flash-cooling in liquid nitrogen. X-ray diffraction dataset was collected at 100 K using synchrotron radiation at the Proxima-1 beam line (SOLEIL, Gif-sur-Yvette, France) and a PILATUS-6M detector (DECTRIS, Switzerland). X-ray diffraction data were integrated and scaled with the *XDS* package [31] (**Table 1**). The phases were obtained by molecular replacement with *PHASER* [32] as previously described, using the MPH structure as a starting model (PDB ID 1P9E) [20]. The model was subsequently built with *Coot* [33] and refined using *REFMAC5* [34] and *PHENIX* [35]. A total of five monomers (two dimers and one monomer of a symmetry related dimer) were found per asymmetric unit. One of these dimers is highly agitated in the crystal, resulting in a poor electron density. The model and structure factors were deposited under the Protein Data Bank (PDB) code 4LE6.

Structural Modeling

The region 168 to 210, lacking from OPHC2 structure, was modelled using *CHIMERA* [36] and *Modeller 9.11* [37] with the structure of MPH as template.

Anomalous X-ray Scattering Experiments

The chemical nature of the bi-metallic center was studied using anomalous X-ray fluorescence. Two datasets were collected consisting of 3600×0.1° at 2.6 and 3.1 Å resolution at respective wavelengths lower (1.2835 Å) and higher (1.2822 Å) than the Zn-K absorption edge. Moreover, the X-ray fluorescence spectrum of OPHC2 crystal has been collected.

Table 1. Data collection and refinement statistics of OPHC2 structures.

Data collection	
PDB ID	4LE6
Beamline	PROXIMA-1
Wavelength (Å)	0.980
Detector	PILATUS 6M
Oscillation (°)	0.15
Number of frames	1200
Resolution (Å) (last bin)	2.1 (2.2–2.1)
Space group	C2
Unit-cell parameters (Å)	a = 109.9, b = 63.8, c = 221.3, β = 101.8
No. of observed reflections (last bin)	252270 (24317)
No. of unique reflections (last bin)	82530 (9469)
Completeness (%)(last bin)	93.7 (82.6)
R_{meas} (%) (last bin)	6.5 (50.1)
I/σ(I) (last bin)	13.67 (3.07)
Redundancy (last bin)	3.06 (2.57)
Mosaicity (°)	0.508
Refinement statistics	
Rfree/Rwork	20.99/17.32
No. of total model atoms	19946
Ramachandran favored	93.5
Ramachandran outliers	0.8
Generously allowed rotamers	5.7
Rmsd from ideal	
Bond lengths (Å)	0.008
Bond angles (°)	1.111

doi:10.1371/journal.pone.0077995.t001

Structure Analysis

Structural comparisons were made using the crystal structures of MPH (PDB ID 1P9E) and AiiA (PDB ID 2A7M). Structure illustrations, analysis and comparisons were performed using *PyMOL* [38]. Vacuum electrostatic potentials and surface representation were computed under *PyMOL* using a solvent probe of 1.4 Å radius. The surface of the dimer interface and the number of hydrogen bonds and salt bridges were computed using *PISA* [39] available from *PDBe* web interface [40]. Root mean square deviations (RMSD) were calculated on α-carbon using the *align* command under *PyMOL* interface [38].

Results

OPHC2 belongs to the metallo-β-lactamase superfamily and shares significant homology with other representatives such as MPH (identity = 48%; similarity = 58.6%), and lower sequence identity with the lactonases AiiA (17–18%) and AiiB (14%) (**Table S1**) [41]. A phylogenetic tree (**Fig. 2A**) clearly shows that AiiAs and AiiBs in the one hand, MPHs and OPHC2s on the other, form different clades. A sequence alignment between OPHC2, MPH, AiiA and AiiB sequences (**Fig. 2B**) highlights the common HXHXDH motif typical of the bi-metallic catalytic center of the metallo-β-lactamase superfamily [42]. The main variable regions are concentrated in the helix/loop parts of the enzymes.

Biochemical Characterization

Size exclusion chromatography experiments performed on OPHC2 revealed an apparent molecular weight of 58.3 kDa corresponding to an intermediate size between monomeric (32 kDa) and dimeric (64 kDa) forms (**Fig. S2A**). This discrepancy may be due to a slightly anomalous Stokes radius relative to its actual mass, or may reflect a rapid equilibrium between monomeric and dimeric forms of the enzyme as previously proposed [43]. DLS experiments revealed an apparent size of 74.9±11.3 kDa (**Fig. S2B**), suggesting that OPHC2 is a dimer in solution. OPHC2 melting temperature (T_m) was also determined to 97.8±3.2°C by circular dichroïsm (**Fig. S2C**).

Enzymatic Characterization

OPHC2 enzyme was initially characterized for its ability to hydrolyze OPs in crude extracts [19]. We have determined the enzyme kinetic parameters for several insecticides: ethyl/methyl-paraoxon (**Fig. S1I–II**), ethyl/methyl-parathion (**Fig. 1SIII–IV**) and malathion (**Fig. 1SV**) (**Table 2**). Methyl-paraoxon ($k_{cat}/K_M = 1.48(\pm0.34)\times10^3\ M^{-1}s^{-1}$) and methyl-parathion ($k_{cat}/K_M = 2.68(\pm0.73)\times10^3\ M^{-1}s^{-1}$) are the best substrates. As previously observed in PLLs [28], the K_M for methyl-parathion is better than for methyl-paraoxon. Ethyl-paraoxon ($k_{cat}/K_M = 13.3\pm9.2\ M^{-1}s^{-1}$), and malathion (specific activity = 329±82 μmol.mol^{-1}.s^{-1}) are poor substrates for OPHC2, whereas CMP-coumarin (**Fig. 1B**) is hydrolyzed with significant rates ($k_{cat}/K_M = 2.96(\pm0.48)\times10^3\ M^{-1}s^{-1}$). Overall, OPHC2 exhibits rather low organophosphate hydrolase activity ($k_{cat}/K_M \sim 10^3\ M^{-1}s^{-1}$) as compared to other enzymes such as PTEs, mainly because of a low catalytic rate ($k_{cat} \sim 10^{-1}\ s^{-1}$).

Concomitantly to the phosphotriesterase activity, esterase or lactonase activities are systematically observed in other enzyme superfamilies such as paraoxonases or PLLs [12,13]. We have thus characterized OPHC2's activity against various esters (**Fig. 1C**) and lactones (**Fig. 1D–F**) (**Table 2**). OPHC2 hydrolyzes phenyl-acetate, *p*NP-acetate and *p*NP-decanoate with low catalytic efficiencies ($k_{cat}/K_M < 10^2\ M^{-1}s^{-1}$) because of low catalytic rates ($k_{cat} \sim 10^{-2}\ s^{-1}$). The best ester substrate for OPHC2 is *p*NP-decanoate ($k_{cat}/K_M = 2.33(\pm0.83)\times10^2\ M^{-1}s^{-1}$). Concerning lactones, no hydrolysis of AHLs (**Fig. 1D**) or oxo-lactones (**Fig. 1EF**) could be detected, even at high enzyme concentration (*i.e.* 250 μg/mL). However, interestingly, the best substrate for OPHC2 of all tested molecules is the lactone dihydrocoumarin, with a catalytic efficiency of $5.93(\pm1.55)\times10^3\ M^{-1}s^{-1}$.

Structural Characterization

X-Ray structure of OPHC2. The structure of OPHC2 was solved at 2.1 Å resolution (**Table 1**) and reveals that OPHC2 forms a homodimer in the crystal. The dimer interface consists in a large, mainly hydrophobic, contact area between the two monomers (2453.2 Å^2) (**Fig. 3A**), which is bigger than that of MPH (2243.9 Å^2). The dimer is reinforced by the interaction of the N-terminal extremities of the chain that contact the second monomer (**Fig. 3A**). Both monomers interact intensively, performing 29 hydrogen bonds and 15 salt bridges, involving 61 residues (256 atoms). In comparison, MPH monomers perform 45 hydrogen bonds and 8 salt bridges. OPHC2 exhibits a very charged surface (**Fig. 3B**) with several surface salt bridges (**Fig. S3**) that stabilize, for example, the protein extremities (**Fig. S3B**). Finally, the presence of a disulphide bridge (Cys110-Cys146), absent from MPH, may contribute to the higher thermostability of OPHC2 [44].

The monomer of OPHC2 is roughly globular with overall dimensions of approximately 44 Å×50 Å×37 Å. As for MPH, its

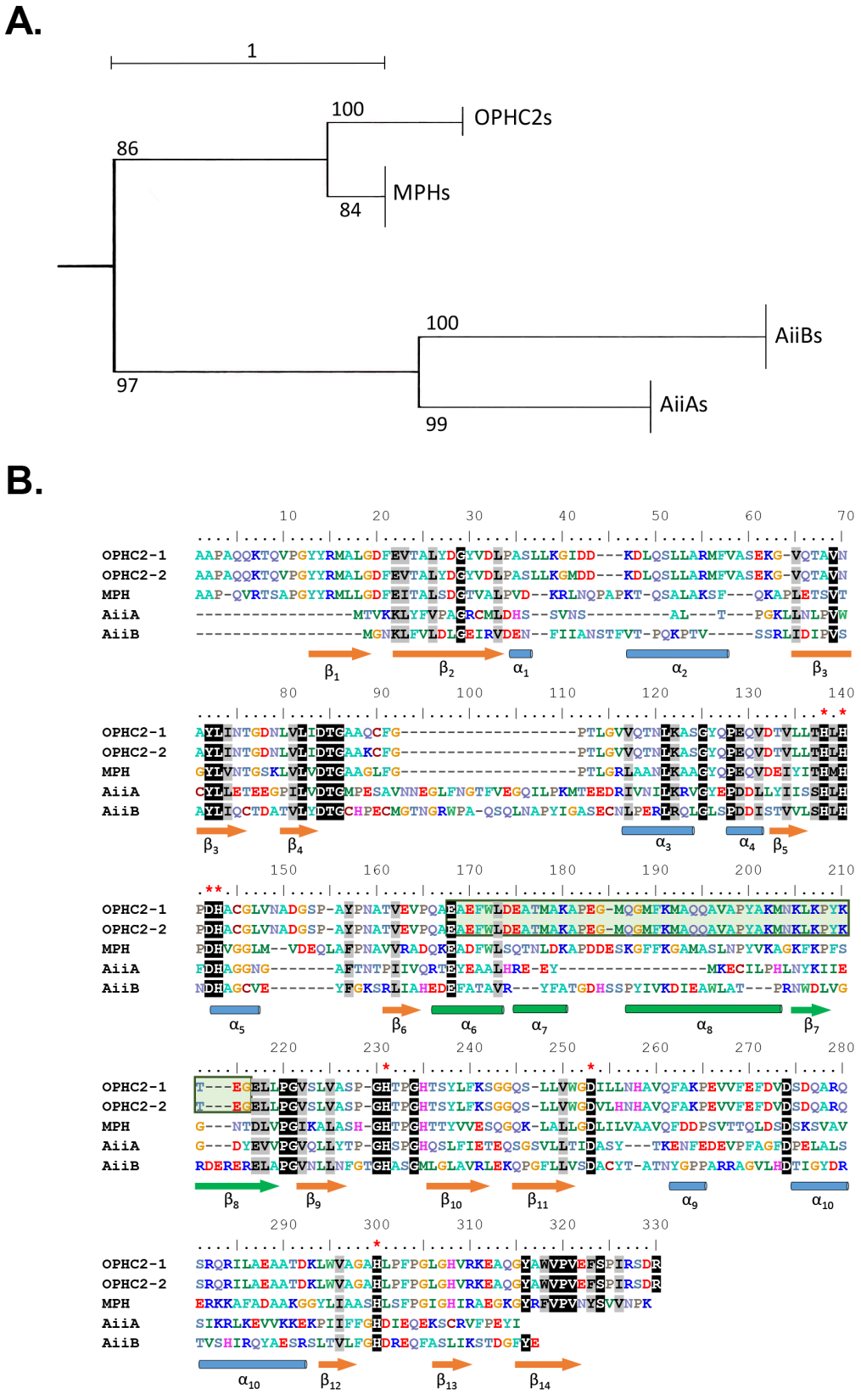

Figure 2. Phylogenetic analysis of OPHC2 enzymes. A. Simplified phylogenetic tree of several OPHs (OPHC2s and MPHs) and lactonases (AiiAs and AiiBs) exhibiting a αβ/βα topology. Sequences were selected from NCBI blast (sequence identity>40%) using input query of OPHC2 from *P. pseudoalcaligenes*, MPH from *Stenotrophomonas* sp. Dsp-4, AiiA from *B. thuringiensis* and AiiB from *A. fabrum* str. C58. Alignment was performed using the *T-coffee* server and the tree was built using *PhyML*. The tree has been arbitrarily rooted for clarity. Bootstraps values are indicated. **B**. Sequence alignment of OPHC2 from *P. pseudoalcaligenes* (OPHC2-1) and *Stenotrophomonas* sp. SMSP-1 (OPHC2-2), MPH from *Stenotrophomonas* sp. Dsp-4, AiiA

from *B. thuringiensis* and AiiB from *A. fabrum* str. C58. Conserved residues are represented with black font while similar residues are represented with grey font. Secondary structures are annotated according to OPHC2 structure (**Fig. 3C & S4) (**β-sheets are represented by orange arrows and α-helices are represented by light blue tubes). Conserved residues involved in the divalent cations coordination are indicated by red stars. Modeled parts of OPHC2 are represented in green (see also **Fig. S4**). This lacking part is also highlighted by a green font.
doi:10.1371/journal.pone.0077995.g002

structure could be described as an αβ/βα sandwich topology, typical of the metallo-β-lactamase superfamily [42]. Two mixed twisted β-sheets, each composed of six strands, are flanked by seven α-helices exposed to the solvent (**Fig. 3C**). The catalytic center is located between the two β-sheets and surrounded by the connecting αβ-loops. In OPHC2 structure, residues 168 to 210 are absent from the electron density maps and therefore have not been modelled. A tentative model of these missing residues based on MPH structure yielded a model that is unfortunately not compatible with OPHC2's crystal packing (**Fig. S4**).

The superposition of OPHC2 with MPH and AiiA yields RMSD values for α-carbon atoms of 0.74 Å (over 213 residues) and 2.41 Å (over 105 residues), respectively. While OPHC2 and MPH structures are very similar, major structural differences are visible between OPHC2 and AiiA. These differences mainly concern the loops size and conformations (**Fig. 3D**).

Active site description. The active site of OPHC2 consists of a cavity with two metal cations: one buried (α metal) and one more solvent exposed (β metal). The α metal is coordinated by His294, His144, Asp143 and the Asp247, the latter coordinates also the β metal together with His226, His139, His141 and a water molecule (**Fig. 4A**). Both metals are bridged by the putative catalytic water molecule. The chemical nature of metal cations was investigated using anomalous X-ray data collection at the Zn-K edge (1.2822 Å) and under (1.2835 Å) (**Table S2**). The presence of two peaks for each metals in Bijvoet difference Fourier maps at the Zn-K edge (18.5 and 14.7 σ in height) and their drop in the maps calculated from data collected under the Zn-edge (8.9 and 11.6 σ) clearly indicates the presence of zinc cations in the active site, but not only (**Table S2**). Indeed, the residual fluorescence observed under the Zn absorption edge may be due to the presence of iron or cobalt, as observed in the X-ray fluorescence spectrum (**Fig. S5**). Therefore, the active site of OPHC2 contains, at both α and β positions, a mixture of zinc and possibly cobalt and/or iron.

The substrate binding pocket is mainly composed of hydrophobic residues. It can be subdivided, based on the MPH structure [45], into three subsites: the leaving group pocket (Phe111, Met188 and Trp172), a first specificity subsite (Leu250, Leu61, Phe263 and Phe265) and a second specificity subsite (Val55 and Leu67) (**Fig. 4B** and **Fig. S6**). Residues Met188 and Trp172 that belong to the leaving group subsite in MPH, belong to the disordered protein fragment that has not been modelled. Residues Cys110 and Cys146 that form a disulphide bridge comprise second shell active site residues (**Fig. 4B**). It covalently bridges helix α_5 and loop $\beta_4\alpha_3$, and may thus rigidify the active site, especially Phe111, a residue possibly involved in the leaving group subsite.

Discussion

OPHC2 is a Dimeric, Thermostable Enzyme

OPHC2 enzyme, as observed for MPH [22], crystallizes as a homodimer, and biochemical evidences suggests that this dimer exists in solution. This homodimer exhibits (i) a very important surface interaction, (ii) a high number of intermolecular hydrogen bonds and salt bridges. The higher thermal stability of OPHC2, as compared to its closest known homologue MPH, may stem from a high dimer interface area and an intramolecular disulfide bridge. Moreover, the structure reveals several ionic bridges at the protein surface, a feature commonly observed in thermostable enzymes [46,47] and usually linked to thermal stability. Altogether, these structural determinants may contribute to the enzyme thermal stability (T_m of 97.8±3.2°C). Because of this very high stability, OPHC2 can be purified by a fast and easy procedure: a heating step followed by ammonium sulfate precipitation, and a polishing step by gel filtration. Moreover, being a thermostable enzyme [47], OPHC2 is expected to exhibit high stability toward various chemicals like organic solvent, and resist to long-term storage. These properties and its measured organophosphate-degrading

Table 2. Enzymatic characterisation of OPHC2 enzyme.

	Substrates	k_{cat} (s^{-1})	K_M (μM)	k_{cat}/K_M ($M^{-1}s^{-1}$)
Phosphoesters	**Ethyl-paraoxon (I)**	$4.05(\pm0.01)\times10^{-3}$	94±19	$1.33(\pm0.92)\times10^{1}$
	Methyl-paraoxon (II)	$3.87(\pm0.29)\times10^{-1}$	261±56	$1.48(\pm0.34)\times10^{3}$
	Ethyl-parathion (III)	ND	ND	ND
	Methyl-parathion (IV)	$5.71(\pm0.33)\times10^{-2}$	21±6	$2.68(\pm0.73)\times10^{3}$
	Malathion (V)	ND	ND	VLH
	CMP-coumarin (VI)	$3.38(\pm0.19)\times10^{-1}$	114±17	$2.96(\pm0.48)\times10^{3}$
Esters	**Phenyl-acetate (VII)**	$9.03(\pm1.26)\times10^{-2}$	1620±563	$5.56(\pm2.08)\times10^{1}$
	***p*NP-Acetate (VIII)**	ND	ND	$2.17(\pm0.08)\times10^{1}$
	***p*NP-Decanoate (IX)**	$3.22(\pm0.25)\times10^{-2}$	138±48	$2.33(\pm0.83)\times10^{2}$
Lactones	**AHLs (X–XV)**	ND	ND	ND
	oxo-lactones (XVI–XX)	ND	ND	ND
	Di-hydrocoumarin (XXI)	2.39±0.20	403±100	$5.93(\pm1.55)\times10^{3}$

Roman numbers correspond to the related chemical structure of the substrate presented in **Figure S1**. Data obtained with cobalt as cofactor. ND corresponds to not determined values because of no or too low catalytic rate. VLH correspond to Very Low Hydrolysis observed without the possibility to record a value.
doi:10.1371/journal.pone.0077995.t002

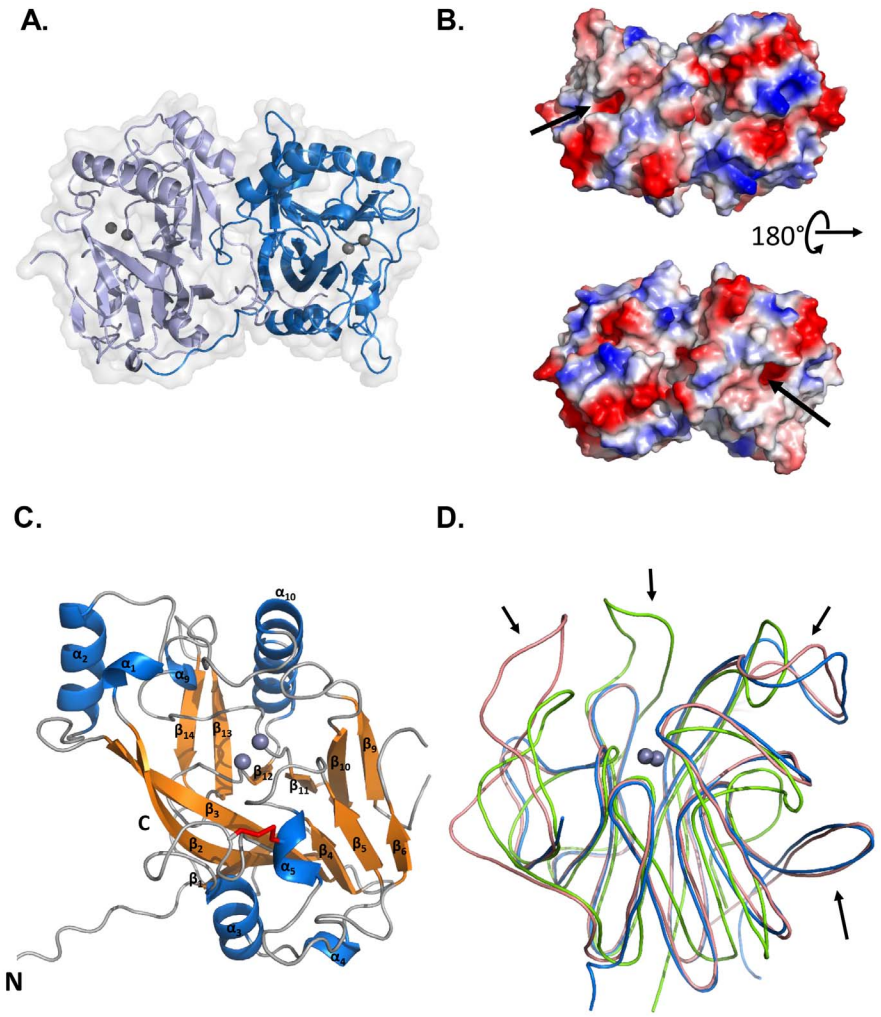

Figure 3. Structure of OPHC2. A. General representation of the OPHC2 dimer. Monomers are colored in light and dark blue. The two metals of the active site are represented as grey spheres. Enzyme surface is also represented. B. Electrostatic surface of OPHC2 dimer. Positive and negative potentials are colored in blue and red, respectively. The active sites are indicated by black arrows. C. Cartoon representation of an OPHC2 monomer with α helices colored in blue, β sheets in orange and loops in grey. The secondary structures are numbered from the alignment present in Fig. 2B. The bimetallic centre is shown as two grey spheres and the disulphide bridge is shown as red sticks. N- and C-terminal extremities are also indicated. D. Structural comparison of OPHC2 (in blue) with MPH (in salmon) and AiiA (in green). Major differences concern loops sizes and conformations.
doi:10.1371/journal.pone.0077995.g003

ability make OPHC2 an interesting candidate for developing an efficient OP biodecontaminant by protein engineering.

OPHC2 Exhibits Esterase and Phosphotriesterase Activities

We here show that OPHC2 hydrolyzes a broad range of esters, from phosphotriesters to the lactone dihydrocoumarin. Being isolated as a phosphotriesterase [19], we show that the enzyme hydrolyzes various insecticides and a nerve agent analogue with relatively low catalytic efficiencies. OPHC2 exhibits clear preference for small substituents (*e.g.* OPHC2 processes methyl-parathion better than ethyl-parathion). Notably, OPHC2 is a less efficient phosphotriesterase than its closest homologue MPH (*e.g.*, against methyl parathion), catalytic efficiencies of OPHC2 and MPH are $\sim 10^3$ $M^{-1}s^{-1}$ and $\sim 10^5$ $M^{-1}s^{-1}$ [22], respectively. This lower activity seems to reside in low k_{cat} values of OPHC2 for phosphotriesters. While structures of MPH and OPHC2 are overall similar (RMSD = 0.74 Å), some differences are observed in active site residues, loops lengths, and second shell residues. Laboratory evolution studies have repeatedly shown that substrate preferences are mediated, at least partly, by length and conformation of active site surrounding loops [16,48–50]. OPHC2's active site comprises a highly hydrophobic substrate binding pocket which thus seems well adapted for the accommodation of the hydrophobic molecules that comprise OPs. The sub-sites architecture of OPHC2 was established on the basis of that of MPH [7,22] (see **Fig. S6**). Comparison of both active site highlights amino acids differences in the leaving group pocket (*e.g.* $Met188_{OPHC2}$ instead of $Phe196_{MPH}$), in the side pockets (*e.g* $Phe265_{OPHC2}$ instead of $Leu273_{OPHC2}$ and $Leu61_{OPHC2}$ instead of $Arg72_{MPH,}$ and the presence of an additional $Phe263_{OPHC2}$ in the binding pocket), as well as the floppy region 168–210. All these differences probably account for the differences in substrate specificity and catalytic efficiencies of both proteins. These residues may thus represent interesting targets for mutational studies, with the aim of increasing the phosphotriesterase activity and widening the specificity spectrum of OPHC2.

A.

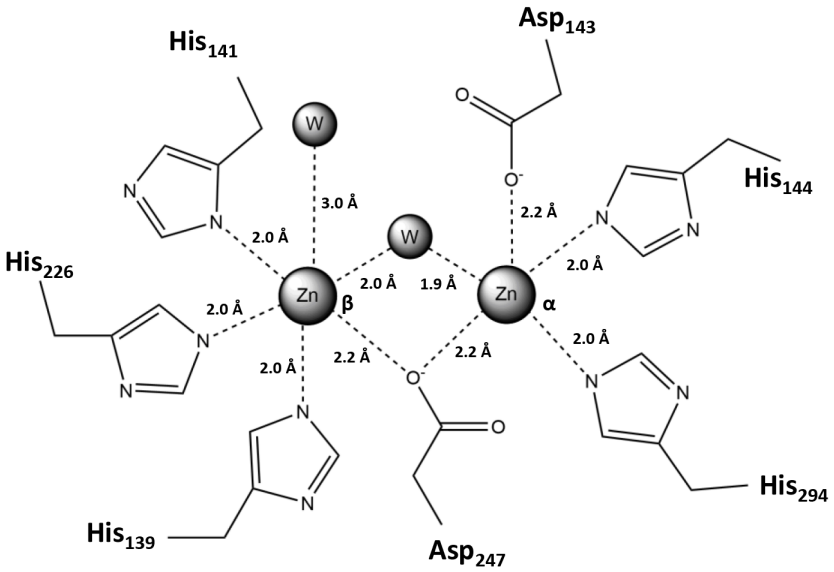
His141
Asp143
W
3.0 Å
2.0 Å
2.2 Å
His144
W
His226
2.0 Å
2.0 Å
1.9 Å
Zn
β
Zn
α
2.0 Å
2.0 Å
2.2 Å
2.2 Å
2.0 Å
His139
Asp247
His294

B.

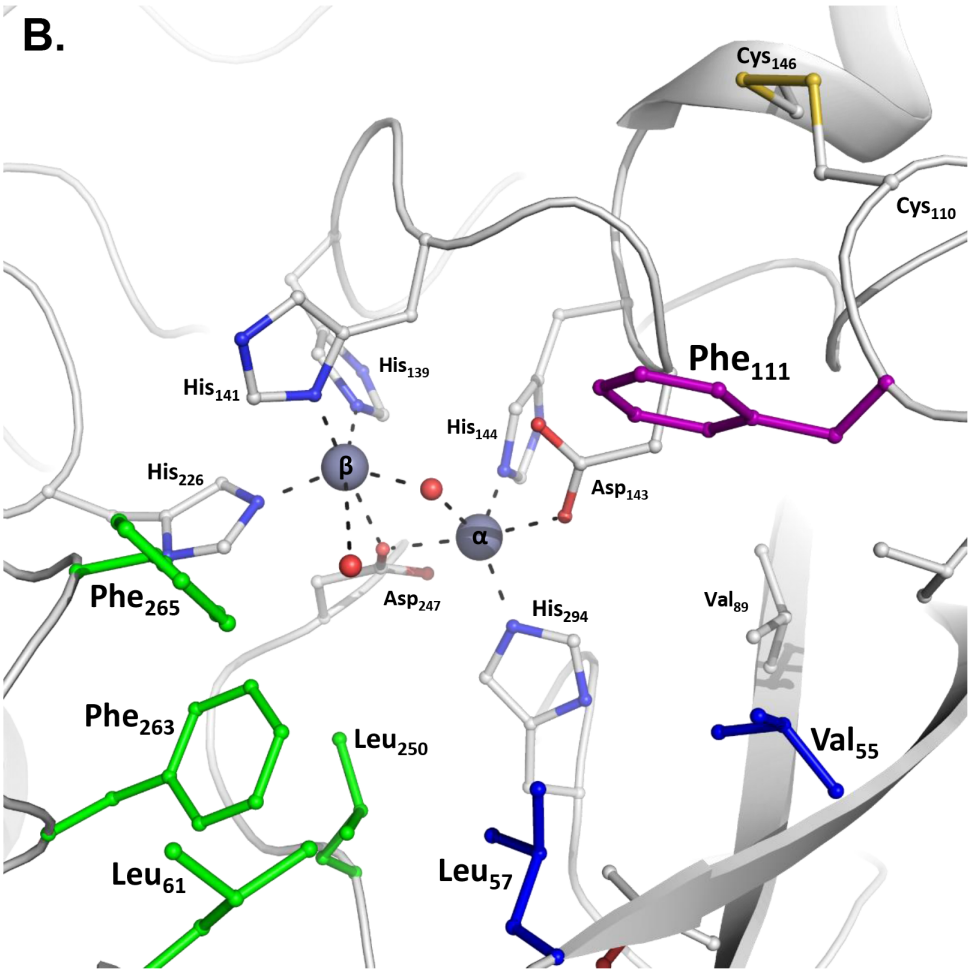
Cys146
Cys110
Phe111
His139
His141
His144
His226
β
Asp143
α
Phe265
Asp247
His294
Val89
Phe263
Leu250
Val55
Leu61
Leu57

Figure 4. Active site of OPHC2. A. Schematic representation of the bi-metallic centre of OPHC2. The two metals and the two water molecules are represented as grey balls. **B.** Three dimensional representation of the OPHC2 active site cavity. Residues are shown as sticks. The metal coordination sphere is shown as dashed lines. The disulphide bridge between Cys110 and Cys146 is colored in yellow. The leaving group subsite of OPHC2 is colored in purple, and the two side pockets are colored in green and blue.
doi:10.1371/journal.pone.0077995.g004

The similarities between catalytic centers of OPHC2 and others OPHs, however, suggest a similar enzymatic chemistry. The catalytic center is composed of two metals bridging an activated water molecule as observed in MPH and AiiA structures [22,51], but also other esterases such as *Sso*Pox or *Sis*Lac [17,18]. Consequently, the hydrolysis mechanism of OPHC2 might be common to these related enzymes.

Additionally, OPHC2 exhibits lactonase activity. Amongst the 12 tested lactones, OPHC2 processes, however, only dihydrocoumarin. Despite the absence of the conserved Tyr residue, characteristic of lactonases in the metallo-β-lactamase superfamily [52] and in the PLLs [16,17,53], the catalysis of dihydrocoumarin is significant ($k_{cat}/K_M = 5.93\times10^3$ $M^{-1}s^{-1}$). A low lactonase activity, interestingly, has been recorded for many phosphotriesterases, the molecular promiscuity between both activities being hypothesized to stem from a molecular overlap between substrate binding of the phosphotriesters and the transition state of the lactone hydrolysis [13].

Finally, we here show that OPHC2 exhibits relatively low catalytic efficiencies against the range of tested substrates ($\sim10^3$ $s^{-1}M^{-1}$ against the best substrates). The average catalytic efficiency of enzymes being $\sim10^5$ $s^{-1}M^{-1}$ [54], this work suggests that OPHC2 natively processes a substrate, yet unknown, that is different in chemical nature from the tested molecules of this study. OPHC2 may therefore have a different biological function than being a lactonase, a phosphotriesterase or an esterase.

Supporting Information

Figure S1 Chemical structure of phosphoesters (I-VI), esters (VII-IX) and lactones (X-XXI).
(DOCX)

Figure S2 Biochemical characterization of OPHC2.
(DOCX)

Figure S3 Surface salt bridges of OPHC2.
(DOCX)

Figure S4 Modelization of the missing part of OPHC2.
(DOCX)

Figure S5 X-ray fluorescence spectrum of OPHC2 crystal.
(DOCX)

Figure S6 Substrate specificity and subsites comparison between MPH (A.) and OPHC2 (B.).
(DOCX)

Table S1 Protein sequence identity between OPHC2, MPH and AiiA-B.
(DOCX)

Table S2 Anomalous X-ray data collection.
(DOCX)

Acknowledgments

We are grateful to Prof. Dan S. Tawfik and Dr. Moshe Goldsmith for the kind gift of CMP -coumarin. We thank the AFMB laboratory (Marseille, France) for the access to protein production and crystallization platforms. We thank also Jeremy Robin and Charlotte Champion for their valuable inputs, and the reviewers for their comments and corrections of our manuscript.

Author Contributions

Conceived and designed the experiments: GG JH ME. Performed the experiments: GG JH DG. Analyzed the data: GG JH DG ME EC. Wrote the paper: GG JH ME.

References

1. Singh BK (2009) Organophosphorus-degrading bacteria: ecology and industrial applications. Nat Rev Microbiol 7: 156–164.
2. Raushel FM (2002) Bacterial detoxification of organophosphate nerve agents. Curr Opin Microbiol 5: 288–295.
3. Gupta RC (2009) Handbook of Toxicology of Chemical Warfare Agents. Handbook of Toxicology of Chemical Warfare Agents.
4. Sapozhnikova Y, Zubcov N, Hungerford S, Roy LA, Boicenco N, et al. (2005) Evaluation of pesticides and metals in fish of the Dniester River, Moldova. Chemosphere 60: 196–205.
5. Sapozhnikova Y, Bawardi O, Schlenk D (2004) Pesticides and PCBs in sediments and fish from the Salton Sea, California, USA. Chemosphere 55: 797–809.
6. LeJeune KE, Wild JR, Russell AJ (1998) Nerve agents degraded by enzymatic foams. Nature 395: 27–28.
7. Bigley AN, Raushel FM (2013) Catalytic mechanisms for phosphotriesterases. Biochim Biophys Acta 1834: 443–453.
8. Goldsmith M, Ashani Y, Simo Y, Ben-David M, Leader H, et al. (2012) Evolved stereoselective hydrolases for broad-spectrum G-type nerve agent detoxification. Chem Biol 19: 456–466.
9. Pakala SB, Gorla P, Pinjari AB, Krovidi RK, Baru R, et al. (2007) Biodegradation of methyl parathion and p-nitrophenol: evidence for the presence of a p-nitrophenol 2-hydroxylase in a Gram-negative Serratia sp. strain DS001. Appl Microbiol Biotechnol 73: 1452–1462.
10. Cheng TC, DeFrank JJ, Rastogi VK (1999) Alteromonas prolidase for organophosphorus G-agent decontamination. Chem Biol Interact 119–120: 455–462.
11. Vyas NK, Nickitenko A, Rastogi VK, Shah SS, Quiocho FA (2010) Structural insights into the dual activities of the nerve agent degrading organophosphate anhydrolase/prolidase. Biochemistry 49: 547–559.
12. Ben-David M, Elias M, Filippi JJ, Dunach E, Silman I, et al. (2012) Catalytic versatility and backups in enzyme active sites: the case of serum paraoxonase 1. J Mol Biol 418: 181–196.
13. Elias M, Tawfik DS (2012) Divergence and Convergence in Enzyme Evolution: Parallel Evolution of Paraoxonases from Quorum-quenching Lactonases. J Biol Chem 287: 11–20.
14. Omburo GA, Kuo JM, Mullins LS, Raushel FM (1992) Characterization of the zinc binding site of bacterial phosphotriesterase. J Biol Chem 267: 13278–13283.
15. Jackson CJ, Carr PD, Kim HK, Liu JW, Herrald P, et al. (2006) Anomalous scattering analysis of Agrobacterium radiobacter phosphotriesterase: the prominent role of iron in the heterobinuclear active site. Biochem J 397: 501–508.
16. Afriat-Jurnou L, Jackson CJ, Tawfik DS (2012) Reconstructing a Missing Link in the Evolution of a Recently Diverged Phosphotriesterase by Active-Site Loop Remodeling. Biochemistry.
17. Elias M, Dupuy J, Merone L, Mandrich L, Porzio E, et al. (2008) Structural basis for natural lactonase and promiscuous phosphotriesterase activities. J Mol Biol 379: 1017–1028.
18. Hiblot J, Gotthard G, Chabriere E, Elias M (2012) Structural and enzymatic characterization of the lactonase SisLac from Sulfolobus islandicus. PLoS One 7: e47028.
19. Chu XY, Wu NF, Deng MJ, Tian J, Yao B, et al. (2006) Expression of organophosphorus hydrolase OPHC2 in Pichia pastoris: purification and characterization. Protein Expr Purif 49: 9–14.
20. Gotthard G, Hiblot J, Gonzalez D, Chabriere E, Elias M (2013) Crystallization and preliminary X-ray diffraction analysis of the organophosphorus hydrolase OPHC2 from Pseudomonas pseudoalcaligenes. Acta Crystallogr Sect F Struct Biol Cryst Commun 69: 73–76.

21. Shen YJ, Lu P, Mei H, Yu HJ, Hong Q, et al. (2010) Isolation of a methyl parathion-degrading strain Stenotrophomonas sp. SMSP-1 and cloning of the ophc2 gene. Biodegradation 21: 785–792.
22. Dong YJ, Bartlam M, Sun L, Zhou YF, Zhang ZP, et al. (2005) Crystal structure of methyl parathion hydrolase from Pseudomonas sp. WBC-3. J Mol Biol 353: 655–663.
23. Monias BL (1928) Classification of bacterium alcaligenes, pyocyaneum, and fluorescens. The Journal of Infectious Diseases 43: 330–334.
24. Poirot O, O'Toole E, Notredame C (2003) Tcoffee@igs: A web server for computing, evaluating and combining multiple sequence alignments. Nucleic Acids Res 31: 3503–3506.
25. Notredame C, Higgins DG, Heringa J (2000) T-Coffee: A novel method for fast and accurate multiple sequence alignment. J Mol Biol 302: 205–217.
26. Gouy M, Guindon S, Gascuel O (2010) SeaView version 4: A multiplatform graphical user interface for sequence alignment and phylogenetic tree building. Mol Biol Evol 27: 221–224.
27. Larkin MA, Blackshields G, Brown NP, Chenna R, McGettigan PA, et al. (2007) Clustal W and Clustal X version 2.0. Bioinformatics 23: 2947–2948.
28. Hiblot J, Gotthard G, Chabriere E, Elias M (2012) Characterisation of the organophosphate hydrolase catalytic activity of SsoPox. Sci Rep 2: 779.
29. Wilkins MR, Gasteiger E, Bairoch A, Sanchez JC, Williams KL, et al. (1999) Protein identification and analysis tools in the ExPASy server. Methods Mol Biol 112: 531–552.
30. Copeland RA (2000) Enzymes, A Practical Introduction to Structure, Mechanism, and Data Analysis. New York, Chichester, Weiheim, Brisbane, Singapore, Toronto: WILEY-VCH. 390 p.
31. Kabsch W (2010) Xds. Acta Crystallogr D Biol Crystallogr 66: 125–132.
32. McCoy AJ, Grosse-Kunstleve RW, Adams PD, Winn MD, Storoni LC, et al. (2007) Phaser crystallographic software. J Appl Crystallogr 40: 658–674.
33. Emsley P, Lohkamp B, Scott WG, Cowtan K (2010) Features and development of Coot. Acta Crystallogr D Biol Crystallogr 66: 486–501.
34. Murshudov GN, Skubak P, Lebedev AA, Pannu NS, Steiner RA, et al. (2011) REFMAC5 for the refinement of macromolecular crystal structures. Acta Crystallogr D Biol Crystallogr 67: 355–367.
35. Adams PD, Afonine PV, Bunkoczi G, Chen VB, Davis IW, et al. (2010) PHENIX: a comprehensive Python-based system for macromolecular structure solution. Acta Crystallogr D Biol Crystallogr 66: 213–221.
36. Pettersen EF, Goddard TD, Huang CC, Couch GS, Greenblatt DM, et al. (2004) UCSF Chimera–a visualization system for exploratory research and analysis. J Comput Chem 25: 1605–1612.
37. Sali A, Blundell TL (1993) Comparative protein modelling by satisfaction of spatial restraints. J Mol Biol 234: 779–815.
38. Schrodinger LLC (2010) The PyMOL Molecular Graphics System, Version 1.3r1.
39. Krissinel E, Henrick K (2007) Inference of macromolecular assemblies from crystalline state. J Mol Biol 372: 774–797.
40. Velankar S, Alhroub Y, Best C, Caboche S, Conroy MJ, et al. (2012) PDBe: Protein Data Bank in Europe. Nucleic Acids Res 40: D445–452.
41. Amara N, Krom BP, Kaufmann GF, Meijler MM (2011) Macromolecular inhibition of quorum sensing: enzymes, antibodies, and beyond. Chem Rev 111: 195–208.
42. Aravind L (1999) An evolutionary classification of the metallo-beta-lactamase fold proteins. In Silico Biol 1: 69–91.
43. Merone L, Mandrich L, Rossi M, Manco G (2005) A thermostable phosphotriesterase from the archaeon Sulfolobus solfataricus: cloning, overexpression and properties. Extremophiles 9: 297–305.
44. Su Y, Tian J, Wang P, Chu X, Liu G, et al. (2011) Improving the thermostability of a methyl parathion hydrolase by adding the ionic bond on protein surface. Appl Biochem Biotechnol 165: 989–997.
45. Bigley AN, Raushel FM (2012) Catalytic mechanisms for phosphotriesterases. Biochim Biophys Acta.
46. Del Vecchio P, Elias M, Merone L, Graziano G, Dupuy J, et al. (2009) Structural determinants of the high thermal stability of SsoPox from the hyperthermophilic archaeon Sulfolobus solfataricus. Extremophiles 13: 461–470.
47. Vieille C, Zeikus GJ (2001) Hyperthermophilic enzymes: sources, uses, and molecular mechanisms for thermostability. Microbiol Mol Biol Rev 65: 1–43.
48. Park HS, Nam SH, Lee JK, Yoon CN, Mannervik B, et al. (2006) Design and evolution of new catalytic activity with an existing protein scaffold. Science 311: 535–538.
49. Dellus-Gur E, Toth-Petroczy A, Elias M, Tawfik DS (2013) What makes a protein fold amenable to functional innovation? Fold polarity and stability tradeoffs. J Mol Biol.
50. Toth-Petroczy A, Tawfik DS (2013) Protein insertions and deletions enabled by neutral roaming in sequence space. Mol Biol Evol 30: 761–771.
51. Kim MH, Choi WC, Kang HO, Lee JS, Kang BS, et al. (2005) The molecular structure and catalytic mechanism of a quorum-quenching N-acyl-L-homoserine lactone hydrolase. Proc Natl Acad Sci U S A 102: 17606–17611.
52. Liu D, Lepore BW, Petsko GA, Thomas PW, Stone EM, et al. (2005) Three-dimensional structure of the quorum-quenching N-acyl homoserine lactone hydrolase from Bacillus thuringiensis. Proc Natl Acad Sci U S A 102: 11882–11887.
53. Afriat L, Roodveldt C, Manco G, Tawfik DS (2006) The latent promiscuity of newly identified microbial lactonases is linked to a recently diverged phosphotriesterase. Biochemistry 45: 13677–13686.
54. Bar-Even A, Noor E, Savir Y, Liebermeister W, Davidi D, et al. (2011) The moderately efficient enzyme: evolutionary and physicochemical trends shaping enzyme parameters. Biochemistry 50: 4402–4410.

SUPPLEMENTAL MATERIAL FOR

Structural and enzymatic characterization of the phosphotriesterase OPHC2 from *Pseudomonas pseudoalcaligenes*

Guillaume GOTTHARD[1*], Julien HIBLOT[1*], Daniel GONZALEZ[1], Jeremy ROBIN[1], Mikael ELIAS[2#], Eric CHABRIERE[1#]

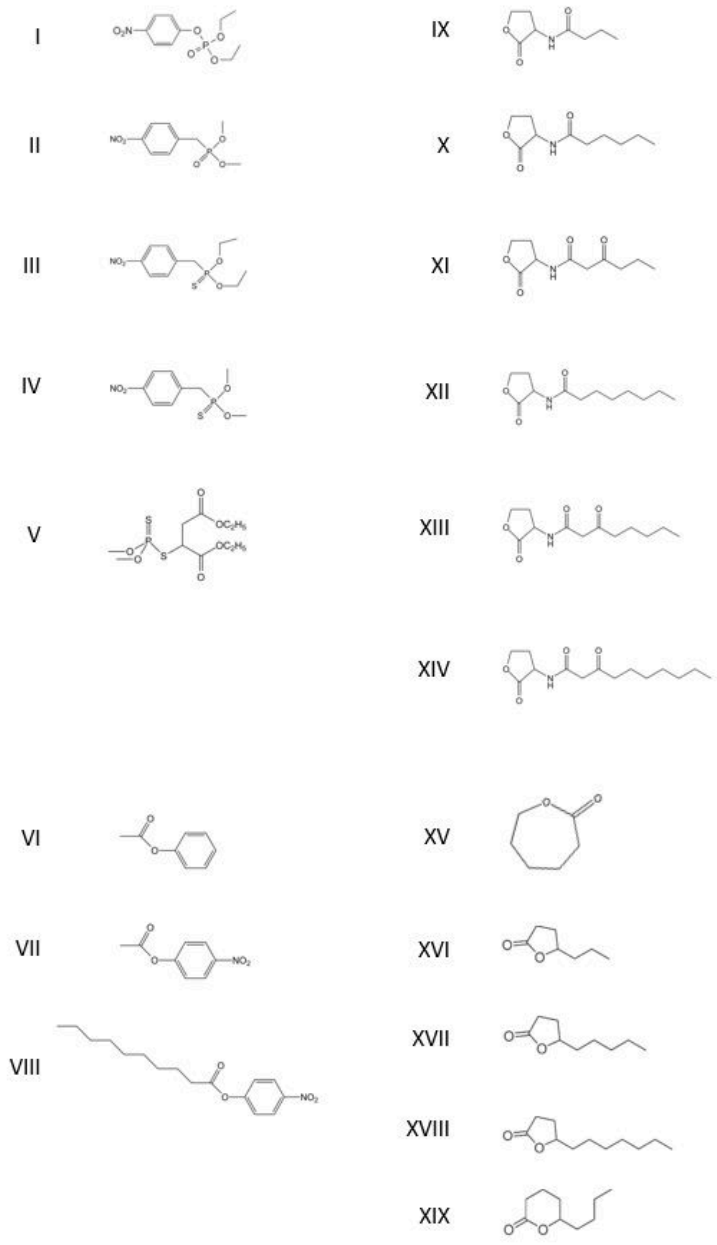

Figure S1: Chemical structure of phosphoesters (I-VI), esters (VII-IX) and lactones (X-XXI)

Chemical structure of ethyl-paraoxon (I), methyl-paraoxon (II), ethyl-parathion (III), methyl-parathion (IV), malathion (V), phenyl-acetate (VI), *p*NP-acetate (VII), *p*NP-decanoate (VIII), .C4-AHL (IX), C6-AHL (X), 3-oxo-C6-AHL (XI), C8-AHL (XII), 3-oxo-C8-AHL (XIII), 3-oxo-C12-AHL (XIV), ε-caprolactone (XV), γ-heptanolide (XVI), Nonanoic-γ-lactone (XVII), Undecanoic-γ-lactone (XVIII) and Nonanoic-δ-lactone (XIX).

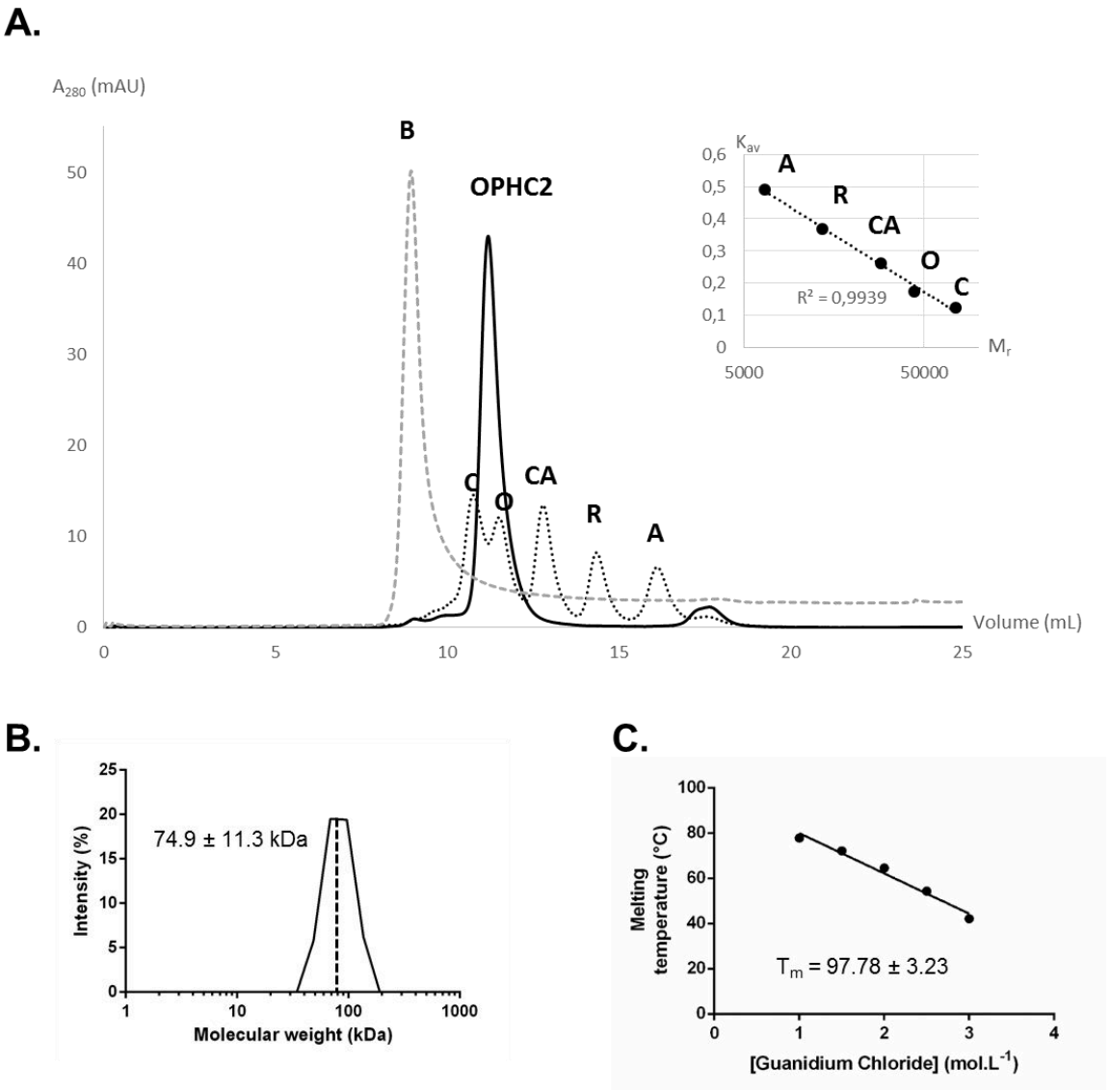

Figure S2: Biochemical characterization of OPHC2

A. Oligomerization state analysis of OPHC2 by exclusion size chromatography. Black line corresponds to the elution profile of 145 µg of OPHC2 on the S75 10/300 GL chromatography column. Black dashed lines correspond to the elution profile of the gel filtration low molecular weight calibration kit (GE-Healthcare): Conalbumin (C), Ovalbumin (O), Carbonic Anhydrase (CA), Ribonuclease A (R), Aprotinin (A). Grey dashed lines correspond to the elution profile of the Blue Dextran 2000 (B) used to obtain the void volume

of the column. The apparent molecular weight of OPHC2 was inferred from the calibration curve of the K_{av} function of the molecular weight (M_r). K_{av} was calculated from the formula: $K_{av} = \frac{V_e - V_0}{V_c - V_0}$, where V_e is the elution volume of each protein, V_0 is the void volume of the column and V_c is the geometric volume of the column. **B.** Oligomerisation state analysis of OPHC2 by DLS experiment. DLS profile of 30 µL OPHC2 enzyme at 5 $mg.ml^{-1}$ averaged on 5 experiments. **C.** Melting temperature (T_m) determination of OPHC2 enzyme. Linear regression of the OPHC2 T_m *versus* guanidinium chloride concentration which allow to extrapolate the T_m of the protein at 97.8 ± 3.2 °C at the y-intercept.

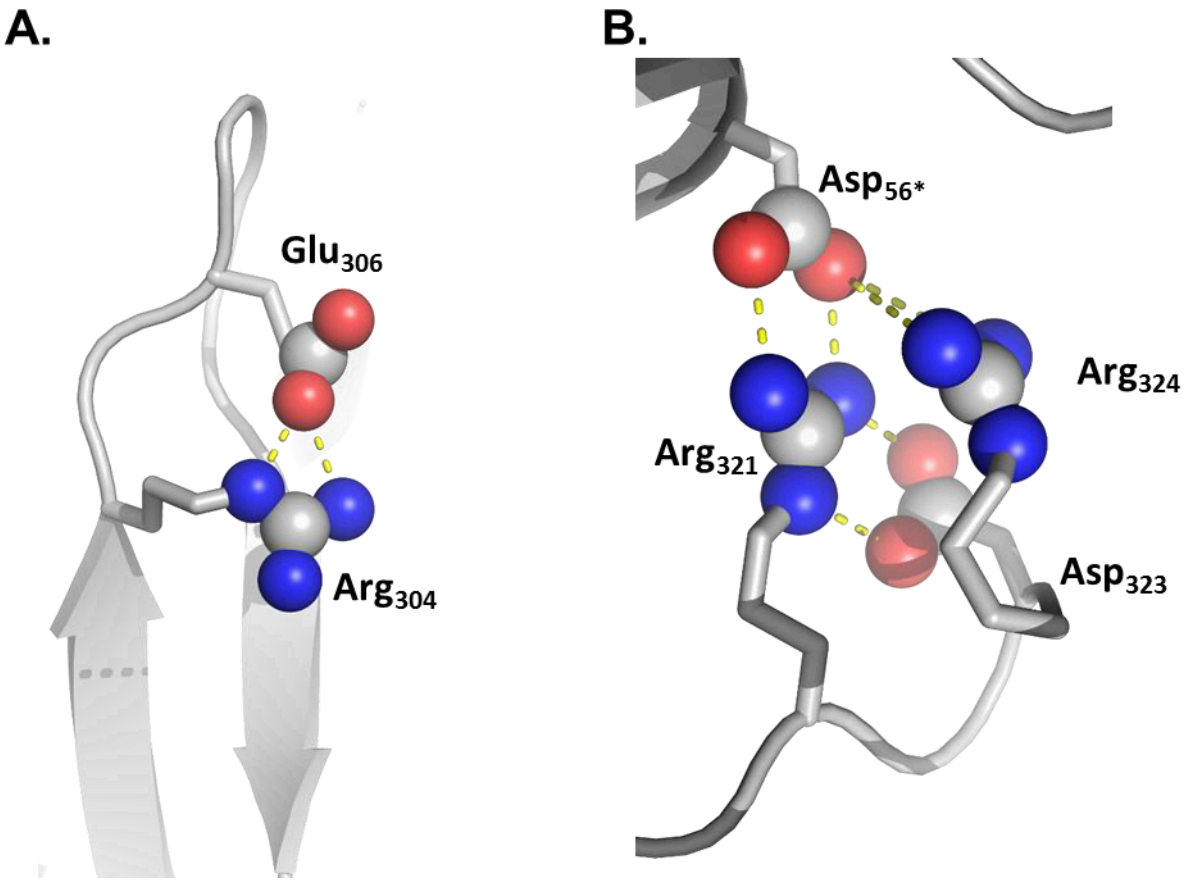

Figure S3: Surface salt bridges of OPHC2

Some surface salt bridges in OPHC2 structure. Main chain and carbon atoms are colored in grey. Oxygen and nitrogen atoms are represented as red and blue spheres respectively. Interactions between complementary charges are indicated by yellow dashes. **A.** Typical salt bridge at the surface of the OPHC2 structure. **B.** Complex salt bridge network linking the extremity of one monomer to its associated monomer (indicated by a star).

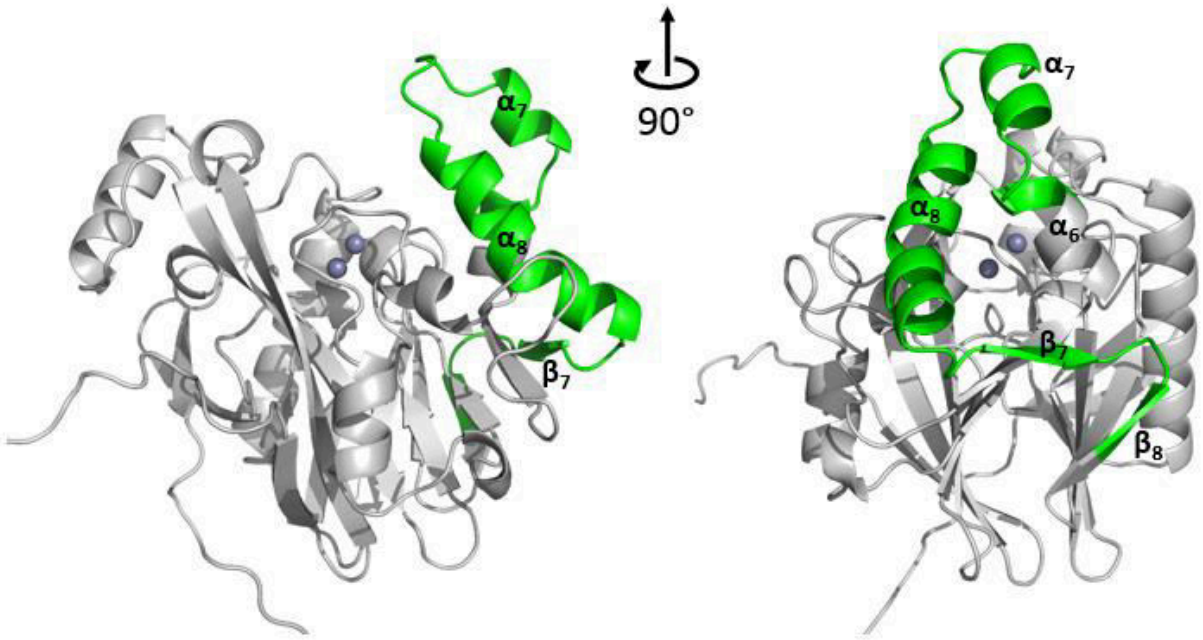

Figure S4: Modelization of the missing part of OPHC2

Cartoon representation of the OPHC2. The part missing from the crystallographic structure is colored in green and secondary structures are numbered as in the alignment of **Fig. 2B**. This part was modelled using *MODELLER* and MPH structure as a model. The two metals are shown as spheres. The quality of the structure was validated using Rampage software from the CCP4 suite (Ramachandran favoured regions, 93.6 %; Allowed region, 4.4 %; generously allowed, 2.0 %).

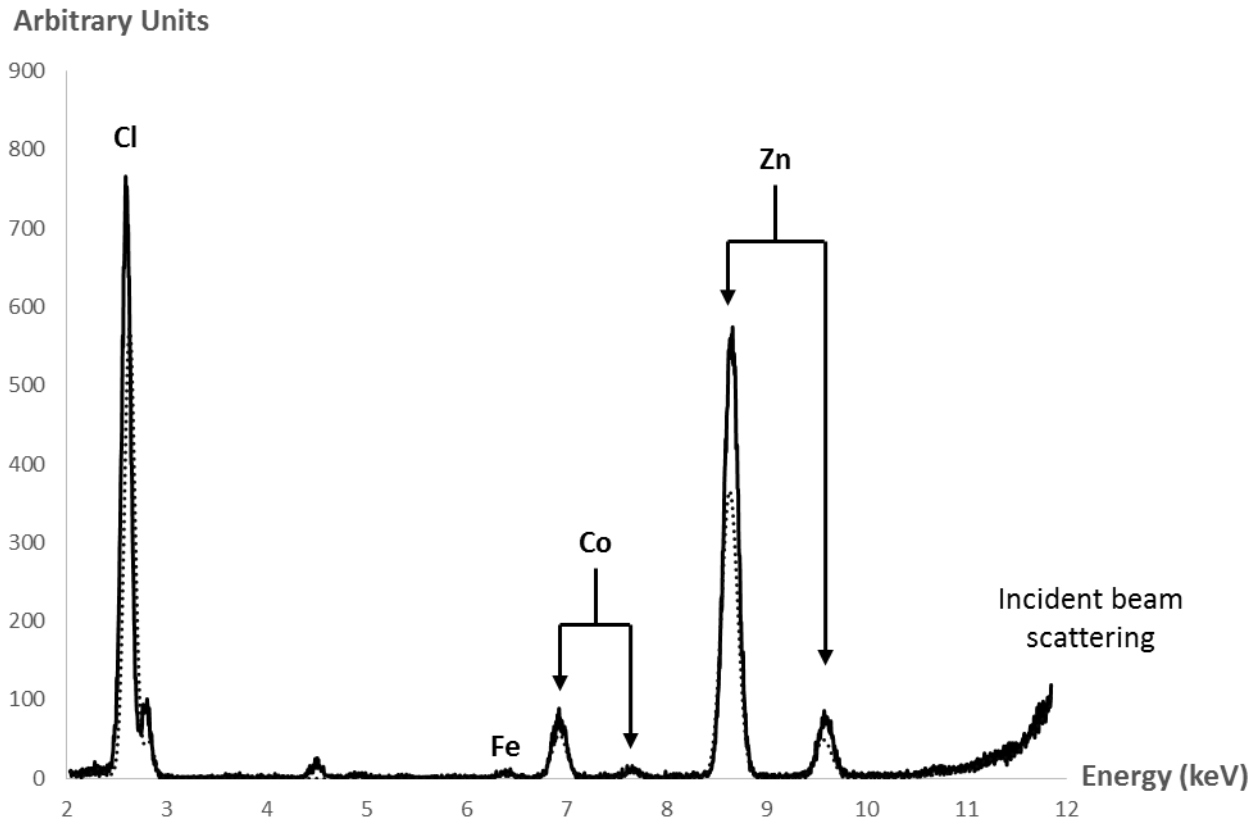

Figure S5: X-ray fluorescence spectrum of OPHC2 crystal

X-ray fluorescence spectrum of OPHC2 crystals. Data have been analysed using *PyMCA* software [53] revealing the presence of chloride, cobalt, zinc and iron. Doubled arrows indicate the characteristic Kα and Kβ edges of compounds.

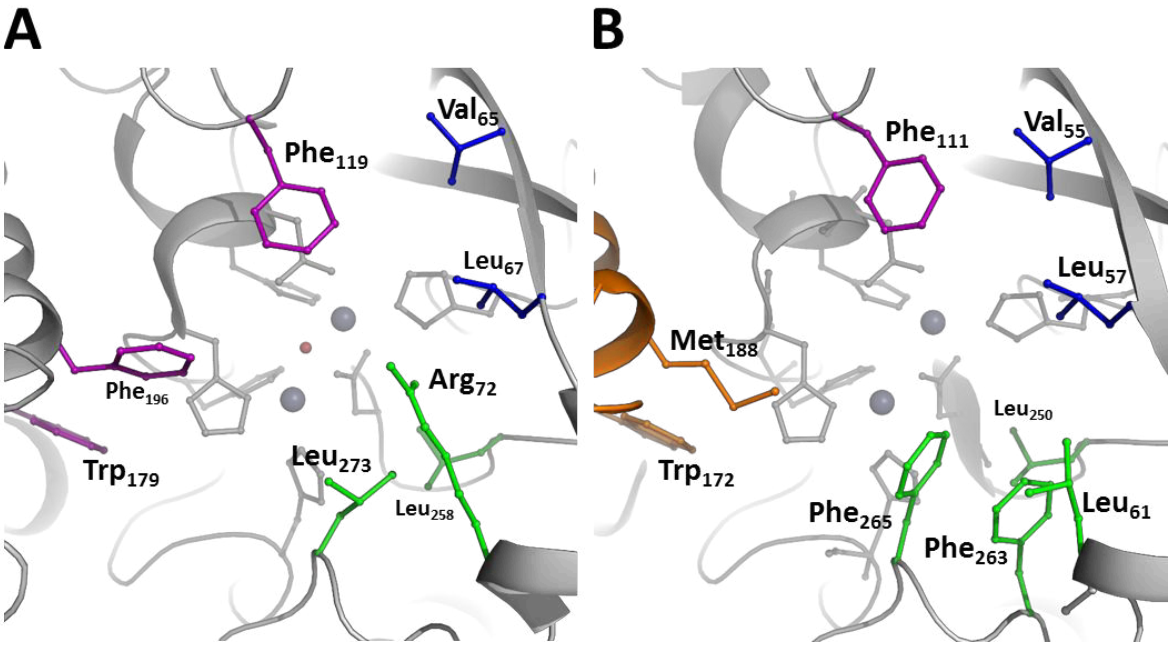

Figure S6: Substrate specificity and subsites comparison between MPH (A.) and OPHC2 (B.)

Leaving group pocket residues are colored in purple, side pockets are colored in green and blue. Residues absent from the crystallographic structure but modelled are colored in orange.

Table SI: Protein sequence identity between OPHC2, MPH and AiiA-B

	OPHC2-1	OPHC2-2	MPH	AiiA	AiiB
OPHC2-1	-	98 %	45 %	18 %	14 %
OPHC2-2	-	-	44 %	17 %	14 %
MPH	-	-	-	18 %	9 %
AiiA	-	-	-	-	22 %
AiiB	-	-	-	-	-

OPHC2-1 originates from *P. pseudoalcaligenes*. OPHC2-2 originates from *Stenotrophomonas* sp. SMSP-1. MPH originates from *Stenotrophomonas* sp. Dsp-4. AiiA originates from *B. thuringiensis*. AiiB originates from *A. fabrum* str. C58. Identities were obtained from a sequence alignment preformed using the ClustalW server.

Table SII: Anomalous X-ray data collection

Data collection		
Dataset	Zn-K edge high	Zn-K edge low
Beamline	ID29	ID29
Wavelength (Å)	1.2822 Å	1.2835 Å
Detector	PILATUS 6M	PILATUS 6M
Oscillation (°)	0.1	0.1
Number of frames	3600	3600
Resolution (Å) (last bin)	3.1 (3.2-3.1)	2.6 (2.7-2.6)
Space group	C2	C2
Unit-cell parameters (Å)	a = 111.7, b = 63.8, c = 222.04, β = 101.5	a = 111.2, b = 63.7, c = 222.0, β = 101.7
No. of observed reflections (last bin)	181006 (17769)	312228 (34740)
No. of unique reflections (last bin)	54065 (5015)	91173 (9834)
Completeness (%)(last bin)	99.2 (99.8)	99.3 (99.7)
R_{meas} (%) (last bin)	10.8 (57.5)	9.5 (54.5)
I/σ(I) (last bin)	10.83 (3.1)	11.60 (3.40)
Redundancy (last bin)	3.35 (3.54)	3.42 (3.53)
Mosaicity (°)	0.155	0.120
Anomalous peak (σ)[#]	α metal = 18.5 β metal = 14.7	α metal = 8.9 β metal = 11.6

[#] is the height of the anomalous peak (in σ units) in the Bijvoet difference Fourier map at the location of the metal cations in the structure. The anomalous signal decline at lower energy, showing that the binding pocket is occupied by zinc ions, but not only.

E. Caractérisation de l'activité phosphotriestérase de *Sso*Pox

Characterization of the organophosphate hydrolase activity of *Sso*Pox

Julien HIBLOT, Guillaume GOTTHARD, Eric CHABRIERE, Mikael ELIAS

Dans les travaux décrits, j'ai réalisé :

- partie expérimentale : affinement de la structure cristallographique
- analyses structurales
- écriture de parties de l'article, dépôt de la structure sur la PDB (code pdb : 3UF9)

Résumé : Ce travail concerne l'étude enzymatique et biochimique de *Sso*Pox. Nous avons également obtenu la première structure d'une PLL en complexe avec un OP. L'enzyme avait été caractérisée à haute température (70 °C) (163), mais aucune donnée n'était connue quant aux activités de *Sso*Pox à température ambiante. Nous avons donc caractérisé l'activité phosphotriestérase de *Sso*Pox à 25 °C envers divers insecticides et CWA. *Sso*Pox présente une activité phosphotriestérase à température ambiante (*e.g* $k_{cat}/K_M \sim 10^2$ $M^{-1}.s^{-1}$ envers le paraoxon) avec une préférence pour les substrats peu encombrants (l'activité envers le méthyl-paraoxon est plus élevée qu'envers l'éthyl-paraoxon) et pour les oxono-phosphotriesters (activités plus élevée envers les paraoxons que les parathions). La mise en évidence de cette seconde préférence fut dénommée « thiono-effect ». De nombreux phosphotriesters étant des thiono-phosphotriesters, l'amélioration de l'activité de l'enzyme envers ces substrats constitue un challenge particulier. Au cours de cette caractérisation enzymatique, il fut aussi montré que *Sso*Pox est capable de dégrader certains dérivés coumariniques d'agents G avec des efficacités catalytiques de l'ordre de 10^3 $M^{-1}.s^{-1}$.

Il avait également été montré que *Sso*Pox, tout comme c'est le cas pour d'autres enzymes hyperthermostables, résistait à la dénaturation par les détergents. Nous avons étudié l'activité de *Sso*Pox en présence de différents détergents anioniques et mis en évidence que l'efficacité de l'enzyme peut être stimulée à température ambiante par l'utilisation de détergents comme le SDS et le DOC. Avec une augmentation pouvant aller jusqu'à 33 fois, l'utilisation de détergents permet d'atteindre des efficacités catalytiques de 10^4 $M^{-1}.s^{-1}$ envers l'insecticide paraoxon et de 10^5 $M^{-1}.s^{-1}$ envers certains dérivés coumariniques d'agents G.

Enfin, au cours de cette étude, l'inhibition de l'enzyme par l'insecticide fensulfothion fut étudiée. La structure cristallographique de *Sso*Pox en complexe avec le fensulfothion mis clairement en évidence que celui-ci est un inhibiteur compétitif. Cependant, de façon inattendue, le mode de fixation

du fensulfothion dans le site actif est atypique. Le groupement phosphoré de celui-est orienté loin du cœur catalytique, alors que le groupement sulfinyl mime le mode de fixation des lactones. L'inhibition est donc la résultante d'une accommodation improductive du fensulfothion qui ne peut être hydrolysé.

L'activité envers les phosphotriesters étant une activité de promiscuité (163), l'étude structurale a permis d'identifier des résidus potentiellement impliqués dans une mauvaise accommodation des OPs par l'enzyme. En particulier, la position Trp 263 qui fut proposée pour permettre d'améliorer l'activité de *Sso*Pox envers les OPs.

SCIENTIFIC REPORTS

OPEN

SUBJECT AREAS:
STRUCTURAL BIOLOGY
BIOCHEMISTRY
PROTEINS
ENZYMES

Received
8 June 2012

Accepted
24 September 2012

Published
8 November 2012

Correspondence and requests for materials should be addressed to E.C. (eric.chabriere@univmed.fr) or M.E. (mikael.elias@weizmann.ac.il)

Characterisation of the organophosphate hydrolase catalytic activity of *Sso*Pox

Julien Hiblot[1], Guillaume Gotthard[1], Eric Chabriere[1] & Mikael Elias[2]

[1]URMITE UMR CNRS-IRD 6236, IFR48, Faculté de Médecine et de Pharmacie, Université de la Méditerranée, Marseille, France, [2]Weizmann Institute of Science, Biological Chemistry, Rehovot, Israel.

_Sso_Pox is a lactonase endowed with promiscuous phosphotriesterase activity isolated from *Sulfolobus solfataricus* that belongs to the Phosphotriesterase-Like Lactonase family. Because of its intrinsic thermal stability, _Sso_Pox is seen as an appealing candidate as a bioscavenger for organophosphorus compounds. A comprehensive kinetic characterisation of _Sso_Pox has been performed with various phosphotriesters (insecticides) and phosphodiesters (nerve agent analogues) as substrates. We show that _Sso_Pox is active for a broad range of OPs and remains active under denaturing conditions. In addition, its OP hydrolase activity is highly stimulated by anionic detergent at ambient temperature and exhibits catalytic efficiencies as high as k_{cat}/K_M of 10^5 $M^{-1}s^{-1}$ against a nerve agent analogue. The structure of _Sso_Pox bound to the phosphotriester fensulfothion reveals an unexpected and non-productive binding mode. This feature suggests that _Sso_Pox's active site is sub-optimal for phosphotriester binding, which depends not only upon shape but also on localised charge of the ligand.

Organophosphates (OPs) are well-known potently toxic compounds because they irreversibly inhibit acetylcholinesterase, a key enzyme of the central nervous system[1]. They have been extensively used since the end of World War II, primarily as agricultural insecticides[2]. Their toxic properties have also been exploited for the development of chemical warfare agents (such as sarin, soman and VX). Enzymes that are capable of degrading OPs are therefore attractive as potential anti-dotes because of their intrinsic potential in decontamination/detection systems for organophosphates-based pesticides and nerve agents[3]. Enzymatic detoxification of OPs has become the subject of numerous studies because current methods of removing them, such as bleach treatments and incineration, are slow, expensive and cause environmental concerns. For this application, OP hydrolases are appealing due to their broad substrate specificity and their high catalytic rate[3].

Bacterial phosphotriesterases (PTEs) are members of the amidohydrolase superfamily[4], enzymes catalysing the hydrolysis of a broad range of compounds with different chemical properties (phosphoesters, esters, amides, etc.). PTEs hydrolyse insecticide-derivatives such as paraoxon with diffusion limit like kinetic parameters[5,6]. Moreover, PTEs catalyse the hydrolysis of various nerve agents with high efficiency[7]. Because the widespread dissemination of these man-made chemicals began only in the 1950's, it has been postulated that the PTEs might have evolved specifically to hydrolyse insecticides over a relatively short period of time[8].

A protein from the hyperthermophilic archaeon *Sulfolobus solfataricus*, *Sso*Pox, was cloned, characterised and related to the PTE family (and was accordingly named paraoxonase[9]). *Sso*Pox indeed shares approximately 30% sequence identity with mesophilic PTEs, but hydrolyses paraoxon and other pesticides with a lower efficiency[9]. *Sso*Pox is an extremely thermostable enzyme, with an evaluated Tm of 104°C and a denaturation half-life of 90 minutes at 100°C[9]. The thermostability of *Sso*Pox was mainly attributed to a large hydrophobic dimer interface and an extensive salt bridge network[10], two classical features of hyperthermostable proteins[11]. *Sso*Pox is thus considered as an excellent starting point for biotechnological applications[12] and directed evolution (which was briefly explored[13]). Isolated by virtue of its phosphotriesterase activity, biochemical and phylogenetic evidence later suggested that *Sso*Pox belongs to another closely related protein family, the *Phosphotriesterase-Like Lactonase* (PLLs)[14]. The structure of *Sso*Pox confirmed that it is a natural lactonase with a promiscuous phosphotriesterase activity[15,16]. In particular, the activity detected against *N*-acyl-homoserine lactones (AHLs)[14,17] may relate *Sso*Pox and the PLLs to the AHL-based *quorum* sensing system[18] and its inhibition by *quorum* quenching[17,19]. The crystal structures of *Sso*Pox free and in complex with an AHL mimic have illustrated the molecular adaptation of a dedicated lactonase to an optimised phosphotriesterase within the last few decades[15]. It is

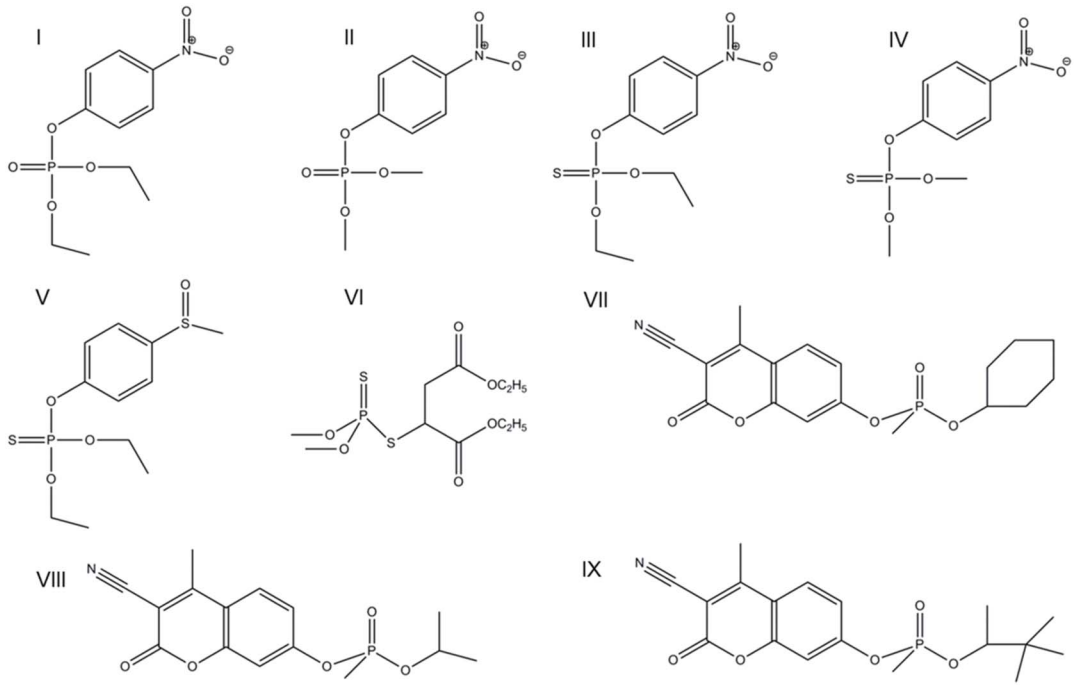

Figure 1 | Chemical structure of organophosphorus compounds used in this study. Chemical structure of (ethyl-)paraoxon (I), methyl-paraoxon (II), (ethyl-)parathion (III), methyl-parathion (IV), fensulfothion (V), malathion (VI), CMP-coumarin (VII), IMP-coumarin (VIII) and PinP-coumarin (IX) generated using ChemDraw software. All these compounds are phosphotriesters with the exception of the last three compounds that are phosphodiesters.

noteworthy that similar adaptations from lactonases to phosphotriesterases have occurred in at least three different families[20], including the PLLs and PTEs (TIM barrel fold), the lactonases with a metallo-β-lactamase fold and the paraoxonase family using directed evolution (β-propeller fold)[21]. However, despite several X-ray structures of representatives for each family, there is no case where structures of the same protein are available with a native substrate mimic and the promiscuous substrate mimic.

In this study, we undertook biochemical studies on *Sso*Pox that further illustrate the potential of this enzyme as an OP biodecontaminant. We performed kinetic characterization of *Sso*Pox with a broad range of organophosphorus compounds including nerve agent analogues, as well as in various detergents and denaturing agents. Furthermore, we discuss the non-productive mode of fensulfothion-binding in the structure and its implications for substrate recognition in *Sso*Pox's active site.

Results

***Sso*Pox OP hydrolase activity characterisation.** Catalytic parameters of *Sso*Pox with (ethyl-)paraoxon (**Fig. 1I**) were characterised at 70°C ($k_{cat}/K_M = (1.22\pm0.21)\times10^3$ $M^{-1}s^{-1}$) (**Table I**). These results are in agreement with previous studies[17] (**Table SI**). Kinetic assays were also performed at 25°C (**Table I**), and reveal, for the first time, that *Sso*Pox is approximately 2.5 times less efficient at 25°C than at 70°C ($k_{cat}/K_M = (5.19\pm1.31)\times10^2$ $M^{-1}s^{-1}$). *Sso*Pox is thus the most efficient PLL against paraoxon at both 70°C and 25°C[9,14,22–24] (**Table SI & SII**). These values, however, are very low compared to the best organophosphate degrading enzyme, PTE from *Pseudomonas diminuta* which exhibits second order rate constants for paraoxon near the diffusion limit ($k_{cat}/K_M \sim 10^8$ $M^{-1}s^{-1}$)[25]. This observation is in agreement with the nature of PLLs which exhibit a promiscuous phosphotriesterase activity, whereas PTEs are natural phosphotriesterases[14,20].

Others OPs were also tested as substrates at 25°C (**Table I**), including the phosphotriesters methyl-paraoxon, (ethyl-)parathion, methyl-parathion, malathion and the phosphodiesters CMP-coumarin, IMP-coumarin and PinP-coumarin (cyclosarin, sarin and soman derivatives, respectively, in which the fluoro substituent of cyclosarin has been replaced by a cyanocoumarin group[26]; see Methods for more details)(**Fig. 1VII, VIII & IX**). These assays showed that *Sso*Pox exhibits about 2.5 times higher catalytic efficiency toward methyl-paraoxon than against (ethyl-)paraoxon ($k_{cat}/K_M = (1.27\pm0.70)\times10^3$ $M^{-1}s^{-1}$ and $(5.19\pm1.31)\times10^2$ $M^{-1}s^{-1}$, respectively). This preference is mainly due to a tenfold lower K_M for methyl-paraoxon than for paraoxon. In a similar fashion, *Sso*Pox shows higher catalytic efficiency for methyl-parathion ($k_{cat}/K_M = 9.09 \pm 0.90$ $M^{-1}s^{-1}$), compared with parathion for which no catalysis could be detected. This result suggests that the bulkiness of the substituent groups of certain phosphotriesters prevents a catalytically efficient binding. This feature was also previously observed for *Sso*Pox and *Sac*Pox at 70°C[22], and for *Dr*OPH at 35°C[24].

Although methyl-paraoxon and methyl-parathion differ by only one atom (the terminal oxygen of the phosphorous moiety is a sulphur atom in parathion (**Fig. 1IV**)), *Sso*Pox hydrolyses methyl-paraoxon approximately 100 times more efficiently ($k_{cat}/K_M = (1.27\pm0.70)\times10^3$ $M^{-1}s^{-1}$ and 9.09 ± 0.90 $M^{-1}s^{-1}$, respectively). The observed K_M values actually suggest that the Michaelis complex formation is more favourable with methyl-parathion than with methyl-paraoxon (approximately ten fold). However, the k_{cat} decreases approximately 1000 times with methyl-parathion compared to methyl-paraoxon, which may reveal a less productive binding of thiono-phosphotriesters compared to that of oxons. This phenomenon was named the thiono-effect and a similar tendency was previously observed in *Agrobacterium radiobacter* PTE with chlorpyrifos and chlorpyrifos oxon[27]. However, PTEs do not exhibit such a drastic difference regarding paraoxon which is only a slightly better substrate than parathion[5,28].

Kinetic parameters were also recorded for the hydrolysis of another sulphur-containing organophosphate, the insecticide malathion ($k_{cat}/K_M = 5.56 \pm 1.26$ $M^{-1}s^{-1}$). This substrate possesses an equivalent K_M value for the enzyme as for methyl-parathion, but the turnover is slower. Finally, *Sso*Pox does not exhibit any detectable activity against PinP-coumarin, but hydrolyses the nerve agent analogs CMP-coumarin and IMP-coumarin with moderate efficiencies

Table 1 | Organophosphate hydrolase activity characterisation of *Sso*Pox

Substrate	k_{cat} (s^{-1})	K_M (μM)	k_{cat}/K_M ($s^{-1}M^{-1}$)
Paraoxon (I) 70°C	3.98 ± 0.23	3270 ± 380	(1.22 ± 0.21) × 10^3
Paraoxon (I) 25°C	12.59 ± 1.26	24250 ± 3616	(5.19 ± 1.31) × 10^2
Paraoxon (I) SDS 0.1% 25°C	40.72 ± 7.70	12340 ± 3630	(3.30 ± 1.59) × 10^3
Paraoxon (I) SDS 0.01% 25°C	24.59 ± 1.77	3830 ± 630	(6.42 ± 1.52) × 10^3
Paraoxon (I) DOC 0.1% 25°C	6.30 ± 0.24	570 ± 70	(1.10 ± 0.16) × 10^4
Paraoxon (I) DOC 0.05% 25°C	4.72 ± 0.13	270 ± 30	(1.72 ±0.21) × 10^4
Paraoxon (I) DOC 0.01% 25°C	10.51 ± 0.75	730 ± 120	(1.44 ± 0.35) × 10^4
Methyl-Paraoxon (II) 25°C	2.71 ± 0.64	2142 ± 676	(1.27 ± 0.70) × 10^3
Parathion (III) 25°C	ND	ND	ND
Methyl-Parathion (IV) 25°C	(1.1±0.02) × 10^{-3}	121 ± 10	9.09 ± 0.9
Malathion (VI) (*r*) 25°C	(8.9±0.4) × 10^{-4}	160 ± 29	5.56 ± 1.26
CMP-coumarin (VII) (*r*) 25°C	ND	ND	(8.13±0.08) × 10^3
CMP-coumarin (VII) (*r*) SDS 0.01% 25°C	25.47 ± 0.42	137.0 ± 7.0	(1.9±0.1) × 10^5
CMP-coumarin (VII) (*r*) DOC 0.01% 25°C	3.3 ± 0.14	71.3 ± 14.8	(4.63±1.16) × 10^4
IMP-coumarin (VIII) (*r*) 25°C	ND	ND	(1.67±0.04) × 10^3
PinP-coumarin (IX) (*r*) 25°C	ND	ND	ND

ND correspond to not dertermined value because of the saturation of the enzyme could not be reached or because there is no or too low hydrolysis of the substrates. (*r*) corresponds to the racemic mix of compounds. Roman numerotation refered to molecules presented in **Figure 1**. The background rates for these reactions are presented in Table SIII.

(k_{cat}/K_M = (8.13±0.08)×10^3 $M^{-1}s^{-1}$ and (1.67±0.04)×10^3 $M^{-1}s^{-1}$, respectively). These values are consistent with those of *P. diminuta* PTE against sarin and soman (k_{cat}/K_M of (9 ± 3)×10^4 $M^{-1}s^{-1}$ and (2.6 ± 0.2)×10^3 $M^{-1}s^{-1}$,respectively)[7], although the coumarin derivatives are more activated substrates.

Anionic detergents enhance paraoxon hydrolysis catalysed by *Sso*Pox. Sso*Pox paraoxonase activity enhancement by SDS.* Previous results have shown that SDS increases paraoxon hydrolysis by *wt Sso*Pox[13]. In this study, we tested various concentrations of SDS (**Fig. 2A**); the highest effect occurs at 0.01% with a velocity enhancement of approximately 5.5 times. The catalytic parameters of *Sso*Pox at 25°C were thus characterised in the presence of 0.01% of SDS (**Table I**) and highlight an approximately 12.5 times catalytic efficiency enhancement compared to that without detergent at 25°C (**Fig. 2H**).

Enhancement of Sso*Pox paraoxonase activity by DOC.* Different DOC concentrations were used during the kinetic experiments (**Fig. 2B**). The greatest effect was obtained with 0.05% DOC (k_{cat}/K_M = (1.72±0.21)×10^4 $M^{-1}s^{-1}$) (**Table I**). With approximately 33 fold catalytic efficiency improvement (**Fig. 2H**), the observed effect with 0.05% DOC is more pronounced than that observed with SDS. These results indicate that despite having two very different chemical structures (**Fig. S1**), the two anionic detergents SDS and DOC improve the kinetic parameters of *Sso*Pox against paraoxon. Interestingly, this improvement might have different causes, because SDS produces an apparently equivalent effect on k_{cat} and K_M whereas DOC positively impacts K_M but decreases k_{cat} (**Table I**).

Effect of anionic detergents on nerve agent analogues hydrolysis. The ability of DOC and SDS to enhance the CMP-coumarin hydrolysis by *Sso*Pox has been tested using 0.01% of each detergent (**Table I**). Catalytic parameters show that DOC and SDS allow catalytic efficiency enhancements of approximately 6 and 23 times, respectively, (DOC: k_{cat}/K_M = (4.63±1.16)×10^4 $M^{-1}s^{-1}$; SDS: k_{cat}/K_M = (1.9±0.1)×10^5 $M^{-1}s^{-1}$), which illustrates the potential of *Sso*Pox for nerve agent decontamination.

*Sso*Pox was characterised to be homodimeric in crystals[15] and a rapid equilibrium between monomeric and dimeric forms was observed with size exclusion chromatography experiments[9]. A possible explanation for the observed paraoxon hydrolysis enhancement is a detergent-induced dissociation of the *Sso*Pox homodimer that could influence the kinetic parameters of the enzyme. Another possibility is a conformational change of the enzyme induced by the detergents. These possibilities were investigated by size exclusion chromatography (**Fig. S2A**), DLS experiments (**Fig. S2B**), and tryptophan fluorescence (**Fig. S2C**), but these studies did not reveal any significant differences with or without SDS.

Effect of other denaturing agents on *Sso*Pox paraoxonase activity. Other denaturing compounds (guanidinium chloride, urea, tween 20, DMSO; see methods for more details) were used and their effect on the paraoxonase activity was recorded. All of the tested compounds can improve the hydrolysis of paraoxon catalysed by *Sso*Pox (**Fig. 2**), albeit with variable amplitudes. Interestingly, unlike the two anionic detergents tested in this study, tween 20 only induces a mild improvement (**Fig. 2C**). Chaotropic agents such as guanidinium chloride (**Fig. 2D**) or urea (**Fig. 2E**), as well as the organic solvent DMSO (**Fig. 2F**), show very little paraoxon hydrolysis enhancement. The highest enhancements are observed with the anionic detergents SDS and DOC (**Fig. 2G**).

Fensulfothion is an inhibitor for *Sso*Pox. Fensulfothion is a substrate for the *P. diminuta* PTE[5] but was previously mentioned as a potent inhibitor for *Sso*Pox[9]. It thus constitutes a good candidate for structural studies, given the very high similarity between the chemical structures of fensulfothion and paraoxon (**Fig. 1V & I**). Preliminary experiments with *Sso*Pox demonstrated that the K_I of fensulfothion, given that this molecule is not water-soluble, is too high to be characterised in classical conditions (data not shown). However, the K_I could be determined in 0.01% SDS (7.78 ± 1.23 mM) (**Fig. S3**). This value is very similar to the K_M values of the enzyme for paraoxon (24 mM without SDS; 4 mM with 0.01% SDS). Because of technical limitations, such as the very low solubility of fensulfothion in water, we were unable to determine experimentally the nature of the inhibition by kinetic experiments.

Unexpected binding mode of the fensulfothion. *Sso*Pox is an enzyme that catalyses two different types of reaction: the hydrolysis of lactones, its preferred substrate, and the hydrolysis of promiscuous substrates, the OPs. The mechanism by which the two different chemical reactions occur within the same active site is not known yet, but some evidence suggests that the promiscuity originates in lactonases from an overlap between the stabilisation of the transition state species of the native substrate and the binding of the promiscuous one[20,29]. To understand how phosphotriesters bind to the active site of *Sso*Pox, we performed co-crystallisation experiments

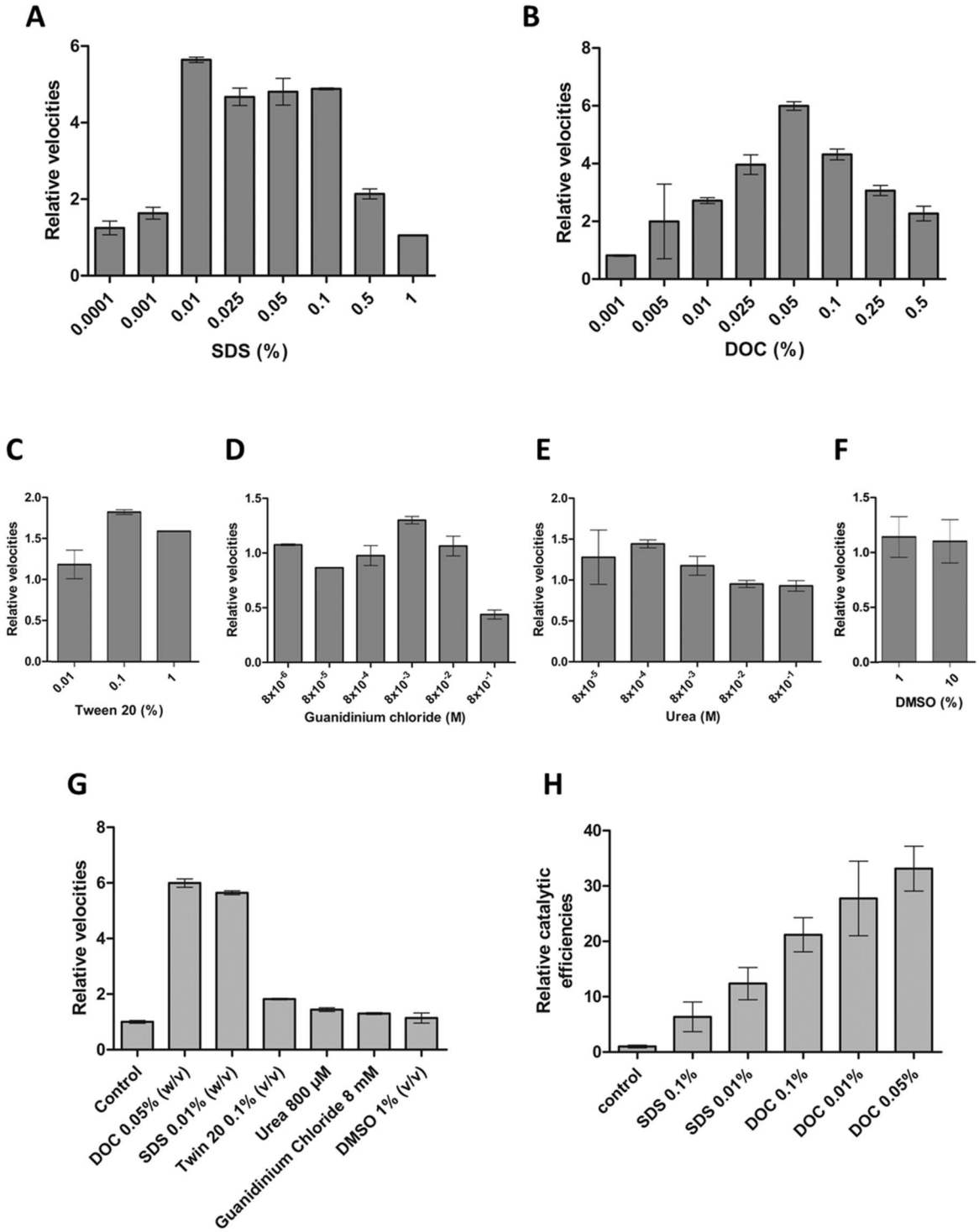

Figure 2 | Enhancement of the paraoxonase activity of *Sso*Pox by different chaotropic agents or detergents. The relative velocity of *Sso*Pox against 1 mM of paraoxon (A., C., D., E., F.) or 100 µM of paraoxon (B) in the presence of various concentrations of destabilising molecules is represented compared to activity without detergent (buffer taking value 1). (G) The highest effect of each compound (DOC, SDS, Tween 20, Urea, Guanidinium Chloride and DMSO) on velocity is represented and the concentrations are indicated. (H) The relative catalytic efficiency of *Sso*Pox against paraoxon at various concentrations of SDS and DOC is represented relative to the catalytic efficiency without detergent (control). The backgrounds for the different reactions are presented in Table SVI.

with various phosphotriesters. Attempts with triethylphosphate and diethyl (4-methylbenzyl) phosphonate failed (Elias *et al.*, unpublished). A complexed *Sso*Pox structure was obtained with the inhibitor fensulfothion at medium resolution (2.68 Å). Interestingly, the binding mode of fensulfothion to the *Sso*Pox's active site is completely unexpected. Indeed, being (i) a very close mimic of paraoxon, and (ii) a substrate for the *P. diminuta* PTE, fensulfothion's binding mode was expected to reveal the phosphotriester-binding mode of *Sso*Pox. However, the structure reveals that the phosphorous moiety of fensulfothion does not bind to the bi-metallic centre, whereas the methyl sulfinyl group occupies the active site (**Fig. 3A**). This unexpected configuration is unambiguous from the

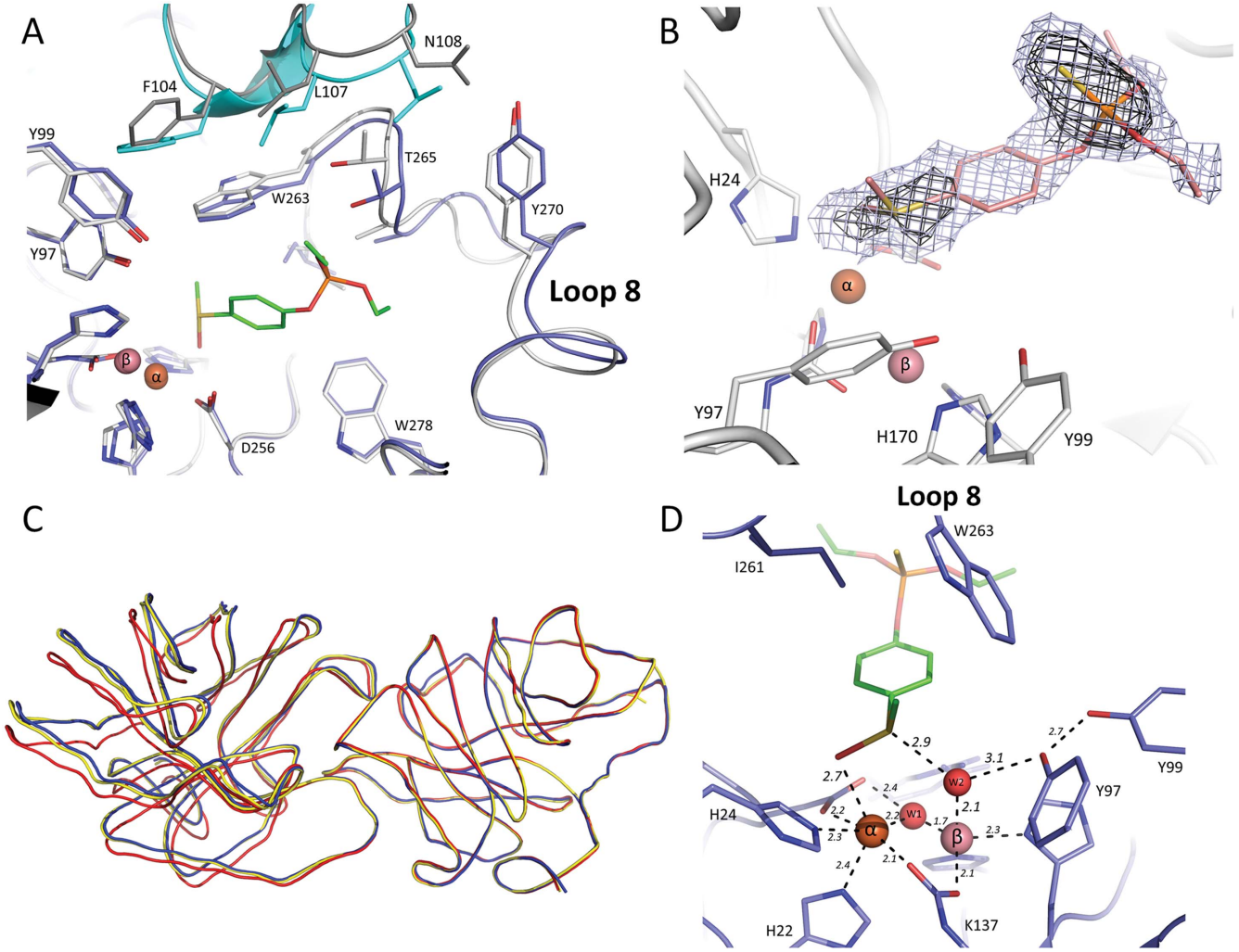

Figure 3 | Structural studies. (A) Structural superposition between the apo structure of *Sso*Pox (PDB ID: 2vc5; monomer A) (in light grey sticks) and the complexed structure of *Sso*Pox with fensulfothion (monomer C; in blue sticks). The contacting monomers (forming the *Sso*Pox homodimer) are shown in dark grey (apo structure) and cyan (fensulfothion-bound structure). The fensulfothion molecule is shown as green sticks, and the two metal ions in the active site are represented by two spheres. (B) Fourier difference electronic density omit map for the bound fensulfothion. The F_{obs}-F_{calc} electronic density map was calculated omitting the fensulfothion molecule from the model in all monomers. The electronic density map is shown as a blue mesh (contoured at 2.5σ) and as a black mesh (contoured at 3.5σ). (C) Ribbon representation of *Sso*Pox homodimers from the apo structure (PDB ID: 2vc5; in red), the C10-homocysteine thiolactone (C10-HTL) bound structure (PDB ID: 2vc7; in yellow), and the fensulfothion-bound structure (in blue). The structures are superposed onto one monomer of the apo structure of *Sso*Pox (right monomer). This enables the observation of the relative re-orientation of the second monomer in the other structures. (D) Close view on the binding of fensulfothion (green sticks; monomer C) in the active site of *Sso*Pox (blue sticks). Metal cations and active site water molecules (in red) are shown as spheres. W2 corresponds to W362 (monomer A) in the deposited PDB coordinate file. Distances are indicated in Ångstrom.

electronic density map, despite the medium resolution of the structure (**Fig. 3B**). Indeed, the presence of two heavy groups on both sides of the molecule (sulfinyl group on one side, the phosphothiomoiety on the other) enables easy interpretation of the electronic density maps. It is noteworthy that putative nonproductive crystallographic complexes were also previously described with bound phosphotriesters to the *P. diminuta* PTE structure[30].

The active site loop (loop 8) adopts a different conformation with fensulfothion binding, altering the dimer orientation. The fensulfothion-bound crystal structure of *Sso*Pox reveals conformational changes within the active site, especially related to the loop 8 conformation. This active site loop has been described as a key feature for lactone binding, because it creates a hydrophobic channel that binds the aliphatic acyl chain of lactones and undergoes conformational changes upon the lactone binding[15]. The structural comparison of the fensulfothion-bound structure with the apo *Sso*Pox structure (**Fig. 3A**) reveals that the whole loop 8 adopts an alternate conformation. Residues W263, T265 and A266 interact with fensulfothion and undergo significant conformational changes (up to 2.5 Å).

The conformational changes that occur in loop 8 upon fensulfothion binding also influence the conformation of residues from the other monomer, because loop 8 is also involved in the dimerization of *Sso*Pox (**Fig. 3A**). Consequently, we observe a relative reorientation of both monomers closer to each other, compared to the apo structure (**Fig. 3C**). Interestingly, the loop 8 conformation observed in the fensulfothion-bound structure is similar to the one observed in the lactone-bound structure. This is further illustrated by the similar dimer orientations of both bound structures compared to the apo structure (**Fig. 3C**).

Active site configuration. The sulfinyl group of fensulfothion binds to the bi-metallic active site, and more precisely to the more buried

metal (2.7 Å) (iron cation, α-metal) (**Fig. 3D**). The free doublet of electrons of the tetrahedral sulphur atom interacts (2.9 Å) with a water molecule (W2) bound to the more exposed metal (2.1 Å) (cobalt cation, β-metal). This water molecule also makes a hydrogen bond with the Y97 hydroxyl group (3.1 Å), a key residue for lactone binding[15] that is conserved amongst all PLLs and known lactonases from the metallo-β-lactamase superfamily[31]. The rest of the fensulfothion molecule is bound in the hydrophobic channel of *Sso*Pox, formed by loop 8.

Discussion

*Sso*Pox, an appealing candidate for OPs biodecontamination, is a native lactonase with promiscuous phosphotriesterase activity that belongs to the PLL family[14]. Our kinetic characterisation experiments highlight the fact that *Sso*Pox exhibits by far the highest paraoxonase activity amongst PLLs at both 70°C and 25°C[9,14,22–24]. Moreover, we provide kinetic characterisations for various organophosphorus compounds, including methyl-paraoxon, methyl-parathion, malathion, IMP-coumarin and CMP-coumarin. Interestingly, *Sso*Pox exhibits very low catalytic efficiency towards P=S containing organophosphates (*e.g.,* the insecticides parathion, methyl-parathion and malathion). Between P=S and corresponding P=O substrates (*e.g.,* methyl-parathion and methyl-paraoxon), the k_{cat} value differs by 3 orders of magnitude. PTEs, albeit preferring paraoxon to parathion as a substrate, do not exhibit this marked thiono-effect[5,28], although some thiono-effect has been observed for *Ar*PTE with chlorpyrifos and its oxon derivative[27]. PTEs constitute a protein family that is believed to have evolved in the last few decades to specifically hydrolyse man-made insecticides[2]. They have possibly emerged from native lactonases such as PLLs[14], and thus may have evolved to suppress this thiono-effect for certain insecticides. Recently, a study succeeded in reconstructing a PLL-like lactonase from the *pd*PTE illustrating this potent evolutionary history[32].

The ability of *Sso*Pox to hydrolyse insecticides as well as nerve agent analogues such as CMP-coumarin and IMP-coumarin strengthens the potential of this enzyme in biodecontamination. Moreover, we show an increase of the catalytic efficiency with the anionic detergents SDS and DOC, whereas very little improvement was observed with Tween 20, various denaturing agents (urea and guanidinium chloride) and DMSO. The highest paraoxon hydrolysis rate was measured at 25°C with 0.05% DOC (k_{cat}/K_M = $(1.72\pm0.21)\times10^4$ $M^{-1}s^{-1}$). SDS and DOC yield similar hydrolysis rate enhancements with CMP-coumarin as a substrate, suggesting that it may be possible to improve the OP hydrolase activity of *Sso*Pox. The improvement observed with detergents on the room temperature activity of a hyperthermostable enzyme is a common feature[11] that serves as evidence that hyperthermostable enzymes are too rigid at room temperature to be highly active[11]. However, in the case of *Sso*Pox, the observed paraoxonase catalytic efficiency increase with temperature (2.5 fold improvement between 25°C and 70°C) and with detergents (33 fold with 0.05% DOC) vary considerably in amplitude, suggesting that detergents may have actions other than mimicking the conformational flexibility provided by the thermal energy. Our investigation of the possible modulation of *Sso*Pox oligomeric state or protein conformation in the presence of SDS did not show any significant changes.

Moreover, we solved the structure of *Sso*Pox in complex with a phosphotriester, fensulfothion. This structure reveals an unexpected binding mode. Fensulfothion binds to the bi-metallic active site by its sulfinyl group, and not by the phosphorous moiety. This unexpected binding most likely explains why fensulfothion is an inhibitor, whereas closely related compounds such as methyl-parathion or paraoxon (differing mainly by having a nitro group instead of the methyl sulfinyl group of fensulfothion) are substrates for *Sso*Pox. In addition, this structure also exemplifies the fact that blind enzymology can lead to misinterpretations in such cases. It also constitutes an interesting case of promiscuous binding to the *Sso*Pox active site that could result in promiscuous chemistry if one substituent of the sulfinyl group is a good leaving group. This unproductive binding also reveals that *Sso*Pox's active site hardly promotes productive binding of phosphotriesters. This feature could be partially explained by a smaller sub-site than PTEs, as previously noted[15]. Indeed, residues such as W263, Y97 and R223, which are key residues for the lactonase activity[15], possibly trade off with the promiscuous activity and may therefore represent interesting mutational targets. This possible steric hindrance is consistent with the poor K_M values of *Sso*Pox for phosphotriesters (24 mM for paraoxon) and may also explain why methyl-paraoxon is a better substrate than ethyl-paraoxon, with a tenfold better K_M.

Furthermore, the binding mode of the inhibitor fensulfothion is interesting because of the close chemical similarity between this molecule and the substrates paraoxon and parathion. Indeed, fensulfothion is less polarised than these two compounds, including at the phosphorous centre. Fensulfothion therefore has a higher propensity to bind according to its shape, yielding to non-productive orientations as has been previously proposed for thiono phosphotriesters compared to oxono which is more polarised[27]. The lower observed K_M for parathion compared to that of paraoxon may also reflect a high affinity for sulphur atoms of the bi-metallic active site that could yield to non-productive binding modes.

Methods

Production-purification of *Sso*Pox. The gene encoding for *Sso*Pox was optimised for *E. coli* expression, synthetised by GeneArt (Germany), and subsequently cloned into the pET22b plasmid using NcoI and HindIII as restriction enzymes. Protein production was performed in *E. coli* BL21(DE_3)-pGro7/GroEL strain cells (TaKaRa) in 8 litres of ZYP medium[33] (100 μg/ml ampicillin, 34 μg/ml chloramphenicol) inoculated by an over-night pre-culture at a 1/20 ratio. Cultures grew at 37°C to reach OD_{600nm} = 1.5. The induction of the protein was made by starting the consumption of the lactose in ZYP medium with an addition of 0.2 mM $CoCl_2$ and a temperature transition to 25°C for 20 hours. Cells were harvested by centrifugation (3000 g, 4°C, 10 min), re-suspended in lysis buffer (50 mM HEPES pH 8, 150 mM NaCl, $CoCl_2$ 0.2 mM, 0.25 mg/ml lysozyme, 0.1 mM PMSF, 10 μg/ml DNAseI and 20 mM $MgSO_4$) and stored at −80°C. Suspended frozen cells were thawed and disrupted by three steps of 30 seconds of sonication (Branson Sonifier 450; 80% intensity and microtip limit of 8). Cell debris was removed by centrifugation (12000 g, 4°C, 30 min). As *Sso*Pox is hyperthermostable[9], host proteins were precipitated by incubation for 30 minutes at 70°C and harvested by centrifugation (12000 g, 4°C, 30 min). A second step of heating at 85°C for 15 minutes and centrifugation was performed to precipitate more host proteins. Thermoresistant proteins from *E. coli* were eliminated by performing ammonium sulphate precipitation (326 g/L). *Sso*Pox was concentrated by ammonium sulphate precipitation (476 g/L) and suspended in buffer 50 mM HEPES pH 8, 150 mM NaCl, 0.2 mM $CoCl_2$. Remaining ammonium sulphate was removed by dialysis against the same buffer and the protein sample was then concentrated for separation on exclusion size chromatography (S75-16-60, GE Healthcare) to obtain pure protein.

Oligomerisation state-interaction analysis. *Size exclusion chromatography*: Experiments were performed in buffer 50 mM HEPES pH 8, 150 mM NaCl and 0.2 mM $CoCl_2$ at room temperature with approximately 5 mg of purified protein using a GE Healthcare S75-16-60 column connected to an ÄKTA-FPLC UPC-900 apparatus and monitored by UNICORN 4.11 software. Experiments were performed in the presence of 0%, 0.1% and 0.01% (w/v) of SDS. The column was previously calibrated with standard proteins (Gel filtration calibration kit, GE Healthcare) of known mass. The resulting elution profile was used as standard to evaluate the molecular weight of species observed during the experiments.

Dynamic light scattering (DLS): Experiments were performed at room temperature using a zetasizer nano series apparatus (Malvern, UK) and the Zetasizer software. A total of 30 μL of purified *Sso*Pox (4 mg/mL) was used in *activity buffer* (50 mM HEPES pH 8, 150 mM NaCl, 0.2 mM $CoCl_2$; pH adjusted with NaOH at 25°C) and different amounts of SDS (0%, 0.1% and 0.01%; w/v) were used to measure the hydrodynamic radius of particles in the protein solution at 633 nm.

Fluorescence experiments: Experiments were performed in *activity buffer* with the addition of 0%, 0.1% or 0.01% (w/v) SDS using a Varian Cary Eclipse apparatus monitored by the Cary Eclipse software. *Sso*Pox protein (0.2 mg/mL) was excited at 280 nm (maximum excitation wavelength of tryptophan) and the emitted fluorescence was measured between wavelengths of 300 to 500 nm.

Kinetic assays. The time course of paraoxon hydrolysis by *Sso*Pox at 70°C was monitored by following the production of *p*-nitrophenolate at 405 nm (ε = 17000 $M^{-1}cm^{-1}$) in a 1-cm path length cell with a Cary WinUV spectrophotometer (Varian, Australia) using the Cary WinUV software. Standard assays (500 μL) were

Table 2 | Data collection and refinement statistics

Data collection	
PDB ID	3uf9
Wavelength (Å)	0. 979
Resolution (Å)	2.68
Space group	P 2_1 2_1 2_1
Unit Cell (Å)	a=85.73 b=103.76 c=151.76
N° observed reflections (last bin)	271688 (33861)
N° unique reflections (last bin)	38674 (4692)
Completeness (last bin) (%)	99.8 (100.0)
R_{merge}[a] (last bin)	0.159 (0.51)
$R_{measured}$[b] (last bin)	0.171 (0.549)
$I/\sigma(I)$ (last bin)	10.18 (3.88)
Last resolution shell	2.68–2.80
Redundancy (last bin)	7.02 (7.22)
Wilson B-factor (Å^2)	38.10
Refinement statistics	
Resolution range (Å)	45.47–2.68
Number of reflections used in refinement	36740
R_{free}/R_{work} [c]	27.54/23.94
N° of protein atoms	10262
N° of water molecules	155
Average B factors (protein/ligand/water) (Å^2)	34.7/31.7/25.3
Average B factor (Å^2)	34.515
rmsd bond length (Å)	0.003
rmsd bond angle (°)	0.731
Ramachandran outliers (%)	0.4
Ramachandran favoured regions (%)	93.1
Allowed regions (%)	6.5

[a] $R_{sym}=R_{merge}=\sum_h|\hat{I}_h-I_{h,i}|\Big/\sum_h\sum_i^{nh}I_{h,i}$.

[b] $R_{meas}=\sum_h\sqrt{\frac{n_h}{n_h-1}}\sum_i^{nh}|\hat{I}_h-I_{h,i}|\Big/\sum_h\sum_i^{nh}I_{h,i}$. with $\hat{I}_h=\frac{1}{n_h}\sum_i^{nh}I_{h,i}$.

[c] $R_{work}=\Sigma\big|\,|F_O|-|F_c|\,\big|/=\Sigma|F_O|$ where F_O denotes the observed structure factor amplitude and F_c denotes the structure factor amplitude calculated from the model. R_{free} is as for R_{work} but calculated with 5% of randomly chosen reflections omitted from the refinement.

performed in buffer 50 mM CHES pH 9, 150 mM NaCl, 0.2 mM $CoCl_2$, 6% (v/v) EtOH, with pH adjusted with NaOH at 70°C and using 5 µL of *Sso*Pox (1.5 mg/mL) for each experiment. Catalytic parameters were evaluated using a substrate (paraoxon) concentration range from 0 to 6 mM. The initial velocities at each substrate concentration were calculated using Excel software (Microsoft). The background rates of paraoxon hydrolysis have been subtracted from the kinetic experiments (**Table SIII**) at each substrate concentration. The catalytic parameters were obtained by fitting velocities *versus* substrate concentration to the Michaelis-Menten (MM) equation using Graph-Pad Prism 5 software.

At 25°C, the paraoxonase, methyl-paraoxonase, parathionase and methyl-parathionase hydrolysis activity was followed at 405 nm (ε = 17000 $M^{-1}cm^{-1}$) with a microplate reader (Synergy HT) and Gen5.1 software in a 6.2 mm path length cell for 200 µL reactions in a 96-well plate. Paraoxonase activity was followed over the concentration range 0–18 mM, methyl-paraoxonase and methyl-parathionase activity have been followed over the concentration range 0–1 mM. Paraoxonase activity assays were also performed using 0.01% and 0.1% (w/v) SDS [sodium dodecyl sulphate (Sigma-Aldrich, France)(**Fig. S1A**)] and 0.1%, 0.05% and 0.01% (w/v) DOC [sodium deoxycholate (Sigma-Aldrich, France)(**Fig. S1B**)] over a range of paraoxon concentrations between 0 and 2 mM. Standard assays were performed in *activity buffer*. The substrate solvent final concentration (ethanol) is below 1% (v/v). Malathionase activity was performed in *activity buffer* supplemented with DTNB 2 mM to follow the malathion hydrolysis at 412 nm (ε = 13400 $M^{-1}cm^{-1}$) over concentrations ranging between 0 and 2 mM. The substrate solvent final concentration (DMSO) was 1% (v/v)). Time course hydrolysis of CMP-coumarin (methylphosphonic acid 3-cyano-4-methyl-2-oxo-2H-coumarin-7-yl ester cyclohexyl ester), IMP-coumarin (methylphosphonic acid 3-cyano-4-methyl-2-oxo-2H-coumarin-7-yl ester isopropyl ester) and PinP-courmarin (methylphosphonic acid 3-cyano-4-methyl-2-oxo-2H-coumarin-7-yl ester pinacolyl ester)[26] were evaluated by following the release of cyanocoumarin at 412 nm (ε = 37000 $M^{-1}cm^{-1}$) in the *activity buffer*. Experiments of CMP-coumarin hydrolysis in the presence of 0.01% SDS and DOC were performed in the same conditions as previously explained. Catalytic parameters were evaluated over the substrate concentration range 0–750 µM. All kinetic experiments were performed in triplicate.

The initial velocities of these experiments were calculated using Gen5.1 software, the backgrounds of substrate hydrolysis subtracted (**Table SIII**) and catalytic parameters were obtained by fitting the data to the MM equation using Graph-Pad Prism 5 software.

Detergent assays. Simple kinetic experiments were performed in the presence of various detergents: SDS (w/v) (1%, 0.5%, 0.1%, 0.05%, 0.025%, 0.01% and 0.001%), tween 20 (v/v) (1%, 0.1% and 0.01%); denaturing agents such as guanidinium chloride (800 mM, 80 mM, 8 mM, 800 µM, 80 µM and 8 µM), urea (800 mM, 80 mM, 8 mM, 800 µM, 80 µM) and the solvent DMSO (v/v) (10% and 1%), and buffer 50 mM CHES pH 9, 150 mM NaCl, 0.2 mM $CoCl_2$, 6% (v/v) EtOH in the presence of 1 mM of paraoxon using 5 µL of *Sso*Pox (3.5 mg/mL or 0.35 mg/mL when the enhancement effect of the paraoxonase activity was too high). At 25°C, the paraoxonase activity was followed at 430 nm (ε = 8970 $M^{-1}cm^{-1}$) with a microplate reader (Tecan) and Magellan software in a 6.2 mm path length cell for 200 µL reactions in a 96-well plate. Kinetic experiments in the presence of DOC were performed as previously described except that kinetics were performed with 1 µL of *Sso*Pox (0.3 mg/mL), 100 µM of paraoxon and detergent concentrations of 0.001%, 0.005%, 0.01%, 0.025%, 0.05%, 0.1%, 0.25% and 0.5% (w/v). At 25°C, the paraoxonase activity was followed at 405 nm (ε = 17000 $M^{-1}cm^{-1}$) in *activity buffer* with a microplate reader (Synergy HT) and Gen5.1 software in a 6.2 mm path length cell for 200 µL reaction in 96-well plate. The average velocities and their respective errors were obtained from duplicate or triplicate experiments and the background rates of substrate hydrolysis (Table SIV) were subtracted from the recorded velocities.

Inhibition assay. The inhibition of the enzyme by fensulfothion was evaluated by performing kinetic assays against paraoxon (concentration range 0–300 µM) and by using different fensulfothion concentrations in buffer 50 mM CHES pH 9, 150 mM NaCl, 0.2 mM $CoCl_2$, 6% (v/v) EtOH with 0.01% (w/v) of SDS. Because of the low solubility of fensulfothion in water, it was dissolved in 100% acetonitrile and the kinetics were measured at final concentration of 10% (v/v) of acetonitrile. Experiments were performed with concentrations of 0, 1, 2, 3, 4, 5 and 6 mM to evaluate the K_I of fensulfothion.

Because of the low solubility of the substrate and the inhibitor, the velocities at high substrate concentration cannot be reached. Catalytic parameters (k_{cat}; K_M) cannot be determined directly. However, by fitting to linear regression the linear part of the MM plot (Graph-Pad Prism 5 software), the catalytic efficiencies (k_{cat}/K_M) have been determined. A Dixon plot cannot be made to determine the inhibition constant (K_I); however, as previously performed[34], the representation of the inverse of the catalytic efficiency at each fensulfothion concentration allows the fit of a linear regression where inhibition constant corresponds to the x-intercept ($-K_I$).

Crystallisation. For the crystallisation studies presented herein, recombinant *Sso*Pox was used. The enzyme was concentrated at 6 mg/mL. Co-crystallisation assays with fensulfothion were performed by adding 1 µL of a 100 mM fensulfothion solution (1:1 ratio in acetonitrile) in 30 µL of the protein solution (approximately 3.2 mM final). Crystallisation was performed using the hanging drop vapour diffusion method. Equal volumes (0.5–1 µL) of protein and reservoir solutions were mixed, and the resulting drops were equilibrated against an 800 µL reservoir solution containing 23–25% (w/v) PEG 8000 and 50 mM Tris-HCl buffer (pH 8). Thin crystals appeared after one week at 277 K.

Data collection and structure determination. Crystals were first transferred to a cryoprotectant solution composed of the reservoir solution and 25% (v/v) glycerol containing a 1/30 (v/v) ratio of a 100 mM fensulfothion solution. Crystals were then flash-cooled in liquid nitrogen. X-ray diffraction data were collected at 100 K using synchrotron radiation at the ID23-1 beam line (ESRF, Grenoble, France) with a ADSC Q315r detector. A data set was recorded at 2.68 Å resolution (**Table II, Fig. S4**). X-ray diffraction data were integrated, scaled and merged with the XDS program[35] and the CCP4 program suite[36]. The phases were obtained using the native structure of *Sso*Pox (PDB ID: 2vc5), performing a molecular replacement with MOLREP[37]. The model was built with Coot[38] and refined using REFMAC[39]. The anisotropic displacement parameters were refined via four groups of translation-liberation-screw (TLS) parameterisation identified by REFMAC[40]. The final stereochemistry was checked using the MOL-PROBITY program[41]. Structure illustrations were performed using PyMol[42]. The coordinate file and the structure factors file of the fensulfothion bound *Sso*Pox structure have been deposited to the Protein Data Bank under the accession number 3uf9.

1. Singh, B. K. Organophosphorus-degrading bacteria: ecology and industrial applications. *Nat Rev Microbiol* **7** (2), 156–64 (2009).
2. Raushel, F. M. Bacterial detoxification of organophosphate nerve agents. *Current opinion in microbiology* **5**(3), 288–95 (2002).
3. LeJeune, K. E., Wild, J. R. & Russell, A. J. Nerve agents degraded by enzymatic foams. *Nature* **395** (6697), 27–8 (1998).
4. Seibert, C. M. & Raushel, F. M. Structural and catalytic diversity within the amidohydrolase superfamily. *Biochemistry* **44** (17), 6383–91 (2005).
5. Dumas, D. P., Caldwell, S. R., Wild, J. R. & Raushel, F. M. Purification and properties of the phosphotriesterase from Pseudomonas diminuta. *J Biol Chem* **264** (33), 19659–65 (1989).
6. Raushel, F. M. Chemical biology: Catalytic detoxification. *Nature* **469** (7330), 310–1 (2011).
7. Tsai, P. C. *et al*. Stereoselective hydrolysis of organophosphate nerve agents by the bacterial phosphotriesterase. *Biochemistry* **49** (37), 7978–87 (2010).

8. Ghanem, E. & Raushel, F. M. Detoxification of organophosphate nerve agents by bacterial phosphotriesterase. *Toxicology and applied pharmacology* **207** (2 Suppl), 459–70 (2005).
9. Merone, L., Mandrich, L., Rossi, M. & Manco, G. A thermostable phosphotriesterase from the archaeon Sulfolobus solfataricus: cloning, overexpression and properties. *Extremophiles* **9** (4), 297–305 (2005).
10. Del Vecchio, P. *et al.* Structural determinants of the high thermal stability of SsoPox from the hyperthermophilic archaeon Sulfolobus solfataricus. *Extremophiles* **13** (3), 461–70 (2009).
11. Vieille, C. & Zeikus, G. J. Hyperthermophilic enzymes: sources, uses, and molecular mechanisms for thermostability. *Microbiol Mol Biol Rev* **65** (1), 1–43 (2001).
12. Demirjian, D. C., Moris-Varas, F. & Cassidy, C. S. Enzymes from extremophiles. *Current opinion in chemical biology* **5** (2), 144–51 (2001).
13. Merone, L. *et al.* Improving the promiscuous nerve agent hydrolase activity of a thermostable archaeal lactonase. *Bioresour Technol* **101** (23), 9204–12 (2010).
14. Afriat, L., Roodveldt, C., Manco, G. & Tawfik, D. S. The latent promiscuity of newly identified microbial lactonases is linked to a recently diverged phosphotriesterase. *Biochemistry* **45** (46), 13677–86 (2006).
15. Elias, M. *et al.* Structural basis for natural lactonase and promiscuous phosphotriesterase activities. *Journal of molecular biology* **379** (5), 1017–28 (2008).
16. Elias, M. *et al.* Crystallization and preliminary X-ray diffraction analysis of the hyperthermophilic Sulfolobus solfataricus phosphotriesterase. *Acta crystallographica* **63** (Pt 7), 553–5 (2007).
17. Ng, F. S., Wright, D. M. & Seah, S. Y. Characterization of a phosphotriesterase-like lactonase from Sulfolobus solfataricus and its immobilization for quorum quenching. *Appl Environ Microbiol* (2010).
18. Popat, R., Crusz, S. A. & Diggle, S. P. The social behaviours of bacterial pathogens. *Br Med Bull* **87**, 63–75 (2008).
19. Dong, Y. H. *et al.* Quenching quorum-sensing-dependent bacterial infection by an N-acyl homoserine lactonase. *Nature* **411** (6839), 813–7 (2001).
20. Elias, M. & Tawfik, D. S. Divergence and Convergence in Enzyme Evolution: Parallel Evolution of Paraoxonases from Quorum-quenching Lactonases. *The Journal of biological chemistry* **287** (1), 11–20 (2012).
21. Gupta, R. D. *et al.* Directed evolution of hydrolases for prevention of G-type nerve agent intoxication. *Nat Chem Biol* **7** (2), 120–5 (2011).
22. Porzio, E., Merone, L., Mandrich, L., Rossi, M. & Manco, G. A new phosphotriesterase from Sulfolobus acidocaldarius and its comparison with the homologue from Sulfolobus solfataricus. *Biochimie* **89** (5), 625–36 (2007).
23. Hawwa, R., Aikens, J., Turner, R. J., Santarsiero, B. D. & Mesecar, A. D. Structural basis for thermostability revealed through the identification and characterization of a highly thermostable phosphotriesterase-like lactonase from Geobacillus stearothermophilus. *Arch Biochem Biophys* **488** (2), 109–20 (2009).
24. Hawwa, R., Larsen, S. D., Ratia, K. & Mesecar, A. D. Structure-based and random mutagenesis approaches increase the organophosphate-degrading activity of a phosphotriesterase homologue from Deinococcus radiodurans. *Journal of molecular biology* **393** (1), 36–57 (2009).
25. Omburo, G. A., Kuo, J. M., Mullins, L. S. & Raushel, F. M. Characterization of the zinc binding site of bacterial phosphotriesterase. *The Journal of biological chemistry* **267** (19), 13278–83 (1992).
26. Ashani, Y. *et al.* Stereo-specific synthesis of analogs of nerve agents and their utilization for selection and characterization of paraoxonase (PON1) catalytic scavengers. *Chemico-biological interactions* **187** (1–3), 362–9 (2010).
27. Jackson, C. J., Liu, J. W., Coote, M. L. & Ollis, D. L. The effects of substrate orientation on the mechanism of a phosphotriesterase. *Org Biomol Chem* **3** (24), 4343–50 (2005).
28. Jackson, C. J. *et al.* Anomalous scattering analysis of Agrobacterium radiobacter phosphotriesterase: the prominent role of iron in the heterobinuclear active site. *The Biochemical journal* **397** (3), 501–8 (2006).
29. Ben-David, M. *et al.* Catalytic versatility and backups in enzyme active sites: the case of serum paraoxonase 1. *Journal of molecular biology* **418** (3–4), 181–96 (2012).
30. Benning, M. M., Hong, S. B., Raushel, F. M. & Holden, H. M. The binding of substrate analogs to phosphotriesterase. *The Journal of biological chemistry* **275** (39), 30556–60 (2000).
31. Momb, J. *et al.* Mechanism of the quorum-quenching lactonase (AiiA) from Bacillus thuringiensis. 2. Substrate modeling and active site mutations. *Biochemistry* **47** (29), 7715–25 (2008).
32. Afriat-Jurnou, L., Jackson, C. J. & Tawfik, D. S. Reconstructing a missing link in the evolution of a recently diverged phosphotriesterase by active-site loop remodeling. *Biochemistry* (2012).
33. Studier, F. W. Protein production by auto-induction in high density shaking cultures. *Protein Expr Purif* **41** (1), 207–34 (2005).
34. Walsh, H. A., O'Shea, K. C. & Botting, N. P. Comparative inhibition by substrate analogues 3-methoxy- and 3-hydroxydesaminokynurenine and an improved 3 step purification of recombinant human kynureninase. *BMC Biochem* **4**, 13 (2003).
35. Kabsch, W. Automatic processing of rotation diffraction data from crystals of initially unknown symmetry land cell constants. *Journal of Applied Crystalography* **26**, 795–800 (1993).
36. Collaborative Computational Project Number 4, The CCP4 suite: programs for protein crystallography. *Acta crystallographica* **50**, 760–3 (1994).
37. Vagin, A. & Teplyakov, A. An approach to multi-copy search in molecular replacement. *Acta Crystallogr D Biol Crystallogr* **56** (Pt 12), 1622–4 (2000).
38. Emsley, P. & Cowtan, K. Coot: model-building tools for molecular graphics. *Acta Crystallogr D Biol Crystallogr* **60** (Pt 12 Pt 1), 2126–32 (2004).
39. Murshudov, G. N., Vagin, A. A. & Dodson, E. J. Refinement of macromolecular structures by the maximum-likelihood method. *Acta Crystallogr D Biol Crystallogr* **53** (Pt 3), 240–55 (1997).
40. Lamzin, V. S. & Wilson, K. S. Automated refinement of protein models. *Acta crystallographica. Section D, Biological crystallography* **49** (Pt 1), 129–47 (1993).
41. Chen, V. B. *et al.* MolProbity: all-atom structure validation for macromolecular crystallography. *Acta crystallographica. Section D, Biological crystallography* **66** (Pt1), 12–21 (2010).
42. DeLano, W. L. The PyMOL Molecular Graphics System. *DeLano Scientific, San Carlos, CA, USA* (2002).

Acknowledgements

We are grateful to Dr. Moshe Goldsmith for the kind gift of CMP-coumarin, IMP-coumarin and PinP-coumarin. We thank Professor Dan Tawfik for constructive discussions on the project and for hosting J.H. in its laboratory. We thank the AFMB laboratory (Marseille, France) for the access to protein production and crystallisation platforms. This work was granted by DGA, France (REI. 2009 34 0045). J.H. and G.G. are PhD students granted by DGA. M.E. is a fellow supported by the IEF Marie Curie program (grant No. 252836).

Author contributions

JH, GG and ME designed the experiments. JH, GG and ME performed the experiments. JH, GG, ME and EC analysed the results. JH, ME and EC wrote the paper. All the authors offer a critical review of the paper.

Additional information

Supplementary information accompanies this paper at http://www.nature.com/scientificreports

Competing financial interests: The authors declare no competing financial interests.

How to cite this article: Hiblot, J., Gotthard, G., Chabriere, E. & Elias, M. Characterisation of the organophosphate hydrolase catalytic activity of *Sso*Pox. *Sci. Rep.* **2**, 779; DOI:10.1038/srep00779 (2012).

F. Etudes structurales des mutants de l'évolution dirigée de *Sso*Pox

Differential active site loop conformations mediate promiscuous activities in the lactonase *Sso*Pox

Guillaume GOTTHARD, Julien HIBLOT*, Mikael ELIAS et Eric CHABRIERE*

* Contribution égale

Article accepté dans le journal « Plos One »

Dans les travaux décrits, j'ai réalisé :

- partie expérimentale : résolution de la structure cristallographique des mutants sélectionnés et affinements, dichroïsme circulaire
- analyses structurales
- écriture de parties de l'article, dépôt des structures des variants sélectionnés sur la PDB (codes pdb : 4KER, 4KES, 4KET, 4KEU, 4KEV, 4KEZ, 4KF1)

Résumé : Ce travail concerne l'étude structurale, enzymatique et biochimique de la mutagénèse à saturation de site sur la position Trp 263 de *Sso*Pox. Au cours de cette étude, l'activité lactonase de *Sso*Pox fut caractérisée révélant que l'enzyme hydrolyse aussi efficacement les AHLs que les oxo-lactones (avec des efficacités catalytiques d'environs $k_{cat}/K_M \sim 10^{3-5}\ M^{-1}.s^{-1}$). *Sso*Pox présente tout de même une préférence pour les lactones à longue chaine aliphatique (8 à 10 carbones pour les AHLs et 4 à 6 carbones pour les oxo-lactones). De plus, il fut montré que l'enzyme est plus spécifique pour l'énantiomère d'AHLs (*l*), qui est l'énantiomère naturellement impliqué dans le *quorum* sensing bactérien à base d'AHLs. Cette énantio-spécificité suggère que *Sso*Pox soit une AHL lactonase naturelle.

Au cours de l'étude précédente, présentée en partie **III. E.**, nous avons mis en évidence l'importance de certains résidus tels que le Trp 263 dans l'accommodation des substrats. Afin d'améliorer les activités de l'enzyme, une mutagénèse à saturation fut réalisée sur cette position et les 19 mutants obtenus furent criblés pour leur activité envers les OPs et envers les lactones. De façon intéressante, l'ensemble des variants criblés possède une activité catalytique plus élevée que la protéine sauvage envers les substrats de promiscuité OPs. En présence de détergents ceux-ci atteignent des efficacités catalytiques d'environ $10^4\ M^{-1}.s^{-1}$ envers le paraoxon. Envers les oxo-lactones, qui sont également des substrats de promiscuité, les variants obtenus permirent d'atteindre une efficacité catalytique de $10^5\ M^{-1}.s^{-1}$. Les variants sélectionnés phosphotriestérase et lactonase constituent deux

groupes distincts (Trp 263 Leu, Met, Phe et Trp 263 Val, Ile, Thr, respectivement) possédant des propriétés de thermorésistance différentes de l'enzyme sauvage.

La structure cristallographique des variants améliorée fut ensuite résolue afin de comprendre l'origine structurale de l'amélioration. Bien que les mutations sélectionnées permettent de créer de l'espace au sein du site actif, la place générée n'explique qu'en partie l'amélioration d'activité observée. L'analyse structurale mit en évidence une augmentation du facteur B moyen de la chaine polypeptidique au niveau de la boucle 8, traduisant une flexibilisation locale de l'enzyme. Cette flexibilité est accrue au niveau de la boucle 8, impliquée dans la spécificité de substrat de *Sso*Pox, avec une flexibilisation plus importante chez les améliorés phosphotriestérase. Ainsi, il est proposé que la flexibilisation de la boucle 8 permet d'élargir le paysage conformationel de *Sso*Pox par rapport à l'enzyme sauvage. Les différents mutants étant alors plus peuplés dans des états conformationels plus aptes à hydrolyser les substrats de promiscuité.

OPEN ACCESS Freely available online

PLOS ONE

Differential Active Site Loop Conformations Mediate Promiscuous Activities in the Lactonase *Sso*Pox

Julien Hiblot[1☯], Guillaume Gotthard[1☯], Mikael Elias[2*], Eric Chabriere[1*]

1 URMITE UMR CNRS-IRD 6236, Faculté de Médecine et de Pharmacie, Université de la Méditerranée, Marseille, France, **2** Weizmann Institute of Science, Biological Chemistry, Rehovot, Israel

Abstract

Enzymes are proficient catalysts that enable fast rates of Michaelis-complex formation, the chemical step and products release. These different steps may require different conformational states of the active site that have distinct binding properties. Moreover, the conformational flexibility of the active site mediates alternative, promiscuous functions. Here we focused on the lactonase *Sso*Pox from *Sulfolobus solfataricus*. *Sso*Pox is a native lactonase endowed with promiscuous phosphotriesterase activity. We identified a position in the active site loop (W263) that governs its flexibility, and thereby affects the substrate specificity of the enzyme. We isolated two different sets of substitutions at position 263 that induce two distinct conformational sampling of the active loop and characterized the structural and kinetic effects of these substitutions. These sets of mutations selectively and distinctly mediate the improvement of the promiscuous phosphotriesterase and oxo-lactonase activities of *Sso*Pox by increasing active-site loop flexibility. These observations corroborate the idea that conformational diversity governs enzymatic promiscuity and is a key feature of protein evolvability.

Citation: Hiblot J, Gotthard G, Elias M, Chabriere E (2013) Differential Active Site Loop Conformations Mediate Promiscuous Activities in the Lactonase *Sso*Pox. PLoS ONE 8(9): e75272. doi:10.1371/journal.pone.0075272

Editor: Fernando Rodrigues-Lima, University Paris Diderot-Paris 7, France

Received May 16, 2013; **Accepted** August 14, 2013; **Published** September 23, 2013

Funding: This work was granted by Direction Générale de l'Armement (DGA), France (REI. 2009 34 0045) and Vaincre La Mucoviscidose, France. JH and GG are PhD students granted by DGA. ME is a fellow supported by the IEF Marie Curie program (grant No. 252836). The funders had no role in study design, data collection and analysis, decision to publish, or preparation of the manuscript.

Competing interests: The authors have declared that no competing interests exist.

* E-mail: mikael.elias@gmx.fr (ME); eric.chabriere@univmed.fr (EC)

☯ These authors contributed equally to this work.

Introduction

Enzymes are considered as highly efficient catalysts, so substrate recognition has long been referred to as the key-lock model with the simple view of "one sequence-one structure-one function" [1] which was subsequently refined by the induce-fit model [2]. Indeed, the protein flexibility indicates that proteins exist as a sampling of similar conformations with discrete energy levels [3,4]. Protein dynamics are essential for protein function and define its conformational landscape. Dynamics enable fast rates of Michaelis-complex formation and products release [4]. In certain cases, the transition step between conformations is the rate limiting step of enzyme catalysis [5]. Moreover, the structural diversity linked to protein flexibility constitutes a foundation of protein evolvability [4]. Indeed, the sampling of enzyme conformations allows the accommodation of different substrates within the same active site or the existence of promiscuous activities [5]. Under selective pressure, conformations allowing promiscuous binding/activities can be selected by evolution. Promiscuity is thus considered to be one of the potential engines of enzyme evolution [1,4,6-8]. Laboratory evolution can successfully exploit promiscuous activity to generate highly efficient and specialized enzymes [9,10]. However, the molecular mechanisms underlining these specializations are still under investigation.

With the aim of understanding the molecular origin of enzymatic promiscuity, we focused on the Phosphotriesterase-Like Lactonases (PLLs) family. PLLs are natural lactonases endowed with promiscuous phosphotriesterase activity [6,11,12]. Isolated from bacterial [11,13-16] or archaeal [17-20] organisms, their physiological function might be related to the bacterial communication system (or *quorum* sensing) by hydrolyzing the *N*-Acyl-Homoserine-Lactones (AHLs; Figure 1AB & S1) [21,22], a *quorum* sensing molecular mediator. Other lactones (oxo-lactones; Figure 1CD & S1) are substrates for these enzymes [23], due to a coincidental binding in their active site [19]. Moreover, PLLs have long been confounded with structurally closely related bacterial phosphotriesterases (PTEs) [11], which hydrolyze paraoxon with a catalytic constant near the physical limit (i.e., k_{cat}/K_M ~ 10^8 $M^{-1}s^{-1}$) [24,25]. PTEs have rapidly evolved from PLLs to

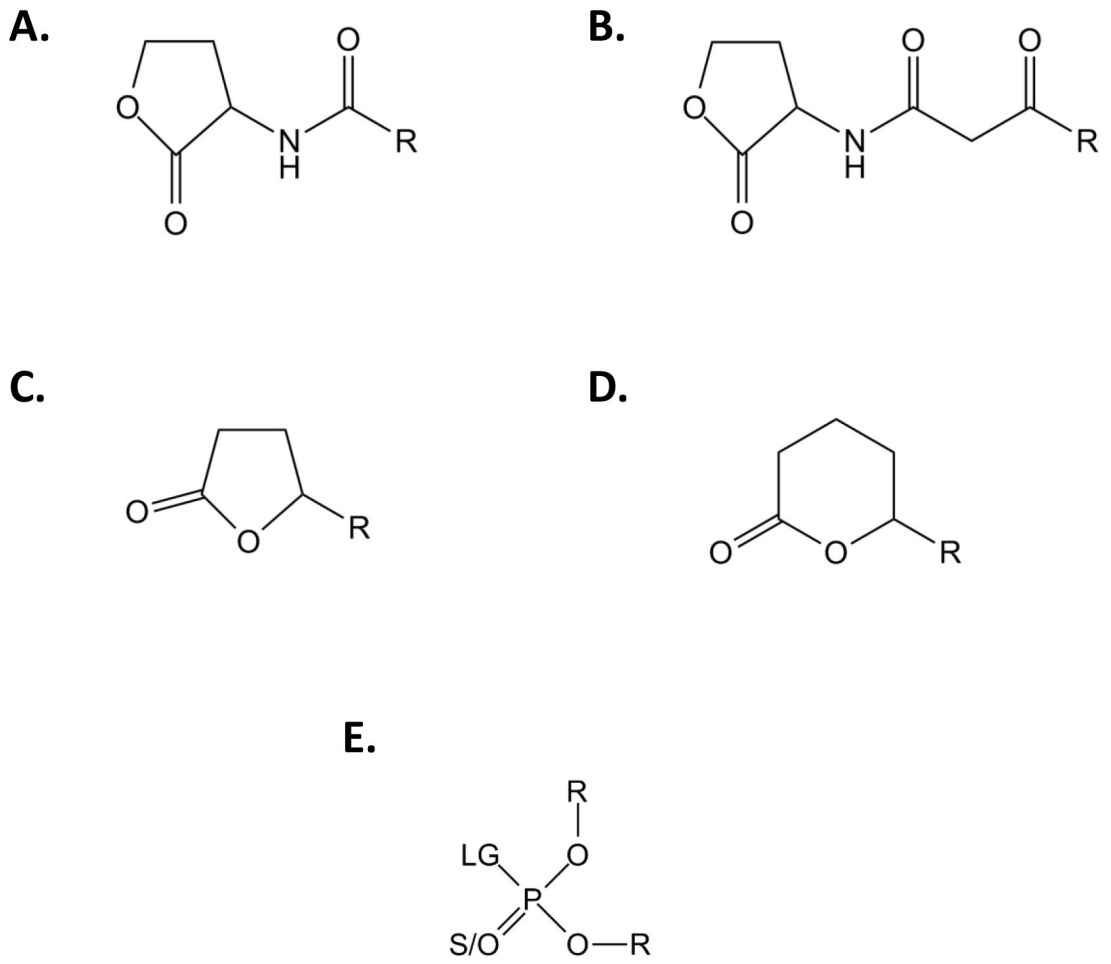

Figure 1. Generic chemical structure of *Sso*Pox substrates. Chemical structures of (A) Acyl-Homoserine Lactones, (B) 3-oxo-Acyl-Homoserine Lactones, (C) γ-lactones, (D) δ-lactones and (E) phosphotriesters are presented. For AHLs and γ/δ-lactones, R corresponds to the different size of the acyl chain. For phosphotriesters, R corresponds to the different nature of substituents; LG corresponds to the leaving group which can be F, S-R, O-R or CN. The terminal substituent could be a S atom if the molecule is a thiono-phosphotriester or an O atom if the molecule is an oxono-phosphotriester.

doi: 10.1371/journal.pone.0075272.g001

very efficiently hydrolyze phosphotriesters (Figure **1E & S1**), a promiscuous activity of PLLs [6,12].

PTEs and PLLs belong to the amidohydrolase superfamily and, exhibit a $(\alpha/\beta)_8$-barrel fold (the so-called TIM-barrel) [24,26]. This fold consists of 8 β-sheets flanked by 8 α-helixes with the catalytic center localized at the C-terminus of the barrel. The catalytic center contained two metal cations coordinated by four histidines, an aspartic acid and a carboxylated lysine residue. These metals activate a bridging water molecule, which, *via* a nucleophilic attack onto the reactive center, allows the substrate hydrolysis. The substrate specificity is mainly governed by variations in the connecting loops of the barrel. Indeed, the major structural differences between PTEs and PLLs reside in the active site loop size and conformation [27]. A structural analysis of *Sso*Pox, a hyperthermostable counterpart of the PLL family from *Sulfolobus solfataricus* [17,27,28], has revealed that loop 7 is shorter in *Sso*Pox than in PTEs; linking the active site to the loop 8, which forms a hydrophobic channel that accommodates AHLs aliphatic chain [22]. The residue W263, located in this cavity, plays a central role in substrate binding in the *Sso*Pox active site. Indeed, W263 is located at the start of loop 8, involved in the dimer interface of the enzyme and positions the lactone cycle of the substrate onto the bi-metallic catalytic center [22]. In this study, we deciphered position 263 contributions to the protein stability, enzymatic activity and promiscuity. We exhaustively mutated this position and selected the most improved variants for both phosphotriesterase and lactonase activities. By cross-analyzing the enzymatic, biochemical and structural properties of the selected variants, we isolated two distinct groups of variants and we propose structural features that may underline these improvements.

Results

Lactonase activity characterization of wild-type SsoPox

PLLs are subdivided into two different subfamilies based on their structures and catalytic preferences: the PLL-A (natural AHLases) and the PLL-B (natural oxo-lactonases) [12]. If lactonases such as PPH and AhlA [11] (PLL-A) exhibit equivalent AHLases and oxo-lactonase activities, *Dr*OPH [29] and *Gk*L [15] (PLL-B) comprise exclusive oxo-lactonases. The lactonase activity of *Sso*Pox, belonging to PLL-A, was assayed with various lactone substrates i.e., AHLs, δ-lactones, γ-lactones with various acyl chain lengths and other lactones (Table **1**). *Sso*Pox is an efficient enzyme against the various lactones, with catalytic efficiencies in the range of 10^4 $M^{-1}s^{-1}$ for nonanoic-δ-latones (r) (6 atoms ring-size), 3-oxo-C10-AHLs (l) and γ-hepetanolide (r) (5 atoms ring-size) (Table **1**). As previously observed for the closely related *Sis*Lac PLL [19], *Sso*Pox exhibits an acyl chain length dependency, preferring AHLs with 8 to 10 carbon aliphatic chains and oxo-lactones with 4 to 6 carbon aliphatic chains. This feature reveals distinct accommodation modes of AHLs and oxo-lactones in the *Sso*Pox active site.

PLLs are believed to be natural AHL lactonases, possibly involved in *quorum* quenching [12,22]. Interestingly, PLLs enzymes, such as *Sso*Pox, hydrolyze a broad spectrum of different lactones. Noteworthy, anionic detergents, which probably increase protein flexibility, strongly stimulate *Sso*Pox promiscuous phosphotriesterase activity (up to 33-fold) [30,31], whereas they have an opposite effect on lactonase activities. In the presence of 0.1% SDS, the enzyme activity towards the best AHL substrate (3-oxo-C10 AHL (*l*)) is severely compromised (161-fold decrease), and, the activity towards undecanoic-γ-lactone (r) is mildly affected (1.3-fold decrease) (Table **1**). Lower SDS concentrations (0.01%) yield to milder but similar effects: the catalytic efficiency against 3-oxo-C10 AHL (l) (10-fold) is decreaed, and undecanoic-γ-lactone (r) hydrolysis is increased (2-fold) (Table **1**). Alterations in substrate specificity induced by detergent were previously observed in enzymes [32], and were mainly attributed to detergent-induced protein flexibility that enlarged the protein conformational landscape [33]. As for *Sso*Pox, detergent-induced flexibility could promotes the increase of promiscuous phosphotriesterase activity but dramatically compromised the AHLase activity, possibly by altering the specific loop conformational sampling required for the proper binding / hydrolysis of AHLs. This result is consistent with AHLs as the native substrates of *Sso*Pox.

Additionally, we investigated the enantiospecificity of *Sso*Pox towards AHLs by using racemic and pure levorotatory 3-oxo-C8 AHLs (Figure **S2**). The levorotatory enantiomer (Specific Activity for the levorotatory enantiomer [i.e., $SA_{(l)}$] = 5.5 (±0.5)x10^{-1} s^{-1}) is hydrolyzed at approximately 2-fold higher velocity than the racemic one ($SA_{1(r)}$ = 3.69 (±0.01)x10^{-1} s^{-1}). Moreover, racemic AHLs hydrolysis by wild-type *Sso*Pox exhibits a biphasic curve. The second recorded velocity ($SA_{2(r)}$ = 1.47 (±0.02)x10^{-2} s^{-1}) presents an approximately 20-fold lower hydrolysis of the dextrorotatory enantiomer highlighting the wild-type *Sso*Pox preference for levorotatory AHLs. The

Table 1. *Sso*Pox lactonase activity characterization.

Substrate		wild-type *Sso*Pox				
	Name	Additive	k_{cat} (s^{-1})	K_M (μM)	K_I (μM)	k_{cat}/K_M ($s^{-1}M^{-1}$)
AHLs	**C4-AHL (r) (V)**	-	ND	ND	ND	11.62 ± 0.72
	C6-AHL (r) (VI)	-	0.36 ± 0.01	459 ± 49	-	7.84 (±0.87)x10^2
	C8-AHL (r) (VII)	-	1.00 ± 0.04	145 ± 26	-	6.90 (±1.27)x10^3
	C12-AHL (r) (VIII)	-	1.70 ± 0.31	345 ± 90	-	4.93 (±1.56)x10^2
3-oxo-AHLs	**3-oxo-C6-AHL (l) (IX)**	-	0.083 ± 0.003	558 ± 68	-	1.49 (±0.20)x10^2
	3-oxo-C6-AHL (r) (IX)	-	0.041 ± 0.005	592 ± 176	-	6.87 (±2.20)x10^1
	3-oxo-C8-AHL (*l*) (X)	-	0.54 ± 0.02	123 ± 22	-	4.39 (±0.80)x10^3
	3-oxo-C8-AHL (r) (X)	-	0.42 ± 0.02	256 ± 55	-	1.63 (±0.36)x10^3
	3-oxo-C10-AHL (l) (XI)	-	4.52 ± 0.10	143 ± 15	-	3.16 (±0.33)x10^4
		+ 0.1% SDS	ND	ND	-	1.96 (±0.04)x10^2
		+ 0.01% SDS	0.75 ±0.03	243±43	-	3.09 (±0.56)x10^3
	3-oxo-C12-AHL (l) (XII)	-	1.01 ± 0.13	456 ± 128	-	2.22 (±0.68)x10^3
γ-lactones	**γ-butyrolactone (XIII)**	-	ND	ND	ND	1.20 (±0.12)x10^3
	γ-heptanolide (r) (XIV)	-	2.92 ± 0.08	166 ± 21	-	1.76 (±0.23)x10^4
	Nonanoic-γ-lactone (r) (XV)	-	5.54 ± 0.57	2 943 ± 436	-	1.88 (±0.34)x10^3
	Undecanoic-γ-lactone (r) (XVI)	-	4.95 ± 0.26	2 099 ± 230	-	2.36 (±0.29)x10^3
		+ 0.1% SDS	2.23 ± 0.47	1 250 ± 361	1 470 ± 440	1.78 (±0.64)x10^3
		+ 0.01% SDS	0.46 ± 0.01	94 ± 10	-	4.89 (± 0.53)x10^3
	Dodecanoic-γ-lactone (r) (XVII)	-	2.72 ± 0.13	1 220 ± 144	-	2.23 (± 0.28)x10^3
δ-lactones	**δ-valerolactone (XVIII)**	-	ND	ND	ND	ND
	Nonanoic-δ-lactone (r) (XIX)	-	15.32 ± 0.52	359 ± 63	-	4.27 (±0.77)x10^4
	Undecanoic-δ-lactone (r) (XX)	-	7.38 ± 0.28	94 ± 18	-	7.86 (±1.53)x10^4
	Dodecanoic-δ-lactone (r) (XXI)	-	12.65 ± 0.44	1 678 ± 133	-	7.54 (±0.65)x10^3
Others	**ε-caprolactone (XXII)**	-	4.45 ± 0.08	234 ± 18	-	1.90 (±0.15)x10^4

Table 1 (continued).

Substrate		wild-type *Sso*Pox			
Name	Additive	k_{cat} (s^{-1})	K_M (μM)	K_I (μM)	k_{cat}/K_M ($s^{-1}M^{-1}$)
Dihydrocoumarin (XXIII)	-	7.32 ± 1.25	1 376 ± 455	-	5.32 (±1.98)x10^3

Roman numbers indicate the chemical structures of indicated molecules presented in Figure **S1**. *r* corresponds to racemic solution and *l* at the pure levorotatory enantiomer. Data obtained with cobalt as cofactor. ND corresponds to an undetermined value. When V_{max} could not be reached, the linear part of the MM plot was fitted to a linear regression and corresponded to the catalytic efficiency. *Sso*Pox clearly preferred the levorotatory enantiomer of the AHLs; kinetics performed for the racemic mix resulted in characterization for the levorotatory enantiomer.

doi: 10.1371/journal.pone.0075272.t001

catalytic efficiencies obtained for racemic 3-oxo-C8 AHLs and 3-oxo-C6 AHLs are approximately half of pure levorotatory AHLs. These results confirm the enantiopreference of wild-type *Sso*Pox (Table **1**) for naturally used molecules in bacterial *quorum* sensing [34].

Isolation of W263 variants with improved phosphotriesterase and lactonase activities

Phosphotriesterase activity screening. All selected variants of the saturation site of position 263 have been produced and partially purified in a heating step (see methods). This method might induce a bias resulting from the different expression of variants, but has the merit of enabling fast selection and comparison of the activities of the various expressed proteins. The ability of each variant to hydrolyze paraoxon has been evaluated with 1 mM (Figure **2A**) and 100 μM (Figure **S3A**). Compared to wild-type *Sso*Pox, variants W263L, W263M and W263F are the most efficient at improving specific activities, ranging from 30-50 and 20-35-fold at 1 mM and 100 μM, respectively. These variants constitute the *Phosphotriesterase Selected Variants* group (*PteSV*). Notably, all 19 substitutions of position 263 increase paraoxonase activity (Figure **2A**). These variants are also the most proficient at hydrolyzing CMP-coumarin (an organophosphate nerve agent analogue; Figure **S1-II**) with specific activity improvements ranging from 4- to 11-fold compared to wild-type enzyme (Figure **S3B**).

Lactonase activity screening. The lactonase activity of each variant has been screened using a genetically modified *Pseudomonas aeruginosa*-based bioluminescence screening method (Figure **S4**). Variants W263I, W263T and W263V were selected (Figure **2B**) and constitute the *Lactonase Selected* Variant group (*LacSV*).

Phosphotriesterase kinetic characterization of selected variants

Catalytic efficiencies of paraoxon hydrolysis have been determined for the selected variants (*PteSV* group) (Table **2**). Variant W263F is the most proficient (k_{cat}/K_M = 1.21 (±0.26)x10^4 $M^{-1}s^{-1}$), followed by W263M and W263L with increased efficiencies of 23.3, 14.1 and 4.6-fold, respectively, as compared to wild-type enzyme. In contrast, variants isolated for their improved lactonase activity (*LacSV*) all exhibit mild catalytic improvement compared to wild-type enzyme ranging from 2.3-1.7 times, respectively, for W263I-W263V (Table **2**; Figure **2C & S5AB**).

The most active variant W263F has been further assayed using other organophosphates as substrates (Table **3**). The catalytic parameters obtained for CMP-coumarin (k_{cat}/K_M = 8.23 (±1.04)x10^4 $M^{-1}s^{-1}$), IMP-coumarin (k_{cat}/K_M = 8.85 (±2.99)x10^4 $M^{-1}s^{-1}$) and PinP-coumarin (k_{cat}/K_M = 7.08 (±2.58)x10^3 $M^{-1}s^{-1}$) hydrolysis enhanced catalytic efficiency 10- and 60-fold compared to the wild-type enzyme for which no activity was reported for PinP-coumarin [30]. The variant W263F was also assayed in the presence of SDS, because anionic detergents have been shown to increase the phosphotriesterase activity of wild-type *Sso*Pox [30,31]. Interestingly, SDS has lower influence on the kinetic parameters of variant W263F against paraoxon and CMP-coumarin (with a catalytic efficiency increase ranging from 1.7 to 6.1-fold) than that observed for wild-type *Sso*Pox (ranging from 6.4 to 12.4-fold) [30]. Activity improvement by SDS is caused by a global increase of the protein flexibility [30]. Thus, the W263F mutation might then mimic the SDS effect, by bringing local flexibility into the active site.

Lactonase kinetic characterization of selected variants

Selected variants have been characterized with the best, possibly natural, substrate of wild-type *Sso*Pox (3-oxo-C10 AHL), the worse AHL substrate (3-oxo-C12) and promiscuous oxo-lactones with long aliphatic chains (undecanoic-δ-lactones and undecanoic-γ-lactones) (Table **2**). The kinetic experiments reveal a mild decrease in the 3-oxo-C10 AHLase activity for all variants (ranging from 2- to 3-fold for the W263F variant to undetectable activities for W263L-M variants) (Figure **S5A**). On the contrary, the moderate 3-oxo-C12 AHLase activity of wild-type *Sso*Pox was improved by 1.3- to 55-fold (W263F and W263V, respectively), but no activity was detected for variants W263L-M (Figure **S5A**). Regarding the other lactones, all selected variants possess higher catalytic efficiencies than the wild-type enzyme, ranging from 1.4- (W263V) to 148-fold for undecanoic-γ-lactone (W263T) (Figure **S5**) and from 3.3- (W263L) to > 74-fold for undecanoic-δ-lactones (W263I) (Figure **2C & Figure S5AC**). Notably, contrary to the wild-type enzyme, all selected variants (with the exception of W263F) exhibit a substrate inhibition for undecanoic-δ-lactones with K_I values ranging between 789 ± 186 μM and 7 400 ± 2 475 μM, respectively, for the W263V and W263M variants. This substrate inhibition has not been observed for undecanoic-γ-lactones and AHLs. Because these mutants dramatically increase the δ- and γ-lactonase activities (up to 148-fold), but have a less important effect on AHLs (up to 55-fold improvement for 3-oxo-C12 AHL) or even decrease this activity (with 3-oxo-C10 AHL), these classes of lactones may utilize a different binding mode to the active site and/or a different active site conformation.

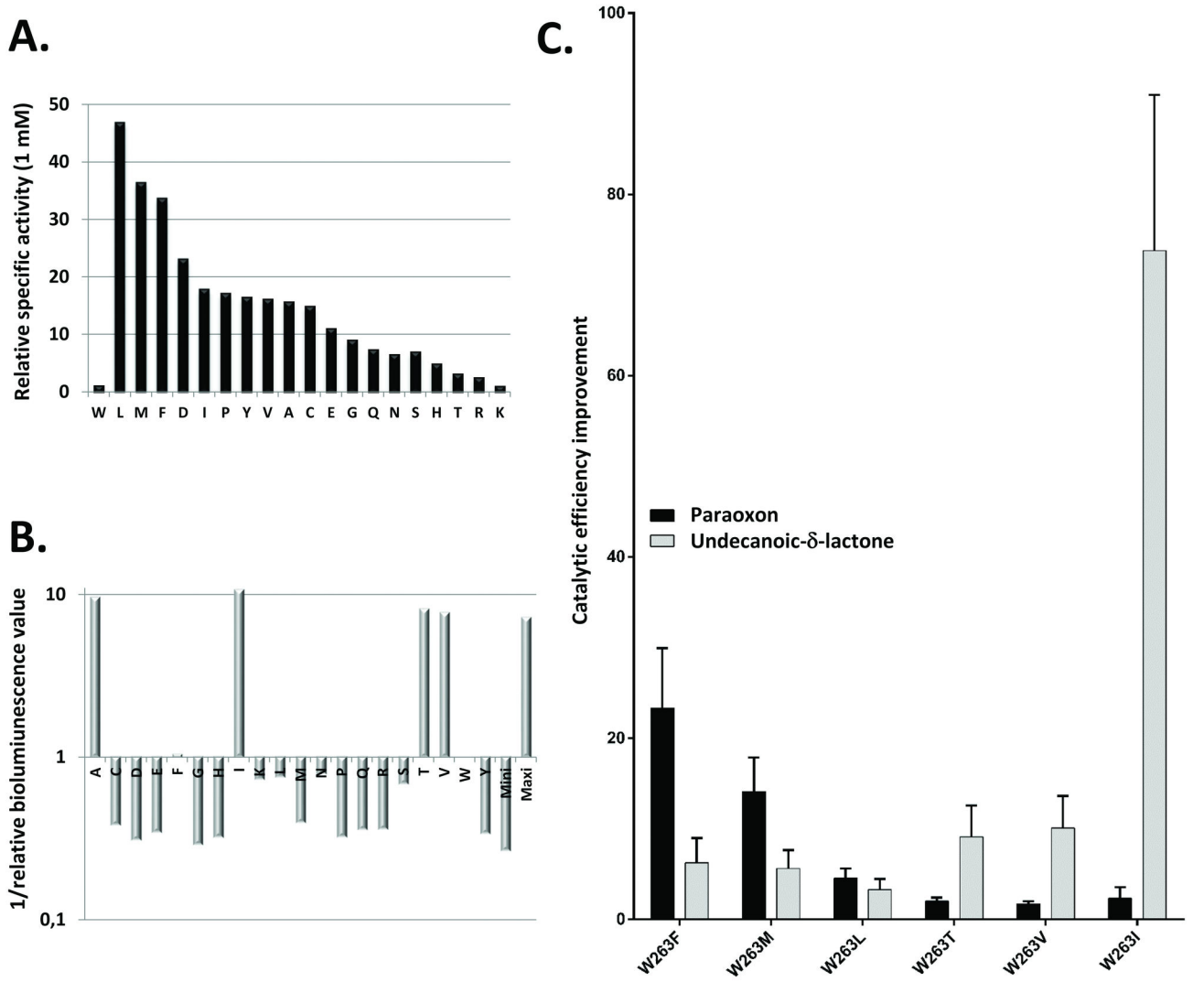

Figure 2. *Sso*Pox W263 saturation site screening and characterization. **A**. Relative phosphotriesterase activities of W263 saturation site variants are screened with 1 mM of paraoxon substrate. **B**. Relative lactonase activity of W263 saturation site variants screened for 3-oxo-C12 AHL hydrolysis (see methods for more details). **C**. Catalytic efficiency comparisons between best selected variants. For screening experiments (A-B.), partially purified enzymes (> 70%) were used.

doi: 10.1371/journal.pone.0075272.g002

Thermal stability and thermophilicity of *SsoPox* variants

*Sso*Pox is an extremely thermostable enzyme (melting temperatures (T_m) = 106 °C) [27]. We here show that substitutions at position 263 are destabilizing (Figure **3**; Table **S1**). Indeed, all variants exhibit a lower T_m compared to the wild-type enzyme (between 92.0 ± 2.1 °C for *Sso*Pox-W263L to 84.1 ± 1.6 °C for *Sso*Pox-W263V). In addition to *Sso*Pox-W263M, *PteSV* variants possess a higher thermal stability than *LacSV* variants. Contrary to the wild-type enzyme that did not lose any paraoxonase activity with an increase in temperature [17], the selected variants possess different profiles (Figure **3**). Interestingly, the loss of paraoxonase activity for the variants *PteSV* occurs before the loss of structure (corresponding to the T_m value). On the contrary, the paraoxonase activity of *LacSV* variants exhibit a behavior that is similar to that of the wild-type enzyme, i.e., the activity keeps increasing with temperature (or remains higher than ambient temperature activity for W236T around its T_m). The temperature-induced behaviors of *LacSV* and *PteSV* confirm their respective distinct behaviors observed in enzyme kinetics.

Structural characterization

In order to understand the structural consequences of variations at position 263, the crystal structures of all selected variants have been solved. No major differences in the wild-type enzyme structure are observed. Position 263 is located at the dimer interface [22]; and it modulates the relative

Table 2. Enzymatic characterization of wild-type *Sso*Pox and its variants.

	*Sso*Pox variant	k_{cat} (s^{-1})	K_M (μM)	K_I (μM)	k_{cat}/K_M ($M^{-1}s^{-1}$)	Enhancement/wt
Paraoxon (I)	*wt**	(1.26 ± 0.13)x10^1	24250 ± 3716	-	5.19 (±0.95)x10^2	1
	W263F	8.47 ± 0.53	700 ± 146	-	1.21 (±0.26)x10^4	23.3 ± 6.6
	W263M	6.82 ± 0.57	931 ± 163	-	7.33 (±1.42)x10^3	14.1 ± 3.8
	W263L	ND	ND	-	2.37 (±0.33)x10^3	4.6 ± 1.0
	W263I	ND	ND	-	1.21 (±0.06)x10^3	2.3 ± 0.4
	W263V	ND	ND	-	8.83 (±0.3)x10^2	1.7 ± 0.3
	W263T	ND	ND	-	1.06 (±0.03)x10^3	2.0 ± 0.4
3-oxo-C12 AHL (I) (XII)	*wt*	1.01 ± 0.13	456 ± 128	-	2.22 (±0.68)x10^3	1
	W263F	0.41 ± 0.02	146 ± 33	-	2.81 (±0.65)x10^3	1.3 ± 0.5
	W263M	ND	ND	-	ND	ND
	W263L	ND	ND	-	ND	ND
	W263I	1.80 ± 0.05	17.8 ± 4.9	-	1.01 (±0.28)x10^5	45.5 ± 18.8
	W263V	3.00 ± 0.07	24.7 ± 5.2	-	1.21 (±0.26)x10^5	54.5 ± 20.4
	W263T	6.44 ± 0.22	137 ± 19	-	4.70 (±0.67)x10^4	21.2 ± 7.2
3-oxo-C10 AHL (I) (XI)	*wt*	4.52 ± 0.10	143 ± 15	-	3.16 (±0.40)x10^4	1
	W263F	3.96 ± 0.18	288 ± 56	-	1.38 (±0.28)x10^4	4.4 (±1.0)x10^{-1}
	W263M	ND	ND	-	ND	0
	W263L	ND	ND	-	ND	0
	W263I	(6.00 ± 0.90)x10^{-1}	1605 ± 443	-	3.74 (±1.17)x10^2	1.2 (±0.4)x10^{-2}
	W263V	(1.90 ± 0.09)x10^{-1}	1346 ± 298	-	1.41 (±0.32)x10^2	4.5 (±1.2)10^{-3}
	W263T	(1.07 ± 0.16)x10^{-1}	1000 ± 343	-	1.06 (±0.40)x10^2	3.4 (±1.3)10^{-3}
Undecanoic-δ-lactone (r) (XX)	*wt*	7.38 ± 0.28	94 ± 18	-	7.86 (±1.53)x10^4	1
	W263F	(6.65 ± 0.32)x10^1	135.2 ± 52.8	-	4.92 (±1.93)x10^5	6.3 ± 2.7
	W263M	(7.12 ± 0.66)x10^1	161 ± 47	7 400 ± 2 475	4.42 (±1.35)x10^5	5.6 ± 2.0
	W263L	(5.68 ± 0.58)x10^1	219 ± 62	4 253 ± 1 152	2.59 (±0.78)x10^5	3.3 ± 1.2
	W263I	(5.80 ± 0.74)x10^1	<10	803 ± 213	>5.80 (±0.74)x10^6	>73.8 ± 17.2
	W263V	(4.48 ± 0.50)x10^1	57 ± 16	789 ± 186	7.92 (±2.34)x10^5	10.1 ± 3.6
	W263T	(9.33 ±0.80)x10^1	130 ± 41	3047 ± 576	7.17 (±2.34)x10^5	9.1 ± 3.5
Undecanoic-γ-lactone (r) (XVI)	*wt*	4.95 ± 0.26	2 099 ± 230	-	2.36 (±0.38)x10^3	1
	W263F	4.63 ± 0.27	373 ± 111	-	1.24 (±0.38)x10^4	5.3 ± 1.8
	W263M	4.25 ± 0.22	334 ± 61	-	1.27 (±0.24)x10^4	5.4 ± 1.3
	W263L	3.92 ± 0.17	371.8 ± 69.2	-	1.05 (±0.20)x10^4	4.4 ± 1.1
	W263I	1.94 ± 0.08	361 ± 47	-	5.37 (±0.73)x10^3	2.3 ± 0.5
	W263V	5.64 ± 0.53	1 760 ± 404	-	3.20 (±0.80)x10^3	1.4 ± 0.4
	W263T	4.55 ± 0.10	13.0 ± 4.2	-	3.49 (±1.13)x10^5	147.9 ± 53.5

Roman numbers indicate the chemical structures of indicated molecules presented in Figure **S1**. * Catalytic parameters are from Hiblot et al. (2012). ND corresponds to an undetermined value. When V_{max} could not be reached, the linear part of the MM plot was fitted to a linear regression and correspond to the catalytic efficiency.

doi: 10.1371/journal.pone.0075272.t002

orientation of its contacting residues, F104, in the second monomer (Figure **S6A**). Consequently, substitutions of W263 affect the relative orientation of both monomers; for each mutant, the monomers are closer to each other compared to the wild-type enzyme (with the exception of W263L). The dimer reorientation yields significant movements that, ranging from 3.4 Å (W263T) to 4.7 Å (W263I) compared to wild-type *Sso*Pox (Figure **S6C**; Table **S1**).

The active sites of variant structures superimpose well with the wild-type enzyme structure (**Figure S6AB**). However, the different residues selected at position 263 modulate the size of the active site cavity, which is increased as compared to wild-type enzyme. The active site cavity is globally larger for *LacSV* than for *PteSV* (Figure **S7**). The HTL-bound structure (Figure **S8A**) of the lactonase variant W263I exhibits the same binding mode than that observed in the wild-type *Sso*Pox structure [22]: both structures are well superimposed (Figure **S8B**). This feature suggests that the observed catalytic enhancements are related to substrate binding, rather than to catalysis improvement. The loss of the interaction of the lactone ring with W263 is compensated by an interaction with a polyethylene glycol molecule that fills the cavity created by the W263I mutation (Figure **S8A**).

The main difference, albeit subtle, between all structures relate to the conformation of the active site loop 8, which carries the position 263 [22]. Indeed, all selected variants present a slightly altered loop 8 conformation compared to wild-type enzyme (**Figure 4ACE**). All variants possess loop 8 conformations that are similar (Figure **4E**) with the exception of the W263L variant (Figures 4C & **S9A**). Moreover, the

Table 3. Phosphotriesterase activity comparison between wild-type and W263F *Sso*Pox.

Substrate		*Sso*Pox *wt**			*Sso*Pox W263F		
Name	**Additive**	k_{cat} (s^{-1})	k_M (μM)	k_{cat}/k_M ($s^{-1}M^{-1}$)	k_{cat} (s^{-1})	k_M (μM)	k_{cat}/k_M ($s^{-1}M^{-1}$)
Paraoxon (I)	-	12.59 ± 1.26	24 250 ± 3 716	5.19 (±0.95)x10^2	8.47 ± 0.53	700 ± 146	1.21 (±0.26)x10^4
	+ SDS 0.1%	40.72 ± 7.70	12 340 ± 3 625	3.30 (±1.15)x10^3	117.7 ± 6.0	2 462 ± 302	4.78 (±0.64)x10^4
	+ SDS 0.01%	24.59 ± 1.77	3 832 ± 626	6.42 (±1.15)x10^3	85.85 ± 4.85	1 168 ± 194	7.35 (±1.29)x10^4
CMP-coumarin (II)	-	ND	ND	8.13 (±0.08)x10^3	9.41 ± 0.38	114.3 ± 13.7	8.23 (±1.04)x10^4
	+ SDS 0.01%	25.47 ± 0.42	137.0 ± 7.0	1.86 (±0.10)x10^5	8.64 ± 0.39	60.0 ± 9.5	1.44 (±0.24)x10^5
IMP-coumarin (III)	-	ND	ND	1.67 (±0.04)x10^3	8.39 ± 1.63	94.8 ± 26.2	8.85 (±2.99)x10^4
PinP-coumarin (IV)	-	ND	ND	ND	0.11 ±0.02	16.1 ± 5.49	7.08 (±2.58)x10^3

Roman numbers indicate the chemical structures of indicated molecules presented in Figure **S1**. * Catalytic parameters are from Hiblot et al. (2012). ND corresponds to an undetermined value. When V_{max} could not be reached, the linear part of the MM plot was fitted to a linear regression and correspond to the catalytic efficiency.

doi: 10.1371/journal.pone.0075272.t003

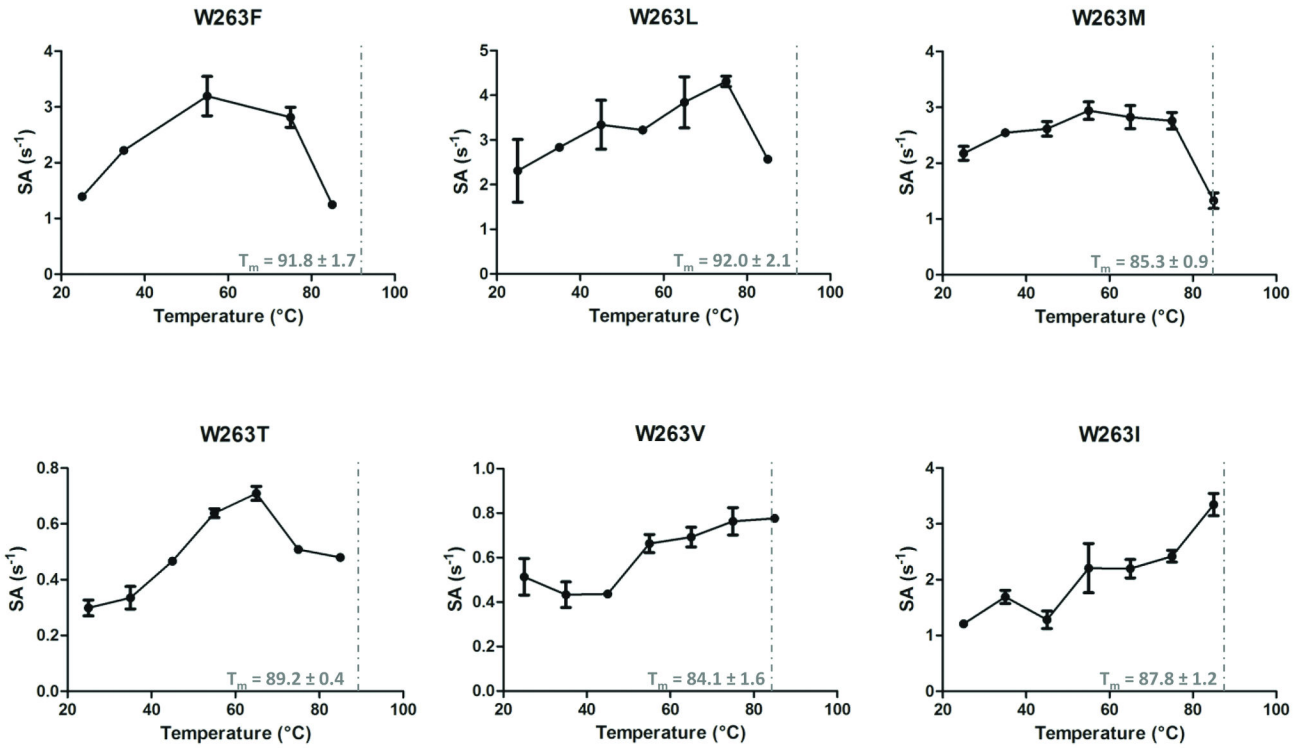

Figure 3. Thermoresistance and thermophilicity of *Sso*Pox variants. Specific activities (in mol. $mol^{-1}.s^{-1}$) for 50 μM of paraoxon are represented at several temperatures ranging from 25 to 85 °C for each selected variants. The T_m value is indicated by a grey dashed line. The wild-type enzyme has a reported T_m of 106 °C [28], and its paraoxonase activity continuously increases with temperature [17].

doi: 10.1371/journal.pone.0075272.g003

normalized B-factor confirms that the substitution of W263 is highly destabilizing, because the normalized B-factor of the loop is increased in all variants, compared to the wild-type structure (**Figure 4BDF & S9B**). The increased flexibility (or increased normalized B-factor) is even more pronounced in *PteSV* variants than in *LacSV* variants (**Figure 4BD**).

Discussion

W263 substitutions increase *SsoPox* promiscuous activities

A single mutation of W263 can significantly increase the paraoxonase activity of the enzyme (by 23-fold with the W263F substitution), the oxo-lactonase activity (by 148-fold with the W263T substitution) and the activity toward the poor AHL

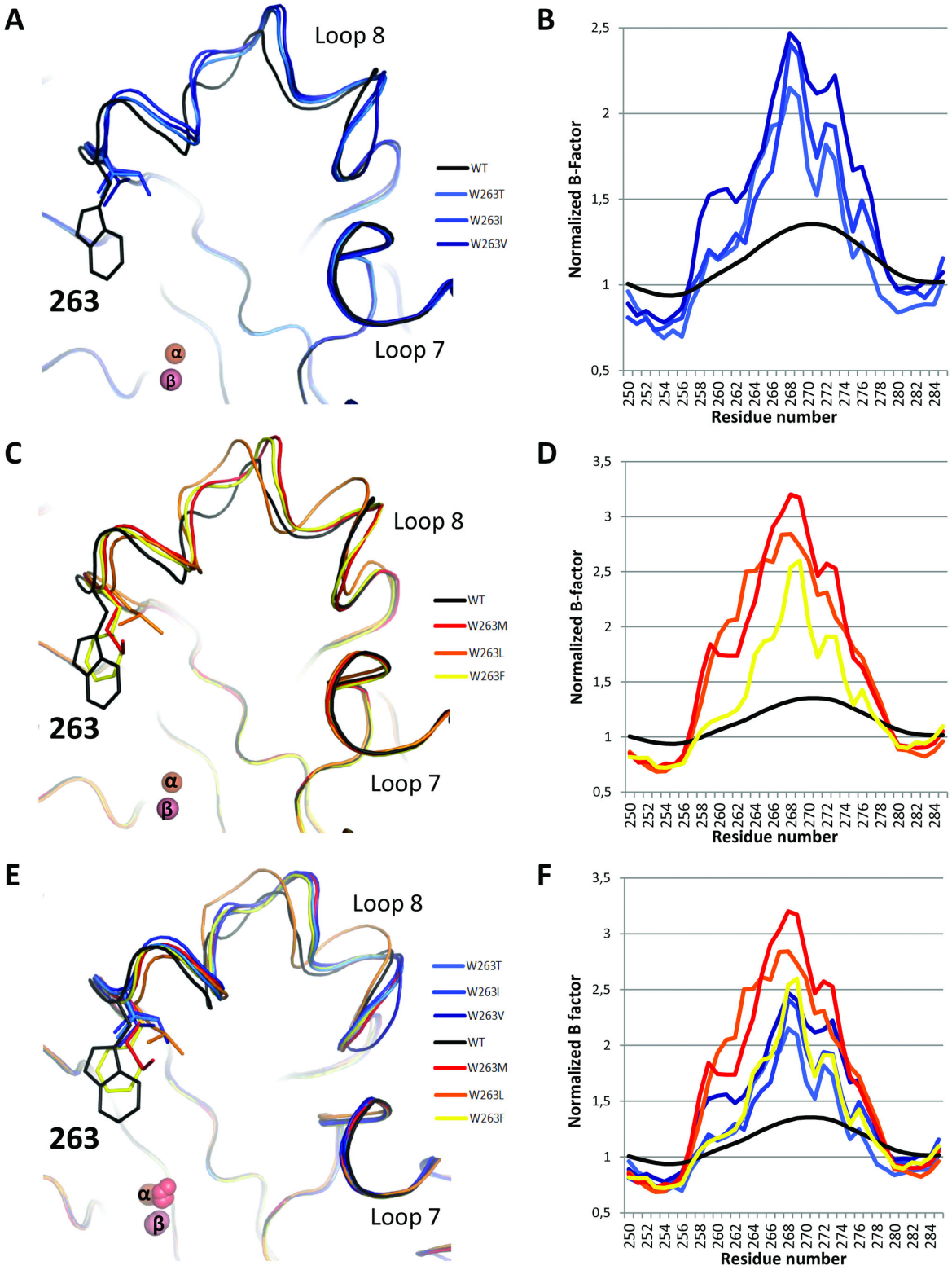

Figure 4. Different loop 8 conformations of W263 mutants. Backbone representation of superposition (**A**-**C**-**E**) and normalized B-factors (**B**-**D**-**F**) of *LacSV* (**A**-**B**). *PteSV* (**C**-**D**) and all selected variants (**E**-**F**) compared to wild-type *Sso*Pox in the active site region (Loop 8). Normalized B-factors are represented on the region 250-285; it corresponds to the B-factor of each residue normalized by the mean B-factor of the structure.

doi: 10.1371/journal.pone.0075272.g004

substrate (3-oxo-C12 AHL; by 55-fold (W263V)). The impact of this substitution is such that *Sso*Pox-W263F hydrolyzes nerve agent analogs with remarkable efficiency (k_{cat}/K_M is 8.85 (±2.99)x10^4 $M^{-1}s^{-1}$ against IMP-coumarin), whereas the wild-type *Sso*Pox is unable to hydrolyze this compound [19]. Noteworthy, subtle changes, such as W263L or W263I, yield to a large tradeoff in catalytic activities.

The W263 substitution seems to have similar effect as SDS on *Sso*Pox: promiscuous phosphotriesterase activity is increased in both cases. Interestingly, SDS has a small stimulatory effect on *Sso*Pox-W263F catalytic efficiency (1.7-6.1-fold increase), whereas it strongly stimulates the wild-type enzyme (with paraoxon and CMP-coumarin as substrates; 6.4- to 12.4-fold increase) [19]. Thus, the detergent induced-flexibility and substitutions of W263 may have overlapping structural effects on the enzyme. However, whereas detergent-induced flexibility has no effect on the lactonase activity, we isolated variants of W263 that exhibit increased lactonase activities (W263T/V/I). These variants exhibit dramatic improvement of their oxo-lactonase catalytic efficiencies (148-fold for variant W263T), while the activity for the best AHL substrate is compromised (3-oxo-C10 AHL; for the wild-type enzyme).

Residue W263 of *Sso*Pox is a key position that interacts with the substrate, is located in loop 8 and is involved in the dimer interface [22] (Figure **S6**). The effects of W263 substitutions on the enzyme structure are numerous, because the W263 mutation provokes a reshaping of the active site cavity (Figure **S7**) and, for some variants a slight re-orientation of the protein homodimer (Figure **S6**). These structural features may contribute to the observed variation of catalytic activities in the W263 variants, compared to the wild-type enzyme. However, the modulation of the enzyme dimer are not systematic for all variants, and therefore cannot explain the systematic effect of W263 on promiscuous activities. Additionally, our study demonstrates that all 19 possible substitutions of the W263 residue increase the *Sso*Pox paraoxonase activity. Such a global effect suggests a non-specific effect of the substitutions on the catalytic cycle, and eliminates a specific role of W263 mutants in the promiscuous substrates accommodation. Moreover, the substitutions of W263 have another effect on the enzyme: all substitutions are consistently destabilizing (Figure **3**) and dramatically increase the active site loop 8 flexibility (Figure **4**).

A given promiscuous activity requires a given conformational subset of the active site loop

Interestingly, the selected mutations for increased phosphotriesterase and lactonase activities (*PteSV* and *LacSV*) are overall mutually exclusive and constitute two distinct groups. Regarding the *PteSV* group, while these variants exhibit higher phosphotriesterase activity, they demonstrate mild improvements for the oxo-lactones and no or wild-type-like AHLase activity (W263L-M and W263F, respectively). Conversely, the *LacSV* group dramatically increases oxo-lactonase activity and 3-oxo-C12 AHLase activities, while the phosphotriesterase activity is mildly modulated and 3-oxo-C10 AHLase is decreased. This dichotomy between the two groups of substitutions is further illustrated by different active-site loop conformational properties. The residues selected in the *LacSV* group (T, V, I) are overall smaller than those selected in the *PteSV* group (F, L, M) with the exception of isoleucine (I). Mutations W263V-T therefore yield enlarged active site cavities for the lactone variants. The analysis of the normalized B-factors of the variants clearly reveal that the substitution W263 is destabilizing (as confirmed by the T_m of the variants), but also that the active site loops of *PteSV* are significantly more disordered than those of *LacSV*. This feature is nicely illustrated by the thermophilicity profile of these variants. *PteSV* lose their activity before the loss of the global structure (T_m), whereas *LacSV* do not, and exhibit a similar thermophilicity profile to that of the wild-type enzyme [17]. These data strongly suggest that the increased disorder in loop 8 caused by the *PteSV* substitutions collapses the loop as the temperature increase, whereas it does not occur with the *LacSV*.

The consequences of the W263 substitution are a decrease in the overall protein stability, a reshaping of the active-site cavity, a slight re-orientation of the enzyme homodimer, a very important increase in loop 8 flexibility and concomitantly an increase in the enzyme's promiscuous activities. The different group of W263 substitutions yield to different conformational loop samplings that possess different structural and physical properties, and are distinct from wild-type behavior. Moreover, because the activity profiles of *LacSV* and *PteSV* show little overlap, the promiscuous activities may then require not only different loop conformations, but also different subsets of the conformational loop landscape. The enzyme would then use a given conformational subset of the active-site to process a given molecule. More precisely, this conformational subset would produce one specific loop conformation that allows the productive binding of the given substrate and another that permits an efficient release of corresponding products. The fact that all selected mutations, for both group of activities, dramatically lower the K_M of the enzyme is consistent with the idea that the conformational flexibility required for enhancing promiscuous activities mainly improves the substrate binding (or reduces non-productive bindings), and/or products release but not catalysis (i.e. the chemical step).

Similarly to the case of paraoxonase 1, the promiscuous activities utilize the catalytic machinery in different combinations [6-8]. This different usage of the active site enables the proper alignment of the promiscuous substrates and the catalytic residues [1,7,8]. Position W263 thus exemplifies a point mutation that can dramatically alter enzyme specificity without the complete loss of the native function (weak tradeoff) [4]. Such a mutation may then provide an evolutionary advantage to the organism, and give birth to a specialized novel enzyme after gene duplication. Flexible loops in the enzyme support the notion of fold polarity [35], whereby a part of the active site (the loop) is weakly connected to the protein scaffold and thus provides the potential, with little mutational events, for evolving new functions.

Material and Methods

Screening methods

Sample preparation for the screening steps. A site-saturation of position W263 of *Sso*Pox was ordered to a service provider (GeneArt, Invitrogen, Germany). Each variant were checked by sequencing and stored as *Escherichia coli* DH5α cell glycerol stocks. The 20 plasmids (pET22b-*Sso*Pox-W263X [30]) have been purified from *E. coli* DH5α cells and transformed into the BL21(DE_3)-pLysS strain for protein production. Protein production was performed in 3 mL of ZYP medium [36] (100 µg/ml ampicillin, 34 µg/ml chloramphenicol) as previously described [19,20,30]. Cells were harvested by centrifugation (3 000 ×g, 4 °C, 10 min), re-suspended in 500 µL of *lysis buffer* (50 mM HEPES pH 8, 150 mM NaCl, 0.2 mM $CoCl_2$, 0.25 mg/ml lysozyme, 0.1 mM PMSF and 10 µg/ml DNAseI) and stored at -80°C. Suspended frozen cells were thawed and disrupted by three steps of 45 seconds of sonication (Ultrasonic processor xl; power 5). Cell debris were removed by centrifugation (13 000 ×g, 25 °C, 30 min). Partial purification of the protein was performed by 15 minutes incubation at 70 °C, which exploited *Sso*Pox extreme thermal stability [17,27,28]. Aggregated proteins were harvested by centrifugation (13 000 ×g, 25 °C, 30 min), and the estimated purity was evaluated as > 70%. The total protein quantity of samples was evaluated using a nanospectrophotometer (Nanodrop, Thermofisher Scientific; France). These protein amounts were used to calculate specific activities. This method enables fast comparison of variants' activities, even if it might introduce a bias due to potential differences in expression/ purification yields of the variants.

Phosphotriesterase activity screening. Phosphotriesterase activity was monitored using paraoxon (1 mM and 100 µM; Fig. **S1-1**) and CMP-coumarin (50 µM; methylphosphonic acid 3-cyano-4-methyl-2-oxo-2H-coumarin-7-yl ester cyclohexyl ester [37]; Fig. **S1-II**), a cyclosarin analog, as substrates. Kinetics experiments were performed in triplicate using 10 µL (for paraoxon hydrolysis) or 2 µL (for CMP-coumarin hydrolysis) of partially purified protein and recorded for 10 minutes. The time course of paraoxon ($\varepsilon_{405\ nm}$ = 17 000 $M^{-1}cm^{-1}$) and CMP-coumarin ($\varepsilon_{412\ nm}$ = 37 000 $M^{-1}cm^{-1}$) hydrolysis was performed at 25 °C and measured with a microplate reader (Synergy HT; BioTek, USA) and the Gen5.1 software in a 6.2 mm path length cell for a 200 µL reaction in a 96-well plate. Standard assays were performed in *pte buffer* (50 mM HEPES pH 8, 150 mM NaCl, 0.2 mM $CoCl_2$ with pH adjusted at 25 °C using NaOH).

Lactonase activity screening. AHL lactonase activity has been screened using a genetically modified strain PAO1 of *P. aeruginosa* (JP2-pKD201) [38]. The pKD201 plasmid encodes proteins coding for bioluminescence production in the presence of 3-oxo-C12 AHLs in *P. aeruginosa*; the *las*I-*rhl*I genes, responsible of AHLs synthesis in wild-type *P. aeruginosa* [39], is deleted in the strain PAO1-JP2 (Fig. **S4**). *Sso*Pox variants (5 µL of tenfold diluted partially purified variants) are mixed in 100 µL of *pte buffer* with 3-oxo-C12 AHL (I) (100 nM; Fig. **S1-XII**) and incubated for 20 minutes at room temperature. A volume of 450 µL of LB media (Trimethoprime lactate 300 µg/mL to maintain the pKD201 plasmid) was inoculated by an overnight preculture of *P. aeruginosa* PAO1-JP2-pKD201 (1/50) and supplemented with the mixture protein/ AHLs (50 µL). The final concentration of 3-oxo-C12 AHLs is 20 nM, prior to enzymatic hydrolysis by *Sso*Pox. After 270 minutes of culture at 37 °C, the cell density ($OD_{600\ nm}$) and bioluminescence (460-40 nm; intensity 100) from 200 µL aliquots of culture are measured in a 96-well plate using a microplate reader (Synergy HT, BioTek, USA) monitored using the Gen5.1 software. Controls in the same experiment are without enzyme and/or without AHLs.

Purification of *SsoPox* and its variants for kinetic measurements and crystallographic studies

Protein production was performed using the *E. coli* strain BL21(DE_3)-pGro7/GroEL (Takara Bio). Productions have been performed in 500 mL of ZYP medium [36] (100 µg/ml ampicillin, 34 µg/ml chloramphenicol) as previously explained [19,20,30], but 0.2% (w/v) arabinose (Sigma-Aldrich, France) was added to induce the expression of the chaperones GroEL/ES. Purification was performed as previously explained [30]. Briefly, a single step of 30 minutes incubation at 70 °C was performed, followed by differential ammonium sulfate precipitation, dialysis and exclusion size chromatography. Proteins were quantified using a nanospectrophotometer (Nanodrop, Thermofisher Scientific, France) and a protein molar extinction coefficient generated with the protein primary sequence in PROT-PARAM (Expasy Tool software) [40].

Enzyme kinetics

Experiments were performed in triplicate at 25 °C and recorded using a microplate reader (Synergy HT, BioTek, USA) and the Gen5.1 software in a 6.2 mm path length cell for a 200 µL reaction in a 96-well plate as previously explained [19]. Catalytic parameters were obtained by fitting the data to the Michaelis-Menten (MM) equation [41] using the Graph-Pad Prism 5 software. When the V_{max} could not be reached in the experiments, the catalytic efficiency (k_{cat}/K_M) was obtained by fitting the linear part of MM plot to a linear regression using Graph-Pad Prism 5 software.

Phosphotriesterase kinetics. Phosphotriesterase activities have been determined as previously explained [19]. Briefly, standard assays were performed in *pte buffer* measuring the time course of hydrolysis of paraoxon ($\varepsilon_{405\ nm}$ = 17 000 $M^{-1}cm^{-1}$) and the nerve agent coumarin derivatives (CMP-coumarin, IMP-coumarin, PinP-coumarin) (Figure **S1-II-III-IV**) [37] ($\varepsilon_{412\ nm}$ = 37 000 $M^{-1}cm^{-1}$). Paraoxon and CMP-coumarin hydrolysis by *Sso*Pox-W263F were also evaluated in *pte buffer* supplemented with 0.1 and/or 0.01% SDS.

Lactonase kinetics. Lactonase kinetics were performed using a previously described protocol [11,19]. The time course hydrolysis of lactones were performed in *lac buffer* (2.5 mM Bicine pH 8.3, 150 mM NaCl, 0.2 mM $CoCl_2$, 0.25 mM Cresol purple and 0.5% DMSO) over a concentration range 0-2 mM for AHLs and 0-5 mM for δ/γ-lactones. Time course hydrolysis of undecanoic-γ-lactone (*d*, I) (Figure **S1-XVI**) and 3-oxo-C10 AHLs (I) (Figure **S1-XI**) in presence of 0.1 and 0.01% SDS has also been performed in *lac buffer*. Duplicate kinetics of *Sso*Pox

with 250 µM of racemic (*d*, l) and enantiopure (l) 3-oxo-C8 AHLs (Figure **S1-X**) have been performed to determine the enantioselectivity of *Sso*Pox. Cresol purple (pK_a 8.3 at 25 °C) is a pH indicator used to follow lactone ring hydrolysis by acidification of the medium. Its molar coefficient extinction ($\varepsilon_{577\ nm}$ = 2 923 $M^{-1}cm^{-1}$) was evaluated by recording the absorbance of the buffer over a range of acetic acid concentrations (0-0.35 mM). For some *Sso*Pox variants, the MM plots have been fitted to the substrate inhibition equation [41] using the Graph-Pad Prism 5 software to determine a K_I for undecanoic-δ-lactone. Consequently, the calculated catalytic efficiencies in these conditions are valid only at low substrate concentrations.

Biophysical studies

Melting temperature determination. Circular Dichroism spectra were recorded as previously explained [19] using a Jasco J-810 spectropolarimeter equipped with a Pelletier type temperature control system (Jasco PTC-4235) in a 1 mm thick quartz cell and using the Spectra Manager software. Briefly, measurements were performed in 10 mM sodium phosphate buffer at pH 8 with a protein concentration of 0.1 mg/mL. Denaturation was recorded at 222 nm by increasing the temperature from 20 to 95 °C (at 5 °C/min) in 10 mM sodium phosphate buffer at pH 8 containing increasing concentrations (1.5-4 M) of guanidinium chloride. The theoretical T_m without guanidinium chloride was extrapolated by a linear fit using the GraphPadPrism 5 software.

Thermophilicity analysis. The temperature dependence of the paraoxonase activity of *Sso*Pox variants were studied over the range of temperatures 25-85 °C with a 10 °C increment. The paraoxon hydrolysis (50 µM) ($\varepsilon_{405\ nm}$ = 17 000 $M^{-1}cm^{-1}$) was monitored in 500 µL with 1-cm path length cell and a Cary WinUV spectophotometer (Varian, Australia) using the Cary WinUV software in *pte buffer* pH adjusted with NaOH to pH 8 at each temperature. Measurements were performed in triplicate.

Structural analysis

Crystallization. Crystallization assays were performed as previously described [30,42] using enzymes concentrated at 6 mg/mL^{-1}. Co-crystallization assays with C10-HTL were performed using the same protocol [22] but adding 4 µL of a 60 mM C10-HTL solution (in Ethyl acetate:DMSO; 1:1) to 120 µL of the protein solution. Crystallization was performed using the hanging drop vapor diffusion method in 96 well plates (Greiner Microplate, 96 well, PS, F-bottom) on ViewDrop II seals (TPP Labtech). Equal volumes (0.5 µL) of protein and reservoir solutions were mixed using a HoneyBee X-8 (Cartesian) crystallization instrument, and the resulting drops were equilibrated against a 150 µL reservoir solution containing 20-30% (w/v) PEG 8000 and 50 mM Tris-HCl buffer (pH 8). Thin crystals appeared after few days at 277 K.

Data collection and structure determination. Crystals were first transferred to a cryoprotectant solution composed of the reservoir solution and 20% (v/v) glycerol, a 1/30 (v/v) ratio of a 60 mM C10 HTL solution was added to the cryo-protectant solution for co-crystallization trials. Crystals were then flash-cooled in liquid nitrogen. X-ray diffraction data were collected for W263L, W263M, W263I, and W263V crystals at 100 K using synchrotron radiation at the ID23-1 beam line (ESRF, Grenoble, France) and an ADSC Q315r detector. The diffraction data for W263F and W263I-C10 HTL crystals were collected at the Proxima-1 beam line (SOLEIL, Gif-sur-Yvette, France) using a PILATUS-6M detector. X-ray diffraction data were integrated and scaled with the *XDS* package [43] (Table **4**). The phases were obtained using the native structure of *Sso*Pox (PDB code 2vc5) as a starting model, performing a molecular replacement with *MOLREP* [44] or *PHASER* [45]. The models were built with *Coot* [46] and refined using *REFMAC* [47]. Structure illustrations were performed using *PyMOL* [48]. B-averages of structures were evaluated using B-average software from CCP4 suite [49]. RMSD were evaluated comparing all structures to wild-type structure (2vc5) using Swiss Prot PDB Viewer software [50].

Table 4. Data collection and refinement statistics of *Sso*Pox variants structures.

Data collections	**W263T**	**W263V**	**W263I**	**W263M**	**W263L**	**W263F**	**W263I-HTL**
PDB ID	4KES	4KER	4KET	4KEU	4KEV	4KEZ	4KF1
Beamline	ID23-EH1	ID23-EH1	ID23-EH1	ID23-EH1	ID23-EH1	Proxima-1	Proxima-1
Wavelength (A°)	0.99987	0.99987	0.99987	0.99987	0.99987	1.00882	0.954
Resolution (A°) (last bin)	2.1	2.6	2.0	2.2	2.65	1.85	2.0
Space group	$P2_12_12_1$						
Unit cell dimensions							
a (A°)	84.2	87.2	87.4	86.8	86.60	87.13	86.78
b (A°)	103.6	103.50	103.9	103.9	105.00	103.62	103.53
c (A°)	151.8	151.60	150.5	151.6	153.60	151.66	151.71
No. observed reflections	501100 (63243)	301273 (30897)	552123 (67740)	566547 (70185)	256359 (39151)	878146 (68071)	688907 (93622)
No. unique reflections	78058 (10044)	42787 (4506)	92731 (12507)	70219 (8674)	39816 (5986)	117479 (8927)	92509 (12379)
Completeness (%)	99.9 (100)	99.7 (99.6)	99.6 (99.8)	99.9 (99.9)	99.5 (99.8)	100 (100)	99.6 (99.1)
Rsym (%)	8.6 (37.6)	12.5 (45.3)	10.7 (37.9)	11.1 (44.6)	10.2 (54.5)	7.1 (47.1)	10.1 (45.9)
Rmeasure (%)	8.2 (48.9)	11.9 (55.4)	10.4 (44.2)	10.6 (55.8)	7.3 (54.5)	7.7 (50.5)	10.8 (49.2)
I/σ(I)	16.43 (4.66)	16.46 (4.40)	13.19 (4.15)	15.78 (4.59)	19.31 (4.17)	18.28 (4.58)	15.05 (4.79)
Last resolution shell	2.2 - 2.1	2.7 - 2.6	2.1 - 2.0	2.3 - 2.2	2.8 - 2.65	1.9 - 1.85	2.1 - 2.0
Redundancy	6.41 (6.30)	7.04 (6.86)	5.95 (5.42)	8.07 (8.09)	6.44 (6.54)	7.47 (7.63)	7.45 (7.56)
Refinement statistics							
Resolution range (last bin) (A °)	49.52 - 2.1 (2.154 - 2.100)	45.41 - 2.6 (2.667 - 2.600)	44.66 - 2.0 (2.052 - 2.000)	49.14 - 2.2 (2.257 - 2.200)	86.776 - 2.652 (2.721 - 2.652)	49.03 - 1.85 (1.898 - 1.850)	45.44 - 2.0 (2.052 - 2.000)
No. Reflections	74154	40646	88093	66708	37816	111605	121721
Rwork (last bin) (%)	16.26 (19.8)	16.83 (22.5)	14.47 (16.8)	17.02 (21.6)	20.30 (32.2)	15.13 (18.9)	14.75 (18.0)
Rfree (last bin) (%)	20.54 (23.0)	23.74 (31.1)	18.95 (22.9)	21.53 (27.0)	26.70 (40.3)	18.64 (22.5)	18.81 (23.0)
No. protein atoms	10280	10146	10263	10225	10058	10151	10346
No. water molecules	579	365	900	332	132	1049	1042
Average B factor ($A°^2$)	38.74	36 .60	24.11	35.62	75.95	25.67	22.24
RMSD from ideal							
Bond lengths (A°)	0.0041	0.0172	0.0052	0.0216	0.0146	0.0040	0.0081
Bond angles (°)	0.8481	0.5669	0.9531	0.6745	0.5081	0.8958	0.6012

doi: 10.1371/journal.pone.0075272.t004

Supporting Information

Figure S1. Chemical structure of OPs (I-IV), AHLs (V-XII), γ-lactones (XIII-XVII), δ-lactones (XVIII-XXI) and other lactones (XXII-XIII).
(DOCX)

Figure S2. Enantiopreference of wild-type *Sso*Pox for AHLs.
(DOCX)

Figure S3. Supplemental *Sso*Pox-W263 saturation site OP hydrolase activity screening.
(DOCX)

Figure S4. Schematic representation of *P. aeruginosa* based AHLase screening method.
(DOCX)

Figure S5. Further catalytic efficiency comparisons between selected variants.
(DOCX)

Figure S6. Structural comparisons of selected variants and *wt Sso*Pox.
(DOCX)

Figure S7. Active site cavity representation of wild-type *Sso*Pox and all selected variants.
(DOCX)

Figure S8. Structural analysis of *Sso*Pox-W263I HTL bound structure.
(DOCX)

Figure S9. RMSD and B-average comparison of wild-type *Sso*Pox and its variants.
(DOCX)

Table S1. Biophysics parameters of *wt Sso*Pox and its variants.
(DOCX)

Acknowledgements

We are grateful to Prof. Dan S. Tawfik for fruitful discussions, inspirations and inputs, to Dr. Moshe Goldsmith for the kind gift of CMP, IMP and PinP-coumarin, to Eynat Dellus-Gur for critical reading of the manuscript and to Dr. Hagit Bar for the help in the lactonase screening manipulation. We thank the AFMB laboratory (Marseille, France) for access to protein production and crystallization platforms.

Author Contributions

Conceived and designed the experiments: JH GG ME. Performed the experiments: JH GG. Analyzed the data: JH GG ME. Contributed reagents/materials/analysis tools: JH GG. Wrote the manuscript: JH GG ME EC.

References

1. Khersonsky O, Tawfik DS (2010) Enzyme promiscuity: a mechanistic and evolutionary perspective. Annu Rev Biochem 79: 471-505. doi: 10.1146/annurev-biochem-030409-143718. PubMed: 20235827.
2. Koshland DE (1995) The Key–Lock Theory and the Induced Fit Theory. Angew Chem Int Ed Engl 33: 2375-2378. doi:10.1002/anie.199423751.
3. Tokuriki N, Tawfik DS (2009) Stability effects of mutations and protein evolvability. Curr Opin Struct Biol 19: 596-604. doi:10.1016/j.sbi.2009.08.003. PubMed: 19765975.
4. Tokuriki N, Tawfik DS (2009) Protein dynamism and evolvability. Science 324: 203-207. doi:10.1126/science.1169375. PubMed: 19359577.
5. Jackson CJ, Foo JL, Tokuriki N, Afriat L, Carr PD et al. (2009) Conformational sampling, catalysis, and evolution of the bacterial phosphotriesterase. Proc Natl Acad Sci U S A 106: 21631-21636. doi: 10.1073/pnas.0907548106. PubMed: 19966226.
6. Elias M, Tawfik DS (2012) Divergence and Convergence in Enzyme Evolution: Parallel Evolution of Paraoxonases from Quorum-quenching Lactonases. J Biol Chem 287: 11-20. doi:10.1074/jbc.R111.257329. PubMed: 22069329.
7. Ben-David M, Elias M, Filippi JJ, Duñach E, Silman I et al. (2012) Catalytic versatility and backups in enzyme active sites: the case of serum paraoxonase 1. J Mol Biol 418: 181-196. doi:10.1016/j.jmb.2012.02.042. PubMed: 22387469.
8. Ben-David M, Wieczorek G, Elias M, Silman I, Sussman JL et al. (2013) Catalytic metal ion rearrangements underline promiscuity and evolvability of a metalloenzyme. J Mol Biol 425: 1028-1038. doi: 10.1016/j.jmb.2013.01.009. PubMed: 23318950.
9. Gupta RD, Goldsmith M, Ashani Y, Simo Y, Mullokandov G et al. (2011) Directed evolution of hydrolases for prevention of G-type nerve agent intoxication. Nat Chem Biol 7: 120-125. doi:10.1038/nchembio.510. PubMed: 21217689.
10. Tokuriki N, Jackson CJ, Afriat-Jurnou L, Wyganowski KT, Tang R et al. (2012) Diminishing returns and tradeoffs constrain the laboratory optimization of an enzyme. Nat Communications 3: 1257. doi:10.1038/ncomms2246.
11. Afriat L, Roodveldt C, Manco G, Tawfik DS (2006) The latent promiscuity of newly identified microbial lactonases is linked to a recently diverged phosphotriesterase. Biochemistry 45: 13677-13686. doi:10.1021/bi061268r. PubMed: 17105187.
12. Afriat-Jurnou L, Jackson CJ, Tawfik DS (2012) Reconstructing a missing link in the evolution of a recently diverged phosphotriesterase by active-site loop remodeling. Biochemistry.
13. Hawwa R, Aikens J, Turner RJ, Santarsiero BD, Mesecar AD (2009) Structural basis for thermostability revealed through the identification and characterization of a highly thermostable phosphotriesterase-like lactonase from Geobacillus stearothermophilus. Arch Biochem Biophys 488: 109-120. doi:10.1016/j.abb.2009.06.005. PubMed: 19615330.
14. Hawwa R, Larsen SD, Ratia K, Mesecar AD (2009) Structure-based and random mutagenesis approaches increase the organophosphate-degrading activity of a phosphotriesterase homologue from Deinococcus radiodurans. J Mol Biol 393: 36-57. doi:10.1016/j.jmb.2009.06.083. PubMed: 19631223.
15. Chow JY, Xue B, Lee KH, Tung A, Wu L et al. (2010) Directed evolution of a thermostable quorum-quenching lactonase from the amidohydrolase superfamily. J Biol Chem 285: 40911-40920. doi: 10.1074/jbc.M110.177139. PubMed: 20980257.
16. Chow JY, Wu L, Yew WS (2009) Directed evolution of a quorum-quenching lactonase from Mycobacterium avium subsp. paratuberculosis K-10 in the amidohydrolase superfamily. Biochemistry 48: 4344-4353. doi:10.1021/bi9004045. PubMed: 19374350.
17. Merone L, Mandrich L, Rossi M, Manco G (2005) A thermostable phosphotriesterase from the archaeon Sulfolobus solfataricus: cloning, overexpression and properties. Extremophiles 9: 297-305. doi:10.1007/s00792-005-0445-4. PubMed: 15909078.
18. Porzio E, Merone L, Mandrich L, Rossi M, Manco G (2007) A new phosphotriesterase from Sulfolobus acidocaldarius and its comparison

with the homologue from Sulfolobus solfataricus. Biochimie 89: 625-636. doi:10.1016/j.biochi.2007.01.007. PubMed: 17337320.
19. Hiblot J, Gotthard G, Chabriere E, Elias M (2012) Structural and enzymatic characterization of the lactonase SisLac from Sulfolobus islandicus. PLOS ONE 7: e47028. doi:10.1371/journal.pone.0047028. PubMed: 23071703.
20. Gotthard G, Hiblot J, Elias M, Chabrière E (2011) Crystallization and preliminary X-ray diffraction analysis of the hyperthermophilic Sulfolobus islandicus lactonase. Acta Crystallogr Sect Struct Biol Cryst Commun 67: 354-357. doi:10.1107/S0108270111027867. PubMed: 21393842.
21. Amara N, Krom BP, Kaufmann GF, Meijler MM (2011) Macromolecular inhibition of quorum sensing: enzymes, antibodies, and beyond. Chem Rev 111: 195-208. doi:10.1021/cr100101c. PubMed: 21087050.
22. Elias M, Dupuy J, Merone L, Mandrich L, Porzio E et al. (2008) Structural basis for natural lactonase and promiscuous phosphotriesterase activities. J Mol Biol 379: 1017-1028. doi:10.1016/j.jmb.2008.04.022. PubMed: 18486146.
23. Ng FS, Wright DM, Seah SY (2010) Characterization of a phosphotriesterase-like lactonase from Sulfolobus solfataricus and its immobilization for quorum quenching. Appl Environ Microbiol.
24. Seibert CM, Raushel FM (2005) Structural and catalytic diversity within the amidohydrolase superfamily. Biochemistry 44: 6383-6391. doi:10.1021/bi047326v. PubMed: 15850372.
25. Dumas DP, Caldwell SR, Wild JR, Raushel FM (1989) Purification and properties of the phosphotriesterase from Pseudomonas diminuta. J Biol Chem 264: 19659-19665. PubMed: 2555328.
26. Roodveldt C, Tawfik DS (2005) Shared promiscuous activities and evolutionary features in various members of the amidohydrolase superfamily. Biochemistry 44: 12728-12736. doi:10.1021/bi051021e. PubMed: 16171387.
27. Hiblot J, Gotthard G, Chabriere E, Elias M (2012) Characterisation of the organophosphate hydrolase catalytic activity of SsoPox. Sci Rep 2: 779. PubMed: 23139857.
28. Del Vecchio P, Elias M, Merone L, Graziano G, Dupuy J et al. (2009) Structural determinants of the high thermal stability of SsoPox from the hyperthermophilic archaeon Sulfolobus solfataricus. Extremophiles 13: 461-470. doi:10.1007/s00792-009-0231-9. PubMed: 19247785.
29. Xiang DF, Kolb P, Fedorov AA, Meier MM, Fedorov LV et al. (2009) Functional annotation and three-dimensional structure of Dr0930 from Deinococcus radiodurans, a close relative of phosphotriesterase in the amidohydrolase superfamily. Biochemistry 48: 2237-2247. doi:10.1021/bi802274f. PubMed: 19159332.
30. Hiblot J, Gotthard G, Chabriere E, Elias M (2012) Characterisation of the organophosphate hydrolase catalytic activity of SsoPox. Sci Rep 2: 779-. PubMed: 23139857.
31. Merone L, Mandrich L, Porzio E, Rossi M, Müller S et al. (2010) Improving the promiscuous nerve agent hydrolase activity of a thermostable archaeal lactonase. Bioresour Technol 101: 9204-9212. doi:10.1016/j.biortech.2010.06.102. PubMed: 20667718.
32. Sigman JA, Patwa TH, Tablante AV, Joseph CD, Glucksman MJ et al. (2005) Flexibility in substrate recognition by thimet oligopeptidase as revealed by denaturation studies. Biochem J 388: 255-261. doi:10.1042/BJ20041481. PubMed: 15647004.
33. Hou L, Honaker MT, Shireman LM, Balogh LM, Roberts AG et al. (2007) Functional promiscuity correlates with conformational heterogeneity in A-class glutathione S-transferases. J Biol Chem 282: 23264-23274. doi:10.1074/jbc.M700868200. PubMed: 17561509.
34. Dickschat JS (2009) Quorum sensing and bacterial biofilms. Nat Prod Rep 27: 343-369. PubMed: 20179876.
35. Dellus-Gur E, Toth-Petroczy A, Elias M, Tawfik DS (2013) What Makes a Protein Fold Amenable to Functional Innovation? Fold Polarity and Stability Trade-offs. J Mol Biol.
36. Studier FW (2005) Protein production by auto-induction in high density shaking cultures. Protein Expr Purif 41: 207-234. doi:10.1016/j.pep.2005.01.016. PubMed: 15915565.
37. Ashani Y, Gupta RD, Goldsmith M, Silman I, Sussman JL et al. (2010) Stereo-specific synthesis of analogs of nerve agents and their utilization for selection and characterization of paraoxonase (PON1) catalytic scavengers. Chem Biol Interact 187: 362-369. doi:10.1016/j.cbi.2010.02.039. PubMed: 20303930.
38. Duan K, Surette MG (2007) Environmental regulation of Pseudomonas aeruginosa PAO1 Las and Rhl quorum-sensing systems. J Bacteriol 189: 4827-4836. doi:10.1128/JB.00043-07. PubMed: 17449617.
39. Popat R, Crusz SA, Diggle SP (2008) The social behaviours of bacterial pathogens. Br Med Bull 87: 63-75. doi:10.1093/bmb/ldn030. PubMed: 18723587.
40. Xue B, Chow JY, Baldansuren A, Yap LL, Gan YH et al. (2012) Correction to Structural Evidence of a Productive Active Site Architecture for an Evolved Quorum-quenching GKL Lactonase. Biochemistry 51: 10120. doi:10.1021/bi3011829. PubMed: 23088324.
41. Copeland RA (2000) Enzymes, A Practical Introduction to Structure, Mechanism, and Data Analysis. New York, Chichester, Weiheim. Brisbane, Singapore, Toronto: Wiley-VCH Verlag. 390pp.
42. Elias M, Dupuy J, Merone L, Lecomte C, Rossi M et al. (2007) Crystallization and preliminary X-ray diffraction analysis of the hyperthermophilic Sulfolobus solfataricus phosphotriesterase. Acta Crystallogr Sect Struct Biol Cryst Commun 63: 553-555. doi:10.1107/S0108270107048937. PubMed: 17620708.
43. Kabsch W (1993) Automatic processing of rotation diffraction data from crystals of initially unknown symmetry land cell constants. J Appl Crystallogr 26: 795-800. doi:10.1107/S0021889893005588.
44. Vagin A, Teplyakov A (2000) An approach to multi-copy search in molecular replacement. Acta Crystallogr D Biol Crystallogr 56: 1622-1624. doi:10.1107/S0907444900013780. PubMed: 11092928.
45. McCoy AJ, Grosse-Kunstleve RW, Adams PD, Winn MD, Storoni LC et al. (2007) Phaser crystallographic software. J Appl Crystallogr 40: 658-674. doi:10.1107/S0021889807021206. PubMed: 19461840.
46. Emsley P, Cowtan K (2004) Coot: model-building tools for molecular graphics. Acta Crystallogr D Biol Crystallogr 60: 2126-2132. doi:10.1107/S0907444904019158. PubMed: 15572765.
47. Murshudov GN, Vagin AA, Dodson EJ (1997) Refinement of macromolecular structures by the maximum-likelihood method. Acta Crystallogr D Biol Crystallogr 53: 240-255. doi:10.1107/S0907444996012255. PubMed: 15299926.
48. DeLano WL (2002) The PyMOL Molecular Graphics System. DeLano. San Carlos, CA, USA: Scientific Publishing House.
49. Winn MD, Ballard CC, Cowtan KD, Dodson EJ, Emsley P et al. (2011) Overview of the CCP4 suite and current developments. Acta Crystallogr D Biol Crystallogr 67: 235-242. doi:10.1107/S0907444910045749. PubMed: 21460441.
50. Guex N, Peitsch MC (1997) SWISS-MODEL and the Swiss-PdbViewer: an environment for comparative protein modeling. Electrophoresis 18: 2714-2723. doi:10.1002/elps.1150181505. PubMed: 9504803.

III. Conclusions :

Lorsque j'ai débuté ma thèse sur le sujet, la seule structure cristallographique de PLL hyperthermostable connue était celle de *Sso*Pox (163, 177). L'homologie structurale observée avec la *Bd*PTE et l'établissement de ses deux mécanismes enzymatiques permit de jeter les bases d'un projet d'amélioration rationalisée de l'activité de promiscuité phosphotriestérase de *Sso*Pox. L'enzyme étant d'origine extrêmophile, un protocole simple d'expression hétérologue (chez *E. coli*) et de purification à bas coût fut mis en place (197). Ce protocole facilita les différentes études structurales qui furent menées au cours de mes travaux sur *Sso*Pox. De plus, au cours de ma thèse, plusieurs nouvelles enzymes furent étudiées dans le but de mieux comprendre les activités des OPs hydrolases. La structure d'une nouvelle PLL fut obtenue (*Sis*Lac), ainsi que celle d'une nouvelle OP hydrolase à topologie sandwich αββα (OPHC2) et plus de 20 structures de *Sso*Pox et de ses variants (**voir partie « Bilan de la thèse »**). Les travaux menés permirent de mieux comprendre l'origine structurale des améliorations catalytiques observée au cours des protocoles d'évolution dirigée. Ainsi, ces travaux permettent d'améliorer le pouvoir de convergence de la base de données de mutations utilisée pour l'ingénierie rationalisée de *Sso*Pox.

A. Caractérisation de nouvelles OP hydrolases d'intérêt biotechnologique

1. Étude des PLLs *Sis*Lac et *Sso*Pox

a. Comparaison structurales

*Sis*Lac fut identifiée dans les bases de données génomiques sur la base de l'identité de séquence qu'elle partage avec *Sso*Pox (plus de 91 %). De par son origine, l'archaea extrêmophile *S. islandicus*, *Sis*Lac présentait un intérêt biotechnologique potentiel comparable à celui de *Sso*Pox (148, 149). De ce fait, l'un des objectifs de ma thèse fut de réaliser une caractérisation biochimique et enzymatique de cette enzyme et d'en résoudre sa structure cristallographique. L'obtention de sa structure par cristallographie aux rayons X présenta une difficulté technique qui fut surmontée (présence d'une macle) (**article présenté en partie III. A.**).

Bien que *Sis*Lac présente une structure essentiellement comparable à *Sso*Pox, l'analyse structurale révéla une compaction du dimère de *Sis*Lac plus importante que celui d'*Sso*Pox. Cette différence fut imputée à une position « pivot », c'est-à-dire une position se trouvant en interaction avec son équivalent au sein du second monomère du dimère. Chez *Sso*Pox, cette position correspond à une glutamine ($Gln34_{SsoPox}$) alors qu'il s'agit d'une tyrosine dans le contexte *Sis*Lac ($Tyr34_{SisLac}$). Ainsi, chez *Sso*Pox, la présence des résidus de glutamine à cette position permet une interaction entre les chaines latérales des deux monomères. Chez *Sis*Lac, la présence de tyrosine ne permet pas aux chaines latérales d'adopter la même orientation, engendrant ainsi une contrainte au niveau de l'interface à l'origine d'une augmentation de la surface de dimérisation. Ces éléments, bien connus pour contribuer à la thermostabilité des enzymes, sont en contrepartie compensés par des différences au sein du réseau de pont-salins de surface (147). Ainsi, afin de mieux comprendre les facteurs influençant la thermostabilité de ces enzymes, l'influence des différentes mutations fut étudiée en mimant la position 34 de *Sso*Pox dans le contexte *Sis*Lac (198). De façon intéressante, les simples mutants ($Glu14Lys_{SisLac}$ et $Tyr34Gln_{SisLac}$) présentent une thermostabilité inférieure à la protéine sauvage alors que la combinaison des deux mutations permet de recouvrer en partie la thermostabilité initiale. Ce phénomène traduit la nature hautement épistatique de ces positions. En effet, l'épistasie dénomme la relation qu'il peut y avoir entre des positions n'ayant à priori aucune relation directe (ici, éloignées dans la structure) mais dont la combinaison révèle des effets pouvant être coopératifs (épistasie positive) ou s'annulant (épistasie négative) (199-201). Ces phénomènes d'épistasie, largement sous-estimés, semblent être des éléments important de l'évolution naturelle des protéines. Ainsi, une mutation peut n'avoir aucun effet observable dans un contexte précis (qualifiée alors à tort de « neutral drift » ou « dérive neutre ») et avoir des conséquences dramatiques dans un autre contexte. Un autre exemple de position épistatique au sein de cette famille d'enzyme a été montré pour la position 254 chez *Bd*PTE. En effet, des expériences visant à reconstituer l'enzyme ancestrale progénitrice de la *Bd*PTE (dont la boucle 7 est raccourcie à l'instar des PLLs) montrèrent que la présence d'une arginine à cette position est essentielle pour l'activité lactonase alors qu'aucun effet direct n'est observable dans le contexte de la *Bd*PTE normale (161).

L'obtention de la structure cristallographique de *Sis*Lac permit d'identifier des positions aux relations épistatiques complexes chez *Sso*Pox et *Sis*Lac (position pivot 34), deux protéines extrêmement proches en séquence, et qui influencent fortement les activités et la thermostabilité des deux enzymes.

b. Caractérisations d'activités phosphotriestérase

L'étude d'*Sso*Pox commença avant le début de ma thèse dans l'équipe et seule une *primo* caractérisation de l'enzyme à haute température avait été effectuée (163, 177). De plus, *Sis*Lac ayant été identifiée par notre équipe, aucune donnée concernant les activités enzymatiques de cette protéine n'était connue. Nous avons donc entrepris de caractériser ces deux enzymes à température ambiante envers les insecticides et les agents neurotoxiques de guerre.

Bien que les deux enzymes soient des lactonases (160, 161), elles présentent toutes deux des activités de promiscuité phosphotriestérase. L'efficacité catalytique varie en fonction des composés; *Sso*Pox présentant une efficacité allant jusqu'à 10^3 $M^{-1}.s^{-1}$ envers certains dérivés coumariniques d'agents neurotoxiques de guerre (*e.g* CMP). Certaines tendances concernant les préférences de substrat de *Sso*Pox ont pu être mises en évidence. Notamment, l'enzyme exhibe des activités plus élevées envers les substrats possédant un groupement partant peu volumineux (*i.e* méthyl parathion plutôt qu'éthyl parathion). Cette observation est en accord avec l'étroitesse du canal hydrophobe de l'enzyme qui est parfaitement adapté au positionnement de la chaine acyl des AHLs. Un autre phénomène également marqué concerne la préférence de l'enzyme pour les oxono-phosphotriesters au détriment des thiono-phosphotriesters (*i.e* paraoxon plutôt que parathion). Ce comportement, également présent chez OpdA, est peu observé chez la *Bd*PTE. L'origine moléculaire de cette particularité est en cours d'étude. C'est un élément important à prendre en compte puisqu'une part importante des OPs sont des thiono-OPs. La structure de *Sso*Pox fut obtenue avec le fensulfothion, un thiono-OP caractérisé comme un inhibiteur de l'enzyme. De façon inattendue, le fensulfothion est accommodé de telle manière que le groupement sulfinyl mime la fixation des lactones dans le site actif. Cette structure permit également de proposer certains positions (*e.g* Trp 263) comme constituant des positions clés à muter afin d'améliorer l'accommodation des OPs dans le site actif de l'enzyme.

Enfin, l'utilisation de SDS avait été montrée comme stimulant de l'activité phosphotriestérase chez *Sso*Pox (178). Nous avons affiné l'étude en montrant que de faibles concentrations de détergents anioniques (*e.g* SDS ou DOC) permettent d'augmenter sensiblement l'efficacité d'hydrolyse de l'enzyme (jusqu'à 33 fois). Bien que l'hypothèse la plus vraisemblable soit que les détergents entrainent une flexibilisation de l'enzyme (147) qui, de nature hyperthermostable, est plus rigide à température ambiante, les expériences effectuées afin de confirmer cette hypothèse ne furent pas concluantes. Néanmoins, l'utilisabilité de l'enzyme en détergents présente des avantages importants pour des applications en décontamination externe (**voir partie IV. C. 2.**). En effet, les détergents sont des tensio-actifs entrainant un « effet mouillant » plus important, permettant alors aux solutions d'être mieux réparties sur des surfaces.

***Sso*Pox et *Sis*Lac sont des lactonases naturelles hyperthermostables présentant des activités de promiscuité phosphotriestérase pouvant faire l'objet d'une amélioration d'activités par ingénierie (180, 184).**

c. Caractérisations d'activités lactonase

*Sso*Pox et *Sis*Lac sont des enzymes appartenant à la famille des PLLs (**voir partie I. C. 2.**) (160, 161) dont l'activité naturelle est l'hydrolyse des lactones. Le mécanisme catalytique fut décrypté par l'équipe avant mon arrivée en thèse (163) suite à l'obtention d'une structure cristallographique en complexe avec un analogue d'AHL (code pdb 2VC5). Néanmoins, il fut récemment établi que les PLLs se différencient en deux sous-familles aux propriétés enzymatiques différentes : les PLL-A, décrites comme des AHL-lactonases naturelles; les PLL-B, exhibant une nette préférence pour les oxo-lactones. Dans le but de mieux évaluer les potentialités biotechnologiques de *Sso*Pox, nous avons élargi la caractérisation de son activité lactonase. En effet, les AHLs sont des molécules naturelles, utilisées dans la communication interbactérienne (*quorum* sensing) impliquées dans développement des facteurs de virulence. Ainsi, les enzymes présentant des activités AHL-lactonases pourraient constituer un moyen de lutte contre les pathogènes utilisant ce type de lactones en hydrolysant ces molécules (*quorum* quenching).

Au cours de nos travaux, nous avons cartographié le répertoire enzymatique lactonase de *Sso*Pox et montré que l'enzyme hydrolyse aussi efficacement les AHLs que les oxo-lactones ($k_{cat}/K_M \sim 10^4$ $M^{-1}.s^{-1}$). De plus, nous avons étudié la préférence énantiomérique de l'enzyme envers une AHL et montré une préférence pour la *l*-AHL qui est l'énantiomère naturellement utilisé dans le QS bactérien (202). Enfin, au cours des travaux d'amélioration d'activité de *Sso*Pox, l'activité oxo-lactonase fut améliorée de façon plus importante (jusqu'à 400 fois d'amélioration), suggérant que celle-ci n'est pas optimisée et serait une activité de promiscuité. En effet, les activités non naturelles sont en général plus facilement/rapidement améliorables puisque celles-ci n'ont fait l'objet d'aucune pression de sélection (180, 184, 203). Ainsi, ces deux éléments tendent à suggérer que l'activité naturelle de *Sso*Pox serait l'activité AHL-lactonase, ciblant plus particulièrement les molécules du QS.

L'analyse bioinformatique des séquences présentes dans les bases de données des génomes séquencé révèle la présence de PLLs chez d'autres archaea extrémophiles (*e.g Vulcanisaeta moutnoskia*, pH 3-6, 60-98 °C (204) (**voir article annexe VI. B.**) et *Sulfolobus acidocaldarius*, pH 2-3, 75-80°C (164, 205, 206)). Néanmoins, la présence de QQ lactonases chez ce type d'archaea soulève la question de l'existence d'un QS dans ces milieux de vie extrêmes (*i.e* pH acide, haute température) (207). En effet, il n'existe actuellement aucun système de QS établi chez ces archaeas. De plus, en dépit d'un

environnement acide favorable, la haute température de ces milieux pourrait diminuer stabilité des AHLs. Néanmoins, la présence d'un QS à base d'AHLs chez une archaea méthanogène mésophile offre des arguments en faveur de l'hypothèse d'un QS/QQ à base d'AHL chez les archaea extrémophiles (208).

2. Étude de OPHC2

a. Comparaison structurale d'OPHC2 et MPH

OPHC2 fut isolée à partir de bactéries provenant de sols pollués en Chine pour sa capacité à dégrader les organophosphorés (**voir partie introductive I. C. 2.**). Présentant une identité de séquence de 45 % avec MPH, elle présente des similitudes avec la superfamille des métallo-β-lactamases. Bien que d'origine mésophile (*i.e Pseudomonas pseudoalcaligenes* et *Stenotrophomonas sp. SMSP-1*), une caractérisation succincte enzymatique de l'enzyme avait été effectuée et indiquait que l'enzyme pouvait être thermorésistante (optimum de température à 66 °C) (158). Pouvant ainsi constituer un potentiel bio-décontaminant d'OPs présentant naturellement à la fois stabilité et activité, nous avons entrepris une caractérisation enzymatique, biochimique et structurale d'OPHC2 (**voir article présenté en partie II. D.**).

OPHC2 démontre une extrême résistance à la température qui fut utilisée pour la purification de l'enzyme à partir du lysat d'*E. coli* (chauffage à 70 °C et précipitation différentielle au sulfate d'ammonium). L'étude par dichroïsme circulaire de sa thermo-dénaturation, classe OPHC2 parmi les enzymes hyperthermostables (Tm ~ 98 °C). La structure cristallographique de l'enzyme fut résolue (**article II. C.**), nous permettant ainsi d'investiguer les éléments à l'origine de sa thermostabilité (**article II. D.**). OPHC2 présente une structure compacte avec une topologie de type sandwich αβ/βα avec un site actif bi-métallique. Bien qu'essentiellement superposable avec celle de MPH, une partie de la structure d'OPHC2 ne fut pas définie dans les cartes de densité électronique, probablement du fait d'une agitation. L'enzyme est dimérique dans le cristal et en solution avec une surface de dimérisation plus étendue que chez MPH et impliquant de nombreux ponts salins. De plus, les extrémités de chaque monomère interagissent avec le second monomère du dimère *via* un complexe réseau de ponts salins. OPHC2 présente également un pont disulfure supposé rigidifier l'une des boucles du site actif. Tous ces éléments sont connus pour contribuer de façon importante à la thermostabilité des protéines (147).

OPHC2 est particulièrement thermostable et constitue ainsi une enzyme d'intérêt biotechnologique pour développer un bio-décontaminant d'OPs.

b. Caractérisations enzymatiques

De par ses propriétés d'hyperthermostabilité, OPHC2 constitue un candidat intéressant pour le développement d'un bio-épurateur d'insecticides et d'agents neurotoxiques de guerre. Ainsi, nous avons entrepris de caractériser les activités enzymatiques à température ambiante envers divers insecticides OPs, analogues d'agents neurotoxiques de guerre et lactones. OPHC2 présente une efficacité catalytique d'environ 10^3 $M^{-1}.s^{-1}$ envers le méthyl-paraoxon et le méthyl-parathion, principalement due à des constantes catalytiques faibles ($k_{cat} \sim 10^{-1}$ s^{-1}). De façon analogue aux PLLs, l'enzyme présente une préférence pour les substrats peu encombrants (activité envers l'éthyl-paraoxon 100 fois plus faible). Cependant, de façon intéressante elle hydrolyse le CMP, un dérivé coumarinique du cyclosarin ($k_{cat}/K_M \sim 10^3$ $M^{-1}.s^{-1}$). Chez les PTE/PLLs et les paraoxonases, les activités envers les OPs s'accompagnant souvent des activités estérases et lactonases. En ce sens, nous avons réalisé une caractérisation de l'enzyme envers divers substrats esters et lactones. OPHC2 présente des activités estérases faibles ($k_{cat}/K_M < 10^2$ $M^{-1}s^{-1}$) et une activité lactonase uniquement envers la dihydroxycoumarine ($k_{cat}/K_M \sim 10^3$ $M^{-1}s^{-1}$). Cependant, il fut récemment mis en évidence chez la praoxonase, que le mode d'hydrolyse de cette molécule pourrait être plus proche de celui des OPs que des lactones (66).

Afin de mieux comprendre l'origine des différences de spécificité d'OPHC2 par rapport aux protéines homologues (*i.e* MPH et AiiA), nous avons comparé les sites catalytiques des enzymes. OPHC2 présente un centre bimétallique comparable à celui d'MPH, constitué de deux cations pontant une molécule d'eau impliquée dans l'hydrolyse des OPs selon un mécanisme similaire aux PTEs (106). Le site catalytique d'OPHC2 est constitué d'une poche hydrophobe globalement similaire à celui d'MPH et comporte quelques différences présentes dans les sous-sites de spécificités putativement responsables des différences de spécificité de l'enzyme. Comparée à AiiA, OPHC2 ne présente pas de canal hydrophobe permettant l'accommodation de la chaine acyl des lactones. De plus, le résidu Tyr 194, essentiel à l'activité lactonase (185) est substitué par la Leu 250 chez OPHC2. Enfin, la présence du pont disulfure impliquant la rigidification de l'une des boucles du site actif pourrait être une cause de sa faible vitesse d'hydrolyse envers les substrats testés.

OPHC2 présente un spectre de spécificité d'hydrolyse intéressant envers les OPs; elle hydrolyse notamment le CMP, un analogue du cyclosarin. De plus, son importante stabilité constitue un avantage pour son amélioration qui pourrait être effectuée *via* des mutations basées, entre autres, sur la comparaison structurale avec MPH.

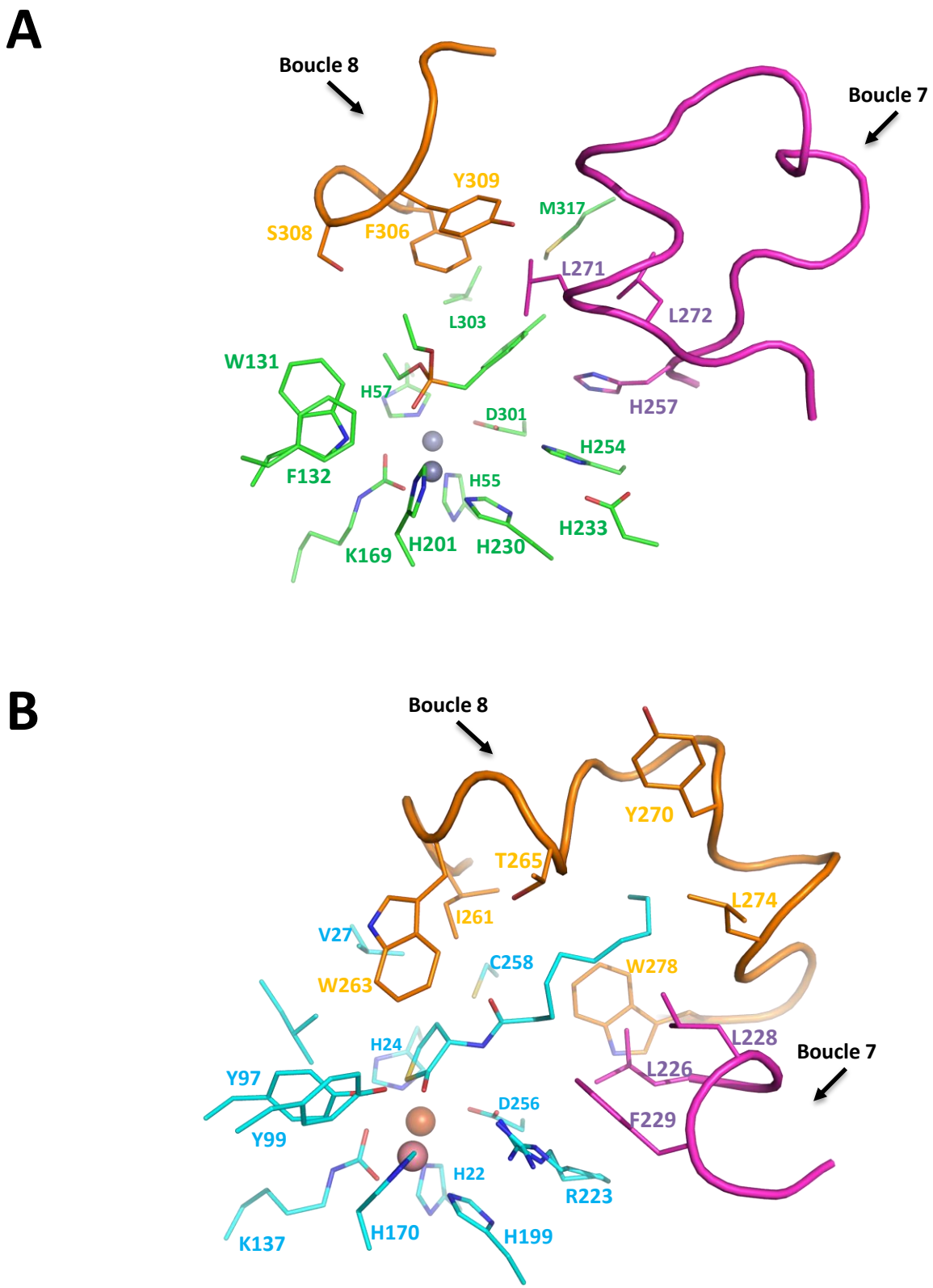

Figure III.1: *Comparaisons des sites actifs de* Bd*PTE et* Sso*Pox*

Comparaison structurale des sites actifs de la *Bd*PTE (**A**) et de *Sso*Pox (**B**). Les boucles 7 et 8 sont indiquées en couleur. On dénote d'importantes différences dans la longueur des boucles et la nature des acides aminés.

B. La promiscuité chez les OP hydrolases

La promiscuité enzymatique se définit comme la capacité fortuite d'une enzyme à prendre en charge des substrats différents de son activité naturelle (**voir partie introductive I. C. 3. a. et b.**). Il est désormais admis que les OPs hydrolases de la famille des amidohydrolases, (*i.e Bd*PTE et OpdA) ont évolué par promiscuité à partir d'une lactonase ancestrale possédant une activité de promiscuité phosphotriestérase (160, 161). La promiscuité enzymatique peut s'exercer de deux manières différentes : l'ambiguïté (ou confusion) de substrat et la chimie de promiscuité (66). L'ambiguïté de substrat concerne la prise en charge d'un substrat chimiquement analogue au substrat naturel et ne requérant pas une chimie de réaction différente. C'est le type de promiscuité le plus répandu et permet par exemple aux lactonases d'hydrolyser des lactones de chaine aliphatique de longueur différente. En revanche, la chimie de promiscuité concerne la prise en charge de substrats nécessitant une chimie de réaction différente de l'activité naturelle. En général, ce type de promiscuité implique la ressemblance géométrique des substrats avec l'état de transition ou l'état intermédiaire intervenant dans l'autre activité (**voir partie introductive, Figure I.20**). La promiscuité d'activité lactonase-phosphotriestérase observée chez les PLLs illustre parfaitement cette seconde catégorie (**voir partie introductive I. C. 3. b.**).

Cependant, l'évolution des PTEs n'est pas un cas isolé au sein des OP hydrolases, puisque au cours de la même période, une évolution parallèle par promiscuité semble avoir eu lieu dans une autre famille structurale (sans relation avec les PLLs) : les métallo-β-lactamases à topologie αβ/βα (185). En effet, MPH et OPHC2 sont des enzymes capable de dégrader les insecticides présents dans les sols pollués qui ont été isolées près de différentes usines de production d'insecticides (106). Ces enzymes présentent des homologies structurales avec les lactonases à repliement métallo-β-lactamases telles qu'AiiA isolée de *B. thuringiensis* (189) et AiiB issue d'*Agrobacterium tumefaciens* (209). La comparaison de leurs structures cristallographiques met en évidence une divergence similaire à celle qui a eu lieu entre les PLLs et les PTEs (**Figures III.1 et 2**). On remarque que la cavité du site actif chez MPH s'est élargie par rapport à AiiA, avec, de plus, le remplacement d'un résidu caractéristique de l'activité lactonase : la Tyrosine 194. La longue crevasse présente chez AiiA et permettant le placement de la chaine alyphatique des lactones a disparu chez MPH et OPHC2 et laisse place à une cavité comparable à celle de la PTE. De plus, les reconstructions phylogénétiques que nous avons effectuées, montrent que les lactonases AiiA/AiiB et MPH/OPHC2 partagent un ancêtre commun. Ainsi, l'hypothèse la plus vraisemblable est que les OP hydrolases de cette famille (*i.e* OPHC2 et MPH) sont issue d'une lactonase ancestrale dont l'activité de promiscuité phosphotriestérase aurait servi comme point de départ de leur évolution (**Figure III.3**) (185).

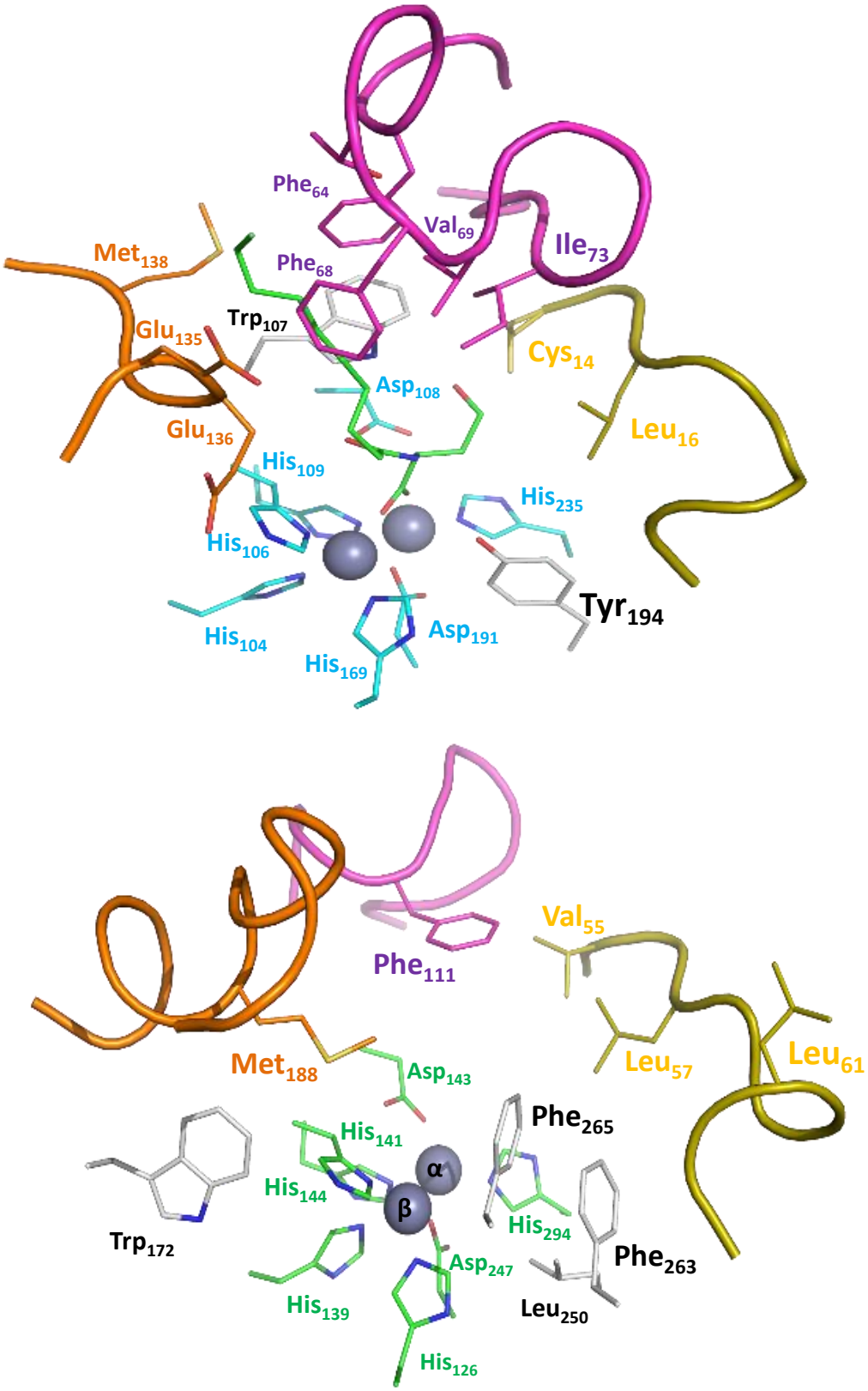

Figure III.2: *Site actif de AiiA et d'OPHC2*

Les sites actifs d'AiiA (en haut) et d'OPHC2 (en bas) présentent principalement des différences au niveau des boucles (orange, mauve et or), à l'origine de la spécificité des deux enzymes. Le résidu Tyr 194, essentiel à l'activité lactonase d'AiiA est absent chez OPHC2.

Cette évolution divergente et simultanée ayant eu lieu dans deux familles structurales distinctes illustre bien que la Nature peut utiliser des solutions équivalentes, façonnées par la chimie (ici, l'hydrolyse des OPs), pour produire des enzymes optimisées (Figure III.4).

C. Ingénierie rationalisée de *Sso*Pox

1. Bilan de la mutagénèse à saturation de la position Trp 263

Au cours des travaux de caractérisation de l'activité phosphotriestérase de *Sso*Pox, une position particulière (Trp 263) fut identifiée comme étant potentiellement responsable d'une gêne stérique pour le positionnement des OPs au sein du site actif de *Sso*Pox (**article présenté en partie II. E.**). Critique également pour l'accommodation des AHLs (163), cette position est située dans la boucle 8 de l'enzyme et à l'interface dimérique. Ainsi, une première stratégie visant à tester la pertinence de cette position clé, fut de réaliser une saturation de site sur la position 263, c'est-à-dire, générer et tester tous les mutants de cette position. Les propriétés enzymatiques et biochimiques des meilleurs mutants obtenus furent ensuite étudiées et leur structure résolue par cristallographie aux rayons X afin de mieux comprendre les déterminants structuraux responsables de l'amélioration (**article présenté en partie II. F.**).

A la fois impliquée dans l'activité lactonase et phosphotriestérase de *Sso*Pox, l'efficacité catalytique des mutants de cette position fut investiguée envers le paraoxon et envers une AHL impliquée dans le QS (3-oxo-C12 AHL). Ainsi, il fut mis en évidence que parmi les 19 acides aminés possibles, tous les acides aminés différents du tryptophane permettent une amélioration de l'activité de promiscuité phosphotriestérase. Trois améliorés phosphotriestérase et trois améliorés lactonase furent sélectionnés pour une caractérisation biochimique et structurale : les variants Trp 263 Phe-Leu-Met constituant le groupe des améliorés phosphotriestérase (PteSV) et Trp 263 Thr-Ile-Val constituant le groupe des améliorés lactonase (LacSV). Cette stratégie permit d'obtenir des augmentations d'activité allant jusqu'à 23 fois pour les PteSV ($k_{cat}/K_M \sim 10^{3-4}$ $M^{-1}s^{-1}$ envers l'éthyl-paraoxon) et de 66 fois pour les LacSV ($k_{cat}/K_M \sim 10^5$ $M^{-1}s^{-1}$ envers les 3-oxo-C12 AHLs). Les efficacités catalytiques observées pour les mutants LacSV sont parmi les plus élevées recensées dans la bibliographie envers les AHLs utilisées dans le QS chez *P. aeruginosa*.

L'unique mutation de la position clé 263 permet d'augmenter à la fois les activités phosphotriestérase et lactonase de *Sso*Pox. Les augmentations obtenues permettent d'atteindre des efficacités catalytiques qui sont parmi les plus élevées recensées dans la bibliographie.

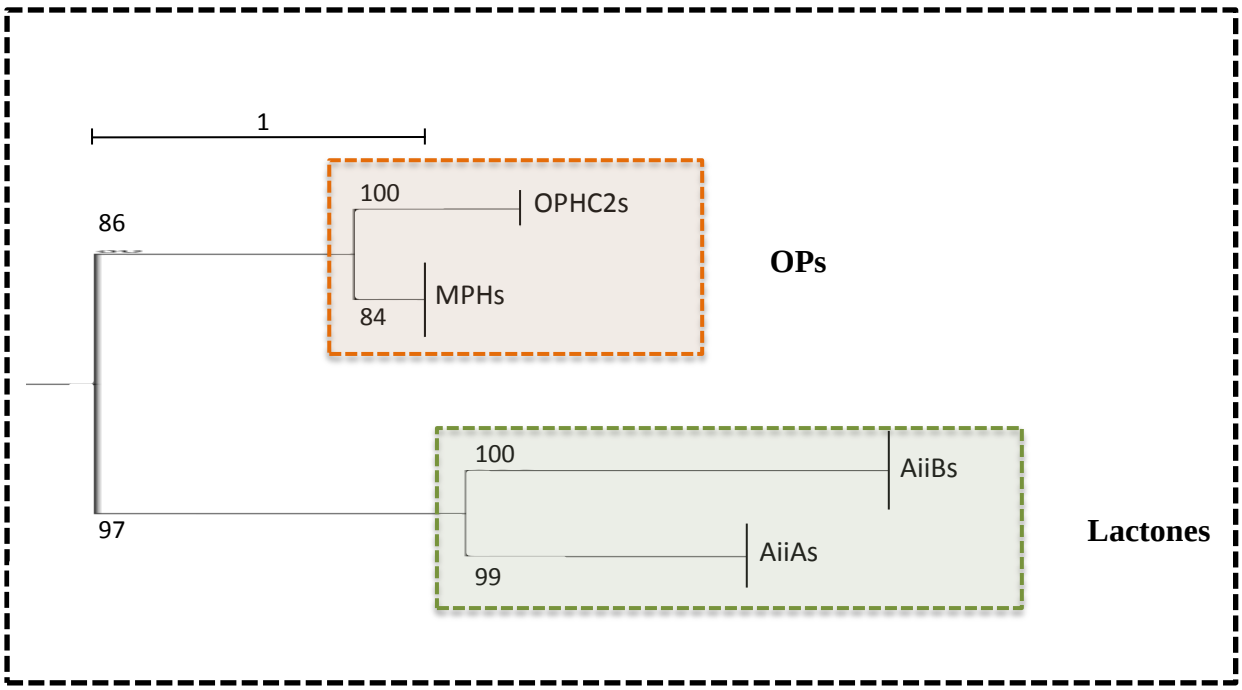

Figure III.3: *Arbre phylogénétique simplifié des enzymes à sandwich αβ/βα*

L'analyse des séquences de lactonases et d'OPs hydrolases à topologie de type sandwich αββα met en évidence le lien phylogénétique entre ces deux types d'enzymes. Les MPHs et OPHC2 pourraient avoir évolué à partir de lactonases ancestrale.

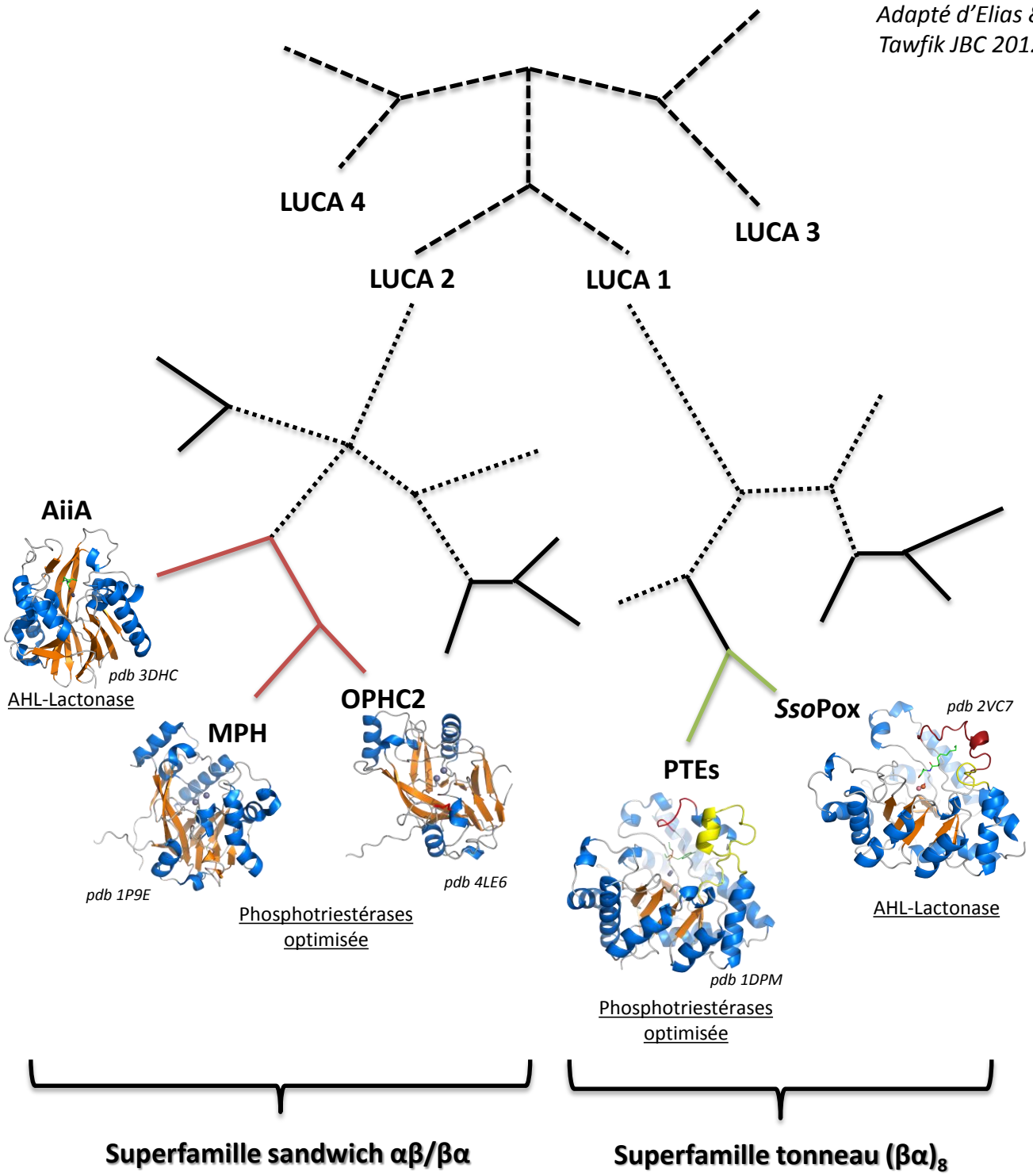

Figure III.4 : *Représentation schématique de l'évolution des OP hydrolases et des lactonases*

Le cas de l'évolution parallèle/convergente des activités OP hydrolase et lactonase au sein de deux superfamilles d'enzymes est illustré (les sandwichs αβ/βα et les tonneaux $(\beta\alpha)_8$). Les protéines progénitrices de chaque famille (numérotées de 1 à 4) qui étaient présentes chez LUCA (Last Universal Common Ancestor) ont divergé à partir de protéines ancestrales inconnues par des voies inconnues (pointillets). Dans les deux superfamilles, des OP hydrolases ont évolué de façon parallèle et divergente à partir de lactonases ancestrales (traits continus de couleur).

2. Rôle de la flexibilisation locale dans l'amélioration

A l'origine, le but de la saturation de site sur la position 263 était d'éliminer un potentiel clash stérique induit par la présence de ce résidu encombrant et ainsi créer l'espace nécessaire à l'accommodation des OPs. Afin de mieux comprendre l'impact des mutations sur cette position, la structure cristallographique des différents variants PteSV et LacSV fut obtenue et comparée à l'enzyme sauvage.

Tel qu'attendu, les structures obtenues des différents variants montrent un élargissement de la cavité du site actif permettant à l'enzyme une meilleure accommodation des substrats possédants un groupement partant encombrant. Cependant, il fut également observé une flexibilisation de la boucle portant la mutation (boucle 8), traduite par une augmentation du facteur B cristallographique et une diminution de la stabilité globale des mutants (T_m). Ce phénomène, également observé pour les mutants du premier cycle d'évolution (**voir partie perspectives IV. A. 4.**), semble être à la base de l'amélioration des activités de *Sso*Pox. En effet, les enzymes ont pendant longtemps été considérées comme des modèles « figés », selon le modèle clé-serrure (Emil Fischer, prix Nobel de chimie organique, 1902) dans lequel une enzyme adopte une conformation permettant l'hydrolyse d'un substrat donné (181) (**Figure III.5**). Celles-ci doivent être suffisamment flexibles pour permettre le repliement induit par la formation du complexe Michaelien et le relargage du produit en fin de réaction (210, 211). Cependant, la promiscuité enzymatique et la nécessité d'adaptation à l'état de transition ébranlant ce modèle, la preuve de l'existence d'une flexibilité conformationnelle permet maintenant de les considérer comme l'échantillonnage d'un ensemble de conformations (211, 212) (**Figure III.6**).

De plus, les protéines, et en particulier les enzymes, présentent deux caractères s'opposant : une rigidité de la charpente protéique nécessaire pour conserver la structure et des acides aminés impliqués dans l'acte chimique, une flexibilité des composantes (*i.e* les boucles) impliquées dans les étapes d'accommodation des substrats et du relargage des produits (210-213). Cette flexibilité est essentielle à l'existence des activités de promiscuité, puisqu'une même enzyme échantillonnant un ensemble de conformations, elle permet ainsi l'accommodation et l'hydrolyse de substrats différents de son activité naturelle : origine de la promiscuité enzymatique (210-212). Ainsi, les enzymes présentant une polarité structurale entre un corps rigide associé à des boucles flexibles constituant le site actif, vont pouvoir accumuler des mutations sans perte de fonction (robustesse envers les mutations). Dans le même temps, de par le caractère flexible d'une partie de leur site actif, elles pourront, en l'espace d'une poignée de mutation, se spécialiser envers une nouvelle fonction enzymatique (213).

Les protéines que nous avons étudiées au cours de ma thèse (*i.e Sso*Pox, *Sis*Lac et OPHC2) appartiennent à des familles structurales présentant typiquement ce type de polarité « corps/site actif » : les TIM-barrels et les sandwichs αββα. En effet, les TIM-barrels constitue une superfamille de protéines

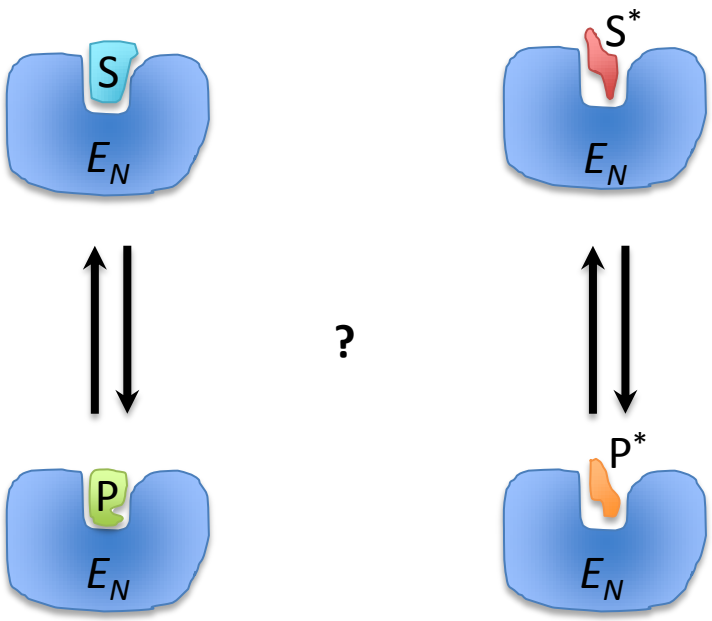

Figure III.5 : *Représentation schématique du modèle clé-serrure*

Dans le modèle clé-serrure, l'enzyme existe sous une seule conformation lui permettant l'accommodation de son substrat naturel. Les changements structuraux nécessaires à la catalyses ne sont pas pris en compte. De même, ce modèle ne permet pas d'expliquer comment une même enzyme peut accommoder un substrat différent de son activité naturelle et réaliser la réaction.

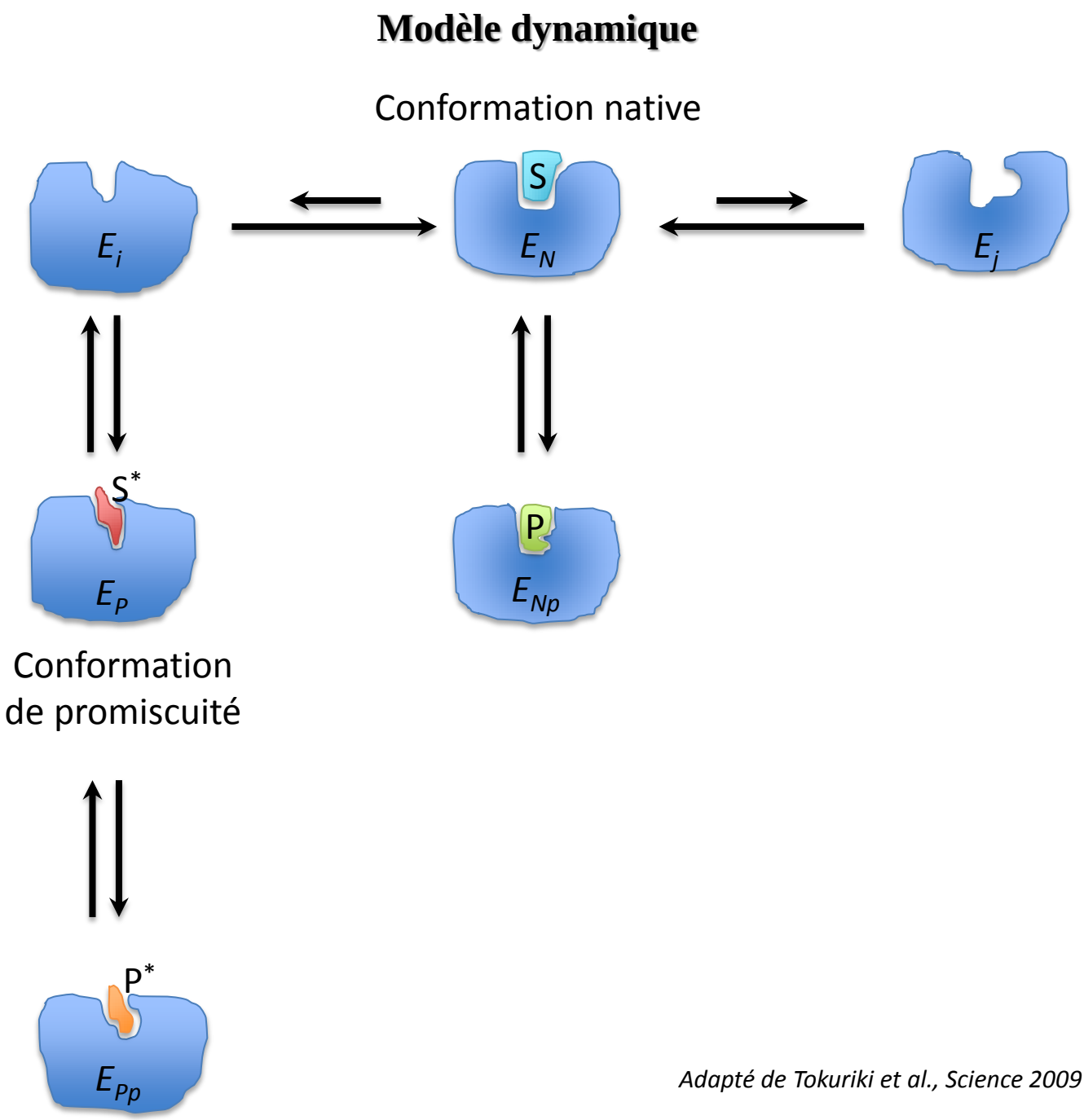

Figure III.6 : *Représentation schématique du modèle dynamique des enzymes*

Dans ce modèle, l'enzyme existe sous une conformation majoritaire (E_N) lui permettant son activité envers le substrat natif (S). L'enzyme est vue comme un objet dynamique, dont les changements conformationels des boucles et les changements de rotamères de certains résidus du site actif lui permettent l'accommodation de l'état de transition et le relargage du produit issu de la réaction native (E_{Np}). D'autres conformations minoritaires se différentiant par des changements équivalents (rotamères, conformation de boucle) (E_i, E_j) permettent l'activité de promiscuité, l'accommodation des substrats de promiscuité (S^*) et tous les changements nécessaires à la réaction catalysée (E_{Pp}).

comprenant plus de 120 familles d'enzymes différentes ne présentant pas d'identité de séquence (213). *Sso*Pox présente ainsi deux caractéristiques principales lui conférant un potentiel évolutif important : sa topologie tonneau $(\beta/\alpha)_8$ connue pour être évolutive et sa nature hyperthermostable, lui conférant une importante stabilité, capable de tolérer un nombre important de mutations sans perdre son intégrité structurale, nécessaire à l'acquisition de nouvelles fonctions enzymatiques (214).

L'amélioration de l'activité de *Sso*Pox fut permise par la flexibilisation de la boucle 8 du site actif, entrainant un élargissement du paysage conformationnel de l'enzyme et permettant à l'enzyme d'hydrolyser plus efficacement les substrats de promiscuité.

***Sso*Pox présente un potentiel évolutif important du fait de ses deux caractéristiques principales : une topologie favorable à l'émergence de nouvelles activités et une extrême stabilité capable d'accumuler un nombre important de mutations. Ainsi, *Sso*Pox constitue un candidat intéressant à l'évolution *in vitro* dans le but d'améliorer son activité envers les OPs.**

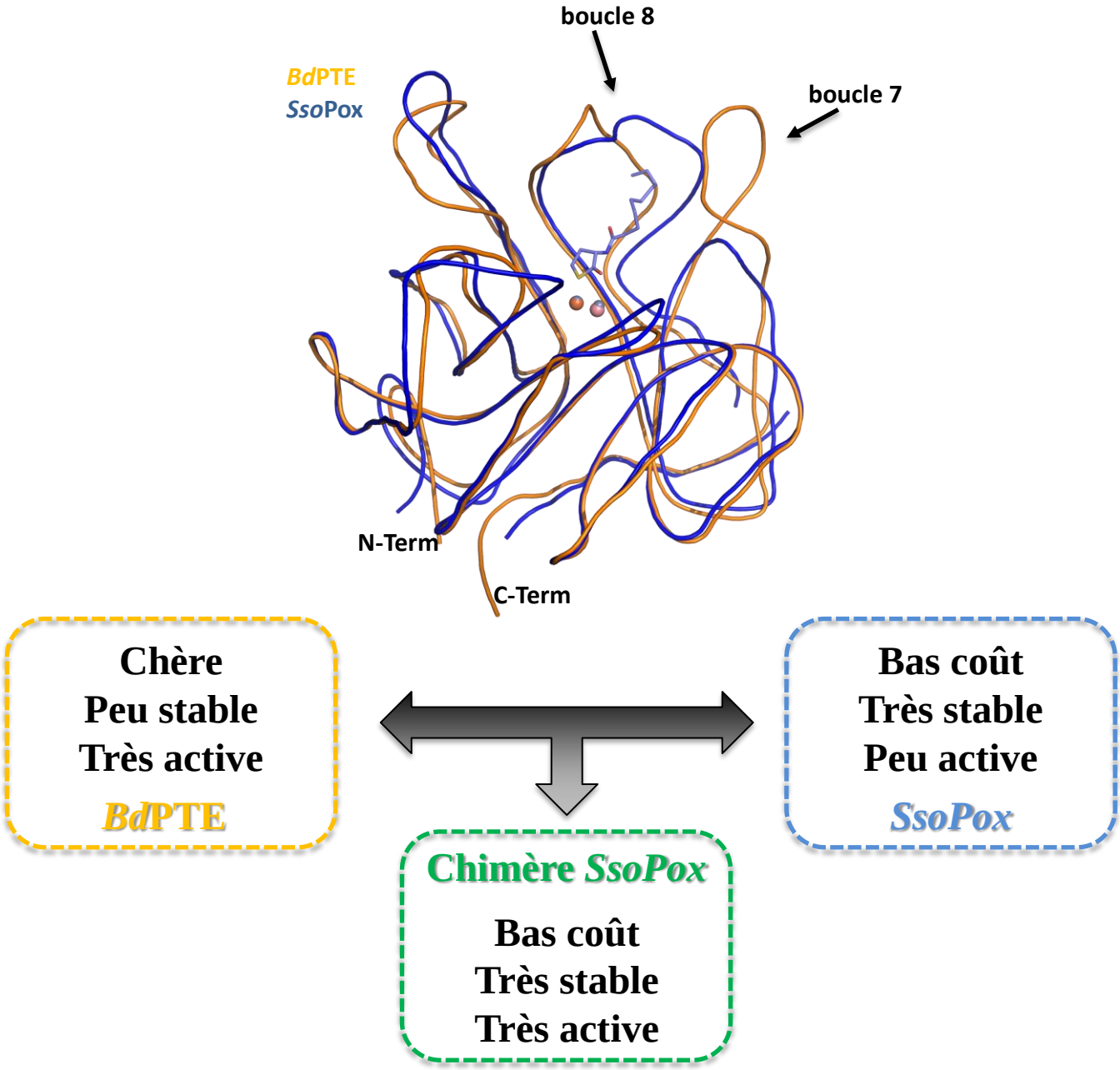

Figure IV.1 : *Concept de transfert de site actif*

*Sso*Pox et *Bd*PTE présentent des topologies similaires (tonneau $(\alpha/\beta)_8$) parfaitement superposable sur la majorité du corps protéique et dont les principales différences résident dans les boucles du site actif. En particulier, la boucle 7 est plus courte chez *Sso*Pox que chez *Bd*PTE ainsi que des conformations différentes pour la boucle 8. Partant de ce constat, une base de données permettant de transférer le site actif de la *Bd*PTE, optimisé pour hydrolyser les OPs, dans l'architecture hyperthermostable de *Sso*Pox. L'objectif final étant d'obtenir une enzyme présentant le meilleur compromis entre les avantages respectifs des deux enzymes.

IV. Perspectives :

A. Ingénierie rationnalisée par la structure

1. Stratégie d'évolution

Afin de développer un bio-décontaminant d'OPs à la fois robuste et efficace, la ressemblance structurale entre les PLLs hyperthermostables et les PTEs fut exploitée (**Figure IV.1**). En effet, approchant la vitesse limite de diffusion dans le cas de certains substrats, les PTEs sont capables d'hydrolyser très efficacement ces composés (215). A contrario, les PLLs sont des lactonases qui ne sont pas optimisées pour hydrolyser les OPs (160, 161). Or, la spécificité de substrat dans cette famille d'enzyme est en grande partie assurée par les boucles proches du site actif qui leur permettent d'accommoder les substrats (161). Les principales différences structurales entre les PTEs et les PLLs résident ainsi dans la longueur des boucles 7 et 8 (**voir Figure III.1**). Afin de conférer les propriétés catalytiques des PTEs aux PLLs, la principale stratégie adoptée dans la littérature fut d'effectuer un transfert direct des boucles de la *Bd*PTE dans le contexte de PLLs telles que *Dr*OPH (162, 216). Cependant, les résultats obtenus furent décourageants puisqu'ils ne résultèrent qu'en l'obtention de protéines instables et/ou inactives envers les OPs. Récemment, un travail inverse impliquant des changements par étapes successives permit de reconstituer le chemin évolutif de la *Bd*PTE en réalisant la résurrection de son ancêtre lactonase dont la boucle 7 est plus courte (161). Cette étude mit également en évidence l'existence de la position 254 (équivalent Arg 223 chez *Sso*Pox) dont les relations épistatiques sont critiques pour les activités enzymatiques des PTEs/PLLs (**voir partie III. A. 1. a.**).

Ainsi, le transfert direct de boucles ne permettant pas d'obtenir le produit biotechnologique voulu, une stratégie alternative fut développée par notre équipe. Tout d'abord par comparaison des structures de la *Bd*PTE et de *Sso*Pox et par le choix d'acides aminés appropriés, nous avons tenté de remodeler le site actif de *Sso*Pox afin qu'il ressemble au plus près à celui de la *Bd*PTE. L'avantage majeur de cette approche était de ne pas modifier la longueur des boucles du site actif mais d'adapter localement la nature des résidus. Il s'agissait ainsi de modeler les formes et les charges locales du site actif par analogie avec la *Bd*PTE afin de redessiner *in silico* le site actif de *Sso*Pox. Enfin en combinant cette analyse structurale avec des méthodologies d'évolution plus douces l'objectif fut de transférer le site actif très efficace de la *Bd*PTE dans l'architecture très stable de *Sso*Pox (**Figure IV.2**).

Le travail d'analyse qui fut effectué permit de constituer une base de données comprenant 14 mutations (brevet n° 07/0304; PCT/FR2008/000596) permettant de mimer le site actif de la *Bd*PTE dans le contexte *Sso*Pox. Grâce à l'utilisation d'une méthode de pointe en biologie moléculaire (217),

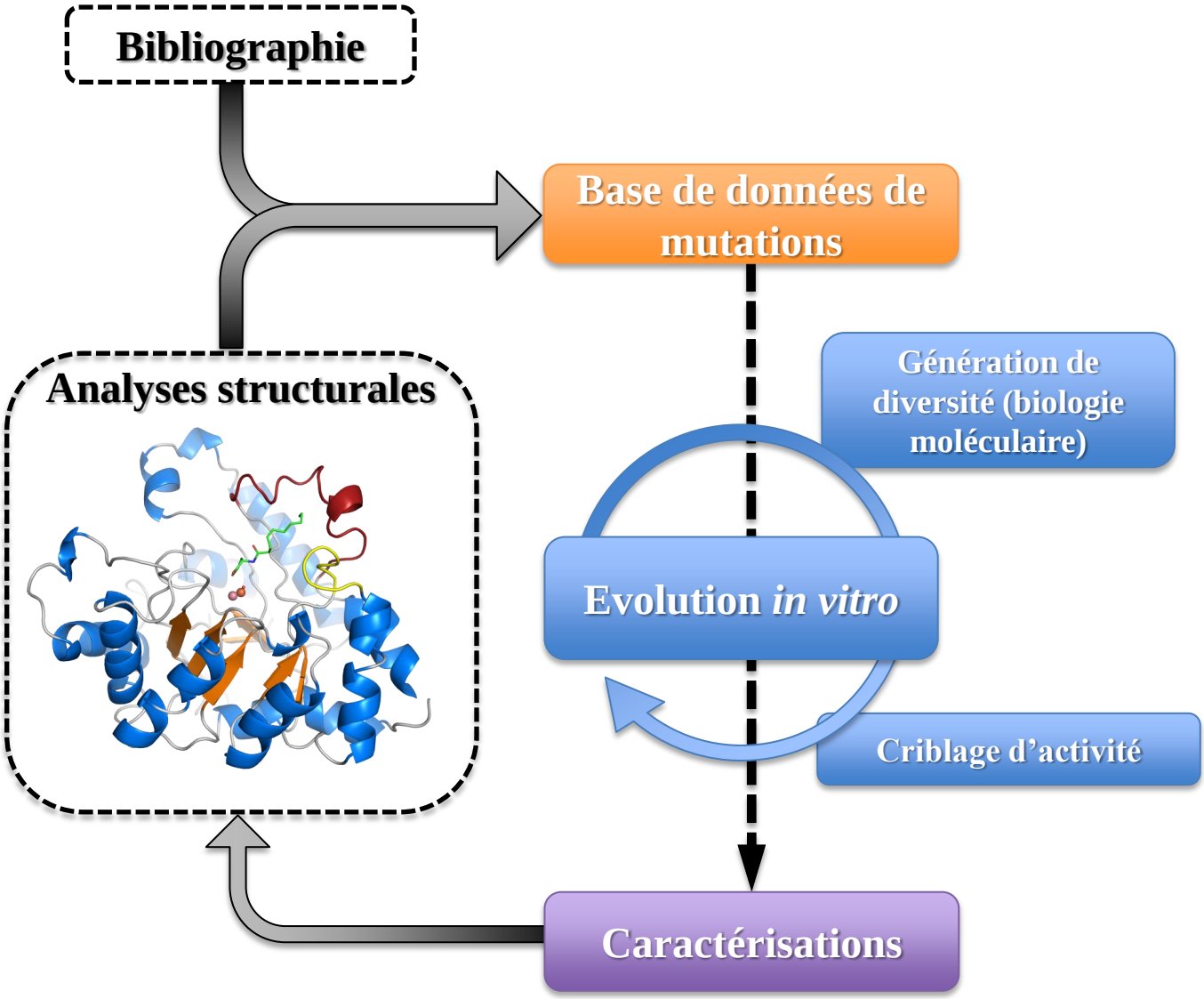

Figure IV.2 : *Stratégie générale utilisée pour l'amélioration rationalisée de* SsoPox

En utilisant les informations issues de la bibliographie et de l'analyse structurale, une base de données permettant de faire évoluer l'activité de *Sso*Pox fut établie. Un protocole d'évolution *in vitro* de l'enzyme (ISOR) fut développé afin de générer la diversité génétique permettant de brasser les mutations contenues dans la base de données. Les variants générés sont criblés pour leur activité phosphotriestérase envers différents OPs. Enfin, les variants les plus intéressants font l'objet d'une caractérisation biochimique, enzymatique et structurale complète. Les informations issues de l'analyse structurale des variants permettent d'améliorer continuellement notre base de données de mutations.

l'ensemble des mutations contenues dans la base de données sont brassées. Ce protocole permet d'obtenir des combinaisons aléatoires de mutations. Les gènes générés sont clonés dans un plasmide permettant l'expression des différents variants. La banque obtenue est criblée en microcultures, des variants améliorés sont sélectionnés, recriblés, séquencés puis les meilleurs d'entre eux font l'objet d'une caractérisation complète (**Figure IV.2**).

Grâce à l'analyse structurale et au dessein intelligent, il fut possible de développer une base de données de mutations dans le but de transférer le site actif très efficace de la *Bd*PTE dans l'architecture très stable de *Sso*Pox. La méthodologie développée a permis d'obtenir des variants améliorés comportant des combinaisons aléatoires de mutations.

2. Résultats préliminaires du premier cycle d'évolution rationalisée

A la fin du premier cycle d'évolution rationalisée de l'enzyme, sur plus de 200 clones criblés, 24 furent recriblés, 14 de ces variants séquencés et 5 d'entre eux furent considérés comme les plus intéressants du fait de leur activité améliorée (**Figure IV.3**). D'un point de vue statistique, parmi les 14 positions de la base de données de mutations, 6 positions furent sélectionnées dans plus de 30 % des cas (Val 27, Leu 72, Tyr 97, Tyr 99, Leu 228, Trp 263). En particulier, la position du Trp 263 que nous avions déjà identifiée comme étant critique dans l'accommodation des substrats, fut même sélectionnée dans plus de 70 % des variants séquencés.

Les différents variants obtenus au cours de ce premier cycle d'évolution furent caractérisés pour leur activité envers différents OPs (**Tableau IV.1**). D'une façon générale, ils présentent des efficacités accrues envers tous les substrats testés (augmentation aussi bien du k_{cat} que du K_M). Le meilleur variant sélectionné (*Sso*Pox-αsD6, V27A/Y97W/L228M/W263M) hydrolyse aussi efficacement le methyl-paraoxon que le methyl-parathion ($k_{cat}/K_M \sim 10^4$ $M^{-1}.s^{-1}$, augmentation de 2210 fois). Cette capacité illustre que l'enzyme semble avoir perdu le « thiono-effect », c'est-à-dire la préférence pour les oxono-OPs au détriment des thiono-OPs. L'origine moléculaire de cette préférence est actuellement en cours d'étude et semble impliquer des modifications de la distribution électronique des métaux constituants le site bi-métallique bien que la sphère de coordination des métaux n'ait pas été touchée par les mutations. La préférence de l'enzyme pour les substrats possédant des substituants peu encombrants fut réduite ($k_{cat}/K_M > 10^4$ $M^{-1}.s^{-1}$ envers le méthyl- et l'éthyl- paraoxon). Ainsi, la stratégie employée semble également avoir permis d'aménager l'espace nécessaire pour l'accommodation des substrats plus volumineux tels que les OPs alors que l'enzyme est à l'origine optimisée pour la fixation des lactones. Enfin, en présence de détergent, le variant asD6 présente une activité 857 fois supérieure à l'enzyme sauvage envers le paraoxon ($k_{cat}/K_M = 4{,}45\ (\pm 0{,}34) \times 10^5$ $M^{-1}.s^{-1}$) et des efficacités catalytiques d'environ 10^4 $M^{-1}.s^{-1}$ envers la plupart des OPs caractérisés. Néanmoins, l'amélioration d'activité obtenue en

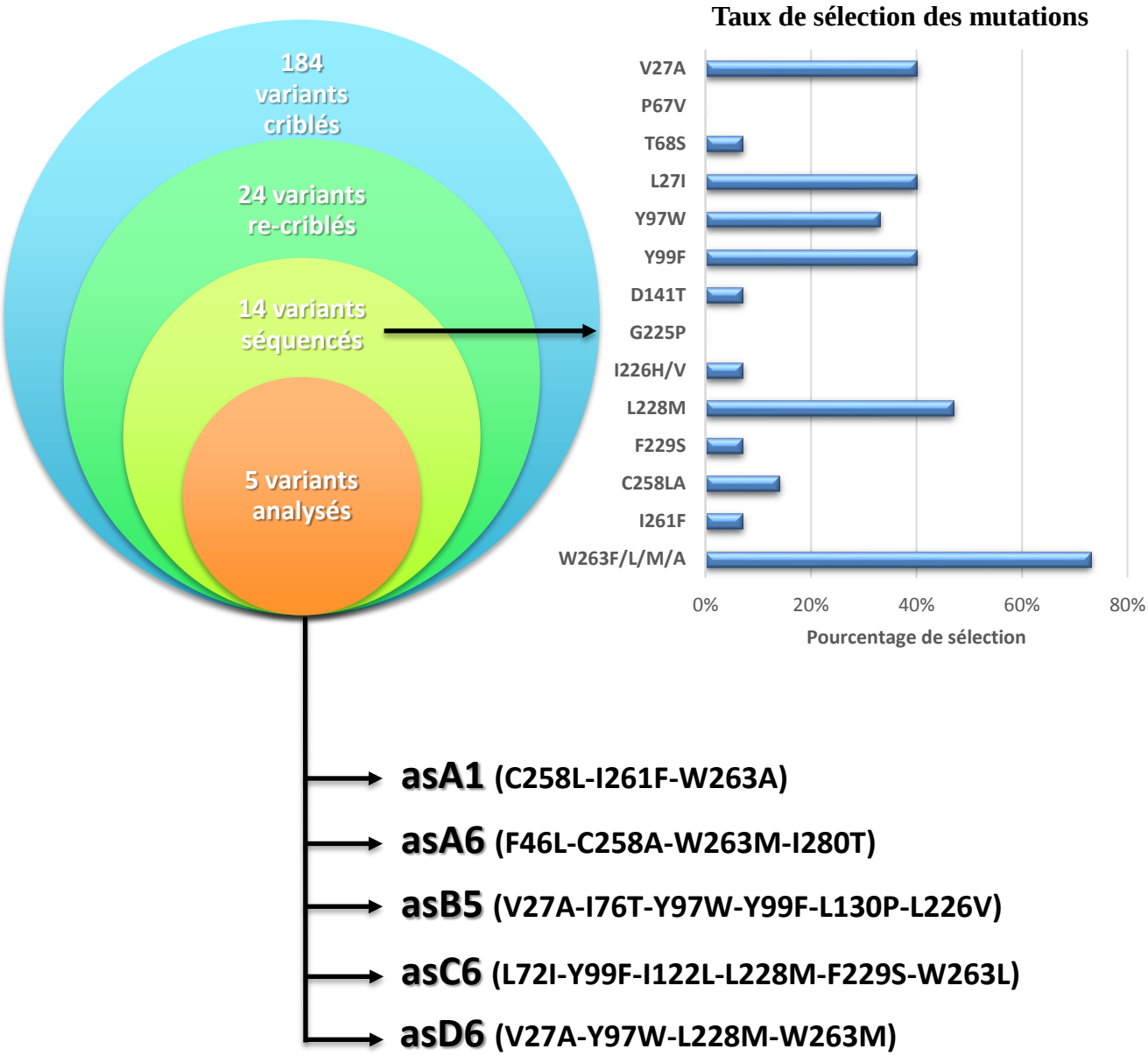

Figure IV.3 : *Variants sélectionnés au premier cycle d'évolution*

184 variants furent criblés au premier cycle d'évolution rationalisée, les 24 variants les plus intéressants furent re-criblés envers le methyl-paraoxon et l'ethyl-paraoxon. Parmi eux, 14 furent alors séquencés révélant un taux de sélection élevé pour la mutation Trp 263 Phe/Leu/Met/Ala et un faible taux pour Thr 68 Ser et Asp 141Thr. En revanche, aucun variant portant la mutation Pro 67 Val et Gly 225 Pro ne furent sélectionnés. Enfin, les 5 meilleurs variants de ce cycle (asA1, asA6, asB5, asC6 et asD6) firent l'objet d'une caractérisation biochimique, enzymatique et structurale poussée.

	Protéine	$k_{cat}(s^{-1})$	$K_M(\mu M)$	$K_I(\mu M)$	$k_{cat}/K_M(M^{-1}.s^{-1})$	amélioration/wt
Ethyl-paraoxon	**wt***	12,6 ± 1,26	2,43(±0,37)x10^4	-	512 ± 131	1 ± 0,36
	αsA1	27 ± 2,27	800 ± 155	-	3,37(±0,71)x10^4	64,98 ± 21,38
	αsA6	5,87 ± 0,47	1630 ± 631	-	3,61(±1,43)x10^3	6,95 ± 3,26
	αsB5	36,4 ± 2,04	731 ± 98	-	4,98(±0,72)x10^4	95,86 ± 27,91
	αsC6	42,7 ± 2,53	1500 ± 161	-	2,86(±0,35)x10^4	55,05 ± 15,45
	αsD6	38,8 ± 1,77	624 ± 73	-	6,22(±0,78)x10^4	119,89 ± 33,79
Methyl-paraoxon	**wt***	2,71 ± 0,64	2140 ± 676	-	1,27(±0,70)x10^3	1 ± 0,78
	αsA1	43,5 ± 8,72	1900 ± 523	-	2,29(±0,78)x10^4	18,08 ± 11,74
	αsA6	5,89 ± 0,55	546 ± 102	-	1,08(±0,23)x10^4	8,53 ± 5,04
	αsB5	ND	ND	-	4,31(±0,14)x10^3	3,41 ± 1,89
	αsC6	23,6 ± 3,68	759 ± 204	-	3,11(±0,97)x10^4	24,57 ± 15,59
	αsD6	42,5 ± 5,2	2080 ± 343	-	2,04(±0,42)x10^4	16,11 ± 9,51
Ethyl-parathion	**wt***	ND	ND	ND	ND	ND
	αsA1	ND	ND	ND	ND	ND
	αsA6	3,2(±0,2)x10^{-2}	134 ± 18	3250 ± 1020	239 ± 35	ND
	αsB5	1,10(±0,04)x10^{-1}	118 ± 14	-	932 ± 116	ND
	αsC6	8,53(±0,30)x10^{-3}	77 ± 11	-	110 ± 16,2	ND
	αsD6	1,21 ± 0,07	200 ± 38	-	6,05(±1,20)x10^3	ND
Methyl-parathion	**wt***	1,10(±0,02)x10^{-3}	121 ± 10	-	9,09 ± 0,9	1 ± 0,14
	αsA1	1,3(±0,5)x10^{-2}	353 ± 34	-	36,8 ± 14,6	4,05 ± 1,66
	αsA6	1,55(±0,15)x10^{-2}	254 ± 39	1520 ± 384	61 ± 11,1	6,71 ± 1,39
	αsB5	1,5(±0,04)x10^{-1}	158 ± 15	-	949 ± 93,6	104,43 ± 14,59
	αsC6	3,00(±0,10)x10^{-3}	121 ± 15	-	24,8 ± 3,18	2,72 ± 0,44
	αsD6	6,89 ± 0,35	343 ± 44	-	2,01(±0,28)x10^4	2209,62 ± 375,22
Malathion	**wt***	8,90(±0,40)x10^{-4}	160 ± 29	-	5,56 ± 1,26	1 ± 0,32
	αsA1	7,1(±0,4)x10^{-4}	222 ± 35	-	3,2 ± 0,54	0,57 ± 0,16
	αsA6	ND	ND	ND	ND	ND
	αsB5	1,55(±0,12)x10^{-2}	498 ± 85	-	31,1 ± 5,8	5,59 ± 1,65
	αsC6	2,47(±0,44)x10^{-2}	32 ± 19	820 ± 343	772 ± 478	138,76 ± 91,58
	αsD6	9,99(±0,29)x10^{-2}	238 ± 21	-	420 ± 39	75,46 ± 18,47

Tableau IV.1 : *Caractérisation de l'activité phosphotriestérase des variants de* Sso*Pox*

Les paramètres catalytiques de l'enzyme sauvage (*) sont issus de *Hiblot et al.* (2012), les valeurs indiquées par ND correspondent aux valeurs non déterminées. Certains substrats entrainent une inhibition par le substrat, le K_I est indiqué mais les efficacités catalytiques ne sont justes qu'à basse concentration en substrat.

présence de détergent est d'une ampleur plus faible que celle observée pour l'enzyme sauvage, suggérant ainsi que les mutations sélectionnées au cours du premier cycle ont un effet partiellement comparable à celui des détergents (*i.e* une flexibilisation de l'enzyme) (147). D'une façon générale, les améliorations d'efficacité catalytique obtenues sont parmi les plus importantes recensées dans la bibliographie pour les PLLs (162, 166-168, 218). De plus, parmi les positions sélectionnées dans la littérature, très peu d'entre elles sont communes avec celles que nous avons sélectionnées avec notre approche. Seules les positions Tyr 99 et Asn 269 sélectionnées chez GkL et Val 235 sélectionnées chez *Dr*OPH ont leurs équivalents structuraux également sélectionnés chez *Sso*Pox (correspondant à Tyr 97, Leu 228 et Cys 258). Ces différences proviennent à la fois de la différence de méthodologie employée mais également de la différence intrinsèque entre *Sso*Pox (PLL-A) et GkL/*Dr*OPH (PLL-B). L'étude approfondie de ces mutations pourrait néanmoins permettre d'améliorer notre base de données de mutations. Cela met également en évidence la pertinence de notre base de données de mutations qui pourra de plus être améliorée grâce aux informations recueillies dans la bibliographie.

Notre stratégie d'évolution rationnalisée permit d'obtenir des valeurs d'efficacité proches de la médiane des efficacités mesurées pour l'activité naturelle des enzymes ($(k_{cat}/K_M \sim 10^5\ M^{-1}.s^{-1}$) (219). Ceci dénote l'élargissement du spectre d'activité de l'enzyme qui pourra alors être respécialisée par la suite envers les OPs. La puissance de notre stratégie permet d'envisager de l'utiliser pour améliorer son efficacité envers de nouvelles molécules. Dans le futur du projet, nous envisageons de combiner notre technique à des méthodes d'évolution dirigée aléatoire et à l'utilisation de banques de mutations ancestrales. De plus, les différents variants étant purifiés par la chaleur, les propriétés biotechnologiques liées à la thermostabilité de l'enzyme sont conservées.

3. Caractérisation structurale préliminaire des mutants améliorés

Au cours de ce premier cycle d'évolution rationalisée, 5 variants d'intérêt furent sélectionnés pour une caractérisation enzymatique, biochimique et structurale complète. Afin de comprendre les bases structurales des améliorations et augmenter le pouvoir de convergence de notre base de données de mutation, les structures cristallographiques des différents mutants furent résolues (ceux-ci cristallisants dans des conditions analogues à celles utilisées précédemment) (197, 198). L'un de ces mutants (*Sso*Pox-asA6) présenta deux faciès cristallins différents présents au sein de la même condition de cristallisation. Les données de diffraction aux rayons X furent obtenues respectivement à 2,1 Å, 2,5

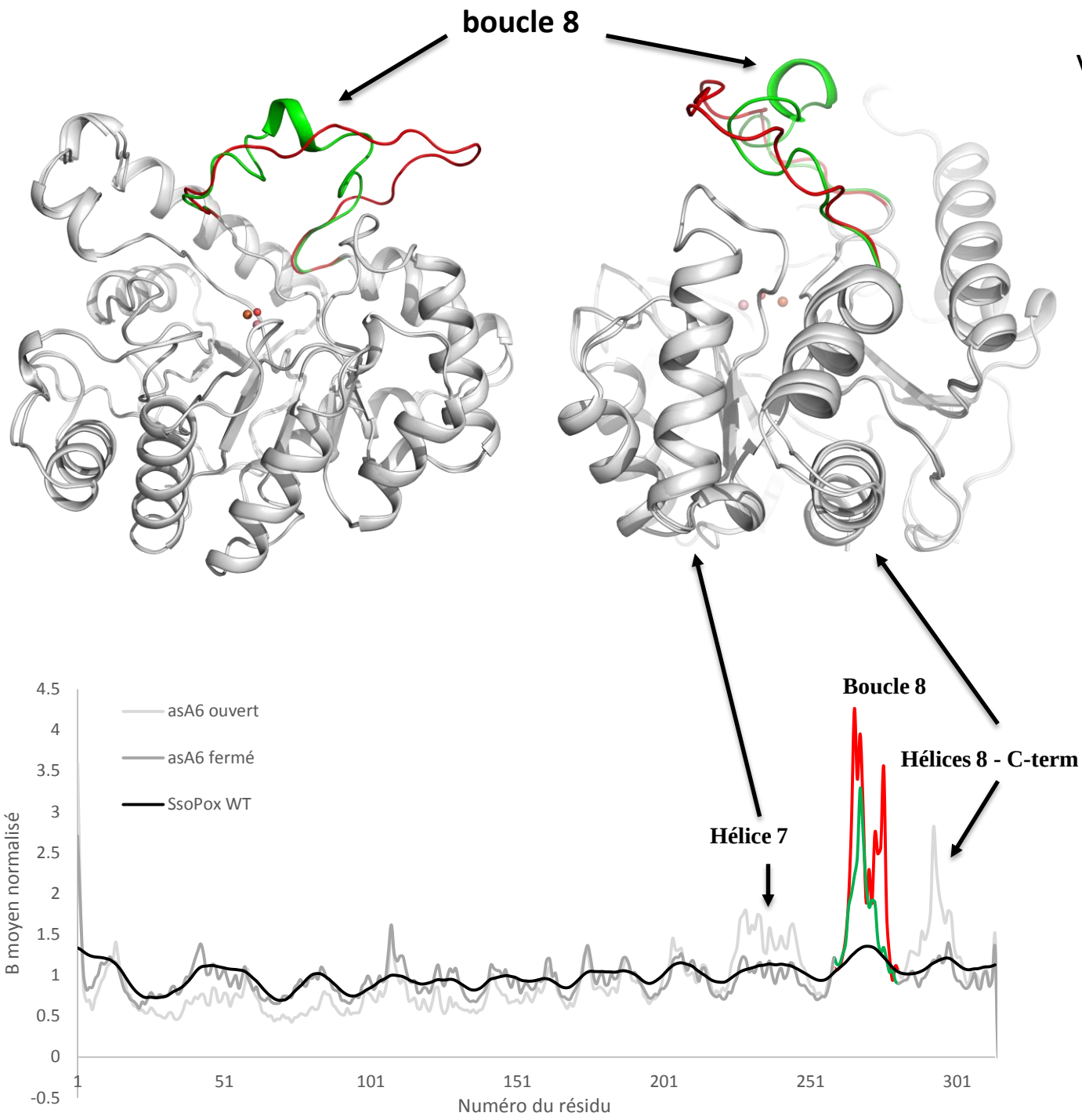

Figure IV.4 : *Structures des variants du premier cycle d'évolution rationnalisée*

L'analyse structurale du variant *Sso*Pox asA6 mit en évidence l'existence de deux conformations alternatives de l'enzyme, la première (dite fermée) où la boucle 8 adopte une conformation analogue à l'enzyme sauvage, la seconde (dite ouverte) où la boucle 8 adopte une conformation relachée, ouvrant l'entrée du site catalytique. L'analyse de la flexibilité (traduite par le facteur B cristallographique) montre une flexibilisation principalement localisée au niveau de la boucle 8 pour la conformation fermée et ouverte, à laquelle s'ajoute une flexibilisation plus élevée des hélices 7 et 8-C-terminal dans la structure fermée.

Å, 2,55 Å, 2,95 Å, 2,15 Å et 1,4 Å pour les variants asA1, asB5, asC6, asD6, asA6 sous la forme cristalline classique et asA6 sous une autre forme cristalline (**voir bilan Tableau V.I**).

Bien que les structures des mutants asA1, asB5, asC6 et asD6 soient toujours en cours d'affinement, celles-ci révélèrent un phénomène analogue aux variants issus de la saturation de site sur la position du Trp 263, une flexibilisation des boucles du site actif. La première structure du variant *Sso*Pox-αsA6 (résolution 2,15 Å) fut ainsi obtenue dans le groupe d'espace classique pour *Sso*Pox ($P2_12_12_1$) révélant après affinement, le même phénomène de flexibilisation au niveau de la boucle 8 (tels qu'en témoignent des facteurs B élevés). La seconde structure de ce variant (obtenue à 1,6 Å) fut obtenue dans un groupe d'espace différent ($P2_1$). L'affinement de cette structure révéla une conformation différente de la boucle 8 qui est dans une conformation dite « ouverte » (**Figure IV.4**). Ainsi, l'échantillonnage de conformations de la boucle 8 est tellement important que l'enzyme fut cristallisée dans deux conformations différentes.

Or les enzymes ont longtemps été vues comme des objets figés, considérés selon le modèle clé-serrure : une enzyme, une conformation, un substrat donné (**voir Figure III.5**). Or, l'existence même de plusieurs activités au sein d'un même site catalytique, la preuve de l'existence de différentes conformations et de la flexibilité permet de les considérer comme des objets échantillonnant différentes conformations aux probabilités d'existence plus ou moins élevées (**voir Figure III.6**) (211, 212). Ainsi, notre stratégie d'évolution de l'activité de l'enzyme a permis, en introduisant des mutations au sein des boucles, d'augmenter l'échantillonnage de conformations en flexibilisant localement l'enzyme. Cette flexibilisation permet de changer la probabilité d'existence de certaines conformations et par exemple de peupler un peu plus certains états dans lesquels l'enzyme peut accommoder les substrats de promiscuité. Ainsi même un changement très faible de cette probabilité d'existence permet d'augmenter de façon importante l'activité de l'enzyme envers ces substrats sans compromettre l'activité naturelle de l'enzyme (**Figure IV.5**). De nouveaux cycles d'évolution rationalisée seront néanmoins nécessaires afin d'obtenir une enzyme spécialisée envers les OPs.

L'analyse préliminaire de la structure cristallographique des variants du premier cycle d'évolution rationalisée mit en évidence une flexibilisation des boucles du site actif analogue à celle obtenue avec la saturation de site sur la position du Trp 263. Cette flexibilisation permet d'élargir le paysage conformationnel de l'enzyme augmentant ainsi la probabilité d'existence de conformations capables d'accommoder les OPs.

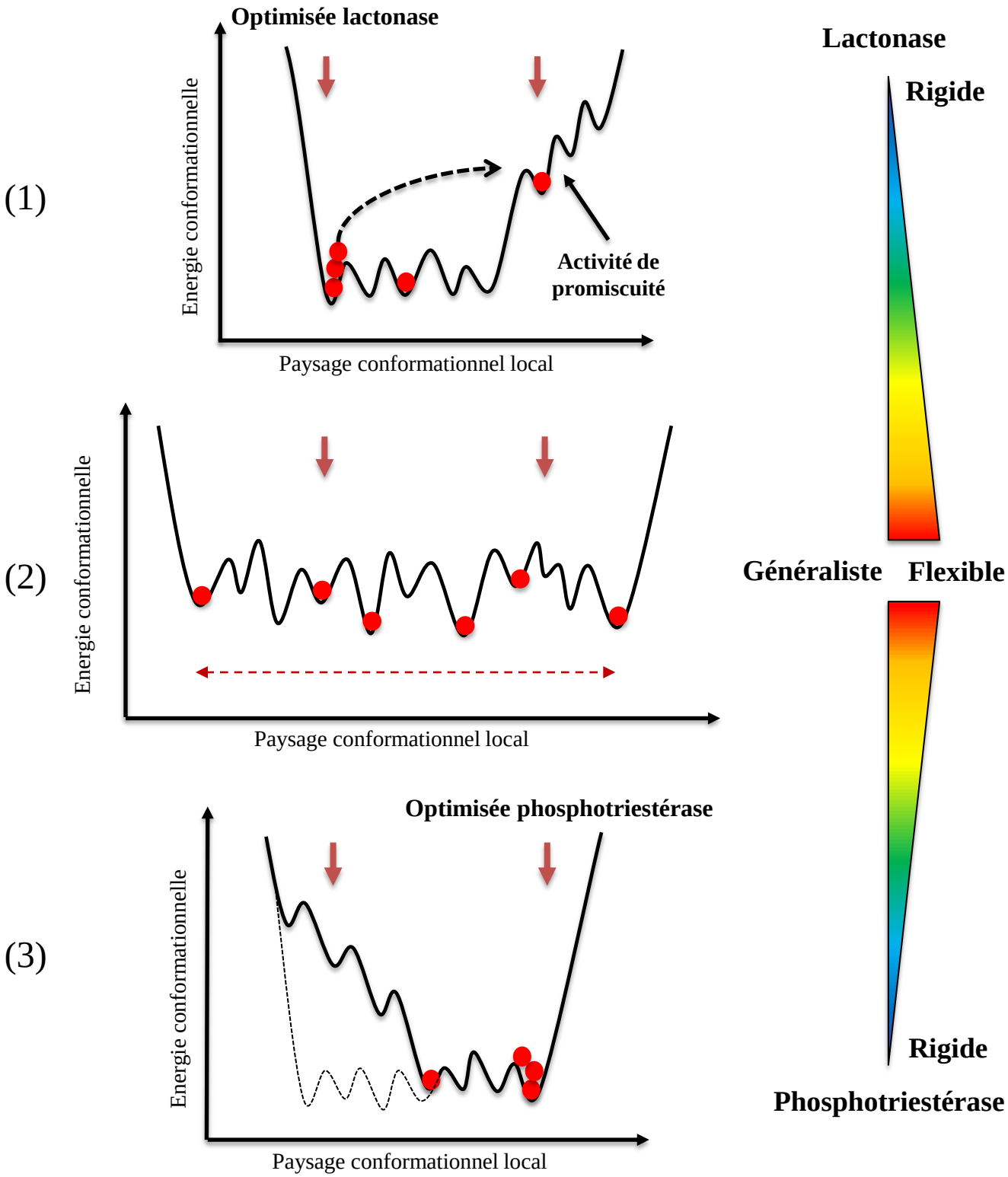

Figure IV.5 : *Représentation schématique de l'exploration du paysage conformationnel d'une enzyme au cours de l'évolution de son activité*

Le paysage conformationnel local (*e.g* boucle du site actif) est représenté en fonction de l'énergie nécessaire pour atteindre la conformation. **(1)** L'enzyme est une lactonase naturelle, présentant une activité de promiscuité phosphotriestérase dont l'énergie de conformation est plus élevée. **(2)** Au cours des protocoles d'évolution, il fut observé une flexibilisation de l'enzyme, lui permettant d'élargir son espace conformationnel et ainsi d'augmenter la probabilité d'existence de conformations permettant l'hydrolyse des OPs. **(3)** Lors de la respécialisation de l'enzyme envers les OPs, l'enzyme sera stabilisée pour hydrolyser ces substrats (*i.e* énergie conformationnelle plus basse), rigidifiant l'enzyme dans ces nouvelles conformations.

B. Activités lactonases de *Sso*Pox

1. Étude de l'activité lactonase de *Sso*Pox

*Sso*Pox fut caractérisée avant mon arrivée en thèse comme étant une lactonase naturelle présentant une activité de promiscuité phosphotriestérase (160, 163). Cependant, il existe différents types de lactones (**voir partie introductive, Figure I.19**) et cette activité ne fut que succinctement caractérisée (220). Ainsi, nous avons réalisé une étude plus étendue de l'activité lactonase de *Sso*Pox envers les AHLs (lactones utilisées dans le QS bactérien) et les oxo-lactones (molécules naturelles constituant des arômes). Or, nous avons pu montrer que l'enzyme hydrolyse aussi efficacement les AHLs ($k_{cat}/K_M \sim 10^4\ M^{-1}.s^{-1}$) que les oxo-lactones. Cette caractéristique est observée chez les autres lactonases appartenant au clade des PLL-A qui sont décrites comme des AHL lactonases naturelles (161). De plus, au cours de notre étude présentée en partie **II. F.**, il fut montré que *Sso*Pox hydrolyse plus efficacement les AHLs lévogyres qui sont celles naturellement utilisées dans le QS (202). De même, la caractérisation des variants de la position du Trp 263 montra que les améliorations obtenues furent les plus importantes pour l'activité oxo-lactonase. Or, il est reconnu que les activités de promiscuité sont celles qui peuvent être le plus facilement améliorées puisque celles-ci ne sont pas optimisées (181). Ces éléments combinés tendent ainsi à suggérer que l'activité AHL lactonase est l'activité naturelle sous pression de sélection.

Néanmoins, bien que l'activité de *Sso*Pox semble être une activité AHL-lactonase, cette observation soulève de nombreuses questions quant à son rôle physiologique chez les *Sulfolobus*. D'autant plus qu'étant donné la nature de l'environnement de ces archaeas extrémophiles (pH acide (~ 3), température > 80 °C), des molécules telles que les lactones pourraient être instables et être rapidement hydrolysées. Un élément allant tout de même dans ce sens est la découverte récente d'un système de QS archaea à base d'AHLs chez certaines archaeas méthanogènes mésophiles (208). Ainsi il pourrait exister un système de QS chez les *Sulfolobus* ou d'autres organismes appartenant à la même niche écologique. Afin d'explorer cette possibilité, des travaux sont en cours afin de déterminer la stabilité des AHLs dans les milieux extrêmes.

2. Étude structurale de l'activité de promiscuité oxo-lactonase

L'activité oxo-lactonase de *Sso*Pox fut précédemment caractérisée comme étant une activité de promiscuité. Un mutant, *Sso*Pox-D256N, fut identifié par analogie avec d'autres lactonases caractérisées dans la littérature (position 266 chez GkL (167, 221) et 108 chez AiiA (185, 190, 191)) et rendant ces enzymes incapables d'hydrolyser ces molécules. La caractérisation enzymatique du mutant ponctuel *Sso*Pox-D256N confirma la perte d'activité lactonase de l'enzyme qui fut alors utilisée afin de mieux

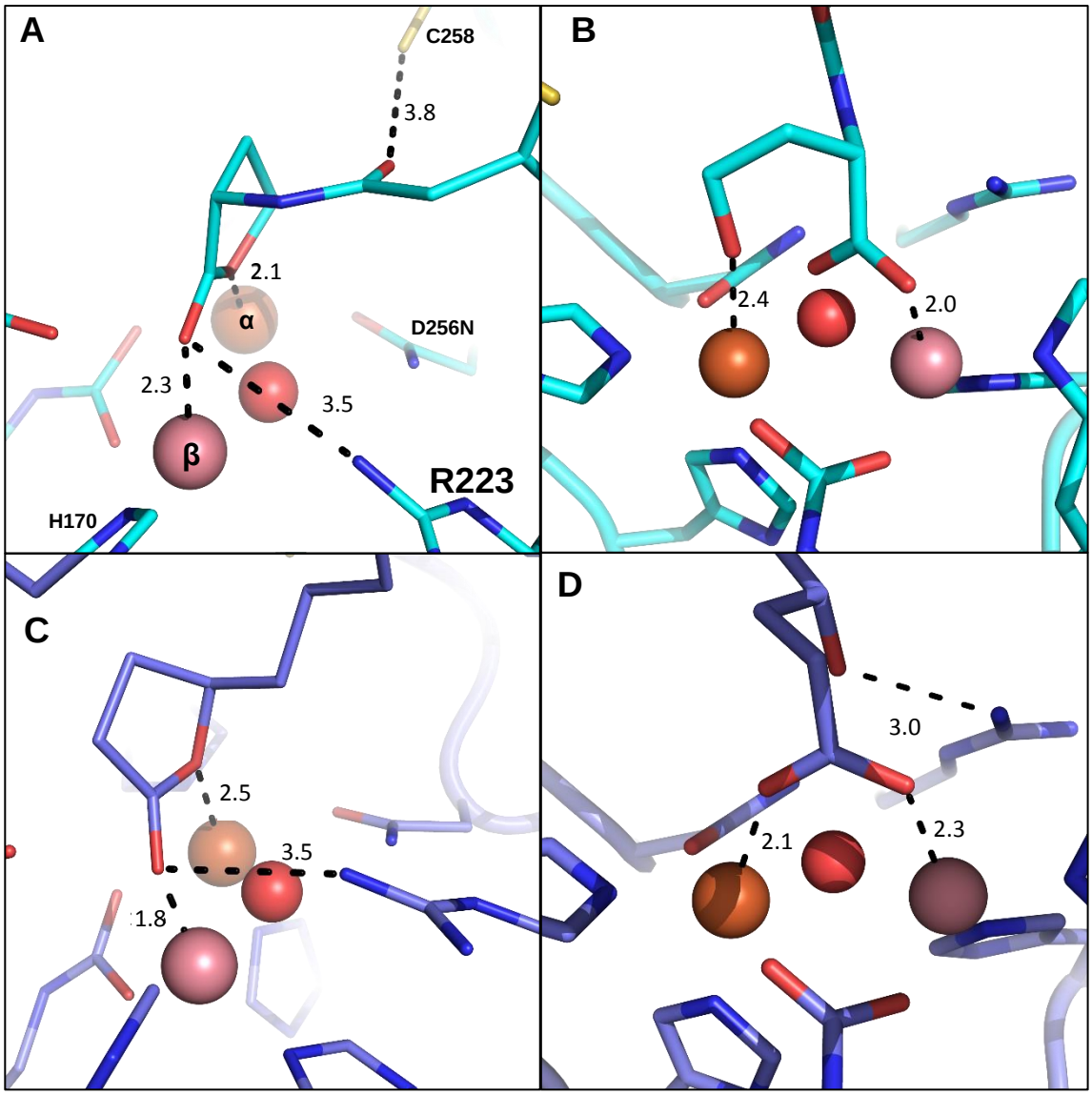

Figure IV.6 : *Structures du variant D256N obtenues en présence de diverses lactones*

Le variant Asp 256 Asn fut obtenu en complexe avec différentes molécules : **A** complexe avec le substrat 3-oxo-C10 AHL (par trempage), et **B** son produit d'hydrolyse (co-cristallisation), C complexe avec le substrat de undecanoic γ-lactone (trempage) et **D** son produit d'hydrolyse (co-cristallisation). Les distances interatomiques sont représentées par des tirets et indiquées en Å. L'accommodation des substrats est relativement équivalente entre les deux types de lactones avec les métaux tandis que les produits d'hydrolyse sont stabilisés de façon différente. Pour le produit d'hydrolyse de l'AHL, les fonctions carboxyliques et alcoolate sont accommodées par les métaux β et α alors que pour le produit d'hydrolyse de l'oxo-lactone, l'acide carboxylique est accommodé par les deux métaux du centre bimétallique et la fonction alcoolate est accommodée par l'Arg 223.

comprendre les bases structurales du mécanisme oxo-lactonase de *Sso*Pox. Des co-cristallisations et des trempages de cristaux furent effectués en présence de différents substrats lactones : une AHL (3-oxo-C12 AHL) et deux oxo-lactones (undecanoic δ-lactone et undecanoic γ-lactone). Les différentes structures furent résolues (**voir Bilan Tableau V.1**) et permirent d'obtenir la structure de l'enzyme complexée aux différents substrats et produits d'hydrolyse des molécules utilisées (**Figure IV.6**).

L'analyse structurale préliminaire suggère que la fixation des substrats (AHL et oxo-lactones) est principalement analogue au niveau du centre bi-métallique tandis que l'accommodation est très différente pour les produits (**Figure IV.6**). En particulier, le résidu Arg 223 semble impliqué dans la stabilisation de l'alcoolate qui est généré lors de l'hydrolyse des oxo-lactones alors qu'il ne semble pas intervenir dans l'accommodation des produits d'hydrolyse des AHLs. De plus, en comparant l'efficacité d'hydrolyse des deux types de thio-lactones (dont le pKa est plus faible), des différences furent mises en évidence. En effet, alors que les Homoserine-ThioLactones (HTLs) sont des inhibiteurs de l'enzyme, les oxo-thiolactones sont mieux hydrolysése que leurs équivalents oxo-lactones. Afin de compléter notre étude et proposer le mécanisme d'hydrolyse de ces deux molécules, nous envisageons d'étudier des mutants de la position Arg 223.

C. Applications biotechnologiques envisagées

1. Applications concernant l'activité lactonase de *Sso*Pox

*Sso*Pox fut caractérisée comme une AHL-lactonase naturelle capable d'hydrolyser efficacement les molécules impliquées dans le QS bactérien ($k_{cat}/K_M \sim 2{,}2 \times 10^3\ M^{-1}.s^{-1}$) (**voir article présenté en II. F.**). La capacité de telles enzymes à effectuer le QQ fut démontrée chez différentes bactéries à coloration de Gram négative (192, 222, 223). Notamment, il avait été montré que *Sso*Pox est capable d'inhiber par QQ la production de facteurs de virulence chez *P. aeruginosa* (220). Nous avons exploré plusieurs voies d'application potentielles : diminution de la pathogénicité d'espèces bactériennes impliquées dans les infections nosocomiales, inhibition de la formation de bio-film pour des applications en santé publique et en tant qu'agent anti-biofouling.

Tout d'abord, en collaboration avec l'équipe du Dr. Bregeon (URMITE, Marseille, France), nous effectuons des travaux montrant que l'utilisation prophylactique de *Sso*Pox permet de réduire significativement la létalité due à l'infection respiratoire aigüe à *P. aeruginosa* chez le rat (diminution de 80 % à 10 %). Les AHLs étant utilisées dans le QS chez de nombreuses espèces bactériennes (*e.g*

Vibrio, *Erwinia*, *Acinetobacter*, *Serratia*), il s'agira désormais d'établir le spectre d'action de l'enzyme envers les espèces pathogènes.

Le problème de l'émergence de souches bactériennes multi- voire pan-résistantes est un problème majeur de santé publique. Touchant particulièrement le milieu hospitalier, les brûlures et les bio-matériaux sont le siège privilégiés des pathogènes nosocomiaux. L'utilisation de lactonases sur des espèces bactériennes devenues multi- voire toto-résistantes aux antibiotiques permet de restaurer une sensibilité de ces souches envers les antibiotiques (222, 224). Le projet va ainsi s'orienter vers la fonctionnalisation de l'enzyme pour un greffage sur des biomatériaux, des dispositifs médicaux (*e.g* pansements). L'objectif étant d'utiliser *Sso*Pox en tant que complément à l'arsenal thérapeutique du médecin.

Se déroulant principalement en milieu marin, le biofouling est un phénomène d'incrustation de matière biologique à la surface des matériaux immergés. A l'origine d'un coût d'entretien évalué à plusieurs milliards d'euros par ans, différentes stratégies visant à empêcher ou réduire ce phénomène sont à l'étude. L'une des composantes principales du biofouling est l'établissement d'un biofilm bactérien complexe. Du fait des avantages biotechnologiques liés à l'extrême robustesse de l'enzyme qui peut être fonctionnalisée dans des peintures, le projet explorera la capacité de *Sso*Pox à inhiber ou ralentir la formation de ce biofilm sur des coques de bateau.

Enfin, l'utilisation de lactonases exprimées chez différentes espèces de plantes permet de lutter contre la virulence de certains phytopathogènes (192, 225). *Sso*Pox pourrait ainsi constituer un moyen de protection face au feu bactérien répondant ainsi à une problématique agroalimentaire importante.

2. Applications concernant l'activité phosphotriestérase de *Sso*Pox

Les OPs sont des composés toxiques neurotoxiques utilisés en tant qu'insecticides et CWA, responsables d'un problème écologique et de santé publique important et constituant une menace terroriste (**voir partie introductive I. A. 1.**). Les méthodes actuellement disponibles pour les décontaminer sont archaïques car polluantes et couteuses. L'alternative élégante à ces solutions réside dans l'utilisation d'enzymes capables de les dégrader (20, 137). Or, au cours du travail de thèse, nous avons caractérisé des enzymes présentant à la fois la robustesse nécessaire dans le cadre d'une utilisation biotechnologique et l'activité de dégradation des OPs. De plus nous avons amélioré l'activité de l'enzyme *Sso*Pox afin de dégrader spécifiquement les insecticides OPs. *Sso*Pox présente ainsi plusieurs applications potentielles principales.

L'activité de l'enzyme fut améliorée envers les principaux insecticides utilisés en agriculture intensive (k_{cat}/K_M ~ 6 x 10^3 $M^{-1}.s^{-1}$ envers le parathion). Les insecticides OPs sont responsables

d'intoxications du fait de leur manipulation, d'empoisonnement (suicide) et constituent une menace terroriste importante du fait de leur relative accessibilité (1, 6). L'enzyme étant de plus active en présence de détergent, ceux-ci sont des tensio-actifs capables de solubiliser les OPs et pourraient permettre de dépolluer des surfaces contaminées (*e.g* matériels, bâtiments). *Sso*Pox pourrait ainsi constituer une réponse écologique à une problématique sociétale majeure ayant des répercutions aussi bien dans l'industrie agroalimentaire qu'en terme de sécurité civile.

L'amélioration d'activité permit également de dégrader efficacement certains analogues d'agents de type G. Le projet d'amélioration aura ainsi pour objectif de développer un bio-décontaminant de CWA OPs. La stratégie que nous avons employée avec succès sera utilisée en étroite collaboration avec la DGA MNRBC (Centre d'Etudes du Bouchet) afin de cribler l'activité des variants envers les agents neurotoxiques de guerre réels. A terme, nous envisageons de développer un cocktail enzymatique efficace contre les agents les plus problématiques (sarin, soman, tabun) qui pourra être inclus dans l'équipement du soldat ou utilisé dans le but de détruire les stocks de CWA OPs. Enfin, les travaux effectués au cours de cette thèse ont conduit au dépôt d'un brevet protégeant la séquence des variants sélectionnés, leurs applications pour la décontamination' des OPs et leurs applications en tant qu'agent d'antivirulence bactérienne. Le projet de développement d'un bio-épurateur d'OPs a été lauréat du concours d'émergence à la création d'entreprise (OSEO). Actuellement, celui-ci est incubé par l'incubateur Impulse à Marseille et une start-up visant à valoriser les produits développés vient tout juste d'être créée.

V. Bilan :

A. Résumé des travaux

Les travaux présentés dans cette thèse de doctorat s'inscrivent dans un projet de développement d'un bio-épurateur d'insecticides organophosphorés qui fut soutenu par un financement REI (Recherche et Innovation) de la DGA (Délégation Générale pour l'Armement) et par le financement de ma thèse *via* une bourse doctorale de la DGA. Au commencement de ma thèse en octobre 2009, la structure de *Sso*Pox avait été résolue (163). *Sso*Pox est une enzyme hyperthermostable appartenant à la famille des PLLs et présentant une activité lactonase naturelle et de promiscuité phosphotriestérase. De l'analyse structurale, se dessina la stratégie que nous allions employer dans l'objectif d'ingénieuriser l'enzyme et d'augmenter son activité envers les insecticides. Mon travail de thèse consista principalement à l'amélioration des connaissances structurales sur les OP hydrolases et comprendre les améliorations obtenues au cours du protocole d'évolution afin d'optimiser la convergence vers un bio-épurateur d'intérêt biotechnologique.

Dans cette optique, l'amélioration des connaissances sur les OPs hydrolases débuta avec la caractérisation enzymatique, biochimique et structurale de la PLL *Sis*Lac (**article II. A.**, (226)). L'étude mit en évidence l'importance du contexte protéique (épistasie) dont les influences sur la thermostabilité et les activités sont souvent sous-estimées (**article II. B.**, (198)). Une nouvelle phosphotriestérase à topologie sandwich αββα fut caractérisée (**article II**. **C.**, (227)). Sa similarité avec l'enzyme MPH et les lactonases de type AiiA témoignant d'un phénomène évolutif parallèle à l'évolution des PTEs à partir de PLLs au sein d'une seconde famille structurale (**article II. D**.). Ainsi, la nature aurait développé des solutions équivalentes guidées par la chimie afin de produire des protéines optimisées à partir d'enzymes promiscuitaires. La promiscuité d'activité phosphotriestérase – lactonase est due à la ressemblance géométrique de l'état de transition d'hydrolyse des lactones et la configuration du groupement phosphoré des OPs. Dans l'objectif final d'améliorer l'activité de promiscuité phosphotriestérase de *Sso*Pox, une caractérisation structurale et enzymatique de l'enzyme fut réalisée (**article II. E**., (197)). Cette étude apporta des informations essentielles sur notre enzyme telles que l'existence d'une préférence oxono-OPs au détriment des thiono-OPs qui sont moins bien hydrolysés et pour les OPs possédant un groupement partant peu encombrant. Le mode d'accommodation d'un OP inhibiteur au sein du site actif permit également d'identifier des résidus clés à muter afin d'optimiser l'enzyme envers les OPs (*e.g* Trp 263).

De la comparaison structurale avec la *Bd*PTE émergea l'idée de transférer son site actif optimisé dans l'architecture hyperthermostable de *Sso*Pox. Pour ce faire, une base de données comportant 14

Structures déposées			
Code PDB		Protéine	Résolution
3UF9		Crystal structure of SsoPox in complex with the phosphotriester fensulfothion	2.68 Å
4G2D		Crystal structure of the hyperthermophilic Sulfolobus islandicus PLL SisLac	2.7 Å
4KEZ		Crystal structure of SsoPox W263F	1.85 Å
4KEV		Crystal structure of SsoPox W263L	2.65 Å
4KEU		Crystal structure of SsoPox W263M	2.2 Å
4KER		Crystal structure of SsoPox W263V	2.6 Å
4KES		Crystal structure of SsoPox W263T	2.1 Å
4KET		Crystal structure of SsoPox W263I	2.0 Å
4KF1		Crystal structure of SsoPox W263I in complex with C10 HTL	2.0 Å
4LE6		Crystal structure of the phosphotriesterase OPHC2 from Pseudomonas pseudoalcaligenes	2.1 Å
Structures non déposées			
		Protéine	
Projet phosphotriestérases	Mutants évolution dirigée cycle 1 – Mutant D256N	D256N apo	2.0 Å
		D256N en complexe avec 3-oxo C10 AHL	2.1 Å
		D256N en complexe avec γ-undecanoic lactone	2.2 Å
		D256N en complexe avec δ-undecanoic lactone	2.0 Å
		D256N en complexe avec le produit d'hydrolyse de 3-oxo C10 AHL	2.1 Å
		D256N en complexe avec le produit d'hydrolyse de γ-undecanoic lactone	2.25 Å
		D256N en complexe avec le produit d'hydrolyse de δ-undecanoic lactone	1.9 Å
	Mutants évolution dirigée cycle 1	Alpha Spike C6	2.55 Å
		Alpha Spike D6	2.95 Å
		Alpha Spike B5	2.5 Å
		Alpha Spike A6 "fermé"	2.15 Å
		Alpha Spike A6 "ouvert"	1.4 Å
		VmoLac	2.4 Å
Projet DING	PfluDING	PfluDING S32G	1.4 Å
		PfluDING T148N	1.5 Å
		PfluDING sauvage en complexe avec phosphosérine	1.55 Å
		Variant soluble HPBP	1.3 Å

Figure V.1 : *Bilan des structures résolues au cours de la thèse*

mutations fut établie permettant de redessiner *in silico* le site actif de l'enzyme. Afin de tester la pertinence des positions identifiées, nous avons réalisé une mutagénèse à saturation de site sur la position du Trp 263 (**article II.F**.). L'unique mutation de ce résidu permit d'augmenter l'activité de promiscuité phosphotriestérase de l'enzyme à température ambiante. Nous avons alors ensuite développé un protocole d'évolution dirigée et de criblage permettant d'incorporer de manière indépendante chaque mutation de la base de données. En un unique cycle d'évolution, les améliorations obtenues furent de plus de 2000 fois envers certains OPs, atteignant jusqu'à 5 x 10^5 $M^{-1}.s^{-1}$. Les variants obtenus ne présentent plus les préférences de substrat observées chez l'enzyme sauvage suggérant la déspécialisation de l'enzyme. Ceux-ci conservent toujours les propriétés de thermostabilité gage de la maniabilité biotechnologique de notre enzyme. Ils offrent des perspectives de valorisation pour la décontamination d'urgence en cas d'utilisation terroriste d'insecticides OPs.

L'analyse structurale des variants obtenus au premier cycle d'évolution mit en évidence que l'amélioration de l'activité de promiscuité est principalement due à la flexibilisation locale de l'enzyme. Pour l'un des variants (asA6), cette flexibilisation résulta en l'obtention de la structure dans deux conformations différentes (boucle ouverte et fermée). Ainsi, cette flexibilisation entraine l'élargissement du paysage conformationnel de l'enzyme, lui permettant ainsi d'adopter des conformations plus aptes à accommoder les substrats de promiscuité. *Sso*Pox étant une enzyme hyperthermostable, elle peut accumuler un nombre important de conformation sans compromettre la stabilité globale, en faisant ainsi une enzyme au fort potentiel évolutif. C'est également une enzyme dont la topologie est modulaire (*i.e* séparation du corps protéique rigide et des boucles flexibles constituants le site actif), capable d'acquérir de nouvelles fonctions par mutation dans les boucles du site actif. A l'avenir, le projet s'orientera afin de développer l'activité de l'enzyme envers les agents neurotoxiques de guerre réels.

*Sso*Pox appartient à la famille des PLLs, caractérisées par leur activité naturelle lactonase. Au cours de nos protocoles d'évolution, l'activité de l'enzyme fut améliorée envers les 3-oxo-C12 AHLs (d'un facteur 60), atteignant une efficacité catalytique d'environ 10^5 $M^{-1}.s^{-1}$. Ces molécules sont principalement utilisées dans la communication bactérienne par *QS*. Notamment, nous avons montré que *Sso*Pox permet d'inhiber le *QS* chez *P. aeruginosa* (par mécanisme de *QQ*), réduisant ainsi *in vitro* et *in vivo* la virulence de la bactérie. Les résultats préliminaires montrent que l'enzyme permet de réduire la létalité dans un modèle d'infection respiratoire chez le rat (collaboration avec le Dr Silby, Etats-Unis et avec le Dr. Bregeon, URMITE, France). Ces résultats offrent des perspectives de valorisation dans la lutte contre les infections nosocomiales dues à *P. aeruginosa*, offrant une alternative élégante à l'utilisation d'antibiotiques. Il sera désormais nécessaire de définir le spectre d'action de l'enzyme en évaluant la capacité de l'enzyme à inhiber la virulence chez d'autres organismes.

Au cours de la thèse, trente structures furent résolues (dix structures déposées, vingt en cours d'affinement) et plus de 200 paramètres catalytiques permirent de décrire nos enzymes. Ces travaux de thèse débouchèrent sur le dépôt de deux brevets protégeant les applications liés à l'activité

phosphotriestérase (*i.e* bio-décontamination des OPs) et lactonase (*i.e* inhibition de la virulence bactérienne). Une start-up (Gene & GreenTech) vient d'être crée afin de valoriser vers le tissu économique le produit développé au cours du projet.

B. Bilan personnel

J'ai rejoint l'équipe du Pr. Eric Chabrière en 2008 lorsque j'ai effectué mon stage de Master 1 et Master 2 Recherche au sein de l'équipe de « Biocristallographie, Enzymologie Structurale et Biotechnologie ». Ces stages furent un avant-goût à la recherche qui me décida à effectuer un doctorat en biologie structurale au sein de l'équipe. Je compris rapidement que les compétences acquises au cours de mon cursus universitaire ne constituaient que les bases permettant d'acquérir les savoir-faire techniques requis par les projets qui m'ont été confiés. Très vite, différents projets me furent confiés faisant appel à d'autres techniques et savoir-faire que la cristallographie des protéines et la biologie structurale. Cette approche pluridisciplinaire des projets me permit d'acquérir des connaissances dans des domaines différents de la biologie tels que la chimie en passant par la physique. La biologie structurale servit de fil conducteur aux différents projets qui s'inscrivent dans des contextes biologiques plus larges. Elle fut étroitement liée à la stratégie employée afin de répondre aux différentes questions biologiques.

Certaines qualités m'ont semblé indispensables au cours de la thèse telles que l'adaptabilité, l'ingéniosité et la patience. En effet, la biologie n'est pas une science linéaire où les résultats sont toujours prévisibles. Les plus belles découvertes sont souvent le fruit du hasard. Sachant cet état de fait, mon directeur de thèse permet beaucoup de liberté à partir du moment où les principaux objectifs sont atteints. Ainsi, de nombreux résultats obtenus furent le fruit de la curiosité. La thèse fut également un moment où j'ai dû apprendre à transmettre le savoir, en formant des étudiants (Licence et Master 1 & 2) et en réalisant des TPs (module de cristallographie du Master 2 BBSG). Au cours de ma thèse j'ai également pu prendre part à un module de cristallographie de l'école doctorale (EDSVS) organisée au laboratoire AFMB en réalisant les TPs de construction et modélisation sous *Coot*.

Sachant aussi que les présentations orales et posters font partie intégrante des capacités nécessaires pour les métiers de la recherche, mon directeur de thèse me permit également de participer à plusieurs colloques nationaux et internationaux dans lesquels j'ai eu la possibilité de présenter mes travaux. Au-delà du travail personnel à fournir pour réussir en thèse, j'ai également eu beaucoup de plaisir à travailler avec les autres membres du groupe (Julien Hiblot, Daniel Gonzalez, Ahmed Djeghader, Jérémy Robin, Magali Richez et Charlotte Champion). L'esprit d'équipe et l'entraide m'ont semblé essentiels à la réussite. Forts des compétences complémentaires de chacun, les différents projets du groupe ne s'en sont retrouvés que mieux abordés. Ce travail de groupe m'a permis de publier un

nombre d'articles plus important mais ce fut également un enrichissement personnel en me permettant de tisser des liens d'amitié.

Dès le début de ma thèse je fus sensibilisé à l'importance de maitriser tous les aspects des compétences nécessaires à tout chercheur, allant de la rédaction des articles scientifiques, des demandes de financement et depuis ma prise de fonction la rédaction d'appels d'offres. Un autre aspect important auquel je fus aussi formé fut la gestion des collaborations et les relations avec les collaborateurs qui permettent souvent de surmonter plus rapidement les difficultés techniques.

Depuis maintenant un an, je gère en parallèle de ma thèse la plateforme d'étude biophysique des protéines au laboratoire où je mets en place les outils et technologies nécessaires pour développer la cristallographie au sein de l'unité.

Ainsi, je considère ces quatre années de thèse comme une expérience unique m'ayant permis de développer mes compétences scientifiques, mais m'ayant également montré l'importance de l'organisation et de la stratégie, d'une bonne gestion, de la rédaction et de la communication.

VI. Fiche résumé de la thèse :

Financement de la thèse : allocation de recherche de la Délégation Générale pour l'Armement

Durée : Octobre 2009 à Octobre 2013 soit 4 ans

Collaborations principales :

Collaborations nationales :

- Université de Strasbourg « Institut de Parasitologie et de Pathologie Tropicale », Pr. Olivier Rohr et Dr. Christian Schwartz.
- Unité d'enzymologie, Département de Toxicologie, Centre de recherche du service de santé des armées, Pharmacien Général Patrick Masson

Collaborations internationales :

- The University of Auckland, Faculty of Science, Dr. Ken Scott
- Weizmann Institute of Science, Dr. Dan S. Tawfik & Dr. Mikael Elias

Articles publiés : 14 articles dans des revues à comités de lectures, 9 en premier auteur

Projet « Phosphotriestérases » :

Crystallization and preliminary x-ray diffraction analysis of the hyperthermophilic *Sulfolobus islandicus* Lactonase (2011)
Gotthard G, Hiblot J, Elias M, Chabriere E
Acta Crystallogr Sect F Struct Biol Cryst Commun. 2011 Mar 1;67(Pt 3):354-7

Structural and enzymatic characterization of the lactonase *Sis*Lac from *Sulfolobus islandicus*
Gotthard G*, Hiblot J*, Chabriere E, Elias M.
PLoS One. 2012;7(10):e47028. doi: 10.1371/journal.pone.0047028. Epub 2012 Oct 10

Characterisation of the organophosphate hydrolase catalytic activity of *Sso*Pox
Hiblot J, Gotthard G, Chabriere E, Elias M.
Sci Rep. 2012;2:779. doi: 10.1038/srep00779. Epub 2012 Nov 8.

Crystallization and preliminary X-ray diffraction analysis of the organophosphorus hydrolase OPHC2 from *Pseudomonas pseudoalcaligenes*
G. Gotthard*, J. Hiblot*, D. Gonzalez, E. Chabrière, M. Elias
Acta Cryst. (2013). F69, 73-76

Differential active site loop conformations mediate promiscuous activities in the lactonase *Sso*Pox (2013)
Gotthard G*, Hiblot J*, Elias M, Chabriere E.

PLoS One. 2013;8(9):e75272. doi: 10.1371/journal.pone.0075272
Epub 2013 Sep 23

Structural and enzymatic characterization of the phosphotriesterase OPHC2 from *Pseudomonas pseudoalcaligenes* (2013)
Gotthard G*, Hiblot J*, Gonzalez D, Robin J, Elias M, Chabriere E.
PLoS One. 2013;8(11):e77995. doi: 10.1371/journal.pone.0077995.
Epub 2013 Nov 4

Crystallization and preliminary X-ray diffraction analysis of the lactonase *Vmo*Lac from *Vulcanisaeta moutnovskia*
Gotthard G*, Hiblot J*, Champion C, Chabriere E, Elias M.
Acta Cryst (2013). F69, 1235-8.

Projet « Protéines DING » :

Crystallization and preliminary X-ray diffraction analysis of a DING protein from Pseudomonas aeruginosa PA14. (2013)
Gotthard G*, Djeghader A*, Suh A, Gonzalez D, Scott K, Elias M, Chabriere E.
Acta Cryst Sect F Apr 1;69(Pt 4):425-9.

Structural insights and ab initio sequencing within the DING proteins family (2011)
Elias M, Liebschner D, Gotthard G, Chabriere E
J. Synchrotron Rad 18(1) 45-9

Eukaryotic DING proteins are endogenous: an immunohistological study in mouse tissues (2010)
Collombet JM, Elias M, Gotthard G , Four E, Renault F, Joffre A, Baubichon D, Rochu D, Chabriere E
PLoS One. 2010 Feb 8;5(2):e9099

Human-Phosphate-Binding-Protein inhibits HIV-1 gene transcription and replication (2011)
Thomas Cherrier, Mikael Elias, Alicia Jeudy, Guillaume Gotthard, Valentin Le Douce, Houda Hallay, Patrick Masson, Andrea Janossy, Ermanno Candolfi, Olivier Rohr, Eric Chabrière and Christian Schwartz
Virology Journal 2011, 8:352

The Level of DING proteins is increased in HIV-infected patients: *in vitro* and *in vivo* studies (2012)
Ahmed Djeghader, Gerard Aragonès, Nune Darbinian, Mikael Elias, Daniel Gonzalez, Anabel García-Heredia, Raúl Beltrán-Debón, Rafal Kaminski, Guillaume Gotthard; Julien Hiblot, Anna Rull, Olivier Rohr, Christian Schwartz, Carlos Alonso-Villaverde, Jorge Joven, Jordi Camps and Eric Chabriere
PlosOne. 2012;7(3):e33062. doi: 10.1371/journal.pone.0033062.

Epub 2012 Mar 9.

Crystallization and preliminary X-ray diffraction analysis of a high affinity phosphate-binding protein endowed with phosphatase activity from *Pseudomonas aeruginosa* PAO1
Gotthard G*, Djeghader A*, Suh A, Gonzalez D, Scott K, Chabriere E, Elias M.
Acta Cryst F (2013) Oct;69(Pt 10):1143-6.

Autres publications :

Long-range DHPS mutations unexpectedly increase *Mycobacterium chimaera* susceptibility to sulfonamides (2013)
Gotthard G, Muhamed Ameen S, Drancourt M, Chabriere E
sous presse dans JGAR

VII. Annexes :

Notre équipe s'intéresse à deux problématiques principales auxquelles j'ai participé activement tout au long de mon master et de ma thèse. Cette partie d'annexe comprend ainsi, une partie expliquant le protocole d'évolution rationnalisée qui fut utilisé au cours des travaux (**partie VII. A.**), un article supplémentaire lié à l'étude des PLLs et de leurs applications (**article présenté en VII. B.**), un article de revue concernant l'autre sujet d'étude que sont les protéines DING et 5 articles de recherche sur cette thématique (**articles VII. C. à VII. H.**).

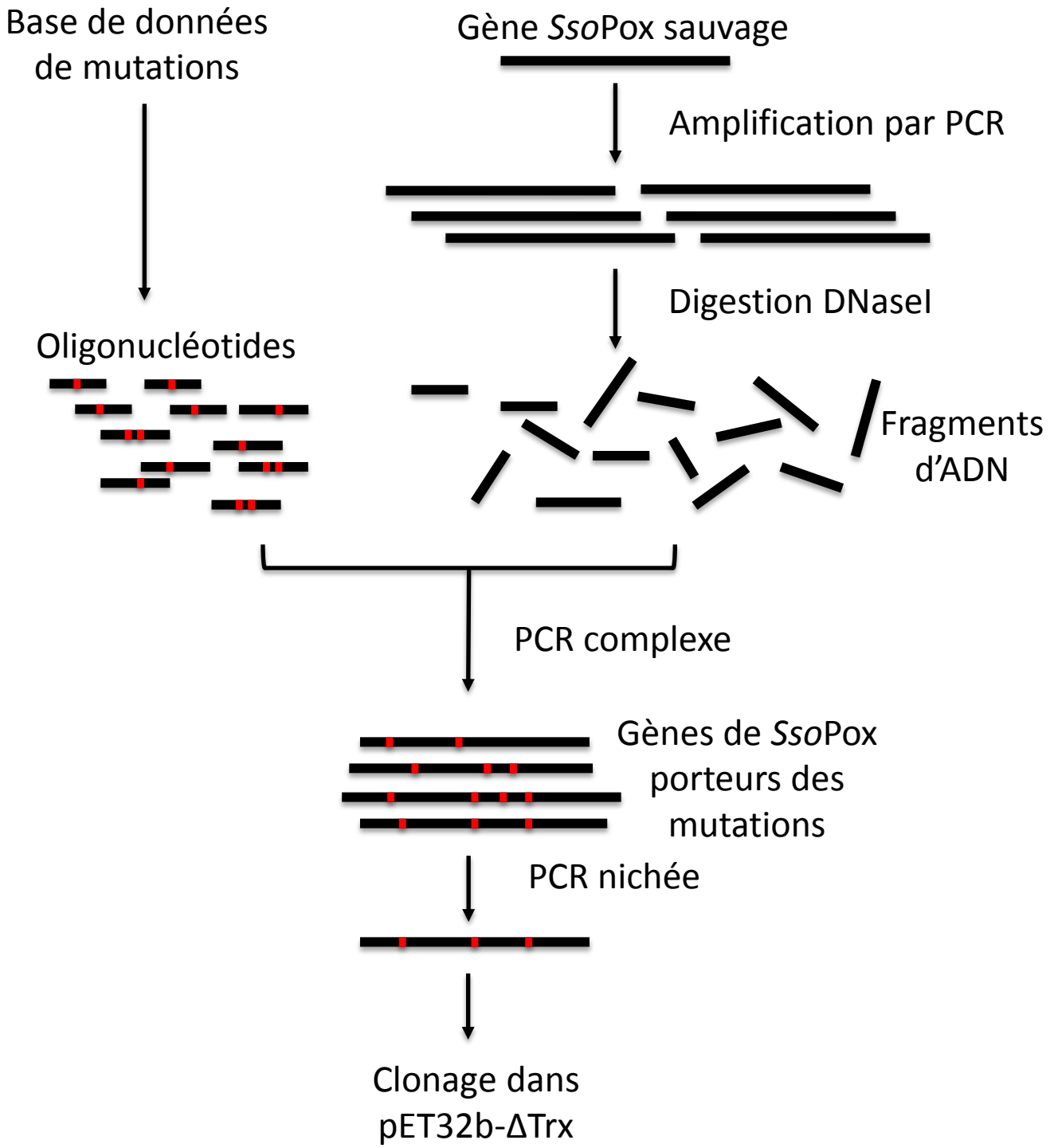

Figure VII.1 : *Représentation schématique du protocole utilisé pour l'évolution rationalisée de* Sso*Pox*

Brièvement, le gène *ssopox* est amplifié par PCR classique puis digéré grâce à la DNaseI de manière à générer ~ 100 ng de fragment d'ADN (~70 paires de bases en moyenne). Ceux-ci sont mélangés à 2 pmol du mélange d'amorces de la base de données puis assemblés grâce à un protocole de PCR plus complexe impliquant de nombreuses étapes à des températures d'hybridation décroissantes (65 – 45 °C). *In fine*, l'objectif est d'obtenir des amplifiats de taille équivalente à *ssopox* en utilisant chaque fragment et chaque oligonucléotide muté comme amorce servant à l'amplification. Enfin, après une PCR nichée, la banque de mutants est reclonée dans un plasmide d'expression.

A. Protocole d'évolution rationnelle de *Sso*Pox

Afin de générer la banque de gènes variants de *Sso*Pox portant des combinaisons aléatoires de mutations, un protocole de pointe en biologie moléculaire fut utilisé. Ce protocole, dénommé ISOR, pour « Incorporating Synthetic Oligonucleotide via gene Reassembly » (217) (**Figure VII.1**), consiste en différentes étapes de biologie moléculaire : (i) amplifier par réaction de polymérisation en chaine (PCR) le gène de *Sso*Pox à partir d'une matrice plasmidique (type pET-22b) (197, 198) en utilisant des amorces externes au gène (amorces T7-prom et pET-RP), (ii) digérer les amplicons à la DNaseI de manière à générer des fragments de gènes d'environ 70 paires de bases, (iii) des oligonucléotides codant pour chacune des 14 mutations (**Figure VII.2**) ont au préalable été synthétisées et sont mélangées avec les fragments d'ADN amplifiés/digérés de manière à ce que chaque position soit représentée de manière équiprobable, (iv) une PCR complexe est ensuite réalisée de manière à reconstituer des gènes de taille équivalentes à ceux de *Sso*Pox en utilisant chaque fragment d'ADN comme amorce servant à l'amplification, (v) enfin, une PCR « nichée » est ensuite effectuée afin de cloner la librairie de gènes dans le plasmide pET32b-ΔTrx (87).

A la fin de ce protocole, la librairie d'ADN obtenue comporte des combinaisons aléatoires des mutations de la base de données. La librairie d'ADN est ensuite transformée par électroporation dans des *E. coli*, mises en cultures en milieu gélosé sélectif puis, les plasmides sont ensuite extraits afin d'obtenir une banque de plasmides codant pour la librairie de gènes variants de *Sso*Pox. Cette banque de plasmides fut ensuite transformée en cellules de production (*E. coli* BL21(DE3)-pGro7/EL, Takara) afin d'obtenir des colonies isolées sur milieu gélosé. Puis, des micro-cultures des colonies (184 colonies choisies au hasard) sont effectuées en milieu auto-inducteur (228)(500 µL en plaques 96 puits). La production des variants protéiques est effectuée selon un protocole analogue à celui utilisé précédemment (197, 198) (5 heures de culture à 37 °C puis transition à 25 °C avec ajout de CoCl2 (0,2 mM) et d'arabinose (0,2 % poids/volume)). Les micro-cultures sont ensuite centrifugées puis lysées après culture sur la nuit. Le lysat est resuspendu dans un tampon de lyse puis partiellement purifié par chauffage (15 min, 70 °C) avant d'être utilisé pour l'étape de criblage d'activité envers l'ethyl-paraoxon (100 µM) (197, 198). Une deuxième étape de criblage est effectuée en utilisant des cultures plus importantes (3 mL) en utilisant cette fois-ci un tampon de lyse ne contenant pas de cobalt et envers un autre substrat, le méthyl-paraoxon. L'absence de cobalt dans le tampon de lyse est destinée à sélectionner des variants conservant l'affinité du site actif pour les métaux. Enfin, afin de valider les mutants sélectionnés, ceux-ci sont produits et purifiés en gros volume puis caractérisés enzymatiquement envers les OPs (197, 198).

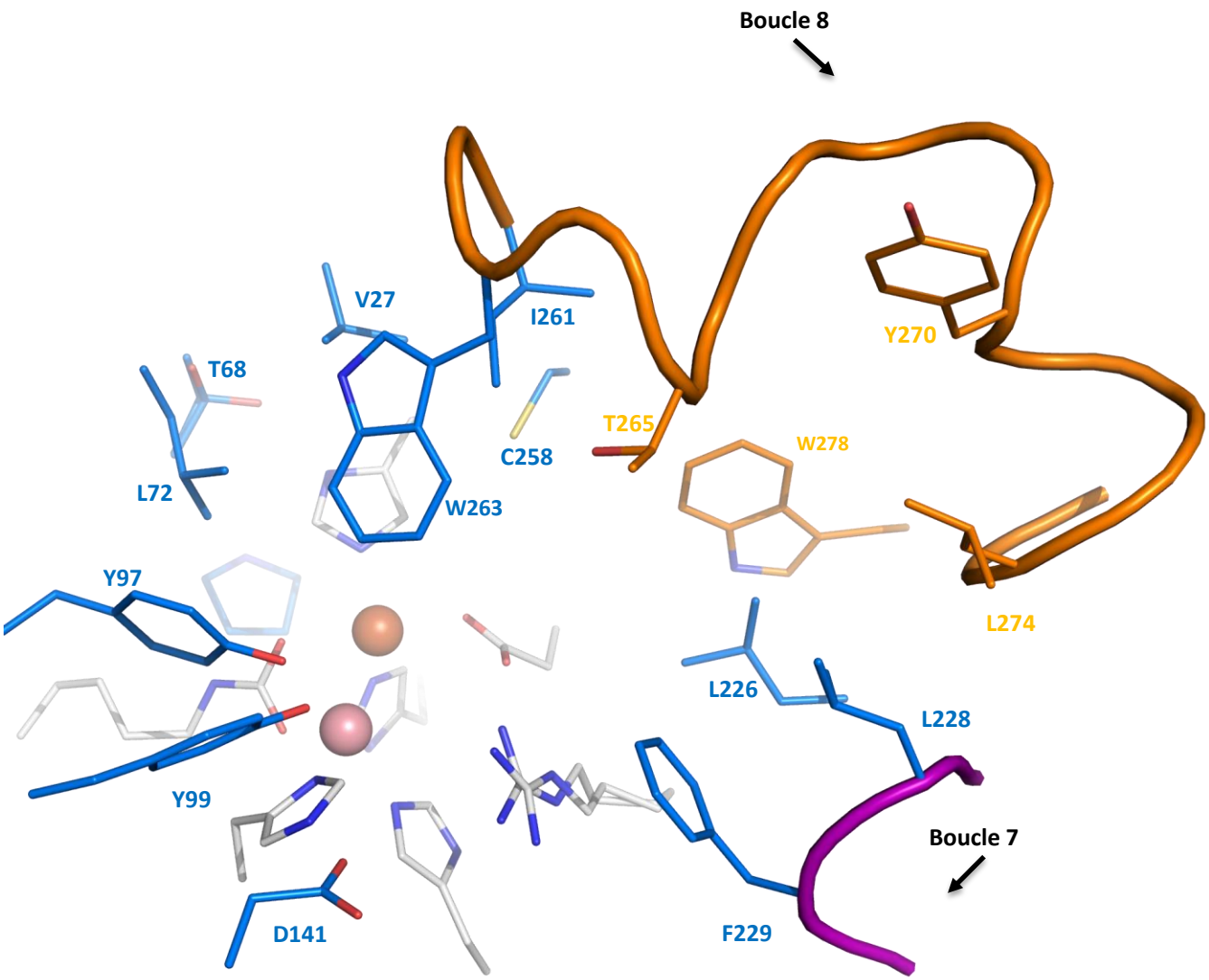

Figure VII.2 : *Positions du site actif de* Sso*Pox comprises dans la base de données*

Les positions ciblées par la base de données de mutations sont représentées en bleu. Bien que celles-ci furent toutes incluses dans le protocole de mutations, seules certaines positions furent sélectionnées au premier cycle d'évolution rationalisée.

La méthodologie d'évolution utilisée permet de générer des variants possédant des combinaisons aléatoires des mutations contenues dans la base de données. Le criblage d'activité permet de sélectionner des variants présentant une efficacité catalytique plus élevée envers le substrat OP voulu.

B. Cristallisation et collectes de données de *Vmo*Lac

Crystallization and preliminary X-ray diffraction analysis of the lactonase *Vmo*Lac from Vulcanisaeta moutnovskia

Guillaume GOTTHARD, Julien HIBLOT*, Charlotte CHAMPION, Eric CHABRIERE and Mikael ELIAS*

* Contribution égale

Article soumis dans le journal « *Acta Crystallographica* section F »

Dans les travaux décrits, j'ai réalisé :

- partie expérimentale : identification dans les bases de données, cristallisation de l'enzyme (conseils), collecte des données, traitement des données, résolution de la structure

Résumé : Les bases de données génomiques comportent d'autres enzymes présentant un intérêt biotechnologique potentiel pour des applications en décontamination des OPs et en tant qu'inhibiteur de virulence bactérienne. Ce travail concerne la mise au point de conditions expérimentales permettant l'expression et la purification de *Vmo*Lac (environs 50 % d'identité de séquence avec *Sso*Pox), enzyme issue de l'archaea extrêmophile *Vulcanisaeta moutnovskia*. Il décrit en particulier les travaux de cristallisation de l'enzyme qui ont nécessité l'identification de nouvelles conditions de cristallisation. Il est également rapporté les conditions de diffraction (cryoprotectant) et la qualité du jeu de données obtenu.

Bien que l'enzyme soit toujours en cours de caractérisation, celle-ci présente des avantages biotechnologiques majeurs (T_m évalué à plus de 120 °C) et une architecture similaire à celle de *Sso*Pox pouvant faire l'objet d'une amélioration rationalisée (brevet en cours de dépôt).

Acta Crystallographica Section F
Structural Biology and Crystallization Communications
ISSN 1744-3091

Crystallization and preliminary X-ray diffraction analysis of the lactonase *Vmo*Lac from *Vulcanisaeta moutnovskia*

Julien Hiblot, Guillaume Gotthard, Charlotte Champion, Eric Chabriere and Mikael Elias

Acta Cryst. (2013). F**69**, 1235–1238

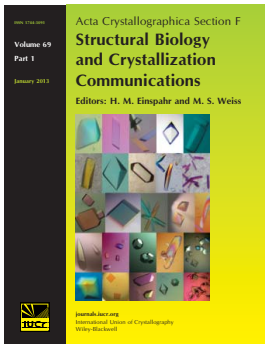

Acta Crystallographica Section F
Structural Biology and Crystallization Communications
ISSN 1744-3091

Crystallization and preliminary X-ray diffraction analysis of the lactonase *Vmo*Lac from *Vulcanisaeta moutnovskia*

Julien Hiblot,[a]‡ Guillaume Gotthard,[a]‡ Charlotte Champion,[a] Eric Chabriere[a]* and Mikael Elias[b]*

[a]Unité de Recherche sur les Maladies Infectieuses et Tropicales Emergents (URMITE), UMR CNRS–IRD–INSERM, IHU Méditerranée Infection, Aix–Marseille Université, 7 Boulevard Jean Moulin, 13385 Marseille CEDEX 05, France, and [b]Biological Chemistry, Weizmann Institute of Science, Rehovot, Israel

‡ These authors made equal contributions.

Correspondence e-mail: eric.chabriere@univmed.fr, mikael.elias@weizmann.ac.il

Received 29 July 2013
Accepted 5 September 2013

Phosphotriesterase-like lactonases (PLLs) are native lactonases that are capable of hydrolyzing lactones such as aliphatic lactones or acyl-homoserine lactones, which are involved in bacterial quorum sensing. Previously characterized PLLs are moreover endowed with a promiscuous phosphotriesterase activity and are therefore able to detoxify organophosphate insecticides. A novel PLL representative, dubbed *Vmo*Lac, has been identified from the hyperthermophilic crenarchaeon *Vulcanisaeta moutnovskia*. Because of its intrinsic high thermal stability, *Vmo*Lac may constitute an appealing candidate for engineering studies with the aim of producing an efficient biodecontaminant for organophosphorus compounds and a bacterial antivirulence agent. In combination with biochemical studies, structural information will allow the identification of the residues involved in substrate specificity and an understanding of the enzymatic catalytic mechanisms. Here, the expression, purification, crystallization and X-ray data collection at 2.4 Å resolution of *Vmo*Lac are reported.

1. Introduction

Organophosphates (OPs) are well known neurotoxic compounds that irreversibly inhibit acetylcholinesterase, a key enzyme of the central nervous system (Masson *et al.*, 2009). These compounds, which are massively used as pesticides, are responsible for soil and water pollution, for which no satisfactory means of remediation are available (Singh, 2009). Indeed, existing methods for removing them are cost-prohibitive and cause environmental concerns (LeJeune *et al.*, 1998). Moreover, before World War 2 these compounds were engineered as chemical warfare agents and were used in the Iran–Iraq war and in the terrorist attack on the Tokyo subway (Gupta, 2009). The use of enzymes that are capable of hydrolyzing these compounds represents an appealing alternative to chemical methods (Singh, 2009). Several organophosphate hydrolases (OPHs) belonging to different enzyme superfamilies have been identified and studied [*e.g.* organophosphate acid anhydrolase (OPAA; Vyas *et al.*, 2010), OPHC2 (Gotthard *et al.*, 2013) and paraoxonases (PONs; Ben-David *et al.*, 2012)]. The most studied OPHs comprise the bacterial phosphotriesterases (PTEs) isolated from *Brevundimonas diminuta* (*Bd*PTE; Benning *et al.*, 1994) and *Agrobacterium radiobacter* (OpdA; Jackson *et al.*, 2006). These enzymes, which exhibit near-diffusion-limit kinetic rates against the insecticide paraoxon (*i.e.* $k_{cat}/K_M \simeq 10^8\ M^{-1}\ s^{-1}$; Omburo *et al.*, 1992), are believed to have emerged from the first uses of OPs as insecticides in the 1950s.

Recently, a protein family sharing ∼30% sequence identity with PTEs was identified by virtue of their ability to hydrolyze insecticides and were initially dubbed paraoxonases (Merone *et al.*, 2005). A detailed biochemical and phylogenetic analysis later revealed that these proteins, named phosphotriesterase-like lactonases (PLLs), are in fact native lactonases endowed with promiscuous phosphotriesterase activity (Afriat *et al.*, 2006; Elias & Tawfik, 2012). PLLs are likely to be the progenitors of PTEs (Afriat-Jurnou *et al.*, 2012). PLLs hydrolyze various lactones, including aliphatic lactones and acyl-homoserine lactones (AHLs), that are involved in bacterial quorum sensing (Hiblot *et al.*, 2012*a*; Hawwa, Larsen *et al.*, 2009). The ability of lactonases such as PLLs to hydrolyze AHLs enables these enzymes

to interfere with bacterial communication (Dong *et al.*, 2001) and they therefore offer interesting potentialities to develop new approaches in order to fight against several pathogens (Amara *et al.*, 2011).

PTEs and PLLs, which belong to the amidohydrolase superfamily (Seibert & Raushel, 2005), share the same $(\alpha/\beta)_8$ topology in which a bimetallic centre is coordinated by four histidines, an aspartic acid and a carboxylated lysine (Elias *et al.*, 2008; Del Vecchio *et al.*, 2009). The bimetallic centre activates a water molecule into a hydroxide ion, which serves as a nucleophile for the hydrolysis of OPs or AHLs. The catalytic centre is surrounded by two loops involved in the substrate specificity: loops 7 and 8 (Elias *et al.*, 2008; Jackson *et al.*, 2009). PTEs and PLLs differ mainly in the relative size and conformations of these loops, which account for the different substrate specificity of these enzymes (Afriat-Jurnou *et al.*, 2012). PLLs hydrolyze organophosphate compounds with poor to moderate efficiency (Hiblot *et al.*, 2012*b*; Hawwa, Larsen *et al.*, 2009; Zhang *et al.*, 2012) compared with PTEs (Omburo *et al.*, 1992; Jackson *et al.*, 2006; Donarski *et al.*, 1989). Some PLL representatives, however, offer interesting biotechnological potentialities for engineering an efficient organophosphate biodecontaminant because of their high thermal stability (Hiblot *et al.*, 2012*a*,*b*; Hawwa, Larsen *et al.*, 2009; Hawwa, Aikens *et al.*, 2009), as illustrated by several engineering studies on these enzymes (Merone *et al.*, 2010; Hawwa, Larsen *et al.*, 2009; Xue *et al.*, 2013; Chow *et al.*, 2010).

*Vmo*Lac (YP_004245953) is an enzyme identified from the recently sequenced crenarchaeon *Vulcanisaeta moutnovskia* strain 768-28 (Gumerov *et al.*, 2011). This organism was isolated from solfataric fields close to the Moutnovsky volcano in Kamchatka, Russia. Its growth temperature ranges between 333 and 371 K (Gumerov *et al.*, 2011). *Vmo*Lac shares ∼50% sequence identity with other PLLs. Here, we report the protein production, purification, crystallization and preliminary X-ray diffraction of *Vmo*Lac.

2. Cloning, expression and purification of *Vmo*Lac

The gene encoding *Vmo*Lac (YP_004245953) was optimized for *Escherichia coli* expression by the GeneArt service provider (Life Technologies, France). The optimized gene included N-terminal tags [a *Strep*-tag (M**SAWSHPQFEK**) for affinity chromatography purification and a TEV cleavage site (**ENLYFQ/G**) for removal of the tag; Gotthard *et al.*, 2011] and was synthesized by GeneArt (Life Technologies, France). This construct leaves an N-terminal Gly residue after cleavage of the tag by TEV protease. The complete gene was subsequently cloned by the same provider into a custom version of pET-22b(+) (Novagen) using *Nde*I and *Xho*I as cloning sites. Recombinant *Vmo*Lac protein was overexpressed using a protocol that was previously used for another PLL (Gotthard *et al.*, 2013; Hiblot *et al.*, 2012*a*). Briefly, recombinant *Vmo*Lac protein was overproduced in *E. coli* BL21 (DE3)-pGro7/GroEL strain (TaKaRa). Protein expression was performed in 4 l ZYP medium (100 µg ml^{-1} ampicillin, 34 µg ml^{-1} chloramphenicol) inoculated with a 50 ml overnight pre-culture. The culture was grown at 310 K until the $OD_{600\ nm}$ reached 0.6. Induction of the protein was conducted by consumption of the lactose in the ZYP medium, a temperature transition to 298 K over 20 h and the addition of 0.2 m*M* $CoCl_2$.

The cells were harvested by centrifugation (4500*g*, 277 K, 15 min). The pellets were resuspended in lysis buffer [50 m*M* HEPES pH 8, 150 m*M* NaCl, 0.2 m*M* $CoCl_2$, 0.25 mg ml^{-1} lysozyme, 10 µg ml^{-1} DNAse I, 0.1 m*M* phenylmethylsulfonyl fluoride (PMSF)] and stored at 193 K for 2 h. The suspended frozen cells were thawed at 310 K for 15 min and disrupted by three sonication steps of 30 s (Branson Sonifier 450; 80% intensity and micro tip limit at 8). Cell debris was removed by centrifugation (14 500*g*, 277 K, 30 min). The cell lysate was then loaded onto a StrepTrap column (GE Healthcare) at a flow rate of 5 ml min^{-1} and protein elution was performed using elution buffer (50 m*M* HEPES pH 8, 150 m*M* NaCl, 0.2 m*M* $CoCl_2$, 2.5 m*M* desthiobiotin). Because of the low binding capacity of the column, this step was repeated five times and all of the protein was then cleaved by TEV protease (1250 µg, 20 h, 310 K; van den Berg *et al.*, 2006). Spontaneously precipitated TEV protease was harvested by centrifugation (12 000*g*, 277 K, 10 min). The protein was subsequently concentrated using a centrifugation device (Amicon Ultra MWCO 10 kDa; Millipore, Ireland) prior to a size-exclusion chromatography step (Superdex 75 16/60, GE Healthcare) in 50 m*M* HEPES pH 8, 150 m*M* NaCl, 0.2 m*M* $CoCl_2$. Fractions containing pure protein were pooled and concentrated prior to crystallization trials using a centrifugation device (Amicon Ultra MWCO 10 kDa; Millipore, Ireland). The yield of production was about 5 mg per litre of culture.

The purity of the protein was checked with Coomassie-stained 15% SDS–PAGE (Fig. 1), which revealed two main bands (35 and 70 kDa). Both bands were subjected to mass-spectrometric analysis (MS Platform Timone, Marseille, France) and both were identified as the *Vmo*Lac protein. The molecular mass of the *Vmo*Lac monomer being 35 548 Da, the two bands on the gel at 35 and 70 kDa were attributed to monomers and dimers of *Vmo*Lac, respectively. As the *Vmo*Lac dimer originates from an extremely thermophilic organism, its dimer may resist the denaturing conditions of sample preparation for SDS–PAGE experiments (368 K incubation for 10 min, 715 m*M* β-mercaptoethanol).

3. Protein crystallization

*Vmo*Lac was concentrated to 20 mg ml^{-1} for crystallization trials. Crystallization assays were performed using the sitting-drop vapour-diffusion method setup in a 96-well plate and the commercial screen conditions Structure Screen 1 + 2 (Molecular Dimensions). The plate was incubated at 277 K. Crystals appeared after 1 d at 277 K in a

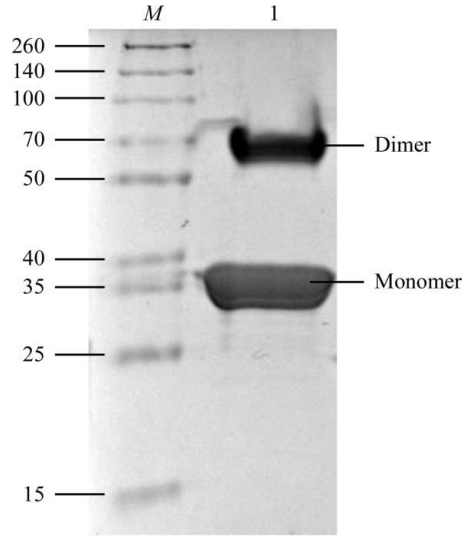

Figure 1
15% SDS–PAGE of *Vmo*Lac protein performed under denaturing conditions and stained with Coomassie Blue. Lane *M* contains molecular-weight markers (Thermo Scientific Spectra Multicolor broad-range protein ladder; labelled in kDa). Lane 1 contains *Vmo*Lac protein.

condition consisting of 400 m*M* ammonium dihydrogen phosphate. Crystals grew in drops containing a 2:1 protein:reservoir ratio (Fig. 2).

4. Data collection

A cryoprotectant solution consisting of the crystallization solution supplemented with 30%(*v*/*v*) glycerol was added to the drop in order to exchange the solution containing the crystal. The crystal was subsequently mounted on a CryoLoop (Hampton Research) and flash-cooled in liquid nitrogen. X-ray diffraction intensities were collected on the ID29 beamline at the ESRF, Grenoble, France using a wavelength of 0.800 Å and a PILATUS 6M detector (DECTRIS, Switzerland) with 50 ms exposures. Diffraction data were collected using the fine-slicing method; individual frames consisted of 0.1° steps over a range of 100° (Fig. 3).

5. Results and conclusions

X-ray diffraction data were integrated and scaled using the *XDS* package (Kabsch, 1993; Table 1). The *Vmo*Lac crystals belonged to the hexagonal space group $P6_4$, with unit-cell parameters $a = b = 174.06$, $c = 61.32$ Å. *Vmo*Lac being a 35 kDa protein, the calculated Matthews coefficient (Matthews, 1968) suggests that between two and three monomers are present per asymmetric unit (3.78 and 2.52 Å^3 Da^{-1}, corresponding to 67.49 and 51.24% solvent content, respectively). An initial molecular replacement was performed using *Phaser* (McCoy *et al.*, 2007) with the structure of *Sso*Pox (52% sequence identity; PDB entry 2vc5; Elias *et al.*, 2008) from which the fragment 265–277 was deleted as a starting model. Two molecules were initially placed in the asymmetric unit (R = 47.25%, R_{free} = 48.1%). The initial solution was then submitted to *ARP*/*wARP* (Morris *et al.*, 2003) for automated model construction. After 50 cycles of *ARP*/*wARP* and 20 cycles of refinement using *REFMAC* (Murshudov *et al.*, 2011), the R and R_{free} factor values were 18.95 and 22.38%, respectively. The electron-density maps revealed that, with the exception of some rotamers and loop conformations, the model is near final. The asymmetric unit contains one homodimer of *Vmo*Lac. The construction, refinement and interpretation of the structure are in progress.

Figure 2
Crystals of *Vmo*Lac (average dimensions of 100 × 50 × 40 µm).

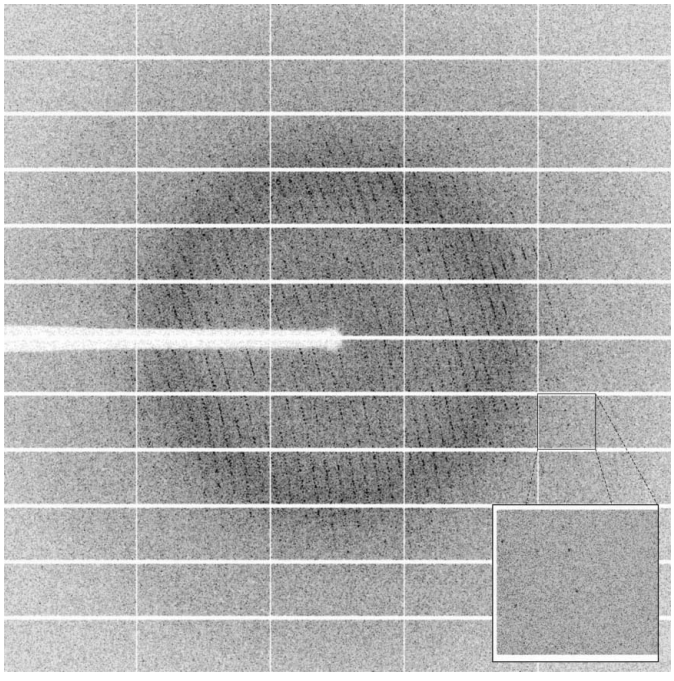

Figure 3
A diffraction pattern from a crystal of *Vmo*Lac. The edge of the frame is at 2.0 Å resolution.

Table 1
Data-collection statistics.

Values in parentheses are for the last bin.

Beamline	ID29, ESRF
Wavelength (Å)	0.800
Detector	PILATUS 6M
Oscillation (°)	0.1
No. of frames	1000
Resolution (Å)	47.6–2.4 (2.5–2.4)
Space group	$P6_4$
Unit-cell parameters (Å)	$a = b = 174.06$, $c = 61.32$
No. of observed reflections	231397 (26406)
No. of unique reflections	41676 (4740)
Completeness (%)	99.6 (99.3)
R_{meas}† (%)	13.4 (63.5)
$CC_{1/2}$‡	99.6 (81.8)
$\langle I/\sigma(I)\rangle$	14.55 (3.22)
Multiplicity	5.55 (5.57)
Mosaicity (°)	0.201

† $R_{meas} = \sum_{hkl}\{N(hkl)/[N(hkl)-1]\}^{1/2}\sum_i |I_i(hkl) - \langle I(hkl)\rangle|/\sum_{hkl}\sum_i I_i(hkl)$. ‡ $CC_{1/2}$ is the intra-data-set correlation coefficient calculated from the percentage of correlation between intensities (I_1 and I_2) from random half data sets (Karplus & Diederichs, 2012): $CC_{1/2} = \mathrm{Corr}(I_1, I_2)$.

This research was supported by a grant to EC from Délégation Générale pour l'Armement (REI #2009 34 0045). GG and JH are supported by Délégation Générale pour l'Armement.

References

Afriat, L., Roodveldt, C., Manco, G. & Tawfik, D. S. (2006). *Biochemistry*, **45**, 13677–13686.
Afriat-Jurnou, L., Jackson, C. J. & Tawfik, D. S. (2012). *Biochemistry*, **51**, 6047–6055.
Amara, N., Krom, B. P., Kaufmann, G. F. & Meijler, M. M. (2011). *Chem. Rev.* **111**, 195–208.
Ben-David, M., Elias, M., Filippi, J. J., Duñach, E., Silman, I., Sussman, J. L. & Tawfik, D. S. (2012). *J. Mol. Biol.* **418**, 181–196.
Benning, M. M., Kuo, J. M., Raushel, F. M. & Holden, H. M. (1994). *Biochemistry*, **33**, 15001–15007.
Berg, S. van den, Löfdahl, P. A., Härd, T. & Berglund, H. (2006). *J. Biotechnol.* **121**, 291–298.
Chow, J. Y., Xue, B., Lee, K. H., Tung, A., Wu, L., Robinson, R. C. & Yew, W. S. (2010). *J. Biol. Chem.* **285**, 40911–40920.
Del Vecchio, P., Elias, M., Merone, L., Graziano, G., Dupuy, J., Mandrich, L., Carullo, P., Fournier, B., Rochu, D., Rossi, M., Masson, P., Chabriere, E. & Manco, G. (2009). *Extremophiles*, **13**, 461–470.
Donarski, W. J., Dumas, D. P., Heitmeyer, D. P., Lewis, V. E. & Raushel, F. M. (1989). *Biochemistry*, **28**, 4650–4655.

Dong, Y.-H., Wang, L.-H., Xu, J.-L., Zhang, H.-B., Zhang, X.-F. & Zhang, L.-H. (2001). *Nature (London)*, **411**, 813–817.
Elias, M., Dupuy, J., Merone, L., Mandrich, L., Porzio, E., Moniot, S., Rochu, D., Lecomte, C., Rossi, M., Masson, P., Manco, G. & Chabriere, E. (2008). *J. Mol. Biol.* **379**, 1017–1028.
Elias, M. & Tawfik, D. S. (2012). *J. Biol. Chem.* **287**, 11–20.
Gotthard, G., Hiblot, J., Elias, M. & Chabrière, E. (2011). *Acta Cryst.* F**67**, 354–357.
Gotthard, G., Hiblot, J., Gonzalez, D., Chabrière, E. & Elias, M. (2013). *Acta Cryst.* F**69**, 73–76.
Gumerov, V. M., Mardanov, A. V., Beletsky, A. V., Prokofeva, M. I., Bonch-Osmolovskaya, E. A., Ravin, N. V. & Skryabin, K. G. (2011). *J. Bacteriol.* **193**, 2355–2356.
Gupta, R. C. (2009). *Handbook of Toxicology of Chemical Warfare Agents*. London: Academic Press.
Hawwa, R., Aikens, J., Turner, R. J., Santarsiero, B. D. & Mesecar, A. D. (2009). *Arch. Biochem. Biophys.* **488**, 109–120.
Hawwa, R., Larsen, S. D., Ratia, K. & Mesecar, A. D. (2009). *J. Mol. Biol.* **393**, 36–57.
Hiblot, J., Gotthard, G., Chabriere, E. & Elias, M. (2012*a*). *PLoS One*, **7**, e47028.
Hiblot, J., Gotthard, G., Chabriere, E. & Elias, M. (2012*b*). *Sci. Rep.* **2**, 779.
Jackson, C. J., Carr, P. D., Kim, H.-K., Liu, J.-W., Herrald, P., Mitić, N., Schenk, G., Smith, C. A. & Ollis, D. L. (2006). *Biochem. J.* **397**, 501–508.
Jackson, C. J., Foo, J.-L., Tokuriki, N., Afriat, L., Carr, P. D., Kim, H.-K., Schenk, G., Tawfik, D. S. & Ollis, D. L. (2009). *Proc. Natl Acad. Sci. USA*, **106**, 21631–21636.
Kabsch, W. (1993). *J. Appl. Cryst.* **26**, 795–800.
Karplus, P. A. & Diederichs, K. (2012). *Science*, **336**, 1030–1033.
LeJeune, K. E., Wild, J. R. & Russell, A. J. (1998). *Nature (London)*, **395**, 27–28.
Masson, P., Carletti, E. & Nachon, F. (2009). *Protein Pept. Lett.* **16**, 1215–1224.
Matthews, B. W. (1968). *J. Mol. Biol.* **33**, 491–497.
McCoy, A. J., Grosse-Kunstleve, R. W., Adams, P. D., Winn, M. D., Storoni, L. C. & Read, R. J. (2007). *J. Appl. Cryst.* **40**, 658–674.
Merone, L., Mandrich, L., Porzio, E., Rossi, M., Müller, S., Reiter, G., Worek, F. & Manco, G. (2010). *Bioresour. Technol.* **101**, 9204–9212.
Merone, L., Mandrich, L., Rossi, M. & Manco, G. (2005). *Extremophiles*, **9**, 297–305.
Morris, R. J., Perrakis, A. & Lamzin, V. S. (2003). *Methods Enzymol.* **374**, 229–244.
Murshudov, G. N., Skubák, P., Lebedev, A. A., Pannu, N. S., Steiner, R. A., Nicholls, R. A., Winn, M. D., Long, F. & Vagin, A. A. (2011). *Acta Cryst.* D**67**, 355–367.
Omburo, G. A., Kuo, J. M., Mullins, L. S. & Raushel, F. M. (1992). *J. Biol. Chem.* **267**, 13278–13283.
Seibert, C. M. & Raushel, F. M. (2005). *Biochemistry*, **44**, 6383–6391.
Singh, B. K. (2009). *Nature Rev. Microbiol.* **7**, 156–164.
Vyas, N. K., Nickitenko, A., Rastogi, V. K., Shah, S. S. & Quiocho, F. A. (2010). *Biochemistry*, **49**, 547–559.
Xue, B., Chow, J. Y., Baldansuren, A., Yap, L. L., Gan, Y. H., Dikanov, S. A., Robinson, R. C. & Yew, W. S. (2013). *Biochemistry*, **52**, 2359–2370.
Zhang, Y., An, J., Ye, W., Yang, G., Qian, Z.-G., Chen, H.-F., Cui, L. & Feng, Y. (2012). *Appl. Environ. Microbiol.* **78**, 6647–6655.

C. Etude des protéines DING, aspect structural et implications biologiques

Structural insights and *ab initio* sequencing within the DING proteins family

Mikael ELIAS, Dorothée LIEBSCHNER, Guillaume GOTTHARD, Eric CHABRIERE

Résumé : Cet article de revue fait la synthèse bibliographique de la famille des protéines DING. C'est une famille de protéine retrouvée chez les eucaryotes, les procaryotes et les archaeas, principalement découvertes fortuitement, du fait de leurs propriétés biologiques ou leur implication dans des pathologies. Notamment, HPBP découverte chez l'homme de par son association avec la paraoxonase hPON1 fut séquencée par une approche originale couplant la spectrométrie de masse MS/MS, le séquençage d'Edman et la cristallographie aux rayons X. Chez les procaryotes, *Pflu*DING fut isolée chez la bactérie *Pseudomonas fluorescens* SW25 et stimule la prolifération des fibroblastes. La structure cristallographique de cette protéine fut résolue à résolution subatomique permettant ainsi d'élucider le mécanisme de fixation du phosphate chez les protéines de haute affinité.

Journal of
Synchrotron
Radiation

ISSN 0909-0495

Received 27 May 2010
Accepted 7 September 2010

Structural insights and *ab initio* sequencing within the DING proteins family

Mikael Elias,[a]* Dorothee Liebschner,[b] Guillaume Gotthard[c] and Eric Chabriere[c]

[a]Weizmann Institute of Science, Rehovot, Israel, [b]CRM2, Nancy Université, France, and [c]AFMB, Université Aix-Marseille II, France. E-mail: mikael.elias@weizmann.ac.il

DING proteins constitute an intriguing family of phosphate-binding proteins that was identified in a wide range of organisms, from prokaryotes and archae to eukaryotes. Despite their seemingly ubiquitous occurrence in eukaryotes, their encoding genes are missing from sequenced genomes. Such a lack has considerably hampered functional studies. In humans, these proteins have been related to several diseases, like atherosclerosis, kidney stones, inflammation processes and HIV inhibition. The human phosphate binding protein is a human representative of the DING family that was serendipitously discovered from human plasma. An original approach was developed to determine *ab initio* the complete and exact sequence of this 38 kDa protein by utilizing mass spectrometry and X-ray data in tandem. Taking advantage of this first complete eukaryotic DING sequence, a immunohistochemistry study was undertaken to check the presence of DING proteins in various mice tissues, revealing that these proteins are widely expressed. Finally, the structure of a bacterial representative from *Pseudomonas fluorescens* was solved at sub-angstrom resolution, allowing the molecular mechanism of the phosphate binding in these high-affinity proteins to be elucidated.

Keywords: serendipity; DING protein; *ab initio* sequencing; sub-angstrom crystallography; HIV inhibition.

1. The DING proteins

DING proteins constitute an intriguing family of phosphate-binding proteins named DING according to their four conserved N-terminal residues (Berna *et al.*, 2002). Surprisingly, the genes coding for these proteins are systematically missing from eukaryotic sequenced genomes, despite the fact that these proteins seem ubiquitous in eukaryotes, being isolated in animals (human, monkey, rat, turkey), in plants (*Arabidopsis thaliana*, potato, tobacco) and in fungi (*Candida albicans*, *Ganoderma lucidum*) (Berna *et al.*, 2002; Riah *et al.*, 2000; Belenky *et al.*, 2003; Blass *et al.*, 1999; Kumar *et al.*, 2004; Adams *et al.*, 2002; Weebadda *et al.*, 2001; Scott & Wu, 2005; Morales *et al.*, 2006; Du *et al.*, 2007; Chen *et al.*, 2007). Furthermore, the DING proteins family extends to prokaryotes (Berna *et al.*, 2008), as some representatives and their corresponding genes have been identified in *Pseudomonads* (Ahn *et al.*, 2007), whereas in some other bacteria the encoding gene remains unidentified (Pantazaki *et al.*, 2008). In eukaryotes, partial DNA sequences coding for this protein family have been cloned or identified in unannotated parts of genomes (Berna *et al.*, 2008; Berna, Bernier *et al.*, 2009), and another interesting point in genetics concerns the sequence conservation. Indeed, between distant species such as potato (a higher plant) and *Leishmania major* (a protozoan) the sequence identity between the known DING representatives is about 90% at the nucleotidic level, over more than 600 base pairs (Morales *et al.*, 2006). This high conservation raised controversy about their prokaryotic (Lewis & Crowther, 2005) or eukaryotic origins (Berna, Scott *et al.*, 2009).

DING proteins have been mostly isolated by virtue of a biological function. One of the best illustrations is the search for a new HIV inhibitor in St John's wort that led to the characterization of a novel DING protein named $p27^{sj}$ (Darbinian-Sarkissian *et al.*, 2006). In humans, several DING proteins have been identified from different tissues, including the crystal adhesion inhibitor (CAI), the human synovial stimulatory protein (SSP), X-DING-CD4+ from human CD4+ T lymphocytes and the human phosphate binding protein (HPBP). Comparison of available peptides sequences of HPBP, CAI, SSP and X-DING-CD4+ strongly suggests that these proteins are encoded by four different genes, all lacking the sequenced human genome. The CAI, isolated from human kidney cells, is assumed to prevent the growth of kidney stones (Kumar *et al.*, 2004). The SSP, isolated from human synovial liquid, possesses auto-antigen activity, lymphocyte stimulatory activity and a putative role in the etiology of rheumatoid arthritis (Hain *et al.*, 1990, 1996). X-DING-CD4+ was isolated from CD4+ T cells that are resistant to HIV infection and was shown to block the HIV-1 LTR promoted expression and the

replication of HIV-1 (Lesner *et al.*, 2009). HPBP is a serendipitously discovered plasma lipoprotein that binds phosphate and was isolated from human plasma (Fokine *et al.*, 2003; Contreras-Martel *et al.*, 2006). HPBP structure was solved (Morales *et al.*, 2006) and its physiological function, *i.e.* its association with the paraoxonase (HPON1), an enzyme involved in atherosclerosis (Shih *et al.*, 1998), has been extensively studied (Renault *et al.*, 2010; Rochu *et al.*, 2008; Rochu, Renault *et al.*, 2007; Rochu, Chabriere *et al.*, 2007). The involvement of DING proteins in a large spectrum of diseases enhances the potential therapeutic value of this specific protein family, but the lack of sequences has considerably hampered the functional studies within this protein family.

2. *Ab initio* sequencing of HPBP

HPBP is a plasmatic protein interacting with HPON1 and possibly involved in inflammation and atherosclerosis processes (Webb, 2006). HPBP was serendipitously discovered while performing structural studies on supposedly pure HPON1 samples purified from human plasma. Crystals were obtained and the resolved structure was not that of HPON1 but rather that of an unexpected and unknown protein: HPBP. As for other DING proteins, the lack of genetic sequence encoding for HPBP has considerably hindered functional studies. In order to overcome this difficulty, HPBP's sequence was determined experimentally. However, the *ab initio* sequencing of a protein of 38 kDa is not a trivial task, and can barely be achieved using only one technique, *i.e.* mass spectrometry, mainly because some of the protein peptides are too hydrophobic and barely observed in this experiment. A new strategy was developed, utilizing mass spectrometry sequencing and available X-ray data in tandem (Diemer *et al.*, 2008).

2.1. Limitations of the X-ray sequencing

The first HPBP sequence was inferred from electronic density maps at 1.9 Å (Fig. 1*a*). However, this sequence contains some ambiguities. The electronic density map is related to the electron number of the atoms, but at this resolution it is not possible to clearly discriminate C, N and O atoms as they possess roughly the same number of electrons (six, seven and eight electrons, respectively). This limitation implies that some amino acids possess similar electronic density shapes at such a resolution, such as Asn and Asp, Gln and Glu, and Val and Thr (Fig. 1*b*), and are thus difficult to discriminate. Furthermore, some protein residues possess multiple conformations. Agitation modifies the electronic density shape. As an illustration, a double serine conformation causes similar electronic density shapes as threonine or valine residues (Fig. 1*c*). A third cause of ambiguity concerns disordered atoms. Indeed, disordered atoms contribute less than ordered atoms in diffraction. Consequently, these agitated atoms disappear from the electronic density maps. This mainly concerns residues located at the protein extremities or surface, and causes truncated electronic density, which can be assimilated to the density corresponding to shorter residue (Fig. 1*d*).

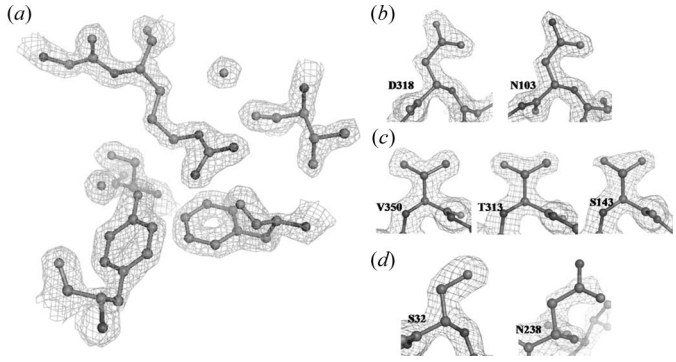

Figure 1
(*a*) Close view of a ball-and-stick representation of the R374 region in the HPBP structure at 1.9 Å resolution. The $2f_{obs} - f_{calc}$ electronic density map is contoured at 1.75σ. (*b*) Comparison between the electronic density shapes of N103 and D318. The $2f_{obs} - f_{calc}$ electronic density map is contoured at 1.5σ. (*c*) Comparison between electronic density shapes of V350, T313 and S143. The $2f_{obs} - f_{calc}$ electronic density map is contoured at 1.5σ. (*d*) Comparison between the electronic density shapes of N238 and S32. The $2f_{obs} - f_{calc}$ electronic density map is contoured at 1.5σ.

2.2. Combination of X-ray data and mass spectrometry data

A series of enzymatic digestions was performed on HPBP to generate peptides, allowing a maximum of sequence information by mass spectrometry (MS) fragmentation in LC-MS/MS and MALDI-MS/MS experiments to be obtained. The primary sequence obtained by X-ray crystallography was used like an 'Ariane wire', useful to align peptide sequences subsequently obtained by mass spectrometry, without the need of having overlapping peptides. It can be noted that X-ray crystallography techniques provided important information that can barely be obtained using MS, such as the exact number of amino acids and the presence of the disulfide bridges, and the discrimination of residues that possess the same mass (Leu, Ile, *etc.*). MS experiments, including ESI-MS on intact HPBP, were used to correct errors from crystallographic sequencing, including those for the few peptides that could not be sequenced. Finally, this technique allowed, *ab initio* and without ambiguities, the 38 kDa HPBP to be sequenced (Diemer *et al.*, 2008), showing that this method could be applied to other DING proteins.

3. The tissue localization of DING proteins

Taking advantage of obtaining the HPBP sequence (Diemer *et al.*, 2008), several polyclonal and monoclonal antibodies targeted against HPBP were developed. Because of the very high sequence identity between DING proteins sequences, the polyclonal antibodies are able to cross-react with other DING proteins. This property was used to map the DING proteins localization in several mouse tissues by immunohistochemistry.

DING proteins were observed in all tested tissues, namely brain, skin, heart, aorta, lung and liver, suggesting that these proteins are widely expressed within the organism (Collombet *et al.*, 2010). A western blot study on these samples also confirms previous assumptions, stemming from the partial

gene found in *Leishmania* major genome and western blot studies on plant tissues (Perera *et al.*, 2008), suggesting that DING proteins exists also as high-molecular-weight proteins (HMW-DING). Indeed, if most of the characterized DING proteins are 38 kDa proteins, our western blot study shows that several HMW-DINGs exists, such as the 140 kDa, the 71 kDa, the 62 kDa and the 52 kDa DING (Collombet *et al.*, 2010). The presence of several isoforms of DING proteins might be linked with different biological activities. Indeed, it was shown for a bacterial DING representative named PfluDING that the truncated form possesses higher stimulation effects on human fibroblasts proliferation than the 38 kDa form (Ahn *et al.*, 2007). This result suggests that there is still a lot to do to understand the physiological involvements of these putatively uncharacterized proteins.

The immunohistochemistry study also reveals that the DING protein cellular localization is tissue-dependent, being exclusively nuclear in neurons, and nuclear and cytoplasmic in the heart muscle. The nuclear localization of DING proteins fits well with previous observations concerning biological activities of DING proteins, showing a clear involvement of these proteins in complex processes within the nucleus. For example, $p27^{SJ}$ suppresses expression of HIV-1 genome (Darbinian *et al.*, 2008). This suppression of expression is mediated by the physical and functional association of $p27^{SJ}$ with human C/EBPβ transcription factor and viral Tat transactivator. Moreover, $p27^{SJ}$ possesses a phosphatase activity inducing a dysregulation at S and G2/M phases in cell cycles related to alteration of the Erk1/2 phosphorylation state (Darbinian *et al.*, 2009). In addition, X-DING-CD4+ seems to interact with transcription factors in the nucleus, and is believed to be involved in the resistance to HIV infection of non-progressive patients (Lesner *et al.*, 2005, 2009).

4. The structure of DING proteins

Two structures of DING representatives are available: the structure of HPBP (Morales *et al.*, 2006) and the structure of a bacterial representative from *Pseudomonas fluorescens* called PfluDING (Ahn *et al.*, 2007; Moniot *et al.*, 2007). These two structures confirm the ability of these proteins to bind a single phosphate ion, in the same manner as the bacterial pstS, which sequesters phosphate for cellular uptake by the ABC phosphate transporter. These two structures and the pstS fit a model known as the 'Venus flytrap', in which the structure can adopt an open and a closed form depending on the phosphate binding (Luecke & Quiocho, 1990). The DING proteins structures reveal an elongated fold composed of two globular domains (Fig. 2*a*). Each domain constitutes a central β-sheet core flanked by α-helices and contains a disulfide bridge that is conserved among the family. Interconnected by an antiparallel two-stranded β-sheet acting as a hinge, the two domains form a deep cleft wherein a phosphate molecule is bound. This fold, known as the Venus flytrap, is very similar to those of the sixth family of solute binding proteins (SBP) (Felder *et al.*, 1999). Structural superposition shows a high correspondence between PfluDING, HPBP and the *Escherichia coli* phosphate-binding protein. Interestingly, the unique feature of DING proteins compared with pstS is the presence of four protruding loops at the protein surface (Fig. 2*b*).

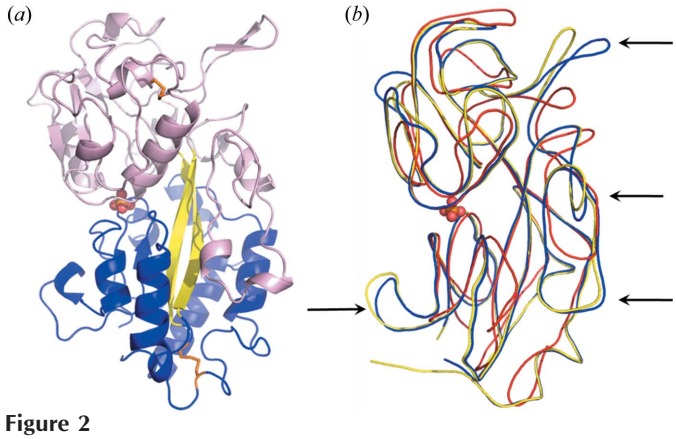

Figure 2
(*a*) X-ray structure of HPBP. The two globular domains are shown in pink and blue. They are hinged by an antiparallel two-stranded β-sheet acting as a hinge (in yellow), and form a deep cleft wherein a phosphate molecule is bound (red balls). The two disulfide bridges (C113–C158 and C306–C359) are shown by orange sticks. (*b*) Structural comparison of different known phosphate-SBPs: HPBP [Protein Data Bank (PDB) ID: 2v3q] is shown in blue, PfluDING (PDB ID: 2q9t) is shown in yellow, *E. coli* PstS protein (PDB ID: 1ixh) is shown in red. The four protruding DING protein-specific loops are indicated by black arrows.

5. Elucidation of the phosphate-binding mechanism

Although their phosphate-binding ability has not been clearly related to their biological functions until now, DING proteins are able to bind phosphate with high affinity. Indeed, it has been shown that HPBP and PfluDING bind phosphate with a K_D of approximately 1 μM (Ahn *et al.*, 2007; Luecke & Quiocho, 1990), of the same order as bacterial phosphate solute binding protein (Poole & Hancock, 1984; Luecke & Quiocho, 1990). As PfluDING yields crystals diffracting to very high resolution, it offers the most convenient model for investigating the molecular mechanism of the phosphate binding in these high-affinity binding proteins. The sub-angstrom resolution structures of PfluDING (0.98 Å and 0.88 Å) at two different pH values (4.5 and 8.5) have been successfully obtained (Liebschner *et al.*, 2009).

The quality of the obtained data allows most of the H atoms in the protein structure to be located precisely (Fig. 3*a*). Moreover, the H atoms involved in the binding of the phosphate ion are clearly visible in both structures. Surprisingly, and despite the intrinsic pK_a values of the phosphate moiety, PfluDING binds only dibasic phosphate both at acidic and basic pH. The structures show that the phosphate ion is bound *via* 11 normal hydrogen bonds plus a highly energetic hydrogen bond, between a phosphate oxygen and the carboxylate side chain of Asp62 (Fig. 3*b*). This very short bond (2.50 Å) belongs to the low barrier hydrogen bond (LBHB) type, where the H atom is almost perfectly shared between the two heavy atoms. This work, combined with electrostatic potential computations, demonstrates the capacity of the protein to alter the pK_a of atoms in the binding site. Indeed,

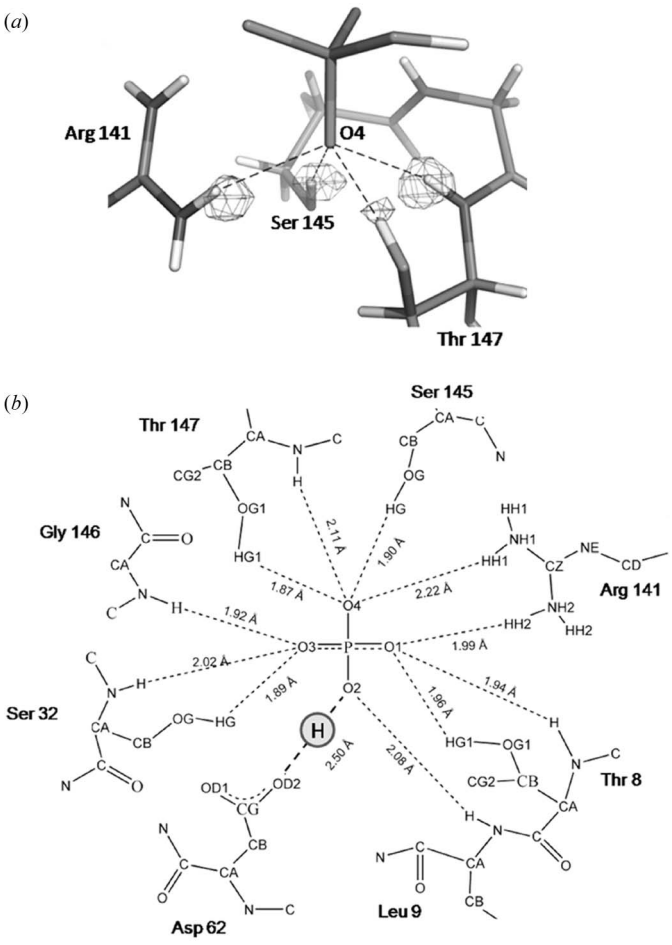

Figure 3
(*a*) Close view of phosphate O4 in the PfluDING structure obtained at pH 4.5. The $F_{obs} - F_{calc}$ map is contoured at 2.6σ. (*b*) Experimentally determined hydrogen bond network involving the phosphate molecule bound in the PfluDING structure.

the fact that PfluDING binds only dibasic phosphate both at acidic and basic pH can be explained by the finding of a very positively charged binding site, capable of altering dramatically the phosphate pK_a.

6. Conclusion

The DING proteins family is an intriguing protein family that seems ubiquitous in eukaryotes, albeit their coding genes are missing. This unconventional protein family requires, for its investigation, some methodological developments. For example, an original approach was developed in order to sequence *ab initio* HPBP using mass spectrometry and X-ray data in tandem. Taking advantage of the very high diffracting power of DING protein crystals, we elucidated the molecular mechanism of phosphate binding in high-affinity proteins. These studies illustrate that DING proteins are widely expressed in eukaryotic tissues, and their cellular localization is tissue-dependent, albeit being mostly nuclear. This nuclear localization partly explains some observed biological activities, such as the role in the cell cycle and the inhibition of the HIV replication by interacting with the viral protein Tat and the human transcription factor CEBP/β. The involvement of DING proteins in several important human diseases, together with their genetic mystery and our findings of unknown HMW-DING in eukaryotes, enhance the emerging scientific interest on this protein family.

ME is a Fellow supported by the FEBS. DL is a doctoral fellow supported by the French Ministry of Research. GG is a doctoral fellow supported by the DGA. EC is supported by a grant from the DGA (grant REI no. 09C7002).

References

Adams, L., Davey, S. & Scott, K. (2002). *Biochim. Biophys. Acta*, **1586**, 254–264.
Ahn, S., Moniot, S., Elias, M., Chabriere, E., Kim, D. & Scott, K. (2007). *FEBS Lett.* **581**, 3455–3460.
Belenky, M., Prasain, J., Kim, H. & Barnes, S. (2003). *J. Nutr.* **133**, 2497S–2501S.
Berna, A., Bernier, F., Chabriere, E., Elias, M., Scott, K. & Suh, A. (2009). *Cell Mol. Life Sci.* **66**, 2205–2218.
Berna, A., Bernier, F., Chabriere, E., Perera, T. & Scott, K. (2008). *Intl. J. Biochem. Cell Biol.* **40**, 170–175.
Berna, A., Bernier, F., Scott, K. & Stuhlmuller, B. (2002). *FEBS Lett.* **524**, 6–10.
Berna, A., Scott, K., Chabriere, E. & Bernier, F. (2009). *Bioessays*, **31**, 570–580.
Blass, S., Schumann, F., Hain, N. A., Engel, J. M., Stuhlmuller, B. & Burmester, G. R. (1999). *Arthritis Rheum.* **42**, 971–980.
Chen, Z., Franco, C. F., Baptista, R. P., Cabral, J. M., Coelho, A. V., Rodrigues, C. J. Jr & Melo, E. P. (2007). *Appl. Microbiol. Biotechnol.* **73**, 1306–1313.
Collombet, J. M., Elias, M., Gotthard, G., Four, E., Renault, F., Joffre, A., Baubichon, D., Rochu, D. & Chabriere, E. (2010). *PLoS One*, **5**, e9099.
Contreras-Martel, C., Carpentier, P., Morales, R., Renault, F., Chesne-Seck, M.-L., Rochu, D., Masson, P., Fontecilla-Camps, J. C. & Chabrière, E. (2006). *Acta Cryst.* F**62**, 67–69.
Darbinian, N., Czernik, M., Darbinyan, A., Elias, M., Chabriere, E., Bonasu, S., Khalili, K. & Amini, S. (2009). *J. Cell Biochem.* **107**, 400–407.
Darbinian, N., Popov, Y., Khalili, K. & Amini, S. (2008). *Antiviral Res.* **79**, 136–141.
Darbinian-Sarkissian, N., Darbinyan, A., Otte, J., Radhakrishnan, S., Sawaya, B. E., Arzumanyan, A., Chipitsyna, G., Popov, Y., Rappaport, J., Amini, S. & Khalili, K. (2006). *Gene Ther.* **13**, 288–295.
Diemer, H., Elias, M., Renault, F., Rochu, D., Contreras-Martel, C., Schaeffer, C., Van Dorsselaer, A. & Chabriere, E. (2008). *Proteins*, **71**, 1708–1720.
Du, M., Zhao, L., Li, C., Zhao, G. & Hu, X. (2007). *Eur. Food Res. Technol.* **224**, 659–665.
Felder, C. B., Graul, R. C., Lee, A. Y., Merkle, H. P. & Sadee, W. (1999). *AAPS PharmSci.* **1**, E2.
Fokine, A., Morales, R., Contreras-Martel, C., Carpentier, P., Renault, F., Rochu, D. & Chabriere, E. (2003). *Acta Cryst.* D**59**, 2083–2087.
Hain, N., Alsalameh, S., Bertling, W. M., Kalden, J. R. & Burmester, G. R. (1990). *Rheumatol. Intl.* **10**, 203–210.
Hain, N. A., Stuhlmuller, B., Hahn, G. R., Kalden, J. R., Deutzmann, R. & Burmester, G. R. (1996). *J. Immunol.* **157**, 1773–1780.
Kumar, V., Yu, S., Farell, G., Toback, F. G. & Lieske, J. C. (2004). *Am. J. Physiol.* **287**, F373–F383.
Lesner, A., Li, Y., Nitkiewicz, J., Li, G., Kartvelishvili, A., Kartvelishvili, M. & Simm, M. (2005). *J. Immunol.* **175**, 2548–2554.

Lesner, A., Shilpi, R., Ivanova, A., Gawinowicz, M. A., Lesniak, J., Nikolov, D. & Simm, M. (2009). *Biochem. Biophys. Res. Commun.* **389**, 284–289.
Lewis, A. P. & Crowther, D. (2005). *FEMS Microbiol. Lett.* **252**, 215–222.
Liebschner, D., Elias, M., Moniot, S., Fournier, B., Scott, K., Jelsch, C., Guillot, B., Lecomte, C. & Chabriere, E. (2009). *J. Am. Chem. Soc.* **131**, 7879–7886.
Luecke, H. & Quiocho, F. A. (1990). *Nature (London)*, **347**, 402–406.
Moniot, S., Elias, M., Kim, D., Scott, K. & Chabriere, E. (2007). *Acta Cryst.* F**63**, 590–592.
Morales, R., Berna, A., Carpentier, P., Contreras-Martel, C., Renault, F., Nicodeme, M., Chesne-Seck, M. L., Bernier, F., Dupuy, J., Schaeffer, C., Diemer, H., Van-Dorsselaer, A., Fontecilla-Camps, J. C., Masson, P., Rochu, D. & Chabriere, E. (2006). *Structure*, **14**, 601–609.
Pantazaki, A. A., Tsolkas, G. P. & Kyriakidis, D. A. (2008). *Amino Acids*, **34**, 437–448.
Perera, T., Berna, A., Scott, K., Lemaitre-Guillier, C. & Bernier, F. (2008). *Phytochemistry*, **69**, 865–872.
Poole, K. & Hancock, R. E. (1984). *Eur. J. Biochem.* **144**, 607–612.
Renault, F., Carus, T., Clery-Barraud, C., Elias, M., Chabriere, E., Masson, P. & Rochu, D. (2010). *J. Chromatogr.* **878**, 1346–1355.
Riah, O., Dousset, J. C., Bofill-Cardona, E. & Courriere, P. (2000). *Cell. Mol. Neurobiol.* **20**, 653–664.
Rochu, D., Chabriere, E., Elias, M., Renault, F., Clery-Barraud, C. & Masson, P. (2008). *The Paraoxonases: Their Role in Disease Development and Xenobiotic Metabolism*, pp. 171–183. Dordrecht: Springer.
Rochu, D., Chabriere, E., Renault, F., Elias, M., Clery-Barraud, C. & Masson, P. (2007). *Biochem. Soc. Trans.* **35**, 1616–1620.
Rochu, D., Renault, F., Elias, M., Hanne, S., Cléry-Barraud, C., Chabriere, E. & Masson, P. (2007). *Toxicology*, 142.
Scott, K. & Wu, L. (2005). *Biochim. Biophys. Acta*, **1744**, 234–244.
Shih, D. M., Gu, L., Xia, Y. R., Navab, M., Li, W. F., Hama, S., Castellani, L. W., Furlong, C. E., Costa, L. G., Fogelman, A. M. & Lusis, A. J. (1998). *Nature (London)*, **394**, 284–287.
Webb, M. R. (2006). *Structure*, **14**, 391–392.
Weebadda, W. K., Hoover, G. J., Hunter, D. B. & Hayes, M. A. (2001). *Compar. Biochem. Physiol.* **130**, 299–312.

D. Origine endogène des protéines DING eucaryotes

Eukaryotic DING proteins are endogenous: an immunohistological study in mouse tissues

Jean-Marc COLLOMBET, Mikael ELIAS, Guillaume GOTTHARD, Elise FOUR, Frédérique RENAULT, Aurélie JOFFRE, Dominique BAUBICHON, Daniel ROCHU, Eric CHABRIERE

Dans les travaux décrits, j'ai réalisé :

- partie expérimentale : Westerns Blots sur les souris « Germ free » et souris normales

Résumé : Ce travail concerne l'étude immuno-histochimique des protéines DING chez la souris et apporte des éléments permettant de conclure quant à l'origine endogène des protéines DING.

Au cours de mon Master 2, j'ai eu pour objectif de déterminer l'origine des protéines DING en utilisant la souris comme animal modèle. Pour ce faire, des westerns blots d'échantillons de sérums de souris normales furent comparés à des sérums de souris élevées en conditions stériles (« germ-free »). L'étude montra qu'il n'y a pas de différence significative dans les profils de western blots entre les deux types de sérums. De plus, l'étude immuno-histochimique réalisée sur différents tissus (*e.g* cœur, poumons, cerveau…), met en évidence la présence de protéines DING dont la localisation cellulaire varie d'un type cellulaire à l'autre.

OPEN ACCESS Freely available online

PLoS one

Eukaryotic DING Proteins Are Endogenous: An Immunohistological Study in Mouse Tissues

Jean-Marc Collombet[1], Mikael Elias[2¤], Guillaume Gotthard[2], Elise Four[1], Frédérique Renault[1], Aurélie Joffre[3], Dominique Baubichon[1], Daniel Rochu[1], Eric Chabrière[2]*

1 Département de Toxicologie, Institut de Recherche Biomédicale des Armées, Centre de Recherche du Service de Santé des Armées, La Tronche, France, **2** Architecture et Fonction des Macromolécules Biologiques, Centre National de la Recherche Scientifique-Aix Marseille Université, Marseille, France, **3** Service de Microscopie et d'Imagerie Médicale, Institut de Recherche Biomédicale des Armées, Centre de Recherche du Service de Santé des Armées, La Tronche, France

Abstract

Background: DING proteins encompass an intriguing protein family first characterized by their conserved N-terminal sequences. Some of these proteins seem to have key roles in various human diseases, e.g., rheumatoid arthritis, atherosclerosis, HIV suppression. Although this protein family seems to be ubiquitous in eukaryotes, their genes are consistently lacking from genomic databases. Such a lack has considerably hampered functional studies and has fostered therefore the hypothesis that DING proteins isolated from eukaryotes were in fact prokaryotic contaminants.

Principal Findings: In the framework of our study, we have performed a comprehensive immunological detection of DING proteins in mice. We demonstrate that DING proteins are present in all tissues tested as isoforms of various molecular weights (MWs). Their intracellular localization is tissue-dependant, being exclusively nuclear in neurons, but cytoplasmic and nuclear in other tissues. We also provide evidence that germ-free mouse plasma contains as much DING protein as wild-type.

Significance: Hence, data herein provide a valuable basis for future investigations aimed at eukaryotic DING proteins, revealing that these proteins seem ubiquitous in mouse tissue. Our results strongly suggest that mouse DING proteins are endogenous. Moreover, the determination in this study of the precise cellular localization of DING proteins constitute a precious evidence to understand their molecular involvements in their related human diseases.

Citation: Collombet J-M, Elias M, Gotthard G, Four E, Renault F, et al. (2010) Eukaryotic DING Proteins Are Endogenous: An Immunohistological Study in Mouse Tissues. PLoS ONE 5(2): e9099. doi:10.1371/journal.pone.0009099

Editor: Art J. Lustig, Tulane University Health Sciences Center, United States of America

Received September 29, 2009; **Accepted** January 20, 2010; **Published** February 8, 2010

Funding: This research was supported by grants to E.C. by Délégation Générale pour l'Armement (CO n°010807/03-10) and by the C.N.R.S. D.R. is under contract with the German Bundesministerium der Verteidigung (M/SABX/8A001). M.E. is a post-doctoral fellow supported by the F.E.B.S. The funders had no role in study design, data collection and analysis, decision to publish, or preparation of the manuscript.

Competing Interests: The authors have declared that no competing interests exist.

* E-mail: eric.chabriere@afmb.univ-mrs.fr

¤ Current address: Department of Biological Chemistry, Weizmann Institute of Science, Rehovot, Israel

Introduction

DING proteins, named according to their four conserved N-terminal amino-acid residues, encompass a recently discovered protein family [1]. Intriguingly, eukaryotic DING genes are consistently missing from genomic databases although proteins belonging to this family seem to be ubiquitous in eukaryotes: they have been identified in animals (human, monkey, rat, turkey), plants (*Hypericum perforatum*, *Arabidopsis thaliana*, potato, tobacco) and fungi (*Candida albicans*, *Ganoderma lucidum*) [2,3] mostly as a 40 kDa protein or higher molecular weight DING proteins [4]. Although no complete eukaryotic DING coding sequence is available in databases, few partial DNA sequences have been either cloned [3] or identified in non-annoted parts of genomes [2]. These few pieces of sequences show that DING proteins are strongly conserved [2]. DING proteins have also been isolated from several prokaryotes [5,6], and their coding genes are in some cases available, such as the gene encoding PfluDING, the protein isolated from *P. fluorescens* [7,8,9]. The high sequence identity between known eukaryotic DING sequences and available prokaryotic DING sequences (>70% sequence identity) and the systematic absence of eukaryotic DING genes raised a controversy about their prokaryotic [10] or eukaryotic origins [11].

DING proteins have been mostly isolated by virtue of a biological function. One of the most striking examples as such, remains the search for a new HIV inhibitor in St John's Wort that led to the characterization of a novel DING protein named $p27^{sj}$ [3]. In humans, several DING proteins have been identified from different tissues [2,12,13]. The human phosphate binding protein (HPBP) is a serendipitously discovered plasma apolipoprotein that binds phosphate and is isolated from human plasma [14,15]. HPBP structure was solved [16] and its physiological function, i.e. its association with paraoxonase (HPON1), an enzyme involved in atherosclerosis [17], has been extensively studied [18,19,20]. The complete protein sequence of HPBP was recently determined by a tandem use of mass spectrometry and X-ray crystallography [21]. Such a sequence stands out as the single complete eukaryotic sequence of a DING representative, known to date. Three other

human DING proteins involve the crystal adhesion inhibitor (CAI), the human synovial stimulatory protein (SSP), and the X-DING-CD4$^+$ from human CD4$^+$ T lymphocytes [22]. Comparison of sequenced N-terminal and internal HPBP, CAI SSP, and X-DING-CD4$^+$ peptides strongly suggests these stem from 4 different genes, all lacking from the sequenced human genome. The CAI isolated from human kidney cells is assumed to prevent the growth of kidney stones [23]. The SSP, isolated from human synovial liquid, possesses auto-antigen activity, lymphocyte stimulatory activity and a putative role in the etiology of rheumatoid arthritis [24,25]. The X-DING-CD4$^+$ was isolated from CD4+ T cells that are resistant to HIV infection and was shown to block the HIV-1 LTR promoted expression and the replication of HIV-1 [22]. The involvement of DING proteins in a large spectrum of diseases enhances the potential therapeutic value of this specific protein family, and further raises the question of the molecular mechanisms involved in such biological properties.

Although the amount of data concerning this protein family has increased over the last few years, their physiological functions remain largely unknown, and their origin in eukaryotes is still under debate. Hence, we performed a mapping of the DING localization in a murine model.

This study focused on several mouse tissues i.e. brain, liver, lung, heart, aorta, artery and skin. Findings revealed that eukaryotic DING proteins have an intracellular localization. It also provides an essential background for future investigations as regards the numerous biological roles of eukaryotic DING proteins.

Material and Methods

Animal Care and Sample Collection

Nine-week old adult male B6D2F1/j@rj mice (Janvier Laboratories - France) were housed in cages under standard conditions of temperature (24°C) and humidity (50–60%), with lights on between 07:00 and 19:00. Mice had free access to water and standard laboratory chow.

All the experiments in our study were reviewed and approved by the Institutional Animal Care and Research Advisory Committee in accordance with French law and leading international guidelines.

Pentobarbital (80 mg/kg) anaesthetized mice were sacrificed by intracardiac perfusion of saline with heparin (5 UI/ml) followed by a fixative solution of 4% formaldehyde and 3% acetic acid in saline. Brain, liver, lung, heart, aorta artery and skin were collected, post-fixed in 4% formaldehyde for 48 hours and then processed for paraffin embedding. For the brain tissue, coronal sections (6 µm thick) were serially cut with a microtome at +0.74 mm (ventricular and striatal areas) and –1.82 mm (hippocampus area) from the bregma, as shown in the Franklin and Paxinos stereotaxic mouse brain atlas [26]. For all other collected tissues (liver, lung, heart, aorta artery and skin), transverse sections were prepared.

Plasma was purified from wild-type and germ-free C57BL/6 mouse blood using standard protocols. Wild-type and germ-free C57BL/6 mouse plasma was kindly provided by the European Mouse Mutant Archive (EMMA; http://emmanet.org).

Histological Staining

Hemalun-phloxin (H&P) staining was performed on paraffin-embedded tissue sections as previously described by Lillie and Fullmer [27]. For skin and lung sections, a saffron staining step was added after the H&P staining (incubation of sections in 2% saffron solution in ethanol for 10 min).

Immunohistochemistry

HPBP was purified from human blood plasma as previously described [28]. Rabbit polyclonal and mouse monoclonal antibodies raised against HPBP were prepared by the Genecust Company (Dudelange, Luxembourg) using standard protocols. All polyclonal antibodies and some monoclonal antibodies raised against HPBP are able to recognize other eukaryotic DING proteins, because of the high sequence identity existing in this family.

For DING protein immunohistochemistry, sections from all tested tissues were deparaffinized, rehydrated and treated for 10 min in TBS containing 0.3% v/v H_2O_2. For brain tissue, a demasking step in boiling 1 mM EDTA pH 8.0 for 20 min was added. Sections were then successively incubated for 1 h at room temperature in TBS-BSA (TBS containing 1% w/v BSA) and overnight at +4°C in TBS-BSA containing primary antibodies. After 3 washes (15 min each) in TBS, secondary biotinylated IgG antibodies in TBS-BSA were applied to sections for 1 h at room temperature. Visualisation was performed using Vectastain ABC Elite kit (Vector) and diaminobenzidine (DAB; Sigma). Dilutions for primary and secondary antibodies were: as follows 1:1000 rabbit polyclonal anti-HPBP (antibody C); 1:50 mouse monoclonal anti-HPBP (antibody 1D3 targeting the N-terminal peptide of HPBP); 1:400 biotinylated anti-rabbit IgG (Vector) and 1:1000 biotinylated anti-mouse IgG (Vector). To ensure proper control processing, some sections from all tested tissues were similarly treated except for the fact that the incubation step in monoclonal or polyclonal HPBP primary antibodies was omitted. In addition, to assess the specificity of polyclonal HPBP antibody, a competition experiment was conducted by adding 0.4, 2, 10 or 40 µg of purified HPBP on brain section slides (3 brain sections per slide) in the primary antibody incubation step.

The following markers were considered for visualization of the main types of specific brain cells: GFAP for activated astroglia, *Griffonia simplifolia* lectin (GSA) for activated microglia and NeuN for mature neurons. Double-labeling detections were achieved on deparaffinized and hydrated sections by performing DAB-stained DING protein immunochemistry (brown staining) as described above, followed by GFAP or NeuN immunolabeling using SG vector dye (blue staining) for visualization [29]. For the detection of DING protein in activated microglia, GSA staining was carried out as previously described by Streit [30] with DAB-staining, followed by DING protein immunochemistry using SG vector as dye revelator.

In control mice, GFAP or GSA staining is very faint since activated astroglial and microglial cells are almost completely absent. Therefore, for the specific detection of DING protein in activated glial cells, brain sections from soman-intoxicated mice were used. Soman, an irreversible cholinesterase inhibitor, is a powerful warfare neurotoxicant triggering epileptic seizures leading to neuronal cell death and subsequent glial activation [29]. For this purpose, nine week old adult male B6D2F1/j@rj mice were subcutaneously injected with 110 µg/kg soman (200 µl in saline buffer; soman was provided by the "Centre d'Etudes du Bouchet" - France) followed 1 min. later by an intraperitoneal injection (200 µl in saline) of 5.0 mg/kg atropine methyl nitrate. Pentobarbital (80 mg/kg) anaesthetized mice were sacrificed on day 3 (pick of microglial cell activation) and day 8 (pick of astroglial cell activation) post-poisoning using intracardiac perfusion of formaldehyde and collected brains were processed for immunohistochemistry as described above for control mice.

Western Blots Assays

Anaesthetized mice were decapitated and tissues such as the whole brain without cerebellum, liver, lung, shaven skin and heart

ventricle were immediately collected. Brain and liver were homogenized with a mini-potter in 5 volumes of cold RIPA buffer containing 20 mM Tris-HCl pH 8.0, 150 mM NaCl, 1 mM EDTA, 1% v/v NP40, 0.5% w/v SDS, 0.5% w/v deoxycholic acid and 0.5% v/v protease inhibitor cocktail set III (Calbiochem - Merck). Lung, skin or heart were disrupted using a mixer mill (Retsch MM301) calibrated for two sessions of 2 min shaking each, at 30 Hz. For disruption, tissues were transferred in a 2 ml microfuge tube containing 5 volumes of cold RIPA buffer (see above) and two 3 mm tungsten carbide beads (Retsch). Subsequently, homogenates were centrifuged at 14000 g for 20 min at +4°C and supernatants were frozen at −20°C for further western blot analysis. Prior to freezing, protein concentrations were determined in the supernatants, using the Lowry method [31].

Western immunoblotting was achieved as previously described [32]. For each tissue homogenate or plasma sample, 20 µg of total protein per well were loaded onto a 10% SDS-PAGE gel. Gel electro-transfer was performed onto 0.2 µm nitrocellulose membrane using a specific transfer buffer (48 mM Tris; 39 mM glycine; 20% methanol; 1.3 mM SDS; pH 9.2). For DING proteins detection on tissues, membranes were incubated with 1:400 monoclonal HPBP antibody and 1:1000 biotinylated-IgG anti-mouse (Vector). Western blots on plasma samples were performed using 1:2000 polyclonal anti-DING antibodies and 1:2500 anti-rabbit antibodies (BioRad). The size of DING proteins bands was calculated according to the migration of Precision plus protein kaleidoscope standard (BioRad) on the same gel for all experiments, except for the western blot on plasma samples, where Prestained Protein Ladder was used (Fermentas life science).

Results

Western Blot Analysis

Western blot analysis was performed on brain, shaven skin, lung, heart and liver prepared from B6D2F1 mouse samples. Anti-DING monoclonal antibody revealed several bands ranging from 41 to 140 kDa in all tested mouse tissues (**Figure 1**). The 41 kDa protein band corresponds to the size of eukaryotic DING proteins already described in the literature [1]. Intensities of 41 kDa bands were very similar in all tested mouse tissues except in shaven skin where the band intensity is weaker. Other bands between 52 and 140 kDa are more likely high molecular weight DING proteins (HMW-DING) comparable to the ones already observed in plants [4]. A similar band pattern was found in mouse lung, heart and liver with 4 major HMW-DING bands located at 140 kDa, 71 kDa (double band of HMW-DING), 62 kDa and 52 kDa. In the heart, the intensity of the double 71 kDa band is more important than the one detected in lung and liver. In the brain, the 3 HMW-DING bands at 140 kDa, 71 kDa (double band) and 62 kDa are revealed but the 52 kDa HMW-DING protein was not present. In the shaven skin, only one HMW-DING was identified with a very intense band located at 52 kDa (**Figure 1**).

Furthermore, western blot analysis was carried out on plasma purified from wild-type or germ-free C57BL/6 mice to determine whether or not the presence of DING proteins in rodent was due to a symbiotic or contaminating microbe. In both wild-type and germ-free C57BL/6 plasma, a similar pattern was observed (**Figure 2**). This indicates that plasma DING proteins do not originate from bacteria but are directly produced by eukaryotic cells and are subsequently secreted in the circulating blood. Anti-DING polyclonal antibody revealed several bands ranging from 35 to 130 kDa, with a slightly different pattern from that observed in mouse tissues. As a case in point, 2 bands of HMW-DING at 130 kDa and 100 kDa and a shorter DING protein of 35 kDa

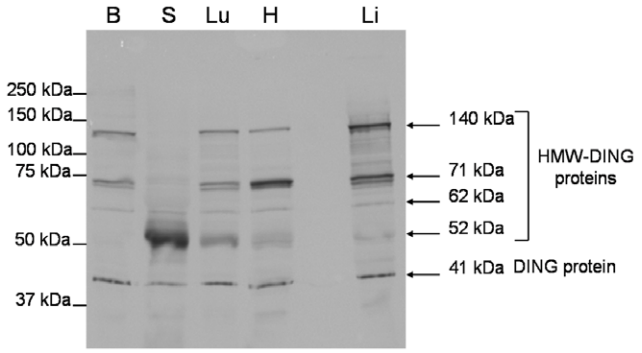

Figure 1. Characterization of DING proteins by western blot analysis. Western blots were achieved with protein homogenates prepared from B6D2F1 mouse brain, shaven skin, lung, heart and liver (loading of 20 µg total proteins in each well). DING proteins were identified with mouse monoclonal anti-DING antibody. Diaminobenzidine was used for the band revelation. Abbreviations are: B = brain; S = shaven skin; Lu = lung; H = heart; Li = liver; HMW = high molecular weight.
doi:10.1371/journal.pone.0009099.g001

were specifically observed. On the other hand, 2 bands corresponding to HMW-DING at 52 kDa and 71 kDa were shared with other mouse tissues. The band at 71 kDa is very strong, suggesting that this isoform is widely predominant in mouse plasma.

DING Protein Detection in the Mouse Brain

DING protein staining was detected in all cerebral regions of brain sections using polyclonal antibody. The specificity of the polyclonal antibody was verified in competition experiments where various quantities of purified HPBP (ranging from 0.4 to 10 µg per brain section) were added in the primary antibody incubation step (**Figure 3**). The addition of 0.4 µg HPBP (**Figure 3B**) is sufficient enough to induce a significant reduction of the intensity of DING immunolabeling previously observed in brain sections in absence of purified HPBP competitor (**Figure 3A**). An almost complete depletion of DING protein immunolabeling was obtained by the addition of either 2 or 10 µg

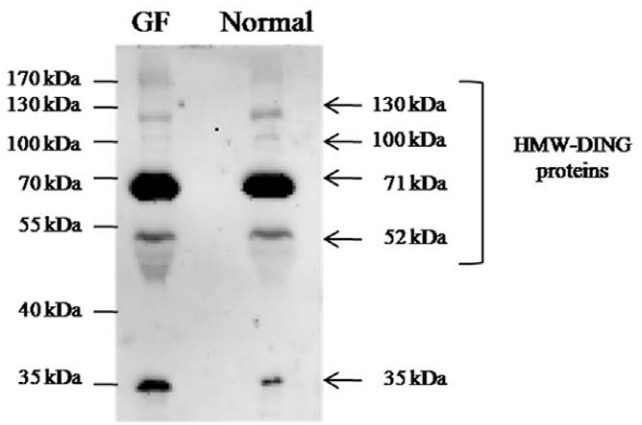

Figure 2. Western blot analysis on plasma samples from normal and germ-free mouse. Western blot was achieved with plasma from wild type and germ-free C57BL/6 mice (loading of 20 µg total proteins in each well). Abbreviations are: normal = wild-type and GF = germ-free.
doi:10.1371/journal.pone.0009099.g002

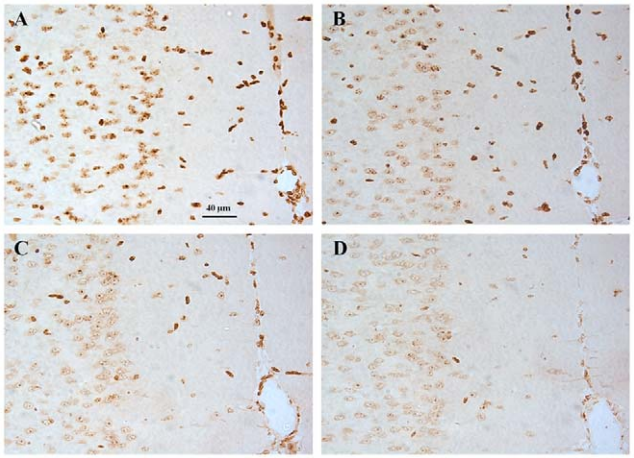

Figure 3. Competition assays to assess polyclonal antibody specificity. Anti-DING immunohistochemistry was performed on brain sections from control mice (panel A). In a competition experiment, 0.4 μg (panel B), 2 μg (panel C) or 10 μg (panel D) of human purified HPBP protein was added in the primary antibody incubation step. In each panel, the same brain area (cingulate cortex area) was photographed with the same magnification (see scale bar on panel A).
doi:10.1371/journal.pone.0009099.g003

of purified HPBP competitor (**Figures 3C and 3D**). This demonstrates the high specificity of polyclonal antibody raised against mouse DING proteins and HPBP.

In the brain, DING labeling was exclusively detected in cell nuclei but following two different staining patterns. In the first one, the whole nucleus is strongly labeled (**Figure 4A**). This labeling can be either evenly distributed throughout the nucleus or some more intensely stained patches can be spotted in the labeled nuclei. In the second pattern, detected DING proteins appeared as small patches scattered in a poorly labeled nucleus (**Figure 4A**). The relative proportion of strongly- or poorly-labeled nuclei is dependent on the considered cerebral regions. For example, strongly-labeled nuclei are almost entirely present in epithelial cells constituting blood vessels (**Figure 4F**) and are dominant in cells located in the subventricular zone and the cerebral cortex (**Figures 4B and 4C**). In contrast, the majority of ''poorly''-labeled nuclei are found in the lateral septum, the striatum and the hippocampus (dentate gyrus and CA1, CA2 or CA3 hippocampal fields). Regardless of the strongly- or poorly-stained status of nuclei, the distribution of DING protein-positive cells is also dependent on the related brain areas. In a semi-qualitative study, the highest number of labeled cells was observed in the granular layer of the dentate gyrus (**Figure 4E**), the CA1, CA2 and CA3 fields of the hippocampus and the subventricular zone (**Figure 4B**). To a lesser extent, the density of DING protein-labeled cells is also important in the hypothalamus, the corpus callosum, the amygdala, the choroid plexus and all cortices including cingular, piriform and cerebral cortices (**Figure 4C**). The quantity of DING protein-positive cells was low in the thalamus (**Figure 4D**), the lateral septum, the striatum and some hippocampal areas deprived of pyramidal neurons such as the stratum radiatum, the lacunosum moleculare layer and the molecular layer of the dentate gyrus.

Both H&P staining and DING protein immunochemistry were combined on same brain sections (co-labeling experiments) to ensure that all brain nuclei are positively labeled with anti-DING antibody (data not shown). In all checked cerebral regions, non-

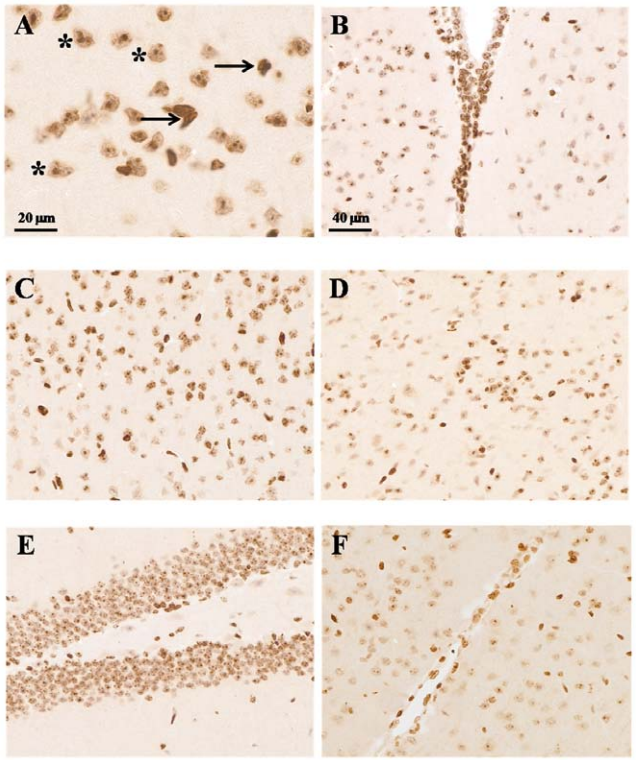

Figure 4. DING immunochemistry in the mouse brain. Different brain areas were photographed on control mouse brain sections labeled by anti-DING immunochemistry, using diaminobenzidine as revelator dye. The different brain regions are: the cerebral cortex (panels A and C), the sub-ventricular zone or SVZ (panel B), the thalamus (panel D), the granular layer of the dentate gyrus (panel E) and epithelial cells from blood vessels (panel F). Scale bars represent 20 μm for panel A or 40 μm for panels B to F. In panel A, black arrows indicate brain cells with intense DING labeling throughout the whole nucleus while black asterisks refer to brain cells with small patches of DING labeling in poorly labeled nuclei.
doi:10.1371/journal.pone.0009099.g004

H&P-stained nuclei were deprived of DING protein labeling. Therefore, the density of DING protein labeling in a given brain area is directly correlated to the density of cell nuclei in the specific cerebral region.

The presence of large numbers of DING protein-positive cells in the hippocampal CA1 field or in the granular layer of the dentate gyrus undoubtedly means that these positively-stained cells are neurons since these brain areas involve pyramidal neurons for the most part. As assessed by DING protein/NeuN double labeling (**Figures 5A and 5B**), co-localization of NeuN and DING proteins was observed in many cell nuclei confirming the presence of DING protein in neurons throughout the brain.

To address the issue as to whether DING protein was also present in astroglial or microglial cells, DING protein/GFAP or DING protein/lectin GSA double staining were performed in the brain of soman-poisoned mice, respectively. Usually, resting glial cells are not easy to detect due to the thinness of their perinuclear cytoplasmic processes and the smallness of their nuclei. Therefore, a mouse model containing activated glial cells with prominent cytoplasmic branching processes and hypertrophied nuclei, namely the soman-intoxicated mouse, was chosen. The presence of DING protein was demonstrated in numerous activated microglial or astroglial cells after soman poisoning, as shown in **Figures 5C and 5D**, respectively.

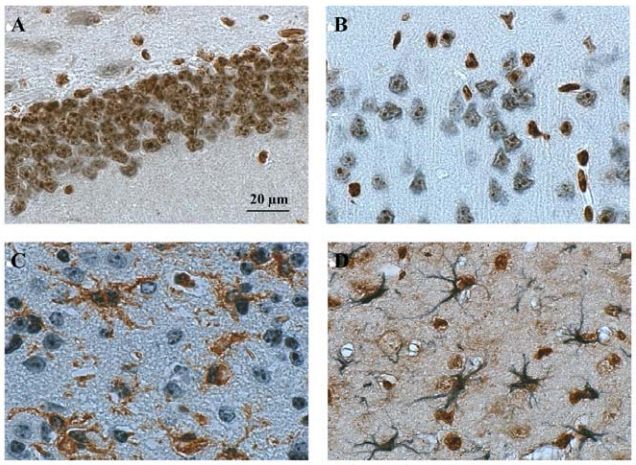

Figure 5. Characterization of DING-labeling in brain cells. Anti-DING/anti-NeuN double staining was performed in brain sections of control mice to detect DING-expressing neurons (panel A: granular layer of the dentate gyrus; panel B: cerebral cortex). Diaminobenzidine (brown labeling) and SG vector dye (blue labeling) were used to view DING and NeuN, respectively. Activated microglia (panel C) and astroglia (panel D) expressing DING proteins were revealed in brain sections of soman-poisoned mice with anti-DING/GSA lectin or anti-DING/anti-GFAP double staining immunochemistry, respectively. Blue staining was obtained with SG vector (labeling of DING proteins in microglia and GFAP in astrocytes) while brown staining was achieved using diaminobenzidine (labeling of DING proteins in astroglia and GSA lectin in microglia).
doi:10.1371/journal.pone.0009099.g005

DING Protein Detection in Other Mouse Tissues

In the skin, a massive DING protein-positive staining was observed in the *stratum corneum*, epidermis (including basal keratinocytes) and cutaneous underlying muscles (**Figures 6A and 6B**). In the dermis, only fibroblasts were strongly labeled with anti-DING antibody. However, a weak DING protein labeling was found in the dermis extracellular matrix mainly consisting of collagen fibers (**Figures 6A and 6B**).

In the heart, muscle fibers were mildly stained with anti-DING antibody in their entirety, including cardiomyocyte nuclei. DING protein was also detected in the nuclei of endothelial cells from blood vessels (data not shown).

The presence of a heterogeneous DING protein labeling was observed in the aortic media and adventitia. An intense labeling was evidenced in the myocyte and fibrocyte nuclei while a slighter labeling was displayed in the aortic amorphous ground substance enriched in chondroitin sulfate. We observed a lack of DING protein staining in elastic concentric membranes and collagen fibrils of the aorta (data not shown).

In the lung, a positive DING protein labeling was identified in cells of the pulmonary alveoli and bronchioles with folded mucous membranes (**Figures 6C and 6D**). DING protein labeling is mainly concentrated in cell nuclei. A positive staining is also present in cytoplasm but in a more diffuse pattern.

In the liver, all the hepatocytes are stained with anti-DING antibody. A strong staining was localized in the nucleus and plasma membrane of hepatocytes while a weaker staining was noticed in the cytoplasm (**Figures 6E and 6F**).

Altogether, these results clearly substantiate the presence of DING protein in all tested mouse tissues. At the cellular level, the strongest labeling was generally localized in nuclei and to a lesser extent in the cytoplasm of considered cells. Moreover, it is noteworthy that DING proteins were rarely spotted in the extracellular matrix. Indeed, DING proteins were only found in the aortic amorphous ground substance or in the skin epidermis.

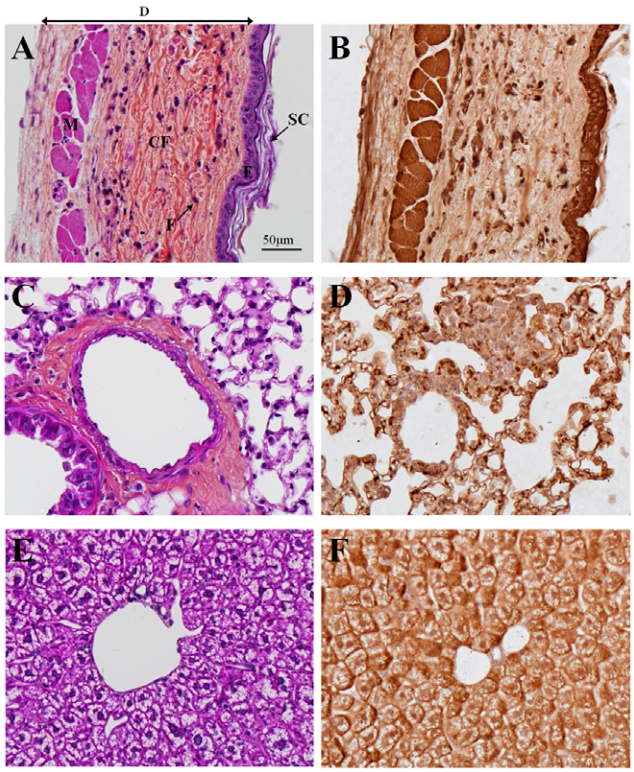

Figure 6. DING immunochemistry in different mouse tissues. Skin (panels A and B), lung (panels C and D) and liver (panels E and F) were collected from control mice and processed for hemalun-phloxin-saffron staining (panels A, C and E) or anti-HPBP immunochemistry (panels B, D and F). The same magnification was used for all the photographs (see scale bar on panel A). Abbreviations are: SC = *stratum corneum*; E = epidermis; D = dermis; F = fibroblast; CF = collagen fibers and M = cutaneous underlying muscles.
doi:10.1371/journal.pone.0009099.g006

Discussion

Origin of Mice DING Proteins

The origin of DING proteins is prone to controversy [11]. Indeed, in the post-genomic era, their genes are still consistently missing from databases and the few partial nucleic sequences identified in non-annoted parts of genomes are highly similar to bacterial DING representatives, such as *Pseudomonas* DING proteins. In addition, their codon usage is similar to that of *Pseudomonas*, leading to the hypothesis of a bacterial origin [10]. Because of the numerous biological implications of DING proteins in eukaryotes, the hypothesis of *Pseudomonas* contamination has been discarded [11,33], but the hypothesis of an unknown microbial symbiosis with eukaryotes remains a viable hypothesis [11]. In order to investigate the possibility of microbial symbiotic origin of DING proteins in eukaryotes, we analyzed wild-type and germ-free mouse plasma samples using western blot assays. The specificity of the used antibodies has been checked using competition assays (**Figure 3**). In addition, the experiment was performed using different kind of polyclonal antibodies, targeted against HPBP (**Figure 2**), and targeted against the very conserved N-terminal peptide of DING proteins (**supporting document – Figure S1**). The similar patterns obtained in both experiments

evidence the specificity of antibodies against DING proteins. The DING protein profiles were compared in both wild-type and germ-free C56BL/6 mouse plasma. The present study shows a similar distribution of DING proteins in either wild-type or germ-free C57BL/6 mouse plasma. This indicates that the presence of DING proteins in eukaryotes is likely not to be related to microbial symbiosis nor to contaminations. Therefore, regarding data provided in this study, the more likely hypothesis concerning the origin of eukaryotic DING proteins is a synthesis by eukaryotic cells themselves.

In addition, the presence of mouse plasma DING protein is consistent with the recent purification of a human DING representative HPBP in the blood as published by Morales et al. [16]. The existence of DING proteins in mammalian plasma suggests therefore that these proteins are synthesized by eukaryotic cells and are subsequently secreted in the circulating blood. To date, the secretion route of DING proteins remains unidentified. The sequence of DING protein genes or the full sequencing of HMW-DING proteins is likely to shed light on the understanding of mechanisms involved in the secretion of these proteins.

Omnipresence of DING Proteins in Mouse Tissues

As assessed by western blot analysis, DING proteins were detected in all explored mouse tissues, namely: brain, skin, heart, aorta, lung and liver. Our present results provide substantial evidence that the omnipresence of DING proteins in various mouse tissues is consistent with data previously published in other mammalian models. Indeed, the 40 kDa cotinine receptor, a member of the DING protein family, was purified from rat brains and sequenced [34]. More recently, the 38 kDa apolipoprotein HPBP has been isolated from human blood and its structure was solved using X-ray crystallography [16,35]. HPBP being a apolipoprotein [16], it could be produced by hepatocytes and could be subsequently secreted in the circulating blood. Therefore, it is not surprising to detect DING proteins in both the mouse liver and plasma, in keeping with substantiated evidence from our experiments.

As mentioned above, only the 41 kDa DING protein was present in mouse liver, heart, brain, skin or lung. Further, the quantity of this protein was more or less similar in all investigated tissues. However, the distribution pattern of HMW-DING proteins was different depending on the nature of the related tissue. A total of four major HMW-DING at 140 kDa, 71 kDa (double bands), 62 kDa and 52 kDa were revealed in tissues, and two others at 130 kDa and 100 kDa were revealed in plasma samples. For example, the 52 kDa HMW-DING was predominant in the skin while the quantities of 140 and 71 kDa HMW-DING were more important in the liver as compared to the other tested mouse tissues. The diversity of HMW-DING proteins possibly results in different physiological involvements. The various forms of DING proteins detected in these assays, different than the classical 41 kDa form, might correspond to higher molecular weight DING protein precursors and truncated or maturated DING proteins. Because of the high sequence conservation within the DING protein family, these bands might also correspond to uncharacterized mouse DING proteins.

Intracellular Localization of Mouse DING Proteins

DING proteins are mainly localized in the nucleus of every cell types present in all investigated mouse tissues. Generally, nuclear stainings are very intense, except in the brain where neuronal nuclei exhibit either strong or reduced labeling. However, as regards other cerebral cells such as microglia or astroglia, all nuclei are deeply stained with anti-DING antibody. Since we investigated the cellular localization of DING proteins with antibodies that recognizes various DING protein forms, the observed signal could be derived from any of these forms. The presence of DING proteins in cell nucleus is consistent with biological activities identified for some of these proteins. For example, bacterial PfluDING protein isolated from *Pseudomonas fluorescens* is competent to stimulate the proliferation of cultured human fibroblasts as assessed by ^{3}H-thymidine incorporation experiment [7]. Another DING protein, p27^{SJ}, suppresses expression of HIV-1 genome [36]. This suppression of expression is mediated by the physical and functional association of p27^{SJ} with human C/EBPβ transcription factor and viral Tat transactivator. C/EBPβ is a factor stimulating HIV-1 gene transcription and regulating the expression of several genes involved in mammalian cell proliferation or differentiation [3,36,37]. Tat transactivator is a viral protein triggering the transcription of HIV-1 viral genes. Moreover, p27SJ possess a phosphatase activity inducing a dysregulation at S and G2/M phases in cell cycles related to alteration of Erk1/2 phosphorylation state [38]. In addition, the X-DING-CD4^{+} seems to interact with transcription factors in the nucleus, and is believed to be involved in the resistance to HIV infection of non-progressive patients [22,39]. Since DING proteins are clearly involved in cell cycle regulation and cell proliferation which are complex processes within the nucleus, it may implies a nuclear localization of these proteins for an optimal activity. Our present investigation provides substantial evidence of the nuclear localization of DING proteins.

The nuclear localization of DING proteins raises the issue of the pathways for these proteins to the nucleus after synthesis in the cytoplasm. The import of proteins into the nucleus is tightly regulated and specific nuclear localization signals (NLS) are required for the transport process [40,41]. Concerning DING proteins, none of the available protein sequences indicate the presence of such a NLS. However, despite being mostly isolated, sequenced and characterized as 38–41 kDa proteins, DING proteins exist also as higher molecular weight proteins [4]. Our study provides evidence to that effect. Then, it could be assumed that NLS might be present in HMW-DING proteins rather than in mature DING proteins. The sequencing of these HMW-DING proteins would be useful to address this issue. DING proteins are also detected in the cytoplasm of liver, lung, skin and aortic cells. Nevertheless, the quantity of DING proteins in cytoplasm is much lower than the quantity revealed in nucleus. DING proteins are completely absent in the cytoplasm of cerebral cells, including neurons, microglia and astroglia. Moreover, the liver is the only tested tissue of our study for which DING proteins was massively localized in the plasma membrane, reinforcing the hypothesis of a possible secretion of these proteins from liver cells to the circulating blood, via a secretion of the DING protein through cell plasma membrane. Since our study demonstrates that 52 kDa and 71 kDa-DING proteins are both intracellular and secreted, this could argue in favor of an unconventional route for DING proteins secretion rather than a secretion pathway via N-terminal secretion signal peptides.

Conclusion

Our study hereby, provides extensive data as regards intracellular DING protein localization in several mouse tissues. DING proteins seem to be ubiquitous in all tested tissues (i.e. brain, skin, heart, aorta, liver and lung) and exists as different isoforms, since we identified, in addition to the common 41 kDa-DING protein, High Molecular Weight DING proteins in all

tested mice tissues. The localization of DING proteins is tissue-dependant: such proteins exhibit an intracellular localization in the brain while these proteins are detected either in the nucleus or cytoplasm of other investigated tissues. As for liver, DING proteins were also recovered in the plasma membrane, findings back up therefore the hypothesis of a possible secretion of DING proteins from liver to circulating blood, as evidenced by the presence of DING proteins both in intracellular and in plasma. Finally, the comparison of western blot profiles performed on blood plasma purified from wild-type and germ-free mice further evidenced the assumption that DING proteins are likely to be produced by eukaryotic cells.

Supporting Information

Figure S1 Western Blot assays on mouse plasmas using anti-N-term antibodies.

Found at: doi:10.1371/journal.pone.0009099.s001 (0.08 MB DOC)

Author Contributions

Conceived and designed the experiments: JMC ME DR EC. Performed the experiments: JMC ME GG EF FR AJ DB. Analyzed the data: JMC ME GG FR AJ DB DR EC. Contributed reagents/materials/analysis tools: JMC ME GG EF FR AJ DB. Wrote the paper: JMC ME DR EC.

References

1. Berna A, Bernier F, Scott K, Stuhlmuller B (2002) Ring up the curtain on DING proteins. FEBS Lett 524: 6–10.
2. Berna A, Bernier F, Chabriere E, Perera T, Scott K (2008) DING proteins; novel members of a prokaryotic phosphate-binding protein superfamily which extends into the eukaryotic kingdom. Int J Biochem Cell Biol 40: 170–175.
3. Darbinian-Sarkissian N, Darbinyan A, Otte J, Radhakrishnan S, Sawaya BE, et al. (2006) p27(SJ), a novel protein in St John's Wort, that suppresses expression of HIV-1 genome. Gene Ther 13: 288–295.
4. Perera T, Berna A, Scott K, Lemaitre-Guillier C, Bernier F (2008) Proteins related to St. John's Wort p27SJ, a suppressor of HIV-1 expression, are ubiquitous in plants. Phytochemistry 69: 865–872.
5. Scott K, Wu L (2005) Functional properties of a recombinant bacterial DING protein: comparison with a homologous human protein. Biochim Biophys Acta 1744: 234–244.
6. Pantazaki AA, Tsolkas GP, Kyriakidis DA (2007) A DING phosphatase in Thermus thermophilus. Amino Acids.
7. Ahn S, Moniot S, Elias M, Chabriere E, Kim D, et al. (2007) Structure-function relationships in a bacterial DING protein. FEBS Lett 581: 3455–3460.
8. Moniot S, Elias M, Kim D, Scott K, Chabriere E (2007) Crystallization, diffraction data collection and preliminary crystallographic analysis of DING protein from Pseudomonas fluorescens. Acta Crystallograph Sect F Struct Biol Cryst Commun 63: 590–592.
9. Liebschner D, Elias M, Moniot S, Fournier B, Scott K, et al. (2009) Elucidation of the Phosphate Binding Mode of DING Proteins Revealed by Subangstrom X-ray Crystallography. J Am Chem Soc 131: 7879–7886.
10. Lewis AP, Crowther D (2005) DING proteins are from Pseudomonas. FEMS Microbiol Lett 252: 215–222.
11. Berna A, Scott K, Chabriere E, Bernier F (2009) The DING family of proteins: ubiquitous in eukaryotes, but where are the genes? Bioessays 31: 570–580.
12. Belenky M, Prasain J, Kim H, Barnes S (2003) DING, a genistein target in human breast cancer: a protein without a gene. J Nutr 133: 2497S–2501S.
13. Adams L, Davey S, Scott K (2002) The DING protein: an autocrine growth-stimulatory protein related to the human synovial stimulatory protein. Biochim Biophys Acta 1586: 254–264.
14. Contreras-Martel C, Carpentier P, Morales R, Renault F, Chesne-Seck ML, et al. (2006) Crystallization and preliminary X-ray diffraction analysis of human phosphate-binding protein. Acta Crystallograph Sect F Struct Biol Cryst Commun 62: 67–69.
15. Fokine A, Morales R, Contreras-Martel C, Carpentier P, Renault F, et al. (2003) Direct phasing at low resolution of a protein copurified with human paraoxonase (PON1). Acta Crystallogr D Biol Crystallogr 59: 2083–2087.
16. Morales R, Berna A, Carpentier P, Contreras-Martel C, Renault F, et al. (2006) Serendipitous discovery and X-ray structure of a human phosphate binding apolipoprotein. Structure 14: 601–609.
17. Shih DM, Gu L, Xia YR, Navab M, Li WF, et al. (1998) Mice lacking serum paraoxonase are susceptible to organophosphate toxicity and atherosclerosis. Nature 394: 284–287.
18. Rochu D, Renault F, Elias M, Hanne S, Cléry-Barraud C, et al. (2007) Functional states, storage and thermal stability of human paraoxonase: Drawbacks, advantages and potential. Toxicology 142.
19. Rochu D, Chabriere E, Renault F, Elias M, Clery-Barraud C, et al. (2007) Stabilization of the active form(s) of human paraoxonase by human phosphate-binding protein. Biochem Soc Trans 35: 1616–1620.
20. Rochu D, Chabriere E, Elias M, Renault F, Clery-Barraud C, et al. (2008) Stabilisation of Active Form of Natural Human PON1 Requires HPBP in The Paraoxonases: Their Role in Disease Development and Xenobiotic Metabolism Springer Netherlands: pp 171–183.
21. Diemer H, Elias M, Renault F, Rochu D, Contreras-Martel C, et al. (2008) Tandem use of X-ray crystallography and mass spectrometry to obtain ab initio the complete and exact amino acids sequence of HPBP, a human 38-kDa apolipoprotein. Proteins 71: 1708–1720.
22. Lesner A, Shilpi R, Ivanova A, Gawinowicz MA, Lesniak J, et al. (2009) Identification of X-DING-CD4, a new member of human DING protein family that is secreted by HIV-1 resistant CD4+ T cells and has antiviral activity. Biochem Biophys Res Commun.
23. Kumar V, Yu S, Farell G, Toback FG, Lieske JC (2004) Renal epithelial cells constitutively produce a protein that blocks adhesion of crystals to their surface. Am J Physiol Renal Physiol 287: F373–383.
24. Hain N, Alsalameh S, Bertling WM, Kalden JR, Burmester GR (1990) Stimulation of rheumatoid synovial and blood T cells and lines by synovial fluid and interleukin-2: characterization of clones and recognition of a co-stimulatory effect. Rheumatol Int 10: 203–210.
25. Hain NA, Stuhlmuller B, Hahn GR, Kalden JR, Deutzmann R, et al. (1996) Biochemical characterization and microsequencing of a 205-kDa synovial protein stimulatory for T cells and reactive with rheumatoid factor containing sera. J Immunol 157: 1773–1780.
26. Franklin KBJ, Paxinos G (1997) The mouse brain in stereotaxic coordinates. Academic Press, San Diego.
27. Lillie RD, Fullmer HM (1976) Histopathologic technique and practice. McGraw-Hill, New-York. pp 208–209.
28. Renault F, Chabriere E, Andrieu JP, Dublet B, Masson P, et al. (2006) Tandem purification of two HDL-associated partner proteins in human plasma, paraoxonase (PON1) and phosphate binding protein (HPBP) using hydroxyapatite chromatography. J Chromatogr B Analyt Technol Biomed Life Sci 836: 15–21.
29. Collombet JM, Four E, Bernabe D, Masqueliez C, Burckhart MF, et al. (2005) Soman poisoning increases neural progenitor proliferation and induces long-term glial activation in mouse brain. Toxicology 208: 319–334.
30. Streit WJ (1990) An improved staining method for rat microglial cells using the lectin from Griffonia Simplicifolia (GSA I-B4). J Histochem Cytochem 38: 1683–1686.
31. Lowry OH, Rosebrough NJ, Farr AL, Randall RJ (1951) Protein measurement with the Folin phenol reagent. J Biol Chem 193: 265–275.
32. Collombet JM, Masqueliez C, Four E, Burckhart MF, Bernabe D, et al. (2006) Early reduction of NeuN antigenicity induced by soman poisoning in mice can be used to predict delayed neuronal degeneration in the hippocampus. Neurosci Lett 398: 337–342.
33. Berna A, Bernier F, Chabriere E, Elias M, Scott K, et al. (2009) For whom the bell tolls? DING proteins in health and disease. Cell Mol Life Sci.
34. Riah O, Dousset JC, Bofill-Cardona E, Courriere P (2000) Isolation and microsequencing of a novel cotinine receptor. Cell Mol Neurobiol 20: 653–664.
35. Morales R, Berna A, Carpentier P, Contreras-Martel C, Renault F, et al. (2007) Discovery and crystallographic structure of human apolipoprotein. Ann Pharm Fr 65: 98–107.
36. Darbinian N, Popov Y, Khalili K, Amini S (2008) Creation of a bi-directional protein transduction system for suppression of HIV-1 expression by p27SJ. Antiviral Res 79: 136–141.
37. Mukerjee R, Deshmane SL, Darbinian N, Czernik M, Khalili K, et al. (2008) St. John's Wort protein, p27(SJ), regulates the MCP-1 promoter. Mol Immunol 45: 4028–4035.
38. Darbinian N, Czernik M, Darbinyan A, Elias M, Chabriere E, et al. (2009) Evidence for phosphatase activity of p27SJ and its impact on the cell cycle. J Cell Biochem 107: 400–407.
39. Lesner A, Li Y, Nitkiewicz J, Li G, Kartvelishvili A, et al. (2005) A soluble factor secreted by an HIV-1-resistant cell line blocks transcription through inactivating the DNA-binding capacity of the NF-kappa B p65/p50 dimer. J Immunol 175: 2548–2554.
40. Kalderon D, Roberts BL, Richardson WD, Smith AE (1984) A short amino acid sequence able to specify nuclear location. Cell 39: 499–509.
41. Dingwall C, Robbins J, Dilworth SM, Roberts B, Richardson WD (1988) The nucleoplasmin nuclear location sequence is larger and more complex than that of SV-40 large T antigen. J Cell Biol 107: 841–849.

E. HPBP est un inhibiteur puissant du VIH-1

Human-Phosphate-Binding-Protein inhibits HIV-1 gene transcription and replication

Thomas CHERRIER, Mikael ELIAS, Alicia JEUDY, Guillaume GOTTHARD, Valentin LE DOUCE, Houda HALLAY, Patrick MASSON, Andrea JANOSSY, Ermanno CANDOLFI, Olivier ROHR, Eric CHABRIÈRE, Christian SCHWARTZ

Dans les travaux décrits, j'ai réalisé :

- partie expérimentale : purification de HPBP à partir de plasma humain

Résumé : Ce travail concerne la mise en évidence d'une activité anti-VIH-1 chez la protéine DING humaine HPBP. Les travaux réalisés dans cet article ont été réalisés en collaboration avec l'équipe du Pr. Oliver Rohr (Université de Strasbourg, Strasbourg, France).

La HPBP est une protéine DING humaine co-purifiée du plasma humain avec la paraoxonase hPON1. Sa structure cristallographique, résolue par le Pr. Eric Chabrière, la relie à la famille des protéines de haute affinité pour le phosphate (PBP). Une protéine DING isolée du Millepertuis, fut isolée en vertu de sa capacité à inhiber la prolifération du VIH-1. Le travail présenté dans cet article met en évidence que HPBP inhibe l'étape de transcription du virus, une étape encore non ciblée par les thérapies actuelles. HPBP est de plus active sur des souches VIH-1 résistantes à l'AZT, un antirétroviral ciblant la transcriptase inverse du virus.

VIROLOGY JOURNAL

SHORT REPORT Open Access

Human-Phosphate-Binding-Protein inhibits HIV-1 gene transcription and replication

Thomas Cherrier[1,2,6†], Mikael Elias[7†], Alicia Jeudy[1], Guillaume Gotthard[2], Valentin Le Douce[1], Houda Hallay[1], Patrick Masson[3], Andrea Janossy[1], Ermanno Candolfi[1], Olivier Rohr[1,4,5], Eric Chabrière[2*†] and Christian Schwartz[1,4*†]

Abstract

The Human Phosphate-Binding protein (HPBP) is a serendipitously discovered lipoprotein that binds phosphate with high affinity. HPBP belongs to the DING protein family, involved in various biological processes like cell cycle regulation. We report that HPBP inhibits HIV-1 gene transcription and replication in T cell line, primary peripherical blood lymphocytes and primary macrophages. We show that HPBP is efficient in naïve and HIV-1 AZT-resistant strains. Our results revealed HPBP as a new and potent anti HIV molecule that inhibits transcription of the virus, which has not yet been targeted by HAART and therefore opens new strategies in the treatment of HIV infection.

Keywords: HIV-1, HPBP, transcription, HAART

Introduction

Human immunodeficiency 1 (HIV-1), identified in 1983 [1], remains a global health threat responsible for a world-wide pandemic. The introduction of the highly active antiretroviral therapy (HAART) in 1996 exhibited the potential of curing acquired immune deficiency syndrome (AIDS). Even though an effective AIDS vaccine is still lacking, HAART has greatly extended survival [2]. AIDS pandemic has stabilized on a global scale in 2008 with an estimated 33 million people infected worldwide (data from UN, 2008).

However, several problems have been encountered since the introduction of HAART, and improvements in the design of drugs for HIV-1 are needed. A drawback of HAART is that the treatment is very expensive with limitation of its use to western countries. HAART has also several serious side effects leading to treatment interruption. Another major concern is related to the emergence of multidrug resistant viruses which has been reported in patients receiving HAART [3-5]. Therefore, new antiviral drugs are needed with activities against both wild type and mutant viruses. Two major cellular targets for HIV-1 are currently known which have critical role in HIV pathogenesis, i.e. CD4+ T lymphocytes and monocytes/macrophages including microglial cells, which are the central nervous system resident macrophages [6-8]. However, several drugs being active in CD4+ T lymphocytes are ineffective in chronically infected macrophages (i.e. several reverse transcriptase inhibitors) [9], and protease inhibitors have significantly lower activities in macrophages compared to lymphocytes [10]. Finally, many observations strongly suggest that even long term suppression of HIV-1 replication by HAART cannot totally eliminate HIV-1. The virus persists in cellular reservoirs because of viral latency, cryptic ongoing replication or poor drug penetration [11-13]. Moreover, these cellular reservoirs are often found in tissue sanctuary sites where penetration of drugs is restricted, like in the brain [14-16]. All these considerations (existence of several reservoirs, tissue-sanctuary sites and multidrug resistance) urge the search for new and original anti HIV-1 treatment strategies. Currently there are seven classes of antiretroviral (ARV) drugs available in the treatment of HIV-1-infected patients: nucleoside/nucleotide reverse transcriptase inhibitors (NRTIs), nucleotide reverse transcriptase inhibitors (NtRTIs), non-nucleoside reverse transcriptase inhibitors (NNRTIs), protease inhibitors (PIs), entry/fusion inhibitors (EIs), co-receptor inhibitors (CRIs) and integrase inhibitors (INIs) [17]. The therapy of HIV-1-infected patients is based on a combination of

* Correspondence: eric.chabriere@univmed.fr; schwartz.christian@unistra.fr
† Contributed equally
[1]Institut de Parasitologie et Pathologie Tropicale, EA 4438, Université de Strasbourg, 3 rue Koeberlé, 67000 Strasbourg, France
[2]Laboratoire URMITE - UMR 6236 Faculté de Médecine, 27, Bvd Jean Moulin, 13385 Marseille Cedex 5 France
Full list of author information is available at the end of the article

three or more drugs from two or more classes [18]. There have been attempts without success to develop vaccines against HIV- 1 and this field of research needs new directions [19-21]. Improvement of HAART is therefore crucial.

We believe that new drugs should target other steps of the HIV-1 cycle such as transcription since there is no drug currently available targeting this step. An increasing number of studies suggest that inhibitors of cellular LTR-binding factors, such as NF-KB and Sp1 repress LTR-driven transcription [19,21-24]. Recently, it has been shown that proteins of the DING family are good candidates to repress HIV-1 gene transcription [25,26].

More than 40 DING proteins have now been purified, mostly from eukaryotes [[27] and personal communication] and most of them are associated with biological processes and some diseases [28]. The ubiquitous presence in eukaryotes of proteins structurally and functionally related to bacterial virulence factors is intriguing, as is the absence of eukaryotic genes encoding DING proteins in databases. However, theoretical arguments together with experimental evidences supported an eukaryotic origin for DING proteins [29,30]. A member of the DING family proteins, HPBP, was serendipitously discovered in human plasma while performing structural studies on another target, the HDL-associated human paraoxonase hPON1 [31-33]. The structure topology is similar to the one described for soluble phosphate carriers of the ABC transporter family [32-36] that makes HPBP the first potential phosphate transporter identified in human plasma. Moreover, the association with hPON1 has been hypothesized to be involved in inflammation and atherosclerosis processes [37]. Later, the *ab initio* sequencing of HPBP by tandem use of mass spectrometry and X-ray crystallography confirmed that its gene was missing from the sequenced human genome [38]. Immunohistochemistry studies performed in mouse tissues demonstrate that DING proteins are present in most of tissues, spanning from neurons to muscle cells and their cellular localization is largely variable, being exclusively nuclear in neurons, or nuclear and cytoplasmic in muscle cells [30]. Altogether, these localizations are consistent with the biological function that was associated to these proteins, especially the regulation/alteration of cell cycle.

To test whether HPBP is a potential HIV-1 repressor we carried out experiments in a lymphoblastoid cell line (Jurkat) and in primary cells (Peripherial Blood Lineage and macrophage cultures). We report that HPBP represses HIV-1 replication through the inhibition of its gene transcription. Furthermore, HPBP is also active against mutant viruses. Evidence that HPBP can block HIV-1 LTR promoted expression and replication should lead to the design of new drugs which target a not yet targeted step of the virus cycle i.e. transcription.

Materials and methods

Protein purification

HPBP/HPON1-containing fractions were obtained following previously described HPON1 purification protocol [39]. Then HPBP was purified from these fractions according to Renault *et al.* protocol [33]. HPBP/HPON1-containing fraction in 25 mM Tris buffer containing 0.1% Triton X-100, were injected on Bio-Gel HTP hydroxyapatite (BioRad Laboratories, Munich, Germany) equilibrated with 10 mM sodium phosphate pH 7.0. This step was followed by washing with the same buffer and elution by 400 mM sodium phosphate allowed to separate the two proteins. HPBP was not retained on hydroxyapatite equilibrated without $CaCl_2$ and was collected in the filtrate. On the contrary, HPON1 was retained and subsequently eluted by higher phosphate concentrations.

Cell culture

1G5 cells (a Jurkat stable cell line for LTR-luciferase) were grown in RPMI 1640 medium supplemented with 10% fetal calf serum and in the presence of penicillin and streptomycin (100 U/ml). Primary Macrophages were cultured and prepared as previously described [40].

Antiretroviral compounds

Stock of AZT (Glaxo Wellcome) was prepared as 0.1 mM solution in dimethylsulfoxide (Pierce) and stored at -70°C. Stock solutions were further diluted in culture medium immediately prior to use.

Luciferase assays

1G5 cells (a Jurkat stable cell line for LTR-luciferase) were transfected (5×10^6-10^7 cells/transfection) using DEAE-dextran transfection method with HIV-1 pNL4.3. Two days later, cells were collected and luciferase activity was determined using the Dual-GloTM Luciferase Assay System (Promega). Values correspond to an average of at least three independent experiments performed in duplicate.

HIV-1 infection and viral replication

1G5 cells (a Jurkat stable cell line for LTR-luciferase) were transfected (5×10^6-10^7 cells/transfection) using DEAE-dextran transfection method with HIV-1 pNL4.3. After 24 h indicated amount of HPBP was added to cell culture medium. HIV-1 replication was monitored as described previously [41].

Purified PBLs were prepared from peripheral blood of healthy donors as described previously [42]. For purified PBL preparation, Ficoll-Hypaque (Pharmacia, Uppsala, Sweden)-isolated PBMCs were incubated for 2 h on 2% gelatincoated plates. Nonadherent cells, 98% that were PBLs, as assessed by CD45/CD14 detection by flow cytometry analysis (Simultest Leucogate, Becton

Dickinson, San Jose, CA, USA), were harvested after Ficoll-Hypaque isolation and adherence. PBLs were cultivated in RPMI with 10% (v/v) FBS supplemented with human recombinant IL-2 (20 IU/ml) following treatment with PHA (5 μg/ml) for 48 h. Cultured in 24-well plates, cells were electroporated (Biorad Gene Pulser X Cell) with the complete HIV-1 infectious molecular clone pNL4.3. For infection experiments, cells were infected (50 ng/million cells) with a wt lymphotropic strain pNL4.3 or an AZT resistant lymphotropic strain (purchased by NIH AIDS research and reference program (lot number 0014 A018-G910-6, post AZT isolates) [43]. HIV-1 replication was monitored as described previously [40].

Macrophages cells were cultured and prepared as previously described [40]. Cultured in 24-well plates, cells were transfected using Lipofectamine 2000 reagent (Invitrogen, Carlsbad, CA, USA) with the complete HIV-1 infectious molecular clone pNL4.3. For infection experiments, cells were infected (50 ng/million cells) with the pseudo typed pNL4.3-VSV 1 virus. Vesicular stomatitis virus G protein (VSV-G) pseudotyped virions were produced by cotransfection of 293T cells with 500 ng of VSV-G expressed with plasmid pHCMVg along with 2 μg of the proviral clone. HIV-1 replication was monitored as described previously [40]. Values correspond to an average of at least three independent experiments carried out in duplicates.

MTT assay

Jurkat cells, as well primary cells, i.e PBL and macrophages, were seeded in 96-well plates and indicated amount of HPBP was added to cell culture medium. The possible cytotoxic effect of the antiretroviral compounds tested was examined using a 3- [4,5-Dimethylthiazol-2-yl]-2,5-diphenyltetrazolium bromide (MTT) assay [44]. Cells were grown at 37°C/5% CO2 for 6 days in the presence of antiretroviral compounds at individual concentrations of 100, 20, 5, or 0 nM, before removal of the supernatant and replacement with 0.25 mg/ml MTT (Sigma) in phenol red-free RPMI-1640 (Life Technologies). After incubation at 37°C/5% CO2 for 1 h, the MTT-containing supernatant was removed and the cells lysed with 5 ml of isopropanol:1M HCl (96:4 v/v). Triplicate 100 _l volumes of dye-containing supernatant were transferred to a 96-well ELISA-plate (Nunc) and the absorption measured at 570 nm, using background subtraction at 630 nm.

Statistical analysis

Values are the means and SDs of independent experiments. Statistical analysis was performed by Student's t test, and differences were considered significant at a value of $p < 0.05$.

Results

1. HPBP represses HIV-1 gene transcription and replication

In order to assess the anti HIV-1 activity of HPBP, we tested HPBP, HPON1 and the complex HPBP/HPON1, for their activities on HIV-1 gene transcription and replication. The complex HPBP-HPON (Figure 1.A and 1.B lane 2) and the purified HPON1 (Figure 1.A and 1.B lane 4) did not have significant impact neither on HIV-1 replication nor on HIV-1 gene transcription. However, purified HPBP strongly repressed HIV-1 replication and transcription (respectively 60 and 70% as shown in Figure 1.A and 1.B lane 3). AZT treatment (10 μM), used as a control, was efficient to repress HIV-1 replication but not HIV-1 gene transcription (Figure 1.A and 1.B lane 5). Heat-inactivated HPBP, used in another control experiment, had no effect on HIV-1 replication (data not shown).

2. Dose response and cytotoxicity assay for HPBP

Figure 2 shows the dose response effect of HPBP on the Jurkat cells with an IC50 (50% inhibitory concentration) equal to 5 nM. To measure the cytotoxic effect of HPBP on these cells we used the MTT [3-(4,5-dimethylthiazol-2-yl)-2,5-diphenyltetrazolium bromide] cytotoxicity assay [44]. Results, shown in Figure 2 (green line), allowed us to calculate CC50 (50% toxicity concentration) to be equal to 526 nM. We next performed dose response experiments and MTT cytotoxicity assays in primary cells. In Peripherical Blood Cells (PBL), the IC50 is estimated to 5 nM and the CC50 is estimated to 200 nM. Comparable results were obtained in primary macrophages with an IC50 of 5 nM and a CC50 of 140 nM (see table 1).

3. HPBP is efficient against drug-resistant strain of HIV-1

To assess the anti HIV-1 activity of HPBP against mutant viruses, we performed a dose response effect of HPBP on PBL infected with an HIV-1 AZT-resistant strain (lot number 0014 A018-G910-6, post AZT isolates) [43]. As shown in Figure 3, HPBP is active against the mutant strain with an IC50 (5 nM) to the same extent as observed for the wild type strain.

Discussion

HPBP is a member of the DING protein family identified in eukaryotes for their implication in diverse biological processes [28,37]. Here, we show that the human phosphate binding protein has a potent anti HIV-1 activity. Previous observations suggested that $p27^{SJ}$, another member of the DING protein family isolated from the plant *Hypericum perforatum*, represses HIV-1 replication and transcription [25,45,46]. However, it is noteworthy to precise that this inhibitor effect is dose dependent. Indeed it was shown by the same group that

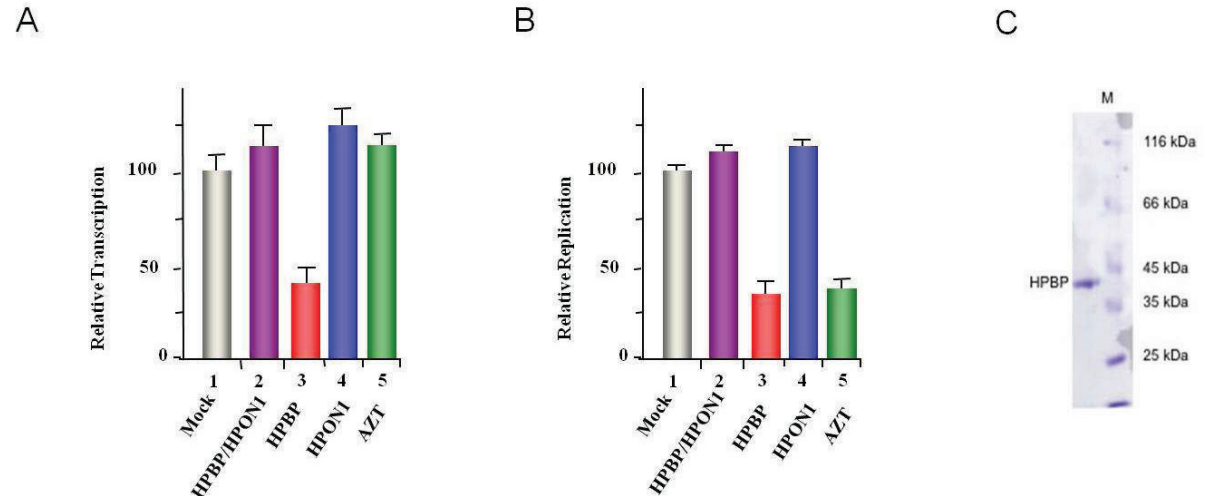

Figure 1 HPBP represses HIV-1 gene transcription and replication. 1G5 cells were transfected with the pNL4.3 provirus. (1) Mock, (2) HPBP/HPNO1 (50 nM), (3) HPBP (50 nM), (4) HPON1 (50 nM), and (5) AZT (10 μM) was added 24 h post transfection. Luciferase activity (A) and HIV-1 replication (B) were monitored 48 h post transfection. Values correspond to an average of at least three independent experiments carried out in duplicate. The purity and the size of purified-HPBP were controlled by SDS-PAGE and coomassie blue staining (C).

p27^{SJ} has a dual role on MCP1(monocyte chemoattractant protein 1) gene transcription being an activator at low concentration and an inhibitor at high concentration [47]. This lead us to hypothesize that HPBP might also have antiviral activities. Since CD4+ T lymphocytes and cells from monocyte-macrophage lineages are major targets for HIV-1, we assessed the *in vitro* antiviral activity of HPBP in lymphoblastoid cell lines (Jurkat), primary monocyte/macrophage cells and peripheral blood lymphocytes presenting laboratory and clinical isolates of HIV-1. The inhibitory effect of HPBP on HIV-1 replication is very strong, the IC50 value being in the range of 5 nM to 10 nM, and also compared to other canonical drugs currently used in HAART (15 nM to 6.7 μM for AZT and 40 nM to 8.5 μM for tenofivir) [48]. At this concentration HPBP is also a potent anti HIV-1 drug in PBL and in primary macrophages, which is not true for several other anti HIV-1 drugs. For example, 3 RT inhibitors, i.e. Lamivudine, entricitabine and AZT have different IC50 values when assessed for their antiviral activity in PBL and macrophages [49]. Furthermore, the CC50 values for HPBP were in the range of 140 nM to 200 nM and the selectivity index CC50/IC50 (ratio between the toxic dose and the inhibitory dose) of HPBP was in the range of 28 to 40. This high ratio indicates that the therapeutical index should therefore be high enough for use in *in vivo studies*.

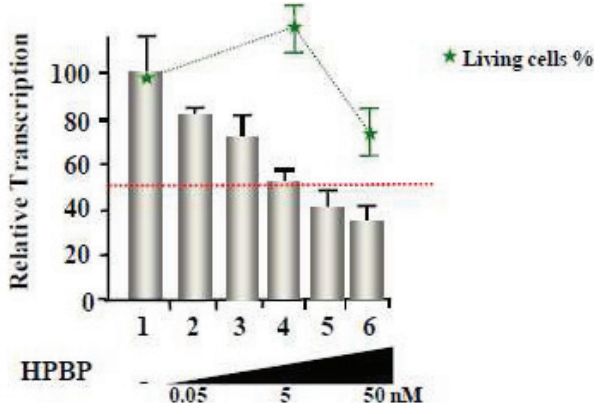

Figure 2 Dose response and cytotoxicity test. 1G5 cells were infected with NL4-3 and treated with increasing amount of HPBP 24 h post transfection. Luciferase activity was assessed 48 h post transfection. MTT test were performed in the same conditions than the dose response experiment. HIV-1 inhibition (grey columns) and percentage of living cell (green line) are shown relative to the mock treated conditions as 100%. Values correspond to an average of at least three independent experiments performed in duplicate.

HPBP also emerged as a promising candidate for drug development as it targets HIV-1 transcription, a phase of the HIV-1 cycle not yet targeted by other drugs. In productive cells, the transcription of the provirus DNA is regulated by the interplay of a combination of viral and cellular transcription factors [50-53]. Darbinian and coll. have identified the protein P27^{SJ}, which belongs to the DING protein family and inhibits the activity of the

Table 1 CC50 and IC50 values in peripheral blood lymphocytes and in primary macrophages

	Peripheral Blood Lymphocytes	Primary Macrophages
CC50	200 nM	140 nM
IC50	5 nM	5 nM

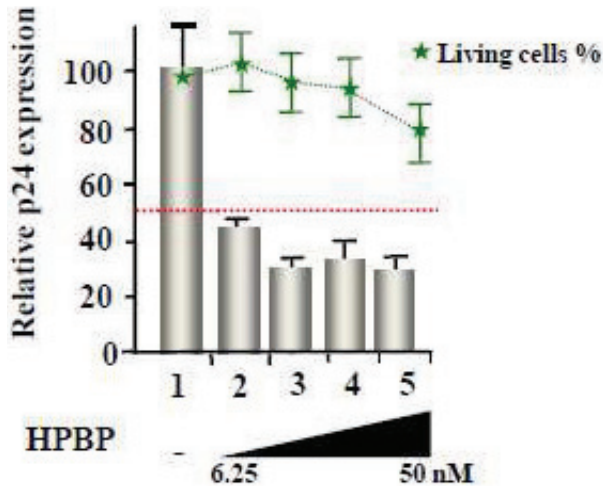

Figure 3 Dose response of HPBP on an AZT-resistant HIV-1 strain. PBL were infected with AZT resistant strain of HIV-1. Different concentrations of HPBP were added 24 h post infection and the HIV-1 replication was monitored 3 days post infection by quantification of the viral p24 protein. HIV-1 inhibition (grey columns) and percentage of living cell (green line) are shown relative to the mock treated conditions as 100%. The 100% level of replication correspond to an average 1.1 ng of p24 protein/ml. Values correspond to an average of at least three independent experiments performed in duplicate.

HIV-1 promoter by interfering with NF-IL6, RNA pol II and Tat [45,46]. Targeting cellular factors, i.e. NF-IL6 has the advantage that resistance to these new drugs should evolve with a lower probability. More importantly, interfering with Tat will ensure a strong and selective repression of HIV-1 replication.

Since its introduction in 1996, antiretroviral therapy has changed the clinical course of HIV and AIDS. However drug resistance has occurred with all of the antiretroviral agents. It is now a major public health concern and it is crucial to design new antiretroviral drugs [54,55]. These new drugs should inhibit HIV replication by targeting new steps within the viral life cycle. Of great interest HPBP, which targets transcription, is as effective against drug resistant HIV strains as to wild type strains, highlighting the potential therapeutic advantage of HPBP. The molecular mechanism of action is unknown but currently under investigation. In the future, pharmacophores ("part of a molecule that is necessary to ensure the optimal interactions with a specific biological target and to trigger (or block) its biological response") can be inferred from the characterization of these biochemical studies.

In conclusion, this work indicates that HPBP has a potent anti HIV activity through the inhibition of transcription a not yet targeted phase of the virus cycle. However additional experiments regarding the HPBP impact on HIV replication and gene transcription have to be performed on other viral strains including several other mutant strains (NRTIs, NNRTIs and protease inhibitors). We believe that this protein or its derivatives are potentially interesting molecules and deserve further studies. As suggested for X-DING-CD4 [26], this work could also uncover a new function for proteins belonging to the DING protein family, that is a role in the innate response to infection including HIV-1. New investigations will be needed in order to precise the importance of the DING proteins. It has been previously shown that HPBP is tightly associated with HPON1 [56]. The search of a correlation between the HPBP abundance, its biologic availability, the HPBP/HPON ratio and the non progression in the disease AIDS in the "elite non progressors cohort" will be of great interest. Finally DING proteins may constitute a marker for AIDS progression since it has been shown that both HPON activity and its concentration have been altered in the presence of HIV-1 [57,58].

Acknowledgements
This work was supported by grants from the Agence Nationale de Recherche sur le SIDA (ANRS), Sidaction and Institut Universitaire de France to OR and from CNRS to TC. ME is a fellow supported by the IEF Marie Curie program (grant No. 252836). TC is a fellow supported by the Belgian Fund for Scientific Research (FRS-FNRS, Belgium). Andrea J is a fellow supported by the "Région Alsace". VLD is supported by a doctoral grant from the French Ministry of Research.

Author details
[1]Institut de Parasitologie et Pathologie Tropicale, EA 4438, Université de Strasbourg, 3 rue Koeberlé, 67000 Strasbourg, France. [2]Laboratoire URMITE - UMR 6236 Faculté de Médecine, 27, Bvd Jean Moulin, 13385 Marseille Cedex 5 France. [3]Unité d'enzymologie, Département de Toxicologie, centre de recherche du service de santé des armées, 38702 la Tronche, France. [4]IUT Louis Pasteur de Schiltigheim, 1 Allée d'Athènes, 67300 Schiltigheim, France. [5]Institut Universitaire de France, 103 Bvd St-Michel, 75005 Paris, France. [6]Cellular and Molecular Biology Unit, FUSAGx, Gembloux, Belgium. [7]Weizmann Institute of Science, Biological Chemistry, Rehovot, Israel.

Authors' contributions
TC, ME, Alicia J, carried out dose response and cytotoxicity assays in lymphocytes and macrophages. Andrea J participated in dose response and cytotoxicity assays in macrophages. VLD and HH carried experiments with heat-inactivated HPBP. CS carried out experiments in Jurkat cell line. GG and PM purified HPBP. Ermanno C and OR participated in the design of the study. Eric C and CS conceived of the study, participated in its design and coordination and wrote the paper. All authors read and approved the final manuscript.

Competing interests
The authors declare that they have no competing interests.

Received: 19 April 2011 Accepted: 15 July 2011 Published: 15 July 2011

References
1. Barre-Sinoussi F, Chermann JC, Rey F, Nugeyre MT, Chamaret S, Gruest J, Dauguet C, Axler-Blin C, Vezinet-Brun F, Rouzioux C, *et al*: **Isolation of a T-lymphotropic retrovirus from a patient at risk for acquired immune deficiency syndrome (AIDS).** *Science* 1983, **220**:868-871.
2. Geeraert L, Kraus G, Pomerantz RJ: **Hide-and-seek: the challenge of viral persistence in HIV-1 infection.** *Annu Rev Med* 2008, **59**:487-501.
3. Hermankova M, Ray SC, Ruff C, Powell-Davis M, Ingersoll R, D'Aquila RT, Quinn TC, Siliciano JD, Siliciano RF, Persaud D: **HIV-1 drug resistance**

profiles in children and adults with viral load of <50 copies/ml receiving combination therapy. *Jama* 2001, **286**:196-207.
4. Kieffer TL, Finucane MM, Nettles RE, Quinn TC, Broman KW, Ray SC, Persaud D, Siliciano RF: **Genotypic analysis of HIV-1 drug resistance at the limit of detection: virus production without evolution in treated adults with undetectable HIV loads.** *J Infect Dis* 2004, **189**:1452-1465.
5. Nettles RE, Kieffer TL, Kwon P, Monie D, Han Y, Parsons T, Cofrancesco J Jr, Gallant JE, Quinn TC, Jackson B, *et al*: **Intermittent HIV-1 viremia (Blips) and drug resistance in patients receiving HAART.** *Jama* 2005, **293**:817-829.
6. Le Douce V, Herbein G, Rohr O, Schwartz C: **Molecular mechanisms of HIV-1 persistence in the monocyte-macrophage lineage.** *Retrovirology* 2010, **7**:32.
7. Redel L, Le Douce V, Cherrier T, Marban C, Janossy A, Aunis D, Van Lint C, Rohr O, Schwartz C: **HIV-1 regulation of latency in the monocyte-macrophage lineage and in CD4+ T lymphocytes.** *J Leukoc Biol* 2009.
8. Herbein G, Varin A: **The macrophage in HIV-1 infection: from activation to deactivation?** *Retrovirology* 2010, **7**:33.
9. Aquaro S, Calio R, Balzarini J, Bellocchi MC, Garaci E, Perno CF: **Macrophages and HIV infection: therapeutical approaches toward this strategic virus reservoir.** *Antiviral Res* 2002, **55**:209-225.
10. Perno CF, Newcomb FM, Davis DA, Aquaro S, Humphrey RW, Calio R, Yarchoan R: **Relative potency of protease inhibitors in monocytes/macrophages acutely and chronically infected with human immunodeficiency virus.** *J Infect Dis* 1998, **178**:413-422.
11. Chun TW, Carruth L, Finzi D, Shen X, DiGiuseppe JA, Taylor H, Hermankova M, Chadwick K, Margolick J, Quinn TC, *et al*: **Quantification of latent tissue reservoirs and total body viral load in HIV-1 infection.** *Nature* 1997, **387**:183-188.
12. Finzi D, Hermankova M, Pierson T, Carruth LM, Buck C, Chaisson RE, Quinn TC, Chadwick K, Margolick J, Brookmeyer R, *et al*: **Identification of a reservoir for HIV-1 in patients on highly active antiretroviral therapy.** *Science* 1997, **278**:1295-1300.
13. Zhang L, Ramratnam B, Tenner-Racz K, He Y, Vesanen M, Lewin S, Talal A, Racz P, Perelson AS, Korber BT, *et al*: **Quantifying residual HIV-1 replication in patients receiving combination antiretroviral therapy.** *N Engl J Med* 1999, **340**:1605-1613.
14. McGee B, Smith N, Aweeka F: **HIV pharmacology: barriers to the eradication of HIV from the CNS.** *HIV Clin Trials* 2006, **7**:142-153.
15. Sawchuk RJ, Yang Z: **Investigation of distribution, transport and uptake of anti-HIV drugs to the central nervous system.** *Adv Drug Deliv Rev* 1999, **39**:5-31.
16. Solas C, Lafeuillade A, Halfon P, Chadapaud S, Hittinger G, Lacarelle B: **Discrepancies between protease inhibitor concentrations and viral load in reservoirs and sanctuary sites in human immunodeficiency virus-infected patients.** *Antimicrob Agents Chemother* 2003, **47**:238-243.
17. De Clercq E: **Antiretroviral drugs.** *Curr Opin Pharmacol* 2010, **10**:507-515.
18. Taiwo B, Murphy RL, Katlama C: **Novel antiretroviral combinations in treatmentexperienced patients with HIV infection: rationale and results.** *Drugs* **70**:1629-1642.
19. Baba M: **Recent status of HIV-1 gene expression inhibitors.** *Antiviral Res* 2006, **71**:301-306.
20. Gatignol A: **Transcription of HIV: Tat and cellular chromatin.** *Adv Pharmacol* 2007, **55**:137-159.
21. Stevens M, De Clercq E, Balzarini J: **The regulation of HIV-1 transcription: molecular targets for chemotherapeutic intervention.** *Med Res Rev* 2006, **26**:595-625.
22. Baba M: **Cellular factors as alternative targets for inhibition of HIV-1.** *Antiviral Res* 1997, **33**:141-152.
23. De Clercq E: **New anti-HIV agents and targets.** *Med Res Rev* 2002, **22**:531-565.
24. Daelemans D, Vandamme AM, De Clercq E: **Human immunodeficiency virus gene regulation as a target for antiviral chemotherapy.** *Antivir Chem Chemother* 1999, **10**:1-14.
25. Darbinian-Sarkissian N, Darbinyan A, Otte J, Radhakrishnan S, Sawaya BE, Arzumanyan A, Chipitsyna G, Popov Y, Rappaport J, Amini S, Khalili K: **p27 (SJ), a novel protein in St John's Wort, that suppresses expression of HIV-1 genome.** *Gene Ther* 2006, **13**:288-295.
26. Lesner A, Shilpi R, Ivanova A, Gawinowicz MA, Lesniak J, Nikolov D, Simm M: **Identification of X-DING-CD4, a new member of human DING protein family that is secreted by HIV-1 resistant CD4(+) T cells and has anti-viral activity.** *Biochem Biophys Res Commun* 2009, **389**:284-289.
27. Berna A, Bernier F, Chabriere E, Elias M, Scott K, Suh A: **For whom the bell tolls? DING proteins in health and disease.** *Cell Mol Life Sci* 2009, **66**:2205-2218.
28. Elias M, Liebschner D, Gotthard G, Chabriere E: **Structural insights and ab initio sequencing within the DING proteins family.** *J Synchrotron Radiat* 2011, **18**:45-49.
29. Berna A, Bernier F, Chabriere E, Perera T, Scott K: **DING proteins; novel members of a prokaryotic phosphate-binding protein superfamily which extends into the eukaryotic kingdom.** *Int J Biochem Cell Biol* 2008, **40**:170-175.
30. Collombet JM, Elias M, Gotthard G, Four E, Renault F, Joffre A, Baubichon D, Rochu D, Chabriere E: **Eukaryotic DING proteins are endogenous: an immunohistological study in mouse tissues.** *PLoS One* 2010, **5**:e9099.
31. Contreras-Martel C, Carpentier P, Morales R, Renault F, Chesne-Seck ML, Rochu D, Masson P, Fontecilla-Camps JC, Chabriere E: **Crystallization and preliminary X-ray diffraction analysis of human phosphate-binding protein.** *Acta Crystallogr Sect F Struct Biol Cryst Commun* 2006, **62**:67-69.
32. Morales R, Berna A, Carpentier P, Contreras-Martel C, Renault F, Nicodeme M, Chesne-Seck ML, Bernier F, Dupuy J, Schaeffer C, *et al*: **Serendipitous discovery and X-ray structure of a human phosphate binding apolipoprotein.** *Structure* 2006, **14**:601-609.
33. Renault F, Chabriere E, Andrieu JP, Dublet B, Masson P, Rochu D: **Tandem purification of two HDL-associated partner proteins in human plasma, paraoxonase (PON1) and phosphate binding protein (HPBP) using hydroxyapatite chromatography.** *J Chromatogr B Analyt Technol Biomed Life Sci* 2006, **836**:15-21.
34. Fokine A, Morales R, Contreras-Martel C, Carpentier P, Renault F, Rochu D, Chabriere E: **Direct phasing at low resolution of a protein copurified with human paraoxonase (PON1).** *Acta Crystallogr D Biol Crystallogr* 2003, **59**:2083-2087.
35. Liebschner D, Elias M, Moniot S, Fournier B, Scott K, Jelsch C, Guillot B, Lecomte C, Chabriere E: **Elucidation of the phosphate binding mode of DING proteins revealed by subangstrom Xray crystallography.** *J Am Chem Soc* 2009, **131**:7879-7886.
36. Morales R, Berna A, Carpentier P, Contreras-Martel C, Renault F, Nicodeme M, Chesne-Seck ML, Bernier F, Dupuy J, Schaeffer C, *et al*: **[Discovery and crystallographic structure of human apolipoprotein].** *Ann Pharm Fr* 2007, **65**:98-107.
37. Webb MR: **A tale of the unexpected.** *Structure* 2006, **14**:391-392.
38. Diemer H, Elias M, Renault F, Rochu D, Contreras-Martel C, Schaeffer C, Van Dorsselaer A, Chabriere E: **Tandem use of X-ray crystallography and mass spectrometry to obtain ab initio the complete and exact amino acids sequence of HPBP, a human 38-kDa apolipoprotein.** *Proteins* 2008, **71**:1708-1720.
39. Gan ZR, Lewis SD, Stone JR, Shafer JA: **Reconstitution of catalytically competent human zeta-thrombin by combination of zeta-thrombin residues A1-36 and B1-148 and an Escherichia coli expressed polypeptide corresponding to zeta-thrombin residues B149-259.** *Biochemistry* 1991, **30**:11694-11699.
40. Leone C, Le Pavec G, Meme W, Porcheray F, Samah B, Dormont D, Gras G: **Characterization of human monocyte-derived microglia-like cells.** *Glia* 2006, **54**:183-192.
41. Rohr O, Lecestre D, Chasserot-Golaz S, Marban C, Avram D, Aunis D, Leid M, Schaeffer E: **Recruitment of Tat to heterochromatin protein HP1 via interaction with CTIP2 inhibits human immunodeficiency virus type 1 replication in microglial cells.** *J Virol* 2003, **77**:5415-5427.
42. Herbein G, Mahlknecht U, Batliwalla F, Gregersen P, Pappas T, Butler J, O'Brien WA, Verdin E: **Apoptosis of CD8+ T cells is mediated by macrophages through interaction of HIV gp120 with chemokine receptor CXCR4.** *Nature* 1998, **395**:189-194.
43. Larder BA, Darby G, Richman DD: **HIV with reduced sensitivity to zidovudine (AZT) isolated during prolonged therapy.** *Science* 1989, **243**:1731-1734.
44. Mosmann T: **Rapid colorimetric assay for cellular growth and survival: application to proliferation and cytotoxicity assays.** *J Immunol Methods* 1983, **65**:55-63.
45. Darbinian N, Czernik M, Darbinyan A, Elias M, Chabriere E, Bonasu S, Khalili K, Amini S: **Evidence for phosphatase activity of p27SJ and its impact on the cell cycle.** *J Cell Biochem* 2009, **107**:400-407.
46. Darbinian N, Gomberg R, Mullen L, Garcia S, White MK, Khalili K, Amini S: **Suppression of HIV-1 transcriptional elongation by a DING phosphatase.** *J Cell Biochem* 2011, **112**:225-232.

47. Mukerjee R, Deshmane SL, Darbinian N, Czernik M, Khalili K, Amini S, Sawaya BE: **St. John's Wort protein, p27SJ, regulates the MCP-1 promoter.** *Mol Immunol* 2008, **45**:4028-4035.
48. Cihlar T, Birkus G, Greenwalt DE, Hitchcock MJ: **Tenofovir exhibits low cytotoxicity in various human cell types: comparison with other nucleoside reverse transcriptase inhibitors.** *Antiviral Res* 2002, **54**:37-45.
49. Hazen R, Lanier ER: **Relative anti-HIV-1 efficacy of lamivudine and emtricitabine in vitro is dependent on cell type.** *J Acquir Immune Defic Syndr* 2003, **32**:255-258.
50. Garcia JA, Harrich D, Soultanakis E, Wu F, Mitsuyasu R, Gaynor RB: **Human immunodeficiency virus type 1 LTR TATA and TAR region sequences required for transcriptional regulation.** *Embo J* 1989, **8**:765-778.
51. Kingsman SM, Kingsman AJ: **The regulation of human immunodeficiency virus type-1 gene expression.** *Eur J Biochem* 1996, **240**:491-507.
52. Pereira LA, Bentley K, Peeters A, Churchill MJ, Deacon NJ: **A compilation of cellular transcription factor interactions with the HIV-1 LTR promoter.** *Nucleic Acids Res* 2000, **28**:663-668.
53. Rohr O, Marban C, Aunis D, Schaeffer E: **Regulation of HIV-1 gene transcription: from lymphocytes to microglial cells.** *J Leukoc Biol* 2003, **74**:736-749.
54. Deeks SG: **Treatment of antiretroviral-drug-resistant HIV-1 infection.** *Lancet* 2003, **362**:2002-2011.
55. Kozal MJ: **Drug-resistant human immunodefiency virus.** *Clin Microbiol Infect* 2009, **15(Suppl 1)**:69-73.
56. Rochu D, Chabriere E, Renault F, Elias M, Clery-Barraud C, Masson P: **Stabilization of the active form(s) of human paraoxonase by human phosphate-binding protein.** *Biochem Soc Trans* 2007, **35**:1616-1620.
57. Parra S, Alonso-Villaverde C, Coll B, Ferre N, Marsillach J, Aragones G, Mackness M, Mackness B, Masana L, Joven J, Camps J: **Serum paraoxonase-1 activity and concentration are influenced by human immunodeficiency virus infection.** *Atherosclerosis* 2007, **194**:175-181.
58. Parra S, Marsillach J, Aragones G, Beltran R, Montero M, Coll B, Mackness B, Mackness M, Alonso-Villaverde C, Joven J, Camps J: **Paraoxonase-1 gene haplotypes are associated with metabolic disturbances, atherosclerosis, and immunologic outcome in HIV-infected patients.** *J Infect Dis* 2010, **201**:627-634.

doi:10.1186/1743-422X-8-352
Cite this article as: Cherrier *et al.*: Human-Phosphate-Binding-Protein inhibits HIV-1 gene transcription and replication. *Virology Journal* 2011 **8**:352.

F. Etude *in vitro* et *in vivo* du niveau d'expression des protéines DING chez les patients infectés par le VIH-1

The level of DING proteins is increased in HIV-infected patients: *in vitro* and *in vivo* studies

Ahmed DJEGHADER, Gerard ARAGONÈS, Nune DARBINIAN, Mikael ELIAS, Daniel GONZALEZ, Anabel GARCÍA-HEREDIA, Raúl BELTRÁN-DEBÓN, Rafal KAMINSKI, Guillaume GOTTHARD, Julien HIBLOT, Anna RULL, Olivier ROHR, Christian SCHWARTZ, Carlos ALONSO-VILLAVERDE C, Jorge JOVEN, Jordi CAMPS, Eric CHABRIERE

Dans cet article, j'ai été associé à la conception des expériences et l'interprétation des résultats.

Résumé : Cet article de recherche concerne l'étude *in vitro* et *in vivo* du taux d'expression des protéines DING chez l'homme.

Cette étude part du constat suivant : alors que HPBP est purifiée à partir du plasma humain et inhibe le VIH-1, l'homme n'est pas immunisé contre ce virus. Pour répondre à cette question, un dosage ELISA des protéines DING dans des cohortes de patients infectés ou non par le VIH-1 fut réalisé. Il fut mis en évidence que l'expression des protéines DING est corrélée à l'infection par le virus, les patients présentant un taux de protéines DING environs trois fois supérieurs aux non-infectés. De plus, l'étude tend à suggérer que le taux de protéines DING plasmatiques soit également lié à l'infection par d'autres virus tels que l'HCV. Les données *in vivo* furent confirmées par des westerns blots des protéines DING en modèle cellulaire infecté par le VIH-1 qui montra également l'induction des protéines DING.

OPEN ACCESS Freely available online

PLoS one

The Level of DING Proteins Is Increased in HIV-Infected Patients: *In Vitro* and *In Vivo* Studies

Ahmed Djeghader[1], Gerard Aragonès[2], Nune Darbinian[3], Mikael Elias[4], Daniel Gonzalez[1], Anabel García-Heredia[2], Raúl Beltrán-Debón[2], Rafal Kaminski[3], Guillaume Gotthard[1], Julien Hiblot[1], Anna Rull[2], Olivier Rohr[5], Christian Schwartz[5], Carlos Alonso-Villaverde[6], Jorge Joven[2], Jordi Camps[2]*, Eric Chabriere[1]*

1 Unité de Recherche sur les Maladies Infectieuses et Tropicales Emergentes, Centre National de la Recherche Scientifique, Faculté de Médecine Aix-Marseille University, Marseille, France, **2** Centre de Recerca Biomèdica, Hospital Universitari de Sant Joan, Institut d'Investigació Sanitària Pere Virgili, Universitat Rovira i Virgili, Reus, Catalonia, Spain, **3** Department of Neuroscience, Center for Neurovirology, Temple University School of Medicine, Philadelphia, Pennsylvania, United States of America, **4** Department of Biological Chemistry, Weizmann Institute of Science, Rehovot, Israel, **5** Institut de Parasitologie et Pathologie Tropicale, Université de Strasbourg, Strasbourg, France, **6** Servei de Medicina Interna, Hospital de Son Llàtzer, Ciutat de Palma, Mallorca, Spain

Abstract

DING proteins constitute an interesting family, owing to their intriguing and important activities. However, after a decade of research, little is known about these proteins. In humans, at least five different DING proteins have been identified, which were implicated in important biological processes and diseases, including HIV. Indeed, recent data from different research groups have highlighted the anti-HIV activity of some DING representatives. These proteins share the ability to inhibit the transcriptional step of HIV-1, a key step of the viral cycle that is not yet targeted by the current therapies. Since such proteins have been isolated from humans, we undertook a comprehensive study that focuses on the relationship between these proteins and HIV-infection in an infectious context. Hence, we developed a home-made ELISA for the quantification of the concentration of DING proteins in human serum. Using this method, we were able to determine the concentration of DING proteins in healthy and HIV-infected patients. Interestingly, we observed a significant increase of the concentration of DING proteins in non treated and treated HIV-infected patients compared to controls. In addition, cell cultures infected with HIV also show an increased expression of DING proteins, ruling out the possible role of antiretroviral treatment in the increase of the expression of DING proteins. In conclusion, results from this study show that the organism reacts to HIV-infection by an overexpression of DING proteins.

Citation: Djeghader A, Aragonès G, Darbinian N, Elias M, Gonzalez D, et al. (2012) The Level of DING Proteins Is Increased in HIV-Infected Patients: *In Vitro* and *In Vivo* Studies. PLoS ONE 7(3): e33062. doi:10.1371/journal.pone.0033062

Editor: Derya Unutmaz, New York University, United States of America

Received November 22, 2011; **Accepted** February 3, 2012; **Published** March 9, 2012

Funding: This study was supported by grants from the Instituto de Salud Carlos III (PI 05/1607, 08/1032 and 08/1175), Madrid, Spain. M.E. is a fellow supported by the IEF Marie Curie program (grant No. 252836). The funders had no role in study design, data collection and analysis, decision to publish, or preparation of the manuscript.

Competing Interests: The authors have declared that no competing interests exist.

* E-mail: jcamps@grupsagessa.com (JC); eric.chabriere@univmed.fr (EC)

Introduction

DING proteins constitute an intriguing family of proteins that were named for their highly conserved N-terminal sequence DINGGG- [1,2]. The first DING protein was discovered in humans [3], and other members have been further identified in the three kingdoms of life [4]. To date, about 40 different DING proteins have been reported, mainly in eukaryotes [5]. Despite the wide presence of these proteins, DING genes have never been identified in eukaryotes, even in the human genome [5]. Attempts to sequence eukaryotic DING genes have encountered many difficulties since no ORF or locus coding these proteins has been identified. Nevertheless, some partial nucleic sequences have been amplified from humans and plants [4] [Genbank HM171537 and Genbank HM572267 to HM572271]. Because of the lack of available genetic information, eukaryotic DING proteins sequences are very sparse and comprise, for the most of them, only some N-terminal and internal peptides [5]. This lack of sequence information has considerably hampered studies on DING proteins, but opens a large field of investigation onto this family of proteins.

In humans, at least five different DING proteins have been reported, generally identified in relation with a broad range of diseases or biological processes [4]. The sequence divergence observed between available pieces of sequences suggests that they are not products of polymorphisms, editing or splicing mechanisms. The Synovial Stimulatory Protein (SSP) was the first discovered DING protein and was hypothesized to be related to the etiology of rheumatoid arthritis [3]. The Crystal Adhesion Inhibitor (CAI) was isolated by virtue of its capacity to inhibit the formation of kidney stones [6]. Khan *et al.* reported the discovery of the Steroidogenisis-Inducing Protein (SIP) and its potent activity toward ovarian surface epithelium [7]. Recently, studies to define the resistant factor from HIV resistant cells led to identification of a new DING protein, X-DING CD4, that exhibits a human immunodeficiency virus-1 (HIV-1) inhibition activity [8]. This protein was only detectable in HIV-resistant cells, and its anti-HIV-mediated activity was blocked by specific antibodies [8]. Finally, the Human Phosphate Binding Protein (HPBP) was serendipitously discovered while performing structural studies on human paraoxonase-1 (PON1), a high-density lipoprotein (HDL)

associated apolipoprotein with anti-atherogenic activity [9]. PON1 is an extensively studied protein that exhibits paraoxonase, lactonase and arylesterase activity, and participates in the antioxidant defense system [10,11]. HPBP was found to form a very tight complex with PON1 [12], and it has been shown to be necessary for the stabilization of this protein [13,14,15]. The X-ray structure of HPBP has been solved [9], and the combination of crystallographic and mass spectrometry data has lead to the obtaining of the first complete sequence of a DING protein [9,16]. Structural analysis of HPBP showed that DING proteins belong to a superfamily of high affinity phosphate binding proteins. Thus, HPBP may be considered as the first phosphate transporter identified so far in humans. However, the function related to this ability is still unknown. Recently, it has been shown that HPBP, as for X-DING CD4, has an anti-HIV activity. Interestingly, HPBP was also able to inhibit specific strains of HIV which are resistant to treatment with zidovudine (AZT), an antiretroviral drug [17].

The HIV inhibition activity within the DING family has also been described outside humans, for p27SJ and its full-length form p38SJ, a plant DING protein from *Hypericum perforatum* [18]. The biological role of this protein is not fully understood, but it is however clear that its phosphatase activity influences the cell cycle [19,20]. Additionally, it has been shown that p27SJ/p38SJ interact with the viral protein Tat, the transcription factor C/EBP and the RNA Polymerase II to inhibit HIV proliferation [18,20]. In fact, p27SJ as well as X-DING CD4 and HPBP inhibit HIV replication by targeting the transcription step in HIV cycle, a viral step that is not yet targeted by the currently used therapies.

HIV-infection is still a public health problem, affecting more than 33 million peoples in the world [21]. Current HIV therapies are based on the using of at least three drugs belonging to two different classes of antiretroviral drugs. Antiretroviral drugs can be divided in seven classes: a) nucleoside reverse transcriptase inhibitors (NRTIs); b) nucleotide reverse transcriptase inhibitors (NtRTIs); c) nonnucleoside reverse transcriptase inhibitors (NNRTIs); d) protease inhibitors (PIs); e) fusion inhibitors; f) co-receptor inhibitors, and g) integrase inhibitors [21,22]. Drugs from each class target a different stage of HIV replication cycle, but none of them targets the transcription step. The discovery that some DING proteins target this step of HIV cycle opens new insights to understand the development of the disease, and might be useful to develop new anti-HIV treatment strategies. The presence in humans of two proteins with anti-HIV activity (HPBP and X-DING CD4) is intriguing and request more investigations. Thus, we carried out this study with the aim of exploring the relationship between HIV infection and the DING proteins concentration.

Materials and Methods

Study population

The study was performed on 207 HIV-infected patients (139 men, 68 women; mean age 38 years; range 22 to 66) attending the outpatients clinics of the Hospital Universitari de Sant Joan. Of these patients, 122 were co-infected by the hepatitis C virus (HCV). HIV-infected patients were undergoing two different treatment regimens. Fifty-two subjects were currently not receiving any type of antiretroviral therapy for at least 6 months (13 patients have never been treated and the 39 others stopped treatment more than 6 months), and 155 had received continuous treatment with an antiretroviral regimen containing zidovudine, stavudine or lamivudine (NRTIs). In addition to this antiretroviral treatment, HIV-infected patients were taking lopinavir/ritonavir (PIs; n = 71) or efavirenz (NNRTI; n = 84) for at least 6 months. The exclusion criteria were age under 18 years, renal function impairment defined as creatinine levels higher than 106 μmol/l, or presence of an AIDS-related opportunistic disease at the time of the study. The main clinical characteristics of these patients are summarized in Table S1. The control group consisted of 130 healthy volunteers who participated in an ongoing epidemiological study being conducted in our geographical area, and the details of which have been previously reported [23]. All the volunteers had been invited to attend a clinical examination and to provide a fasting blood sample. There was no clinical or analytical evidence of renal insufficiency, liver damage, neoplasia, or neurological disorders.

A fasting venous sample blood was obtained from all the participants and serum was stored at −80°C until measurements were performed. All the participants provided fully-informed written consent to participation in the study on the understanding that anonymity of all data is guaranteed. The study was approved by the Ethics Committee of the Hospital Universitari de Sant Joan de Reus (Institutional Review Board).

Determination of serum concentration of DING proteins

Serum concentration of DING proteins was measured by in-house ELISA using rabbit polyclonal antibodies generated against HPBP. Details of the purification methods and antibody production have been previously reported [12,24]. Because of the high sequence conservation between DING proteins, anti-HPBP antibodies are able to recognize several representatives of the DING family. As a standard, we used PfluDING (a DING protein from *Pseudomonas fluorescens* that shares 77% sequence identity with HPBP), with an initial concentration of 204 ng/ml, prepared in phosphate buffered saline (PBS). The secondary antibody was an anti-rabbit-IgG peroxidase conjugate (Invitrogen, Carlsbad, USA), diluted 1:3,000 in PBS/1% BSA. The enzyme substrate was tetramethylbenzidine (Sigma, St. Louis, MO, USA) plus hydrogen peroxide. Tetramethylbenzidine (2 mg) was diluted in 200 μl of dimethylsulfoxide (DMSO) (Sigma, St. Louis, MO, USA) and added to 20 ml of 0.1 M citrate/acetate buffer, pH 6.0, with 72 μl urea hydrogen peroxide.

The ELISA procedure was the following: human serum samples were diluted 1:1,000 in PBS. One hundred μl of sample or standard were added to the plate wells and incubated overnight at room temperature. After one wash with PBS, we added 150 μl of PBS/1% BSA to block the remaining absorption sites, and left for 1 hour at room temperature. After three washes, we added 100 μl of primary antibody (1:3,000) and incubated for 1 hour at room temperature. After washing, we added 200 μl of secondary antibody, and incubated the plates again for 1 hour at room temperature. After washing, we added 200 μl of enzyme/substrate solution and incubated for 15 min. The reaction was stopped with 50 μl of 2 M H_2SO_4, and the absorbance was read at 450 nm in an automated microplate reader (BioTek Instruments Inc., Winooski, VT, USA). All the incubations were under gentle shaking. The assays were performed on 96-well low binding plates (Scientific Laboratory Supplies Ltd., Yorkshire, UK).

Other biochemical and serological measurements

Serum PON1 concentration was determined by in-house ELISA with rabbit polyclonal antibodies generated against a synthetic peptide with the sequence CRNHQSSYQTRLNAL-REVQ that is specific of mature PON1 [25]. Serum PON1 lactonase activity was analyzed by measuring the hydrolysis of 5-thiobutyl butyrolactone (TBBL) as previously described [26,27]. Serum PON1 paraoxonase activity was determined by measuring the rate of hydrolysis of paraoxon [28]. Plasma HIV-1 viral load was measured with the COBAS® TaqMan® HIV-1 assay (Roche,

Basel, Switzerland) and CD4+ T-cell and CD8+ T cell counts by flow cytometry (Coulter Epics XL-MLC, Beckman Coulter, Fullerton, CA, USA). Antibodies against HCV, serum β-2-microglobulin, a marker of lymphocyte destruction and progression of HIV-infection [29], and serum cholesterol, triglycerides, HDL-cholesterol, and apolipoprotein A-I were measured in an automated analyzer (UniCel^{TM} DxI 800, Beckman Coulter, Fullerton, CA, USA). LDL-cholesterol concentration was estimated by the Friedewald formula [30].

FPLC lipoprotein fractionation

DING proteins distribution in lipoproteins was investigated by FPLC (Bio-Rad BioLogic DuoFlow 10 system, Bio-Rad Laboratories, Inc. Hercules, CA). Sera from 2 control subjects and 2 HIV-infected patients were pooled separately, 200 µl from each pool were injected into a Superose 6/300 GL column (GE Healthcare Europe GmbH, Glattbrugg, Switzerland), and 500 µl fractions were collected. DING proteins levels, cholesterol and triglycerides were analyzed in every fraction as previously described.

Statistical analysis

The normality of distributions was determined with the Kolmogorov-Smirnov test. Differences between two groups were assessed with the Student's *t*-test (parametric) or the Mann-Whitney *U* test (non-parametric). Differences between multiple groups were analyzed by the Kruskal-Wallis test. Pearson or Spearman correlation coefficients were used to evaluate the degree of association between variables. The SPSS 18.0 package was employed for all statistical calculations. Receiver Operating Characteristics (ROC) analysis was employed to investigate the ability of DING proteins measurement to distinguish between HIV-infected patients and controls [31]. The curve was plotted using Xlstat software (Addinsoft, http://www.xlstat.com/en/home/).

Infection of peripheral blood mononuclear cells (PBMC) with HIV-1

PBMC were maintained in modified RPMI media. PBMC were infected with the JR-FL strain of HIV-1 as follows. In all, 50 ng of p24-containing virus stock was added to every 1×10^6 cells. Cells were incubated with virus stock in a small volume of serum-free medium for 2 h at 37°C. The cells were then washed twice PBS, and fresh medium was added. In parallel, control uninfected cells were prepared four days post-HIV-1-infection. Cells were harvested and analyzed by western-blot assay and ELISA as described below. Western blot analysis was performed with protein extracts using anti-HPBP, and anti-tubulin antibodies according to standard procedures.

p24 ELISA

Approximately 1×10^6 PBMC were infected with HIV-1 JF-RL. Six days post-infection, supernatants were collected and analyzed for the presence of p24 by ELISA assay using p24 ELISA Assay kit purchased from BioChain (BioChain Institute, Inc., Hayward, CA). The assay was measured spectrophotometrically using 450 nm filter to indicate the concentration of p24 reactive determinants present in samples.

Results

DING proteins concentration is increased in HIV-infected patients

Serum DING proteins concentration was significantly increased in HIV-infected patients with respect to the control group [18.3 (11.0–28.3) vs. 7.9 (4.2–11.2) mg/l, respectively; $p<0.001$] (Fig. 1A). The diagnostic value of our ELISA dosage was investigated using ROC curve by plotting the true positive rate (sensitivity) against the false positive rate (1- specificity). The best diagnostic test is a test in which the curve is the most closer to the upper left corner of the graph. The accuracy of the test is measured by the area under the curve (AUC) which could be different from 0.5 (non discrimination) and the closest to 1. Our ROC analysis showed an AUC of 0.813 (95%CI: 0.769 to 0.858). This value, close to 1.0 indicates that measuring DING proteins concentration may be considered as a potential predictive factor for HIV-infection (Fig. 1B).

Relationships between serum DING proteins concentration, PON1 status and lipoprotein alterations

Results are summarized in Fig. 2 and Table 1. HIV-infected patients had an altered lipoprotein profile with an increase in

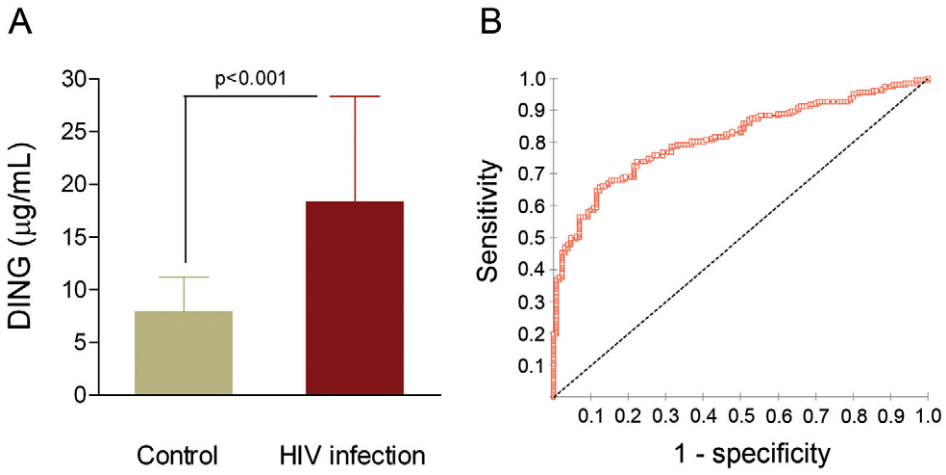

Figure 1. DING proteins concentrations and ROC curve obtained for the ELISA assay. (**A**) Variation of concentration between HIV-infected patients and controls; results are represented as medians and interquartile range (IQR). (**B**) ROC curve obtained for the ELISA assay; dashed line show the line of non discrimination.
doi:10.1371/journal.pone.0033062.g001

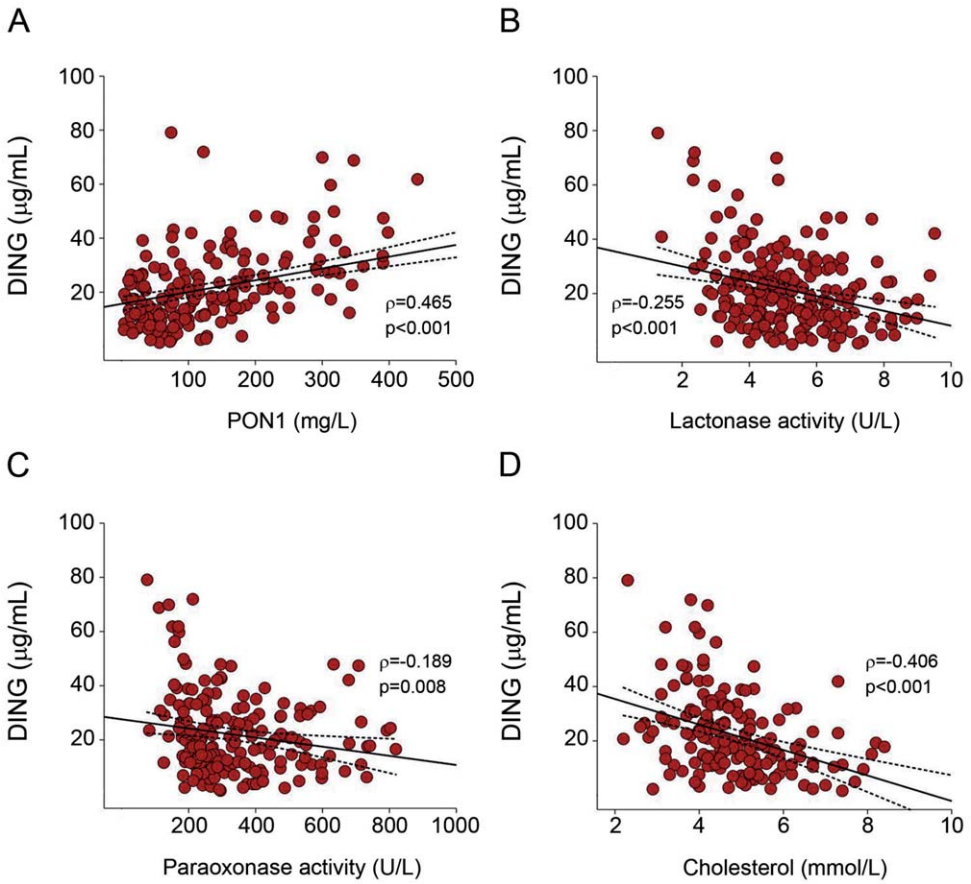

Figure 2. Relationship between DING proteins concentration, PON1 status and cholesterol. Correlation of DING proteins concentration with: (**A**) serum PON1 concentrations, (**B**) PON1 lactonase activity, (**C**) PON1 paraoxonase activity and (**D**) cholesterol concentration in HIV-infected patients.
doi:10.1371/journal.pone.0033062.g002

serum triglycerides concentration and a decrease in cholesterol in LDL and HDL fractions. A significant direct relationship was observed between serum DING proteins and PON1 concentrations in HIV-infected patients ($r = 0.465$; $p<0.001$; Fig. 2A), and an inverse relationship between DING proteins and PON1 lactonase ($r = -0.255$; $p<0.001$; Fig. 2B) and paraoxonase activities ($r = -0.189$; $p = 0.008$; Fig. 2C). DING proteins concentration was also inversely associated with serum cholesterol ($r = -0.406$; $p<0.001$; Fig. 2D), LDL-cholesterol ($r = -0.310$; $p<0.001$), HDL-cholesterol ($r = -0.174$; $p = 0.016$), serum triglycerides ($r = -0.146$; $p = 0.050$), and apolipoprotein A-I ($r = -0.221$; $p = 0.002$) concentrations.

Table 1. Selected biochemical parameters in the control group and in HIV-infected patients.

Parameter	Control group (n = 130)	HIV-infected patients (n = 207)	p*	Untreated (n = 52)	Treated (n = 155)	p†
Cholesterol (mmol/L)	5.28 (0.98)	4.89 (1.23)	<0.001	4.47 (0.93)	5.03 (1.29)	0.007
Triglycerides (mmol/L)	1.1 (0.5–2.6)	1.5 (0.6–8.5)	<0.001	1.1 (0.6–4.1)	1.8 (0.7–8.6)	<0.001
HDL-cholesterol (mmol/L)	1.48 (0.39)	1.18 (0.45)	<0.001	1.19 (0.37)	1.17 (0.46)	NS
LDL-cholesterol (mmol/L)	3.20 (0.95)	2.75 (0.96)	<0.001	2.57 (0.79)	2.82 (1.01)	NS
Apolipoprotein A-I (g/L)	1.69 (0.28)	1.38 (0.31)	<0.001	1.38 (0.31)	1.38 (0.31)	NS
PON1 concentration (mg/L)	96.5 (43.6–291)	98.9 (14.1–347)	NS	115.9 (13.7–571)	93.5 (13.7–338)	0.06
PON1 lactonase activity (U/L)	5.4 (3.2–8.8)	5.2 (2.8–8.5)	NS	4.9 (2.3–8.1)	5.1 (2.9–8.3)	NS
PON1 paraoxonase activity (U/L)	278.2 (161–580)	285.7 (153–679)	NS	275.3 (123–678)	285.9 (171–709)	NS

Results are presented as means and SD in parentheses (parametric) or as medians and 95% CI in parenthesis (nonparametric). NS: Not significant.
*Control group *versus* all HIV-infected patients.
†Treated *versus* untreated HIV-infected patients.
doi:10.1371/journal.pone.0033062.t001

FPLC lipoproteins fractionation

In the control pool, DING proteins were eluted in HDL fractions, together with PON1, but also in IDL particles, an intermediate form between VLDL and LDL. A substantial amount of DING proteins was observed in the lipoprotein deficient serum (LPDS) from fractions 25 to 45, corresponding to soluble, free or DING proteins bound to albumin or other serum proteins. The HIV-infected pool showed a similar pattern of distribution, but with a global increase that was especially marked in the HDL and free DING proteins fractions (Fig. 3).

Relationships between serum DING proteins concentration and the immunological and virological outcomes

DING proteins concentration was directly associated with viral load ($r = 0.332$; $p<0.001$). HIV-infected patients with a negative HIV-1 plasma viral load had significantly lower serum DING proteins concentration than those with a positive viral load [14.6 (2.7–48.0) vs. 24.1 (7.5–50.5) mg/l, respectively; $p<0.001$]. A highly significant inverse association was observed between serum DING proteins concentration and CD4+ T cell counts ($r = -0.275$; $p<0.001$) (Fig. 4A), and with the CD4+/CD8+ ratio ($r = -0.270$; $p = 0.001$). There was a highly significant linear direct relationship between serum DING proteins and β-2-microglobulin concentrations ($r = 0.666$; $p<0.001$; Fig. 4B). Co-infection with HCV was also associated with a significantly higher serum DING proteins concentration [21.0 (4.8–56.8) vs. 14.6 (3.5–44.5) mg/l, respectively; $p = 0.016$].

Influence of treatments on serum DING proteins concentrations in HIV-infected patients

Serum DING proteins concentration was significantly affected by the type of antiretroviral treatment followed. As shown in Fig. 5A, both untreated HIV-infected patients and patients treated with PIs had higher levels of DING proteins than those undergoing a NNRTIs-based antiretroviral treatment regimen [26.9 (17.4–38.9) and 24.0 (15.4–34.5) vs 17.2 (8.4–26.3) mg/l; respectively]. Moreover, we observed a significant inverse

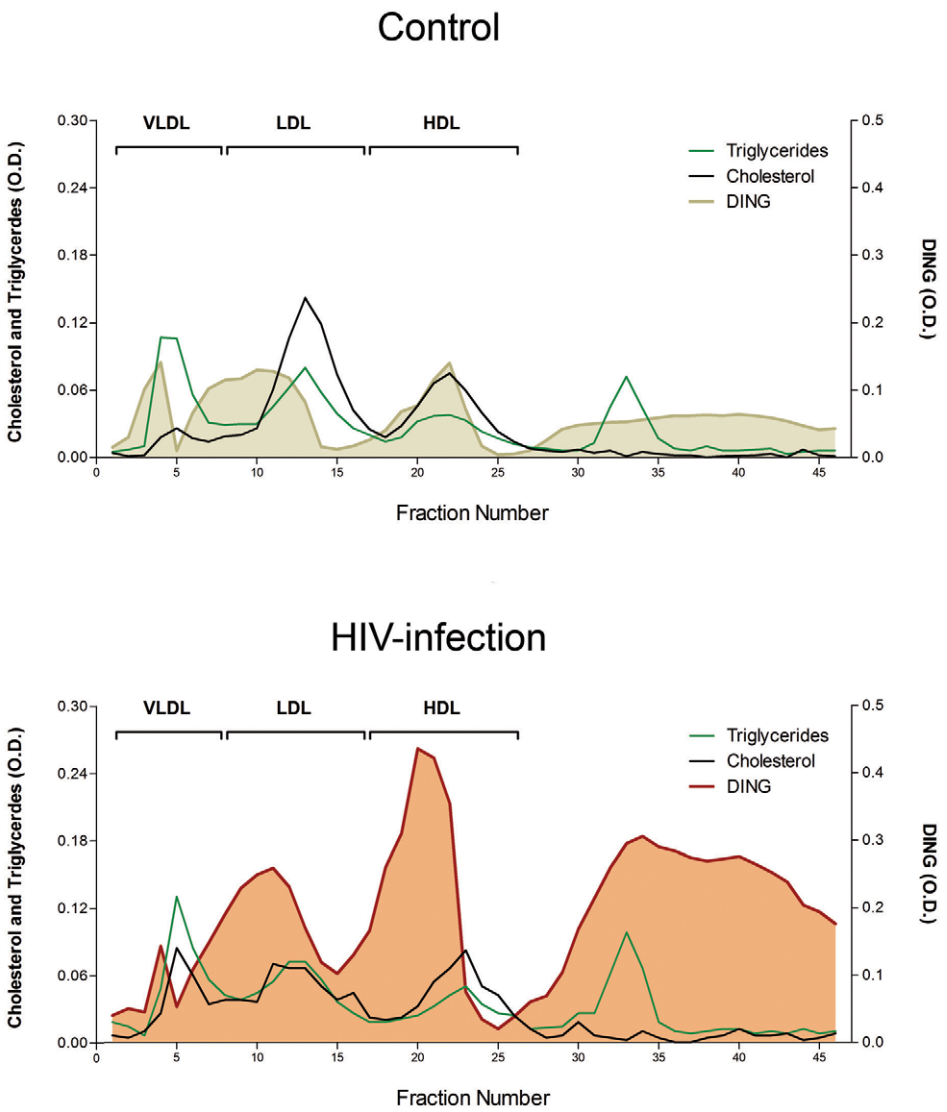

Figure 3. DING proteins distribution in lipoproteins fractions from HIV-infected and control pool. Pools of two HIV-infected patients and two controls were used in this experiment; results are represented as the optical densities at 450 nm.
doi:10.1371/journal.pone.0033062.g003

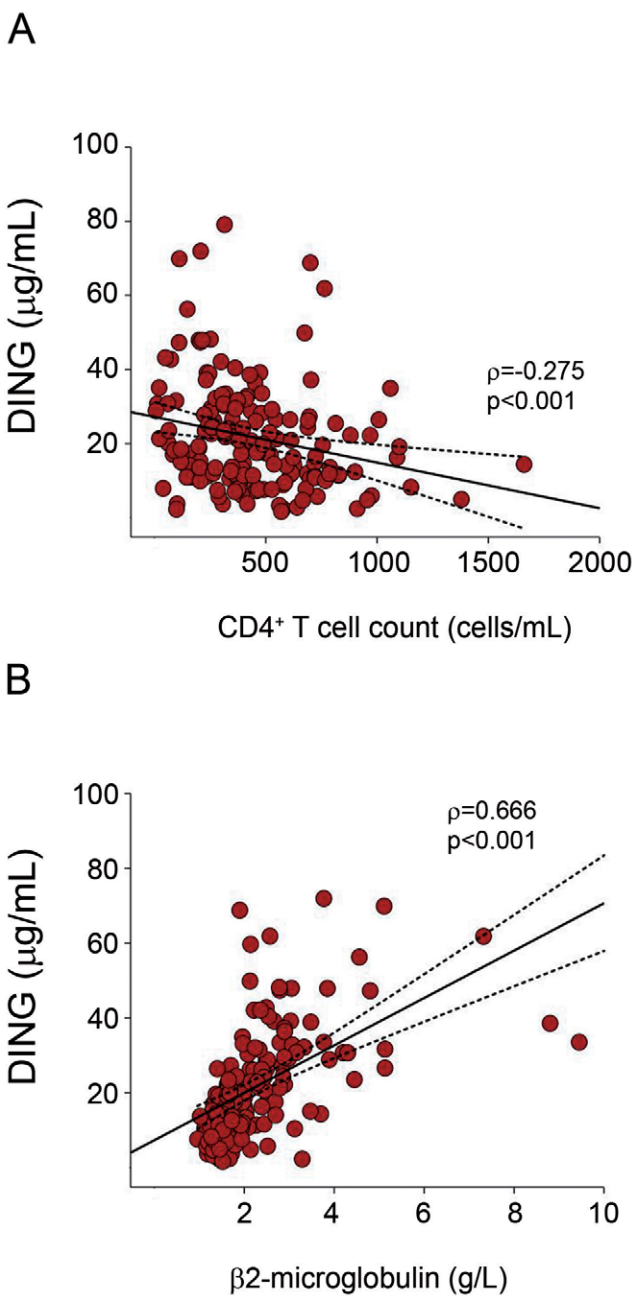

Figure 4. Relationship between DING proteins concentrations and some HIV markers. Correlation of DING proteins concentration with (**A**) CD4+ T cell counts and (**B**) β-2-microglobulin in HIV-infected patients.
doi:10.1371/journal.pone.0033062.g004

relationship between serum DING proteins concentration and the duration of the antiretroviral treatment with NNRTI ($r = -0.309$; $p = 0.012$), but not in HIV-infected patients receiving PIs ($r = -0.059$; $p = 0.408$) (Fig. 5B).

In vitro HIV-infection of cell culture

Infection of human PBMC with HIV-1 caused overproduction of DING proteins detected by monoclonal anti-HPBP antibody (Figure 6 A, top panel, lane 2) compared to uninfected cells (Lane 1). HIV-1 replication on the sixth day post-infection was also confirmed by p24 ELISA for the presence of HIV-1 p24 protein (Figure 6 B). Data from this experiment suggest that DING proteins seem to be expressed in response to HIV infection.

Discussion

Recent studies on DING proteins have highlighted the anti-HIV potential of some members of this family [8,17,18,20]. During this study, we have developed a homemade ELISA for the quantification of serum DING proteins. Using this method, we were able to measure for the first time the concentration of serum DING proteins in healthy people (7.9 (4.27–11.24) mg/l). In contrast, our results show that DING proteins concentration was increased in both serum and lipoproteins fractions of HIV-infected patients with respect to controls. This increase is likely to be a response of the organism to HIV infection. However, the pathophysiological significance of this increase remains unclear. In addition, cell cultures infected with HIV show also an overexpression of DING proteins. This overexpression was not related to treatment side effects since these cells were not treated with any antiretroviral medication.

Expression of DING proteins in response to HIV-infection has been previously reported by Simm et al. [32,33]. Indeed, it has been shown that primary CD4+ T cells exposed to an attenuated form of HIV-1 (*Δvif* HIV-1) acquire resistance to the wild-type virus [32,33]. Interestingly, these resistant cells were permissive to virus entry, reverse transcription of RNA, integration of the viral genome in the DNA of the cell, but were able to block transcription of HIV-1 genes [33]. Moreover, it has been shown that this phenotype was mediated via the production of a DING protein that they have named X-DING CD4 (formerly HIV resistance factor or HRF) [8]. Recently, it has been shown that HIV-exposure of these resistant cells causes a rapid up-regulation of X-DING CD4 at the mRNA level [34]. Given this potent anti-HIV activity, the author proposed that this factor may be considered as a part of an ancient defense mechanism of the organism against HIV [34,35]. In fact, recent discoveries have shown that human cells are able to produce a so called "restriction factors" that interfere with HIV and other retroviruses replication. Particularly, APOBEC3, Tethrin, TRIM5, defensins and other antiretroviral factors has been shown to block HIV at different stages of its replication cycle [35,36,37,38]. It has been proposed that these factors could be part of an ancient defense mechanism against HIV, which has otherwise evolved a "toolkit" to overcome their effects. From the known anti-HIV potential of some human DING representatives, it is not to be excluded that DING proteins may make part of this unusual defense mechanism against HIV or other viruses.

We have also observed a significant direct relationship between DING proteins and PON1 concentration in HIV-infected patients. This increase may be explained by the recently described association between PON1 and the DING protein HPBP. Indeed, in human plasma HPBP and PON1 were found to be tightly associated, and it has been shown that this association is required for the stability of each other [13,14]. However, an inverse relationship was observed between the concentration of DING proteins and both PON1 lactonase and paraoxonase activities. In fact, it is known that PON1 activities are greatly modulated by its molecular environment on HDL particles. In addition, PON1 need to be bound to HDL for its optimum activity [39]. Since PON1 can be tightly associated with HPBP on HDL surface, a modulation of its activity by HPBP seems to be possible.

Our experiments on the fractionation of lipoproteins give new information about DING proteins localization. Our results show that DING proteins are localized mainly on HDL and IDL

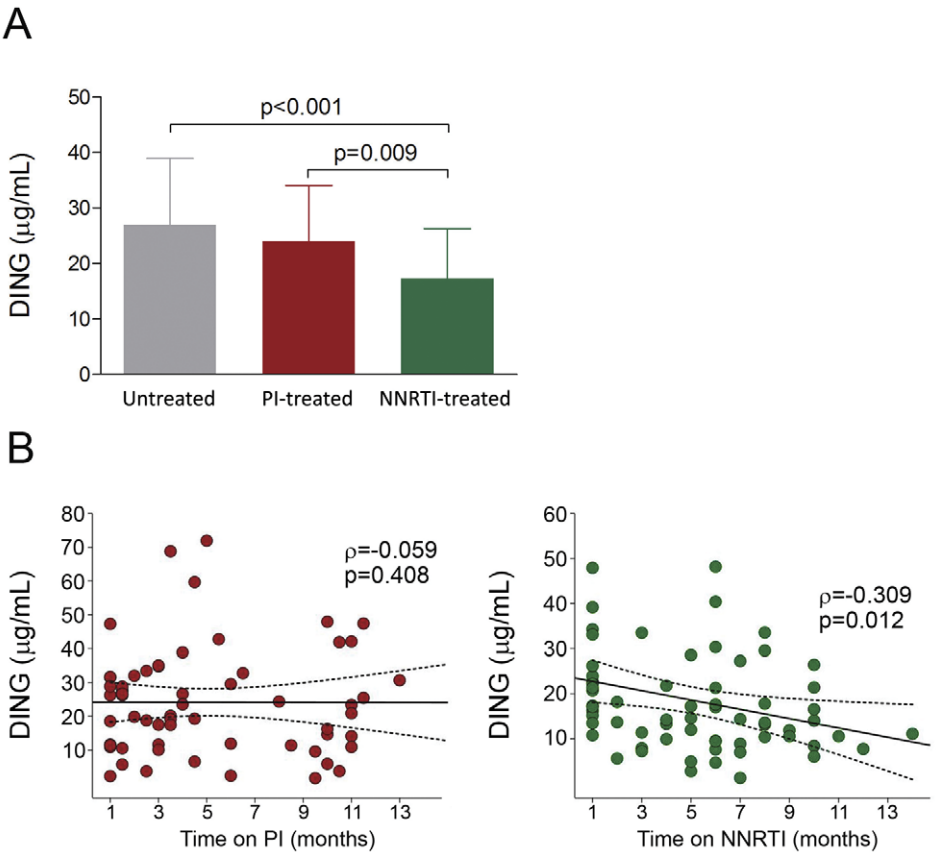

Figure 5. Influence of treatment on DING proteins concentration. (**A**) Effect of PIs and NNRTIs based treatment on DING proteins concentration compared to naives HIV-infected patients; results are represented as medians and IQRs. (**B**) Relationship between DING proteins concentration and type/duration of NNRTIs or PIs treatment.
doi:10.1371/journal.pone.0033062.g005

particles, an intermediate form between VLDL and LDL. Given the association between HPBP and the HDL-associated PON1, it seems that DING proteins found on IDL are directly linked or in association with other proteins. We found also a substantial amount of DING proteins in a free form in the LPDS fractions. This finding indicates that DING proteins may also be present in free form as circulating proteins, maybe in association with other proteins, but not linked to any lipoprotein particle. Identification of these putative partners will be helpful to better understand their physiological functions.

We investigated the relationship between DING proteins concentration and several HIV markers like CD4 counts, β-2-microglobulin and viral load. Our results show an inverse relationship between DING proteins concentration and CD4 counts. Interestingly, a very strong direct association with β-2-microglobulin has been observed. It is worth to be noted that

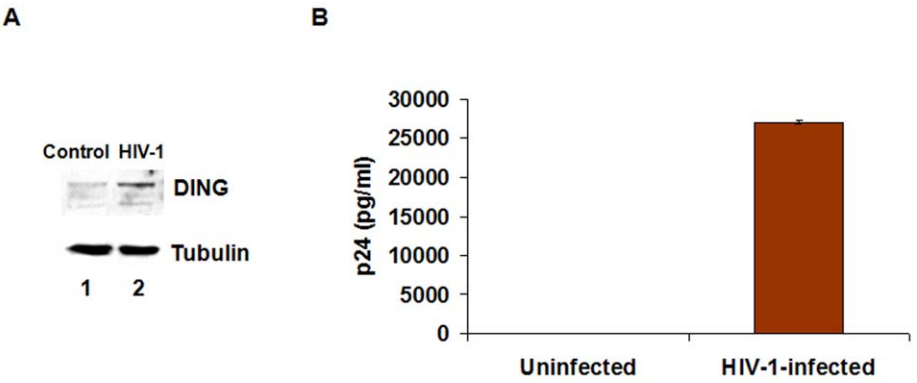

Figure 6. *In vitro* HIV-infection of cell culture and its impact on the expression of DING proteins. (**A**) Expression of DING proteins detected by western blot using anti-HPBP antibody in HIV-infected cells (right panel) or non infected control cells (left panel). (**B**) p24 antigen quantified 6 days post-infection using a p24-ELISA.
doi:10.1371/journal.pone.0033062.g006

many studies consider β-2-microglobulin as an effective marker of HIV disease progression [29,40]. Combined with our results from ROC curve analysis, we suggest that serum DING proteins dosage may be considered as a potential predictor factor of HIV. In addition, DING proteins concentration was directly associated with the viral load. Interestingly, HIV-infected patients with a negative viral load kept a relatively high concentration of DING proteins compared to controls. It seems that once infected, the organism stay producing relatively high amounts of DING proteins. The molecular mechanisms responsible of this response are still unknown and need to be further studied.

Another intriguing finding was the effect of treatment on the DING proteins concentration. In fact, in contrary to antiproteases, treatment with non-nucleoside reverse transcriptase inhibitors was correlated with a decrease of DING proteins concentration. It seems possible that overexpression of DING proteins occurs between these two steps targeted by the therapy. May viral genome integration induce DING proteins overexpression? Indeed, many studies have shown that HIV infection can modulate the expression of several genes [41,42]. Hence, a direct implication of HIV on the expression of DING proteins is not to be excluded.

Our results, together with the presence in humans of DING proteins with anti-HIV activity (HPBP and X-DING CD4), raise a major question of why this increase is not correlated with a resistance to HIV infection. One possibility is that DING proteins are not "bioavailable" and cannot inhibit HIV when associated with other proteins. For instance, HPBP is not active against HIV when associated with PON1 [17]. So we can think about a mechanism in which DING proteins need to be released from their partners to be able to exercise their functions.

In summary, results from this study show that human organism reacts to HIV infection by an overexpression of DING proteins. This overexpression was also observed in the in vitro infection of cell cultures, ruling out any influence of treatment on this increase. This may have a prognostic value to assess HIV infection in newly or already treated HIV-infected patients. Anyway, DING proteins stay enigmatic, and further studies are needed to deepen our knowledge on this family of proteins.

Supporting Information

Table S1 General characteristics of the HIV-infected patients (n = 207).
(DOC)

Acknowledgments

We thank Dr. Armine Darbinyan from Temple University School of Medicine for providing human primary cultures and consultations throughout this work, Drs. Dan Tawfik, Olga Khersonsky and Leonid Gaidukov, from the Weizmann Institute of Rehovot, Israel, for the generous gift of the TBBL reagent.

Author Contributions

Conceived and designed the experiments: EC JC JJ CAV ND AD GA ME. Performed the experiments: AD GA AGH RBD AR ND RK DG. Analyzed the data: EC AD JC GA ND RK GG JH OR CS. Contributed reagents/materials/analysis tools: JC JJ EC ND OR CS. Wrote the paper: AD EC JC GA ND. Critical read: OR CS JH GG ME.

References

1. Adams L, Davey S, Scott K (2002) The DING protein: an autocrine growth-stimulatory protein related to the human synovial stimulatory protein. Biochim Biophys Acta 1586: 254–264.
2. Berna A, Bernier F, Scott K, Stuhlmuller B (2002) Ring up the curtain on DING proteins. FEBS Lett 524: 6–10.
3. Hain NA, Stuhlmuller B, Hahn GR, Kalden JR, Deutzmann R, et al. (1996) Biochemical characterization and microsequencing of a 205-kDa synovial protein stimulatory for T cells and reactive with rheumatoid factor containing sera. J Immunol 157: 1773–1780.
4. Berna A, Bernier F, Chabriere E, Elias M, Scott K, et al. (2009) For whom the bell tolls? DING proteins in health and disease. Cell Mol Life Sci 66: 2205–2218.
5. Berna A, Scott K, Chabriere E, Bernier F (2009) The DING family of proteins: ubiquitous in eukaryotes, but where are the genes? Bioessays 31: 570–580.
6. Kumar V, Yu S, Farell G, Toback FG, Lieske JC (2004) Renal epithelial cells constitutively produce a protein that blocks adhesion of crystals to their surface. Am J Physiol Renal Physiol 287: F373–383.
7. Khan SA, Matysiak-Zablocki E, Ball R, Krtolica A, Hawkins G, et al. (1997) Steroidogenesis-inducing protein, isolated from human ovarian follicular fluid, is a potent mitogen for cell lines derived from ovarian surface epithelial carcinomas. Gynecol Oncol 66: 501–508.
8. Lesner A, Shilpi R, Ivanova A, Gawinowicz MA, Lesniak J, et al. (2009) Identification of X-DING-CD4, a new member of human DING protein family that is secreted by HIV-1 resistant CD4(+) T cells and has anti-viral activity. Biochem Biophys Res Commun 389: 284–289.
9. Morales R, Berna A, Carpentier P, Contreras-Martel C, Renault F, et al. (2006) Serendipitous discovery and X-ray structure of a human phosphate binding apolipoprotein. Structure 14: 601–609.
10. Khersonsky O, Tawfik DS (2005) Structure-reactivity studies of serum paraoxonase PON1 suggest that its native activity is lactonase. Biochemistry 44: 6371–6382.
11. Camps J, Marsillach J, Joven J (2009) The paraoxonases: role in human diseases and methodological difficulties in measurement. Crit Rev Clin Lab Sci 46: 83–106.
12. Renault F, Chabriere E, Andrieu JP, Dublet B, Masson P, et al. (2006) Tandem purification of two HDL-associated partner proteins in human plasma, paraoxonase (PON1) and phosphate binding protein (HPBP) using hydroxyapatite chromatography. J Chromatogr B Analyt Technol Biomed Life Sci 836: 15–21.
13. Rochu D, Chabriere E, Renault F, Elias M, Clery-Barraud C, et al. (2007) Stabilization of the active form(s) of human paraoxonase by human phosphate-binding protein. Biochem Soc Trans 35: 1616–1620.
14. Rochu D, Renault F, Clery-Barraud C, Chabriere E, Masson P (2007) Stability of highly purified human paraoxonase (PON1): association with human phosphate binding protein (HPBP) is essential for preserving its active conformation(s). Biochim Biophys Acta 1774: 874–883.
15. Renault F, Carus T, Clery-Barraud C, Elias M, Chabriere E, et al. (2010) Integrative analytical approach by capillary electrophoresis and kinetics under high pressure optimized for deciphering intrinsic and extrinsic cofactors that modulate activity and stability of human paraoxonase (PON1). J Chromatogr B Analyt Technol Biomed Life Sci 878: 1346–1355.
16. Diemer H, Elias M, Renault F, Rochu D, Contreras-Martel C, et al. (2008) Tandem use of X-ray crystallography and mass spectrometry to obtain ab initio the complete and exact amino acids sequence of HPBP, a human 38-kDa apolipoprotein. Proteins 71: 1708–1720.
17. Cherrier T, Elias M, Jeudy A, Gotthard G, Le Douce V, et al. (2011) Human-Phosphate-Binding-Protein inhibits HIV-1 gene transcription and replication. Virol J 8: 352.
18. Darbinian-Sarkissian N, Darbinyan A, Otte J, Radhakrishnan S, Sawaya BE, et al. (2006) p27(SJ), a novel protein in St John's Wort, that suppresses expression of HIV-1 genome. Gene Ther 13: 288–295.
19. Darbinian N, Czernik M, Darbinyan A, Elias M, Chabriere E, et al. (2009) Evidence for phosphatase activity of p27SJ and its impact on the cell cycle. J Cell Biochem 107: 400–407.
20. Darbinian N, Gomberg R, Mullen L, Garcia S, White MK, et al. (2011) Suppression of HIV-1 transcriptional elongation by a DING phosphatase. J Cell Biochem 112: 225–232.
21. Klimas N, Koneru AO, Fletcher MA (2008) Overview of HIV. Psychosom Med 70: 523–530.
22. De Clercq E (2010) Antiretroviral drugs. Curr Opin Pharmacol 10: 507–515.
23. Ferre N, Camps J, Fernandez-Ballart J, Arija V, Murphy MM, et al. (2003) Regulation of serum paraoxonase activity by genetic, nutritional, and lifestyle factors in the general population. Clin Chem 49: 1491–1497.
24. Collombet JM, Elias M, Gotthard G, Four E, Renault F, et al. (2010) Eukaryotic DING proteins are endogenous: an immunohistological study in mouse tissues. PLoS One 5: e9099.
25. Marsillach J, Mackness B, Mackness M, Riu F, Beltran R, et al. (2008) Immunohistochemical analysis of paraoxonases-1, 2, and 3 expression in normal mouse tissues. Free Radic Biol Med 45: 146–157.
26. Gaidukov L, Tawfik DS (2007) The development of human sera tests for HDL-bound serum PON1 and its lipolactonase activity. J Lipid Res 48: 1637–1646.
27. Marsillach J, Aragones G, Beltran R, Caballeria J, Pedro-Botet J, et al. (2009) The measurement of the lactonase activity of paraoxonase-1 in the clinical evaluation of patients with chronic liver impairment. Clin Biochem 42: 91–98.

28. Ferre N, Camps J, Prats E, Vilella E, Paul A, et al. (2002) Serum paraoxonase activity: a new additional test for the improved evaluation of chronic liver damage. Clin Chem 48: 261–268.
29. Saves M, Morlat P, Chene G, Peuchant E, Pellegrin I, et al. (2001) Prognostic value of plasma markers of immune activation in patients with advanced HIV disease treated by combination antiretroviral therapy. Clin Immunol 99: 347–352.
30. Matas C, Cabre M, La Ville A, Prats E, Joven J, et al. (1994) Limitations of the Friedewald formula for estimating low-density lipoprotein cholesterol in alcoholics with liver disease. Clin Chem 40: 404–406.
31. Zweig MH, Campbell G (1993) Receiver-operating characteristic (ROC) plots: a fundamental evaluation tool in clinical medicine. Clin Chem 39: 561–577.
32. Simm M, Pekarskaya O, Potash MJ, Volsky DJ (2000) Prolonged infection of peripheral blood lymphocytes by Vif-negative HIV type 1 induces resistance to productive HIV type 1 infection through soluble factors. AIDS Res Hum Retroviruses 16: 943–952.
33. Simm M, Miller LS, Durkin HG, Allen M, Chao W, et al. (2002) Induction of secreted human immunodeficiency virus type 1 (HIV-1) resistance factors in CD4-positive T lymphocytes by attenuated HIV-1 infection. Virology 294: 1–12.
34. Shilpi RY, Sachdeva R, Simm M (2011) Cellular resistance to HIV-1 infection in target cells coincides with a rapid induction of X-DING-CD4 mRNA: Indication of the unique host innate response to virus regulated through function of the X-DING-CD4 gene. Innate Immun.
35. Simm M (2007) The innate cellular responses to HIV-1 invasion: emerging molecules of ancient defense mechanisms. Arch Immunol Ther Exp (Warsz) 55: 131–138.
36. Arhel N, Kirchhoff F (2010) Host proteins involved in HIV infection: new therapeutic targets. Biochim Biophys Acta 1802: 313–321.
37. Neil S, Bieniasz P (2009) Human immunodeficiency virus, restriction factors, and interferon. J Interferon Cytokine Res 29: 569–580.
38. Venkataraman N, Cole AL, Ruchala P, Waring AJ, Lehrer RI, et al. (2009) Reawakening retrocyclins: ancestral human defensins active against HIV-1. PLoS Biol 7: e95.
39. Gaidukov L, Tawfik DS (2005) High affinity, stability, and lactonase activity of serum paraoxonase PON1 anchored on HDL with ApoA-I. Biochemistry 44: 11843–11854.
40. Mocroft A, Johnson MA, Sabin CA, Bofill M, Janossy G, et al. (1997) The relationship between beta-2-microglobulin, CD4 lymphocyte count, AIDS and death in HIV-positive individuals. Epidemiol Infect 118: 259–266.
41. van 't Wout AB, Lehrman GK, Mikheeva SA, O'Keeffe GC, Katze MG, et al. (2003) Cellular gene expression upon human immunodeficiency virus type 1 infection of CD4(+)-T-cell lines. J Virol 77: 1392–1402.
42. Wen W, Chen S, Cao Y, Zhu Y, Yamamoto Y (2005) HIV-1 infection initiates changes in the expression of a wide array of genes in U937 promonocytes and HUT78 T cells. Virus Res 113: 26–35.

G. Cristallisation et collecte des données de PA14 DING

Crystallization and preliminary X-ray diffraction analysis of the *Pseudomonas aeruginosa* PA14 DING protein

Ahmed DJEGHADER, Guillaume GOTTHARD*, Andrew SUH, Daniel GONZALEZ, Ken SCOTT, Mikael ELIAS, and Eric CHABRIERE*
* Contribution égale

Dans les travaux décrits, j'ai réalisé :

- partie expérimentale : Mise au point des conditions d'expression, de purification et de cristallisation de la protéine, collecte et traitement des données, remplacement moléculaire
- écriture de parties de l'article

Résumé : Ce travail concerne la production, purification, cristallisation et les premières données de diffraction aux rayons X de la protéine PA14 DING issue de *Pseudomonas aeruginosa* PA14.

Actuellement, seule deux structures de protéines DING ont été résolues, celle de la protéine DING humaine HPBP et celle de la protéine DING bactérienne PfluDING (issue de *Pseudomonas fluorescens*). Les principales différences structurales entre les protéines DING et les PstS résident dans les boucles qui sont protubérantes chez les protéines DING. PA14 DING présente une identité de séquence de 74 % avec PfluDING et un alignement de séquence suggère des boucles plus courtes chez PA14 DING. Enfin, d'un point de vue biologique, les protéines DING présentes chez *P. aeruginosa* constituent des facteurs de virulence pour la bactérie en lui permettant de capturer les ions phosphate de l'hôte. L'obtention de la structure de PA14 DING représente ainsi un intérêt majeur pour l'amélioration des connaissances sur les protéines DING et la compréhension des mécanismes moléculaires de fixation du phosphate chez les bactéries pathogènes.

Acta Crystallographica Section F
Structural Biology and Crystallization Communications
ISSN 1744-3091

Crystallization and preliminary X-ray diffraction analysis of a DING protein from *Pseudomonas aeruginosa* PA14

Ahmed Djeghader,[a]‡ Guillaume Gotthard,[a]‡ Andrew Suh,[b] Daniel Gonzalez,[a] Ken Scott,[b] Mikael Elias[c] and Eric Chabriere[a]*

[a]Aix-Marseille Université, URMITE, UM63, CNRS 7278, IRD 198, Inserm 1095, 27 Boulevard Jean Moulin, 13385 Marseille CEDEX 5, France, [b]School of Biological Sciences, University of Auckland, Auckland, New Zealand, and [c]Department of Biological Chemistry, Weizmann Institute of Science, Rehovot, Israel

‡ These authors contributed equally to this work.

Correspondence e-mail: eric.chabriere@univmed.fr

Received 23 January 2013
Accepted 24 February 2013

DING proteins form an emergent family of proteins consisting of an increasing number of homologues that have been identified in all kingdoms of life. They belong to the superfamily of phosphate-binding proteins and exhibit a high affinity for phosphate. In eukaryotes, DING proteins have been isolated by virtue of their implication in several diseases and biological processes. Some of them are potent inhibitors of HIV-1 replication/transcription, raising the question of their potential involvement in the human defence system. Recently, a protein from *Pseudomonas aeruginosa* strain PA14, named PA14DING or LapC, belonging to the DING family has been identified. The structure of PA14DING, combined with detailed biochemical characterization and comparative analysis with available DING protein structures, will be helpful in understanding the structural determinants implicated in the inhibition of HIV-1 by DING proteins. Here, the expression, purification and crystallization of PA14DING and the collection of X-ray data to 1.9 Å resolution are reported.

1. Introduction

In bacteria, phosphate uptake is mediated by two different systems: the phosphate inorganic transport system (Pit), which is used under high-phosphate conditions, and the phosphate-specific transport system (Pst), which is utilized during phosphate starvation (Willsky & Malamy, 1980). The latter involves an ATP-fueled ABC transporter, in which a periplasmic phosphate-binding protein (PBP or PstS) plays a phosphate-scavenging role (Wanner, 1993). In addition to PstS, which is encoded by the *pst* operon, some bacterial species encode other PBPs such as DING proteins (Berna, Scott *et al.*, 2009) or alkaline phosphatases (APs; Berna *et al.*, 2008), which share about 20–30% sequence identity with PstS. Interestingly, whereas PstS and AP proteins seem to be exclusively prokaryotic, DING proteins have been identified in all kingdoms of life (Berna, Scott *et al.*, 2009).

DING proteins were named according to their highly conserved N-terminal amino-acid sequence DINGGG– (Adams *et al.*, 2002). These proteins were initially identified in eukaryotes by virtue of their implication in numerous diseases and biological mechanisms (rheumatoid arthritis, nephrolithiasis, HIV inhibition and cell-cycle regulation; Adams *et al.*, 2002; Berna, Bernier *et al.*, 2009; Hain *et al.*, 1996; Kumar *et al.*, 2004; Darbinian *et al.*, 2009). However, functional studies of these proteins have been considerably hampered by a lack of genetic information, since neither a gene nor an ORF encoding DING proteins has been identified in eukaryotes (Berna, Scott *et al.*, 2009; Diemer *et al.*, 2008). The explosion of high-throughput genome sequencing in the last decade has revealed that DING proteins are widespread in *Pseudomonas* species. In contrast to eukaryotes, the encoding genes are well sequenced and properly annotated in these genomes and thus constitute a valuable resource for studies of DING proteins.

To date, only two structures of DING proteins have been solved: those of the human phosphate-binding protein (HPBP) isolated from human plasma (Morales *et al.*, 2006) and its homologue PfluDING from *P. fluorescens* SBW25 (Liebschner *et al.*, 2009; Moniot *et al.*, 2007). These proteins exhibit a fold consisting of two globular domains linked together by a flexible hinge (Ahn *et al.*, 2007). Their structures superimpose on those of PstS with the exception of four external protruding loops and two disulfide bridges that are present

in DING proteins but not in PstS (Berna, Bernier *et al.*, 2009; Liebschner *et al.*, 2009; Ahn *et al.*, 2007). The bound phosphate anion resides within a binding cleft formed by the two domains. Anion binding involves eight residues that form a complex network of 12 hydrogen bonds with the phosphate moiety (Liebschner *et al.*, 2009). Amongst these binding residues, an aspartic acid (Asp62) has been shown to play a critical role in discrimination between phosphate and other closely related ions such as sulfate or arsenate (Elias *et al.*, 2012; Liebschner *et al.*, 2009).

In pseudomonads, the gene encoding the DING protein is located in a conserved genomic region between a haemagglutinin-like gene and an Hxc type 2 secretion system. Recently, Ball *et al.* (2012) showed that the DING protein is indeed secreted *via* this machinery in clinical isolates that are closely related to the *P. aeruginosa* strain PA14. Despite their high affinity for phosphate, no clear role in phosphate uptake has been attributed to DING proteins in pseudomonads. However, these proteins are possibly involved, together with PstS, in the adherence of pathogenic *P. aeruginosa* to intestinal epithelial cells (Zaborina *et al.*, 2008). This adherence, which is required for the expression of cytotoxic effectors, is abolished in phosphate-rich media, suggesting regulation by the Pho regulon (Zaborina *et al.*, 2008).

In addition to their potential implication in bacterial virulence, some DING proteins isolated from humans (Lesner *et al.*, 2009; Cherrier *et al.*, 2011) and plants (Darbinian-Sarkissian *et al.*, 2006) show a potent ability to inhibit HIV-1 replication. The molecular mechanism by which viral inhibition occurs is still unknown, although DING proteins may specifically inhibit the transcriptional step of the viral cycle (Cherrier *et al.*, 2011). In this paper, we focus on the DING protein from *P. aeruginosa* strain PA14, which we named PA14DING (or LapC; Ball *et al.*, 2012). The resolution of its structure and the consequent structure–function studies will enable the mechanism of this inhibition to be deciphered. Here, we report the crystallization, data collection and primary crystallographic analysis of PA14DING.

2. Methods and materials

2.1. Cloning, expression and purification of the PA14DING protein

The PA14DING gene was amplified from the genomic DNA of *P. aeruginosa* strain PA14 (accession No. CP000438; locus tag PA14_55410) using the Gateway Cloning System (Invitrogen). Briefly, an initial PCR was performed to amplify the PA14DING gene (primers PA14DINGF, 5′-GGC AGC GGC GCG GAC ATC AAC GGC GGT GGC GCC ACC CTG CCG CAA CAG CTG TAC-3′, and PA14DINGR, 5′-GAA AGC TGG GTG TTA GAG CGG ACG GCC GAT GCC GTT GCA GAC GTT GGA ATG-3′). A second PCR step using primers containing *attB*1 and *attB*2 Gateway recombination sites (GatewayF, 5′-GGGG ACA AGT TTG TAC AAA AAA GCA GGC TTC GAA AAC CTG TAT TTT CAG GGC AGC GGC GCG-3′, and GatewayR, 5′-GGGG AC CAC TTT GTA CAA GAA AGC TGG GTG-3′) was performed to allow cloning into the Gateway pDONR221 vector (Moreland *et al.*, 2005). To allow the removal of fusion tags, a sequence encoding a tobacco etch virus (TEV) cleavage site was added downstream of the GatewayF primer. Finally, the PA14DING gene was subcloned into the destination vector pDEST-periHisMBP (Addgene plasmid 11086; Nallamsetty *et al.*, 2005), allowing the expression of an N-terminal hexa-His-MBP fusion tag for affinity purification of the protein. The resulting vector was transformed into *Escherichia coli* DH5α and extracted using a QIAprep Spin Miniprep Kit (Qiagen). The sequence of the gene was verified by sequencing.

PA14DING in fusion with His-MBP (His-MBP-PA14DING) was overexpressed in *E. coli* strain BL21(DE3)-pLysS. Protein expression was performed in 4 l auto-inducible ZYP medium (Studier, 2005; 100 µg ml^{-1} ampicillin, 34 µg ml^{-1} chloramphenicol; overnight culture at 310 K) inoculated with 100 ml overnight pre-culture. Cells were harvested by centrifugation (5000*g*, 15 min, 277 K), resuspended in lysis buffer (300 m*M* NaCl, 50 m*M* Tris pH 8, 1 m*M* PMSF, 0.25 mg ml^{-1} lysozyme, 10 µg ml^{-1} DNAse I, 20 m*M* $MgSO_4$) and stored at 193 K for 2 h. The frozen suspension was then thawed at 377 K and disrupted by three steps of sonication (Branson Sonifier 450; 30 s, 80% intensity and microtip limit of 8). The cell debris was pelleted by centrifugation (17 500*g*, 30 min, 277 K) and the supernatant was loaded onto a nickel-affinity column (GE Healthcare) at a flow rate of 5 ml min^{-1}. Elution of His-MBP-PA14DING was performed using a buffer consisting of 300 m*M* NaCl, 50 m*M* Tris pH 8, 250 m*M* imidazole. The eluted proteins were checked on a 15% SDS–PAGE gel. The gel revealed the presence of two major proteins migrating with mobilities of ∼80 and ∼40 kDa that could correspond to His-MBP-PA14DING and a partial expression product probably corresponding to His-MBP alone, respectively (data not shown).

```
ggcagcggcgcggacatcaacggcggtggcgccaccctgccgcaacagctgtaccaggagcccggcgtcctgaccgccggctttgccgcctacatcggcgtaggcagtggcaacggcaag
 g s g a D I N G G G A T L P Q Q L Y Q E P G V L T A G F A A Y I G V G S G N G K
gcggccttcctgaacaacgactacaccaagttcgtcgccggcaccaccaacaagaacgtgcattgggctggtagcgactccaaactgagcaagaccaacgaaaccaacccctatctgagc
 A A F L N N D Y T K F V A G T T N K N V H W A G S D S K L S K T N E T N P Y L S
gcccatggctccgcctggggtccgctgatccaggtgccgtcggtagccacttctgtcgctctgccgttcaacaagtcaggtagcaacgccgtcaacttcgcagacgtgaacacccctttgc
 A H G S A W G P L I Q V P S V A T S V A L P F N K S G S N A V N F A D V N T L C
ggtgtcttctccggccgtctgaccgattggagtcagattcctggctcgggccgtagcggcgccatcacagtggtctaccgttccgagagcagcggcaccaccgaactgttcacccgcttc
 G V F S G R L T D W S Q I P G S G R S G A I T V V Y R S E S S G T T E L F T R F
ctcaacgcctcctgctccagcaccctcgaaggtggcaccttcgccatcaccaccagcttcggtagcagcttctccggcggcctgccggctggcgccgtatcggcccagggcagccaggcc
 L N A S C S S T L E G G T F A I T T S F G S S F S G G L P A G A V S A Q G S Q A
gtgatgaatgcgctcaacgccgcccaaggccgcatcacctacatgagcccggacttcgccgcgccgaccctggccggtctcgacgacgccaccaaggtcgcccaggttcgcggcgtatcc
 V M N A L N A A Q G R I T Y M S P D F A A P T L A G L D D A T K V A Q V R G V S
ccggcgccggccaacgtttcggcggccatcggcgccgttactccgccgactactgcccagcgttccgatccgaacaactgggtaccggtcttcgctgccaccgccaaccccaacgacccg
 P A P A N V S A A I G A V T P P T T A Q R S D P N N W V P V F A A T A N P N D P
agcgtgcgtccgtatccgaccagcggctacccgatcctcggcttcaccaacctgatcttcagccagtgctacgccaacgccacccagacccagcaggtgcgcgacttcttcacccgtcac
 S V R P Y P T S G Y P I L G F T N L I F S Q C Y A N A T Q T Q Q V R D F F T R H
tacggcgccaccgccaacaacgacaccgcgatcaccaaccatcgcttcgtgccgctgccggcttcctggaagcttgccgtacgccagtcgttcctgacctccaccaacaacttgtacatc
 Y G A T A N N D T A I T N H R F V P L P A S W K L A V R Q S F L T S T N N L Y I
ggccattccaacgtctgcaacggcatcggccgtccgctc
 G H S N V C N G I G R P L
```

Figure 1
Sequence of the PA14DING protein; the amino acids of the TEV recognition site that remain after cleavage are shown in lower case.

In order to separate these two proteins, a purification step was performed on a size-exclusion chromatography column (Superdex 75 16/60; GE Healthcare) in 20 m*M* Tris pH 8, 50 m*M* NaCl. Fractions containing His-MBP-PA14DING were pooled and incubated with 500 µl TEV protease (2.57 mg ml^{-1}) overnight at 277 K. After centrifugation (5000*g*, 10 min, 277 K), proteins were loaded onto a nickel-affinity column as described previously to eliminate His-MBP and potential remaining His-MBP-PA14DING. The flowthrough containing the PA14DING protein was then recovered and reloaded onto an anion-exchange column (HiTrap QFF GE Healthcare) to eliminate residual MBP, as the two proteins possessed similar molecular weights (∼43 kDa for MBP and ∼40 kDa for PA14DING). At pH 8 MBP is negatively charged and binds to the column, while the PA14DING protein, which is positively charged, can be recovered in the flowthrough. Finally, the PA14DING protein was dialyzed against a buffer consisting of 20 m*M* NaCl, 20 m*M* Tris pH 8 and concentrated to 10 mg ml^{-1} (Amicon Ultra MWCO 10 kDa; Millipore, Ireland) prior to crystallization trials. The sequence of the crystallized protein is shown in Fig. 1.

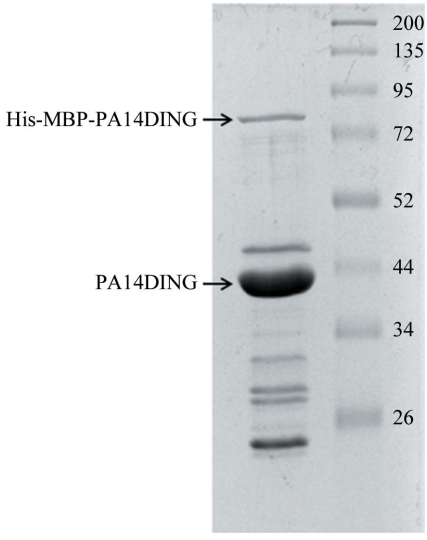

Figure 2
15% SDS–PAGE of PA14DING protein stained with Coomassie Blue. Right lane, molecular-weight markers (Thermo Scientific Spectra Multicolor broad-range protein ladder; labelled in kDa). Left lane, 5 µg PA14DING protein. PA14DING protein and the residual fusion protein His-MBP-PA14DING are indicated by arrows.

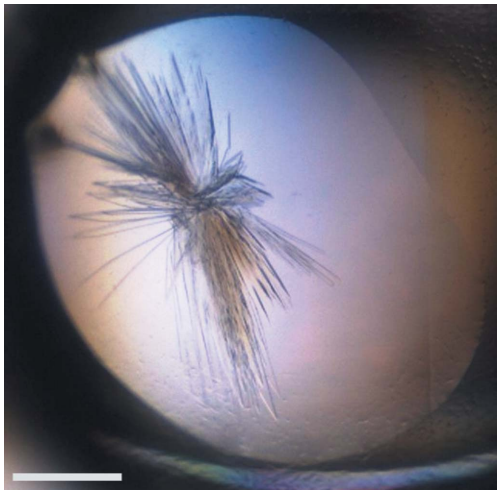

Figure 3
A typical cluster of plate-shaped PA14DING crystals; the scale bar (white) is 0.2 mm in length.

Table 1
Data-collection statistics.

Values in parentheses are for the last bin.

Beamline	ID29, ESRF
Wavelength (Å)	0.976
Detector	PILATUS 6M
Oscillation (°)	0.1
No. of frames	1800
Resolution (Å)	1.9 (2.0–1.9)
Space group	$P2_1$
Unit-cell parameters (Å, °)	a = 53.60, b = 47.81, c = 62.99, β = 98.60
No. of observed reflections	80197 (11338)
No. of unique reflections	24616 (3501)
Completeness (%)	98.1 (98.6)
R_{meas}† (%)	10.7 (43.9)
$\langle I/\sigma(I)\rangle$‡	12.86 (4.75)
Multiplicity	3.26 (3.24)
Mosaicity (°)	0.480

† R_{meas} is the redundancy-independent merging R factor: $R_{meas} = \sum_{hkl}\{N(hkl)/[N(hkl)-1]\}^{1/2}\sum_i |I_i(hkl) - \langle I(hkl)\rangle|/\sum_{hkl}\sum_i I_i(hkl)$. ‡ $I/\sigma(I)$ is the signal-to-noise ratio.

2.2. Protein crystallization

Crystallization assays were performed in 96-well trays incubated at 293 K using the sitting-drop vapour-diffusion method implemented on a nanodrop dispensing robot (Honeybee X8, Genomic Solutions). An initial round of screening (864 drops) was performed using the commercial crystallization screens Wizard I and II (Emerald BioSystems), Structure Screens I and II (Molecular Dimensions) and Stura Footprint Combination HT-96 (Molecular Dimensions). Despite the presence of impurities in this PA14DING preparation (Fig. 2), clusters of plate-shaped crystals appeared under various conditions. The best hit was identified as a condition from the Wizard I and II screens (Emerald BioSystems) containing 1.6 *M* ammonium sulfate. The pH and ammonium sulfate concentration of this condition were optimized (64 drops) using a commercial ammonium sulfate screen (AmSO4 Suite, Qiagen). The plate was incubated at 293 K and monitored using a Rock Imager and *Rock Maker* system (Formulatrix Inc., USA). Clusters of plates appeared after a few months at 293 K in a condition consisting of 100 m*M* MES pH 6.5, 2 *M* ammonium sulfate, 5%(*v*/*v*) PEG 400 (Fig. 3). Attempts to further optimize the crystals by using new screening strategies or by improving the best conditions using additives (Additive Screen HT, Hampton Research) yielded the same clusters of plates.

2.3. Data collection

A cryoprotectant solution consisting of the crystallization solution supplemented with 20%(*v*/*v*) glycerol was added to the drop (1 µl cryoprotectant in 300 nl drops) in order to gently exchange the solution containing the crystal. Next, the crystal was transferred into a drop containing 1 µl of the cryoprotective solution for 1 min prior to mounting on a MicroLoop (MiTeGen) and flash-cooling in liquid nitrogen. X-ray diffraction intensities were collected on the ID29 beamline at the ESRF (Grenoble, France) using a wavelength of 0.976 Å and a PILATUS 6M detector with 0.1 s exposures. Diffraction data were collected from 1800 images using the fine-slicing method; individual frames consisted of 0.1° steps over a range of 180° (Fig. 4).

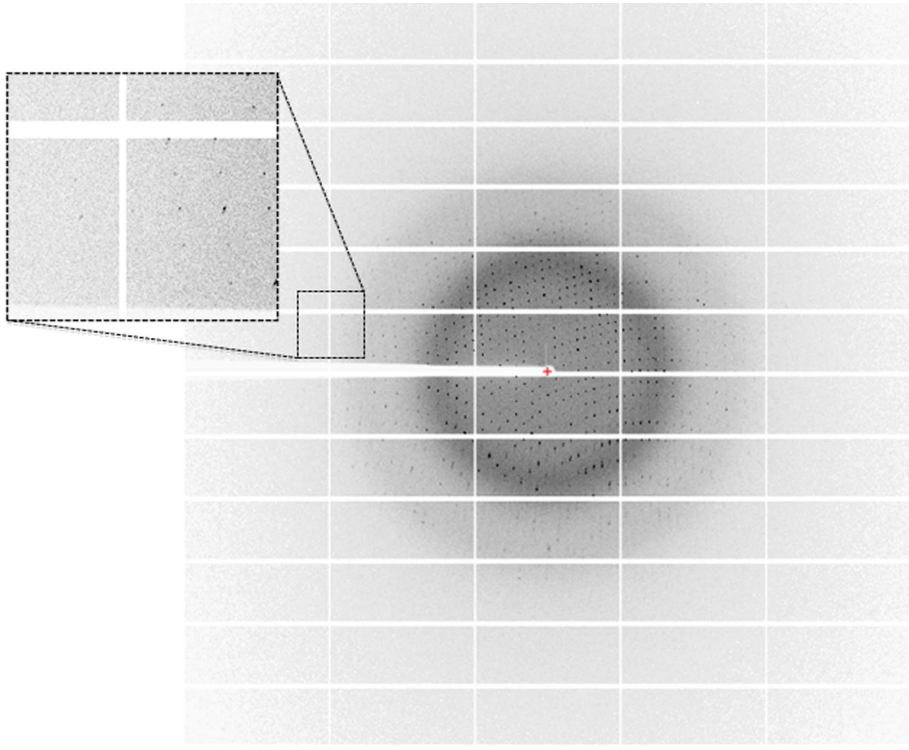

Figure 4
A diffraction pattern from a crystal of the PA14DING protein. The edge of the frame is at 1.30 Å resolution.

3. Results and conclusions

X-ray diffraction data were integrated and scaled using the *XDS* program (Kabsch, 2010; Table 1). The PA14DING crystals belonged to the monoclinic space group $P2_1$, with unit-cell parameters $a = 53.60$, $b = 47.81$, $c = 62.99$ Å, $\beta = 98.60^\circ$. The calculated Matthews coefficient V_M suggests the presence of one monomer per asymmetric unit (with a V_M of 2.1 Å^3 Da^{-1}, corresponding to a solvent content of 41.47%). Molecular replacement was performed with *Phaser* (McCoy *et al.*, 2007) using the structure of PfluDING as a model (74% sequence identity to PA14DING; PDB entry 2q9t; Ahn *et al.*, 2007), from which amino acids 231–238 were deleted. One molecule was placed in the asymmetric unit (R_{free} = 33.29%) and the crystal packing was clearly complete. The solvent content of this crystal is low and is comparable to that observed for the high-resolution crystals of PfluDING (V_M = 1.9 Å^3 Da^{-1}, corresponding to a solvent content of 37.9%; Moniot *et al.*, 2007). Manual model improvement was performed using *Coot* (Emsley & Cowtan, 2004) and refinement was performed with *REFMAC* (Murshudov *et al.*, 2011) and *PHENIX* (Adams *et al.*, 2010). The construction, refinement and interpretation of the structure are in progress.

This research was supported by a grant to EC from 'Agence Nationale pour la Recherche sur le Sida' (Grant No. 12264). AD is a PhD student supported by Aix-Marseille Université. GG and DG are AP-HM engineers (Marseille, France). We thank the AFMB-CNRS UMR 6098 for full access to the expression and crystallization platform. AS and KS thank the Auckland Medical Research Foundation and the University of Auckland for support.

References

Adams, L., Davey, S. & Scott, K. (2002). *Biochim. Biophys. Acta*, **1586**, 254–264.
Adams, P. D. *et al.* (2010). *Acta Cryst.* D**66**, 213–221.
Ahn, S., Moniot, S., Elias, M., Chabriere, E., Kim, D. & Scott, K. (2007). *FEBS Lett.* **581**, 3455–3460.
Ball, G., Viarre, V., Garvis, S., Voulhoux, R. & Filloux, A. (2012). *Res. Microbiol.* **163**, 457–469.
Berna, A., Bernier, F., Chabrière, E., Elias, M., Scott, K. & Suh, A. (2009). *Cell. Mol. Life Sci.* **66**, 2205–2218.
Berna, A., Bernier, F., Chabrière, E., Perera, T. & Scott, K. (2008). *Int. J. Biochem. Cell Biol.* **40**, 170–175.
Berna, A., Scott, K., Chabrière, E. & Bernier, F. (2009). *Bioessays*, **31**, 570–580.
Cherrier, T., Elias, M., Jeudy, A., Gotthard, G., Le Douce, V., Hallay, H., Masson, P., Janossy, A., Candolfi, E., Rohr, O., Chabrière, E. & Schwartz, C. (2011). *Virol. J.* **8**, 352.
Darbinian, N., Czernik, M., Darbinyan, A., Elias, M., Chabriere, E., Bonasu, S., Khalili, K. & Amini, S. (2009). *J. Cell. Biochem.* **107**, 400–407.
Darbinian-Sarkissian, N., Darbinyan, A., Otte, J., Radhakrishnan, S., Sawaya, B. E., Arzumanyan, A., Chipitsyna, G., Popov, Y., Rappaport, J., Amini, S. & Khalili, K. (2006). *Gene Ther.* **13**, 288–295.
Diemer, H., Elias, M., Renault, F., Rochu, D., Contreras-Martel, C., Schaeffer, C., Van Dorsselaer, A. & Chabriere, E. (2008). *Proteins*, **71**, 1708–1720.
Elias, M., Wellner, A., Goldin-Azulay, K., Chabriere, E., Vorholt, J. A., Erb, T. J. & Tawfik, D. S. (2012). *Nature (London)*, **491**, 134–137.
Emsley, P. & Cowtan, K. (2004). *Acta Cryst.* D**60**, 2126–2132.
Hain, N. A., Stuhlmüller, B., Hahn, G. R., Kalden, J. R., Deutzmann, R. & Burmester, G. R. (1996). *J. Immunol.* **157**, 1773–1780.
Kabsch, W. (2010). *Acta Cryst.* D**66**, 125–132.
Kumar, V., Yu, S., Farell, G., Toback, F. G. & Lieske, J. C. (2004). *Am. J. Physiol. Renal Physiol.* **287**, F373–F383.
Lesner, A., Shilpi, R., Ivanova, A., Gawinowicz, M. A., Lesniak, J., Nikolov, D. & Simm, M. (2009). *Biochem. Biophys. Res. Commun.* **389**, 284–289.
Liebschner, D., Elias, M., Moniot, S., Fournier, B., Scott, K., Jelsch, C., Guillot, B., Lecomte, C. & Chabrière, E. (2009). *J. Am. Chem. Soc.* **131**, 7879–7886.
McCoy, A. J., Grosse-Kunstleve, R. W., Adams, P. D., Winn, M. D., Storoni, L. C. & Read, R. J. (2007). *J. Appl. Cryst.* **40**, 658–674.
Moniot, S., Elias, M., Kim, D., Scott, K. & Chabriere, E. (2007). *Acta Cryst.* F**63**, 590–592.
Morales, R. *et al.* (2006). *Structure*, **14**, 601–609.
Moreland, N., Ashton, R., Baker, H. M., Ivanovic, I., Patterson, S., Arcus, V. L., Baker, E. N. & Lott, J. S. (2005). *Acta Cryst.* D**61**, 1378–1385.
Murshudov, G. N., Skubák, P., Lebedev, A. A., Pannu, N. S., Steiner, R. A., Nicholls, R. A., Winn, M. D., Long, F. & Vagin, A. A. (2011). *Acta Cryst.* D**67**, 355–367.

Nallamsetty, S., Austin, B. P., Penrose, K. J. & Waugh, D. S. (2005). *Protein Sci.* **14**, 2964–2971.
Studier, F. W. (2005). *Protein Expr. Purif.* **41**, 207–234.
Wanner, B. L. (1993). *J. Cell. Biochem.* **51**, 47–54.
Willsky, G. R. & Malamy, M. H. (1980). *J. Bacteriol.* **144**, 356–365.
Zaborina, O., Holbrook, C., Chen, Y., Long, J., Zaborin, A., Morozova, I., Fernandez, H., Wang, Y., Turner, J. R. & Alverdy, J. C. (2008). *PLoS Pathog.* **4**, e43.

H. Cristallisation et collecte des données de LapA

Crystallization and preliminary X-ray diffraction analysis of a high affinity phosphate-binding protein endowed with phosphatase activity from *Pseudomonas aeruginosa* PAO1

Ahmed DJEGHADER, Guillaume GOTTHARD*, Andrew SUH, Daniel GONZALEZ, Ken SCOTT, Eric CHABRIERE and Mikael ELIAS*
* Contribution égale

Dans les travaux décrits, j'ai réalisé :

- partie expérimentale : conseils pour la mise au point des conditions d'expression, de purification et de cristallisation de la protéine, collecte et traitement des données, remplacement moléculaire

Résumé : Ce travail concerne la production, purification, cristallisation et les premières données de diffraction à résolution sub-atomique de la protéine LapA issue de *Pseudomonas aeruginosa* PAO1.

La protéine LapA est une protéine de haute affinité pour le phosphate (PBP) présentant une activité phosphatase. Ce sont des facteurs de virulence bactériens présentant environ 45 % d'identité de séquence avec les protéines DING. Elles sont sécrétées en réponse à la carence en phosphate dans l'environnement de la bactérie. Il est proposé que l'activité phosphatase de ces PBPs puisse permettre aux bactéries de convertir le phosphate organique en phosphate inorganique. L'obtention de la structure cristallographique de cette protéine à résolution subatomique (0,87 Å) combinée aux études biochimiques et enzymatiques permettra d'élucider le mécanisme enzymatique de ces protéines dans le but de mieux comprendre leur implication dans l'importation du phosphate.

Acta Crystallographica Section F
Structural Biology and Crystallization Communications
ISSN 1744-3091

Crystallization and preliminary X-ray diffraction analysis of a high-affinity phosphate-binding protein endowed with phosphatase activity from *Pseudomonas aeruginosa* PAO1

Ahmed Djeghader,[a]‡ Guillaume Gotthard,[a]‡ Andrew Suh,[b] Daniel Gonzalez,[a] Ken Scott,[b] Eric Chabriere[a]* and Mikael Elias[c]*

[a]Aix Marseille Université, URMITE, UM63, CNRS 7278, IRD 198, Inserm 1095, 27 Boulevard Jean Moulin, 13385 Marseille CEDEX 5, France, [b]School of Biological Sciences, University of Auckland, Auckland, New Zealand, and [c]Biological Chemistry, Weizman Institute of Science, Rehovot, Israel

‡ These authors made equal contributions.

Correspondence e-mail: eric.chabriere@univmed.fr, mikael.elias@weizmann.ac.il

Received 10 July 2013
Accepted 28 August 2013

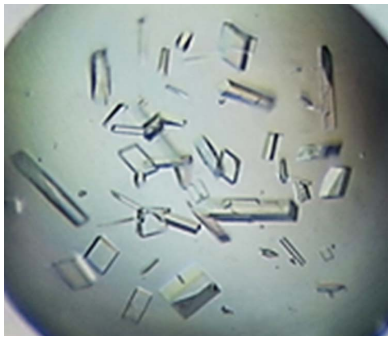

In prokaryotes, phosphate starvation induces the expression of numerous phosphate-responsive genes, such as the *pst* operon including the high-affinity phosphate-binding protein (PBP or pstS) and alkaline phosphatases such as PhoA. This response increases the cellular inorganic phosphate import efficiency. Notably, some *Pseudomonas* species secrete, *via* a type-2 secretion system, a phosphate-binding protein dubbed LapA endowed with phosphatase activity. Here, the expression, purification, crystallization and X-ray data collection at 0.87 Å resolution of LapA are described. Combined with biochemical and enzymatic characterization, the structure of this intriguing phosphate-binding protein will help to elucidate the molecular origin of its phosphatase activity and to decipher its putative role in phosphate uptake.

1. Introduction

Phosphorus is an essential nutrient for all living cells as it is a key component of biomolecules such as DNA. However, although phosphate (P_i) is relatively abundant on Earth, its bioavailability is limited (Cordell & White, 2011). Bacteria therefore possess different tools for cellular phosphate uptake (Wanner, 1993), such as the Pit (phosphate inorganic transport) system that is usually used and expressed when P_i is plentiful (Willsky & Malamy, 1980). On the other hand, under P_i limitation conditions or in the presence of high concentrations of competing anions, the PhoB–PhoR two-component system which senses variation of P_i concentration in the environment induces the transcription of numerous genes related to P_i assimilation (Hsieh & Wanner, 2010). The phosphate-specific transport (Pst) system is highly expressed under such conditions, including the high-affinity extracellular (or periplasmic) phosphate-binding protein (called PstS or PBP), in order to scavenge the phosphate present in the environment (Willsky & Malamy, 1980; Wanner, 1993; Elias *et al.*, 2012). Phosphate starvation also induces the expression of a large variety of genes that enable the extraction of phosphate from sources other than P_i, such as organophosphate compounds (Dyhrman *et al.*, 2006). A well documented example is alkaline phosphatases such as PhoA (Ohtake *et al.*, 1998; VanBogelen *et al.*, 1996).

Alkaline phosphatases (EC 3.1.3.1) are nonspecific esterases that catalyze phosphate monoester hydrolysis *via* a phosphoseryl intermediate to yield P_i and an alcohol (Coleman, 1992; Sun *et al.*, 1999). They thus hydrolyze non-transportable organophosphate compounds to release P_i that may be subsequently taken up by the Pit or Pst systems (Wanner, 1993). Homologous proteins to PhoA exist in many bacterial species, including *Pseudomonas* (Kriakov *et al.*, 2003; Filloux *et al.*, 1988). Interestingly, in addition to PstS and PhoA, some *Pseudomonas* species possess phosphate-binding proteins (PBPs) endowed with phosphatase activity. Indeed, one of these proteins, dubbed low-molecular-weight alkaline phosphatase (LapA), is able to hydrolyze *para*-nitrophenyl phosphate (pNPP; specific activity 46 U mg^{-1}, where 1 U mg^{-1} represents one micromole of pNPP hydrolyzed per minute per milligram of protein; Tan & Worobec, 1993). In contrast to PhoA, which is constitutively produced by *P. aeruginosa* PAO1, LapA expression is induced solely under P_i limitation (Tan & Worobec, 1993; Ball *et al.*, 2002).

LapA-like proteins belong to the PBP superfamily and seem to form a specific clade (Fig. 1). The LapA-encoding gene displays a

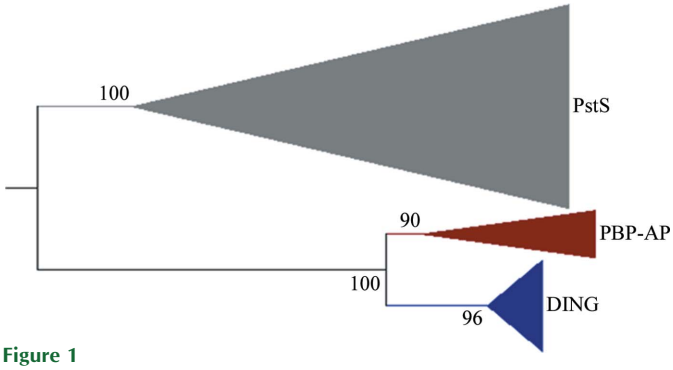

Figure 1
Collapsed phylogenetic tree of the phosphate-binding protein superfamily. PBP-AP represents the family of phosphate-binding proteins endowed with phosphatase activity. The sequences were collected from the NCBI database using the LapA sequence as the query. A total of 153 sequences were subsequently aligned using the *MUSCLE* program (Edgar, 2004). The phylogenetic tree was built using the *MEGA* software (Tamura *et al.*, 2011). Bootstrap values are shown for each node of the tree.

similar genetic organization to that observed for a clade of the PBP superfamily: DING proteins, which are also induced by phosphate starvation (Liebschner *et al.*, 2009; Zhang *et al.*, 2007). These genes locate between an Hxc type-2 secretion system (T2SS) and a haemagglutinin-like protein (Zhang *et al.*, 2007; Djeghader *et al.*, 2013). This specific localization downstream from the T2SS allows the secretion of these proteins by this machinery. Interestingly, this T2SS seems to be dedicated to the unique secretion of LapA-like proteins and DING proteins (Ball *et al.*, 2012; Douzi *et al.*, 2012; Filloux, 2011).

The isolation of PBPs that exhibit phosphatase activity is intriguing, since high-affinity PBPs and alkaline phosphatase are both overexpressed during phosphate starvation. Proteins such as LapA might thus have a unique, as yet unexplored role in phosphate starvation. The determination of its structure, coupled with careful biochemical and functional characterization, will be of great value in deciphering the role of these proteins in phosphate uptake in *Pseudomonas*. Here, we report the crystallization, data collection at 0.87 Å resolution and preliminary crystallographic analysis of LapA.

2. Methods and materials

2.1. Cloning, expression and purification of LapA protein

The LapA-encoding gene was amplified from *P. aeruginosa* PAO1 genomic DNA (accession No. NC_002516; locus tag PA0688) using the same strategy as used for the amplification of the PA14DING gene (Djeghader *et al.*, 2013). Briefly, primers LapAF, 5′-GGC AGC GGC GCG GTC ACC GGC GGT GGC GCT T-3′, and LapAR, 5′-GAA AGC TGG GTG TTA CGG GCG GCC TTT GGT G-3′, were designed according to the *lapA* sequence and used for an initial amplification. Using the obtained product, a second PCR step was performed using primers containing the *att*B1 and *att*B2 Gateway recombination sites (GatewayF, 5′-GGGG ACA AGT TTG TAC AAA AAA GCA GGC TTC GAA AAC CTG TAT TTT CAG GGC AGC GGC GCG-3′; GatewayR, 5′-GGGG AC CAC TTT GTA CAA GAA AGC TGG GTG-3′) which allow cloning into the Gateway pDONR221 vector (Moreland *et al.*, 2005). Downstream of the GatewayF primer, a *Tobacco etch virus* (TEV) protease recognition site was added to allow removal of the fusion tag. Finally, the *lapA* gene was cloned into the destination vector pDEST-periHisMBP (Addgene plasmid 11086; Nallamsetty *et al.*, 2005), allowing the expression of an N-terminal hexa-His-MBP tag for affinity purification of the protein. The resulting vector was transformed into *Escherichia coli* DH5*α* and extracted using the QIAprep Spin Miniprep Kit (Qiagen). The identity of the cloned gene was verified by sequencing.

The fusion protein (His-MBP-LapA) was overexpressed in *E. coli* BL21(DE3)-pLysS strain (see construct sequence in Fig. 2*a*). As in the cases of homologues of LapA, the periplasmic expression of the protein did not require the use of periplasmic extraction protocols (Ahn *et al.*, 2007; Moniot *et al.*, 2007; Djeghader *et al.*, 2013). Protein expression was performed overnight at 310 K in 4 l auto-inducible ZYP medium (Studier, 2005) inoculated with 100 ml overnight preculture in the presence of 100 µg ml^{-1} ampicillin and 34 µg ml^{-1} chloramphenicol. Cells were then harvested by centrifugation (5000*g*, 15 min, 277 K), resuspended in lysis buffer (300 m*M* NaCl, 10 m*M* imidazole, 50 m*M* Tris pH 8, 1 m*M* PMSF, 0.25 mg ml^{-1} lysozyme, 10 µg ml^{-1} DNAse I, 20 m*M* $MgSO_4$) and stored at 193 K for 2 h.

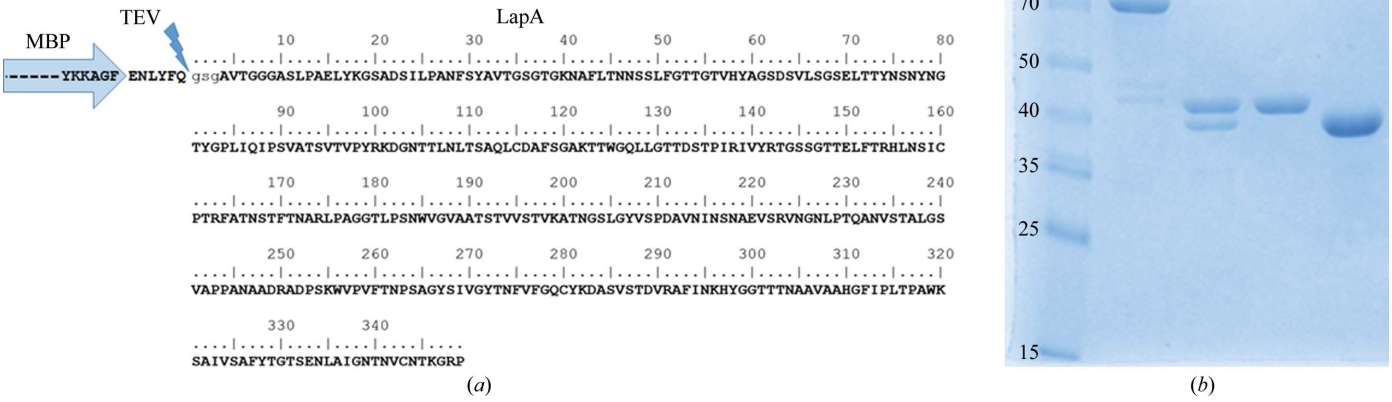

Figure 2
(*a*) View of the expressed construct. It encodes the sequence of the MBP (in blue), the TEV protease cleavage site and the protein sequence (LapA). The three residues from the expression tag that remain on LapA after TEV cleavage are shown in lower case. (*b*) 12% SDS–PAGE related to purification steps of LapA. Lane MWM, molecular-weight markers (Thermo Scientific Spectra Multicolor Broad Range Protein Ladder; labelled in kDa); lane 1, His-MBP-LapA fusion protein; lane 2, TEV protease-cleavage products; lanes 3 and 4, MBP and LapA (5 µg), respectively, separated by the anion-exchange column.

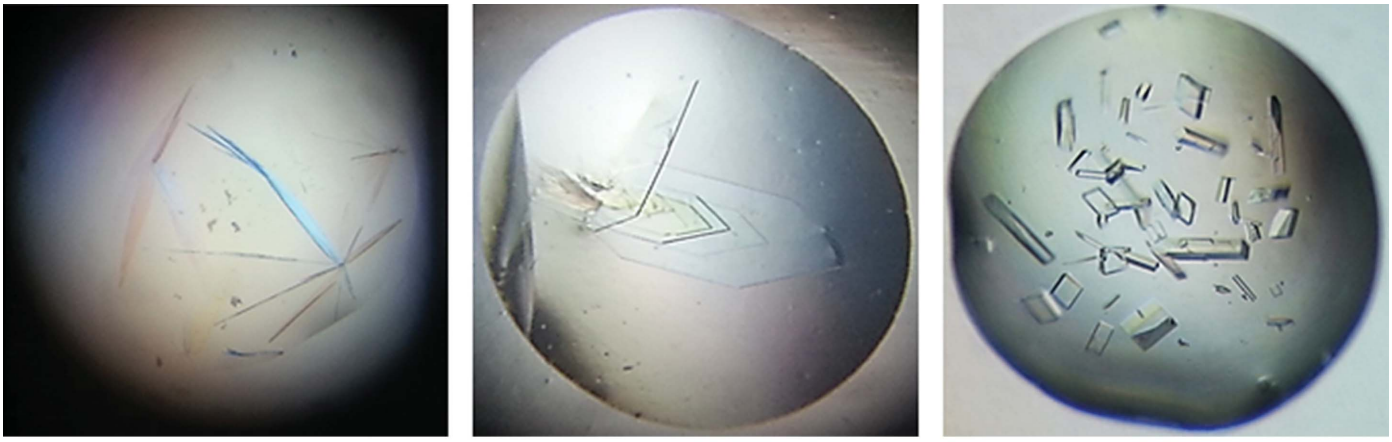

(*a*) (*b*) (*c*)

Figure 3
Evolution of LapA crystals during crystallization. (*a*) Needles from the Wizard I and II screen, (*b*) crystal plates obtained from the optimized conditions, (*c*) LapA crystals improved by re-screening and microseeding.

After thawing, complete lysis of the cells was achieved by sonication (Vibracell 75185; 30 s, 80% intensity). Cell debris was then pelleted by centrifugation (17 000*g*, 30 min, 277 K) and the supernatant was loaded onto a nickel-affinity column (HisTrap FF crude, GE Healthcare) at a flow rate of 5 ml min^{-1}. Elution of His-MBP-LapA protein was performed using a buffer consisting of 300 m*M* NaCl, 500 m*M* imidazole, 50 m*M* Tris pH 8. Eluted proteins were then applied onto a size-exclusion chromatography column (Superdex 75 16/60, GE Healthcare) in 20 m*M* NaCl, 20 m*M* Tris pH 8 buffer to eliminate contaminant proteins. Fractions containing the fusion protein (Fig. 2*b*, lane 1) were pooled and incubated with 1.25 mg TEV protease overnight at 289 K in the presence of 0.5 m*M* EDTA and 1 m*M* DTT. The two proteins resulting from TEV protease cleavage migrated with almost the same mobility (around 40 kDa as observed on 12% SDS–PAGE; Fig. 2*b*, lane 2). Taking advantage of their different isoelectric points (pI 5.0 for MBP and 8.98 for LapA), it was possible to separate them on an anion-exchange column (Resource Q, GE Healthcare; Fig. 2*b*, lanes 3 and 4). Finally, pure LapA was recovered, concentrated to 12.5 mg ml^{-1} (Amicon Ultra MWCO 10 kDa; Millipore, Ireland) and used for crystallization assays.

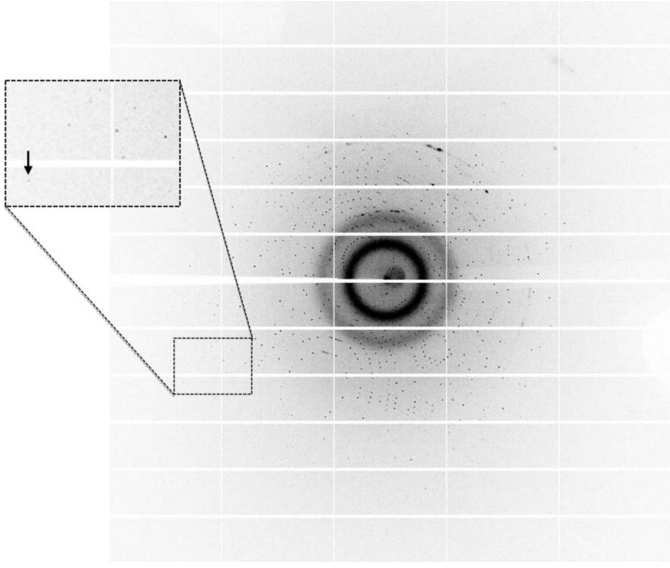

Figure 4
A diffraction pattern from a LapA crystal. The edge of the frame is at 0.8 Å resolution. The spot indicated by the arrow is at 0.86 Å.

2.2. Protein crystallization

Crystallization assays were performed in 96-well trays using the sitting-drop vapour-diffusion method implemented on a nanodrop dispensing robot (Mosquito, TTP Labtech) and incubated at 298 K. Initial screening (192 drops of 750 nl, with protein:crystallization solution ratios of 2:1 and 1:1) was performed using the commercial crystallization screens Wizard I and II (Emerald BioSystems). Needles and clusters appeared in several conditions in a few hours, and the best hit was identified in a condition consisting of 30%(*v*/*v*) PEG 8000, 200 m*M* Li_2SO_4, 100 m*M* sodium acetate/acetic acid pH 4.5 (Fig. 3*a*). This condition was optimized for pH (4.0–5.5) and PEG concentration (15–30%) using the hanging-drop method (64 drops), but only thin plates appeared after 1–2 h in different conditions (Fig. 3*b*). To overcome this issue, a microseeding strategy was undertaken. An initial strategy consisted of crushing a crystal and diluting it in 100 µl crystallization solution (20% PEG 8000, 200 m*M* Li_2SO_4, 100 m*M* sodium acetate/acetic acid pH 4.75). The drops were subsequently inoculated with 25 nl of this seeding solution. However, this strategy did not improve the crystal quality. The same strategy was repeated but adding 10% of the initial commercial screen solution as an additive to the crystallization solution and by using the seeding solution at 1:1000 dilution. Diffraction-quality crystals appeared after 2 d (Fig. 3*c*). The final condition consisted of 20% PEG 8000, 250 m*M* NaCl, 200 m*M* Li_2SO_4, 100 m*M* sodium acetate/acetic acid pH 4.75.

2.3. Data collection

The crystals for the diffraction experiment were cryoprotected using a solution consisting of the crystallization solution containing 20%(*v*/*v*) glycerol prior to mounting on a MicroLoop (MiTeGen) and flash-cooling in liquid nitrogen. X-ray diffraction intensities were collected on the ID23-1 beamline at the European Synchrotron Radiation Facility (ESRF, Grenoble, France) using a wavelength of 0.799 Å and a PILATUS 6M detector with 37 ms exposure. A total of 3600 images were collected using the fine-slicing method and the

Table 1
Data-collection statistics.

Values in parentheses are for the last bin.

Beamline	ID-23-1
Wavelength (Å)	0.799
Detector	PILATUS 6M
Oscillation (°)	0.1
No. of frames	2000
Resolution (Å)	0.87 (0.95–0.87)
Space group	$P2_1$
Unit-cell parameters (Å, °)	a = 40.76, b = 67.63, c = 57.62, β = 110.4
No. of observed reflections	830383 (177520)
No. of unique reflections	231568 (52382)
Completeness (%)	96.8 (94.7)
R_{meas}† (%)	5.3 (42.8)
R_{merge} (%)	4.5 (36.1)
$CC_{1/2}$	99.9 (87.3)
$\langle I/\sigma(I)\rangle$‡	15.25 (3.47)
Multiplicity	3.59 (3.39)
Mosaicity (°)	0.184

† The redundancy-independent merging R factor $R_{meas} = \sum_{hkl}\{N(hkl)/[N(hkl)-1]\}^{1/2}\sum_i |I_i(hkl) - \langle I(hkl)\rangle|/\sum_{hkl}\sum_i I_i(hkl)$. ‡ $I/\sigma(I)$ is the signal-to-noise ratio.

individual frames consisted of 0.1° steps over a range of 360° (Fig. 4). Among these images, 2000 were retained for data integration and scaling to minimize the effect of radiation decay.

3. Results and conclusions

Integration and scaling of X-ray diffraction data were performed using *XDS* (Kabsch, 2010; Table 1). The LapA crystal belonged to the monoclinic space group $P2_1$, with unit-cell parameters a = 40.76, b = 67.63, c = 57.62 Å, β = 110.4°. Molecular replacement was performed with *Phaser* (McCoy *et al.*, 2007) using the structure of *Pseudomonas fluorescens* DING as a model (44% sequence identity to LapA; PDB entry 2q9t; Ahn *et al.*, 2007), in which regions corresponding to protruding loops in the structure were deleted from the PDB model file (residues 217–221, 239–246 and 279–287). One molecule was placed per asymmetric unit (R_{free} = 30.38%) as suggested by the calculated Matthews coefficient (2.07 $Å^3\,Da^{-1}$ corresponding to 40.50% solvent content; Matthews, 1968) and the crystal packing was clearly complete. Manual model improvement was performed using *Coot* (Emsley *et al.*, 2010) and refinement was performed using *REFMAC* (Murshudov *et al.*, 2011). The current R_{free} is 12.40%. The construction, refinement and interpretation of the sub-Å resolution structure of LapA are in progress.

AD is a PhD student supported by Aix-Marseille Université. GG is a PhD student/AP-HM engineer in charge of the protein purification/crystallization platform. DG is a PhD student/AP-HM engineer. AS and KS thank the Auckland Medical Research Foundation and the University of Auckland for support.

References

Ahn, S., Moniot, S., Elias, M., Chabriere, E., Kim, D. & Scott, K. (2007). *FEBS Lett.* **581**, 3455–3460.
Ball, G., Durand, E., Lazdunski, A. & Filloux, A. (2002). *Mol. Microbiol.* **43**, 475–485.
Ball, G., Viarre, V., Garvis, S., Voulhoux, R. & Filloux, A. (2012). *Res. Microbiol.* **163**, 457–469.
Coleman, J. E. (1992). *Annu. Rev. Biophys. Biomol. Struct.* **21**, 441–483.
Cordell, D. & White, S. (2011). *Sustainability*, **3**, 2027–2049.
Djeghader, A., Gotthard, G., Suh, A., Gonzalez, D., Scott, K., Elias, M. & Chabriere, E. (2013). *Acta Cryst.* F**69**, 425–429.
Douzi, B., Filloux, A. & Voulhoux, R. (2012). *Philos. Trans. R. Soc. Lond. B Biol. Sci.* **367**, 1059–1072.
Dyhrman, S. T., Chappell, P. D., Haley, S. T., Moffett, J. W., Orchard, E. D., Waterbury, J. B. & Webb, E. A. (2006). *Nature (London)*, **439**, 68–71.
Edgar, R. C. (2004). *Nucleic Acids Res.* **32**, 1792–1797.
Elias, M., Wellner, A., Goldin-Azulay, K., Chabriere, E., Vorholt, J. A., Erb, T. J. & Tawfik, D. S. (2012). *Nature (London)*, **491**, 134–137.
Emsley, P., Lohkamp, B., Scott, W. G. & Cowtan, K. (2010). *Acta Cryst.* D**66**, 486–501.
Filloux, A. (2011). *Front. Microbiol.* **2**, 155.
Filloux, A., Bally, M., Soscia, C., Murgier, M. & Lazdunski, A. (1988). *Mol. Gen. Genet.* **212**, 510–513.
Hsieh, Y.-J. & Wanner, B. L. (2010). *Curr. Opin. Microbiol.* **13**, 198–203.
Kabsch, W. (2010). *Acta Cryst.* D**66**, 125–132.
Kriakov, J., Lee, S. & Jacobs, W. R. Jr (2003). *J. Bacteriol.* **185**, 4983–4991.
Liebschner, D., Elias, M., Moniot, S., Fournier, B., Scott, K., Jelsch, C., Guillot, B., Lecomte, C. & Chabrière, E. (2009). *J. Am. Chem. Soc.* **131**, 7879–7886.
Matthews, B. W. (1968). *J. Mol. Biol.* **33**, 491–497.
McCoy, A. J., Grosse-Kunstleve, R. W., Adams, P. D., Winn, M. D., Storoni, L. C. & Read, R. J. (2007). *J. Appl. Cryst.* **40**, 658–674.
Moniot, S., Elias, M., Kim, D., Scott, K. & Chabriere, E. (2007). *Acta Cryst.* F**63**, 590–592.
Moreland, N., Ashton, R., Baker, H. M., Ivanovic, I., Patterson, S., Arcus, V. L., Baker, E. N. & Lott, J. S. (2005). *Acta Cryst.* D**61**, 1378–1385.
Murshudov, G. N., Skubák, P., Lebedev, A. A., Pannu, N. S., Steiner, R. A., Nicholls, R. A., Winn, M. D., Long, F. & Vagin, A. A. (2011). *Acta Cryst.* D**67**, 355–367.
Nallamsetty, S., Austin, B. P., Penrose, K. J. & Waugh, D. S. (2005). *Protein Sci.* **14**, 2964–2971.
Ohtake, H., Kato, J., Kuroda, A., Wu, H. & Ikeda, T. (1998). *J. Biosci.* **23**, 491–499.
Studier, F. W. (2005). *Protein Expr. Purif.* **41**, 207–234.
Sun, L., Martin, D. C. & Kantrowitz, E. R. (1999). *Biochemistry*, **38**, 2842–2848.
Tamura, K., Peterson, D., Peterson, N., Stecher, G., Nei, M. & Kumar, S. (2011). *Mol. Biol. Evol.* **28**, 2731–2739.
Tan, A. S. P. & Worobec, E. A. (1993). *FEMS Microbiol. Lett.* **106**, 281–286.
VanBogelen, R. A., Olson, E. R., Wanner, B. L. & Neidhardt, F. C. (1996). *J. Bacteriol.* **178**, 4344–4366.
Wanner, B. L. (1993). *J. Cell. Biochem.* **51**, 47–54.
Willsky, G. R. & Malamy, M. H. (1980). *J. Bacteriol.* **144**, 356–365.
Zhang, X.-X., Scott, K., Meffin, R. & Rainey, P. B. (2007). *BMC Microbiol.* **7**, 114.

VIII. Références bibliographiques

1. Gupta RC (2009) Handbook of Toxicology of Chemical Warfare Agents.
2. Rajaee F (1993) The Iran-Iraq War - The politics of Aggression.
3. Golomb BA (2008) Acetylcholinesterase inhibitors and Gulf War illnesses. *Proc Natl Acad Sci U S A* 105(11):4295-4300.
4. Israeli E, Agmon-Levin N, Blank M, & Shoenfeld Y (2009) Adjuvants and autoimmunity. *Lupus* 18(13):1217-1225.
5. WEAPONS OFTPOC (CONVENTION ON THE PROHIBITION OF THE DEVELOPMENT, PRODUCTION, STOCKPILING AND USE OF CHEMICAL WEAPONS AND ON THEIR DESTRUCTION
6. Krieger R (Handbook of pesticide toxicology - Principles.
7. Sussman JL*, et al.* (1991) Atomic structure of acetylcholinesterase from Torpedo californica: a prototypic acetylcholine-binding protein. *Science* 253(5022):872-879.
8. Curtil C & Masson P (1993) [Aging of cholinesterase after inhibition by organophosphates]. *Annales pharmaceutiques francaises* 51(2):63-77.
9. Masson P (2011) Evolution of and perspectives on therapeutic approaches to nerve agent poisoning. *Toxicology letters* 206(1):5-13.
10. Authority EFS (2012) The 2009 European Union Report on Pesticide Residues in Food. *EFSA Journal* 9(11):2430.
11. Anonymous (Exposition de la population française aux substances chimiques de l'environnement - Tome 2 : Polychlorobiphényles (PCB-NDL) et Pesticides. *Institut de veille sanitaire (INVS)*.
12. A. Grube DD, T. Kiely and L. Wu (2007) Pesticides Industry Sales and Usage 2006 and 2007 Market Estimates. *EPA*.
13. Eyer P (2003) The role of oximes in the management of organophosphorus pesticide poisoning. *Toxicological reviews* 22(3):165-190.
14. Eddleston M & Phillips MR (2004) Self poisoning with pesticides. *Bmj* 328(7430):42-44.
15. Costa LG (2006) Current issues in organophosphate toxicology. *Clinica chimica acta; international journal of clinical chemistry* 366(1-2):1-13.
16. Rauh VA*, et al.* (2012) Brain anomalies in children exposed prenatally to a common organophosphate pesticide. *Proceedings of the National Academy of Sciences of the United States of America* 109(20):7871-7876.
17. MORTUREUX M (2012) AVIS de l'Agence nationale de sécurité sanitaire de l'alimentation, de l'environnement et du travail *Anses* Saisine n° 2012-SA-0222.
18. El-Masry EM & Abou-Donia MB (2006) Interaction of pyridostigmine bromide and N,N-diethyl-m-toluamide alone and in combination with P-glycoprotein expressed in Escherichia coli leaky mutant. *Journal of toxicology and environmental health. Part A* 69(10):919-933.
19. Theriot CM & Grunden AM (2011) Hydrolysis of organophosphorus compounds by microbial enzymes. *Applied microbiology and biotechnology* 89(1):35-43.
20. LeJeune KE, Wild JR, & Russell AJ (1998) Nerve agents degraded by enzymatic foams. *Nature* 395(6697):27-28.
21. diTargiani RC, Chandrasekaran L, Belinskaya T, & Saxena A (2010) In search of a catalytic bioscavenger for the prophylaxis of nerve agent toxicity. *Chemico-biological interactions* 187(1-3):349-354.
22. Lenz DE*, et al.* (2007) Stoichiometric and catalytic scavengers as protection against nerve agent toxicity: a mini review. *Toxicology* 233(1-3):31-39.

23. Lane RM, Potkin SG, & Enz A (2006) Targeting acetylcholinesterase and butyrylcholinesterase in dementia. *The international journal of neuropsychopharmacology / official scientific journal of the Collegium Internationale Neuropsychopharmacologicum* 9(1):101-124.
24. Soreq H & Seidman S (2001) Acetylcholinesterase--new roles for an old actor. *Nature reviews. Neuroscience* 2(4):294-302.
25. Gorelick DA (1997) Enhancing cocaine metabolism with butyrylcholinesterase as a treatment strategy. *Drug Alcohol Depend* 48(3):159-165.
26. Nicolet Y, Lockridge O, Masson P, Fontecilla-Camps JC, & Nachon F (2003) Crystal structure of human butyrylcholinesterase and of its complexes with substrate and products. *The Journal of biological chemistry* 278(42):41141-41147.
27. Raveh L, *et al.* (1993) Human butyrylcholinesterase as a general prophylactic antidote for nerve agent toxicity. In vitro and in vivo quantitative characterization. *Biochem Pharmacol* 45(12):2465-2474.
28. Masson P & Lockridge O (2010) Butyrylcholinesterase for protection from organophosphorus poisons: catalytic complexities and hysteretic behavior. *Archives of biochemistry and biophysics* 494(2):107-120.
29. Lockridge O & Masson P (2000) Pesticides and susceptible populations: people with butyrylcholinesterase genetic variants may be at risk. *Neurotoxicology* 21(1-2):113-126.
30. Masson P, Carletti E, & Nachon F (2009) Structure, activities and biomedical applications of human butyrylcholinesterase. *Protein and peptide letters* 16(10):1215-1224.
31. Saxena A, Luo C, & Doctor BP (2008) Developing procedures for the large-scale purification of human serum butyrylcholinesterase. *Protein Expr Purif* 61(2):191-196.
32. Millard CB, *et al.* (1999) Crystal structures of aged phosphonylated acetylcholinesterase: nerve agent reaction products at the atomic level. *Biochemistry* 38(22):7032-7039.
33. Worek F, *et al.* (2010) Evaluation of medical countermeasures against organophosphorus compounds: the value of experimental data and computer simulations. *Chemico-biological interactions* 187(1-3):259-264.
34. Eyer P, Worek F, Thiermann H, & Eddleston M (2010) Paradox findings may challenge orthodox reasoning in acute organophosphate poisoning. *Chemico-biological interactions* 187(1-3):270-278.
35. Mazor O, *et al.* (2008) Aging-resistant organophosphate bioscavenger based on polyethylene glycol-conjugated F338A human acetylcholinesterase. *Mol Pharmacol* 74(3):755-763.
36. Saxena A, *et al.* (1997) Mutant acetylcholinesterases as potential detoxification agents for organophosphate poisoning. *Biochem Pharmacol* 54(2):269-274.
37. Barelli A, Soave PM, Del Vicario M, & Barelli R (2011) New experimental Oximes in the management of organophosphorus pesticides poisoning. *Minerva anestesiologica* 77(12):1197-1203.
38. Masson P, *et al.* (2008) A collaborative endeavor to design cholinesterase-based catalytic scavengers against toxic organophosphorus esters. *Chemico-biological interactions* 175(1-3):273-280.
39. Lockridge O, *et al.* (1997) A single amino acid substitution, Gly117His, confers phosphotriesterase (organophosphorus acid anhydride hydrolase) activity on human butyrylcholinesterase. *Biochemistry* 36(4):786-795.
40. Trovaslet-Leroy M, *et al.* (2011) Organophosphate hydrolases as catalytic bioscavengers of organophosphorus nerve agents. *Toxicol Lett* 206(1):14-23.
41. Nachon F, *et al.* (2011) X-ray crystallographic snapshots of reaction intermediates in the G117H mutant of human butyrylcholinesterase, a nerve agent target engineered into a catalytic bioscavenger. *The Biochemical journal* 434(1):73-82.
42. Poyot T, *et al.* (2006) Mutant of Bungarus fasciatus acetylcholinesterase with low affinity and low hydrolase activity toward organophosphorus esters. *Biochim Biophys Acta* 1764(9):1470-1478.

43. Angkawidjaja C, Koga Y, Takano K, & Kanaya S (2012) Structure and stability of a thermostable carboxylesterase from the thermoacidophilic archaeon Sulfolobus tokodaii. *The FEBS journal* 279(17):3071-3084.
44. Sanghani SP, Sanghani PC, Schiel MA, & Bosron WF (2009) Human carboxylesterases: an update on CES1, CES2 and CES3. *Protein and peptide letters* 16(10):1207-1214.
45. Marshall SD, Putterill JJ, Plummer KM, & Newcomb RD (2003) The carboxylesterase gene family from Arabidopsis thaliana. *Journal of molecular evolution* 57(5):487-500.
46. Mandrich L, Merone L, & Manco G (2009) Structural and kinetic overview of the carboxylesterase EST2 from alicyclobacillus acidocaldarius: a comparison with the other members of the HSL family. *Protein and peptide letters* 16(10):1189-1200.
47. Coppin CW*, et al.* (2012) Testing the evolvability of an insect carboxylesterase for the detoxification of synthetic pyrethroid insecticides. *Insect biochemistry and molecular biology* 42(5):343-352.
48. Bencharit S, Morton CL, Xue Y, Potter PM, & Redinbo MR (2003) Structural basis of heroin and cocaine metabolism by a promiscuous human drug-processing enzyme. *Nature structural biology* 10(5):349-356.
49. Satoh T & Hosokawa M (2006) Structure, function and regulation of carboxylesterases. *Chemico-biological interactions* 162(3):195-211.
50. Fleming CD*, et al.* (2007) Crystal structures of human carboxylesterase 1 in covalent complexes with the chemical warfare agents soman and tabun. *Biochemistry* 46(17):5063-5071.
51. Newcomb RD, East PD, Russell RJ, & Oakeshott JG (1996) Isolation of alpha cluster esterase genes associated with organophosphate resistance in Lucilia cuprina. *Insect molecular biology* 5(3):211-216.
52. Jackson CJ*, et al.* (2013) Structure and function of an insect alpha-carboxylesterase (alphaEsterase7) associated with insecticide resistance. *Proceedings of the National Academy of Sciences of the United States of America* 110(25):10177-10182.
53. Newcomb RD*, et al.* (1997) A single amino acid substitution converts a carboxylesterase to an organophosphorus hydrolase and confers insecticide resistance on a blowfly. *Proceedings of the National Academy of Sciences of the United States of America* 94(14):7464-7468.
54. Hemmert AC*, et al.* (2011) Nerve agent hydrolysis activity designed into a human drug metabolism enzyme. *PloS one* 6(3):e17441.
55. Aldridge WN (1953) Serum esterases. II. An enzyme hydrolysing diethyl p-nitrophenyl phosphate (E600) and its identity with the A-esterase of mammalian sera. *The Biochemical journal* 53(1):117-124.
56. Aldridge WN (1953) Serum esterases. I. Two types of esterase (A and B) hydrolysing p-nitrophenyl acetate, propionate and butyrate, and a method for their determination. *The Biochemical journal* 53(1):110-117.
57. Hoskin FC, Kirkish MA, & Steinmann KE (1984) Two enzymes for the detoxication of organophosphorus compounds--sources, similarities, and significance. *Fundamental and applied toxicology : official journal of the Society of Toxicology* 4(2 Pt 2):S165-172.
58. Bigley AN & Raushel FM (2013) Catalytic mechanisms for phosphotriesterases. *Biochimica et biophysica acta* 1834(1):443-453.
59. Scharff EI, Koepke J, Fritzsch G, Lucke C, & Ruterjans H (2001) Crystal structure of diisopropylfluorophosphatase from Loligo vulgaris. *Structure* 9(6):493-502.
60. Aharoni A*, et al.* (2004) Directed evolution of mammalian paraoxonases PON1 and PON3 for bacterial expression and catalytic specialization. *Proceedings of the National Academy of Sciences of the United States of America* 101(2):482-487.
61. Harel M*, et al.* (2004) Structure and evolution of the serum paraoxonase family of detoxifying and anti-atherosclerotic enzymes. *Nature structural & molecular biology* 11(5):412-419.

62. Chen CK, Chan NL, & Wang AH (2011) The many blades of the beta-propeller proteins: conserved but versatile. *Trends Biochem Sci* 36(10):553-561.
63. Fulop V & Jones DT (1999) Beta propellers: structural rigidity and functional diversity. *Curr Opin Struct Biol* 9(6):715-721.
64. Blum MM, Lohr F, Richardt A, Ruterjans H, & Chen JC (2006) Binding of a designed substrate analogue to diisopropyl fluorophosphatase: implications for the phosphotriesterase mechanism. *Journal of the American Chemical Society* 128(39):12750-12757.
65. Ben-David M*, et al.* (2013) Catalytic metal ion rearrangements underline promiscuity and evolvability of a metalloenzyme. *Journal of molecular biology* 425(6):1028-1038.
66. Ben-David M*, et al.* (2012) Catalytic versatility and backups in enzyme active sites: the case of serum paraoxonase 1. *Journal of molecular biology* 418(3-4):181-196.
67. Elias M*, et al.* (2013) Hydrogen atoms in protein structures: high-resolution X-ray diffraction structure of the DFPase. *BMC research notes* 6:308.
68. Scharff EI*, et al.* (2001) Crystallization and preliminary X-ray crystallographic analysis of DFPase from Loligo vulgaris. *Acta crystallographica. Section D, Biological crystallography* 57(Pt 1):148-149.
69. Hartleib J & Ruterjans H (2001) High-yield expression, purification, and characterization of the recombinant diisopropylfluorophosphatase from Loligo vulgaris. *Protein expression and purification* 21(1):210-219.
70. Hartleib J & Ruterjans H (2001) Insights into the reaction mechanism of the diisopropyl fluorophosphatase from Loligo vulgaris by means of kinetic studies, chemical modification and site-directed mutagenesis. *Biochimica et biophysica acta* 1546(2):312-324.
71. Blum MM, Timperley CM, Williams GR, Thiermann H, & Worek F (2008) Inhibitory potency against human acetylcholinesterase and enzymatic hydrolysis of fluorogenic nerve agent mimics by human paraoxonase 1 and squid diisopropyl fluorophosphatase. *Biochemistry* 47(18):5216-5224.
72. Koepke J, Scharff EI, Lucke C, Ruterjans H, & Fritzsch G (2002) Atomic resolution crystal structure of squid ganglion DFPase. *Acta Crystallogr D Biol Crystallogr* 58(Pt 10 Pt 1):1757-1759.
73. Blum MM*, et al.* (2009) Rapid determination of hydrogen positions and protonation states of diisopropyl fluorophosphatase by joint neutron and X-ray diffraction refinement. *Proc Natl Acad Sci U S A* 106(3):713-718.
74. Durrington PN, Mackness B, & Mackness MI (2001) Paraoxonase and atherosclerosis. *Arteriosclerosis, thrombosis, and vascular biology* 21(4):473-480.
75. Seo D & Goldschmidt-Clermont P (2009) The paraoxonase gene family and atherosclerosis. *Current atherosclerosis reports* 11(3):182-187.
76. Rochu D, Chabriere E, & Masson P (2007) Human paraoxonase: a promising approach for pre-treatment and therapy of organophosphorus poisoning. *Toxicology* 233(1-3):47-59.
77. Draganov DI*, et al.* (2005) Human paraoxonases (PON1, PON2, and PON3) are lactonases with overlapping and distinct substrate specificities. *Journal of lipid research* 46(6):1239-1247.
78. Khersonsky O & Tawfik DS (2005) Structure-reactivity studies of serum paraoxonase PON1 suggest that its native activity is lactonase. *Biochemistry* 44(16):6371-6382.
79. Bar-Rogovsky H, Hugenmatter A, & Tawfik DS (2013) The Evolutionary Origins of Detoxifying Enzymes: THE MAMMALIAN SERUM PARAOXONASES (PONs) RELATE TO BACTERIAL HOMOSERINE LACTONASES. *The Journal of biological chemistry* 288(33):23914-23927.
80. Shih DM*, et al.* (1998) Mice lacking serum paraoxonase are susceptible to organophosphate toxicity and atherosclerosis. *Nature* 394(6690):284-287.
81. Sorenson RC*, et al.* (1999) Human serum Paraoxonase/Arylesterase's retained hydrophobic N-terminal leader sequence associates with HDLs by binding phospholipids

: apolipoprotein A-I stabilizes activity. *Arteriosclerosis, thrombosis, and vascular biology* 19(9):2214-2225.
82. Morales R, *et al.* (2006) Serendipitous discovery and X-ray structure of a human phosphate binding apolipoprotein. *Structure* 14(3):601-609.
83. Rochu D, Renault F, Clery-Barraud C, Chabriere E, & Masson P (2007) Stability of highly purified human paraoxonase (PON1): association with human phosphate binding protein (HPBP) is essential for preserving its active conformation(s). *Biochim Biophys Acta* 1774(7):874-883.
84. Doctor BP & Saxena A (2005) Bioscavengers for the protection of humans against organophosphate toxicity. *Chem Biol Interact* 157-158:167-171.
85. Renault F, *et al.* (2006) Tandem purification of two HDL-associated partner proteins in human plasma, paraoxonase (PON1) and phosphate binding protein (HPBP) using hydroxyapatite chromatography. *J Chromatogr B Analyt Technol Biomed Life Sci* 836(1-2):15-21.
86. Harel M, *et al.* (2007) 3-D structure of serum paraoxonase 1 sheds light on its activity, stability, solubility and crystallizability. *Arh Hig Rada Toksikol* 58(3):347-353.
87. Gupta RD, *et al.* (2011) Directed evolution of hydrolases for prevention of G-type nerve agent intoxication. *Nature chemical biology* 7(2):120-125.
88. Goldsmith M, *et al.* (2012) Evolved stereoselective hydrolases for broad-spectrum G-type nerve agent detoxification. *Chemistry & biology* 19(4):456-466.
89. Ashani Y, *et al.* (2011) In vitro detoxification of cyclosarin in human blood pre-incubated ex vivo with recombinant serum paraoxonases. *Toxicology letters* 206(1):24-28.
90. Sarkar M, *et al.* (2012) Solubilization and humanization of paraoxonase-1. *Journal of lipids* 2012:610937.
91. Kondo Y, *et al.* (2004) Senescence marker protein-30 is a unique enzyme that hydrolyzes diisopropyl phosphorofluoridate in the liver. *FEBS letters* 570(1-3):57-62.
92. Kondo Y, *et al.* (2006) Senescence marker protein 30 functions as gluconolactonase in L-ascorbic acid biosynthesis, and its knockout mice are prone to scurvy. *Proceedings of the National Academy of Sciences of the United States of America* 103(15):5723-5728.
93. Aizawa S, *et al.* (2013) Structural basis of the gamma-lactone-ring formation in ascorbic acid biosynthesis by the senescence marker protein-30/gluconolactonase. *PloS one* 8(1):e53706.
94. Chen CN, Chin KH, Wang AH, & Chou SH (2008) The first crystal structure of gluconolactonase important in the glucose secondary metabolic pathways. *Journal of molecular biology* 384(3):604-614.
95. Tanaka Y, *et al.* (2007) Structural and mutational analyses of Drp35 from Staphylococcus aureus: a possible mechanism for its lactonase activity. *The Journal of biological chemistry* 282(8):5770-5780.
96. Kitchener RL & Grunden AM (2012) Prolidase function in proline metabolism and its medical and biotechnological applications. *Journal of applied microbiology* 113(2):233-247.
97. Lupi A, Tenni R, Rossi A, Cetta G, & Forlino A (2008) Human prolidase and prolidase deficiency: an overview on the characterization of the enzyme involved in proline recycling and on the effects of its mutations. *Amino acids* 35(4):739-752.
98. Cheng TC, Harvey SP, & Stroup AN (1993) Purification and Properties of a Highly Active Organophosphorus Acid Anhydrolase from Alteromonas undina. *Applied and environmental microbiology* 59(9):3138-3140.
99. DeFrank JJ & Cheng TC (1991) Purification and properties of an organophosphorus acid anhydrase from a halophilic bacterial isolate. *Journal of bacteriology* 173(6):1938-1943.
100. Cheng TC, DeFrank JJ, & Rastogi VK (1999) Alteromonas prolidase for organophosphorus G-agent decontamination. *Chemico-biological interactions* 119-120:455-462.

101. Vyas NK, Nickitenko A, Rastogi VK, Shah SS, & Quiocho FA (2010) Structural insights into the dual activities of the nerve agent degrading organophosphate anhydrolase/prolidase. *Biochemistry* 49(3):547-559.
102. Hsu YT, Su CY, Du HC, Jao SC, & Li WS (2008) Evaluation of organophosphorus chemicals-degrading enzymes: a comparison of Escherichia coli and human cytosolic aminopeptidase P. *Chemistry & biodiversity* 5(7):1401-1411.
103. Cheng T*, et al.* (1997) Nucleotide sequence of a gene encoding an organophosphorus nerve agent degrading enzyme from Alteromonas haloplanktis. *Journal of industrial microbiology & biotechnology* 18(1):49-55.
104. Rani NL & Lalithakumari D (1994) Degradation of methyl parathion by Pseudomonas putida. *Canadian journal of microbiology* 40(12):1000-1006.
105. Fu G, Cui Z, Huang T, & Li S (2004) Expression, purification, and characterization of a novel methyl parathion hydrolase. *Protein expression and purification* 36(2):170-176.
106. Dong YJ*, et al.* (2005) Crystal structure of methyl parathion hydrolase from Pseudomonas sp. WBC-3. *Journal of molecular biology* 353(3):655-663.
107. Cornaglia G, Giamarellou H, & Rossolini GM (2011) Metallo-beta-lactamases: a last frontier for beta-lactams? *Lancet Infect Dis* 11(5):381-393.
108. Wu N*, et al.* (2004) Cloning and expression of ophc2, a new organophosphorus hydrolase gene. *Chinese Science Bulletin* 49(12):1245-1249.
109. Bebrone C (2007) Metallo-beta-lactamases (classification, activity, genetic organization, structure, zinc coordination) and their superfamily. *Biochem Pharmacol* 74(12):1686-1701.
110. Carfi A*, et al.* (1995) The 3-D structure of a zinc metallo-beta-lactamase from Bacillus cereus reveals a new type of protein fold. *EMBO J* 14(20):4914-4921.
111. Benning MM, Shim H, Raushel FM, & Holden HM (2001) High resolution X-ray structures of different metal-substituted forms of phosphotriesterase from Pseudomonas diminuta. *Biochemistry* 40(9):2712-2722.
112. Zhongli C, Shunpeng L, & Guoping F (2001) Isolation of methyl parathion-degrading strain M6 and cloning of the methyl parathion hydrolase gene. *Appl Environ Microbiol* 67(10):4922-4925.
113. Zhang Z, Hong Q, Xu J, Zhang X, & Li S (2006) Isolation of fenitrothion-degrading strain Burkholderia sp. FDS-1 and cloning of mpd gene. *Biodegradation* 17(3):275-283.
114. Liu H, Zhang JJ, Wang SJ, Zhang XE, & Zhou NY (2005) Plasmid-borne catabolism of methyl parathion and p-nitrophenol in Pseudomonas sp. strain WBC-3. *Biochem Biophys Res Commun* 334(4):1107-1114.
115. Zhang R*, et al.* (2006) Cloning of the organophosphorus pesticide hydrolase gene clusters of seven degradative bacteria isolated from a methyl parathion contaminated site and evidence of their horizontal gene transfer. *Biodegradation* 17(5):465-472.
116. Yang C, Liu N, Guo X, & Qiao C (2006) Cloning of mpd gene from a chlorpyrifos-degrading bacterium and use of this strain in bioremediation of contaminated soil. *Fems Microbiol Lett* 265(1):118-125.
117. Su Y*, et al.* (2011) Improving the thermostability of a methyl parathion hydrolase by adding the ionic bond on protein surface. *Applied biochemistry and biotechnology* 165(3-4):989-997.
118. Tian J*, et al.* (2010) Enhanced thermostability of methyl parathion hydrolase from Ochrobactrum sp. M231 by rational engineering of a glycine to proline mutation. *FEBS J* 277(23):4901-4908.
119. Singh BK & Walker A (2006) Microbial degradation of organophosphorus compounds. *FEMS Microbiol Rev* 30(3):428-471.
120. Singh BK, Walker A, Morgan JA, & Wright DJ (2003) Effects of soil pH on the biodegradation of chlorpyrifos and isolation of a chlorpyrifos-degrading bacterium. *Appl Environ Microbiol* 69(9):5198-5206.

121. Singh BK, Walker A, Morgan JA, & Wright DJ (2003) Role of soil pH in the development of enhanced biodegradation of fenamiphos. *Appl Environ Microbiol* 69(12):7035-7043.
122. Caldwell SR, Newcomb JR, Schlecht KA, & Raushel FM (1991) Limits of diffusion in the hydrolysis of substrates by the phosphotriesterase from Pseudomonas diminuta. *Biochemistry* 30(30):7438-7444.
123. Seibert CM & Raushel FM (2005) Structural and catalytic diversity within the amidohydrolase superfamily. *Biochemistry* 44(17):6383-6391.
124. McDaniel CS, Harper LL, & Wild JR (1988) Cloning and sequencing of a plasmid-borne gene (opd) encoding a phosphotriesterase. *J Bacteriol* 170(5):2306-2311.
125. Horne I, Sutherland TD, Harcourt RL, Russell RJ, & Oakeshott JG (2002) Identification of an opd (organophosphate degradation) gene in an Agrobacterium isolate. *Appl Environ Microbiol* 68(7):3371-3376.
126. Benning MM, Kuo JM, Raushel FM, & Holden HM (1994) Three-dimensional structure of phosphotriesterase: an enzyme capable of detoxifying organophosphate nerve agents. *Biochemistry* 33(50):15001-15007.
127. Vanhooke JL, Benning MM, Raushel FM, & Holden HM (1996) Three-dimensional structure of the zinc-containing phosphotriesterase with the bound substrate analog diethyl 4-methylbenzylphosphonate. *Biochemistry* 35(19):6020-6025.
128. Chen-Goodspeed M, Sogorb MA, Wu F, Hong SB, & Raushel FM (2001) Structural determinants of the substrate and stereochemical specificity of phosphotriesterase. *Biochemistry* 40(5):1325-1331.
129. Chen-Goodspeed M, Sogorb MA, Wu F, & Raushel FM (2001) Enhancement, relaxation, and reversal of the stereoselectivity for phosphotriesterase by rational evolution of active site residues. *Biochemistry* 40(5):1332-1339.
130. Tsai PC*, et al.* (2010) Stereoselective hydrolysis of organophosphate nerve agents by the bacterial phosphotriesterase. *Biochemistry* 49(37):7978-7987.
131. Samples CR, Howard T, Raushel FM, & DeRose VJ (2005) Protonation of the binuclear metal center within the active site of phosphotriesterase. *Biochemistry* 44(33):11005-11013.
132. Jackson CJ*, et al.* (2009) Conformational sampling, catalysis, and evolution of the bacterial phosphotriesterase. *Proceedings of the National Academy of Sciences of the United States of America* 106(51):21631-21636.
133. Hong SB & Raushel FM (1996) Metal-substrate interactions facilitate the catalytic activity of the bacterial phosphotriesterase. *Biochemistry* 35(33):10904-10912.
134. Munnecke DM (1976) Enzymatic hydrolysis of organophosphate insecticides, a possible pesticide disposal method. *Appl Environ Microbiol* 32(1):7-13.
135. Sethunathan N & Yoshida T (1973) A Flavobacterium sp. that degrades diazinon and parathion. *Can J Microbiol* 19(7):873-875.
136. Siddavattam D, Khajamohiddin S, Manavathi B, Pakala SB, & Merrick M (2003) Transposon-like organization of the plasmid-borne organophosphate degradation (opd) gene cluster found in Flavobacterium sp. *Applied and environmental microbiology* 69(5):2533-2539.
137. Singh BK (2009) Organophosphorus-degrading bacteria: ecology and industrial applications. *Nature reviews. Microbiology* 7(2):156-164.
138. Hill CM, Li WS, Thoden JB, Holden HM, & Raushel FM (2003) Enhanced degradation of chemical warfare agents through molecular engineering of the phosphotriesterase active site. *Journal of the American Chemical Society* 125(30):8990-8991.
139. Yang H*, et al.* (2003) Evolution of an organophosphate-degrading enzyme: a comparison of natural and directed evolution. *Protein Eng* 16(2):135-145.
140. Jackson CJ*, et al.* (2006) Anomalous scattering analysis of Agrobacterium radiobacter phosphotriesterase: the prominent role of iron in the heterobinuclear active site. *The Biochemical journal* 397(3):501-508.

141. Jackson CJ, *et al.* (2008) In crystallo capture of a Michaelis complex and product-binding modes of a bacterial phosphotriesterase. *J Mol Biol* 375(5):1189-1196.
142. McLoughlin SY, Jackson C, Liu JW, & Ollis D (2005) Increased expression of a bacterial phosphotriesterase in Escherichia coli through directed evolution. *Protein Expr Purif* 41(2):433-440.
143. Bird SB, *et al.* (2008) OpdA, a bacterial organophosphorus hydrolase, prevents lethality in rats after poisoning with highly toxic organophosphorus pesticides. *Toxicology* 247(2-3):88-92.
144. Blatchford PA, Scott C, French N, & Rehm BH (2012) Immobilization of organophosphohydrolase OpdA from Agrobacterium radiobacter by overproduction at the surface of polyester inclusions inside engineered Escherichia coli. *Biotechnol Bioeng* 109(5):1101-1108.
145. Raushel FM (2002) Bacterial detoxification of organophosphate nerve agents. *Current opinion in microbiology* 5(3):288-295.
146. Bigley AN, Xu C, Henderson TJ, Harvey SP, & Raushel FM (2013) Enzymatic Neutralization of the Chemical Warfare Agent VX: Evolution of Phosphotriesterase for Phosphorothiolate Hydrolysis. *Journal of the American Chemical Society* 135(28):10426-10432.
147. Vieille C & Zeikus GJ (2001) Hyperthermophilic enzymes: sources, uses, and molecular mechanisms for thermostability. *Microbiology and molecular biology reviews : MMBR* 65(1):1-43.
148. Niehaus F, Bertoldo C, Kahler M, & Antranikian G (1999) Extremophiles as a source of novel enzymes for industrial application. *Applied microbiology and biotechnology* 51(6):711-729.
149. Demirjian DC, Moris-Varas F, & Cassidy CS (2001) Enzymes from extremophiles. *Current opinion in chemical biology* 5(2):144-151.
150. Gonzalez JM, *et al.* (1998) Pyrococcus horikoshii sp. nov., a hyperthermophilic archaeon isolated from a hydrothermal vent at the Okinawa Trough. *Extremophiles : life under extreme conditions* 2(2):123-130.
151. Maher MJ, *et al.* (2004) Structure of the prolidase from Pyrococcus furiosus. *Biochemistry* 43(10):2771-2783.
152. Jeyakanthan J, *et al.* (2009) Crystal Structural and Functional Analysis of the Putative Dipeptidase from Pyrococcus horikoshii OT3. *Journal of biophysics* 2009:434038.
153. Ghosh M, Grunden AM, Dunn DM, Weiss R, & Adams MW (1998) Characterization of native and recombinant forms of an unusual cobalt-dependent proline dipeptidase (prolidase) from the hyperthermophilic archaeon Pyrococcus furiosus. *Journal of bacteriology* 180(18):4781-4789.
154. Theriot CM, Tove SR, & Grunden AM (2010) Characterization of two proline dipeptidases (prolidases) from the hyperthermophilic archaeon Pyrococcus horikoshii. *Applied microbiology and biotechnology* 86(1):177-188.
155. Theriot CM, Du X, Tove SR, & Grunden AM (2010) Improving the catalytic activity of hyperthermophilic Pyrococcus prolidases for detoxification of organophosphorus nerve agents over a broad range of temperatures. *Applied microbiology and biotechnology* 87(5):1715-1726.
156. Wu N, *et al.* (2004) Isolation, purification and characterization of a new organosphosphorus hydrolase OPHC2. *Chinese Science Bulletin* 49(3):268-272.
157. Shen YJ, *et al.* (2010) Isolation of a methyl parathion-degrading strain Stenotrophomonas sp. SMSP-1 and cloning of the ophc2 gene. *Biodegradation* 21(5):785-792.
158. Chu XY, *et al.* (2006) Expression of organophosphorus hydrolase OPHC2 in Pichia pastoris: purification and characterization. *Protein expression and purification* 49(1):9-14.

159. Chu XY, Tian J, Wu NF, & Fan YL (2010) An intramolecular disulfide bond is required for the thermostability of methyl parathion hydrolase, OPHC2. *Appl Microbiol Biotechnol* 88(1):125-131.
160. Afriat L, Roodveldt C, Manco G, & Tawfik DS (2006) The latent promiscuity of newly identified microbial lactonases is linked to a recently diverged phosphotriesterase. *Biochemistry* 45(46):13677-13686.
161. Afriat-Jurnou L, Jackson CJ, & Tawfik DS (2012) Reconstructing a missing link in the evolution of a recently diverged phosphotriesterase by active-site loop remodeling. *Biochemistry* 51(31):6047-6055.
162. Hawwa R, Larsen SD, Ratia K, & Mesecar AD (2009) Structure-based and random mutagenesis approaches increase the organophosphate-degrading activity of a phosphotriesterase homologue from Deinococcus radiodurans. *Journal of molecular biology* 393(1):36-57.
163. Elias M, *et al.* (2008) Structural basis for natural lactonase and promiscuous phosphotriesterase activities. *Journal of molecular biology* 379(5):1017-1028.
164. Porzio E, Merone L, Mandrich L, Rossi M, & Manco G (2007) A new phosphotriesterase from Sulfolobus acidocaldarius and its comparison with the homologue from Sulfolobus solfataricus. *Biochimie* 89(5):625-636.
165. Uroz S, *et al.* (2008) A Rhodococcus qsdA-encoded enzyme defines a novel class of large-spectrum quorum-quenching lactonases. *Applied and environmental microbiology* 74(5):1357-1366.
166. Chow JY, Wu L, & Yew WS (2009) Directed evolution of a quorum-quenching lactonase from Mycobacterium avium subsp. paratuberculosis K-10 in the amidohydrolase superfamily. *Biochemistry* 48(20):4344-4353.
167. Chow JY, *et al.* (2010) Directed evolution of a thermostable quorum-quenching lactonase from the amidohydrolase superfamily. *The Journal of biological chemistry* 285(52):40911-40920.
168. Zhang Y, *et al.* (2012) Enhancing the promiscuous phosphotriesterase activity of a thermostable lactonase (GkaP) for the efficient degradation of organophosphate pesticides. *Applied and environmental microbiology* 78(18):6647-6655.
169. Hawwa R, Aikens J, Turner RJ, Santarsiero BD, & Mesecar AD (2009) Structural basis for thermostability revealed through the identification and characterization of a highly thermostable phosphotriesterase-like lactonase from Geobacillus stearothermophilus. *Archives of biochemistry and biophysics* 488(2):109-120.
170. McMullan G, *et al.* (2004) Habitat, applications and genomics of the aerobic, thermophilic genus Geobacillus. *Biochemical Society transactions* 32(Pt 2):214-217.
171. Nazina TN, *et al.* (2001) Taxonomic study of aerobic thermophilic bacilli: descriptions of Geobacillus subterraneus gen. nov., sp. nov. and Geobacillus uzenensis sp. nov. from petroleum reservoirs and transfer of Bacillus stearothermophilus, Bacillus thermocatenulatus, Bacillus thermoleovorans, Bacillus kaustophilus, Bacillus thermodenitrificans to Geobacillus as the new combinations G. stearothermophilus, G. th. *International journal of systematic and evolutionary microbiology* 51(Pt 2):433-446.
172. Murray RGE (1992) The family Deinococcaceae. *The prokaryotes*:3732–3744.
173. de Miguel Bouzas T, Barros-Velazquez J, & Villa TG (2006) Industrial applications of hyperthermophilic enzymes: a review. *Protein and peptide letters* 13(7):645-651.
174. van den Burg B (2003) Extremophiles as a source for novel enzymes. *Current opinion in microbiology* 6(3):213-218.
175. Auernik KS, Cooper CR, & Kelly RM (2008) Life in hot acid: pathway analyses in extremely thermoacidophilic archaea. *Current opinion in biotechnology* 19(5):445-453.
176. Merone L, Mandrich L, Rossi M, & Manco G (2005) A thermostable phosphotriesterase from the archaeon Sulfolobus solfataricus: cloning, overexpression and properties. *Extremophiles* 9(4):297-305.

177. Del Vecchio P, *et al.* (2009) Structural determinants of the high thermal stability of SsoPox from the hyperthermophilic archaeon Sulfolobus solfataricus. *Extremophiles : life under extreme conditions* 13(3):461-470.
178. Merone L, *et al.* (2010) Improving the promiscuous nerve agent hydrolase activity of a thermostable archaeal lactonase. *Bioresource technology* 101(23):9204-9212.
179. Meier MM, *et al.* (2013) Molecular Engineering of Organophosphate Hydrolysis Activity from a Weak Promiscuous Lactonase Template. *Journal of the American Chemical Society*.
180. Khersonsky O, Roodveldt C, & Tawfik DS (2006) Enzyme promiscuity: evolutionary and mechanistic aspects. *Current opinion in chemical biology* 10(5):498-508.
181. Khersonsky O & Tawfik DS (2010) Enzyme promiscuity: a mechanistic and evolutionary perspective. *Annual review of biochemistry* 79:471-505.
182. Hult K & Berglund P (2007) Enzyme promiscuity: mechanism and applications. *Trends in biotechnology* 25(5):231-238.
183. O'Brien PJ & Herschlag D (1999) Catalytic promiscuity and the evolution of new enzymatic activities. *Chemistry & biology* 6(4):R91-R105.
184. Aharoni A, *et al.* (2005) The 'evolvability' of promiscuous protein functions. *Nature genetics* 37(1):73-76.
185. Elias M & Tawfik DS (2012) Divergence and convergence in enzyme evolution: parallel evolution of paraoxonases from quorum-quenching lactonases. *The Journal of biological chemistry* 287(1):11-20.
186. Bar-Rogovsky H, Hugenmatter A, & Tawfik DS (2013) The evolutionary origins of detoxifying enzymes: The mammalian serum paraoxonases (PONs) relate to bacterial homoserine lactonases. *The Journal of biological chemistry*.
187. Mackness B & Mackness M (2010) Anti-inflammatory properties of paraoxonase-1 in atherosclerosis. *Advances in experimental medicine and biology* 660:143-151.
188. Kim MH, *et al.* (2005) The molecular structure and catalytic mechanism of a quorum-quenching N-acyl-L-homoserine lactone hydrolase. *Proceedings of the National Academy of Sciences of the United States of America* 102(49):17606-17611.
189. Liu D, *et al.* (2005) Three-dimensional structure of the quorum-quenching N-acyl homoserine lactone hydrolase from Bacillus thuringiensis. *Proceedings of the National Academy of Sciences of the United States of America* 102(33):11882-11887.
190. Liu D, *et al.* (2008) Mechanism of the quorum-quenching lactonase (AiiA) from Bacillus thuringiensis. 1. Product-bound structures. *Biochemistry* 47(29):7706-7714.
191. Momb J, *et al.* (2008) Mechanism of the quorum-quenching lactonase (AiiA) from Bacillus thuringiensis. 2. Substrate modeling and active site mutations. *Biochemistry* 47(29):7715-7725.
192. Dong YH, *et al.* (2001) Quenching quorum-sensing-dependent bacterial infection by an N-acyl homoserine lactonase. *Nature* 411(6839):813-817.
193. Choudhary S & Schmidt-Dannert C (2010) Applications of quorum sensing in biotechnology. *Applied microbiology and biotechnology* 86(5):1267-1279.
194. Rutherford ST & Bassler BL (2012) Bacterial quorum sensing: its role in virulence and possibilities for its control. *Cold Spring Harbor perspectives in medicine* 2(11).
195. Antunes LC, Ferreira RB, Buckner MM, & Finlay BB (2010) Quorum sensing in bacterial virulence. *Microbiology* 156(Pt 8):2271-2282.
196. Krukonis ES & DiRita VJ (2003) From motility to virulence: Sensing and responding to environmental signals in Vibrio cholerae. *Current opinion in microbiology* 6(2):186-190.
197. Hiblot J, Gotthard G, Chabriere E, & Elias M (2012) Characterisation of the organophosphate hydrolase catalytic activity of SsoPox. *Scientific reports* 2:779.
198. Hiblot J, Gotthard G, Chabriere E, & Elias M (2012) Structural and enzymatic characterization of the lactonase SisLac from Sulfolobus islandicus. *PloS one* 7(10):e47028.
199. Salverda ML, *et al.* (2011) Initial mutations direct alternative pathways of protein evolution. *PLoS genetics* 7(3):e1001321.

200. Breen MS, Kemena C, Vlasov PK, Notredame C, & Kondrashov FA (2012) Epistasis as the primary factor in molecular evolution. *Nature* 490(7421):535-538.
201. Bershtein S, Segal M, Bekerman R, Tokuriki N, & Tawfik DS (2006) Robustness-epistasis link shapes the fitness landscape of a randomly drifting protein. *Nature* 444(7121):929-932.
202. Dickschat JS (2010) Quorum sensing and bacterial biofilms. *Natural product reports* 27(3):343-369.
203. Tokuriki N*, et al.* (2012) Diminishing returns and tradeoffs constrain the laboratory optimization of an enzyme. *Nature communications* 3:1257.
204. Gumerov VM*, et al.* (2011) Complete genome sequence of "Vulcanisaeta moutnovskia" strain 768-28, a novel member of the hyperthermophilic crenarchaeal genus Vulcanisaeta. *Journal of bacteriology* 193(9):2355-2356.
205. Chen L*, et al.* (2005) The genome of Sulfolobus acidocaldarius, a model organism of the Crenarchaeota. *Journal of bacteriology* 187(14):4992-4999.
206. Porzio E, Di Gennaro S, Palma A, & Manco G (2013) Mn2+ modulates the kinetic properties of an archaeal member of the PLL family. *Chemico-biological interactions* 203(1):251-256.
207. Reno ML, Held NL, Fields CJ, Burke PV, & Whitaker RJ (2009) Biogeography of the Sulfolobus islandicus pan-genome. *Proceedings of the National Academy of Sciences of the United States of America* 106(21):8605-8610.
208. Zhang G*, et al.* (2012) Acyl homoserine lactone-based quorum sensing in a methanogenic archaeon. *The ISME journal* 6(7):1336-1344.
209. Liu D*, et al.* (2007) Structure and specificity of a quorum-quenching lactonase (AiiB) from Agrobacterium tumefaciens. *Biochemistry* 46(42):11789-11799.
210. Alcolombri U, Elias M, & Tawfik DS (2011) Directed evolution of sulfotransferases and paraoxonases by ancestral libraries. *Journal of molecular biology* 411(4):837-853.
211. Tokuriki N & Tawfik DS (2009) Stability effects of mutations and protein evolvability. *Current opinion in structural biology* 19(5):596-604.
212. Tokuriki N & Tawfik DS (2009) Protein dynamism and evolvability. *Science* 324(5924):203-207.
213. Dellus-Gur E, Toth-Petroczy A, Elias M, & Tawfik DS (2013) What Makes a Protein Fold Amenable to Functional Innovation? Fold Polarity and Stability Trade-offs. *Journal of molecular biology* 425(14):2609-2621.
214. Bloom JD, Labthavikul ST, Otey CR, & Arnold FH (2006) Protein stability promotes evolvability. *Proceedings of the National Academy of Sciences of the United States of America* 103(15):5869-5874.
215. Dumas DP, Caldwell SR, Wild JR, & Raushel FM (1989) Purification and properties of the phosphotriesterase from Pseudomonas diminuta. *The Journal of biological chemistry* 264(33):19659-19665.
216. Xiang DF*, et al.* (2009) Functional annotation and three-dimensional structure of Dr0930 from Deinococcus radiodurans, a close relative of phosphotriesterase in the amidohydrolase superfamily. *Biochemistry* 48(10):2237-2247.
217. Herman A & Tawfik DS (2007) Incorporating Synthetic Oligonucleotides via Gene Reassembly (ISOR): a versatile tool for generating targeted libraries. *Protein engineering, design & selection : PEDS* 20(5):219-226.
218. Meier MM*, et al.* (2013) Molecular engineering of organophosphate hydrolysis activity from a weak promiscuous lactonase template. *Journal of the American Chemical Society* 135(31):11670-11677.
219. Bar-Even A*, et al.* (2011) The moderately efficient enzyme: evolutionary and physicochemical trends shaping enzyme parameters. *Biochemistry* 50(21):4402-4410.
220. Ng FS, Wright DM, & Seah SY (2011) Characterization of a phosphotriesterase-like lactonase from Sulfolobus solfataricus and its immobilization for disruption of quorum sensing. *Applied and environmental microbiology* 77(4):1181-1186.

221. Xue B, *et al.* (2013) Structural evidence of a productive active site architecture for an evolved quorum-quenching GKL lactonase. *Biochemistry* 52(13):2359-2370.
222. Ma F, *et al.* (2009) Heterologous expression of human paraoxonases in Pseudomonas aeruginosa inhibits biofilm formation and decreases antibiotic resistance. *Applied microbiology and biotechnology* 83(1):135-141.
223. Reimmann C, *et al.* (2002) Genetically programmed autoinducer destruction reduces virulence gene expression and swarming motility in Pseudomonas aeruginosa PAO1. *Microbiology* 148(Pt 4):923-932.
224. Landman D, *et al.* (2002) Citywide clonal outbreak of multiresistant Acinetobacter baumannii and Pseudomonas aeruginosa in Brooklyn, NY: the preantibiotic era has returned. *Archives of internal medicine* 162(13):1515-1520.
225. Dong YH, Xu JL, Li XZ, & Zhang LH (2000) AiiA, an enzyme that inactivates the acylhomoserine lactone quorum-sensing signal and attenuates the virulence of Erwinia carotovora. *Proceedings of the National Academy of Sciences of the United States of America* 97(7):3526-3531.
226. Gotthard G, Hiblot J, Elias M, & Chabriere E (2011) Crystallization and preliminary X-ray diffraction analysis of the hyperthermophilic Sulfolobus islandicus lactonase. *Acta crystallographica. Section F, Structural biology and crystallization communications* 67(Pt 3):354-357.
227. Gotthard G, Hiblot J, Gonzalez D, Chabriere E, & Elias M (2013) Crystallization and preliminary X-ray diffraction analysis of the organophosphorus hydrolase OPHC2 from Pseudomonas pseudoalcaligenes. *Acta crystallographica. Section F, Structural biology and crystallization communications* 69(Pt 1):73-76.
228. Studier FW (2005) Protein production by auto-induction in high density shaking cultures. *Protein expression and purification* 41(1):207-234.

Résumé :

Les organophosphorés (OPs) sont des composés synthétiques neurotoxiques qui ont été introduits dans la nature à partir des années 50s et qui sont responsables de pollutions des sols et des eaux. La décontamination de ces composés présente des difficultés liées au coût et aux pollutions secondaires générées. Une solution alternative et élégante aux méthode actuelles réside en l'utilisation d'enzymes capables de dégrader ces composés. Identifiées chez des bactéries du sol, certaines enzymes auraient évolué rapidement (~ 30 ans) pour dégrader ces composés. Bien qu'étant particulièrement actives, celles-ci sont peu stables et chères à produire. Afin de pallier à ces problèmes, nous nous sommes intéressés aux enzymes hyperthermostables, *Sso*Pox et *Sis*Lac, appartenant à la famille des Phosphotriestérases-Like Lactonases (PLLs) présentant des activités de promiscuité phosphotriestérase. L'homologie structurale avec la *Bd*PTE permit de développer une base de données de mutations visant à implanter au sein de *Sso*Pox un cœur catalytique efficace envers les OPs. En utilisant des protocoles de pointe en biologie moléculaire, cette base de données de mutation fut brassée, criblée envers les OPs et permit d'obtenir des variants présentant des amélioration de près de 2000 fois envers certains OPs insecticides. L'analyse structurale effectuée tout au long de ce projet met en évidence des phénomènes de flexibilisation des boucles du site actif permettant d'élargir le paysage conformationnel de l'enzyme lui permettant ainsi d'adopter des conformations plus aptes à hydrolyser les substrats de promiscuité. Les phénomènes de flexibilisation observés au cours de l'évolution *in vitro* de l'enzyme tendent à confirmer certains concepts émergents relatifs à l'évolution naturelle des enzymes. En parallèles, l'activité naturelle lactonase de *Sso*Pox a été caractérisée et améliorée pour hydrolyser les molécules impliquées dans le *quorum* sensing, notamment chez le pathogène *P. aeruginosa*. Les preuves de concept que nous avons effectuées mettent en lumière l'utilisabilité de *Sso*Pox dans le cadre des infections nosocomiales dues à cet organisme.

Summary:

Organophosphorous (OPs) compounds are synthetic nerve agents that have been introduced in Nature from the 50s. OPs compounds are responsible of large soil and water pollutions, making of it a human health problem. Current methods for removing them are cost prohibitive and generate secondary pollutions. An alternative and appealing solution consist in the use of enzymes capable of degrading these compounds. Such enzymes were identified from OPs contaminated soils in which they have evolved to degrade them. Although they evolved to hydrolyze them at high rate, these enzymes are poorly stable and expensive to produce. To overcome these issues, we were interested by hyperthermostable enzymes, *Sso*Pox and *Sis*Lac, belonging to the Phosphotriesterase-Like Lactonase (PLLs) family that are natural lactonase endowed with a promiscuous phosphotriesterase activity. The structural homology with the *Bd*PTE allowed us to develop a mutation database aiming to transfer its highly optimized active site into the highly stable architecture of *Sso*Pox. Using complex molecular biology protocols, this mutation database was screened against OPs hydrolysis, allowing to identify enhanced variant (reaching 2000 times against some insecticides). Structural analysis of these selected variant incriminates active site loops flexibilization resulting in the enlargement of the conformational space of the enzyme. This enlargement then allow the enzyme to better accommodate promiscuous substrates. These flexibilization phenomenon that have been observed during the *in vitro* evolution of *Sso*Pox are in accordance with novel concepts concerning the natural evolution of enzymes. In parallel to these works, the natural lactonase activity of *Sso*Pox was characterized and enhanced to better hydrolyze molecules that are implicated in the *quorum* sensing of *P. aeruginosa*. The proof of concepts that we have carried out, highlights the usability of *Sso*Pox in the fight against nosocomial infections due to this organism.